THE IN SILICO SEARCH FOR AN ENDOGENOUS ANTI-ALZHEIMER'S THERAPEUTIC

by

Autumn Meek

Submitted in partial fulfilment of the requirements
for the degree of Doctor of Philosophy

at

Dalhousie University
Halifax, Nova Scotia
December 2011

DALHOUSIE UNIVERSITY

DEPARTMENT OF CHEMISTRY

The undersigned hereby certify that they have read and recommend to the Faculty of Graduate Studies for acceptance a thesis entitled "THE IN SILICO SEARCH FOR AN ENDOGENOUS ANTI-ALZHEIMER'S THERAPEUTIC" by Autumn Meek in partial fulfilment of the requirements for the degree of Doctor of Philosophy.

Dated: December 9, 2011

External Examiner: _____

Research Supervisor: _____

Examining Committee: _____

_____

Departmental Representative: _____

DALHOUSIE UNIVERSITY

DATE: December 9, 2011

AUTHOR: Autumn Meek

TITLE: THE IN SILICO SEARCH FOR AN ENDOGENOUS ANTI-ALZHEIMER'S THERAPEUTIC

DEPARTMENT OR SCHOOL: Department of Chemistry

DEGREE: PhD CONVOCATION: May YEAR: 2012

_____

Signature of Author

Philippians 4:13

For my family

TABLE OF CONTENTS

LIST OF TABLES

LIST OF FIGURES

ABSTRACT

Alzheimer's disease (AD) is a progressive, degenerative neurological disorder for which there is no cure. The causative agent is β-amyloid (Aβ) which becomes neurotoxic upon conformational change from α-helix to β-sheet. *In silico* methods have been used to indentify endogenous small molecules of the brain that are capable of binding to Aβ to inhibit conformational changes; this is a novel approach to the disease. Through the use of computational methods, several small molecules that are endogenous to the brain, such as phosphoserine, have been identified as being capable of binding to the monomeric forms of Aβ; *in vitro* studies support their role as anti-aggregants. One of the small molecules identified through these *in silico* methods, 3-hydroxyanthranilic acid (3HAA) has been developed through the use of Quantitative Structure-Activity Relationship (QSAR) studies to design more potent analogues. These *in silico* studies have also examined the capacity of synthetic compounds (structurally similar to endogenous molecules) to bind to both Aβ and other proteins affiliated with AD. Results indicate the potential for a single molecule to bind "promiscuously" to multiple proteins bearing a common BBXB (where B is a basic amino acid) motif affiliated with AD. This will allow for the development of molecules to target AD in a multifaceted approach. Furthermore, these small molecules can be selected through the use of "physinformatics" to bind with equal efficacy to the HHQK and LVFF regions (which play a role in the misfolding process) of Aβ; this will prevent conformational changes of the protein. A novel diagnostic imaging agent for AD has also been developed through computational methods; solapsone (formerly used to treat leprosy) has been identified as being structurally similar to species that bind to Aβ to initiate conformational changes. Results show that solapsone can chelate gadolinium, used in MRI, and bind to the soluble forms of Aβ, allowing for imaging of the toxic species in the human brain, and thus a definitive diagnosis of AD (which is not currently possible with living patients). Computational methods have proved useful in developing a new approach to treating AD, and designing a novel imaging agent.

LIST OF ABBREVIATIONS USED

3HAA	3-hydroxyanthranilic acid
A	(in AAXA) an aliphatic or aromatic amino acid
A*	alanine, where * indicates its location on the protein chain
Aβ	β-amyloid
Aβ40	β-amyloid (residues 1-40)
Aβ42	β-amyloid (residues 1-42)
ACh	acetylcholine
AChE	acetylcholinesterase
AChEI	acetylcholinesterase inhibitor
α_1-ACT	alpha-1-antichymotrypsin
AD	Alzheimer's disease
ADDLs	Aβ-derived diffusible ligands
ApoE	Apolipoprotein E
Apoε4	Apolipoprotein ε4
APP	Amyloid precursor protein
APPs	soluble shortened APP fragment
Ar	an aromatic ring
BACE1	beta-site APP cleaving enzyme
B	a basic amino acid (in BBXB)
B7-1	T lymphocyte activation antigen
BBB	blood-brain barrier
BHMT	betaine-homocysteine methyl transferase
C	CO_2^- functional group
C*	cysteine, where * indicates its position on the protein chain
C1qA	complement component 1, q subcomponent, chain A

CD	circular dichroism
CHARMM	Chemistry at HARvard Macromolecular Mechanics
CS	used to indicate the central SO_2 group on solapsone
CSF	cerebrospinal fluid
D*	aspartic acid, where * indicates its position on the protein chain
DPDP	dipyridoxyl diphosphate
E*	glutamic acid, where * indicates its position on the protein chain
EDTA	ethylenediaminetetraacetic acid
EV**HH**Q**K**	amino acid residues glutamic acid11- valine12- histidine13-histidine14-glutamine15-lysine16 of the β-amyloid peptide
F*	phenylalanine, where * indicates its position on the protein chain
FF	phenylalanine-phenylalanine
FAD	familial Alzheimer's disease
G*	glycine, where * indicates its position on the protein chain
H*	histidine, where * indicates its position on the protein chain
HH	histidine-histidine
HHQ**K**	amino acid residues histidine13-histidine14-glutamine15-lysine16 of the β-amyloid peptide
I*	isoleucine, where * indicates its position on the protein chain
ICAM-1	intercellular adhesion molecule 1
IFN-γ	interferon-gamma
IL-1βCE	interleukin-1 β converting enzyme
IL-4	interleukin 4
IL-12	interleukin 12
IL-13	interleukin 13
In	represents interactions with an indole
InB	represents interactions with the benzyl ring of an indole

InP	represents interactions with the pyrrole ring of an indole
K*	lysine, where * indicates its position on the protein chain
L*	leucine, where * indicates its position on the protein chain
LB1	used to indicate the first benzyl ring on the left side of solapsone
LB2	used to indicated the furthest benzyl ring on the left side of solapsone
LNH	used to indicate the –NH- on the left side of solapsone
LS1	used to indicate the first sulfonate group on the left side of solapsone
LS2	used to indicate the furthest sulfonate group on the left side of solapsone
LVFF	amino acid residues leucine17-valine18-phenylalanine19-phenylalanine20
M*	methionine, where * indicates its position on the protein chain
MIP-1α	macrophage inflammatory protein-1α
MIP-1β	macrophage inflammatory protein-1β
MOE	Molecular Operating Environment
MRI	magnetic resonance imaging
N	NH_3^+ functional group
N*	asparagine, where * indicates its position on the protein chain
NCE	novel chemical entity
NEP	neprilysin
NFTs	neurofibrillary tangles
NMDA	N-methyl-D-aspartate
NMR	nuclear magnetic resonance
O	OH functional group
O^1	OH group meta to the ethylamine on dopamine
O^2	OH group para to the ethylamine on dopamine
p3	non-amyloidogenic fragment cleaved from APP
P	PO_3H^- functional group

P*	proline, where * indicates its position on the protein chain
PCA	principal components analysis
PDB	Protein Data Bank
PES	potential energy surface
PET	positron emission tomography
PLS	partial-least squares
PVS	polyvinylsulfonate
Q*	glutamine, where * indicates its position on the protein chain
QSAR	Quantitative Structure-Activity Relationship
R*	arginine, where * indicates its position on the protein chain
RANTES	regulated upon activation, normal T-cell expressed, and secreted
RB1	used to indicate the first benzyl ring on the right side of solapsone
RB2	used to indicate the furthest benzyl ring on the right side of solapsone
RCSB	Research Collaboratory for Structural Bioinformatics
RNH	used to indicate the –NH- on the right side of solapsone
RS1	used to indicate the first sulfonate group on the right side of solapsone
RS2	used to indicate the furthest sulfonate group on the right side of solapsone
S	SO_3^- functional group
S*	serine, where * indicates its position on the protein chain
SDF-1	stromal cell-derived factor-1
T	threonine, where * indicates its position on the protein chain
ThT	thioflavin T
V*	valine, where * indicates its position on the protein chain
V*	valine, where * indicates its position on the protein chain
W*	tryptophan, where * indicates its position on the protein chain
X	a variable representative of any non-specified amino acid
Y*	tyrosine, where * indicates its position on the protein chain

ACKNOWLEDGEMENTS

I would first like to thank God for His strength and guidance throughout this research. Second, the research encompassed in this thesis would not be complete without the assistance of my supervisor, Dr. Don Weaver.

I would like to acknowledge the assistance of Harman Clair for the assembly of the library of endogenous compounds.

Special thanks to Dr. Chris Barden for his assistance in providing the scripts for calculations in QUANTA, and his assistance with many computer crises.

Thanks to Todd Galloway, Rose Chen, and Gordon Simms for providing the biological data presented.

Gordon Simms is also acknowledged for his synthetic contributions with the 3HAA analogues. Arun Yadav is thanked for his synthetic work on solapsone.

Katharine Anderson, Laural Fisher, and Alaina McGrath were of assistance in providing the analogues of NCE-0217 for the QSAR.

I would like to thank my family for all their support and love throughout this process, and my mom for being an excellent proof-reader.

The Nova Scotia Health Research Foundation and the Gunn Family Studentship in Alzheimer's Research are thanked for their funding of this research.

Finally, thanks to the Toronto Maple Leafs for demonstrating that perseverance brings results. Go Leafs!

CHAPTER 1: INTRODUCTION

Computational chemistry is an extremely useful field of chemistry in the realm of medicinal chemistry and drug design. A variety of techniques available to the computational chemist can be utilized in many aspects of the drug design process. The combined use of computationally calculated descriptors and biological activities can be used to perform quantitative structure-activity relationship (QSAR) studies in order to optimize the design of novel therapeutic molecules. Molecular dynamics simulations can be used to examine how certain molecules will interact with lipid membranes, and molecular modelling can be used to optimize systems to determine whether molecules will bind to proteins at a specific targeted region. These techniques are becoming an integral part of modern drug design, and are particularly useful in developing new drugs to treat Alzheimer's disease (AD). The beginning of this chapter will provide background material on Alzheimer's disease, its development, treatment and diagnosis. The latter part of the chapter will detail the background behind the computational methods used, and the goals of this research.

1.1 ALZHEIMER'S DISEASE AND β-AMYLOID

Alzheimer's disease, so named for Alois Alzheimer who first described the disease in 1907, is a neurodegenerative disorder that is both progressive and degenerative and is the leading cause of dementia among the elderly [1, 2]. This disease is becoming increasingly prevalent as the population ages. Currently there is no cure or drug to prevent this disease [3].

The psychological and physical manifestations of the disease are characterized by many symptoms, including behavioural changes and cognitive deterioration that lead to increasing requirements for care, particularly as the disease progresses from a mild to a severe form, which coincides with a decrease in the patient's functional independence [2, 3]. While the primary symptom is dementia, there can also be symptoms such as irritability or mood changes, depression, disinhibition, anxiety, sleep disorders and wandering [2]. The disease is therefore most often diagnosed through tests for these psychological and memory-related changes, along with the use of imaging techniques of which positron emission tomography (PET) is becoming quite useful since it can determine the acetylcholine levels (an important neurotransmitter in AD), available in the brain [3, 4].

1.1.1 Acetylcholine and its Role in Alzheimer's Disease

The neurotransmitter acetylcholine (ACh) (Figure 1.1) is believed to play a role in cognition and memory since the levels of the neurotransmitter have been shown to be decreased in patients with Alzheimer's disease. This loss is due to a severe decrease in the number of cholinergic neurons (where synthesis of acetylcholine occurs) present in the basal forebrain and neocortex as well as decreased enzyme activity of choline acetyltransferase and acetylcholinesterase, which are enzymes involved in the production and degradation of acetylcholine [3, 5].

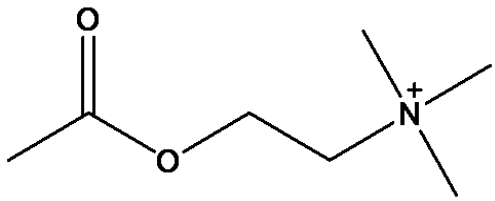

Figure 1.1: Acetylcholine

Acetylcholine is generated in cholinergic nerve terminals from acetyl coenzyme A and choline via the enzymatic activity of choline acetyltransferase. Decreased levels of this enzyme present in the brain means that less acetylcholine will be synthesized [6, 7]. As there is no cellular reuptake mechanism for acetylcholine, the neurotransmitter is catabolized into acetate and choline via the activity of acetylcholinesterase, enabling the choline to be recycled [6, 7]. Current drug treatments for Alzheimer's disease consist mainly of acetylcholinesterase inhibitors (AChEI), whose actions prevent the hydrolysis of acetylcholine thus increasing the concentration of the neurotransmitter in the synaptic cleft [7].

1.1.2 β-Amyloid and the Amyloid Cascade

The most commonly accepted causative agent in the development and progression of Alzheimer's disease is β-amyloid (Aβ). The amyloid cascade hypothesis suggests that a neurotoxic cascade of events is initiated in the brain when Aβ starts aggregating, and genetic evidence from patients with early-onset AD linking the onset of Alzheimer's disease with β-amyloid aggregation has also helped to support this now widely accepted hypothesis [8, 9].

1.1.2.1 The Generation of β-Amyloid from Amyloid Precursor Protein

β-Amyloid is an amphipathic peptide (having both hydrophilic and lipophilic regions) that is 39-43 amino acids in length and is generated by the proteolytic cleavage of the amyloid precursor protein (APP) [8, 10, 11]. APP is an integral membrane glycoprotein composed of a single transmembrane domain with a short cytoplasmic tail (where the C-terminus is located) and a longer extracellular domain (where the N-

terminus is located) and is cleaved enzymatically via one of two pathways: non-amyloidogenic or amyloidogenic [8, 11]. The non-amyloidogenic pathway produces soluble products and involves α-secretase cleavage occurring within the Aβ domain, releasing a soluble shortened form of APP, which is then followed by γ-secretase action at the terminal end of the Aβ domain, releasing another soluble and non-amyloidogenic fragment (see Figure 1.2) [11]. In the amyloidogenic pathway, the initial enzymatic action involves beta-site APP cleaving enzyme (BACE1) that cleaves APP near the N-terminus of the β-amyloid domain, which is then followed by the same γ-secretase action, only in this case along with generating the soluble shortened APP there is also the potentially toxic β-amyloid peptide [11].

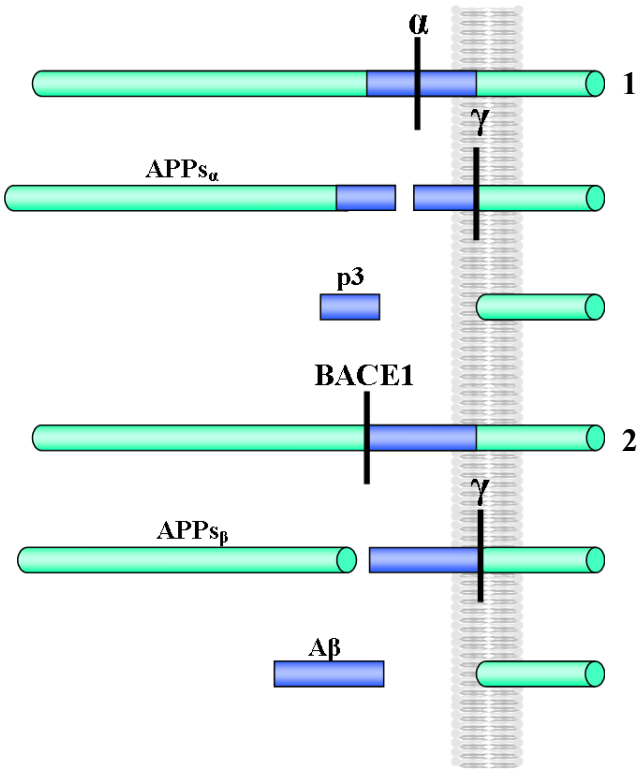

Figure 1.2: Enzymatic cleavage of APP: 1. Non-amyloidogenic pathway. 2. Amyloidogenic pathway. α is the α-secretase enzyme, γ is the γ-secretase enzyme and BACE1 is beta-site APP cleaving enzyme. $APPs_{\alpha}$ and $APPs_{\beta}$ represent soluble shortened fragments of APP, p3 represents a non-amyloidogenic fragment and Aβ is the generated β-amyloid protein.

Generated β-amyloid is between 39 and 43 amino acids in length (see Figure 1.3) and it is this length that plays a role in the self-aggregating nature of the peptide [10, 11]. Most of the Aβ that is generated is 40 amino acids in length (Aβ40), comprising approximately 90 percent of generated β-amyloid, while a smaller portion is the 42 amino acid length peptide (Aβ42) – it is this longer peptide that seems to be of most relevance in the development of Alzheimer's disease [11, 12].

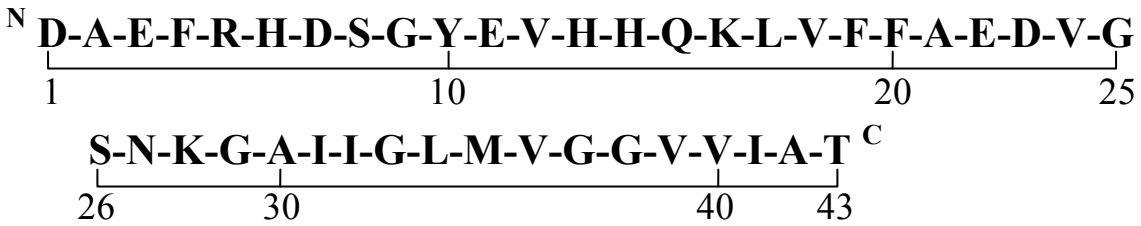

Figure 1.3: The amino acid sequence of β-amyloid.

Production of β-amyloid and its oligomerization appear to begin intracellularly, as APP can be found not only in the plasma membrane, but also in other locations such as the endoplasmic reticulum (ER) and the trans-Golgi network [13, 14]. Interestingly the form of generated Aβ varies with location, as more Aβ42 is produced in the ER and intermediate compartment, while Aβ40 is produced more so in the Golgi apparatus and beyond [13]. The cholesterol content of the various membranes may play a role in influencing length of the produced Aβ [13, 14].

It is of most importance to realize that β-amyloid is a naturally occurring substance found in the brain and cerebrospinal fluid (CSF) in a soluble non-toxic form; only when it undergoes a conformational change from random coil or α-helix to a β-sheet conformation does Aβ begin to take on neurotoxic properties [9, 10]. Given its length, the

42 amino acid length β-amyloid peptide is slightly more hydrophobic than shorter peptide forms, allowing it to self-aggregate more readily [8, 10, 15].

1.1.2.2 β-Amyloid Aggregation and Toxicity

The initiation of β-amyloid aggregation occurs when the peptide takes on a β-sheet conformation, which is possibly instigated by the peptide interacting with lipid membranes [10, 14]. Evidence suggests that Aβ interacts with negatively charged regions on the surface of membranes, causing both misfolding of the protein and damage to the membrane [16, 17]. Figure 1.4 shows where these potential membrane interactions can occur. The positively charged **HHQK** region can interact with negatively charged glycosaminoglycans on the membrane surface to allow conformational changes to occur around the hinge region: the cholesterol binding domains can further facilitate this transformation from α-helix or random coil to β-sheet for the protein.

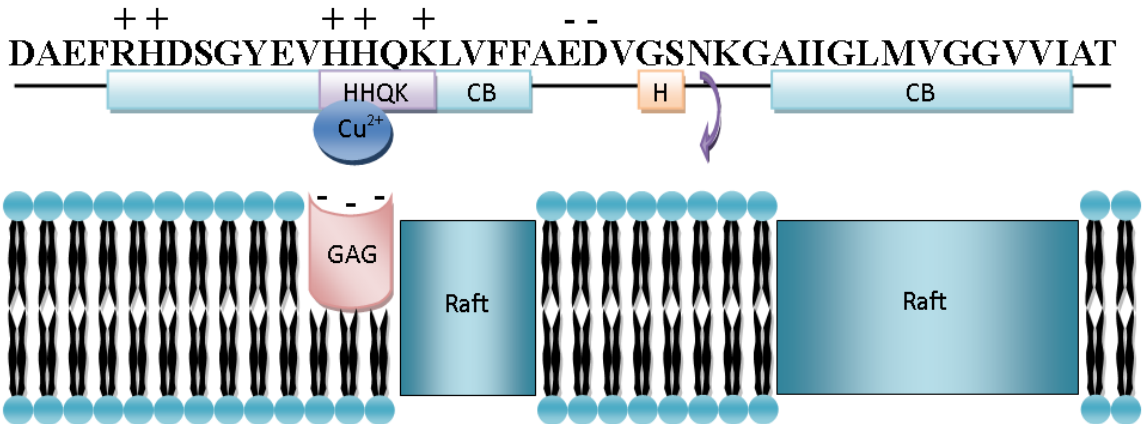

Figure 1.4: Interaction between β-amyloid and a membrane surface. GAG represents glycosaminoglycans; Raft represents cholesterol rafts; CB represents a cholesterol binding domain, and H the hinge region where Aβ folding occurs.

Aβ first forms small aggregates in the form of dimers, trimers, larger oligomers and protofilaments along with other intermediate structures, which then form larger

protofibrils, all of which are soluble, followed by the insoluble fibrils that deposit to form the amyloid plaques that are characteristic of Alzheimer's disease (Figure 1.5) [14, 18]. These plaques are non-toxic and do not correlate to the severity of the disease [31]. It appears that oligomerization of β-amyloid begins intraneuronally, as the intraneuronal Aβ will appear first, and levels of intracellular Aβ decrease as the extracellular levels increase and plaques appear [14, 19]. As well, the oligomerization may be dependent on the cholesterol levels of the membranes Aβ interacts with as it can affect the folding process and speed of fibrillization [15]. It is likely that extracellular Aβ, at least in part, originates from the intracellular Aβ that causes lysis of the neuron as it aggregates [14].

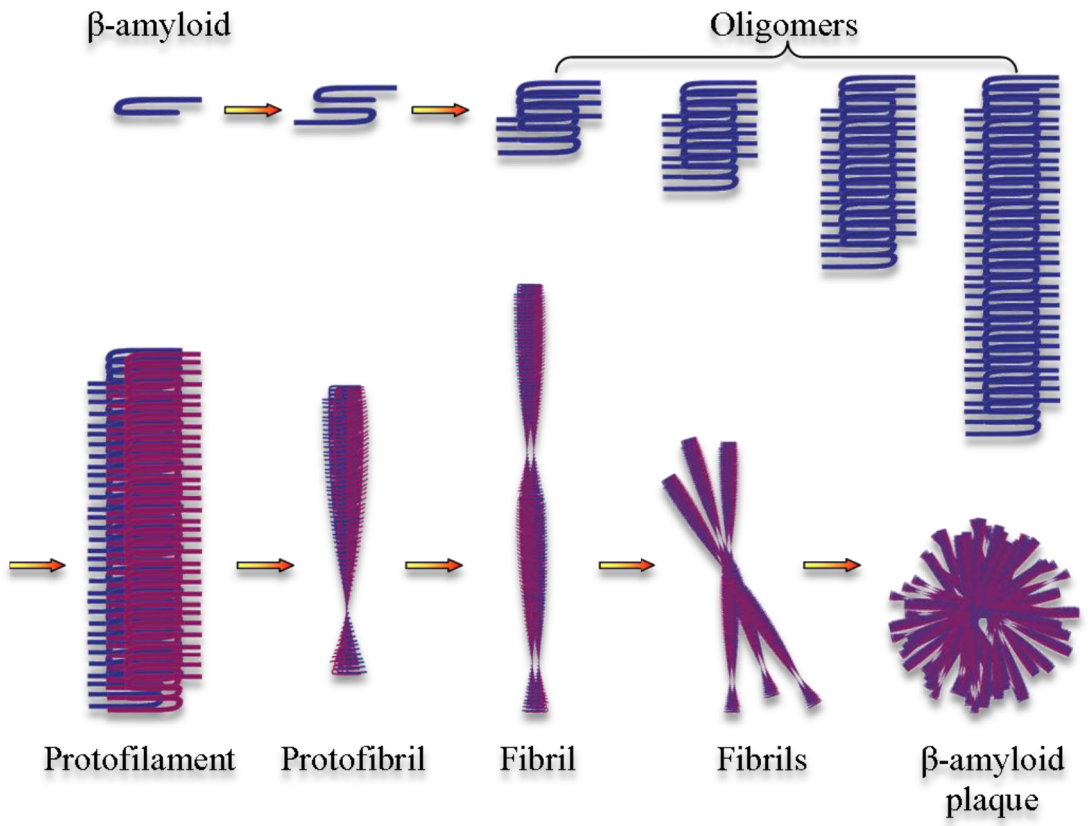

Figure 1.5: The aggregation pathway of β-amyloid from soluble monomer to insoluble amyloid plaque

One of the most stable species of the early soluble stage appears to be the Aβ-derived diffusible ligands (ADDLs), which are now suspected to be some of the neurotoxic species as their presence at even nanomolar concentrations has been shown to be toxic [11, 14, 16]. Other small soluble oligomeric species are considered to be neurotoxic as well [16]. The ADDLs have been shown to inhibit long term potentiation, and can also cause disruption of cellular membranes and calcium dysregulation resulting in neuronal changes in the brain as well as being detrimental to memory; levels of soluble forms of Aβ aggregates are relative to the severity of cognitive impairment and synaptic loss seen in individuals with AD [9, 11, 12, 19]. It has also been reported that the size of the oligomers formed plays a role in which aspects of the brain's functions are affected by the β-amyloid; the smaller oligomers seem to affect the synapses and certain forms of memory while the larger dodecamers appear to influence spatial memory in particular [9]. The oligomeric forms of Aβ are more hydrophobic than the fibrillar species, and can interact more readily with membranes, as well as having a higher diffusability, explaining why the oligomers are the more toxic species [18]. The causative agent in all of this appears in particular to be the longer Aβ42 as is evidenced in cases of early-onset Alzheimer's disease [9].

1.1.2.3 Familial Alzheimer's Disease as Evidence of the Role of β-Amyloid in Disease Initiation

There are several genetic mutations that have been discovered that predispose certain families to early-onset Alzheimer's disease, also known as familial Alzheimer's disease (FAD); sporadic AD has not been linked to any such mutations. It appears that cases of FAD are caused either by an increased production of Aβ42 relative to Aβ40, or an overall increase in the production of all forms of the peptide, giving rise to proof that

certainly in some, if not all, cases the chief instigator of Alzheimer's disease is the β-amyloid peptide [9].

Mutations occurring in the APP gene, which is located on chromosome 21, have been shown to increase the amount or alter the aggregation properties of β-amyloid [8, 9]. As well, some aggressive cases of Alzheimer's disease that occur earlier in life can also be initiated by mutations affecting the presenilin 1 and presenilin 2 genes. Presenilin forms the catalytic site of the γ-secretase enzyme that generates the C terminal end of the β-amyloid fragment; individuals inheriting these mutated genes have shown an increase in the ratio of Aβ42 to Aβ40 that occurs throughout their lifetime [9].

Although it is not guaranteed, there is also an increased chance that individuals with a specific allele of the Apolipoprotein E (ApoE) gene will develop Alzheimer's disease [8, 9, 12]. If an individual possesses the ε4 allele, as opposed to ε2 or ε3, the individuals inheriting the gene are at an increased risk for developing late-onset AD, as opposed to FAD [8, 9, 20]. More recent studies have also indicated a relationship between the CALHM1 gene and an increased susceptibility for late-onset AD [20].

1.1.2.4 β-Amyloid and Neurofibrillary Tangles

The other main feature present in the brains of individuals having Alzheimer's disease are neurofibrillary tangles (NFTs) that are composed primarily of tau protein [1]. These NFTs appear to be the result of processes later on in the neurotoxic cascade and are not an initial factor in the disease, as they cannot themselves cause amyloidosis [12, 18].

Tau is a microtubule-associated protein that is necessary for microtubule stability as well as being involved in their assembly and maintenance [21]. Microtubules are

cellular components that are required for axonal transport, making them critical for neuronal function since breakdown in microtubules prevents vesicles containing molecules such as neurotransmitters being transported to and from the cell body to the synapse; they are also important in forming the cytoskeleton of cells [21, 22]. Therefore the consequences are severe when tau becomes abnormally phosphorylated – it can no longer bind to the microtubules to regulate their polymerization state, and thus can result in the disassembly of these very important support structures [11, 20, 21]. When the microtubules disassemble, the support system needed to maintain cell structure disappears and degradation will occur in the axons and dendrites [11].

The abnormally phosphorylated tau protein self-aggregates to form paired helical filaments that accumulate intraneuronally and thusly causes neuronal degeneration and death [21]. Tau pathology also contributes to the neuronal loss in Alzheimer's patients; however, its abnormal phosphorylation occurs after amyloidosis has started along with other neurotoxic effects [19]. Figure 1.6 shows the pathological artefacts of tau and amyloid in the brain.

Besides the abovementioned neurotoxic effects related to the self-aggregated form of β-amyloid and NFTs, other neurotoxic effects appear to be caused by oxidative stress related to the methionine 35 residue of the β-amyloid peptide [23]. This oxidative stress can result in protein oxidation as well as lipid peroxidation [8]. Inflammation also appears in the vicinity of neurofibrillary tangles and β-amyloid plaques. Overall, the effects of aggregated β-amyloid on the brain are highly unfavourable and as of yet there are no drugs available to halt this aggregation to prevent Alzheimer's disease [11].

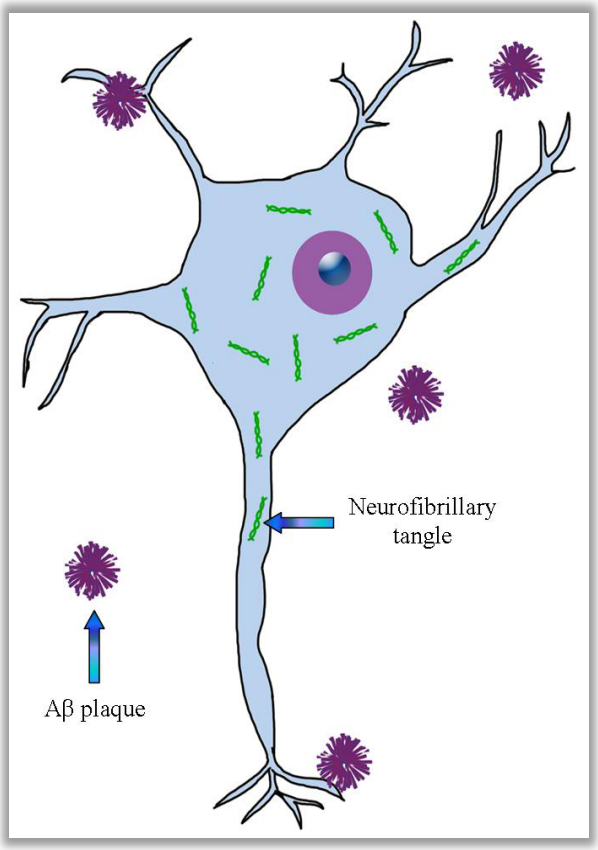

Figure 1.6: Characteristic features of Alzheimer's disease present in the brain: intraneuronal neurofibrillary tangles and extracellular β-amyloid plaques

1.1.3 WHY RESEARCH ALZHEIMER'S DISEASE?

Alzheimer's disease is currently one of the most significant diseases being researched due to its increasing prevalence and an increasingly ageing society. In 2010 approximately 35.6 million people in the world were living with Alzheimer's disease, and this number will almost double every twenty years; in North America those numbers are expected to increase by approximately 63% in that same time frame [24]. In Canada one in twenty people over the age of 65 has AD today, and that number increases to an astounding one in four people over the age of 85 [25].

After the initial diagnosis of Alzheimer's disease, death usually occurs in individuals between seven and ten years later; it should be noted that there are always

exceptions to the rule [25]. It has also been suggested that the progression from mild to severe Alzheimer's disease occurs over a period of six years; however, the older the person is when diagnosed, the shorter the survival rate [3]. Research by Brookmeyer *et al* has predicted that delaying disease progression by therapeutic means for a two year period could decrease the number of late stage cases by about 7 million but the number of new cases would increase by 5.2 million; on the other hand, if the onset of the disease could be delayed by two years, the number of cases of Alzheimer's disease will drop by 22.8 million, and even a one year delay in onset results in 11.8 million fewer cases of AD [3]. Therefore the design and development of drugs capable of preventing, or at least delaying the onset of disease could greatly impact and ease the worldwide burden of Alzheimer's disease as opposed to current methods which can only delay the symptomatic progression.

1.1.3.1 Current Alzheimer's Drugs

In Canada, there are two classes of drugs currently available for the treatment of Alzheimer's disease. The first class of drugs consists of three acetylcholinesterase inhibitors which are used for symptomatic treatment in patients suffering from mild to moderate AD: donepezil, rivastigmine and galantamine [25, 26]. The second class of drugs consists of a single drug which is an N-methyl-D-aspartate (NMDA) receptor antagonist that has been conditionally approved by Health Canada for use in the treatment of moderate to severe Alzheimer's disease: memantine [25, 27].

Donepezil, also known as Aricept or E2020 (Figure 1.7), is a non-competitive and reversible inhibitor of acetylcholinesterase that functions mainly through π-π and cation-π interactions along the gorge of the enzyme wherein the active site (a catalytic triad) is

located [28]. While it does not interact with the active site itself (making it non-competitive) the drug molecule does prevent the Michaelis complex (the enzyme-substrate complex that in this case involves binding interactions forming between acetylcholine and the catalytic triad) from forming or possibly the deacylation process from occurring [28].

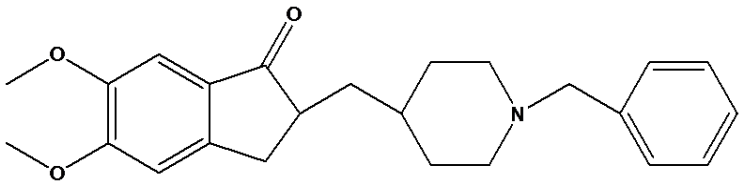

Figure 1.7: Donepezil

Rivastigmine, also known as Exelon (Figure 1.8), is a pseudo-irreversible inhibitor of AChE and acts upon the catalytic triad in a process involving covalent binding where the enzyme treats the drug molecule as a substrate and generates a hydrolytic product, called NAP, which acts as a competitive but reversible inhibitor of the acetylcholinesterase enzyme [29].

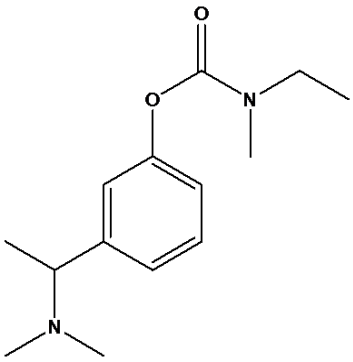

Figure 1.8: Rivastigmine

Galantamine (Figure 1.9), also known as Reminyl, is an extended release formulation; it is also known as galanthamine hydrobromide [25, 30]. Like rivastigmine, galantamine also acts upon the catalytic triad; however, it acts through hydrogen bonding interactions making it reversible [30]. The action of galantamine prevents the enzymatic

activity in that the binding occurs with one of the residues of the catalytic triad, a serine residue, which needs to be activated in order to start the catalytic processing of acetylcholine [28, 30].

Unfortunately all of these current treatments provide only symptomatic relief of the disease, and in the case of the acetylcholinesterase inhibitors are only useful so long as acetylcholine is still being produced in the brain; as of yet there are currently no drugs available on the market to treat the pathological agent of importance – β-amyloid.

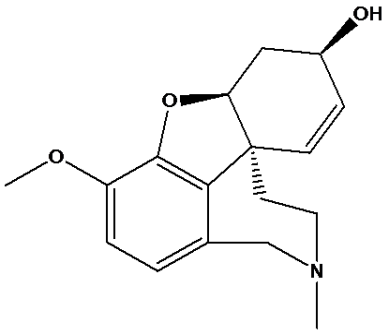

Figure 1.9: Galantamine

Memantine (Figure 1.10), also known as Ebixa, acts by blocking the NMDA receptor channel to prevent excitotoxity due to an increase in the influx of calcium ions which is a result of the channel being opened for prolonged periods of time due to excess glutamate present in the brain [27]. It is believed that although excess glutamate is not the primary cause of Alzheimer's disease, its increased concentrations are partially responsible for the loss of cholinergic neurons and thus memantine is used to help prevent the overstimulation of these neurons [27]. Memantine can be used as a monotherapy or it can also be given in conjunction with one of the available acetylcholinesterase inhibitors [27].

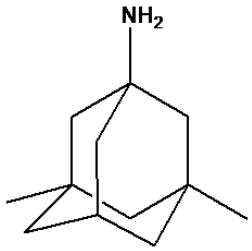

Figure 1.10: Memantine

1.1.4 CURRENT RESEARCH IN TREATING ALZHEIMER'S DISEASE

Current research towards the design and development of new drugs to treat Alzheimer's disease has unfortunately yielded unsuccessful results from clinical trials, even with multiple targets of interest.

1.1.4.1 DRUGS TARGETING β-AMYLOID AGGREGATION

There are currently no drugs on the market approved for treating Alzheimer's disease by targeting Aβ aggregation. Tramiprosate, also known as homotaurine or Alzhemed, was successful in early stage trials, but failed to show efficacy in phase III trials (probably resulting from the methodology of the trial) [31]. PBT2, being developed by Prana Biotechnology Limited, has demonstrated success in phase II trials and works by binding complexes of Aβ and copper or zinc to prevent oligomerization; further trials are awaited [31, 32]. Elan pharmaceuticals has finished phase II trials of *scyllo*-inositol; during the trial, high dosages resulted in deaths, so only low doses were continued in the study [31, 33]. Results of the study have been published and have demonstrated inconclusive results as to the efficacy of the drug due to the small trial size; however, there does seem to be some success in targeting Aβ42, which may be of use in the mild stage of AD [33]. A polyphenol, epigallocatechin-3-gallate, is currently undergoing a

phase II-III study and prevents Aβ aggregation by binding to the monomeric form of β-amyloid [31].

1.1.4.2 Drugs Promoting Clearance of β-Amyloid from the Brain

Research is ongoing in the area of treating AD by removing or reducing the amount of β-amyloid in the brain. This methodology looks at the use of vaccines to target Aβ, either actively or passively [31]. Active immunization involves provoking an immune response by introducing fragments of β-amyloid, however many of these therapies, such as CAD-106 and ACC-001 are only in phase II trials, and most have only completed phase I trials so far [31]. Passive immunization involves the use of monoclonal antibodies or polyclonal immunoglobulins that target the Aβ protein. There is more progress in this field, with several phase III trials ongoing for compounds such as bapineuzumab, solanezumab and intravenously administered immunoglobulins [31]. The difficulty with these vaccination strategies is that there is the potential for more adverse affects occurring in the case of active immunization, while passive immunization is a costly and time-consuming task [31]. While the benefits of vaccination strategies are recognized, there is some risk involved in this scenario as the monomeric form of Aβ may play a neuroprotective role.

1.1.4.3 Drugs Targeting the Reduction of the Production of Aβ

The major focus of drug researchers in the search for new ways to treat Alzheimer's disease is to target the enzymes involved in the secretion of Aβ from APP. There are three enzymes involved in the cleavage of APP: α-secretase is involved in the non-amyloidogenic pathway, BACE1 involved in the amyloidogenic pathway, and γ-secretase, which plays a role in both pathways (see Figure 1.2). Drugs that activate α-

secretase have only reached phase II clinical trials, but have shown indications of reducing the production of Aβ [31]. In terms of γ-secretase inhibitors and modulators, the results have been less than favourable: Eli Lilly halted the phase III trial of semagacestat when it was discovered that the drug had no effect on improving cognition and may lead to increased incidence of skin cancer [34]. Drugs targeting BACE1 have also resulted in little progress; those that have reached phase III trials have demonstrated no efficacy in improving patient outcomes [31]. There are some BACE1 inhibitors in the earlier stages of clinical trials, and it is hoped that they will deliver more promising results [31, 34].

1.1.4.4 Drugs Targeting Other Aspects of Alzheimer's Disease

There is some research focussing on targets other than Aβ to treat AD. Molecules that target the tau protein are being investigated, with Rember (a tau anti-aggregant) being the only drug currently in phase III trials [31, 34]. Results of the only other tau drug to reach phase III, valproate, were disappointing, with no effect on the cognition of Alzheimer's patients [31].

Another phase III trial looking at dimebon as a monotherapy for Alzheimer's disease targeting mitochondria failed to demonstrate any effect on mental status, but is being looked at as part of a combination therapy study for treating AD [31, 34].

Neurotrophins are another target, as nerve growth factor (NGF) is important for the survival of cholinergic neurons that are damaged by the disease [31]. Methods to introduce NGF into the brain are being examined, with phase II trials ongoing.

The current methods for diagnosing Alzheimer's disease and tracking its progression have not been sufficient enough to provide the success desired in curing AD.

1.1.5 Current Methods in Diagnosing Alzheimer's Disease

The diagnosis of Alzheimer's disease in a living patient is dependent on the results of tests that examine the mental status of the individual in question. The decline in cognitive function of an individual is an important factor in diagnosing AD, but is not useful in detecting the disease at a very early stage, before the damage to neurons is significant. While there is a lack of consensus on the use of biomarkers to help diagnose the disease, some methods are available, and others are being investigated.

1.1.5.1 Biomarkers Used to Diagnose Alzheimer's Disease

Currently, there are four identified biomarkers useful to diagnose Alzheimer's disease: Aβ42, Aβ40, total tau, and phospho-tau-181 [35, 36]. Tau and hyperphosporylated tau levels are both increased in patients with AD, while levels of Aβ42 or the Aβ42/Aβ40 ratio are significantly reduced, and all of these are needed to diagnose the disease in its sporadic form [35]. The drawback to collecting these biomarkers is that they are obtained by examining the cerebrospinal fluid of the patient, and therefore require a lumbar puncture [35]. Analysis of these biomarkers also requires the use of costly assays, and to date blood plasma biomarkers have not been useful in identifying sporadic AD [35]. It is likely that in the case of biomarkers, especially if blood plasma is the desired source, a combination of stable elements must be identified to use in combination to diagnose the disease [35].

1.3.5.2 Imaging Agents for Alzheimer's Disease

There are no truly commercial diagnostic imaging agents available on the market for AD; however, there are some currently in development and some are being used in clinical trials of Alzheimer's drugs.

Magnetic resonance imaging (MRI) is used to look at brain volumes, as there is a decrease in the amount of grey matter in individuals with AD as the disease progresses [36]. Studies looking at the use of functional MRI are being expanded to more centres, and this technique is used to determine the effects of drugs on regional brain activation by measuring the blood oxygen-dependent level signals [36].

Positron emission tomography (PET) is the focus of most diagnostic compounds being developed so far. The more noted imaging agent is Pittsburgh compound B (^{11}C-PIB) which binds to amyloid plaques in the brain [36, 37]. There are two notable downfalls to this imaging agent, the first being that ^{11}C-PIB does not bind to the soluble forms of β-amyloid (and the soluble oligomers are the toxic species). The second downfall is that the half-life of ^{11}C-PIB is only 20.4 minutes [36, 37]. PET is also used to look at glucose consumption, as a labelled sugar can be used to identify regions of reduced uptake, indicative of the damaged neurons that occur in AD. Molecules continue to be developed for PET use, such as [^{18}F] AV-45, which also binds to Aβ plaques, and has a significantly longer half-life than ^{11}C-PIB [37].

Single photon emission computed tomography (SPECT) presents an alternative to PET for diagnostic imaging of AD in that it is available in more hospitals than PET scanners, and the half-lives of the radionuclei are significantly longer [38]. Several

imaging agents for Aβ plaques are being developed, and are based largely on Congo Red and thioflavin-T, which are known to bind to amyloid aggregates as they are used in staining and fluorescence studies [38].

1.1.6 Defining the Drug Molecule

To understand what is needed to design and develop a new drug, in particular for Alzheimer's disease, it is relevant to know the features of a drug molecule and what properties it must have in order to be bioavailable.

1.1.6.1 Characteristic Features of Drug Molecules

How each drug molecule interacts with its targeted receptor and moves throughout the body is determined by its functional groups and their geometrical arrangement [39]. The functional groups determine the chemical and physical properties of the drug molecule and their geometry in space should be specific enough that they will only bind with the targeted receptor: this should reduce toxicity. If the molecule is too flexible it will be able to bind to other receptors, which can have potentially negative effects [39]. The biological response elicited by the binding of the drug molecule to the target receptor should be beneficial in nature and can result in many different biological responses depending on the receptor in question: the acetylcholinesterase inhibitors mentioned earlier in this chapter bind to their target receptors to block an enzymatic pathway, while other drug molecules can be used to block neurotransmitter receptors, and so forth [39]. Figure 1.11 shows the interaction between a drug molecule and its target receptor.

The structural frame to which the functional groups of the drug molecule are attached in order to maintain a specific three-dimensional arrangement should not be

involved in the interaction themselves, and thus it is generally preferable to use a chemically inert structure composed of hydrocarbons [39]. Rigidity in the framework is also preferable to minimize geometry changes that could affect the target specificity of the molecule and thereby reduce side-effects [39]. In addition the molecule must be able to traverse the hydrophilic and lipophilic regions of the body in order to reach its desired destination, so this chemistry must also be accounted for when designing novel drugs [39]. In the particular case of Alzheimer's disease, drugs need to enter the brain in order to take action; this presents an added obstacle as the drug molecules must pass through the blood-brain barrier (BBB) which is composed of multiple lipid bilayers – drugs must have a proper balance of hydrophilicity and lipophilicity in order to pass through this barrier [39].

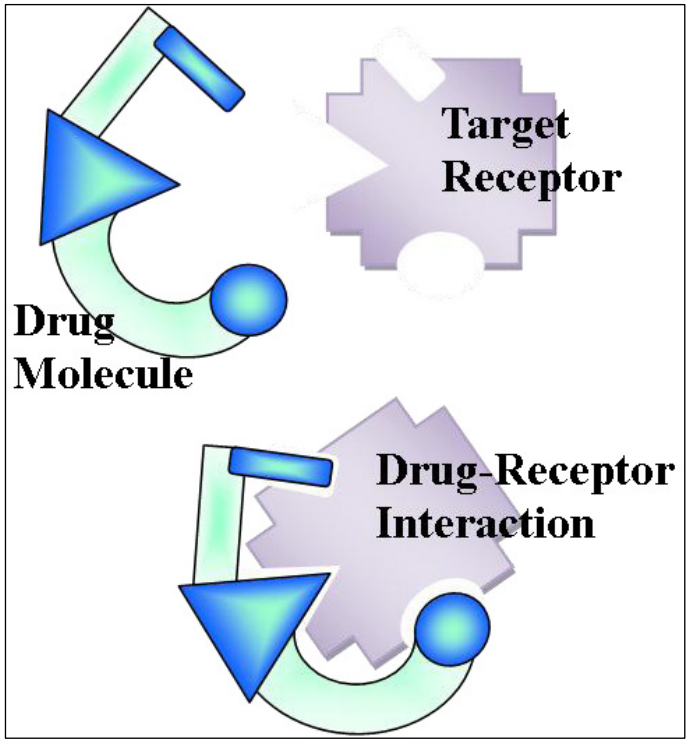

Figure 1.11: Drug molecule interacting with target receptor

1.1.6.2 Requirements for a Bioavailable Drug Molecule

There are certain physical and chemical properties that must be met by a drug-like molecule in order for it to be an effective drug molecule assuming an appropriate receptor can be identified [39]. These properties are best summed up by the Rule of Five as proposed by Lipinski: first the molecular weight should be less than 500 g/mol, since the molecule must be small enough to be transported throughout the body [39, 40]. Second, the molecule should have a logP value less than 5 (where logP is the logarithm of the octanol-water partition coefficient) since the molecule must have a certain lipophilicity in order to allow it to cross lipid layers but also have enough hydrophilicity that it can dissolve in the blood and circulate through the body [39, 40]. Third and fourth the molecule should not have more than five hydrogen bonding donors and no more than ten hydrogen bonding acceptors; too many polar groups results in rapid elimination of the drug from the body since the kidneys will filter out highly polar molecules more quickly, resulting in little therapeutic effect of the drug as its half life would be very short (a drug half life is defined as the time it takes for half of the drug molecules delivered to the desired target to be metabolized) [39, 40]. There are exceptions to the above rules should the drug be an analogue of molecules that are transported actively across cell membranes (as opposed to passive diffusion, which is the normal entry method for most drug molecules) [39, 40].

It should also be noted that if these drug molecules must cross the blood-brain barrier there are further limitations; in particular the logP value must be between 1.5 and 3.0 so as not to be too hydrophilic or consequently so lipophilic that it cannot reach the brain [39]. It is also suggested that there be even fewer hydrogen donors or acceptors

(three is usually the maximum) and it is very unlikely that any charged molecules will be able to pass this barrier if entry is being sought via passive diffusion [39]. If the drug molecule is being transported actively into the brain as a structural analogue of either L-phenylalanine or D-glucose (both being molecules that are actively transported across the BBB), there is more leeway in the type and number of functional groups as well as the size of the drug molecule [39].

Drug molecules can be designed to mimic molecules already present in the body (several such molecules will be examined in the research presented in this thesis) or they can be designed to target pathways involved in the production or elimination of certain molecules [39]. The difficulty with designing drugs for Alzheimer's disease lies in ensuring that they are capable of meeting the above requirements in order to cross the BBB.

1.1.7 The Promiscuous Drug Concept

It has been proposed that a novel way of approaching the treatment of AD would be to design a "promiscuous" drug capable of interacting with many of the proteins involved in disease [41]. Analysis of multiple proteins related to Alzheimer's disease has revealed a common **BB**X**B** motif (or pattern of amino acids), where B represents a basic amino acid [41]. This **BB**X**B** motif is found only on proteins affiliated with AD. The concept is therefore to design or find a small molecule that is capable of binding to this specific pattern of amino acids. A single molecule could thus act in a "promiscuous" manner by binding to the same motif on multiple proteins, allowing for a multifaceted approach to treating the disease using a single drug molecule.

1.1.7.1 HHQK

One of the identified **BB**X**B** motifs is the **HH**Q**K** region of β-amyloid [41]. This region is particularly significant as it is highly positively charged, and can interact with the negatively charged regions (such as glycosaminoglycans) on the surface of membranes to allow for conformational conversions to occur. Designing and developing small molecules to bind to this **HH**Q**K** region should prevent such membrane interactions from occurring, and thereby unwanted conformational changes that result in neurotoxicity.

1.2 Molecular Modelling

Molecular modelling involves the use of empirical molecular mechanics force fields to study the conformational energies of molecules. There are a wide variety of force fields available to the computational chemist, ranging from generic force fields that are applicable to a wide range of molecular systems and atom types to those that are specific to small molecules, nucleic acids or proteins.

1.2.1 What are Force Fields?

A force field is composed of a functional form (energy equations) and parameters that are used to calculate the energy of a system based on the inter- and intramolecular forces of that system [42]. Force fields ignore electron contributions, calculating energies based solely on nuclear contributions [42]. As they are empirical in nature, there is no absolutely correct form for a force field; therefore, a force field can be selected based on its suitability for a particular system given that the parameters can determine how well a particular force field functions with certain systems [42].

Each force field has a functional form and parameters with four basic components being common to all force fields; these can be grouped into terms related to bonding interactions and terms related to nonbonding interactions [42]. Energy terms describing the deviation of bond lengths and angles from specified equilibrium values, as well as torsional changes, are the terms related to bonding interactions, whereas electrostatic and van der Waals energy terms compose the non-bonding interaction terms [42]. Depending on the force field in question, *ad hoc* hydrogen bonding terms can also be included.

The parameters that help define a force field give the various constants necessary for the functional form in terms of atom types [42]. The atom type contains information about the atom such as its hybridization state, the atomic number and, depending on the force field, information about the local environment of the atom [42]. Atom types can be more or less specific, depending on the type of force field being used for molecular modelling. A more generic force field, such as DREIDING2.21, will assign all atoms of the same element the same atomic type, whereas some more specialized force fields, such as CHARMM, will assign different atom types to a particular element depending on the nature of the local environment of the atom; for example, a nitrogen atom in a ring is assigned a different atom type than one in a peptide [42, 43, 44].

Parameters are instituted for force fields based on the properties that the force field is designed to predict [42]. In the realm of molecular modelling, force fields are most typically designed to reproduce structural properties of systems [42]. Another asset of these force fields is that their parameters allow for transferability of the force field – new parameters do not have to be defined for each individual molecule in a system, which is to say that related molecules can be treated using the same force field [42]. An example

of the transferability of force fields would be the CHARMM force field, which can be applied to any protein-based system, and can be used for energy calculations, or dynamics simulations of the proteins interacting with other molecules, or energy minimizations, allowing for optimal protein geometries to be located [44].

1.2.2 THE DREIDING2.21 FORCE FIELD

Optimizations performed in the Cerius^2 molecular modelling environment involve the use of the DREIDING2.21 force field [43, 45]. The DREIDING2.21 force field is a simple, generic force field applicable to a variety of systems from organic and biological molecules to main-group inorganic molecules, and allows for structural predictions as well as dynamics simulations [43]. The force field treats all atoms of the same atomic type identically, with types being assigned automatically based on the topology of the structure in question [43]. The functional form of the DREIDING2.21 force field is as follows:

$$E = E_{val} + E_{nb} \tag{1.1}$$

This equation sums the total energy from the energy of valence interactions (e.g. bonding interactions), E_{val} and the energy of nonbonding interaction energies, E_{nb}.

These two energy terms are summations of various energy interactions as follows:

$$E_{val} = E_B + E_A + E_T + E_I \tag{1.2}$$

and

$$E_{nb} = E_{vdw} + E_Q + E_{hb} \tag{1.3}$$

Looking at the valence energy terms, the bond stretching energy, E_B, is defined by default as a harmonic oscillator where:

$$E_B = \frac{1}{2}k_e(R-R_e)^2 \tag{1.4}$$

In this case, k_e is the stretching constant at equilibrium, R is the variable bond length and R_e is the equilibrium value of the bond length. The bond-angle bending energy, E_A, is calculated using a harmonic cosine function:

$$E_A = E_{IJK} = \frac{1}{2}C_{IJK}[\cos\theta_{IJK} - \cos\theta^0_J]^2 \tag{1.5}$$

θ is defined as the angle between bonds *IJ* and *JK* for two bonds sharing a common atom, and θ^0_J is the equilibrium angle while

$$C_{IJK} = K_{IJK}/(\sin\theta^0_J)^2 \tag{1.6}$$

where K_{IJK} is a force constant, independent of *I*,*J* and *K*, defined as:

$$K_{IJK} = 100 \text{ (kcal/mol)/rad}^2 \tag{1.7}$$

The dihedral angle torsion energy term, E_T, is expressed in the form of a cosine series expansion:

$$E_T = E_{IJLK} = \frac{1}{2}V_{JK}\{1 - \cos [n_{JK}(\varphi - \varphi^0_{JK})]\} \tag{1.8}$$

The periodicity is described by n_{JK}, the dihedral angle by φ, the equilibrium torsional angle by φ^0_{JK}, while V_{JK} is a barrier to the rotation and is dependent on the specific case being calculated [42, 43]. The parameters for the torsional term in DREIDING2.21 are based on hybridization rather than on the particular atoms involved [43]. The energy of

the inversion terms, E_1, which are terms that describe the ease or difficulty of maintaining planarity, is described as follows:

$$E_1 = E^d_{IJKL} = \tfrac{1}{2}C_I(\cos\psi - \cos\psi^0_I)^2 \tag{1.9}$$

IJKL represents four atoms connected together with *I* being the central atom, and ψ is therefore equal to the angle between the *IL* bond and the *JKL* plane. The equilibrium angle is ψ^0_I and

$$C_I = K_I/(\sin\psi^0_I)^2 \tag{1.10}$$

K_I is the force constant and is a parameter determined by the nature of the molecule – whether the system is planar or nonplanar.

The non-bonding energy term has two components, the first being van der Waals interactions, also referred to as dispersion interactions, E_{vdw}, which is expressed by a Lennard-Jones type function as the default:

$$E^{LJ}_{vdw} = D_0[\rho^{-12} - 2\rho^{-6}] \tag{1.11}$$

where

$$\rho = R/R_0 \tag{1.12}$$

The bond length is represented by R, the van der Waals bond length by R_0, and the van der Waals well depth by D_0. The values for D_0 and R_0 are calculated by the following equations:

$$D_{0ij} = [D_{0ii}D_{0jj}]^{1/2} \tag{1.13}$$

$$R_{0ij} = \tfrac{1}{2}(R_{0ii} + R_{0jj}) \tag{1.14}$$

The two atoms being examined in an interaction are represented by *i* and *j* [2]. The other component of the non-bonding energy term is the electrostatic interaction energy, E_Q, which uses Gasteiger charge estimates and is calculated using a version of Coulomb's law for a system in vacuum [42, 43].

$$E_Q = (322.0637)Q_1Q_2/\varepsilon R_{ij} \tag{1.15}$$

The 322.0637 term is a conversion factor used for converting the energy into kcal/mol, Q_1 and Q_2 are the point charges, measured in electron units, the dielectric constant is ε and the distance between the two atoms is R_{ij}, measured in angstroms [43]. The DREIDING2.21 force field also contains a term for calculating energies associated with explicit hydrogen bonding within the non-bonding energy term and is represented by E_{hb}.

$$E_{hb} = D_{hb}[5(R_{hb}/R_{DA})^{12} - 6(R_{hb}/R_{DA})^{10}] \cos^4 (\theta_{DHA}) \tag{1.16}$$

The hydrogen donor, the hydrogen atom, and the hydrogen acceptor are represented by D, H, and A, respectively, while the bond angle between these atoms is θ_{DHA}. The distance between the donor and acceptor atoms (D and A) is given by R_{DA} while the values for D_{hb} and R_{hb} are dependent on the charge calculation method. Further details on the functional form and parameters of this force field are described by Mayo *et al* [43].

1.2.3 The CHARMM Force Field and QUANTA

The QUANTA program, from Accelrys Inc., uses the CHARMM (Chemistry at HARvard Macromolecular Mechanics) force field [3, 5]. The CHARMM22 version of this force field is available from MOE (Molecular Operating Environment Inc.), and has been parameterized specifically for proteins, with an emphasis on solution phase interactions in water [47, 48].

The CHARMM force field calculates the energy of a system using a functional form containing bonded and non-bonded interaction energies based on atomic coordinates [44]. The equation for the force field is as follows:

$$E = E_b + E_\theta + E_\varphi + E_\omega + E_{vdW} + E_{el} + E_{hb} + E_{cr} + E_{c\varphi} \quad (1.17)$$

The energy terms associated with bonding interactions are E_b, E_θ, E_φ, and E_ω, with E_b being the bond potential energy which is calculated via the following:

$$E_b = \Sigma k_b(r - r_0)^2 \quad (1.18)$$

The bond length is r, which is measured in angstroms, and k_b is a force constant which is selected based on the atom type along with r_0 which is the minimal value of the bond length [44, 46]. The energy term associated with bond angles is given the following form [49]:

$$E_\theta = \Sigma k_\theta(\theta-\theta_0)^2 \quad (1.19)$$

The bond angle is represented by θ, and the minimum of the bond angle by θ_0, while k_θ is the force constant specified by the CHARMM parameters [49]. Both the bond length and bond angle energy terms are treated as harmonic oscillators in the form of Hooke's Law [44]. The torsional energy depends on the angle between four connected atoms with rotation occurring around the middle pair of atoms and is calculated by [44, 50]:

$$E_\varphi = \Sigma|k_\varphi| - k_\varphi\cos(n\varphi) \quad (1.20)$$

The n is a geometric constant that is equal to 1, 2, 3, 4, or 6 and is dependent on the parameters selected in CHARMM, the k_φ is the force constant and the φ is the dihedral angle of the system in question [44, 50]. The remaining bonding energy term is the improper inversion term which involves planarity in molecules and takes the form of a harmonic oscillator:

$$E_{\omega} = \Sigma k_{\omega}(\omega-\omega_0)^2 \quad (1.21)$$

The improper torsion angle is represented by ω, and the minimum torsion angle by ω_0 and k_{ω} is the force constant [44].

The non-bonding interaction terms begin with the van der Waals energy term, E_{vdW}, which is calculated via:

$$E_{vdW} = \sum_{excl(i,j)=1} (A_{ij}/r_{ij}^{12} - B_{ij}/r_{ij}^{6})sw(r^2_{ij},r^2_{on},r^2_{off}) \quad (1.22)$$

The equation involves a switching function, sw, which is equal to either 1 or 0 as determined by a set of formulae that are detailed in the CHARMM force field documentation [44].The van der Waals bond length minima are represented by A_{ij} and B_{ij} while the measured distance between two atoms *i* and *j* is represented by r_{ij}. The exclusion term excl(*i,j*) = 1 refers to the excluded list that is generated for the system under study – atoms that are too close (i.e. in a bonding situation) are to be excluded from the calculation; a cutoff distance is also determined such that those atoms too far away to interact are not included [44, 50]. The electrostatic energy term, E_{el}, is given by [44, 50]:

$$E_{el} = \sum_{excl(i,j)=1} q_i q_j/4\pi\varepsilon_0 r_{ij} \quad (1.23)$$

The partial atomic charges on each of the two atoms involved in the calculation are given by q_i and q_j while the distance between the two atoms is given by r_{ij} and the dielectric constant is ε_0 [44, 50].

Although there is a hydrogen bonding term available in the CHARMM force field, it is often excluded as the hydrogen bonding interactions can be accurately represented by the electrostatic and van der Waals terms [48].

The other two energy terms involved in the functional form are related to atom harmonics, E_{cr} and dihedral constraints $E_{c\varphi}$; as these are energies related to constraints

applicable to atoms in the system but were not used in calculations involved in the research for this thesis, the equations will not be given here but are found in Brooks, et al. [44].

1.2.4 Energy Minimization Algorithms

Energy minimization algorithms are used in molecular modelling to assist in identifying the lowest energy, optimal molecular conformation of a system [42]. The use of this energy minimization technique is an essential part of the presented research.

In order for molecular modelling to be viable, the Born-Oppenheimer approximation is applied, which states that for molecules in the electronic ground state, the energy can be considered a function of the nuclear coordinates, and will only change when the nuclear positions change [42]. The energy of a system is thus described by the potential energy surface (PES), where the energy varies with the nuclear coordinates [42]. The goal of these minimization algorithms is to find a local minimum point on the potential energy surface, since a minimum point corresponds to a relatively stable structure or conformation; stable structures are lower in energy than unstable structures and therefore a lower energy conformation will be equivalent to a minimum point on the potential energy surface [42]. These energy minimization techniques, sometimes called geometry optimization algorithms since they find the optimal geometry/conformation for a system, find only the minimum points on the potential energy surface and thus may not actually correspond to the active form of a biological system, particularly since existing in a low energy state is not the only criterion for an active drug molecule [42].

There are many algorithms available for energy minimization [45, 49]. Some of these algorithms are only applicable to small systems. For example, the Newton Raphson algorithm is best suited for systems with 200 or fewer atoms [42]. In the case of molecular modelling, particularly in the case of systems involving explicit solvation, the systems being studied usually contain several thousand atoms, and there are two algorithms particularly suited to the minimization of such large systems: steepest descent and conjugate gradient [42]. These two minimization algorithms are available in QUANTA and Cerius[2] [45, 46]. In the MOE program, however, three consecutive energy minimization algorithms are applied to a system regardless of the number of atoms present: steepest descent, conjugate gradient and truncated Newton [51].

1.2.4.1 The Steepest Descent Algorithm

Steepest descent is a particularly useful algorithm when starting with an initial conformation in a high energy state [42]. It is a first order minimization method that involves the atomic coordinates being changed gradually as the system is moved closer to an energy minimum point; thus the positional shifts are gentler than some of the other methods. However, the steepest descent algorithm is more likely to generate a low energy structure regardless of the system being optimized [42, 44, 52]. Movements along the PES are made in a direction parallel to the net force, and the direction and gradient of each successive step is orthogonal to the previous step – this stepwise manner is the main reason that the steepest descents method tends to be nonconvergent in larger systems (Figure 1.12) [42, 44].

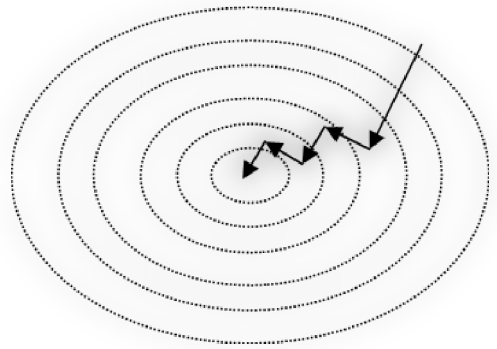

Figure 1.12: Steepest descent approach

One method for taking these steps downhill is the arbitrary step approach. The step size taken for each iteration is also modified, starting off with a predetermined value and then adjusted according to whether the previous step taken resulted in an increase or decrease in the potential energy; a multiplicative factor is applied to the step size which will either augment or diminish the next step taken [42].

More commonly a line search approach is used for both the steepest descents and conjugate gradient methods of minimization; the line search approach is one dimensional and follows along the direction vector that is determined at each iteration [42, 52]. The line search brackets the minimum along the line, where the minimum point is lower in energy than the two points bracketing it; the distance between these points is then gradually decreased by each iterative step [42].

1.2.4.2 The Conjugate Gradient Algorithm

The other very useful algorithm for optimizing the conformational energies of complex biological systems is the conjugate gradient approach. Unlike steepest descents, it is preferable to apply this algorithm only when the system is close to a minimum on the PES, particularly when larger systems are being studied [52]. Like the steepest descent

algorithm, a line search approach is also taken for the conjugate gradient minimization method; however, the direction of the steps taken differs in that, while the gradients are still orthogonal the direction of the steps is conjugate (Figure 1.13) [42, 52]. These conjugate directions will allow the minimum to be reached in fewer steps than in steepest descents; for example, if one is dealing with a quadratic function, containing *M* variables, the minimum will be reached in *M* number of steps – two variables results in two steps until the minimum is achieved [42].

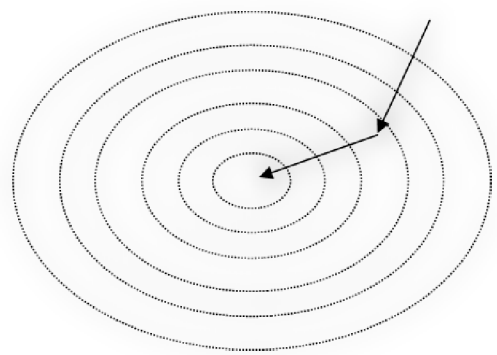

Figure 1.13: Conjugate gradient approach

It is useful to first run steepest descents to relieve strain in high energy systems and then to run the conjugate gradient algorithm to attain a minimum point on the potential energy surface and by doing so, also obtain a stable structure for the system [52]. These algorithms are the most useful for dealing with the large atomic systems that are studied via molecular modelling [42].

1.2.4.3 The Truncated Newton Algorithm

Unlike the steepest descent and conjugate gradient algorithms, the truncated Newton algorithm is a second-order method [42]. Second-order methods use the second derivative, which deals with the curvature of the energy function, to predict where a

minimum will be located along the direction chosen on the PES using the gradient [42, 51, 52]. Given that the algorithm involves solving the Newton equations, which can be an intensive, computationally demanding process, an iterative linear equation solver is employed to solve these equations in an approximate manner that guarantees the minimum will be reached [51, 52, 53]. This iterative solver is terminated after relatively few iterations, leading to the moniker of truncated Newton [51, 53].

The Molecular Operating Environment uses these three algorithms sequentially. Initially several iterations of the steepest descents algorithm are used to bring the gradient down to a more reasonable range and continues only in the direction of energy descent [47, 51, 53]. The conjugate gradients algorithm is then applied to improve the search for a low energy minimum, bringing the gradient down further so that the truncated Newton algorithm can then be applied to find the lowest energy minimum for the energy function [51, 53].

1.3 Quantitative Structure-Activity Relationships

The use of quantitative structure-activity relationship (QSAR) studies is an extremely useful molecular modelling tool for the development of novel drug molecules. The concept of a QSAR involves the assumption that the physical properties of a compound are related to its structure and therefore related compounds (e.g. in the same family of compounds) will have similar properties [54]. The basis is then that mathematical models can be used to first relate and then predict a particular property for sets of compounds: molecular descriptors are calculated for various data sets and then statistical tools are applied to improve the predictive capacity of the descriptors by determining which of the descriptors are relevant to the desired property (for example the

biological activity of the compounds) and eliminating those which have no significant contribution [54]. While techniques related to QSAR have existed since the mid 1800s, molecular modelling allows for an expanded range of descriptors to be calculated for each compound and detailed statistical analyses to be performed at minimal costs in the process of designing new drugs [54].

Molecular descriptors calculated in QSAR studies cover a wide range of properties: physicochemical, electronic, topological and geometric [39]. These descriptors can use the molecular structure to calculate such properties as bond lengths and angles, molecular dipoles and the polar surface area, the number of particular atom types or the logP, all of which can play an important role in the biological activity of a particular compound [39, 55]. Over 330 descriptors can be calculated in MOE for QSAR studies, encompassing two-dimensional (e.g. number of aromatic rings) and three-dimensional descriptors (e.g. the van der Waals volume) [51].

Quantitative structure-activity relationship studies are performed in an iterative fashion in combination with the syntheses of diverse molecules with highly variable biological activity data in order to improve the design of novel drug molecules to obtain maximal efficacy. The process of performing a QSAR requires a set of molecules with known properties. In the case of the presented research this will involve data related to the biological activity of the molecules in question. This training set of molecules contains a selection of compounds with known properties and a significant number of molecular descriptors are calculated for each of the molecules in the set [54, 55].

Statistical analyses in the form of multivariate analyses such as principal components analysis (PCA) and partial-least squares (PLS) are applied to the calculated descriptors to find the most relevant contributions to generate a linear equation capable of predicting the desired property [54]. In PCA, the original data is transformed into linear combinations of the original variables that account for the variance covered by the descriptors, with most of the variance covered in the first principal component (the new variables are referred to as principal components) [56]. In PLS, the data is transformed such that the most variance is represented while retaining the correlation between the dependent and independent variables [56]. In MOE, a binary QSAR model is also available which is non-linear and uses probability distributions to determine how well descriptors can predict the activity or inactivity of molecules [K].

If a large number of descriptors have been calculated for the QSAR, their number is reduced based on their contributions to the predictiveness of the QSAR as otherwise there is a risk of overfitting the data. Overfitting the data means that while the predictions of activity for the training set of compounds will be extremely accurate, the model will be unlikely to provide accurate predictions for the validation set. Descriptors can be "weeded out" based on measures of their importance to correctly predicting activity, and correlation to other descriptors. Two different descriptors may both describe the same property accurately, therefore only one would be needed for the QSAR. As well, some descriptors may provide no information relative to the molecules that are being studied and can thus be eliminated from the QSAR.

The QSAR methods involving linear equations are be validated through the use of statistics such the r^2, bootstrap r^2 and cross-validation methods which deal with the

goodness of fit of the generated mathematical model [54, 56]. The r^2 value, the square of the correlation coefficient, measures the goodness of fit of the data and better prediction are obtained the closer this value is to 1, and the bootstrap r^2 is the average squared correlation coefficient [56]. The cross-validated r^2 value is a variation of this measurement where either one or more molecules from the training set are left out, with the remaining molecules used for a model to predict the property of the excluded compound; this value is usually lower than the r^2 value [56]. Validation of a binary QSAR involves evaluating the sensitivity and the specificity of the model; the sensitivity is measured as the number of correctly predicted actives divided by the number of observed actives, while the selectivity is measured as the number of correctly predicted inactives divided by the number of observed inactives [57]. These two values can be added together and divided by the total number of compounds to determine the overall accuracy of the model [57]. As this is a binary model, Cohen's kappa can also be calculated to determine how accurate the model is by taking into account the correct predictions that could occur by chance; the best model will have a kappa value that is close to 1 [58].

After a mathematical model has been generated for the training set of data with good statistical values, the linear equation is then applied to a validation set of data, which contains a mixture of active and inactive molecules [54]. Successful application of the model will allow for the model to be applied to further related compounds with unknown activity in order to determine which molecules should be selected for synthesis. Unsuccessful models may be the result of not having calculated enough descriptors to adequately relate the structural features to the desired property or may be due to the presence of outliers which will need to be dealt with on an individual basis; overfitting of

the data may also occur when too many descriptors are used [54]. These QSAR studies can be repeated as many times as necessary to improve the activity of lead compounds in the design of novel therapeutics.

Both QSAR studies and molecular mechanics in the field of molecular modelling are useful tools in the development and design of novel therapeutics for Alzheimer's disease.

1.4 Research Goals

This research encompasses several goals related to the design and development of novel therapeutics for the treatment of Alzheimer's disease, and also a novel approach to identifying the disease presence in individuals using a known drug in a new and functional manner.

The β-amyloid peptide, as it exists at physiological pH within the brain, contains a highly positively charged region that is believed to be directly involved in its conformational changes, this region is designated as the **HH**Q**K** peptidic segment. More specifically, this region is concentrated in both aromatic rings capable of π-π interactions, and cationic charged side chains capable of multiple interaction types. Given this knowledge, the use of highly negatively charged molecules as well as aromatic rings capable of forming aromatic-π interactions as potential therapeutics, presents itself as an option for targeting this area of interest, as these functional groups should allow for binding to this charged region on the Aβ peptide.

In this thesis, computational methods will be used to identify endogenous molecules of the brain that may bind to β-amyloid to prevent its aggregation. This is a

new approach to the disease, as no one has examined small molecules that already exist in the brain for their potential anti-AD properties, or even postulated their existence. This research topic is the continuation of work performed in the Master's thesis by the author entitled "Endogenous Therapeutics for Alzheimer's Disease: Zwitterionic Molecules." Others have suggested peptidic macromolecules as supposed endogenous anti-Alzheimer's agents, but none of them are small molecules, and none of them are potential therapeutics [59].

Through the use of these computational methods, an endogenous molecule that exhibits excellent activity in binding to β-amyloid was identified (Chapter 2). The preliminary research in this chapter, encompassing Sections 2.2-2.6, is from the author's Master's thesis work, and is further expanded on in the rest of the chapter. These endogenous molecules present ideal targets as compounds that already exist in the brain are less likely to cause the side effects that non-endogenous molecules may incur. The enzymatic processes involved in the syntheses and metabolism of these molecules can be targeted to increase levels in the brain, or they can be used to design structurally relevant molecules capable of crossing the blood-brain barrier.

The use of computational methods to identify and develop endogenous (and structurally related synthetic) molecules for AD is also a novel approach. These computational techniques have been used to examine the binding of endogenous and synthetic molecules to a common BBXB motif on proteins involved in Alzheimer's disease in order to validate the "promiscuous drug" concept (Chapter 3). Computational methods were also used to develop analogues of endogenous molecules through the use of a QSAR (Chapter 3).

Furthermore, both endogenous and synthetic molecules were examined for their potential to bind to the **HH**Q**K** region of Aβ, due to its role in the protein misfolding process (Chapter 3). The EV**HH**Q**K** region was also targeted for binding studies with endogenous and synthetic molecules via computational methods (Chapter 4).

The nearby LVFF region of β-amyloid was also examined as a potential target for identified molecules to bind to in order to prevent aggregation (Chapter 5). The binding strength of molecules with both the **HH**Q**K** and LVFF regions was compared to determine if a single molecule could target both regions with the same efficacy.

Computational methods have also been used to examine the repurposing of a known drug for use as a diagnostic agent for Alzheimer's disease (Chapter 6). The results of these studies will allow for the development of a novel diagnostic agent for AD, capable of binding to the soluble forms of Aβ, allowing for both earlier diagnosis of the disease and definitive diagnosis.

CHAPTER 2: THE SEARCH FOR AN ENDOGENOUS ANTI-ALZHEIMER'S DRUG TARGETING HHQK: PHOSPHOSERINE

It is understood that the clinical course of Alzheimer's disease is quite variable from one afflicted person to another. One potential explanation for this variability arises from the possibility that there are "endogenous" protective factors; i.e. chemicals naturally occurring within humans that have anti-amyloidogenic properties. The research in this chapter focuses on the concept of an endogenous molecule of the brain that will bind to β-amyloid in its monomeric form to prevent aggregation from occurring.

2.1 THE HHQK REGION OF β-AMYLOID AS A BINDING TARGET

The **HH**Q**K** region of Aβ, residues His13-His14-Gln15-Lys16, is postulated to be a key component in the interactions that lead to the misfolding of Aβ as it has a highly positively charged region that can interact with the surface of membranes [16, 17, 41]. This **HH**Q**K** segment also fits the **BB**X**B** motif identified as being present in various proteins involved in Alzheimer's disease [41]. Molecules containing negatively charged functional groups or aromatic rings should be able to interact with this charged region to block it from other unwanted interactions and thus prevent protein misfolding.

2.2 IDENTIFICATION OF PHOSPHOSERINE AS AN ENDOGENOUS MOLECULE TO TARGET THE HHQK REGION OF β-AMYLOID

To identify a molecule capable of interacting with the **HH**Q**K** region, we put in place an *in silico* library of endogenous compounds. Using standard textbooks of biochemistry and neurochemistry, coupled with an exhaustive review of literature, we assembled a list of 1,451 compounds (having a molecular weight less than 600) that are naturally occurring within the human brain (these are listed in Appendix 1). A library was constructed containing these compounds in energy minimized, fully extended conformations. This library was screened against the identified **BB**X**B** motif and phosphoserine (Figure 2.1) is one of the endogenous molecules that was identified through this virtual screening campaign.

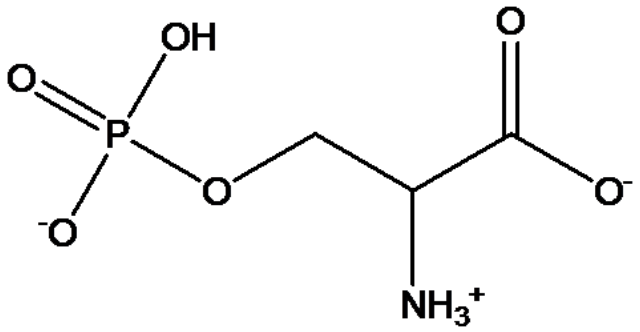

Figure 2.1: Phosphoserine at physiological pH

Phosphoserine is a small endogenous molecule of the brain that is believed to play a role in Alzheimer's disease. Despite suggestions that this role is destructive as proposed by Klunk *et al*, it is in fact possible that phosphoserine has a protective role in the brain by binding to β-amyloid to prevent the conformational conversions that result in neurotoxic aggregates [60, 61]. Given that phosphoserine is already endogenous to the

brain, and is shown to be capable of binding to this **HH**Q**K** region, it presents greater possibilities for developing drugs that will be able to prevent β-amyloid neurotoxicity.

2.3 PHOSPHOSERINE IN THE BRAIN

There is some controversy over the role of phosphoserine in Alzheimer's disease. Studies by Molina *et al* have shown that levels of phosphoserine are decreased in the brains of patients with Alzheimer's disease, while having higher levels of phosphoserine in plasma compared to age- and sex-matched patients [62]. In contrast, studies by Klunk and Mason *et al* have shown a correlation between levels of phosphoserine and the presence of β-amyloid plaques; the highest levels of phosphoserine are located in the regions containing the fewest plaques [60, 61]. Klunk has measured normal levels of phosphoserine in the brain to be 0.3 mM, with an increase of up to 1mM in the brain of Alzheimer's patients [63]. Thus controversy arises over whether brain levels of phosphoserine are actually increased or decreased in the disease.

Klunk suggests since phosphoserine bears structural similarity to glutamate, which is an excitatory neurotransmitter, that phosphoserine could therefore act as an NMDA antagonist and be a cause of the memory disturbances in Alzheimer's patients [60]. According to Mason and Klunk, given that levels of phosphoserine is highest in regions with fewer plaques, it may play a role in the pathogenesis of the disease [60, 63, 64]. They further conclude these increased levels of phosphoserine result in membrane changes that lead to the abnormal processing of APP to generate Aβ [64].

More recent studies by Wu *et al* suggest rather that the excitotoxicity is the result of D-serine, which is a metabolite of phosphoserine and a potent co-agonist of the NMDA receptor [65]. The rate limiting step in the conversion of L-serine to D-serine is suspected

to be the catabolism of phosphoserine to L-serine [66]. If the brain levels of phosphoserine are increased as Klunk *et al* claim, it may be that increased levels of D-serine would have more of an effect than phosphoserine.

None of the studies have actually studied the impact that phosphoserine could have on the aggregation of Aβ. It could be alternatively interpreted that as levels of phosphoserine are higher in regions with fewer plaques, that it plays a neuroprotective role to prevent amyloid aggregation from occurring. It is possible that phosphoserine may not be detrimental but could be part of the brain's response as a preventative agent in order to protect the brain.

At physiological pH, phosphoserine contains three charged functional groups: a positively charged amino group, a negatively charged carboxylate group and a negatively charged phosphate group. These charged residues are therefore capable of interacting with the **HH**Q**K** region of the β-amyloid peptide, which itself is highly positively charged at physiological pH.

2.4 Expansion to Target the EVHHQK Region of β-amyloid

As the phosphoserine molecule is in a zwitterionic state at physiological pH, it was realized that the targeted region of Aβ could be expanded to EV**HH**Q**K,** residues eleven to sixteen which are glutamic acid11 (Glu11), valine12 (Val12), histidine13 (His13), histidine14 (His14), glutamine15 (Gln15), and lysine16 (Lys16). Potential interactions could occur between the positively charged amino group on phosphoserine and the negatively charged glutamic acid residue in EV**HH**Q**K**, while the negatively charged groups could interact with the positively charged histidine and lysine residues. The EV**HH**Q**K** region presents four charged sites (see Figure 2.2) with which

phosphoserine can interact with, in the form of electrostatic interactions, between positively charged amino and negatively charged functional groups and vice versa; hydrogen bonding interactions can also occur as both the charged functional groups and amino acid side chains present themselves as hydrogen bond donors and acceptors.

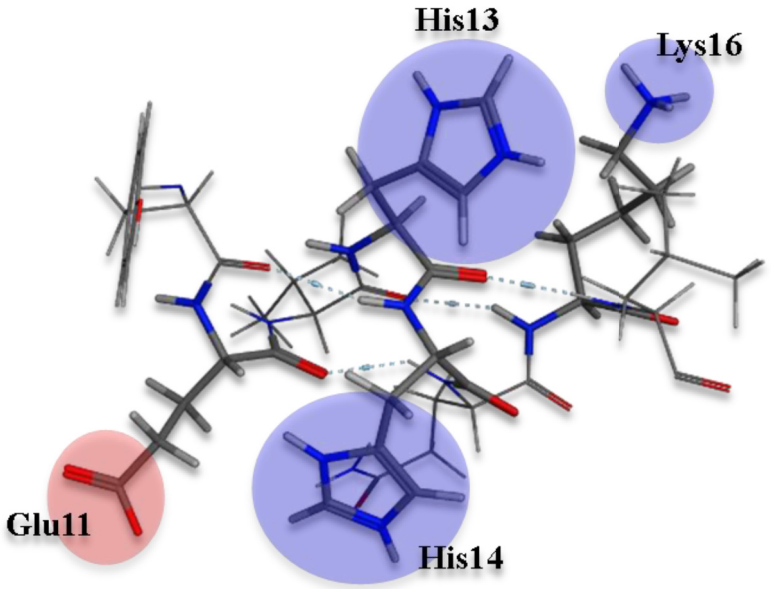

Figure 2.2: The charged amino acid side chains of the EVHHQK region of β-amyloid. The acidic Glu11 group is highlighted in red while the basic His13, His14 and Lys16 residues are highlighted in blue.

2.5 In Vacuo Calculations of Phosphoserine Interacting with β-amyloid

The first phase in determining if phosphoserine could bind to β-amyloid was to minimize Aβ-phosphoserine systems *in vacuo* to determine if stable binding interactions could occur. In calculating the gas phase interaction between phosphoserine and the target

EV**HH**Q**K** region of β-amyloid, some preliminary work was required to set up the molecules in order to perform the molecular modelling tasks.

2.5.1 Selection of β-Amyloid Conformers

Six different conformations of β-amyloid were selected from the RCSB Protein Data Bank (PDB) to be tested for their capacity to bind to and interact with phosphoserine [67]. These six conformers ranged in length from 16 to 42 amino acids long, and the variety of conformers allowed for a better determination as to whether phosphoserine was capable of binding to the EV**HH**Q**K** region of β-amyloid or not.

The six selected conformers, given by their PDB identifications, were as follows: 1AMB, 1AMC, 1AML, 1IYT, IBA4, and 2BP4 [67, 68, 69, 70, 71, 72, 73]. All structures were obtained via the use of NMR and under acidic conditions; therefore the structures required some preparation before they could be used for the gas phase calculations [68-73]. The 1AMB and 1AMC conformers are composed of residues one through 28 of the Aβ and both have α-helical conformations (Figure 2.3 and 2.4) [68, 69]. The 1AML conformer (Figure 2.5) represents the 1-40 length Aβ found in the brain in a random-coil conformation whereas 1BA4 (Figure 2.6), also composed of amino acids 1-40 of Aβ, has a more α-helical form, although there is a kink in the coil due to a hydrogen-bonded turn being present [70, 71]. 1IYT (Figure 2.7) is composed of 42 amino acids residues, and has a conformation closer to the more toxic Aβ form and is composed of two α-helices separated by a sharper hydrogen bonded turn [72]. The shortest conformer studied is the 2BP4 conformer (Figure 2.8) which spans the first through sixteenth residues of the β-amyloid peptide and exists in an α-helical form [73].

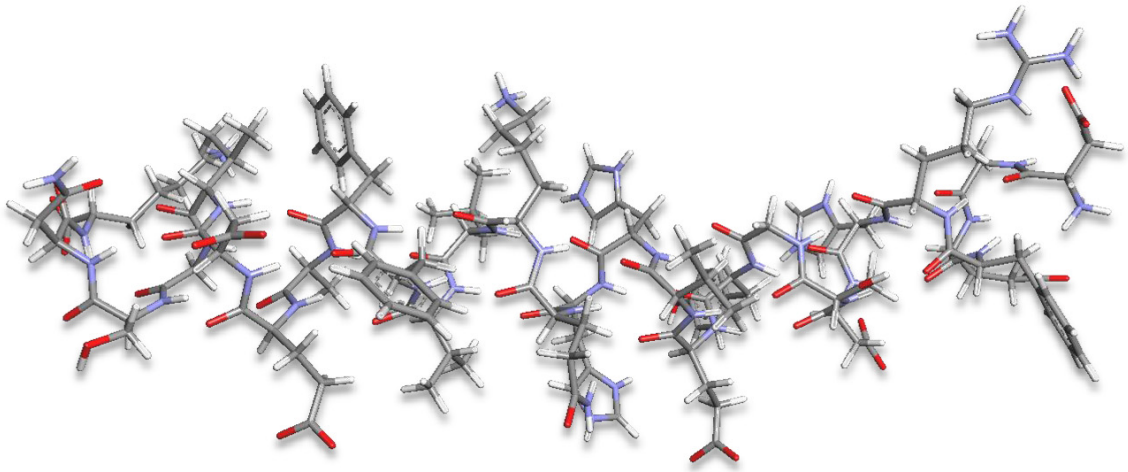

Figure 2.3: The 1AMB conformer of β-amyloid

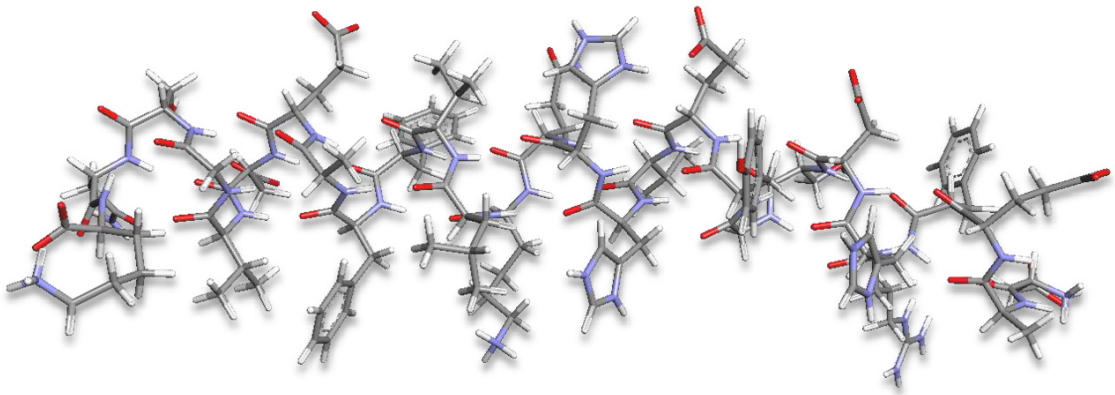

Figure 2.4: The 1AMC conformer of β-amyloid

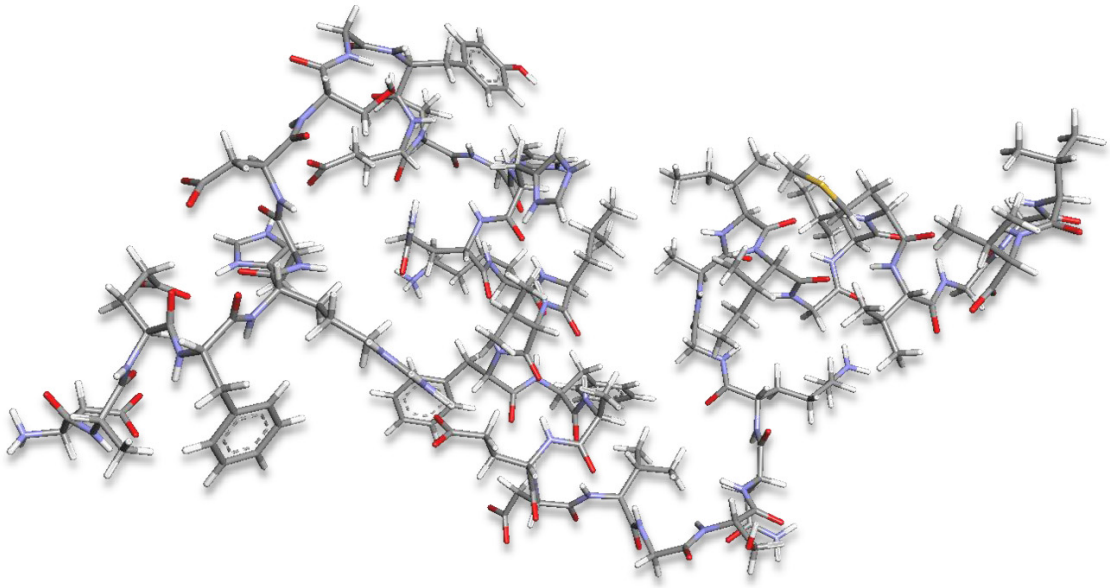

Figure 2.5: The 1AML conformer of β-amyloid

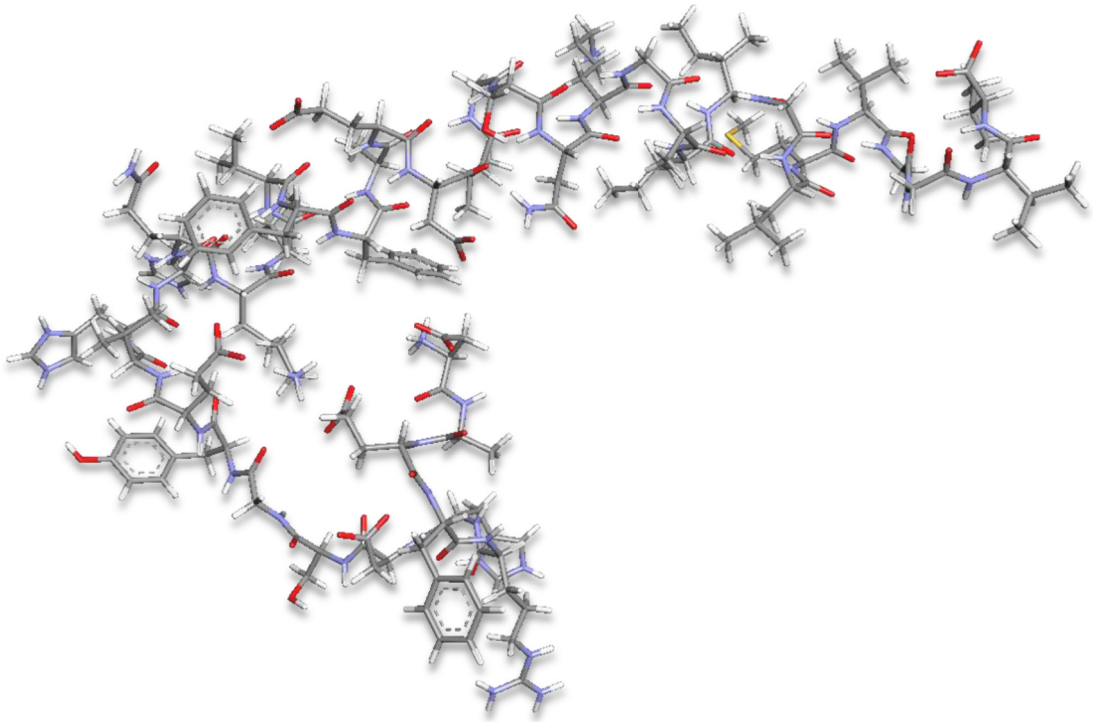

Figure 2.6: The 1BA4 conformer of β-amyloid

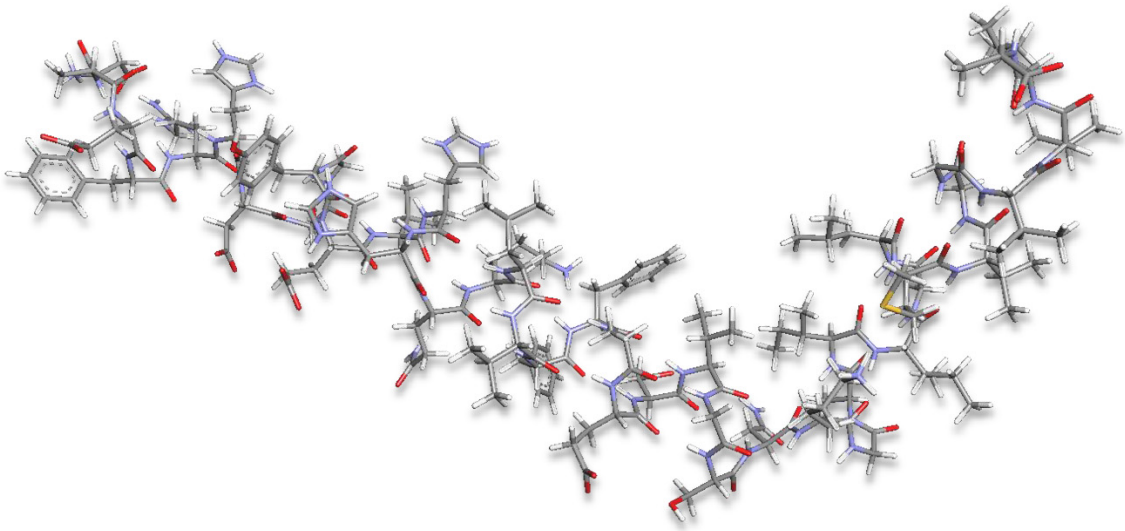

Figure 2.7: The 1IYT conformer of β-amyloid

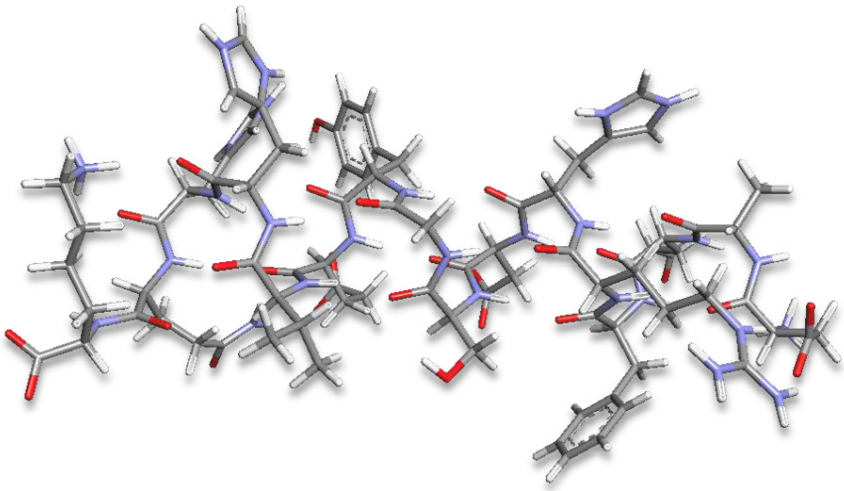

Figure 2.8: The 2BP4 conformer of β-amyloid

The six selected conformers were studied using the Cerius^2 program [45]. The first step was to charge the amino acid side chains such that they would be representative of the charged state as seen at physiological pH. This involved either protonating or deprotonating the side chains and terminal ends as required.

The next step was to locate a structure consistent with an energy minimum on the PES, as this provided a stable, low energy structure with which to work. PDB files of the β-amyloid conformers were downloaded and opened in the Cerius^2 program [45, 67]. Given that the peptide sequences contain polar and charged molecules, the backbones (i.e. the -N-C_α-$C_{=O}$- chain) were constrained to prevent a collapse of the structures during the gas phase calculations, since in a vacuum these elements will be attracted to each other whereas in an aqueous environment the charges will be shielded by the water molecules. Once the backbone of the conformer was constrained, the DREIDING2.21 force field was used to provide energy minimizations using a steepest descent approach [43]. This resulting low energy conformer for the β-amyloid conformation was saved for use both in gas phase and solution phase calculations. The final energies from each conformer that were used in calculating the energy differences for the following gas phase calculations are denoted in Table 2.1.

Table 2.1: Total energies of the six β-amyloid conformers as calculated using the DREIDING2.21 force field for gas phase calculations in Cerius^2

Conformer	Total Energy (kcal/mol)
1AMB	268.7
1AMC	248.3
1AML	443.4
1BA4	268.2
1IYT	298.7
2BP4	101.4

2.5.2 PREPARATION OF THE PHOSPHOSERINE MOLECULE

An optimized molecule of phosphoserine was constructed for use in the calculations. In order to find a low energy, stable structure a conformational search was performed; being a gas phase calculation, a neutral structure of the molecule was constructed in order to prevent self-interactions from occurring.

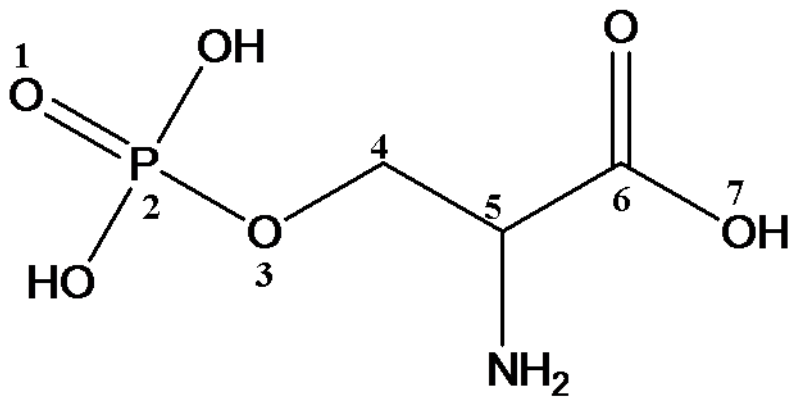

Figure 2.9: Neutral phosphoserine molecule with grid search numbers indicated

An extended, neutral conformation of phosphoserine was constructed, with four torsional angles (1-2-3-4, 2-3-4-5, 3-4-5-6, 4-5-6-7 as shown in Figure 2.9) selected and a grid search was performed in 30° steps from -180.0° to 150.0° [45]. From the resulting structures that were generated during the search, the lowest energy structure was found that was also in an extended conformation (as opposed to being folded in on itself). The selected model was then charged for physiological pH, with a protonated amino group, and deprotonated carboxylate and phosphate groups; the charges were then equilibrated using the Gasteiger algorithm [64]. Finally, all atoms except for the hydrogens were constrained and a steepest descent minimization was performed to ensure the hydrogens were located at the optimal geometries to produce a low energy stable structure. This

model of phosphoserine was used for each of the gas phase calculations, and the total energy of the molecule is given in Table 2.2.

Table 2.2 Total energy of phosphoserine in the gas phase as calculated in Cerius[2] using the DREIDING2.21 force field

Ligand	Total Energy (kcal/mol)
Phosphoserine	-42.0

2.5.3 CALCULATING GAS PHASE INTERACTIONS BETWEEN PHOSPHOSERINE AND VARIOUS CONFORMERS OF β-AMYLOID.

The purpose of the gas phase calculations was to determine which orientations, if any, of phosphoserine and β-amyloid would result in binding interactions. Should these binding interactions occur, a select few of the most energetically favourable systems would then be examined via solution phase calculations to mimic the natural conditions of the brain, where such interactions would occur *in vivo*.

2.5.3.1 SELECTING INITIAL ORIENTATIONS FOR OPTIMIZATION

Before the systems were prepared, it was determined that in order for a favourable interaction to occur, two of the charged functional groups should be oriented towards two of the charged side chains in the EV**HH**Q**K** segment of β-amyloid. Each initial interaction therefore contains two of the charged phosphoserine groups being oriented towards two different charged side chains on Aβ; the overall number of these potential interactions varies between the different conformations of Aβ being examined.

Experimental studies on drug-receptor interactions showed that the best distance to establish favourable interactions was a distance of approximately 3.0 Å between the functional group and the amino acid side chain. Given these distance requirements, any

possible orientation of phosphoserine and β-amyloid that resulted in a distance greater than roughly 3 Å between the two was rejected: in some cases the side chains of the amino acids were on opposite sides of the β-amyloid peptide and were too far apart to be selected for an initial orientation.

2.5.3.2 Optimization of the Gas Phase Systems

Each of the possible binding orientations available was modelled in the Cerius[2] program [45]. Once phosphoserine was oriented appropriately towards the peptide, the backbone of the peptide was constrained (to prevent self-interactions) and the system was then optimized (to find the lowest energy system) using the steepest descent algorithm. The resulting system was then saved, the energies calculated and finally examined for potential binding interactions: given that all of the charged side chains and amino acids are also capable of forming hydrogen bonds, bonding interactions were determined to have formed in some of the orientations between phosphoserine and β-amyloid.

To determine the favourability of the potential binding interactions that occurred following optimization, the binding energy was determined. The binding energy, which is based on the total energy of the system, was calculated as follows:

$$\Delta E_{bind} = E_{A\beta phos} - E_{A\beta} - E_{phos} \tag{2.1}$$

where $E_{A\beta phos}$ is the total energy of the optimized β-amyloid-phosphoserine system, $E_{A\beta}$ is the total energy of the β-amyloid conformer involved in the interaction, and E_{phos} is the total energy of the phosphoserine molecule, all calculated in the gas phase with the DREIDING2.21 force field [43].

2.5.4 GAS PHASE RESULTS OF PHOSPHOSERINE INTERACTING WITH β-AMYLOID

The main results of the gas phase interactions between phosphoserine and β-amyloid were summarized in the following tables according to the selected Aβ conformer. They include the initial orientations that were selected, the resulting orientations after optimization, the binding energy and the number of internal hydrogen bonds that formed. Phosphoserine had a tendency to form internal hydrogen bonds – that is bonds between its charged functional groups, when minimized with β-amyloid in the gas phase. These internal hydrogen bonds needed to be accounted for when determining which interactions were suitable for solution phase calculations: they lowered the energy state of the system, which made the interaction appear more favourable than it truly was with respect to phosphoserine interacting with Aβ.

The initial and final orientations of the functional groups were listed so that the functional group, represented by NH_3^+, CO_2^-, or PO_3^-, is located under columns indicating the Glu11-Lys16 amino acids of β-amyloid: in a few cases bonding interactions occurred outside the specified region and were noted as such. The final orientation observed only shows interactions where bonding interactions have formed. The calculated ΔE_{bind} energies are listed in kcal/mol.

2.5.4.1 RESULTS OF THE GAS PHASE CALCULATIONS OF PHOSPHOSERINE INTERACTING WITH THE 1AMB CONFORMER OF β-AMYLOID

There were twenty-four possible arrangements for phosphoserine to be oriented such that two functional groups were interacting with two of the four charged side chains on the 1AMB conformer of β-amyloid. Results in Table 2.3 showed that not all of these initial orientations resulted in binding interactions. As the purpose of the experiment was

to determine whether or not phosphoserine is capable of binding to β-amyloid, the phosphoserine molecule should bind to Aβ in at least two different places, therefore those systems that did not result in binding at sufficient sites were not selected for future calculations.

Table 2.3: Gas phase results of phosphoserine interacting with the 1AMB conformer of β-amyloid

Initial Orientation						Final Orientation						ΔE_{bind}	Internal
Glu11	Val12	His13	His14	Gln15	Lys16	Glu11	Val12	His13	His14	Gln15	Lys16	(kcal/mol)	H-Bonds
		PO_3^-	CO_2^-					PO_3^-	CO_2^-			-41.2	1
		CO_2^-	PO_3^-					CO_2^-				-34.2	1
		CO_2^-	NH_3^+					CO_2^-				-73.0	3
		NH_3^+	CO_2^-									-61.1	2
		PO_3^-	NH_3^+					PO_3^-				-48.3	1
		NH_3^+	PO_3^-									-5.5	1
NH_3^+			CO_2^-			NH_3^+			CO_2^-			-43.7	1
CO_2^-			NH_3^+			NH_3^+						-25.0	1
CO_2^-			PO_3^-						PO_3^-			1.2	1
PO_3^-			CO_2^-									-22.7	2
PO_3^-			NH_3^+									2.7	1
NH_3^+			PO_3^-			NH_3^+			PO_3^-			-32.8	1
		CO_2^-			PO_3^-						PO_3^-/CO_2^-	-61.3	0
		PO_3^-			CO_2^-						CO_2^-	-56.1	1
		CO_2^-			NH_3^+						CO_2^-	-66.1	4
		NH_3^+			CO_2^-						CO_2^-	-67.2	3
		PO_3^-			NH_3^+			PO_3^-			CO_2^-	-79.7	1
		NH_3^+			PO_3^-			CO_2^-			PO_3^-	-74.8	1
NH_3^+		CO_2^-				NH_3^+						-38.4	1
CO_2^-		NH_3^+							CO_2^-			2.6	1
CO_2^-		PO_3^-							CO_2^-			-28.2	1
PO_3^-		CO_2^-							PO_3^-			-26.2	1
PO_3^-		NH_3^+						CO_2^-	PO_3^-			-54.3	2
NH_3^+		PO_3^-				NH_3^+						-53.2	1

Examination of the results eliminated eighteen of the twenty-four interactions as viable options for the solution phase calculations. The remaining six were ranked in order of energy. The number of internal hydrogen bonds that formed was also taken in to consideration when choosing four of the remaining systems for aqueous treatment (see Table 2.4). The interaction is specified by the initial orientation of the system, where P, N,

and C are not representative of amino acids but rather the charged functional groups present on phosphoserine; the amino acids are identified by their one-letter abbreviation for naming simplicity.

Table 2.4: Potential interactions of phosphoserine and the 1AMB conformer of Aβ for solvation

Interaction	ΔE_{bind}
HPHQKN	-79.7
HNHQKP	-74.8
EPVHN	-54.3
ENVHHC	-43.7
HPHC	-41.2
ENVHHP	-32.8

From this information, the HPHQKN, HNHQKP, ENVHHC, and HPHC interactions were selected for solution phase calculations; EPVHN although seemingly lower in energy than the last two orientations selected, also had two binding interactions forming within the phosphoserine molecule, which made the binding energy seem more favourable than it truly was. Figure 2.10 shows the binding interaction resulting from the minimization of the phosphoserine-Aβ system where the amino and phosphate groups were oriented towards the His13 and Lys16 residues initially.

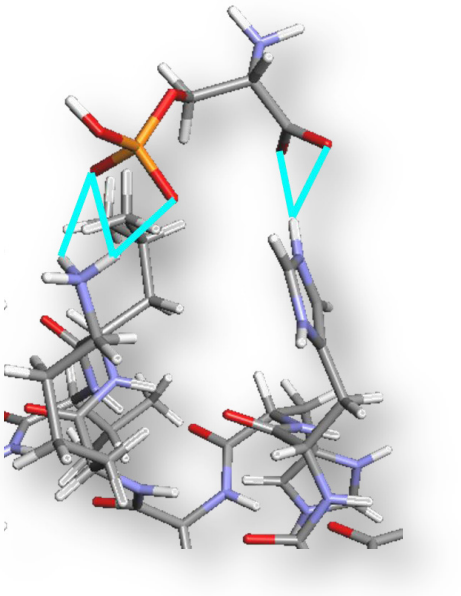

Figure 2.10: The gas phase interaction occurring between phosphoserine and the His13 and Lys16 residues of the 1AMB conformer of β-amyloid. Hydrogen bonds are represented by the turquoise lines.

2.5.4.2 Results of the Gas Phase Calculations of Phosphoserine Interacting with the 1AMC Conformer of β-amyloid

Table 2.5 shows the results of the twenty-four combinations of initial orientations that were available for phosphoserine to interact with the 1AMC conformer of β-amyloid. Three of the interactions resulted in binding occurring between phosphoserine and the Tyr10 amino acid on Aβ.

Table 2.5: Gas phase results of phosphoserine interacting with the 1AMC conformer of β-amyloid

Initial Orientation						Final Orientation							ΔE_{bind}	Internal
Glu11	Val12	His13	His14	Gln15	Lys16	Tyr10	Glu11	Val12	His13	His14	Gln15	Lys16	(kcal/mol)	H-Bonds
NH_3^+			CO_2^-				NH_3^+			CO_2^-			-20.8	1
CO_2^-			NH_3^+										14.3	1
CO_2^-			PO_3^-				NH_3^+			PO_3^-			-20.2	2
PO_3^-			CO_2^-							CO_2^-			-24.4	1
PO_3^-			NH_3^+							CO_2^-			-21.2	4
NH_3^+			PO_3^-				NH_3^+						-30.9	1
PO_3^-		NH_3^+				NH_3^+	PO_3^-		CO_2^-	PO_3^-			-43.6	2
NH_3^+		PO_3^-					NH_3^+						-26.5	1
NH_3^+		CO_2^-							CO_2^-				-23.1	1
CO_2^-		NH_3^+				NH_3^+				CO_2^-			6.6	1
CO_2^-		PO_3^-											-25.1	1
PO_3^-		CO_2^-				PO_3^-			CO_2^-				-32.7	1
		NH_3^+	CO_2^-							CO_2^-			14.8	1
		CO_2^-	NH_3^+						CO_2^-				-12.0	0
		CO_2^-	PO_3^-						CO_2^-				-25.6	1
		PO_3^-	CO_2^-						PO_3^-				-17.5	1
		PO_3^-	NH_3^+						PO_3^-				-20.9	1
		NH_3^+	PO_3^-										1.4	1
		NH_3^+			CO_2^-							CO_2^-	-24.4	1
		CO_2^-			NH_3^+							NH_3^+	-54.3	3
		CO_2^-			PO_3^-				CO_2^-			PO_3^-	-46.2	1
		PO_3^-			CO_2^-							CO_2^-	-34.5	1
		NH_3^+			PO_3^-				CO_2^-			PO_3^-	-69.1	1
		PO_3^-			NH_3^+							CO_2^-	-48.5	1

Only seven of the twenty-four interactions demonstrated potential for solution phase calculations. Table 2.6 summarizes the potential of these interactions according to their binding energy.

Table 2.6: Potential interactions of phosphoserine and the 1AMC conformer of Aβ for solvation

Interaction	ΔE_{bind}
HNHQKP	-69.1
HCHQKP	-46.2
EPVHN	-43.6
EPVHC	-32.7
ENVHHC	-20.8
ECVHHP	-20.2
ECVHN	6.6

Analysis revealed the four best interactions to use for solution phase calculations were HNHQKP, HCHQKP, EPVHC and ENVHHC; due to the presence of two internal bonding interactions in phosphoserine, EPVHN was ruled out as a possible selection since the true energy of interaction was most likely less favourable than indicated. Although EPVHC had one binding interaction outside the EV**HH**Q**K** region, it was still deemed acceptable for use in solution phase calculations due to the fact that binding was occurring at two different amino acid side chains and the favourable energy of the interaction.

2.5.4.3 Results of the Gas Phase Calculations of Phosphoserine Interacting with the 1AML Conformer of β-Amyloid

There were twenty-four possible orientations for phosphoserine to be arranged in to interact with the 1AML conformer of β-amyloid, the results of which are presented in Table 2.7.

Table 2.7: Gas phase results of phosphoserine interacting with the 1AML conformer of β-amyloid

Initial Orientation						Final Orientation							ΔE_{bind}	Internal
Glu11	Val12	His13	His14	Gln15	Lys16	Glu11	Val12	His13	His14	Gln15	Lys16	Other	(kcal/mol)	H-Bonds
NH_3^+			PO_3^-			NH_3^+							-51.8	1
PO_3^-			NH_3^+						PO_3^-	PO_3^-		CO_2^- [a]	-30.0	1
PO_3^-			CO_2^-							PO_3^-		PO_3^- [b]	-20.7	1
CO_2^-			PO_3^-							CO_2^-			-14.2	1
CO_2^-			NH_3^+							CO_2^-			-48.6	3
NH_3^+			CO_2^-									NH_3^+ [a]	-36.0	1
NH_3^+					PO_3^-	NH_3^+					PO_3^-		-32.6	1
PO_3^-					NH_3^+								19.3	1
PO_3^-					CO_2^-						CO_2^-		-37.7	1
CO_2^-					PO_3^-						PO_3^-		-24.6	1
CO_2^-					NH_3^+	NH_3^+						CO_2^- [b]	6.2	1
NH_3^+					CO_2^-	NH_3^+					CO_2^-		-41.0	1
		NH_3^+			PO_3^-						PO_3^-		-50.2	1
		PO_3^-			NH_3^+						CO_2^-		-46.0	2
		CO_2^-			PO_3^-						PO_3^-		-32.5	1
		PO_3^-			CO_2^-						CO_2^-		-34.3	1
		CO_2^-			NH_3^+						CO_2^-		-36.0	3
		NH_3^+			CO_2^-						CO_2^-		-11.6	1
		PO_3^-	NH_3^+					PO_3^-				PO_3^- [c]	-48.9	2
		NH_3^+	PO_3^-										-6.8	1
		CO_2^-	PO_3^-					CO_2^-					-28.3	1
		PO_3^-	CO_2^-										-18.6	1
		NH_3^+	CO_2^-										6.1	1
		CO_2^-	NH_3^+									CO_2^- [c]	-16.3	2

a = Ser8, b = His6, c = Tyr10

Several of the arrangements resulted in binding interactions occurring between phosphoserine and regions outside the area of interest to this study.

Of these twenty-four initial arrangements, only six had binding interactions occurring at two or more sites on β-amyloid, and these are listed in Table 2.8.

Table 2.8: Potential interactions of phosphoserine and the 1AML conformer of Aβ for solvation

Interaction	ΔE_{bind}
HPHN	-48.9
ENVHHQKC	-41.0
ENVHHQKP	-32.6
EPVHHN	-30.0
EPVHHC	-20.7
ECVHHQKN	6.2

The first four, with the lowest binding energies, appear to be the most favourable interactions and were selected for solution phase calculations. Although the HPHN interaction had the lowest energy, it also had two internal bonding interactions that formed in phosphoserine, as opposed to only one for all the other interactions; despite this, the energy minus the extra hydrogen bond should still be more favourable than the two higher energy interactions and so it was selected for further calculations. The HPHN and EPVHHN systems were selected although there were binding interactions occurring outside the region of EV**HH**Q**K,** as they were suitably favourable interactions meeting the requirement that binding occur at a minimum of two different side chains of Aβ.

2.5.4.4 Results of the Gas Phase Calculations of Phosphoserine Interacting with the 1BA4 Conformer of β-Amyloid

Given that the 1BA4 conformer of Aβ has a hydrogen bond turn present, this resulted in the side chains being further apart or on opposite sides of the peptide chain than in a strictly α-helical chain structure. As a result there were only twelve orientations in which phosphoserine was capable of binding to β-amyloid, and the final results of the gas phase minimizations are summarized in Table 2.9.

There were more instances in which the final binding interactions involved amino acid side chains outside the EV**HH**Q**K** region of interest. In particular, initial orientations where phosphoserine was positioned to interact with the Glu11 and Lys16 side chains resulted in several binding interactions occurring with the Asp1 residue; given that the terminal amino acid also has a charged amino group, it was capable of interacting with both the positively and negatively charged functional groups on phosphoserine.

There were only five final binding orientations where phosphoserine formed bonding interactions with Aβ at two or more sites, which are listed in Table 2.10. All of the selected interactions had only one internal hydrogen bond and therefore the four that were selected for further calculations in an aqueous environment were determined based on the binding energy alone.

Table 2.9: Gas phase results of phosphoserine interacting with the 1BA4 conformer of β-amyloid

Initial Orientation						Final Orientation								ΔE_{bind}	Internal
Glu11	Val12	His13	His14	Gln15	Lys16	Asp1	Glu11	Val12	His13	His14	Gln15	Lys16	Other	(kcal/mol)	H-Bonds
NH_3^+					CO_2^-		NH_3^+					CO_2^-		0.7	1
CO_2^-					NH_3^+	NH_3^+						CO_2^-	NH_3^+ [a]	-21.8	1
PO_3^-					CO_2^-	NH_3^+/CO_2^-						CO_2^-	NH_3^+ [b]	-18.6	1
CO_2^-					PO_3^-	PO_3^-						PO_3^-		-9.6	1
PO_3^-					NH_3^+	NH_3^+								-6.9	1
NH_3^+					PO_3^-		NH_3^+							0.1	0
		NH_3^+	CO_2^-									PO_3^-		-25.8	2
		CO_2^-	NH_3^+											-15.9	2
		NH_3^+	PO_3^-						CO_2^-					-41.9	2
		PO_3^-	NH_3^+						PO_3^-					-46.7	2
		CO_2^-	PO_3^-						CO_2^-	PO_3^-				-25.5	1
		PO_3^-	CO_2^-						PO_3^-					-25.3	1

a = Glu3, b = Asp23

Table 2.10: Potential interactions of phosphoserine and the 1BA4 conformer of Aβ for solvation

Interaction	ΔE_{bind}
HCHP	-25.5
ECVHHQKN	-21.8
EPVHHQKC	-18.6
ECVHHQKP	-9.6
ENVHHQKC	0.7

The four binding interactions chosen were HCHP, ECVHHQKN, EPVHHQKC, and ECVHHQKP. While the former had binding interactions within the EV**HH**Q**K** region, the latter three interactions bound more so to amino acid side chains found outside of this focused region. However, given the few number of interactions available for the 1BA4 β-amyloid conformer, they were determined to be acceptable for the solution phase calculations.

2.5.4.5 Results of the Gas Phase Calculations of Phosphoserine Interacting with the 1IYT Conformer of β-Amyloid

Due to the nature of the 1IYT conformer, in which a sharp hydrogen bonded turn is present that separates the two α-helical chains present in the structure, there were only eighteen available orientations in which phosphoserine could be placed for potential interaction. These orientations and the results of their minimization calculations in the gas phase are summarized in Table 2.11.

Of the resulting final binding orientations, only four had bonding interactions that bind phosphoserine to Aβ at two different sites, thus these four were selected for further analysis in the solution phase: HCHP, HNHQKP, HPHQKC and HCHQKP, all of which also had favourable binding energies.

Table 2.11: Gas phase results of phosphoserine interacting with the 1IYT conformer of β-amyloid

Initial Orientation						Final Orientation						ΔE_{bind}	Internal
Glu11	Val12	His13	His14	Gln15	Lys16	Glu11	Val12	His13	His14	Gln15	Lys16	(kcal/mol)	H-Bonds
NH_3^+			PO_3^-			NH_3^+						-33.0	1
PO_3^-			NH_3^+									21.3	1
NH_3^+			CO_2^-			NH_3^+						-25.1	0
CO_2^-			NH_3^+									-4.7	1
PO_3^-			CO_2^-									10.1	1
CO_2^-			PO_3^-									12.8	2
		PO_3^-	NH_3^+									-36.4	2
		NH_3^+	PO_3^-									13.7	1
		NH_3^+	CO_2^-									3.4	1
		CO_2^-	NH_3^+					CO_2^-				-11.2	1
		PO_3^-	CO_2^-						CO_2^-			-23.8	1
		CO_2^-	PO_3^-					CO_2^-	PO_3^-			-26.0	1
		CO_2^-			NH_3^+			CO_2^-				-20.9	1
		NH_3^+			CO_2^-						CO_2^-	-1.1	1
		NH_3^+			PO_3^-			CO_2^-			PO_3^-	-61.0	2
		PO_3^-			NH_3^+			PO_3^-				-10.1	1
		PO_3^-			CO_2^-			PO_3^-			CO_2^-	-48.2	1
		CO_2^-			PO_3^-			CO_2^-			PO_3^-	-43.8	1

2.5.4.6 Results of the Gas Phase Calculations of Phosphoserine Interacting with the 2BP4 Conformer of β-Amyloid

There were twenty-four available orientations for phosphoserine being optimized interacting with the 2BP4 conformer of β-amyloid. Given that the 2BP4 conformer is the shortest of the conformers that was examined (ending at the Lys16 residue that terminates the Glu11-Lys16 region of interest) it is possible that some of the resulting binding positions were not representative of those seen in the brain. With the longer forms of β-amyloid there could be potential for more side chain interactions occurring in the brain with those amino acids following Lys16 in the peptide sequence of amino acids. Table 2.12 summarizes the results of the gas phase optimizations.

Of the twenty-four final binding orientations, fifteen had interactions form between phosphoserine at two or more side chains on Aβ. This higher number of

favourable binding interactions was most likely due to the fact that the terminal region of the peptide chain was more exposed to the empty space around it, resulting in more freedom of movement for the phosphoserine molecule such that it could find more, lower energy, stable structures. Table 2.13 lists these systems resulting in acceptable binding interactions ranked according to their binding energies. Three of the final binding orientations revealed that phosphoserine had formed interactions with the Tyr10 side chain of β-amyloid.

Table 2.12: Gas phase results of phosphoserine interacting with the 2BP4 conformer of β-amyloid

Initial Orientation						Final Orientation							ΔE_{bind}	Internal
Glu11	Val12	His13	His14	Gln15	Lys16	Tyr10	Glu11	Val12	His13	His14	Gln15	Lys16	(kcal/mol)	H-Bonds
PO_3^-			CO_2^-			PO_3^-				CO_2^-			-8.5	1
CO_2^-			PO_3^-										18.7	1
NH_3^+			PO_3^-				NH_3^+			PO_3^-			-41.9	1
PO_3^-			NH_3^+										39.2	1
CO_2^-			NH_3^+			CO_2^-				CO_2^-			-30.4	2
NH_3^+			CO_2^-			CO_2^-	NH_3^+			CO_2^-			-45.9	1
		PO_3^-	NH_3^+						PO_3^-			PO_3^-	-22.9	1
		NH_3^+	PO_3^-									CO_2^-	-56.9	1
		NH_3^+	CO_2^-						CO_2^-				-40.9	4
		CO_2^-	NH_3^+						CO_2^-			CO_2^-/PO_3^-	-42.5	1
		CO_2^-	PO_3^-						CO_2^-			CO_2^-	-50.5	1
		PO_3^-	CO_2^-						PO_3^-			PO_3^-	-59.3	1
		PO_3^-			NH_3^+				PO_3^-				-10.7	1
		NH_3^+			PO_3^-							PO_3^-	-29.2	1
		NH_3^+			CO_2^-							CO_2^-	-44.0	3
		CO_2^-			NH_3^+							CO_2^-	-50.1	3
		CO_2^-			PO_3^-				CO_2^-	CO_2^-		PO_3^-	-41.2	1
		PO_3^-			CO_2^-				PO_3^-	PO_3^-		CO_2^-	-50.8	1
			PO_3^-		CO_2^-				PO_3^-			CO_2^-	-51.1	1
			CO_2^-		PO_3^-				CO_2^-			PO_3^-	-51.3	1
			NH_3^+		PO_3^-					CO_2^-		PO_3^-	-50.7	1
			PO_3^-		NH_3^+				PO_3^-			PO_3^-	-32.5	1
			CO_2^-		NH_3^+				CO_2^-			CO_2^-	-39.1	1
			NH_3^+		CO_2^-							CO_2^-	-43.5	3

Table 2.13: Potential interactions of phosphoserine and the 2BP4 conformer of Aβ for solvation

Interaction	ΔE_{bind}
HPHC	-59.3
HCQKP	-51.3
HPQKC	-51.1
HPHQKC	-50.8
HNQKP	-50.7
HCHP	-50.5
ENVHHC	-45.9
HCHN	-42.5
ENVHHP	-41.9
HCHQKP	-41.2
HCQKN	-39.1
HPQKN	-32.5
ECVHHN	-30.4
HPHN	-22.9
EPVHHC	-8.5

Analysis of the initial orientations that resulted in favourable binding interactions revealed that the four lowest energy interactions were the best choice for calculations in the aqueous phase: HPHC, HCQKP, HPQKC, and HPHQKC all had very favourable binding energies, as well as only having one internal bonding interaction within the phosphoserine molecule, which made them all acceptable interactions for further analysis.

2.6 Solution Phase Calculations of Phosphoserine Interacting with β-Amyloid

To appropriately model the interactions that could occur between phosphoserine and β-amyloid within the brain, solution phase calculations needed to be performed. In the brain, phosphoserine and Aβ are found in an aqueous environment at physiological pH. The presence of water molecules (among other species present in the brain) can therefore alter how these two charged species will interact with each other.

2.6.1 THE USE OF EXPLICIT SOLVATION

To simulate the binding interactions that possibly occur in the brain between phosphoserine and β-amyloid, an explicit solvation method was used.

Given the biological nature of the system, having explicit water molecules present was best to mimic the aqueous environment of the brain. Implicit solvation involves the dielectric constant and although the dielectric constant could be modified to mimic the shielding effects water has on charged species, it was not the best method when looking at systems of this nature [42]. By having explicit water molecules present, the true interactions that could occur between the various species present in a system was better represented since the molecules and the peptide side chains could have interactions with water that would also affect how they interacted with each other, as well as geometric positioning.

The Cerius^2 program that was used for the gas phase calculations of phosphoserine interacting with Aβ was determined to lack the appropriate tools for modelling solvated environments, so the QUANTA program was selected [45, 46]. The QUANTA program uses the CHARMM force field, and explicit solvation of water molecules uses the simple TIP3P water molecule [44, 46].

The TIP3P model of water is a rigid model that involves three electrostatic interaction sites; two positively charged hydrogen atoms that sum up to balance the negatively charged oxygen atom [42]. Van der Waals calculations of the water molecules involve only the oxygen atom and not the hydrogen atoms [42]. This model is most commonly used since it provides a fairly accurate model of the properties of water that

are suitable to the type of calculations being performed in this research, while also minimizing the computational cost that occurs when more complex water models are used [42].

2.6.2 SET-UP OF THE SOLUTION PHASE CALCULATIONS OF PHOSPHOSERINE INTERACTING WITH β-AMYLOID

The method used for modelling the potential binding interactions between phosphoserine and Aβ was selected to minimize computational cost. This was accomplished by selecting four of the resulting interactions of the gas phase calculations that met specific requirements and then solvating these systems. Only four interactions were selected due to the large computational cost associated with running minimization algorithms on solvated systems. Four calculations were determined to be an adequate number to establish whether the binding interactions would be significantly altered between the gas and solution phases. They should also be sufficient to determine favourable binding interactions in trends with a total of twenty-four results for solvated systems.

2.6.2.1 SOLVATING THE SYSTEM

If the gas phase interaction between phosphoserine and the various conformers of β-amyloid resulted in interactions occurring at two or more different amino acid side chains on the peptide, and had a favourable binding energy that was due to the interaction alone and not to the formation of multiple interactions within the phosphoserine molecule, it was selected as a viable option for solvation. The four lowest energy interactions that met these criteria were selected for solvation as this minimized the computational cost involved. By taking a binding interaction known to exist in the gas phase, it could then be

determined what action the presence of water molecules would exert on the system, whether to encourage the binding or to disrupt it. It would have been more computationally demanding to begin again with separated phosphoserine and β-amyloid models and run the same calculations in a solvated environment.

The selected interaction was then solvated, depending on the size of the system, with one or two 30 Å x 30 Å x 30 Å boxes of water molecules. The QUANTA program only has two sizes of water boxes available, 15 Å x 15 Å x 15 Å and 30 Å x30 Å x 30 Å, neither of which was large enough to solvate the entire peptide except in the case of the 2BP4 conformer [46]. This problem was solved by writing a script that allowed for two 30 Å x 30 Å x 30 Å water boxes to be united. The detailed method and scripts used can be found in Appendices 2-4.

For those systems requiring two 30 Å boxes to be solvated, a program was started to capture the commands in QUANTA and a 30 Å water box was positioned over an atom to solvate part of the system, and then the capture program was terminated [46]. This saved file contained information on the position of the atoms and the water molecules that were introduced to the system. Part of this information was selected, saved and read into the above mentioned script: a second atom from the peptide was selected to place a second water box upon and the file was saved. This saved file was then streamed into the QUANTA program and resulted in two water boxes being positioned on the β-amyloid-phosphoserine complex (a detailed methodology is given in Appendix 2) [46]. In most cases this positioning resulted in some overlap of the boxes which caused some of the water molecules to become merged together. These molecules were then separated where possible to regenerate single water molecules that would not be too close to the

other molecules, or they were deleted as some of the overlapping water molecules were quite mangled. All of these molecules were fixed or deleted as necessary before any other operation was performed on the system. Figure 2.11 shows one of the solvated interactions where two 30 Å water boxes were united together for the system.

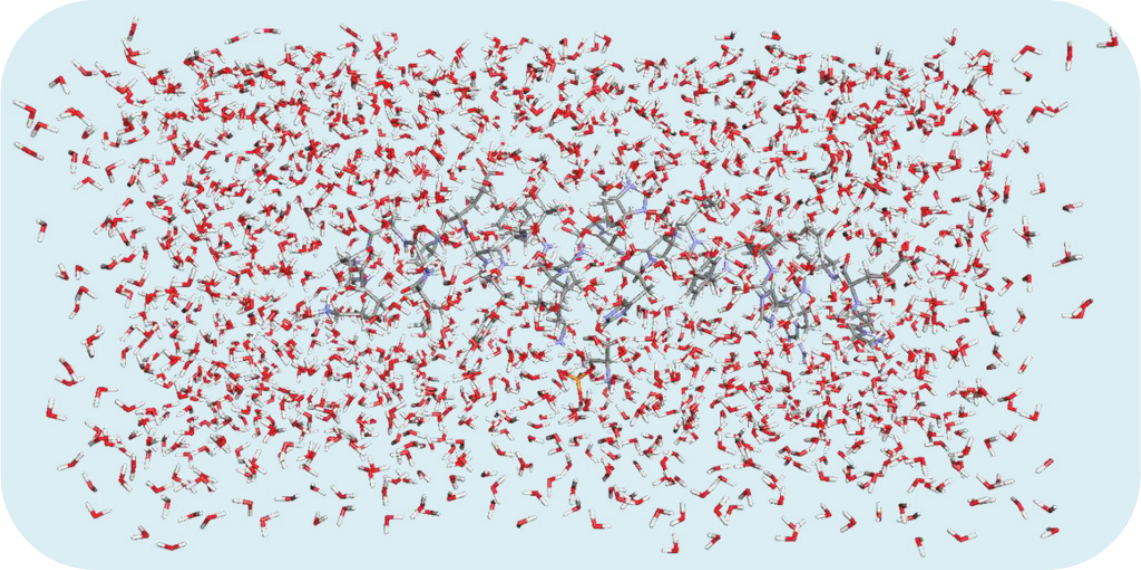

Figure 2.11: The interactions between phosphoserine and the 1AMB conformer of β-amyloid in an aqueous environment

2.6.2.2 Periodic Boundary Conditions

Once the system was solvated, periodic boundary conditions were introduced. The boundary conditions were necessary to prevent the water molecules from expanding infinitely into space once minimization of the system was commenced. The boundary conditions were set to be equal to the size of the water boxes solvating the system and according to the spatial orientation of the boxes. For the 1AMB, 1AMC, 1AML, and 1BA4 conformers the periodic boundary conditions were therefore set to be 60 Å x 30 Å x 30 Å (in the x, y, and z directions). 1IYT had a different spatial orientation of the water boxes and therefore the periodic boundaries were set for 30 Å x 30 Å x 60 Å. Given that

the 2BP4 conformer of β-amyloid was small enough to be solvated by one 30 Å water box, the periodic boundaries were set to 30 Å x 30 Å x 30 Å.

2.6.2.3 Minimization of the Solvated Phosphoserine-β-Amyloid System

Once the interacting systems selected from the gas phase calculations were set up for the calculations, the energy minimization step was performed. Unlike the gas phase calculations, no constraints were placed upon the peptide backbone as the water molecules would help to shield the charged species from interacting with each other; those changes that did occur were more likely reflective of the positioning that could exist in a biological environment.

Given the large size of the system – a few hundred peptide and phosphoserine atoms plus several thousand atoms comprising the water molecules – a minimum on the potential energy surface was unlikely to be attained when using the steepest descent minimization algorithm; therefore the steepest descent energy minimization was used to bring the system close to an energy minimum on the PES until it took at least twenty-five iterative steps for the energy of the system to change by 1 kcal/mol. Upon reaching this slow energy change, the minimization was halted and the conjugate gradient energy minimization algorithm was utilized to bring the system to an energy minimum.

2.6.2.4 Energy Calculations of the Solvated Aβ-Phosphoserine Interactions

Once an energy minimum was attained, the total energy of the system was measured, ignoring the solvent contributions to the energy of the system, and then the electrostatic energy was measured while also ignoring solvent contributions. A third energy was measured while ignoring the solvent contributions and constraining the

protein backbone in order to determine the electrostatic energy based solely on the amino acid side chains and phosphoserine.

The three energies that were calculated for analytical purposes are therefore; the total binding energy of the system ignoring solvent contributions:

$$\Delta E_{tot} = E_{tot} - E_{A\beta} - E_{phos} \tag{2.2}$$

E_{tot} is the total energy of the phosphoserine-Aβ system, $E_{A\beta}$ is the total energy of the β-amyloid conformer and E_{phos} is the total energy of phosphoserine, all of which were calculated after minimization in the solution phase, but ignoring the solvent contributions to the energy.

The electrostatic energy of the system, after minimization in the solution phase and also ignoring the solvent contributions was calculated by:

$$\Delta E_{ele} = E_{ele} - E_{eleA\beta} - E_{elephos} \tag{2.3}$$

The electrostatic energy of the final phosphoserine-Aβ system is given by E_{ele} and subtracting the electrostatic energy of Aβ, $E_{eleA\beta}$, and phosphoserine, $E_{elephos}$, gives the overall change in the electrostatic energy for that particular system.

The final energy calculation examined the electrostatic contributions based solely on the phosphoserine and amino acid side chain contributions, ignoring the backbone contributions to this energy (since the backbone atoms could interact electrostatically in maintaining or altering the conformation of the peptide). The equation used is identical to the previous one except that the electrostatic energy was calculated with a constrained protein backbone:

$$\Delta E_{elecpb} = E_{elecpb} - E_{elecpbA\beta} - E_{elephos} \quad (2.4)$$

E_{elecpb} is the electrostatic energy of the interacting phosphoserine and β-amyloid system with a constrained protein backbone for the peptide involved, $E_{elecpbA\beta}$ is the electrostatic energy of the β-amyloid conformer with the backbone constrained, and the $E_{elephos}$ remains unconstrained since the molecule is not a protein.

2.6.2.5 Determination of Binding Interactions

To determine if binding interactions occurred as a result of the minimization of the solvated phosphoserine-Aβ systems, two methods were used. First the QUANTA program has an option to display hydrogen bonds present in the system. This feature was applied to the final optimized system once the solvent contributions were ignored for better visualization of the possible interactions [46].

It was discovered that MOE (Molecular Operating Environment) allowed for ligand interactions to be determined, including potential π-π and cation-π interactions, as well as electrostatic interactions [47]. The final binding orientations were then imported into the MOE environment to determine if any of the other possible types of binding interactions were present [47].

2.6.3 Solution Phase Results of Phosphoserine Interacting with Six Different β-Amyloid Conformers

The results of the minimizations of phosphoserine interacting with β-amyloid in an aqueous environment are summarized in tables according to the Aβ conformer being examined. The initial binding orientation that resulted from the gas phase calculations is given, followed by the final binding orientation that resulted from the optimized, solvated system. The calculated total energy, electrostatic energy, and electrostatic energy

involving a constrained protein backbone are given (solvent contributions to the system were not included when calculating these energies), as well as the differences in these energies calculated using the previously mentioned equations. Hydrogen bonding interactions are denoted by peach coloured cells, while electrostatic interactions are marked by blue coloured cells in the tables. The energies of the β-amyloid conformers and phosphoserine used to calculate the binding energies of the solution phase interactions are given in Table 2.14.

Table 2.14: Total energies of the six β-amyloid conformers and phosphoserine calculated in a solvated environment

Conformer	E_{tot}	E_{ele}	E_{elecpb}
1AMB	-314.52	-270.43	-55.10
1AMC	-314.53	-280.48	-66.97
1AML	-404.92	-346.18	-54.90
1BA4	-420.10	-369.83	-57.33
1IYT	-530.26	-404.59	-72.85
2BP4	-177.10	-153.70	-39.15

	E_{tot}	E_{ele}
Phosphoserine	-11.31	-12.76

2.6.3.1 Results of the Solution Phase Interaction Between Phosphoserine and the 1AMB Conformer of β-Amyloid

The solution phase calculations resulted in fewer bonding interactions than in the gas phase, but this was understandable given the presence of water molecules in the system. In most cases the functional groups remained in similar orientations to the final result of the gas phase minimizations, with both hydrogen bonding and electrostatic interactions occurring. The results of the final orientations of the functional groups,

binding interactions and the calculated binding energies are tabulated in Table 2.15.

Electrostatic interactions are in blue, while hydrogen bonds are in peach.

Table 2.15: The solution phase results of phosphoserine interacting with the 1AMB conformer of β-amyloid

A) Amino Acid	Glu11	Val12	His13	His14	Gln15	Lys16
Initial Orientation			CO_2^-			PO_3^-
Final Orientation			CO_2^-/PO_3^-			PO_3^-
E_{tot}	-1382.31 kcal/mol					
E_{ele}	-1416.29 kcal/mol					
E_{elecpb}	-586.11 kcal/mol					
ΔE_{tot}	-1056.48 kcal/mol					
ΔE_{ele}	-1133.10 kcal/mol					
ΔE_{elecpb}	-531.00 kcal/mol					

B) Amino Acid	Glu11	Val12	His13	His14	Gln15	Lys16
Initial Orientation			PO_3^-	CO_2^-		
Final Orientation			PO_3^-	CO_2^-		
E_{tot}	-327.32 kcal/mol					
E_{ele}	-284.97 kcal/mol					
E_{elecpb}	-69.12 kcal/mol					
ΔE_{tot}	-1.49 kcal/mol					
ΔE_{ele}	-1.78 kcal/mol					
ΔE_{elecpb}	-14.02 kcal/mol					

C)

Amino Acid	Glu11	Val12	His13	His14	Gln15	Lys16	Leu17
Initial Orientation			PO_3^-			CO_2^-	
Final Orientation			PO_3^-			CO_2^-	CO_2^-

E_{tot}	-346.16 kcal/mol
E_{ele}	-295.17 kcal/mol
E_{elecpb}	-77.42 kcal/mol
ΔE_{tot}	-20.33 kcal/mol
ΔE_{ele}	-11.99 kcal/mol
ΔE_{elecpb}	-22.32 kcal/mol

D)

Amino Acid	Glu11	Val12	His13	His14	Gln15	Lys16
Initial Orientation	NH_3^+			CO_2^-		
Final Orientation	NH_3^+			CO_2^-	CO_2^-	

E_{tot}	-1219.67 kcal/mol
E_{ele}	-1268.40 kcal/mol
E_{elecpb}	-440.86 kcal/mol
ΔE_{tot}	-893.84 kcal/mol
ΔE_{ele}	-985.21 kcal/mol
ΔE_{elecpb}	-385.76 kcal/mol

Three of the four systems examined retained at least one of the initial hydrogen bonding interactions, while two systems also demonstrated electrostatic binding interactions. In some cases the groups were close enough to each other for potential binding interactions to have occurred, even if they were not recognized as such by the molecular modelling programs. Figure 2.12 shows one of the resulting binding interactions from the solution phase calculations (orientation C) with the water molecules

removed for clarity's sake – hydrogen bonds are represent by turquoise lines, while electrostatic interactions are represented by purple lines.

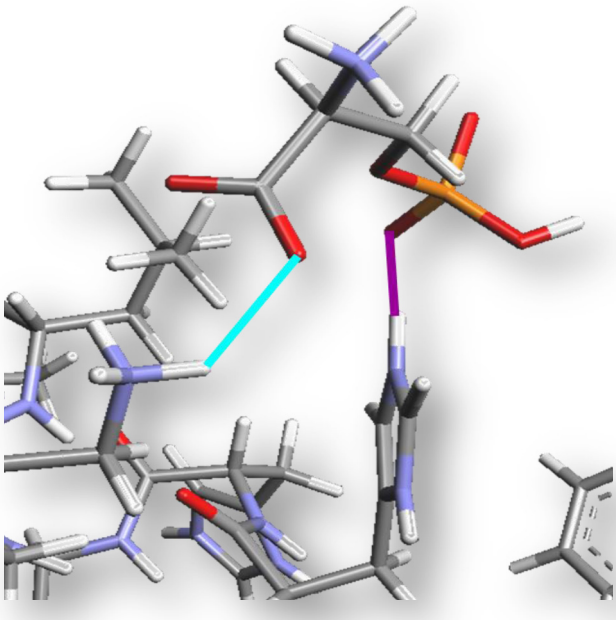

Figure 2.12: The binding interactions occurring between phosphoserine and the 1AMB conformer of β-amyloid upon minimization in an aqueous environment. The hydrogen bond is in turquoise, while the electrostatic interaction is in purple.

There is significant variation in binding energies of the systems which is likely due at least in part to the initial set-up of the system: the positioning of the water boxes was not identical and therefore resulted in varying amounts of overlapping water molecules that needed to be removed in order for calculations to proceed. Given that the numbers hold no true value to real life situations, they were only being used for comparative purposes to determine the favourability of interacting phosphoserine-Aβ systems. The only general conclusion that could be made for all four systems is that the binding interactions were favourable given the low ΔE_{elecpb} energies.

2.6.3.2 Results of the Solution Phase Interaction Between Phosphoserine and the 1AMC Conformer of β-Amyloid

The solution phase results of phosphoserine and the 1AMC conformer of Aβ showed fewer bonding interactions occurred than seen in the gas phase. Table 2.16 summarizes these results and it was seen that only two of the four selected systems retained hydrogen bonding interactions upon optimization in a solvated environment.

Table 2.16: The solution phase results of phosphoserine interacting with the 1AMC conformer of β-amyloid

A)

Amino Acid	Glu11	Val12	His13	His14	Gln15	Lys16
Initial Orientation	NH_3^+			CO_2^-		
Final Orientation	NH_3^+			CO_2^-		

E_{tot}	-326.54 kcal/mol
E_{ele}	-289.86 kcal/mol
E_{elecpb}	-75.52 kcal/mol
ΔE_{tot}	-0.69 kcal/mol
ΔE_{ele}	3.38 kcal/mol
ΔE_{elecpb}	-8.55 kcal/mol

B)

Amino Acid	Tyr10	Glu11	Val12	His13	His14	Gln15	Lys16	Leu17	Val18
Initial Orientation	NH_3^+			CO_2^-					
Final Orientation				CO_2^-	PO_3^-			CO_2^-/NH_3^+	CO_2^-

E_{tot}	-318.06 kcal/mol
E_{ele}	-297.70 kcal/mol
E_{elecpb}	-82.61 kcal/mol
ΔE_{tot}	7.78 kcal/mol
ΔE_{ele}	-4.46 kcal/mol
ΔE_{elecpb}	-15.64 kcal/mol

C)

Amino Acid	Glu11	Val12	His13	His14	Gln15	Lys16
Initial Orientation			CO_2^-			PO_3^-
Final Orientation			CO_2^-			PO_3^-

E_{tot}	-330.66 kcal/mol
E_{ele}	-290.69 kcal/mol
E_{elecpb}	-78.22 kcal/mol
ΔE_{tot}	-4.82 kcal/mol
ΔE_{ele}	2.55 kcal/mol
ΔE_{elecpb}	-11.25 kcal/mol

D)

Amino Acid	Glu11	Val12	His13	His14	Gln15	Lys16	Leu17
Initial Orientation			CO_2^-			PO_3^-	
Final Orientation			CO_2^-			PO_3^-	PO_3^-

E_{tot}	-325.77 kcal/mol
E_{ele}	-287.44 kcal/mol
E_{elecpb}	-72.66 kcal/mol
ΔE_{tot}	0.08 kcal/mol
ΔE_{ele}	5.80 kcal/mol
ΔE_{elecpb}	-5.69 kcal/mol

For the most part, the interactions retained the same orientation of phosphoserine functional groups towards the amino acid side chains they were bonded to in the gas phase. Interestingly, those systems where hydrogen bonding still occurred upon minimization in aqueous solution were higher in energy than those that did not result in bonding interactions. It is possible then that there may indeed have been some electrostatic-type interactions occurring in the EV**HH**Q**K** region of interest for these lower energy systems, or it may have been that the side chains in these particular systems

had engaged in more electrostatic interactions than in those systems where hydrogen bonding occurred.

2.6.3.3 Results of the Solution Phase Interaction Between Phosphoserine and the 1AML Conformer of β-Amyloid

All four solution phase calculations involving phosphoserine and the 1AML conformer of β-amyloid resulted in at least one bonding interaction forming between the two. The results of these interactions are summarized in Table 2.17. The cell in green indicates where a hydrogen bond had formed as well as an electrostatic interaction occurring between the functional groups on phosphoserine and the backbone atoms of the amino acid residue. Peach coloured cells indicate hydrogen bonds. The pink cell represents an electrostatic interaction between the phosphoserine functional groups and atoms forming the peptide backbone.

Table 2.17: The solution phase results of phosphoserine interacting with the 1AML conformer of β-amyloid

A) Amino Acid	Glu11	Val12	His13	His14	Gln15	Lys16
Initial Orientation	NH_3^+					PO_3^-
Final Orientation	NH_3^+					PO_3^-
	PO_3^-					

E_{tot}	-382.18 kcal/mol
E_{ele}	-356.36 kcal/mol
E_{elecpb}	-64.98 kcal/mol
ΔE_{tot}	34.04 kcal/mol
ΔE_{ele}	2.58 kcal/mol
ΔE_{elecpb}	-10.08 kcal/mol

B)

Amino Acid	Ser8	Tyr10	Glu11	Val12	His13	His14	Gln15	Lys16
Initial Orientation	CO_2^-					PO_3^-	PO_3^-	
Final Orientation	PO_3^-	CO_2^-				PO_3^-	PO_3^-	
						CO_2^-		

E_{tot}	-398.17	kcal/mol
E_{ele}	-360.25	kcal/mol
E_{elecpb}	-72.18	kcal/mol
ΔE_{tot}	18.05	kcal/mol
ΔE_{ele}	-1.31	kcal/mol
ΔE_{elecpb}	-17.28	kcal/mol

C)

Amino Acid	Tyr10	Glu11	Val12	His13	His14	Gln15	Lys16	Ile31
Initial Orientation	PO_3^-			PO_3^-				
Final Orientation				PO_3^-				CO_2^-

E_{tot}	-426.12	kcal/mol
E_{ele}	-360.03	kcal/mol
E_{elecpb}	-63.23	kcal/mol
ΔE_{tot}	-9.89	kcal/mol
ΔE_{ele}	-1.10	kcal/mol
ΔE_{elecpb}	-8.33	kcal/mol

D) Amino Acid	Glu11	Val12	His13	His14	Gln15	Lys16
Initial Orientation	NH_3^+					CO_2^-
Final Orientation	NH_3^+	PO_3^-				CO_2^-
						PO_3^-
E_{tot}	-413.13 kcal/mol					
E_{ele}	-357.45 kcal/mol					
E_{elecpb}	-62.14 kcal/mol					
ΔE_{tot}	3.09 kcal/mol					
ΔE_{ele}	1.49 kcal/mol					
ΔE_{elecpb}	-7.24 kcal/mol					

All of the solution phase results for phosphoserine interacting with the 1AML conformer of Aβ resulted in the formation of at least one calculable binding interaction. All except one of the systems (orientation C) had functional groups close enough to the other amino acid side chains in the EV**HH**Q**K** region of interest that electrostatic interactions might be possible. All of the final binding interactions exhibited similar, slightly favourable energies as well, indicating that the orientation of phosphoserine towards β-amyloid may have favourable results.

2.6.3.4 Results of the Solution Phase Interaction Between Phosphoserine and the 1BA4 Conformer of β-Amyloid

Three of the four solvated interactions of phosphoserine interacting with the 1BA4 conformer of β-amyloid resulted in calculable binding interactions, the results of which are summarized in Table 2.18. Hydrogen bonds are represented by peach coloured cells, and electrostatic interactions that occurred between the phosphoserine functional groups and the backbone atoms of the amino acids are given in pink.

Table 2.18: The solution phase results of phosphoserine interacting with the 1BA4 conformer of β-amyloid

A)

Amino Acid	Asp1	Glu3	Glu11	Val12	His13	His14	Gln15	Lys16
Initial Orientation	NH_3^+	NH_3^+						CO_2^-
Final Orientation	NH_3^+	NH_3^+	CO_2^-					CO_2^-/NH_3^+

E_{tot}	-419.52 kcal/mol
E_{ele}	-372.65 kcal/mol
E_{elecpb}	-63.59 kcal/mol
ΔE_{tot}	11.88 kcal/mol
ΔE_{ele}	9.94 kcal/mol
ΔE_{elecpb}	-6.26 kcal/mol

B)

Amino Acid	Asp1	Glu11	Val12	His13	His14	Gln15	Lys16	Phe19	Asp23
Initial Orientation	CO_2^-/NH_3^+						CO_2^-		NH_3^+
Final Orientation	CO_2^-/NH_3^+	PO_3^-					CO_2^-/PO_3^-	PO_3^-	NH_3^+
	CO_2^-								

E_{tot}	-448.74 kcal/mol
E_{ele}	-376.84 kcal/mol
E_{elecpb}	-70.85 kcal/mol
ΔE_{tot}	-17.34 kcal/mol
ΔE_{ele}	5.74 kcal/mol
ΔE_{elecpb}	-13.52 kcal/mol

C)

Amino Acid	Asp1	Glu11	Val12	His13	His14	Gln15	Lys16	Phe19	Glu22
Initial Orientation	PO_3^-						PO_3^-		
Final Orientation	PO_3^-	PO_3^-					PO_3^-	CO_2^-	CO_2^-

E_{tot}	-417.99 kcal/mol
E_{ele}	-372.88 kcal/mol
E_{elecpb}	-68.85 kcal/mol
ΔE_{tot}	13.42 kcal/mol
ΔE_{ele}	9.71 kcal/mol
ΔE_{elecpb}	-11.52 kcal/mol

D)

Amino Acid	Glu11	Val12	His13	His14	Gln15	Lys16
Initial Orientation			CO_2^-	PO_3^-		
Final Orientation			CO_2^-	PO_3^-		

E_{tot}	-417.94 kcal/mol
E_{ele}	-374.37 kcal/mol
E_{elecpb}	-70.41 kcal/mol
ΔE_{tot}	13.46 kcal/mol
ΔE_{ele}	8.22 kcal/mol
ΔE_{elecpb}	-13.08 kcal/mol

The highest energy interaction had no computable hydrogen bonds or electrostatic interactions, although it is very possible that there were some electrostatic interactions occurring between phosphoserine and β-amyloid. The remaining interactions formed hydrogen bonds, as well as possible electrostatic interactions in two cases, and all had similar, somewhat favourable energies, indicating potential binding orientations that may exist in the brain.

2.6.3.5 Results of the Solution Phase Interaction Between Phosphoserine and the 1IYT Conformer of β-Amyloid

The solution phase results of phosphoserine interacting with the 1IYT conformer of β-amyloid revealed that only two of the systems formed bonding interactions. Table 2.19 summarizes the final binding orientations and energies of interaction. Electrostatic interactions are represented by blue coloured cells, and hydrogen bonds by peach coloured cells.

Table 2.19: The solution phase results of phosphoserine interacting with the 1IYT conformer of β-amyloid

A) Amino Acid	Glu11	Val12	His13	His14	Gln15	Lys16
Initial Orientation			CO_2^-			PO_3^-
Final Orientation			CO_2^-			PO_3^-
E_{tot}	-578.21 kcal/mol					
E_{ele}	-543.54 kcal/mol					
E_{elecpb}	-220.07 kcal/mol					
ΔE_{tot}	-53.64 kcal/mol					
ΔE_{ele}	-126.20 kcal/mol					
ΔE_{elecpb}	-146.50 kcal/mol					

B)

Amino Acid	Glu11	Val12	His13	His14	Gln15	Lys16
Initial Orientation			CO_2^-			PO_3^-
Final Orientation			CO_2^-			PO_3^-

E_{tot}	-611.38 kcal/mol
E_{ele}	-571.99 kcal/mol
E_{elecpb}	-245.84 kcal/mol
ΔE_{tot}	-86.81 kcal/mol
ΔE_{ele}	-154.64 kcal/mol
ΔE_{elecpb}	-172.27 kcal/mol

C)

Amino Acid	Glu11	Val12	His13	His14	Gln15	Lys16
Initial Orientation			PO_3^-			CO_2^-
Final Orientation			PO_3^-			CO_2^-

E_{tot}	-573.06 kcal/mol
E_{ele}	-537.38 kcal/mol
E_{elecpb}	-212.69 kcal/mol
ΔE_{tot}	-47.49 kcal/mol
ΔE_{ele}	-120.03 kcal/mol
ΔE_{elecpb}	-139.85 kcal/mol

D) Amino Acid	Glu11	Val12	His13	His14	Gln15	Lys16	Leu17
Initial Orientation			CO_2^-	PO_3^-			
Final Orientation			CO_2^-	PO_3^-			CO_2^-

E_{tot}	-595.40 kcal/mol
E_{ele}	-548.57 kcal/mol
E_{elecpb}	-219.92 kcal/mol
ΔE_{tot}	-70.83 kcal/mol
ΔE_{ele}	-131.23 kcal/mol
ΔE_{elecpb}	-146.34 kcal/mol

Those systems that resulted in binding interactions had lower, more favourable energies than those that did not. The favourable binding interactions also occurred within the EV**HH**Q**K** region of interest, and those that did not still had relatively favourable energies, as well as being oriented towards side chains in the same focused region of Aβ.

2.6.3.6 Results of the Solution Phase Interaction Between Phosphoserine and the 2BP4 Conformer of β-Amyloid

All four systems of phosphoserine and the 2BP4 conformer of Aβ optimized in an aqueous environment resulted in binding interactions. Hydrogen bonds are denoted by a peach colour, electrostatic interactions between phosphoserine and the amino acid side chains in blue, and electrostatic interactions between phosphoserine and the peptide backbone in pink. A cation-π interaction that formed is in periwinkle. The final orientations and energies are given in Table 2.20, note that orientation C also involved the formation of a hydrogen bond within the phosphoserine molecule.

Table 2.20: The solution phase results of phosphoserine interacting with the 2BP4 conformer of β-amyloid

A)

Amino Acid	Glu11	Val12	His13	His14	Gln15	Lys16
Initial Orientation			CO_2^-			PO_3^-
Final Orientation			PO_3^- CO_2^-	CO_2^-		PO_3^-

E_{tot}	-400.63 kcal/mol
E_{ele}	-377.85 kcal/mol
E_{elecpb}	-274.23 kcal/mol
ΔE_{tot}	-212.23 kcal/mol
ΔE_{ele}	-211.39 kcal/mol
ΔE_{elecpb}	-223.77 kcal/mol

B)

Amino Acid	Glu11	Val12	His13	His14	Gln15	Lys16
Initial Orientation			PO_3^-			PO_3^-
Final Orientation			PO_3^- CO_2^-	CO_2^-		PO_3^-

E_{tot}	-381.92 kcal/mol
E_{ele}	-357.66 kcal/mol
E_{elecpb}	-254.75 kcal/mol
ΔE_{tot}	-193.51 kcal/mol
ΔE_{ele}	-191.20 kcal/mol
ΔE_{elecpb}	-204.29 kcal/mol

C)

Amino Acid	Glu11	Val12	His13	His14	Gln15	Lys16
Initial Orientation			PO_3^-	PO_3^-		CO_2^-
Final Orientation			PO_3^-	PO_3^- NH_3^+		CO_2^-

E_{tot}	-405.36 kcal/mol
E_{ele}	-381.41 kcal/mol
E_{elecpb}	-277.56 kcal/mol
ΔE_{tot}	-216.95 kcal/mol
ΔE_{ele}	-214.95 kcal/mol
ΔE_{elecpb}	-227.10 kcal/mol

D)

Amino Acid	Glu11	Val12	His13	His14	Gln15	Lys16
Initial Orientation			PO_3^-			CO_2^-
Final Orientation			CO_2^-/PO_3^-	PO_3^-		CO_2^-

E_{tot}	-405.40 kcal/mol
E_{ele}	-388.24 kcal/mol
E_{elecpb}	-283.13 kcal/mol
ΔE_{tot}	-217.00 kcal/mol
ΔE_{ele}	-221.78 kcal/mol
ΔE_{elecpb}	-232.67 kcal/mol

All four interactions appeared to be favourable in terms of low energy as well as functional group orientation. Every one of the four interacting systems formed hydrogen bonds. There did not appear to be a significant correlation between the binding energies and the types of measureable binding interactions that formed; however, it was unknown what the other unmeasured interactions would also be contributing to these energies.

2.7 Biological Support of Phosphoserine Interacting with β-Amyloid

The computational findings were supported through experimental means using thioflavin T (ThT), circular dichroism (CD) and transmission electron microscopy (TEM) *in vitro* assays (performed by Todd Galloway). The effect of phosphoserine in preventing both β-amyloid aggregation and β-amyloid conformational change (α-helix to β-sheet) was examined via these methods. The methods for these assays are given in Appendix 5.

First, the ThT assay showed that phosphoserine was able to reduce the aggregation of β-amyloid from monomers to oligomers (dimers, trimers … dodecamers) by more than 60% in a dose dependent fashion at concentrations of 0.01-5 mM (See Figure 2.13A). At the same dose range, CD studies showed that phosphoserine was able to inhibit the α-helix to β-sheet conformational change over a time period of 140 hrs. The ThT and CD studies were done with Aβ40. The TEM studies used Aβ42, which is more prone to aggregation than the Aβ40 variant [8, 10, 15]. Images were taken using freshly prepared Aβ42 in the presence of DMSO, the control sample, and in the presence of 1 mM phosphoserine. The TEM images in Figure 2.13B show the effects of the presence of phosphoserine on the aggregation of β-amyloid, after a twenty-four hour incubation period compared to the control sample. It is dramatically apparent from these images that phosphoserine inhibited the aggregation of β-amyloid when compared to the control sample, which shows marked clumping of the peptide.

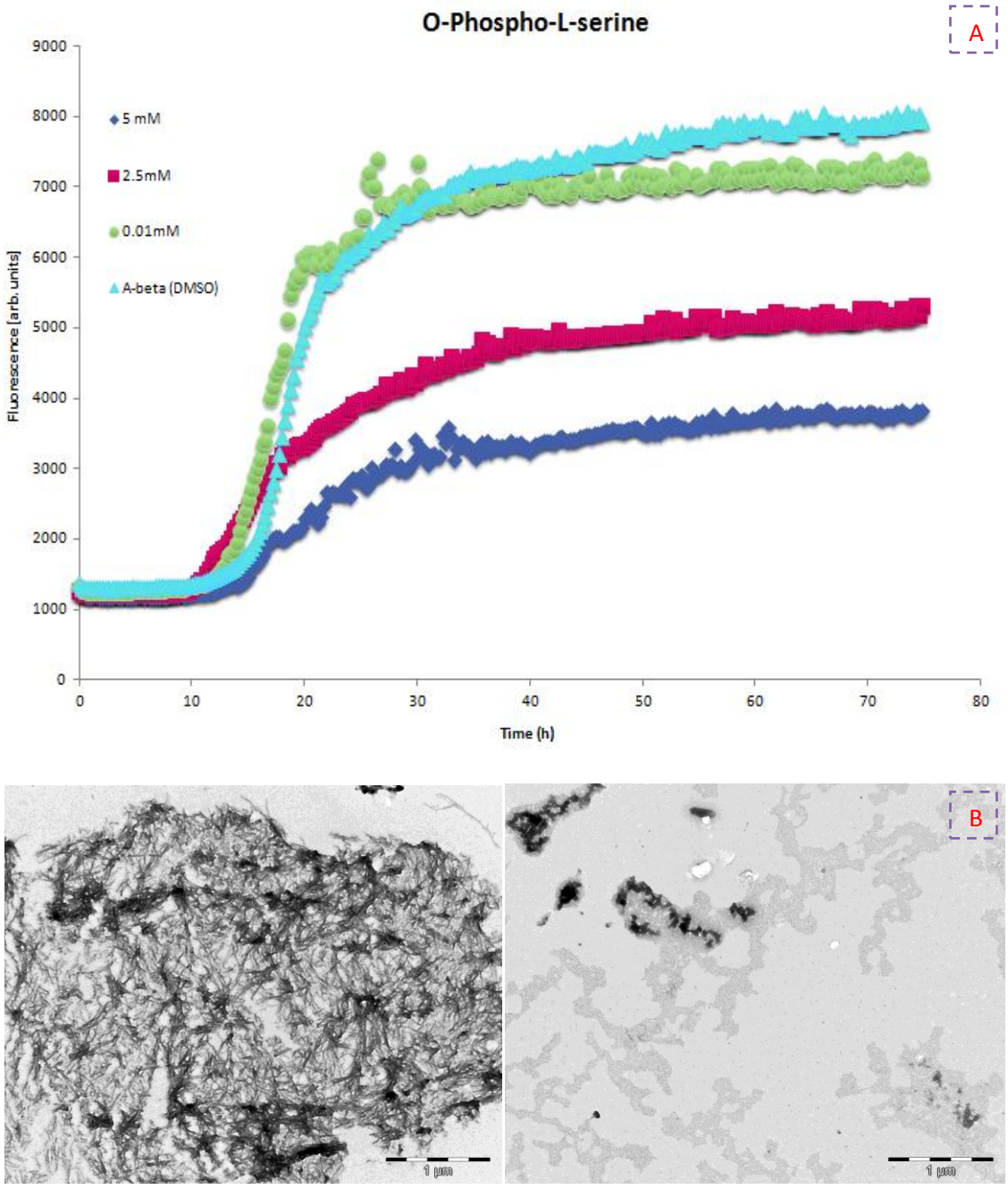

Figure 2.13: (A) ThT assay of phosphoserine at different concentrations; (B) Transmission electron microscopy images of Aβ42 incubated with DMSO (left) and 1 mM phosphoserine (right) for a twenty-four hour period.

2.8 PHOSPHOSERINE INTERACTING WITH BBXB

Additional selected gas phase optimizations were performed looking at whether phosphoserine demonstrates the capacity to bind to **BB**X**B** regions other than the **HH**Q**K** region of β-amyloid. Research by Meier-Stephenson *et al* has suggested that this **BB**X**B** motif is present on a variety of proteins affiliated with Alzheimer's disease; a "promiscuous drug" could be identified to bind to this common motif for a multifaceted approach to treating AD [41].

To this effect, six proteins identified as playing a role in Alzheimer's disease and having the **BB**X**B** motif were selected for optimization with phosphoserine: Interleukin-4, Interleukin-12, Interleukin-13, S100β, RANTES, and ICAM-1[75, 76, 77, 78, 79, 80].

2.8.1 SET-UP OF BBXB OPTIMIZATIONS

Each of the six proteins was optimized in the gas phase for physiological pH conditions. Structures of each of the proteins were first obtained from the RCSB protein data bank and are identified as follows: Interleukin-4 – 2B8U, Interleukin-12 – 1F45, Interleukin-13 – 3BPO, S100β – 1UW0, RANTES – 1HRJ, and ICAM-1 – 1IAM [67, 75-80]. Each protein then underwent specific preparations to be in the correct state for optimization in the QUANTA environment [46].

2.8.1.1 INTERLEUKIN-4

Interleukin-4 (IL-4) is a pleiotropic cytokine that plays a key signalling role in the immune system as well as provoking allergic response that can lead to hypersensitivity [75]. This protein plays a role in immune response and expresses the **BB**X**B** motif in two

places: as histidine-histidine-glutamic acid-lysine and as histidine-arginine-histidine-lysine [41].

The protein structure of interleukin-4 was downloaded from the RSCB website and first edited in MOE [51]. Hydrogen atoms were added to the structure, and extraneous molecules and any solvent atoms present were deleted from the system. The histidine residues present in the protein were protonated and the file format of the structure was then converted and imported into QUANTA [46]. Atoms were retyped as necessary and the system was then optimized via steepest descents with a constrained protein backbone. The optimized structure was then saved for use in further calculations.

2.8.1.2 INTERLEUKIN-12

Interleukin-12 (IL-12) is another cytokine with an immunomodulatory role [76]. This protein is involved in enhancing the cytotoxic activity of natural killer and cytotoxic T-cells, as well as inducing the production of interferon-γ (IFN-γ), another inflammatory protein [76]. The **BB**X**B** motif found in the interleukin-12 amino acid sequence is histidine-lysine-leucine-lysine [41].

The same procedure as in section 2.6.1.1 was followed for the interleukin-12 protein with two exceptions. Before optimization of the system could occur, there were some carboxylate groups that were incorrectly represented as aldehydes, and thus needed to be corrected, and some of the asparagine side chains were missing a proton. Once these adjustments were made, the protein backbone was constrained and then the minimization calculation was run.

2.8.1.3 INTERLEUKIN-13

Interleukin-13 (IL-13) is an inflammatory cytokine with a similar function to IL-4, and presents a **BB**X**B** motif of histidine-leucine-lysine-lysine [41, 77].

The structure of interleukin-13 was downloaded from the protein data bank into MOE, where hydrogen atoms were added, solvent molecules and other unrelated species were deleted, and the histidine residues were protonated [51]. The PDB structure contained more than just the interleukin-13 chain, so the unnecessary chains were deleted from the system, whereupon the file format was converted and then imported into QUANTA [5]. Optimization then proceeded upon atom retyping and the constraint of the protein backbone.

2.8.1.4 S100β

S100β is a calcium binding protein that is found primarily in the cytoplasm of glial cells and plays a role in regulating cellular architecture [78]. Microglia cells are known to cluster at the sites of amyloid deposits in the AD brain, and an increased expression of S100β is seen in these areas [71, 74]. It is postulated that S100β may therefore play a role in the neuropathology of Alzheimer's disease, and it expresses the common **BB**X**B** motif in the form of histidine-lysine-leucine-lysine, and lysine-leucine-lysine-lysine [41].

The structure of S100β was imported directly into QUANTA, whereupon the histidine residues were protonated and some binding situations that were highly unlikely were deleted [46]. The protein backbone was constrained and minimization of the system occurred via steepest descents.

2.8.1.5 RANTES

RANTES (regulated on activation, normal T-cell expressed and secreted) is a member of the interleukin superfamily of proteins, and is an inflammatory cytokine [79]. In its role it can activate leukocytes and incite their accumulation [79]. It appears that in its natural form, RANTES exists as a dimer; this presents two identical **BB**X**B** receptors as targets for interaction in the form of arginine-lysine-asparagine-arginine [41].

The RANTES protein was imported into MOE where the two histidine residues present were protonated, and the file format was then converted for QUANTA [46, 51]. The backbone was constrained the system was optimized using the steepest descents algorithm.

2.8.1.6 ICAM-1

ICAM-1, or intracellular adhesion molecule-1, is a protein that can play two roles in the human body; it can help provide adhesion between white blood cells and endothelial cells to allow the passage of white blood cells to the site of injury or stress, or it can act as a receptor for human rhinovirus [22, 80]. ICAM-1 could therefore play a detrimental role in AD in that it allows for increased inflammation, which can cause further damage to the neurons. The **BB**X**B** motif presents itself twice in ICAM-1 as arginine-arginine-aspartic acid-histidine and as arginine-aspartic acid-histidine-histidine [41].

The protein structure required minimal adjustments with only histidine residues being protonated before the structure was converted to an appropriate format and imported into QUANTA [46]. It was discovered that some of the asparagine residues

were missing hydrogen atoms, so these corrections were made before the system was optimized via steepest descents with a constrained protein backbone.

2.8.1.7 Optimization Methods

Gas phase optimizations were performed to see if potential interactions could occur between phosphoserine and other proteins involved in AD bearing the common **BB**X**B** motif. These optimizations were performed in the gas phase in the QUANTA program using the CHARMM22 force field [46].

For each simulation, the phosphoserine molecule was set at a distance of 3.0 Å away from the **BB**X**B** region on the protein such that two of the charged functional groups were oriented towards two of the charged amino acid side chains. The protein backbone was constrained and the system was optimized using the steepest descents algorithm. The final optimized systems were imported into MOE to determine what interactions could occur between the phosphoserine molecule and the proteins [51]. The total energy of the system was calculated using the following equation:

$$E_{tot} = E_{A\beta prot} - E_{prot} - E_{phos} \tag{2.5}$$

$E_{A\beta prot}$ represents the total energy of the optimized phosphoserine-protein system, E_{prot} the energy of the protein optimized by itself, and E_{phos} the energy of the optimized phosphoserine molecule. Similarly, the van der Waals energy was calculated using the following equation:

$$E_{VdW} = E_{A\beta protVdW} - E_{protVdW} - E_{phosVdW} \tag{2.6}$$

The overall van der Waals energy of the system, E_{VdW}, is calculated by subtracting the individual van der Waals energies from the protein, $E_{protVdW}$, and phosphoserine,

$E_{phosVdW}$, from the van der Waals energy of the optimized phosphoserine-protein system, $E_{A\beta protVdW}$. The electrostatic energy of the binding interactions occurring between phosphoserine and the protein was calculated using equation 2.7.

$$E_{Ele} = E_{A\beta protEle} - E_{protEle} - E_{phosEle} \quad (2.7)$$

The calculated electrostatic energies of the individual protein, $E_{protEle}$, and phosphoserine, $E_{phosEle}$, were subtracted from the electrostatic energy of the optimized system, $E_{A\beta protEle}$, to determine the electrostatic energy of interaction.

2.8.2 Results of the Optimization of Phosphoserine with Selected Proteins Containing BBXB

The results of these optimizations are summarized in Table 2.21. Hydrogen bonds that formed between phosphoserine and the protein are indicated by the orange coloured cells; the darker the colour, the more hydrogen bonding interactions that are occurring.

Table 2.21: Gas phase optimization of phosphoserine interacting with the BBXB motif on various proteins implicated in Alzheimer's disease

Protein	Initial Orientation				Final Orientation						Binding Energy (kcal/mol)		
	R149	R150	D151	H152	R125	L147	**R149**	**R150**	**D151**	**H152**	Total	VdW	Ele
ICAM-1	CO_2^-	PO_3^-					CO_2^-		CO_2^-		-103.69	4.40	-84.81
	CO_2^-			PO_3^-		PO_3^-	CO_2^-			PO_3^-	-103.76	-4.33	-72.99
							PO_3^-						
	PO_3^-			CO_2^-	CO_2^-					CO_2^-	-117.79	1.20	-98.39
	R150	D151	H152	H153	R150	D151	H152	H153					
	CO_2^-			PO_3^-	CO_2^-			PO_3^-			-113.88	3.97	-95.80
IL-4	H58	H59	E60	K61	S57	**H58**	**H59**	**E60**	**K61**				
	CO_2^-	PO_3^-				CO_2^-					-103.87	5.22	-86.86
	PO_3^-	CO_2^-				PO_3^-/CO_2	CO_2^-				-106.32	2.50	-86.59
	PO_3^-	NH_3^+				PO_3^-					-118.33	4.58	-99.18
	NH_3^+	PO_3^-					PO_3^-				-137.13	3.10	-116.26
	CO_2^-			PO_3^-	-	-	-	-	-		-104.92	8.11	-88.43
	PO_3^-			CO_2^-	PO_3^-				CO_2^-		-116.36	4.14	-98.68
	NH_3^+			PO_3^-	NH_3^+	CO_2^-					-123.79	2.54	-101.70
					CO_2^-								
	H74	R75	H76	K77	Q71	**H74**	**R75**	**H76**	**K77**	Q78			
	CO_2^-			PO_3^-		CO_2^-			PO_3^-		-116.28	6.49	-101.56
	PO_3^-			CO_2^-		PO_3^-					-102.88	5.69	-87.38
	NH_3^+			PO_3^-	NH_3^+/CO_2^-						-112.67	5.63	-98.14
	CO_2^-	PO_3^-				CO_2^-				CO_2^-	-117.69	3.21	-99.76
	PO_3^-	CO_2^-			CO_2^-		CO_2^-				-12.49	4.99	-105.74
	NH_3^+	PO_3^-								CO_2^-	-128.46	6.18	-111.69
IL-12	H194	K195	K196	K197	K84	**H194**	**K195**	**L196**	**K197**				
	PO_3^-	CO_2^-			-	-	-	-	-		-127.56	5.92	-110.39
	CO_2^-	PO_3^-				CO_2^-	PO_3^-				-128.89	1.95	-110.86
	NH_3^+	PO_3^-					PO_3^-				-132.38	2.63	-111.75
	CO_2^-			PO_3^-		PO_3^-			PO_3^-		-139.92	5.83	-119.72
	PO_3^-			CO_2^-					CO_2^-		-114.73	3.73	-95.54
	NH_3^+			PO_3^-	PO_3^-				PO_3^-		-152.71	5.35	-134.38
		CO_2^-		PO_3^-		PO_3^-			PO_3^-		-127.84	3.31	-106.43
		PO_3^-		CO_2^-					CO_2^-		-119.50	1.58	-96.72
IL-13	H102	L103	K104	K105	A21	**H102**	**L103**	**K104**	**K105**				
	PO_3^-			CO_2^-	PO_3^-						-100.84	7.75	-86.88
	CO_2^-			PO_3^-	CO_2^-				PO_3^-		-102.01	5.81	-86.00
	NH_3^+			PO_3^-					PO_3^-		-106.51	6.04	-93.18
RANTES	R44	K45	N46	R47	S1	**R44**	**K45**	**N46**	**R47**				
		CO_2^-		PO_3^-			CO_2^-				-228.19	3.03	-198.16
							PO_3^-						
		PO_3^-		CO_2^-	CO_2^-		PO_3^-		CO_2^-		-224.69	-3.95	-199.94
S100β	H25	K26	L27	K28	H25	K26	L27	K28					
	CO_2^-	PO_3^-			CO_2^-						-96.90	4.23	-77.08
	PO_3^-	CO_2^-				CO_2^-					-116.33	1.81	-94.44
	NH_3^+	PO_3^-				PO_3^-					-111.16	5.10	-90.39
	K26	L27	K28	K29	K26	L27	K28	K29					
			CO_2^-	PO_3^-	PO_3^-						-133.40	1.35	-107.59
			PO_3^-	CO_2^-			PO_3^-				-122.05	3.83	-98.47

Although only a sample of some of the proteins involved in Alzheimer's disease containing the **BB**X**B** motif were examined, the results indicate phosphoserine has the potential to bind to the **BB**X**B** motif on more proteins than just Aβ. A more detailed study would allow for trends to be determined; however, the results do indicate binding between phosphoserine and multiple sites within the **BB**X**B** region on five of the six proteins examined.

Energetically speaking, the interactions between phosphoserine and the proteins are favourable. Some of the interactions resulted in a more collapsed phosphoserine molecule where the phosphate and amino groups were interacting within itself. Despite these self interactions, the energies still appear to be more favourable than those between phosphoserine and β-amyloid.

These results indicate that phosphoserine is capable of binding not only to **HH**Q**K** as seen in earlier sections of this chapter, but to other **BB**X**B** motifs as well in a gas phase environment. This indicates that an endogenous molecule such as phosphoserine could bind to multiple proteins involved in the disease process of AD.

2.9 Conclusions

Overall results of the gas phase calculations showed that phosphoserine is capable of binding to β-amyloid in such a manner as to interact with two different amino acids in the Glu11-Val12-His13-His14-Gln15-Lys16 region. Sufficient interactions resulted from the gas phase minimizations for the four most energetically favourable systems, where binding occurred at two or more sites, to be selected and optimized in a solvated environment.

The solution phase calculations resulted in fewer bonding interactions forming between the charged amino acid side chains and the functional groups on phosphoserine, but this was not surprising given the presence of water molecules in the systems which could have altered the sterics of the interactions, as well as modifying conformations depending on the hydrophobicity or hydrophilicity of the amino acids.

Examination of the results of the solution phase calculations revealed that there are three main binding sites within the EV**HH**Q**K** region of β-amyloid: His13, His14 and Lys16. Sixteen of the twenty-four interactions had potential binding interactions with His13, in the form of hydrogen bonding, and possible electrostatic interactions. The carboxylate and phosphate functional groups on phosphoserine seemed to interact almost equally with the His13 residue. Potential binding interactions also occurred at the Lys16 residue in sixteen of the twenty-four possible cases. There were a significant number of hydrogen bonds that formed at this site (eleven) and there was also the potential for non-hydrogen bonding, electrostatic-type interactions to occur. Lys16 favoured binding interactions with the phosphate group slightly more than the carboxylate group of phosphoserine. Binding interactions at the His14 residue involved some hydrogen bonding, as well as possible electrostatic interactions, although they only occurred in eleven of the twenty-four minimized systems. There were an equal number of interactions occurring at the His14 side chain with the phosphate and carboxylate functional groups. Overall, it appeared that there was no significant difference between which of the negative functional groups was interacting with these three residues. The Glu11 amino acid residue was also involved in seven potential binding interactions, mainly occurring with the amino and phosphate groups of phosphoserine. The remaining phosphoserine-

Aβ interactions all involved amino acids outside of the four charged amino acids of interest in the EV**HH**Q**K** region of the peptide.

Closer examination of the results showed that nearly half of the solvated systems had potential binding interactions occurring at both the His13 and Lys16 residues. These interactions favoured carboxylate interactions occurring at the His13 residue and phosphate interactions occurring at the Lys16 residue in a two-to-one ratio over the opposite orientation. Four of these eleven interactions also had the capacity to bind to or interact with the His14 residue. There were another four cases where His13 and His14 were both involved in binding interactions not including Lys16. These interactions involving both histidine and lysine residues appeared to be the most favoured binding interactions, where binding occurs at two or more sites on the peptide, particularly in the EV**HH**Q**K** region.

2.10 INTERPRETATION

It could be suggested based on these observed results, that phosphoserine not only will bind to and interact with β-amyloid *in vacuo*, but also in a solvated environment (such as would exist in the brain). The His13-Lys16 binding interactions are particularly favourable, since it is possible that in binding to these two amino acid side chains, phosphoserine would prevent them from interacting with other proteins or lipid bilayers and thus prevent conformational conversions. Prevention of conversion from α-helical and random coil to β-sheet conformations should prevent the toxic form of β-amyloid from forming so that no soluble aggregates will be available to inflict neurodegeneration and neurotoxicity.

Biological evidence further supports the computational findings that phosphoserine can interact with β-amyloid to prevent aggregation from occurring. It can be seen from the *in vitro* assays that phosphoserine clearly inhibits the aggregation of Aβ, which would indicate a potential neuroprotective role.

Furthermore, there is computational evidence that phosphoserine could also interact with other proteins involved in the AD process. Phosphoserine therefore represents an endogenous molecule of the brain that may play a multi-faceted role in the prevention of Alzheimer's disease. These results also support the idea that a single drug molecule could target multiple receptors involved in a disease in a way that would allow for better success at treating the disease rather than targeting a single receptor alone.

Phosphoserine represents a viable endogenous molecule of the brain that can be exploited in designing a drug to prevent β-amyloid conformational conversions. Given the lowered concentrations in the Alzheimer's brain according to Molina *et al*, and its potential role as the brain's response to amyloid aggregation due to high local concentrations in regions free from plaques, phosphoserine may play a protective role in the brain. It may therefore be possible to develop a drug molecule targeting the enzymatic pathways involved in the synthesis and metabolism of phosphoserine that will increase the levels of phosphoserine in order to prevent β-amyloid aggregation.

If levels of phosphoserine are instead elevated in the brain as Klunk *et al* have observed, then drugs that target the catabolism of phosphoserine may be of use to maintain these higher levels. Alternatively, if levels were to remain sufficiently high as part of the brain's natural response to Aβ aggregation, serine racemase could be targeted

to prevent increased levels of D-serine from forming (as a result of the increased levels of phosphoserine).

Looking at the favourable solution phase results, supported by the biological data, it is therefore likely that increased phosphoserine levels in the brain will allow more phosphoserine to interact with and bind to the stable, non-toxic forms of Aβ and prevent it from taking on neurotoxic properties, and potentially other proteins involved in the disease as well. Phosphoserine therefore presents itself as a possible drug molecule for at least delaying the onset of Alzheimer's disease or at best preventing the disease from commencing.

CHAPTER 3: THE SEARCH FOR AN ENDOGENOUS ANTI-ALZHEIMER'S DRUG TARGETING HHQK

The previous chapter dealt with the potential interactions between a small endogenous molecule of the brain and the HHQK region of β-amyloid. Additional endogenous molecules of the brain were also identified as potential targets for this region.

3.1 THE HHQK AND LVFF REGIONS OF β-AMYLOID AS BINDING TARGETS

Two regions of β-amyloid play an important role in the misfolding of the protein; the region containing residues His13-His14-Gln15-Lys16 (**HH**Q**K**) and the region containing residues Leu17-Val18-Phe19-Phe20 (LVFF).

The highly positively charged region of **HH**Q**K** is postulated to be a key component in the interactions that lead to the misfolding of Aβ and also fits the **BB**X**B** motif identified as being present in various proteins involved in Alzheimer's disease [41]. Molecules that contain negatively charged functional groups or aromatic rings should be able to interact with this charged region through various binding interactions to block unwanted interactions with membrane surfaces from occurring.

Situated immediately next to the **HH**Q**K** region of Aβ is the LVFF region, which also has been identified as another potential region for small molecules to bind to in order to prevent protein misfolding [82]. This represents more of an **AA**X**A** motif, where A is an aliphatic or aromatic amino acid and X is any other amino acid residue. Systems can be visually examined to determine if aliphatic interactions with these side chains may be

occurring, and aromatic-aromatic interactions are capable of being identified within the MOE program [47]. In this chapter, some of the small molecules be examined will also be analyzed for their potential to bind to both the **HH**Q**K** and LVFF regions of β-amyloid.

3.2 Identification of Amino Acids and Their Metabolites as Target Molecules

As stated in Chapter 2, Section 2.2, a library of endogenous compounds of the brain was searched for potential drug targets capable of interacting with the **BB**X**B** motif. Several small molecules were identified in this process including the amino acids tryptophan, phenylalanine and their metabolites. These molecules were examined through *in silico* methods for their potential to bind to both the **HH**Q**K** and LVFF regions of β-amyloid.

3.3 Phenylalanine and β-Amyloid

The library of endogenous molecules of the brain, when screened against the identified **BB**X**B** motif, identified phenylalanine (Figure 3.1) as one of the endogenous molecules which possessed the necessary features to interact with this region. The structure of phenylalanine also presents regions capable of interacting with the LVFF region of Aβ as well.

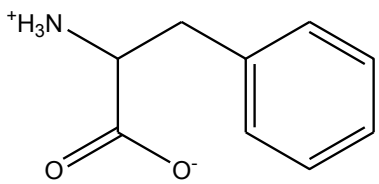

Figure 3.1: Phenylalanine as charged for physiological pH

A geometry optimized phenylalanine structure was built for the following calculations, whereupon a grid scan was performed on the molecule over three possible torsional angles in a stepwise fashion of 30° increments from 0° to 330°. The lowest energy conformation resulting from this search was selected and then minimized via steepest descent followed by conjugate gradient minimization. The resulting structure was considered geometry optimized and used in setting up the systems for energy minimization in the gas phase; the energy is given in Table 3.1.

Table 3.1: Gas phase energy of phenylalanine

	Total Energy (kcal/mol)
Phenylalanine	3.20

Both gas phase and solution phase calculations were performed examining the potential binding interactions between phenylalanine and the **HH**Q**K** and LVFF regions of the β-amyloid peptide and both sets of calculations were performed in QUANTA using the CHARMM force field [46, 48, 50]. Solution phase geometry optimizations were performed to determine if interactions that occurred between phenylalanine and Aβ would still occur in an environment more representative of the brain.

As there are no crystal structures available of β-amyloid to give its exact conformation, six NMR based structures were selected for interacting with the phenylalanine molecule – these six different structures allow for determination of the potential binding interactions with small molecules like phenylalanine in a variety of Aβ conformations. The structures were obtained from the RCSB Protein Data Bank (PDB) and range in length from 28 to 42 amino acids and encapsulate both the **HH**Q**K** and

LVFF regions of interest. The six selected conformers, given by their PDB identifications, were as follows: 1AMB, 1AMC, 1AML, IBA4, 1IYT, and 1Z0Q [67, 68, 69, 70, 71, 72, 83]. While the phosphoserine optimizations looked at the 2BP4 conformer, it was not long enough to be used for these optimizations as LVFF was of interest too and the terminal end was residue 16 [73]. The 1Z0Q conformer was selected as it is composed of residues 1-42 [83]. These structures were imported into QUANTA, charged appropriately for physiological pH and then optimized with a constrained protein backbone to find the lowest energy gas phase conformation [46]. The energies of the proteins can be found in Appendix 6.

3.3.1 Gas Phase Interactions Between Phenylalanine and β-Amyloid

Gas phase optimizations were performed to determine if phenylalanine was capable of binding to the **HH**Q**K** and LVFF regions of β-amyloid. If interactions did occur, selected favourable interactions would be further examined via solution phase calculations to better determine if such interactions would occur *in vivo*.

3.3.1.1 Selection of Initial Orientations for Optimization

Previous research by the author has indicated that separating the phenylalanine molecule from the desired peptide region of β-amyloid by a distance of 3.0 Å is the most effective for determining whether favourable or unfavourable interactions will occur. Systems were set up such that two of the amino, carboxylate or aromatic functional groups of phenylalanine could interact with two of the **HH**Q**K** or LVFF side chains of interest. Some interactions could not be tested as the amino acid side chains were either too far apart for the small phenylalanine molecule to interact with, or were on opposite sides of the peptide.

3.3.1.2 Optimization of the Gas Phase Systems

Each of the potential binding interactions was modelled in the QUANTA program using the CHARMM force field [46, 48, 50]. The phenylalanine molecule was oriented towards the peptide at the appropriate distance and then the backbone of the protein conformation was constrained before the system was optimized. Given the nature of gas phase optimizations, constraining the protein backbone prevents collapse of the protein structure due to intramolecular interactions in the gas phase. Minimization was first performed using the steepest descent algorithm followed by conjugate gradient to ensure a minimum point was reached on the PES. The optimized system was then examined for potential binding interactions. The final interactions were next examined in the Molecular Operating Environment for other possible interactions such as cation-π and π-π interactions [47].

To determine the relative favourability of the optimized systems, the binding energy was determined using the following formula:

$$\Delta E_{bind} = E_{A\beta phen} - E_{A\beta} - E_{phen} \quad (3.1)$$

Where the total binding energy is equal to the energy of the optimized phenylalanine-β-amyloid system, $E_{A\beta phen,}$ minus the individual contributions of separately optimized phenylalanine, $E_{A\beta phen,}$ and β-amyloid, $E_{A\beta}$.

3.3.2 Gas Phase Results of Phenylalanine Interacting with β-Amyloid

The main results of the gas phase optimizations of phenylalanine interacting with different conformations of Aβ are summarized in the following tables according to the

selected β-amyloid conformer and contain information of the initial and final phenylalanine orientations.

The tables also contain the calculated binding energies (in kcal/mol) and the number of measureable binding interactions that have occurred. The amino acid side chains are represented by single letter notations and their position on the peptide chain. The functional groups are also represented by abbreviations where C represents the CO_2^- functional group, N the NH_3^+ functional group and Ar represents the aromatic ring present in phenylalanine.

Tables 3.2 through 3.7 summarize the results of the gas phase minimizations of phenylalanine with each of the six Aβ conformers: 1AMB, 1AMC, 1AML, 1BA4, 1IYT, and 1Z0Q respectively. Interactions covered **HH**Q**K** and LVFF, as well as overlapping possibilities between the two regions. The number of measureable bonds occurring for each system was, respectively, eleven, thirteen, nine, four, ten and ten.

Although interactions between the amino functional group and the lysine side chain are likely to be repulsive, these orientations were still included for comparison of what potential binding interactions could occur, or if rearrangements would happen.

For each of the β-amyloid conformers examined for potential interactions with phenylalanine, the overall binding energies, as well as the electrostatic and van der Waals energies were compared to determine which interactions were most favourable. It was determined that by selecting the overall most energetically favourable binding interactions (where potential binding could occur at two or more sites) would reflect a range of favourable van der Waals interactions, electrostatic interactions and overall

energetically favourable systems. Therefore, for each Aβ conformation, the six systems selected for optimization in the solution phase exhibited the most favourable binding energies and involved phenylalanine interacting with β-amyloid at two or more amino acid side-chains.

Table 3.2: Gas phase results of phenylalanine interacting with the 1AMB conformer of β-amyloid

Initial Orientation								Final Orientation									ΔE_{bind}	Measureable
H13	H14	Q15	K16	L17	V18	F19	F20	H13	H14	Q15	K16	L17	V18	F19	F20	X	(kcal/mol)	Bonds
C	Ar							C	Ar								-12.99	1
Ar	C							Ar	C								-13.66	0
N	Ar								Ar							C/Ar	-10.98	2
Ar	N							Ar	N							Ar	-12.25	0
Ar			C					Ar			C						-8.28	2
C			Ar					C/Ar			Ar					Ar	-10.53	1
Ar			N					N/Ar			N					Ar	-9.15	1
N			Ar					N			Ar						-8.09	1
				Ar			N					Ar			N	N	-10.31	0
					Ar	N							Ar	N		Ar	-13.55	0
						Ar	N							Ar	N	Ar	-11.47	0
						N	Ar							N	Ar		-8.79	0
			C	Ar				C			C	Ar					-9.31	2
			N	Ar							Ar	Ar/N			Ar		-10.48	0
C				Ar				C				Ar/C					-10.16	2
N				Ar				Ar				Ar					-9.15	0
	N				Ar				Ar				Ar				-8.24	0
	C				Ar				C				Ar				-9.70	0
	C			Ar					C			Ar	Ar				-10.87	0
	N			Ar					N			Ar	Ar				-11.36	1
			Ar				N					Ar	Ar	N			-12.80	2
			C				Ar				C	N			Ar		-13.38	2
			N				Ar					N/Ar			Ar		-13.01	0

Table 3.3: Gas phase results of phenylalanine interacting with the 1AMC conformer of β-amyloid

Initial Orientation								Final Orientation									ΔE_{bind}	Measureable
H13	H14	Q15	K16	L17	V18	F19	F20	H13	H14	Q15	K16	L17	V18	F19	F20	X	(kcal/mol)	Bonds
Ar	N							Ar	N							Ar/C/N	-14.07	2
N	Ar							N	Ar							C/Ar	-12.20	2
Ar	C							Ar	C							Ar	-13.88	0
C	Ar							C	Ar							Ar	-14.93	1
Ar			N					Ar/N			N					Ar	-11.30	1
N			Ar					Ar			C	Ar					-10.12	2
Ar			C					Ar			C	Ar					-9.19	1
C			Ar					C			Ar						-6.84	1
				Ar			N					Ar			N		-8.67	0
					Ar	N							Ar	N		Ar	-9.72	0
						N	Ar			Ar	Ar			Ar/N		Ar	-13.19	1
						Ar	N							Ar	N	N	-11.22	0
N				Ar				N/Ar				Ar					-10.90	1
	N				Ar				N				Ar				-9.89	0
	C				Ar				C				Ar				-10.91	0
C				Ar				C				Ar					-12.27	1
			C	Ar				C			C	Ar					-8.89	0
			N	Ar								Ar/N			Ar		-10.42	0
			Ar				N				Ar				N		-12.69	2
			C				Ar	C			C	Ar					-8.88	1
			N				Ar				Ar	Ar			Ar		-9.65	1

Table 3.4: Gas phase results of phenylalanine interacting with the 1AML conformer of β-amyloid

Initial Orientation								Final Orientation									ΔE_{bind}	Measureable
H13	H14	Q15	K16	L17	V18	F19	F20	H13	H14	Q15	K16	L17	V18	F19	F20	X	(kcal/mol)	Bonds
Ar	C							Ar	C							Ar/C	-20.27	1
C	Ar							C	Ar							Ar/N	-12.71	0
N	Ar							N	Ar							Ar/C/N	-17.54	0
Ar	N							Ar/N	N							N/Ar	-15.63	1
Ar			C					Ar			C						-5.70	0
C			Ar					C			Ar						-11.71	0
N			Ar					Ar			Ar						-6.63	0
Ar			N					Ar			N					Ar	-6.72	0
				Ar			N	Ar				Ar			N	N/Ar	-14.02	2
					Ar	N				N				N		Ar/N/C	-18.37	0
						N	Ar							Ar	Ar		-10.43	0
						Ar	N							Ar	N		-8.79	0
	C				Ar				C							N/Ar	-18.57	1
	N				Ar											C	-14.05	1
			Ar			N					Ar			N			-10.96	1
			C			Ar					C			Ar			-6.87	1
			N			Ar								Ar			-7.76	0
Ar							N	Ar							N	N	-14.02	2
C							Ar	C							Ar		-16.01	1
N							Ar								Ar	Ar	-12.92	0

Table 3.5: Gas phase results of phenylalanine interacting with the 1BA4 conformer of β-amyloid

Initial Orientation								Final Orientation									ΔE_{bind}	Measureable
H13	H14	Q15	K16	L17	V18	F19	F20	H13	H14	Q15	K16	L17	V18	F19	F20	X	(kcal/mol)	Bonds
Ar	N							Ar	N								-10.84	0
N	Ar							N/Ar	Ar								-9.69	2
C	Ar							C	Ar								-10.88	2
Ar	C							Ar	Ar/C								-11.99	1
				Ar			N					Ar			N		-6.22	0
					Ar	N				Ar			Ar	N			-8.43	0
	C			Ar					C			Ar					-6.60	0
	N			Ar								Ar/N					-9.34	0
			Ar			N								N		Ar	-15.77	1
	N				Ar				N	Ar		Ar	Ar				-12.04	0
	C				Ar				C	Ar		Ar	Ar				-11.85	0

Table 3.6: Gas phase results of phenylalanine interacting with the 1IYT conformer of β-amyloid

Initial Orientation								Final Orientation									ΔE_{bind}	Measureable
H13	H14	Q15	K16	L17	V18	F19	F20	H13	H14	Q15	K16	L17	V18	F19	F20	X	(kcal/mol)	Bonds
Ar	C							Ar									-11.81	1
C	Ar							C	Ar			Ar					-13.07	0
N	Ar							N/Ar	Ar								-11.39	2
Ar	N							Ar				Ar					-8.61	1
N			Ar								Ar				Ar		-8.50	0
Ar			N					Ar			N						-8.84	0
C			Ar					C			Ar				Ar		-11.98	1
Ar			C					Ar			C					Ar	-10.53	1
				Ar			N					Ar			N/Ar		-8.34	1
					Ar	N							Ar	N			-10.74	0
						Ar	N				Ar			Ar	N		-8.27	0
						N	Ar							Ar	Ar	Ar	-13.15	0
C				Ar				C				Ar					-11.52	0
N				Ar				N				Ar					-8.86	1
	C			Ar					C			Ar					-7.14	0
	N			Ar					N			Ar	Ar				-12.15	1
			C				Ar				C			Ar	Ar/C		-9.81	0
			Ar				N				Ar			Ar			-8.05	1
			N				Ar							Ar	Ar		-8.83	0
			C			Ar					C			Ar/C			-8.95	2
			Ar			N					Ar			N/Ar			-7.92	0
			N			Ar								Ar/N			-9.65	0

Table 3.7: Gas phase results of phenylalanine interacting with the 1Z0Q conformer of β-amyloid

Initial Orientation								Final Orientation									ΔE_{bind}	Measureable
H13	H14	Q15	K16	L17	V18	F19	F20	H13	H14	Q15	K16	L17	V18	F19	F20	X	(kcal/mol)	Bonds
N	Ar							N	Ar							Ar	-13.65	2
Ar	N							Ar									-7.82	0
C	Ar							C	Ar		C						-14.05	1
Ar	C							Ar	C		Ar						-16.10	3
N			Ar					Ar			Ar						-6.49	0
Ar			N					Ar			Ar						-9.62	1
Ar			C					Ar/C			C						-11.24	2
C			Ar					C			Ar						-7.89	1
				Ar			N					Ar			N/C		-13.68	1
				Ar		N						Ar		Ar	Ar		-9.03	0
						N	Ar								Ar		-7.97	0
						Ar	N							Ar			-3.42	0
	N				Ar				Ar				Ar				-10.75	0
	C				Ar				C/Ar				Ar				-14.77	0
	N			Ar					Ar								-14.33	1
	C			Ar					N			C/Ar					-15.88	1
			C			Ar					C			Ar			-13.94	2
			N			Ar					N/Ar			Ar			-13.87	0
			Ar			N					Ar			C			-13.75	0

The interactions that were chosen as the most favourable, with binding occurring at two or more sites for each of the conformers can be summarized in the following table. The amino acid side chains are represented by their single letter abbreviations, and the functional groups of phenylalanine interacting with those side chains are highlighted in purple.

Table 3.8: Selected interactions for optimization of phenylalanine with β-amyloid in the solution phase

Interaction	Binding Energy (kcal/mol)	Interaction	Binding Energy (kcal/mol)
1AMB		1BA4	
HArHC	-13.66	HNQKLVAr	-12.04
VArFN	-13.55	HArHC	-11.99
KCLVFFAr	-13.38	HCQKLVAr	-11.85
HCHAr	-12.99	HCHAr	-10.88
KArLVFFN	-12.80	HArHN	-10.84
HArHN	-12.25	HNHAr	-9.69
1AMC		1IYT	
HCHAr	-14.93	HCHAr	-13.07
HArHN	-14.07	HNQKLAr	-12.15
HArHC	-13.88	HCHQKAr	-11.98
FNFAr	-13.19	HCHQKLAr	-11.52
KArLVFFN	-12.69	HNHAr	-11.39
HCHQKLAr	-12.27	VArFN	-10.74
1AML		1Z0Q	
HArHC	-20.27	HArHC	-16.10
VArFN	-18.37	HCQKLVAr	-14.77
HNHAr	-17.54	HCHAr	-14.05
HCHQKLVFFAr	-16.01	LArVFFN	-13.68
HArHN	-15.63	HNHAr	-13.65
LArVFFN	-14.02	KCLVFAr	-13.94

3.3.3 Solution Phase Optimization of Phenylalanine Interacting with β-Amyloid

Upon completion of the gas phase optimizations, six of the resulting energetically favourable interactions were selected from each Aβ conformer for solution phase minimizations. Using these initial gas phase optimized systems allowed for more efficient solution phase calculations. The solution phase optimizations were also performed in QUANTA using the CHARMM force field [45, 47, 49].

3.3.3.1 Solvation and Minimization Set-Up for Phenylalanine and β-Amyloid

Solution phase calculations were performed using explicit solvation. As discussed in Chapter 2, Section 2.6.1, given the biological nature of the systems being examined, having explicit water molecules present was optimal to mimic the aqueous environment of the brain. The procedure for solvating the systems followed that which was outlined in Chapter 2, Sections 2.6.2.1-2.6.2.3.

The binding energies of the minimized solution phase interactions between phenylalanine and β-amyloid were calculated using three different equations:

$$\Delta E_{tot} = E_{tot} - E_{A\beta} - E_{phen} \tag{3.2}$$

$$\Delta E_{ele} = E_{ele} - E_{eleA\beta} - E_{elephen} \tag{3.3}$$

$$\Delta E_{vdw} = E_{vdw} - E_{vdwA\beta} - E_{vdwphen} \tag{3.4}$$

The measured energies were the total binding energy, ΔE_{tot}, the total electrostatic binding energy, ΔE_{ele}, and the total van der Waals binding energy, ΔE_{vdw}. All followed the same type of calculation where the energy contributions of the peptide conformer and the phenylalanine molecule were subtracted from the energy of the final minimized phenylalanine-Aβ system as calculated via solution phase optimization and all energies were computed ignoring the energy contributions of the water molecules present in the system. The resulting optimized phenylalanine-Aβ systems were examined for measurable binding interactions in both the QUANTA and MOE programs [46, 47].

The types of measurable binding interactions that occurred in these systems comprised hydrogen bonding, cation-π interactions and π-π interactions. Other interactions such as aliphatic-aromatic interactions may have been occurring as well; the

presence of these types of interactions was usually reflected in the system when functional groups remained in their initial orientations and were not displaced by interactions with water molecules.

3.3.4 Solution Phase Results of Phenylalanine Interacting with Six Different Conformations of β-Amyloid

The results of the solution phase optimizations of the phenylalanine-β-amyloid systems have been summarized in tables for each conformation of β-amyloid. Initial and final binding orientations are given; the three calculated energies and any measureable binding interactions that occurred are indicated according to the following colour scheme: hydrogen-bonds are coloured orange, cation-π interactions are green and π-π interactions are blue. Interactions occurring outside the **HH**Q**K** and LVFF regions of interest are also indicated. As in the gas phase calculations, the amino acids are represented in single letter notation with the respective site number on the peptide chain and the phenylalanine functional groups are represented by C, N, and Ar for the carboxylate, amino, and aromatic groups, respectively.

The final energies for the binding interactions were calculated using the following energies for phenylalanine in Table 3.9. The energies of the solvated proteins are given in Appendix 6.

Table 3.9: Total energies of phenylalanine in the solution phase

	Energy (kcal/mol)		
	E_{tot}	E_{ele}	E_{vdw}
Phenylalanine	4.32	2.76	-0.12

The results of the solution phase optimizations between phenylalanine and the 1AMB conformer of Aβ are indicated in Table 3.10. Of the six interactions selected for solution phase optimization, four had measureable binding interactions. Three of the six systems also demonstrated potential binding interactions at His13 and His14. Overall the binding energies are very favourable.

Table 3.11 indicates the results of the solution phase optimization of potential interactions between phenylalanine and the 1AMC conformer of β-amyloid. Each of the six systems had measureable binding interactions when optimized and three of the six also exhibited possible binding at His13 and His14. One of the systems, despite demonstrating multiple binding interactions, had extremely unfavourable binding energies. With this one exception, the rest of the interactions demonstrated both favourable overall binding energies as well as favourable van der Waals energies.

The results of the solution phase interactions between phenylalanine and the 1AML Aβ conformation are given in Table 3.12. Four of the six optimized systems resulted in measureable binding interactions and three of the six also demonstrated potential interactions at His13 and His14. There is no correlation between the number of measured binding interactions and the overall favourability of the total binding energies, which are all relatively favourable. Systems demonstrated a preference for van der Waals interactions over electrostatic interactions as seen in the calculated energies.

Table 3.13 denotes the results of the solution phase minimizations of the phenylalanine and the 1BA4 β-amyloid systems. All of the systems had measureable binding interactions, and four of these also exhibited potential binding at the His13 and

His14 residues. The binding energies are favourable and the van der Waals energies are significantly more favourable than the electrostatic energies.

Table 3.10: The solution phase results of phenylalanine interacting with the 1AMB conformer of β-amyloid

	Amino Acid										E_{tot}	E_{ele}	E_{vdw}	ΔE_{tot}	ΔE_{ele}	ΔE_{vdw}
	Y10	H13	H14	Q15	K16	L17	V18	F19	F20	E22	kcal/mol	kcal/mol	kcal/mol	kcal/mol	kcal/mol	kcal/mol
Initial Orientation	Ar	Ar	C													
Final Orientation	Ar	Ar	C								-365.38	-278.30	-179.14	-55.18	-10.63	-16.74
Initial Orientation				Ar			Ar	Ar/N		Ar						
Final Orientation						Ar	Ar	Ar/N		Ar	-374.49	-279.50	-185.87	-64.28	-11.83	-23.47
Initial Orientation					C	N			Ar							
Final Orientation					C	C/Ar/N			Ar		-375.09	-277.51	-184.14	-64.89	-9.83	-21.75
Initial Orientation	Ar	C	Ar													
Final Orientation	Ar/C	C	Ar								-374.48	-281.38	-185.68	-64.27	-13.71	-23.29
Initial Orientation					Ar	N			N							
Final Orientation					Ar	N			N		-374.06	-281.73	-180.25	-63.86	-14.06	-17.86
Initial Orientation	Ar	Ar	N													
Final Orientation	Ar	Ar	Ar*/N		Ar						-374.31	-281.28	-183.45	-64.11	-13.61	-21.06

*Indicates the functional group involved in the specified interaction that is occurring

Table 3.11: The solution phase results of phenylalanine interacting with the 1AMC conformer of β-amyloid

	Amino Acid											E_{tot}	E_{ele}	E_{vdw}	ΔE_{tot}	ΔE_{ele}	ΔE_{vdw}
	Y10	E11	V12	H13	H14	Q15	K16	L17	V18	F19	F20	kcal/mol	kcal/mol	kcal/mol	kcal/mol	kcal/mol	kcal/mol
Initial Orientation	Ar			C	Ar												
Final Orientation	Ar			C	Ar			C				-378.22	-284.71	-182.41	-68.01	-6.99	-21.62
Initial Orientation	C*/Ar	N		Ar	N				Ar	Ar/N							
Final Orientation	C*/Ar	N		Ar	N				Ar	Ar/N		-381.60	-283.16	-185.76	-71.38	-5.44	-24.97
Initial Orientation	Ar			Ar	C												
Final Orientation	Ar			Ar	C							-317.10	-273.30	-166.17	-6.89	4.42	-5.38
				C													
Initial Orientation			Ar			Ar	Ar			N/Ar							
Final Orientation			Ar			Ar	Ar			N*/Ar		-373.62	-291.48	-177.56	-67.13	-7.20	-22.28
Initial Orientation							Ar				N						
Final Orientation				Ar			Ar	Ar			N*/C	-377.35	-284.93	-183.07	-63.86	-14.06	-17.86
Initial Orientation				C				Ar									
Final Orientation				C				Ar				-377.93	-279.24	-188.35	-67.71	-1.52	-27.56

*Indicates the functional group involved in the specified interaction that is occurring

Table 3.12: The solution phase results of phenylalanine interacting with the 1AML conformer of β-amyloid

	Amino Acid															E_{tot}	E_{ele}	E_{vdw}	ΔE_{tot}	ΔE_{ele}	ΔE_{vdw}
	F4	R5	H6	Y10	H13	H14	Q15	K16	L17	V18	F19	F20	E22	G29	A30	I31	kcal/mol	kcal/mol	kcal/mol	kcal/mol	kcal/mol	kcal/mol
Initial Orientation				C/Ar	Ar	C										C/Ar						
Final Orientation				C/Ar	Ar	C										C/Ar	-476.07	-357.78	-243.39	-75.47	-14.36	-30.78
Initial Orientation					Ar				Ar			N		N	Ar							
Final Orientation					Ar							N			Ar		-456.08	-349.37	-233.34	-55.48	-5.95	-20.73
Initial Orientation	Ar	Ar	C				N				N		N*/Ar									
Final Orientation		Ar	C				N			Ar	N		Ar				-481.81	-356.96	-246.83	-81.21	-13.54	-34.22
Initial Orientation				Ar	N	Ar										N/C						
Final Orientation				Ar	N	Ar			N							C	-474.09	-355.78	-242.46	-73.49	-12.36	-29.85
Initial Orientation					C							Ar										
Final Orientation					C				Ar			Ar		Ar	Ar/C		-472.44	-350.94	-238.93	-71.84	-7.51	-26.31
Initial Orientation				N/Ar	N/Ar*	N										Ar						
Final Orientation				N	N/Ar*	N/C										Ar	-462.18	-346.17	-234.68	-61.58	-2.75	-22.06

*Indicates the functional group involved in the specified interaction that is occurring

Table 3.13: The solution phase results of phenylalanine interacting with the 1BA4 conformer of β-amyloid

	Amino Acid									E_{tot}	E_{ele}	E_{vdw}	ΔE_{tot}	ΔE_{ele}	ΔE_{vdw}
	V12	H13	H14	Q15	K16	L17	V18	F19	F20	kcal/mol	kcal/mol	kcal/mol	kcal/mol	kcal/mol	kcal/mol
Initial Orientation		Ar	Ar/C												
Final Orientation		Ar	Ar*/C	Ar		C				-493.11	-369.69	-247.71	-77.34	-2.61	-41.42
Initial Orientation		C	Ar												
Final Orientation		C	Ar							-489.66	-374.64	-239.99	-73.88	-7.57	-33.70
Initial Orientation		Ar	N												
Final Orientation	Ar	Ar	N	Ar						-484.59	-369.77	-244.80	-68.82	-2.70	-38.51
Initial Orientation		N	Ar												
Final Orientation		N/Ar	Ar	Ar						-487.59	-367.77	-241.49	-71.82	-0.70	-35.20
Initial Orientation			N	Ar		Ar	Ar								
Final Orientation			N	Ar		Ar	Ar			-492.69	-373.03	-244.93	-76.91	-6.01	-38.64
Initial Orientation			C	Ar		Ar	Ar								
Final Orientation			C	Ar		Ar	Ar			-492.58	-372.52	-243.88	-76.80	-5.45	-37.60

*Indicates the functional group involved in the specified interaction that is occurring

Table 3.14: The solution phase results of phenylalanine interacting with the 1IYT conformer of β-amyloid

	Amino Acid									E_{tot}	E_{ele}	E_{vdw}	ΔE_{tot}	ΔE_{ele}	ΔE_{vdw}
	Y10	V12	H13	H14	Q15	K16	L17	V18	F19	F20	kcal/mol	kcal/mol	kcal/mol	kcal/mol	kcal/mol	kcal/mol
Initial Orientation			C	Ar			Ar									
Final Orientation			Ar*/C	Ar			Ar				-525.29	-410.73	-249.48	-16.36	-8.90	-9.36
Initial Orientation				N			Ar	Ar								
Final Orientation				N			Ar	Ar			-529.68	-409.05	-252.02	-20.75	-7.22	-11.91
Initial Orientation			C			Ar				Ar						
Final Orientation	C					Ar		C			-526.69	-406.81	-247.67	-17.75	-4.98	-7.56
Initial Orientation			C				Ar									
Final Orientation			C				Ar				-518.48	-408.13	-244.28	-9.54	-6.30	-4.16
Initial Orientation			N	Ar												
Final Orientation	Ar		N/Ar	Ar							-518.35	-403.71	-250.10	-9.41	-1.89	-9.99
Initial Orientation								Ar	N							
Final Orientation					Ar			Ar	N		-521.91	-406.74	-249.73	-12.97	-4.91	-9.61

*Indicates the functional group involved in the specified interaction that is occurring

Table 3.15: The solution phase results of phenylalanine interacting with the 1Z0Q conformer of β-amyloid

	Amino Acid											E_{tot}	E_{ele}	E_{vdw}	ΔE_{tot}	ΔE_{ele}	ΔE_{vdw}
	G9	V12	H13	H14	Q15	K16	L17	V18	F19	F20	A21	kcal/mol	kcal/mol	kcal/mol	kcal/mol	kcal/mol	kcal/mol
Initial Orientation			Ar	C		Ar											
Final Orientation			Ar	C		Ar						-469.07	-370.87	-253.87	-24.72	-6.70	-16.67
Initial Orientation				C/Ar				Ar									
Final Orientation				C			Ar	Ar			Ar	-462.11	-363.42	-254.05	-17.75	0.75	-16.85
Initial Orientation			C	Ar		C											
Final Orientation			C	Ar		C						-458.21	-365.91	-248.30	-13.86	-1.74	-11.10
Initial Orientation						Ar			N/C								
Final Orientation									N		Ar	-473.22	-372.23	-248.29	-28.87	-8.06	-11.09
Initial Orientation	N		N	Ar													
Final Orientation	N		N	Ar								-470.81	-367.01	-250.96	-26.46	-2.84	-13.76
Initial Orientation						C			Ar								
Final Orientation		Ar			Ar	C			Ar			-474.07	-373.55	-251.84	-29.72	-9.38	-14.63

The results of the optimization of phenylalanine with the 1IYT conformer of β-amyloid in a solvated environment are given in Table 3.14. Half of the systems resulted in measureable binding interactions, and only two exhibited potential binding interactions

at the His13 and His14 residues. The overall binding energies are significantly lower than the previously calculated interactions with other Aβ conformations, and the van der Waals and electrostatic energies are very similar in range.

Phenylalanine and the 1Z0Q conformer of Aβ were optimized in the solution phase and the results are indicated in Table 3.15. Four of the systems exhibited measureable binding interactions when optimized, and three of these also demonstrated the potential to interact with the His13 and His14 residues of β-amyloid. The total binding energies are moderately favourable compared to the others. Van der Waals energies are again slightly more favourable than the electrostatic binding energies.

3.3.5 Conclusions of Phenylalanine Interacting with β-Amyloid.

Overall, the results of the solution phase optimizations of phenylalanine and six different β-amyloid conformers indicate that potential binding interactions can occur. Cation-π interactions tend to be somewhat favoured over hydrogen bonding, with only a few π-π interactions, and most of these measureable interactions occur at the His13 and His14 residues of the peptide. Examining systems for potential binding at two or more sites reveals His13-His14 as the preferred interaction, with a few at His13-Leu17 and His14-Leu17. Overall, interactions occurring strictly within the LVFF region were not as favoured, even though phenylalanine should be capable of forming aromatic-aromatic interactions with the phenyl rings of Phe19 and Phe20.

In general, the measured binding energies did not exhibit a direct correlation to the number of measureable binding interactions; therefore it is possible that there are also

aliphatic-aromatic interactions occurring among other types of interactions that cannot be directly measured and/or visualized in the modelling programs.

3.4 DOPAMINE AND β-AMYLOID

One of the amino acid metabolites identified by screening the library of endogenous compounds is dopamine (Figure 3.2) which is one of the products in the metabolic pathway of phenylalanine [39].

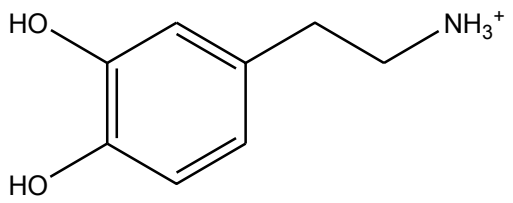

Figure 3.2: Dopamine as charged for physiological pH

Dopamine is a naturally occurring small molecule found in the human brain that plays a role as a neurotransmitter [39]. Although dopamine is often mentioned in relationship to Parkinson's disease, it also has altered levels in the brains of Alzheimer's patients. Research indicates that levels of dopamine in plasma are significantly lower in Alzheimer's patients when compared to controls [84]. It is suggested that while there is no loss of dopaminergic neurons as a result of AD, the enzymes involved in stimulating the release of dopamine from neurons are not as active or are decreased in concentration [84, 85]. As dopamine is a small molecule endogenous to the brain and L-DOPA can be given to patients to generate more dopamine in the brain, studies were performed to see if dopamine was capable of binding to the β-amyloid peptide, specifically at the **HHQK** and LVFF regions.

The neutral dopamine molecule was subjected to a grid search from 0° to 330° in 30° steps, for each of the two torsional angles. The lowest energy structure generated from this search was first charged for physiological pH and was then minimized via steepest descent and conjugate gradient algorithms to find the lowest energy structure in the QUANTA program [46]. The energy of the optimized structure is given in Table 3.16.

Table 3.16: Gas phase energy of dopamine

	Total Energy (kcal/mol)
Dopamine	-3.32

The potential binding interactions between dopamine and the specified regions of the Aβ peptide were examined in both gas and solution phase environments. These optimizations were performed in QUANTA using the CHARMM force field [46, 48, 50]. The same six conformations of β-amyloid selected for use in the phenylalanine calculations were also used to perform these system optimizations.

3.4.1 GAS PHASE INTERACTIONS BETWEEN DOPAMINE AND DIFFERENT CONFORMERS OF β-AMYLOID

Gas phase minimizations were performed to see if dopamine was capable of forming binding interactions with the amino acid side chains in the **HH**Q**K** and LVFF regions of the β-amyloid peptide.

3.4.1.1 SELECTION OF INITIAL ORIENTATIONS FOR OPTIMIZATION

Results from previous research have indicated that the optimal initial distance to separate a molecule of interest from the β-amyloid peptide is 3.0 Å: this distance is close enough that both attractive forces and repulsive forces can be exerted by the protein on

the molecule, which may not occur if they are separated by larger distances. The number of systems minimized depended on the location of the amino acids side chains in the **HH**Q**K** and LVFF regions of interest; some of these were too far apart for dopamine to interact with. The systems were set up such that any two of the three functional groups on dopamine were oriented in a way where they could interact with two different amino acid side chains in the selected Aβ regions.

3.4.1.2 Optimization of the Gas Phase Systems

The potential binding systems were all modelled in the QUANTA program using the CHARMM force field [47, 48, 50]. Systems were set up following the above procedure, the protein backbone was constrained to prevent self interactions, and then the systems were subjected to minimization first via the steepest descent algorithm and then the conjugate gradient algorithm. These optimized systems were saved for future reference and then examined for measureable binding interactions that may have occurred between dopamine and the β-amyloid peptide. The systems were also imported into MOE to determine if aromatic type interactions were occurring [47].

The relative favourability was determined by calculating the binding energy of each system using the following formula:

$$\Delta E_{bind} = E_{A\beta dopa} - E_{A\beta} - E_{dopa} \tag{3.5}$$

Where the total binding energy is equal to the energy of the optimized β-amyloid-dopamine system, $E_{A\beta dopa}$, minus the individual contributions of separately optimized dopamine, E_{dopa}, and β-amyloid, $E_{A\beta}$. The protein energies are given in Appendix 6.

3.4.2 GAS PHASE RESULTS OF DOPAMINE INTERACTING WITH β-AMYLOID

The main results of the gas phase optimizations of dopamine interacting with different conformations of β-amyloid are summarized in the following tables according to the β-amyloid conformer. The initial and final binding orientations of the systems are given, with the amino acid side chains represented by their single letter abbreviation and the location in the peptide sequence. The dopamine functional groups are represented by Ar for the aromatic ring, N for the NH_3^+ group, and the two OH groups are represented by O^1 and O^2 where O^1 is *meta* to the ethylamine (Figure 3.3).

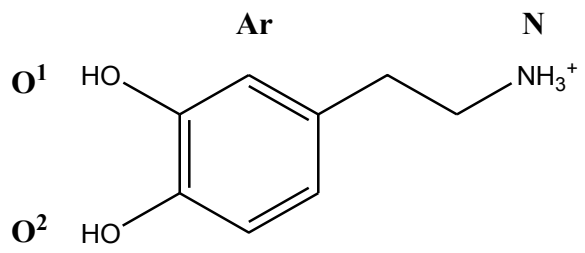

Figure 3.3: Identification of the functional groups on dopamine

The results for each Aβ conformer minimized with dopamine in the gas phase are given in Tables 3.17-3.22. Interactions in the **HH**Q**K** and LVFF regions as well as overlapping possibilities between the two are shown for each system. The number of measureable bonds varied for each system with eight for the 1AMB conformer, eight for 1AMC, eight for 1AML, six systems for 1BA4, ten for 1IYT and six for the 1Z0Q Aβ conformer.

Systems where measureable bonds were present did not always correlate to have the most energetically favourable interactions, therefore the selection of which of these systems would be subjected to solution phase optimization was based on different criteria. For each of the Aβ conformers that were optimized with dopamine, six systems

were selected for minimization in a solvated environment. These six systems had the lowest overall binding energies and the potential to interact with two different amino acid side chains within the specified regions of β-amyloid.

Table 3.17: Gas phase results of dopamine interacting with the 1AMB conformer of β-amyloid

Initial Orientation								Final Orientation									ΔE_{bind}	Measureable
H13	H14	Q15	K16	L17	V18	F19	F20	H13	H14	Q15	K16	L17	V18	F19	F20	X	(kcal/mol)	Bonds
Ar	N							O^2	N			O^1					-11.12	3
N	Ar							O^2	N							Ar/O^1	-11.20	0
Ar			N					Ar			N	N					-10.34	1
N			Ar					N			O^2						-9.46	1
				N			Ar					N			O^2		-9.31	0
				Ar			N					Ar/O^2			N/Ar		-10.42	1
						Ar	N							O^1/O^2			-6.39	0
						N	Ar					Ar			$O^1/O^2/Ar$		-9.16	0
Ar				N				$Ar/O^1/O^2$				N					-11.44	1
N				Ar				Ar/N				C/O^2					-8.02	0
			Ar	N				Ar/N			O^2/Ar	N/Ar					-9.59	1
			N	Ar							N/Ar	O^1/O^2			Ar/O^2		-10.71	1
			Ar				N	O^1/O^2			O^1	O^2			N		-7.30	1
			N				Ar	N			N/Ar				O^1/O^2		-5.51	0

Table 3.18: Gas phase results of dopamine interacting with the 1AMC conformer of β-amyloid

Initial Orientation								Final Orientation									ΔE_{bind}	Measureable
H13	H14	Q15	K16	L17	V18	F19	F20	H13	H14	Q15	K16	L17	V18	F19	F20	X	(kcal/mol)	Bonds
Ar	N							O^1/O^2	N			O^1				Ar	-14.99	1
N	Ar							N	O^2							Ar/O^1	-16.06	2
N			Ar					N/Ar			Ar/O^1						-9.10	3
Ar			N					Ar/N								O^2	-13.32	1
				N			Ar					N			Ar/O^1		-9.13	0
				Ar			N					Ar/O^1			N		-8.30	0
						N	Ar							N	O^2		-6.95	0
						Ar	N								N		-5.58	0
Ar				N				Ar				N					-6.93	1
N				Ar				N/Ar				$Ar/O^1/O^2$					-11.03	2
			Ar	N				O^2			Ar/O^2	N/Ar					-8.95	1
			N	Ar				O^1			N	$Ar/O^1/O^2$					-9.59	0
			N				Ar				N				O^1/O^2		-5.38	0
			Ar				N				Ar/O^2	Ar			N/Ar		-9.28	2

Table 3.19: Gas phase results of dopamine interacting with the 1AML conformer of β-amyloid

Initial Orientation								Final Orientation									ΔE_{bind}	Measureable
H13	H14	Q15	K16	L17	V18	F19	F20	H13	H14	Q15	K16	L17	V18	F19	F20	X	(kcal/mol)	Bonds
N	Ar							N	O^1			O^1				Ar	-17.73	2
Ar	N							O^2	N							Ar/O^1	-14.37	0
Ar			N					O^1/O^2			N						-9.45	0
N			Ar					N			O^1/O^2						-6.89	1
				Ar			N				O^1	O^2			Ar/N	O^2	-21.04	2
				N			Ar					N			O^1/O^2		-8.09	0
						N	Ar							N	O^1/O^2	N	-7.60	0
						Ar	N							O^1/O^2	N		-4.95	0
			N			Ar					N			O^1/O^2			-4.90	0
			Ar			N					O^1			N			-4.93	1
			Ar				N				O^1/O^2	N		Ar	N		-10.72	1
			N				Ar				$N/Ar/O^1$			Ar	O^1/O^2		-14.84	2
N							Ar	N			O^1				O^2	Ar	-17.64	1
Ar							N	O^1/O^2							N	Ar	-12.22	1

Table 3.20: Gas phase results of dopamine interacting with the 1BA4 conformer of β-amyloid

Initial Orientation								Final Orientation									ΔE_{bind}	Meaureable
H13	H14	Q15	K16	L17	V18	F19	F20	H13	H14	Q15	K16	L17	V18	F19	F20	X	(kcal/mol)	Bonds
N	Ar							N	Ar	O^1							-12.16	2
Ar	N							O^1	N/Ar	O^2							-11.01	2
				Ar			N					Ar/O^2			Ar/N		-12.70	1
				N			Ar					N			O^1/O^2		-11.31	0
	N			Ar					N			Ar/O^1					-8.94	1
	Ar			N					Ar/O^1			N					-13.43	0
			Ar			N					O^2			N		O^1/O^2	-13.36	3
			N			Ar					N			Ar		Ar	-17.51	1

Table 3.21: Gas phase results of dopamine interacting with the 1IYT conformer of β-amyloid

Initial Orientation								Final Orientation									ΔE_{bind}	Measureable
H13	H14	Q15	K16	L17	V18	F19	F20	H13	H14	Q15	K16	L17	V18	F19	F20	X	(kcal/mol)	Bonds
Ar	N							O^2	N/O^1			Ar/O^1					-10.78	0
N	Ar							N	O^1/O^2			Ar				O^1	-10.88	3
N			Ar					N			O^1/O^2				Ar/O^1		-11.38	2
Ar			N					O^2			N				Ar/N		-11.23	1
				N			Ar								O^1/O^2	O^1	-8.83	0
				Ar			N					O^1/O^2			Ar/N		-8.15	1
						Ar	N				O^2			O^1/O^2	N		-7.69	0
						N	Ar				Ar/O^1			N	O^1/O^2	Ar	-10.52	0
Ar				N				$Ar/O^1/O^2$				N					-6.46	1
N				Ar				N				O^1/O^2					-7.08	1
	Ar			N					$Ar/O^1/O^2$			N				O^1	-9.15	2
	N			Ar					N			$Ar/O^1/O^2$		Ar	O^1/O^2		-6.78	0
N							Ar	N							$Ar/O^1/O^2$		-8.85	1
Ar							N	$Ar/O^1/O^2$			N	Ar			Ar/N		-11.94	0
			Ar				N				Ar/O^2			Ar/O^2	Ar/N		-6.16	0
			N				Ar								O^1/O^2		-5.99	0
			N			Ar					N			$Ar/O^1/O^2$		O^1	-6.84	1
			Ar			N					O^1/O^2			$Ar/N/O^2$	Ar	Ar	-6.34	1

Table 3.22: Gas phase results of dopamine interacting with the 1Z0Q conformer of β-amyloid

Initial Orientation								Final Orientation									ΔE_{bind}	Measureable
H13	H14	Q15	K16	L17	V18	F19	F20	H13	H14	Q15	K16	L17	V18	F19	F20	X	(kcal/mol)	Bonds
N	Ar							N	O^1/O^2							N	-11.55	2
Ar	N							Ar/O^2	N			O^1/O^2				N	-16.98	0
	Ar		N					Ar	O^1/O^2		N						-14.44	0
	N		Ar						N		O^1/O^2	O^2					-5.94	0
Ar			N					$Ar/O^1/O^2$			N					O^2	-10.75	2
N			Ar					N/Ar			$Ar/O^1/O^2$						-11.46	3
				Ar		N						$Ar/O^1/O^2$		N	N		-12.69	0
				N		Ar						N		$Ar/O^1/O^2$	Ar/O^1		-7.65	0
				N			Ar								O^1/O^2		-5.28	0
				Ar			N					$Ar/O^1/O^2$			N		-9.77	1
						Ar	N							$Ar/O^1/O^2$	N		-8.65	0
						N	Ar							N	$Ar/N/O^1/O^2$		-7.72	0
			Ar	N							O^1/O^2	N/Ar					-8.57	1
			N	Ar							N	O^1/O^2					-5.89	0
			Ar			N				N	$N/O^1/O^2$			N		Ar	-18.50	5
			N			Ar								O^1/O^2			-12.35	0
	N			Ar					N			O^1/O^2					-8.51	0
	Ar			N					O^1/O^2								-9.48	0

The six selected systems from each conformer selected for optimization in a solvated environment are summarized in Table 3.23.

Table 3.23: Selected interactions of dopamine interacting with β-amyloid for optimization in the solution phase

Interaction	Binding Energy (kcal/mol)	Interaction	Binding Energy (kcal/mol)
1AMB		1BA4	
HArHQKLN	-11.44	KNLVFAr	-17.51
HNHAr	-11.20	HArQKLN	-13.43
HArHN	-11.12	KArLVFN	-13.36
KNLAr	-10.71	LArVFFN	-12.70
LArVFFN	-10.42	HNHAr	-12.16
HArHQKN	-10.34	LNVFFAr	-11.31
1AMC		1IYT	
HNHAr	-16.06	HArHQKLVFFN	-11.94
HArHN	-14.99	HNHQKAr	-11.38
HNHQKLAr	-11.03	HArHQKN	-11.23
KArLVFFN	-9.28	HNHAr	-10.88
LNVFFAr	-9.13	HArHN	-10.78
HNHQKAr	-9.10	HArHQKLN	-6.46
1AML		1Z0Q	
HNHAr	-17.73	KArLVFN	-18.50
HNHQKLVFFAr	-17.64	HArHN	-16.98
KNLVFFAr	-14.84	HArQKN	-14.44
HArHN	-14.37	LArVFN	-12.69
HArHQKLVFFN	-12.22	HNHAr	-11.55
KArLVFFN	-10.72	HNHQKAr	-11.46

3.4.3 SOLUTION PHASE RESULTS FOR DOPAMINE INTERACTING WITH β-AMYLOID

Upon completion of the gas phase optimizations, six of the resulting energetically favourable interactions between dopamine and β-amyloid were selected from each Aβ conformer for solution phase minimizations. Using these initial gas phase optimized systems allowed for more efficient solution phase calculations. The solution phase optimizations were also performed in QUANTA using the CHARMM force field [46, 48, 50]. The same procedure as described in section 3.3.3.1 was used for the solution phase optimization of dopamine and β-amyloid systems.

The final energies for the binding interactions were calculated using the energies listed in Table 3.24 and Appendix 6 via the following equations:

$$\Delta E_{tot} = E_{tot} - E_{A\beta} - E_{dopa} \quad (3.6)$$

$$\Delta E_{ele} = E_{ele} - E_{eleA\beta} - E_{eledopa} \quad (3.7)$$

$$\Delta E_{vdw} = E_{vdw} - E_{vdwA\beta} - E_{vdwdopa} \quad (3.8)$$

where the energies of the solution phase optimized β-amyloid conformers and the dopamine molecule were subtracted from the total energies of the optimized system for each of the overall total energy, the electrostatic energy and the van der Waals energy of the systems. The energies were measured with the solvent contributions ignored.

Table 3.24: Total energies of dopamine in the solution phase

	Energies (kcal/mol)		
	E_{tot}	E_{ele}	E_{vdw}
Dopamine	1.89	-1.40	-0.31

All of the resulting minimized systems were examined in MOE after optimization in QUANTA to determine where, if any, cation-π or π-π interactions are occurring [46, 47].

The results of the solution phase optimizations of the dopamine-Aβ systems have been summarized in tables for each conformation of β-amyloid. Initial and final binding orientations are given along with the three calculated energies: the total binding energy, electrostatic binding energy and van der Waals binding energy. Any measureable binding interactions that occurred are indicated according to the following colour scheme: hydrogen-bonds are coloured orange, cation-π interactions are green and π-π interactions

are blue. Interactions occurring outside the **HH**Q**K** and LVFF regions of interest are also indicated according to the amino acid side chain with which binding may be occurring. As in the gas phase calculations, the amino acids are represented in single letter notation with the respective site number on the peptide chain and the dopamine functional groups are represented by N, Ar, O^1 and O^2 for the amino group, the aromatic ring, the OH *meta* to the ethylamine chain and the OH *para* to the ethylamine chain, respectively.

The results of the solution phase optimizations between dopamine and the 1AMB conformer of Aβ are indicated in Table 3.25. All six optimized systems had measureable bonds and favourable binding energies, with the electrostatic and van der Waals energies being very similar in range. Two of the systems had potential binding interactions at His13 and His14. The other two systems exhibited potential binding interactions at both Lys16 and Phe20, one of which can also interact at Leu17 and Phe20.

The results of the solution phase minimized systems of dopamine and the 1AMC conformer of β-amyloid are given in Table 3.26. Five of the six systems demonstrated measureable binding interactions and two had potential interactions at His13 and His14 while one had potential interactions at Lys16 and Phe20 as well as two at Leu17 and Phe20. The total binding energies are favourable; however, the van der Waals energies are significantly lower than the electrostatic energies.

Table 3.27 summarizes the results of the optimization of dopamine and the 1AML conformer of Aβ in a solvated environment. Four of the final systems contained measureable binding interactions. Overall the binding energies are very favourable with the exception of one system, with the electrostatic binding energies being much weaker

than the van der Waals binding energies. Two systems have potential interactions at His13 and His14, two at Leu17 and Phe20, and one at Lys16 and Phe20.

The results of the solution phase optimization of dopamine with the 1BA4 conformer are detailed in Table 3.28. While four of the six systems have measureable bonds forming, the binding energies are very unfavourable; however, the van der Waals energies are still significantly lower than the electrostatic energies. There are two systems presenting possible binding at both Leu17 and Phe20 and one at His13 and His14.

Table 3.25: The solution phase results of dopamine interacting with the 1AMB conformer of β-amyloid

		Amino Acid								E_{tot}	E_{ele}	E_{vdw}	ΔE_{tot}	ΔE_{ele}	ΔE_{vdw}
	Y10	H13	H14	Q15	K16	L17	V18	F19	F20	kcal/mol	kcal/mol	kcal/mol	kcal/mol	kcal/mol	kcal/mol
Initial Orientation					N/Ar*	O^1/O^2			Ar						
Final Orientation					N/Ar*	O^2			O^2	-376.03	-288.44	-177.60	-63.39	-16.60	-15.01
Initial Orientation					Ar/O^2				Ar/N*						
Final Orientation					Ar/O^2				N	-382.25	-284.97	-187.26	-69.61	-13.14	-24.67
Initial Orientation		O^2	N			O^1									
Final Orientation		O^2	N			O^1				-376.35	-283.25	-181.39	-63.72	-11.42	-18.8
Initial Orientation	Ar/O^1	O^2	N												
Final Orientation	Ar	N	Ar							-376.87	-287.27	-181.26	-64.23	-15.44	-18.67
Initial Orientation		Ar			N	N									
Final Orientation		Ar			N					-377.47	-285.45	-182.72	-64.84	-13.62	-20.13
Initial Orientation		$Ar^*/O^1/O^2$				N									
Final Orientation		Ar			Ar	N				-376.77	-285.28	-181.80	-64.13	13.45	-19.21

*Indicates the functional group involved in the specified interaction that is occurring

Table 3.26: The solution phase results of dopamine interacting with the 1AMC conformer of β-amyloid

	Amino Acid										E_{tot}	E_{ele}	E_{vdw}	ΔE_{tot}	ΔE_{ele}	ΔE_{vdw}
	Y10	E11	H13	H14	Q15	K16	L17	V18	F19	F20	kcal/mol	kcal/mol	kcal/mol	kcal/mol	kcal/mol	kcal/mol
Initial Orientation	Ar	O^1	N	O^1												
Final Orientation	Ar	O^1	N	Ar			N				-390.48	-290.97	-192.20	-77.83	-9.09	-31.21
Initial Orientation	Ar		O^1/O^2	N												
Final Orientation	Ar		O^1/O^2	N			O^1				-389.77	-290.15	-193.28	-77.12	-8.26	-32.29
Initial Orientation			N/Ar				$Ar/O^1/O^2$									
Final Orientation			N/Ar				$Ar/O^1/O^2$				-378.27	-292.41	-179.05	-65.62	-10.53	-18.06
Initial Orientation						Ar/O^2*	Ar			N/Ar*						
Final Orientation						Ar/O^2*	Ar			N/Ar*	-376.01	-286.72	-180.12	-63.36	-4.84	-19.13
Initial Orientation							N			Ar/O^1						
Final Orientation							N			Ar/O^1	-377.56	-294.82	-174.90	-64.91	-12.93	-13.91
Initial Orientation			N/Ar			Ar/O^2*										
Final Orientation			N/Ar			Ar/O^2					-376.80	-286.06	-181.15	-64.15	-4.18	-20.17

*Indicates the functional group involved in the specified interaction that is occurring

Table 3.27: The solution phase results of dopamine interacting with the 1AML conformer of β-amyloid

	Amino Acid											E_{tot}	E_{ele}	E_{vdw}	ΔE_{tot}	ΔE_{ele}	ΔE_{vdw}
	Y10	H13	H14	Q15	K16	L17	V18	F19	F20	A30	I31	kcal/mol	kcal/mol	kcal/mol	kcal/mol	kcal/mol	kcal/mol
Initial Orientation					O^1	O^2			Ar*/N	O^2							
Final Orientation					O^1/O^2	O^2			Ar*/N	Ar		-481.26	-356.64	-238.27	-78.22	-9.05	-25.46
Initial Orientation	Ar	N	O^1								Ar						
Final Orientation		N*/Ar	O^1								Ar/N	-479.74	-365.82	-237.77	-76.71	-18.23	-24.96
Initial Orientation		N			O^1				O^2	Ar							
Final Orientation						O^1			O^2	Ar		-478.65	-364.29	-238.87	-75.62	-16.70	-26.05
Initial Orientation					$N/Ar/O^1$*			Ar	O^1/O^2								
Final Orientation					N				O^1/O^2			-477.84	-357.96	-236.74	-74.80	-10.38	-23.93
Initial Orientation		O^1/O^2							N	Ar							
Final Orientation		O^1/O^2				N			N	Ar		-421.21	-352.81	-229.37	-18.17	-5.23	-16.56
Initial Orientation	Ar	O^2	N								Ar/O^1						
Final Orientation	Ar/N	Ar	N			N					Ar	-475.08	-354.34	-240.05	-72.05	-6.80	-27.24

*Indicates the functional group involved in the specified interaction that is occurring

Table 3.28: The solution phase results of dopamine interacting with the 1BA4 conformer of β-amyloid

	Amino Acid									E_{tot}	E_{ele}	E_{vdw}	ΔE_{tot}	ΔE_{ele}	ΔE_{vdw}
	D1	E3	E11	H13	H14	Q15	K16	L17	V18 F19	F20	kcal/mol	kcal/mol	kcal/mol	kcal/mol	kcal/mol	kcal/mol
Initial Orientation			Ar				N			Ar						
Final Orientation			N				N			Ar	-435.47	-370.34	-229.04	-17.26	0.90	-22.55
Initial Orientation		O^2	O^1/O^2				O^2			N						
Final Orientation	Ar		Ar				O^2			N	-421.71	-372.07	-222.58	-3.50	-0.83	-16.10
Initial Orientation								Ar/O^2		Ar/N*						
Final Orientation								O^1/O^2		N	-424.49	-378.33	-219.24	-6.28	-7.10	-12.75
Initial Orientation				N	Ar	O^1										
Final Orientation				N	Ar	O^1					-405.52	-369.45	-214.37	12.69	1.78	-7.89
Initial Orientation					Ar		Ar	N/Ar								
Final Orientation					O^1			N			-418.66	-372.65	-217.06	-0.45	-1.42	-10.45
Initial Orientation								N		O^1/O^2						
Final Orientation								N		O^1	-420.68	-377.04	-217.69	-2.47	-5.80	-11.21

*Indicates the functional group involved in the specified interaction that is occurring

Table 3.29: The solution phase results of dopamine interacting with the 1IYT conformer of β-amyloid

	Amino Acid											E_{tot}	E_{ele}	E_{vdw}	ΔE_{tot}	ΔE_{ele}	ΔE_{vdw}
	Y10	H13	H14	Q15	K16	L17	V18	F19	F20	D23		kcal/mol	kcal/mol	kcal/mol	kcal/mol	kcal/mol	kcal/mol
Initial Orientation		O^1/O^2*			N	Ar			Ar/N								
Final Orientation		Ar/O^2*			N				N			-530.85	-417.92	-249.73	-19.47	-11.93	-9.42
Initial Orientation		N			O^1/O^2				Ar/O^1								
Final Orientation					O^1				O^1			-530.24	-415.49	-246.25	-18.87	-9.50	-5.94
Initial Orientation		O^2			N				Ar/N								
Final Orientation		O^2			N							-531.70	-417.81	-247.16	-20.33	-11.82	-6.85
Initial Orientation	O^1	N	O^1/O^2			Ar											
Final Orientation	O^1	N/Ar	O^1/O^2*									-528.94	-416.04	-248.79	-17.56	-10.05	-8.48
Initial Orientation		O^2	N/O^1			Ar/O^1											
Final Orientation		O^1/O^2	N			O^1						-523.18	-413.40	-248.10	-11.81	-7.41	-7.79
Initial Orientation					Ar/O^1			N	O^1/O^2	Ar							
Final Orientation					Ar/O^1*			N	O^1/O^2	Ar		-527.21	-414.04	-247.33	-15.84	-8.05	-7.02

*Indicates the functional group involved in the specified interaction that is occurring

Table 3.30: The solution phase results of dopamine interacting with the 1Z0Q conformer of β-amyloid

	Amino Acid											E_{tot}	E_{ele}	E_{vdw}	ΔE_{tot}	ΔE_{ele}	ΔE_{vdw}
	G9	Y10	V12	H13	H14	Q15	K16	L17	V18	F19	F20	kcal/mol	kcal/mol	kcal/mol	kcal/mol	kcal/mol	kcal/mol
Initial Orientation			Ar			N	$N/O^1/O^2$			N							
Final Orientation				O^1		N	O^1/O^2			N		-463.78	-376.21	-250.41	-16.99	-7.88	-13.01
Initial Orientation		N		Ar/O^2	N			O^1/O^2									
Final Orientation				O^2	N			O^1/O^2				-478.04	-372.78	-252.32	-31.26	-4.45	-14.93
Initial Orientation				Ar	O^1/O^2		N										
Final Orientation					O^2		N					-467.86	-368.81	-254.28	-21.07	-0.48	-16.88
Initial Orientation								$Ar/O^1/O^2$		N	N						
Final Orientation								O^1/O^2		N	N	-470.21	-372.08	-245.72	-23.42	-3.75	-8.32
Initial Orientation	N			N	O^1/O^2												
Final Orientation				N	O^2							-464.12	-365.87	-252.68	-17.34	2.46	-15.28
Initial Orientation				N/Ar			$Ar/O^1/O^2$*										
Final Orientation	N			N			Ar					-459.77	-370.62	-244.19	-12.99	-2.29	-6.79
							O^2										

*Indicates the functional group involved in the specified interaction that is occurring

Table 3.29 gives the results of the solution phase optimization of the 1IYT conformer of β-amyloid interacting with dopamine. Four of the six systems have measureable binding interactions. Three have binding occurring at both Lys16 and Phe20 and two at His13 and His14. The binding energies are only slightly favourable, and the electrostatic energies are very similar to the van der Waals energies.

The results of the solution phase minimizations of dopamine interacting with the 1Z0Q conformer of Aβ are listed in Table 3.30. Only two of the six systems had measureable binding interactions, and both also had the least favourable binding energies of them. Van der Waals energies are more favourable than electrostatic energies, and two systems had potential interactions at both His13 and His14. There is also one system that presents potential binding at Leu17 and Phe20. The overall binding energies were only moderately favourable relative to the other systems.

3.4.4 Conclusions of Dopamine Interacting with β-Amyloid.

Overall the solution phase optimization of dopamine interacting with various conformations of β-amyloid indicates that binding interactions can occur. Some conformations showed less favourable energies of interactions than others, but measureable binding interactions were still formed. Cation-π interactions are slightly more prevalent than hydrogen bonding interactions, with very few π-π interactions formed. Potential interactions occur most often at both the His13 and His14 side chains in the **HH**Q**K** region, in eleven of the systems in total. Interactions at both Leu17 and Phe20 are most common in the LVFF region with nine of the twenty-four final systems demonstrating potential binding at these sites. Interactions can also occur at Lys16 and Phe20 overlapping both **HH**Q**K** and LVFF regions, as demonstrated in eight of the final systems.

As seen in the phenylalanine results, there does not appear to be a direct correlation between the number of measureable binding interactions and the energetic favourability of the systems. Despite this lack of correlation, these results suggest dopamine is capable of binding to and interacting with the β-amyloid peptide in both regions of interest. This implies that if dopamine levels are prevented from decreasing as part of the disease process, these higher dopamine concentrations could potentially prevent β-amyloid aggregation from occurring.

3.5 Tryptophan and β-Amyloid

Another amino acid identified in the virtual library for having the potential to interact with the **BB**X**B** region of Aβ is tryptophan. Tryptophan (Figure 3.4) is one of the

amino acids involved in protein synthesis and is only obtained through diet and not synthesized in the body [86]. Tryptophan can exert an effect on neurotransmitters such as dopamine (increased tryptophan levels result in increased dopamine levels) and its metabolites can also affect the activity of neurotransmitters [86].

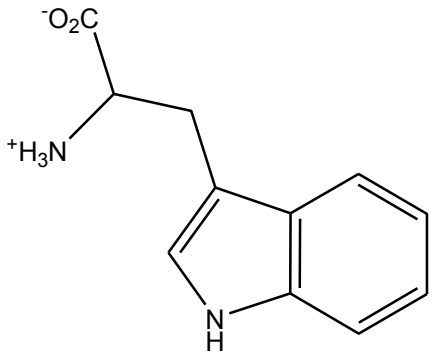

Figure 3.4 Tryptophan charged for physiological pH

Both L-tryptophan and D-tryptophan (Figure 3.5) were studied for their potential to interact with the **HH**Q**K** region of β-amyloid. *In silico* studies examined potential binding in both gas phase and solution phase environments using MOE [87].

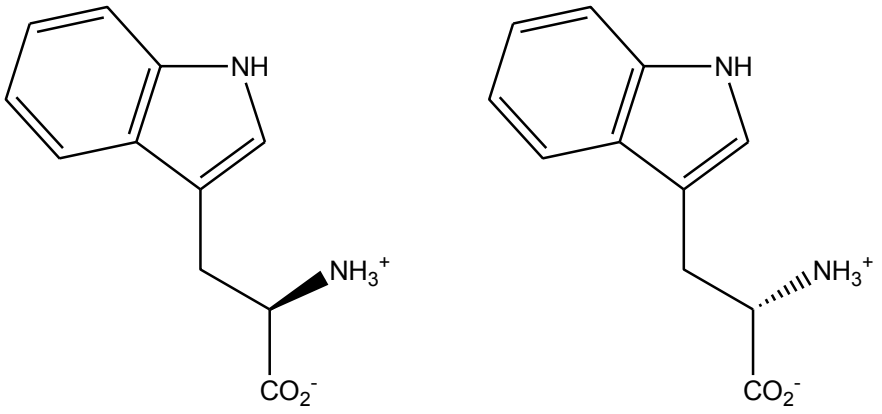

L-Tryptophan D-Tryptophan

Figure 3.5: L-tryptophan and D-tryptophan

3.5.1 Preparation of the β-Amyloid Conformers for Optimization

The protein structures were reoptimized as the optimizations being performed were taking place in the Molecular Operating Environment instead of QUANTA like the previous calculations, as MOE provided a more complete program environment for the studies [46, 87]. For each of the 1AMB, 1AMC, 1AML, and 1BA4 conformations, the histidine residues were protonated, the charges of the system were corrected, the backbone was constrained and the system was minimized [68, 69, 70, 71]. For the 1IYT conformer, the carboxylate groups needed to be deprotonated, then the system charges were corrected, the protein backbone constrained and minimization was performed [72]. For the 1Z0Q conformer, hydrogen atoms needed to be added to the whole system, and the terminal carboxylate residue needed to be fixed; system charges were fixed for the force field and then the protein backbone was constrained before optimization occurred [75]. The total energy for each conformation with the constrained protein backbone is summarized in Appendix 6 and these optimizations were performed in the gas phase.

3.5.2 Gas Phase Interactions Between D- and L-Tryptophan and β-Amyloid

D- and L-tryptophan were examined for their potential to bind to the **HH**Q**K** region of Aβ in the gas phase using the CHARMM22 force field [44, 47]. Initially optimizations were performed between the tryptophan stereoisomers and an isolated V**HH**Q**K**L segment of Aβ; however, these results were inconclusive. It seems likely that the lack of surrounding amino acids left the **HH**Q**K** region too exposed and provided less stability for interactions to occur. It was determined that the whole protein would therefore be best for the calculations.

3.5.2.1 Preparation of D- and L-Tryptophan for Optimization

D-Tryptophan and L-tryptophan were first constructed in a neutrally charged form in a gas phase environment. Each structure was then subjected to a systematic conformational search based on torsional rotations. The lowest energy conformer was selected for each stereoisomer and then charged for physiological pH before minimization. The overall energies for these molecules are summarized in Table 3.31. The total energies of these systems were identical, with very slight variations in the electrostatic and van der Waals energies.

Table 3.31: Gas phase energies of D- and L-tryptophan

	Total Energy (kcal/mol)
D-tryptophan	8.05
L-tryptophan	8.05

3.5.2.2 Selection of Initial Orientations for Optimization of Tryptophan and β-Amyloid

There are three regions on tryptophan capable of interacting with the charged region of **HH**Q**K** on Aβ: The indole group, the positively charged amino group and the negatively charged carboxylate group. Each system was set up such that either the carboxylate group and the indole, or the amino group and the indole were situated approximately 3.0 Å from two of the positively charged amino acids in **HH**Q**K**. Every possible initial orientation was determined, but there are spatial limitations for some of the protein conformations that prevented their usage.

3.5.2.3 Optimization of the Gas Phase Systems

In these gas phase optimizations the protein backbone was constrained for the systems to prevent structural collapse from occurring. Minimization in MOE follows the pattern detailed in Section 1.1.4.3. The final energies for each optimized system were noted as well as any binding interactions that were occurring. The total binding energy for each system was calculated using the following equation:

$$\Delta E_{bind} = E_{trpA\beta} - E_{trp} - E_{A\beta} \tag{3.9}$$

Here the overall binding energy, $\Delta E_{bind,}$ is the result of subtracting the individual energies of the optimized Aβ protein, $E_{A\beta}$, and tryptophan, E_{trp}, from the energy of the optimized system.

3.5.3 Gas Phase Results of the Optimization of D-Tryptophan and L-Tryptophan with β-Amyloid

The results of the gas phase optimizations of D- and L-tryptophan with Aβ are summarized in the following tables. For the sake of clarity, the indole group has been abbreviated to In, the amino group to N and the carboxylate group to C. Each table denotes the initial orientation in which the functional groups were located, the final orientation, the overall binding energy, and the number of measurable bonds that formed. The measured bonds have been split into hydrogen bonds, and aromatic type interactions: cation-π, and π-π. The amino acids are identified by their three letter abbreviation, and any interaction occurring outside of the **HH**Q**K** region is listed as "other".

Table 3.32 summarizes the results of the tryptophan stereoisomers with the 1AMB conformer of Aβ. L-tryptophan was capable of binding to **HH**Q**K** in more

situations than D-tryptophan. Measurable bonds formed in nine of the sixteen systems. The four systems where binding occurred at two or more of the **HH**Q**K** side chains were selected for optimization in the solution phase.

Table 3.33 summarizes the results of D- and L-tryptophan interacting with the 1AMC conformer of β-amyloid. Measurable bonds have formed in seven of the sixteen systems, and both D- and L-tryptophan are capable of binding to/interacting with multiple sites within the **HH**Q**K** region. Therefore, the four systems with the lowest energy and multiple binding interactions were selected for solution phase optimizations.

Table 3.32: The gas phase results of D- and L-tryptophan interacting with the 1AMB conformer of β-amyloid

	Initial Orientation				Final Orientation					ΔE_{bind}	Measureable Bonds	
	His13	His14	Gln15	Lys16	His13	His14	Gln15	Lys16	Other	(kcal/mol)	H-Bond	+-π
D-Tryptophan	In	C				C				-36.63	0	0
	C	In			C	In			In	-45.63	0	1
	In	N				N			In	-35.54	0	1
	N	In				In				-21.92	0	0
	C			In	In					-31.93	0	0
	In			C				C		-31.51	1	0
	N			In	C					-32.58	0	0
	In			N				C		-26.35	1	0
L-Tryptophan	In	C				C			In	-25.14	0	0
	C	In			C	In				-38.13	0	0
	In	N			N					-51.62	0	1
	N	In				In				-33.78	0	2
	C			In	C			In		-32.51	0	1
	In			C	In			C	C	-33.67	1	0
	N			In	-	-	-	-	-	-26.12	0	0
	In			N				C	In	-23.85	0	0

Table 3.33: The gas phase results of D- and L-tryptophan interacting with the 1AMC conformer of β-amyloid

	Initial Orientation				Final Orientation					ΔE_{bind}	Measureable Bonds	
	His13	His14	Gln15	Lys16	His13	His14	Gln15	Lys16	Other	(kcal/mol)	H-Bond	+-π
D-Tryptophan	N	In				In			N	-51.86	0	0
	In	N				N			C	-41.11	1	0
	C	In			C	In			In/C	-42.66	0	1
	In	C				C			In/C	-38.22	0	0
	N			In	-	-	-	-	-	-33.98	0	0
	In			N				C	In	-46.20	1	0
	C			In	C			In		-30.99	0	1
	In			C	In			C		-32.50	2	0
L-Tryptophan	N	In				In			C	-33.69	1	0
	In	N						N	In	-36.84	0	0
	C	In			C	In				-36.09	0	0
	In	C				C			In	-28.38	0	0
	N			In	C			In	In	-38.33	0	0
	In			N	-	-	-	-	-	-32.19	0	0
	C			In	C					-36.01	0	0
	In			C	In			C	C	-34.80	1	0

Table 3.34: The gas phase results of D- and L-tryptophan interacting with the 1AML conformer of β-amyloid

	Initial Orientation				Final Orientation					ΔE_{bind}	Measureable Bonds	
	His13	His14	Gln15	Lys16	His13	His14	Gln15	Lys16	Other	(kcal/mol)	H-Bond	π-π
D-Tryptophan	In	N			C				In	-42.15	0	0
	N	In			C				N	-43.21	0	0
	C	In			C				In/C	-40.08	0	0
	In	C				C			In/C	-45.90	0	0
	N			In	C					-25.35	0	0
	In			N				C		-21.77	1	0
	C			In	C					-29.18	1	0
	In			C	In			C		-33.84	0	0
L-Tryptophan	In	N			-	-	-	-	-	-28.59	0	0
	N	In			C				In	-44.01	0	2
	C	In			C				In	-44.62	0	2
	In	C			In	C			C	-50.11	0	0
	N			In	C					-22.99	0	0
	In			N	In					-12.44	0	0
	C			In	C			In		-32.24	0	0
	In			C				C		-30.62	1	0

Table 3.35: The gas phase results of D- and L-tryptophan interacting with the 1BA4 conformer of β-amyloid

	Initial Orientation				Final Orientation				ΔE_{bind}	Measureable Bonds	
	His13	His14	Gln15	Lys16	His13	His14	Gln15	Lys16	(kcal/mol)	H-Bond	+-π
D-Tryptophan	In	C				C			-21.32	0	0
	C	In			C	In			-29.10	0	0
	In	N			In	C			-27.24	0	1
	N	In			N	In			-23.94	0	2
L-Tryptophan	In	C			In			C	-36.06	1	0
	C	In			C	In			-30.62	0	0
	In	N			In				-24.94	0	0
	N	In				In			-24.10	0	0

Table 3.36: The gas phase results of D- and L-tryptophan interacting with the 1IYT conformer of β-amyloid

	Initial Orientation				Final Orientation					ΔE_{bind}	Measureable Bonds	
	His13	His14	Gln15	Lys16	His13	His14	Gln15	Lys16	Other	(kcal/mol)	H-Bond	+-π
D-Tryptophan	N	In			N	In			In	-23.57	0	2
	In	N			In					-19.12	0	0
	In	C			In					-28.52	0	0
	C	In			C	In				-31.07	0	0
	In			N	In				In	-25.89	0	0
	N			In				In		-12.77	0	0
	In			C	In			C		-30.26	1	0
	C			In	C					-30.04	0	0
L-Tryptophan	N	In			N	In			In	-25.20	0	1
	In	N			In					-38.01	0	0
	C	In			In				In	-43.10	0	0
	In	C			C					-24.82	0	0
	In			N	In			C		-32.00	0	0
	N			In	C			In		-27.06	1	1
	In			C				C	N	-38.01	0	0
	C			In	C			In		-29.87	0	0

Table 3.37: The gas phase results of D- and L-tryptophan interacting with the 1Z0Q conformer of β-amyloid

	Initial Orientation				Final Orientation					ΔE_{bind}	Measureable Bonds	
	His13	His14	Gln15	Lys16	His13	His14	Gln15	Lys16	Other	(kcal/mol)	H-Bond	+-π
D-Tryptophan	In	N			In				In	-26.71	0	0
	N	In			-	-	-	-	-	-21.14	0	0
	In	C				C				-29.97	0	0
	C	In			-	-	-	-	-	-31.37	0	0
	In			N	In					-21.36	0	0
	N			In	-	-	-	-	-	-22.68	0	0
	In			C	In			C		-26.10	2	0
	C			In	C			In		-27.00	0	0
L-Tryptophan	In	N			In			In		-27.66	0	0
	N	In			C			In		-36.78	0	0
	In	C				C				-32.04	0	0
	C	In			C	In				-32.76	1	0
	In			N	In			C		-25.05	1	0
	N			In	C/In					-23.32	0	0
	In			C	In			C		-25.53	1	0
	C			In	C					-30.36	0	0

The results in Table 3.34 summarize the results of tryptophan interacting with the 1AML conformer of Aβ. Measurable interactions only formed in five of the sixteen systems, and binding at two or more sites in **HH**Q**K** only occurred in three systems; these three plus one more system with the lowest overall energy were selected for solution phase optimization.

The interactions of tryptophan with the 1BA4 conformer of β-amyloid are summarized in Table 3.35 and show measured interactions in three of the eight systems. Multiple binding interactions at **HH**Q**K** were noted, particularly for D-tryptophan. The four systems with the most favourable energy as well as binding at two sites within **HH**Q**K** were selected for optimization in a solvated environment.

Table 3.36 demonstrates that when D- and L-tryptophan interact with the 1IYT conformer of Aβ, measured interactions only form in four of the sixteen systems. Both D-tryptophan and L-tryptophan demonstrated the capacity to bind to more than one residue in **HH**Q**K**, and from these the four with the lowest energies were selected for solution phase calculations.

The results of the gas phase optimizations of D-tryptophan and L-tryptophan with the 1Z0Q conformer are given in Table 3.37. Only four systems had measured interactions but seven systems demonstrated binding at two sites in **HH**Q**K**. L-tryptophan interacted more favourably with **HH**Q**K** than D-tryptophan, but both were capable of binding to the region. The four systems with multiple binding interactions and the lowest overall energies were selected for optimization. These selected configurations are summarized in Table 3.38

Table 3.38: Selected systems of D- and L-tryptophan for solution phase optimization

Interaction	Binding Energy (kcal/mol)	Interaction	Binding Energy (kcal/mol)
1AMB		1BA4	
D-HCHIn	-45.63	L-HInHC	-36.06
L-HCHIn	-38.13	L-HCHIn	-30.62
L-HInHQKC	-33.67	D-HCHIn	-29.10
L-HCHQKIn	-32.51	D-HInHN	-27.24
1AMC		1IYT	
D-HCHIn	-42.66	L-HInHQKN	-32.00
L-HNHQKIn	-38.33	D-HCHIn	-31.07
L-HCHIn	-36.09	D-HInHQKC	-30.26
L-HInHQKC	-34.79	L-HCHQKIn	-29.87
1AML		1Z0Q	
L-HInHC	-50.11	L-HNHIn	-36.78
D-HInHC	-45.90	L-HInHN	-32.76
D-HInHQKC	-33.84	L-HCHIn	-27.66
L-HCHQKIn	-32.24	D-HCHQKIn	-27.00

3.5.4 SOLUTION PHASE OPTIMIZATION OF D-TRYPTOPHAN AND L-TRYPTOPHAN WITH β-AMYLOID

From the optimized gas phase results of D-tryptophan and L-tryptophan with β-amyloid, four systems from each Aβ conformer were selected for solution phase optimization. Solution phase optimizations were performed in MOE using the CHARMM22 force field [48, 87].

3.5.4.1 SOLVATION AND MINIMIZATION SET-UP FOR D- AND L-TRYPTOPHAN AND β-AMYLOID

Each of the selected gas phase systems was used as the starting configuration for the solution phase optimizations. In MOE, there are several different solvation methods available to the user [87]. For these optimizations, explicit solvation was selected to surround the entire system in a box of water molecules. The size of the box varied for each system and could be adjusted as necessary to ensure that the system was completely surrounded by water, and periodic boundary conditions were placed on the box to prevent expansion of the system. Given the presence of water molecules, the protein backbone did not need to be constrained for these calculations. Before optimization of the solvated system, verification was made that the charges for the system were calculated appropriately for the force field.

The individual Aβ proteins conformations, D-tryptophan, and L-tryptophan were also optimized in a solvated environment to provide the energies necessary for calculating the binding energies occurring in the optimized systems. The tryptophan energies are summarized in Table 3.39, and the protein energies are given in Appendix 6.

Table 3.39: Energies of solvated D-tryptophan and L-tryptophan

	Energies (kcal/mol)		
	E_{tot}	E_{ele}	E_{vdw}
D-Tryptophan	13.48	11.07	-4.52
L-Tryptophan	12.95	9.29	-4.78

3.5.5 SOLUTION PHASE RESULTS OF D-TRYPTOPHAN AND L-TRYPTOPHAN INTERACTING WITH β-AMYLOID

The results of the solution phase optimizations of the optimized D-tryptophan-Aβ and L-tryptophan-Aβ systems have been summarized in tables for each conformation of β-amyloid. The tables summarize the results by including which conformation of tryptophan was involved in the interaction as well as giving the initial and final binding orientations. The energies of the optimized systems are listed and following are the three calculated energies: the total binding energy, electrostatic binding energy and van der Waals binding energy.

Any measureable interactions that occurred as a result of the optimization are indicated according to the following colour scheme: hydrogen bonds are coloured orange and cation-π interactions are green. Interaction occurring between tryptophan and the –CH_2- region of the amino acids (as opposed to the charged side chain) are shown in indigo. Interactions occurring outside the **HH**Q**K** region of interest are also indicated according to the amino acid side chain where binding may be occurring. The amino acids are represented in single letter notation with the respective site number on the protein chain and the tryptophan functional groups are represented by N, C, and In for the amino group, the carboxylate group, and the indole ring.

The final energies for the binding interactions were calculated using the energies listed in Table 3.39 via the following equations:

$$\Delta E_{tot} = E_{tot} - E_{A\beta} - E_{trp} \tag{3.10}$$

$$\Delta E_{ele} = E_{ele} - E_{eleA\beta} - E_{eletrp} \tag{3.11}$$

$$\Delta E_{vdw} = E_{vdw} - E_{vdwA\beta} - E_{vdwtrp} \tag{3.12}$$

where the energies of the solution phase optimized β-amyloid conformers and the tryptophan molecule were subtracted from the total energies of the optimized system for each of the overall total energy, the electrostatic energy and the van der Waals energy of the systems. These energies were calculated for the systems once the solvent had been removed and the protein backbone was constrained to better show the relationship between tryptophan and β-amyloid. Depending on the nature of the system being examined, the energies for D-tryptophan or L-tryptophan were used as required.

Each system was also examined for the bonding interactions that may have occurred between tryptophan and Aβ following optimization in the solution phase.

Tables 3.40 through 3.45 summarize the results of the solution phase optimization of D-tryptophan and L-tryptophan with the different conformers of β-amyloid.

Table 3.40: The solution phase results of D- and L-tryptophan interacting with the 1AMB conformer of β-amyloid

D- or L-Tryptophan		Tyr10	His13	His14	Gln15	Lys16	Leu17
D	Initial Orientation	In	C	In			
	Final Orientation		C	In			
	Total Energy =	-24.63 kcal/mol					
	van der Waals =	56.19 kcal/mol					
	electrostatic =	-236.28 kcal/mol					
	ΔE_{tot} =	-36.46 kcal/mol					
	ΔE_{vdw} =	-1.65 kcal/mol					
	ΔE_{ele} =	-33.76 kcal/mol					
L	Initial Orientation		C	In			
	Final Orientation	C	C	In			
	Total Energy =	-26.54 kcal/mol					
	van der Waals =	47.49 kcal/mol					
	electrostatic =	-238.70 kcal/mol					
	ΔE_{tot} =	-37.84 kcal/mol					
	ΔE_{vdw} =	-8.57 kcal/mol					
	ΔE_{ele} =	-35.93 kcal/mol					
L	Initial Orientation		C			In	
	Final Orientation		C			In	
	Total Energy =	-31.64 kcal/mol					
	van der Waals =	50.74 kcal/mol					
	electrostatic =	-229.32 kcal/mol					
	ΔE_{tot} =	-42.94 kcal/mol					
	ΔE_{vdw} =	-5.32 kcal/mol					
	ΔE_{ele} =	-26.55 kcal/mol					
L	Initial Orientation		In			C	C
	Final Orientation		In			C	
	Total Energy =	-1.82 kcal/mol					
	van der Waals =	57.45 kcal/mol					
	electrostatic =	-221.64 kcal/mol					
	ΔE_{tot} =	-13.12 kcal/mol					
	ΔE_{vdw} =	1.39 kcal/mol					
	ΔE_{ele} =	-18.87 kcal/mol					

Table 3.41: The solution phase results of D- and L-tryptophan interacting with the 1AMC conformer of β-amyloid

D- or L-Tryptophan		Tyr10	His13	His14	Gln15	Lys16	Leu17	Phe20
L	Initial Orientation		C			In	In	In
	Final Orientation		C			In	In	In
	Total Energy =	-39.29 kcal/mol						
	van der Waals =	56.91 kcal/mol						
	electrostatic =	-263.30 kcal/mol						
	ΔE_{tot} =	-25.02 kcal/mol						
	ΔE_{vdw} =	2.34 kcal/mol						
	ΔE_{ele} =	-38.03 kcal/mol						
L	Initial Orientation		C	I				
	Final Orientation	N	C	C				
	Total Energy =	-4.90 kcal/mol						
	van der Waals =	58.35 kcal/mol						
	electrostatic =	-233.26 kcal/mol						
	ΔE_{tot} =	9.37 kcal/mol						
	ΔE_{vdw} =	3.79 kcal/mol						
	ΔE_{ele} =	-7.98 kcal/mol						
D	Initial Orientation	In/C	C	In				
	Final Orientation	In/C		In				
	Total Energy =	-63.77 kcal/mol						
	van der Waals =	52.22 kcal/mol						
	electrostatic =	-266.21 kcal/mol						
	ΔE_{tot} =	-50.03 kcal/mol						
	ΔE_{vdw} =	-4.13 kcal/mol						
	ΔE_{ele} =	-41.20 kcal/mol						
L	Initial Orientation		In			C	C	
	Final Orientation		In			C	C	
	Total Energy =	-13.59 kcal/mol						
	van der Waals =	57.59 kcal/mol						
	electrostatic =	-247.56 kcal/mol						
	ΔE_{tot} =	0.68 kcal/mol						
	ΔE_{vdw} =	3.02 kcal/mol						
	ΔE_{ele} =	-22.29 kcal/mol						

Table 3.42: The solution phase results of D- and L-tryptophan interacting with the 1AML conformer of β-amyloid

D- or L-Tryptophan		Tyr10	Val12	His13	His14	Gln15	Lys16	Leu17
L	Initial Orientation	C		In	C			
	Final Orientation			In	C			C
	Total Energy =	102.01 kcal/mol						
	van der Waals =	81.00 kcal/mol						
	electrostatic =	-202.40 kcal/mol						
	ΔE_{tot} =	-37.24 kcal/mol						
	ΔE_{vdw} =	3.79 kcal/mol						
	ΔE_{ele} =	-38.50 kcal/mol						
D	Initial Orientation				C			C
	Final Orientation				C			
	Total Energy =	93.72 kcal/mol						
	van der Waals =	79.61 kcal/mol						
	electrostatic =	-208.03 kcal/mol						
	ΔE_{tot} =	-46.05 kcal/mol						
	ΔE_{vdw} =	0.63 kcal/mol						
	ΔE_{ele} =	-44.39 kcal/mol						
D	Initial Orientation			In			C	
	Final Orientation			In			C	
	Total Energy =	92.08 kcal/mol						
	van der Waals =	76.51 kcal/mol						
	electrostatic =	-198.97 kcal/mol						
	ΔE_{tot} =	-47.69 kcal/mol						
	ΔE_{vdw} =	-2.47 kcal/mol						
	ΔE_{ele} =	-35.32 kcal/mol						
L	Initial Orientation			C			In	
	Final Orientation		In	C			In	
	Total Energy =	109.42 kcal/mol						
	van der Waals =	84.74 kcal/mol						
	electrostatic =	-190.30 kcal/mol						
	ΔE_{tot} =	-29.82 kcal/mol						
	ΔE_{vdw} =	7.53 kcal/mol						
	ΔE_{ele} =	-26.39 kcal/mol						

Table 3.43: The solution phase results of D- and L-tryptophan interacting with the 1BA4 conformer of β-amyloid

D- or L-Tryptophan		His13	His14	Gln15	Lys16
L	Initial Orientation	In			C
	Final Orientation	In	C		
	Total Energy =	102.66	kcal/mol		
	van der Waals =	95.50	kcal/mol		
	electrostatic =	-202.78	kcal/mol		
	ΔE_{tot} =	-48.04	kcal/mol		
	ΔE_{vdw} =	8.46	kcal/mol		
	ΔE_{ele} =	-33.28	kcal/mol		
L	Initial Orientation	C	In		
	Final Orientation	C	In		
	Total Energy =	108.75	kcal/mol		
	van der Waals =	76.18	kcal/mol		
	electrostatic =	-195.24	kcal/mol		
	ΔE_{tot} =	-41.96	kcal/mol		
	ΔE_{vdw} =	-10.86	kcal/mol		
	ΔE_{ele} =	-25.73	kcal/mol		
D	Initial Orientation	C	In		
	Final Orientation	C	In		
	Total Energy =	100.33	kcal/mol		
	van der Waals =	87.50	kcal/mol		
	electrostatic =	-200.57	kcal/mol		
	ΔE_{tot} =	-52.15	kcal/mol		
	ΔE_{vdw} =	0.21	kcal/mol		
	ΔE_{ele} =	-31.06	kcal/mol		
D	Initial Orientation	In	C		
	Final Orientation	In	C		
	Total Energy =	81.25	kcal/mol		
	van der Waals =	80.64	kcal/mol		
	electrostatic =	-218.37	kcal/mol		
	ΔE_{tot} =	-71.23	kcal/mol		
	ΔE_{vdw} =	-6.66	kcal/mol		
	ΔE_{ele} =	-48.86	kcal/mol		

Table 3.44: The solution phase results of D- and L-tryptophan interacting with the 1IYT conformer of β-amyloid

D- or L-Tryptophan		Val12	His13	His14	Gln15	Lys16	Leu17
D	Initial Orientation		In			C	
	Final Orientation		In			C	
	Total Energy =	101.36 kcal/mol					
	van der Waals =	85.17 kcal/mol					
	electrostatic =	-213.84 kcal/mol					
	ΔE_{tot} =	11.26 kcal/mol					
	ΔE_{vdw} =	-14.09 kcal/mol					
	ΔE_{ele} =	7.23 kcal/mol					
L	Initial Orientation		In			C	
	Final Orientation		In			C	
	Total Energy =	95.63 kcal/mol					
	van der Waals =	84.52 kcal/mol					
	electrostatic =	-221.83 kcal/mol					
	ΔE_{tot} =	6.03 kcal/mol					
	ΔE_{vdw} =	-12.96 kcal/mol					
	ΔE_{ele} =	-0.51 kcal/mol					
L	Initial Orientation		C			In	
	Final Orientation	In	C			In	
	Total Energy =	75.74 kcal/mol					
	van der Waals =	87.28 kcal/mol					
	electrostatic =	-234.88 kcal/mol					
	ΔE_{tot} =	-13.86 kcal/mol					
	ΔE_{vdw} =	-10.20 kcal/mol					
	ΔE_{ele} =	-13.56 kcal/mol					
D	Initial Orientation		C	In			
	Final Orientation		C				
	Total Energy =	57.96 kcal/mol					
	van der Waals =	79.94 kcal/mol					
	electrostatic =	-248.45 kcal/mol					
	ΔE_{tot} =	-32.17 kcal/mol					
	ΔE_{vdw} =	-19.32 kcal/mol					
	ΔE_{ele} =	-27.38 kcal/mol					

Table 3.45: The solution phase results of D- and L-tryptophan interacting with the 1Z0Q conformer of β-amyloid

D- or L-Tryptophan		Gly9	His13	His14	Gln15	Lys16
L	Initial Orientation		C			In
	Final Orientation	C	C			In
	Total Energy =	120.09 kcal/mol				
	van der Waals =	76.61 kcal/mol				
	electrostatic =	-193.02 kcal/mol				
	ΔE_{tot} =	-14.64 kcal/mol				
	ΔE_{vdw} =	-5.16 kcal/mol				
	ΔE_{ele} =	-2.87 kcal/mol				
L	Initial Orientation		C	In		
	Final Orientation		C	In		
	Total Energy =	119.14 kcal/mol				
	van der Waals =	78.77 kcal/mol				
	electrostatic =	-205.75 kcal/mol				
	ΔE_{tot} =	-15.59 kcal/mol				
	ΔE_{vdw} =	-3.00 kcal/mol				
	ΔE_{ele} =	-15.61 kcal/mol				
L	Initial Orientation		In			In
	Final Orientation	In	In	In		
	Total Energy =	119.57 kcal/mol				
	van der Waals =	70.81 kcal/mol				
	electrostatic =	-205.36 kcal/mol				
	ΔE_{tot} =	-15.16 kcal/mol				
	ΔE_{vdw} =	-10.96 kcal/mol				
	ΔE_{ele} =	-15.22 kcal/mol				
D	Initial Orientation		C			In
	Final Orientation		C			In
	Total Energy =	150.45 kcal/mol				
	van der Waals =	82.82 kcal/mol				
	electrostatic =	-198.13 kcal/mol				
	ΔE_{tot} =	15.19 kcal/mol				
	ΔE_{vdw} =	-0.72 kcal/mol				
	ΔE_{ele} =	-8.24 kcal/mol				

Table 3.40 indicates in the solution phase both D- and L-tryptophan are capable of binding to multiple side chains within **HH**Q**K**. Interactions at His13-His14 and His13-Lys16 are favoured equally.

The results of the solution phase optimization of D-tryptophan and L-tryptophan with the 1AMC conformer of Aβ in Table 3.41 show binding can occur between L-tryptophan and multiple sites of **HH**Q**K**. The interaction with D-tryptophan only resulted in one interaction in **HH**Q**K**.

The results of Table 3.42 show that three of the four systems demonstrate multiple binding interactions with **HH**Q**K**, between both D-tryptophan and L-tryptophan with the 1AML conformer of β-amyloid. Interactions are favoured at His13-Lys16.

Table 3.43 shows that, in the case of D- and L-tryptophan being optimized in the solution phase with the 1BA4 conformer of Aβ, all four systems will bind to **HH**Q**K** at His13-His14.

Three of the four systems shown in Table 3.44 indicated binding at two sites on **HH**Q**K** between D- and L-tryptophan and the 1IYT conformer of β-amyloid. Binding preferentially favours interactions at His13-Lys16.

From the results of the optimization of D- and L-tryptophan with the 1Z0Q conformer of Aβ in a solvated environment in Table 3.45 it can be seen that all four systems show multiple binding interactions at **HH**Q**K**. The binding occurs equally at His13-His14 and His13-Lys16.

3.5.6 Conclusions of D- and L-Tryptophan Interacting with β-Amyloid

Overall it can be observed in a solution phase environment both D-tryptophan and L-tryptophan are capable of binding to and interacting with the **HH**Q**K** region of β-amyloid in its various conformations, but not nearly as well as observed for phenylalanine and dopamine.

In terms of binding site preference, it appears that interactions at His13-His14 and His13-Lys16 are favoured almost equally. Breaking this down into interactions occurring between each of the stereoisomers, interactions with L-tryptophan were favoured over D-tryptophan, but each interacted almost equally between His13-His14 and His13-Lys16. Hydrogen bond formation slightly exceeded the amount of cation-π interactions, but overall not many measureable bonds formed.

There are no discernable trends based on the binding energies of the systems for interactions with 1AMB, 1AMC, 1BA4 and 1IYT. In the case of interactions with the 1AML conformer, the energies of D-tryptophan interactions were more favourable, whereas the opposite was true in the case of the 1Z0Q conformer. The presence of measureable bonds does not impact the binding energies in a noticeable fashion: some systems with measured bonds had extremely favourable energies, whereas others had highly unfavourable energies. The electrostatic energies were more favourable than the van der Waals energies for the optimized systems.

Overall it can be concluded that both D- and L-tryptophan can bind to/interact with the highly charged **HH**Q**K** region of β-amyloid. L-Tryptophan is capable of forming more interactions than D-tryptophan, but both are significantly less efficacious at binding

relative to the earlier examined species. The *in vitro* assay of tryptophan also demonstrated its inability to inhibit β-amyloid aggregation.

3.6 TRYPTAMINE AND β-AMYLOID

Tryptamine (Figure 3.6) is one of the metabolites produced in the catabolism of tryptophan and plays a role in the brain as both a neuromodulator and neurotransmitter [86]. It was also identified in the endogenous library as being capable of interacting with the **HH**Q**K** region of β-amyloid.

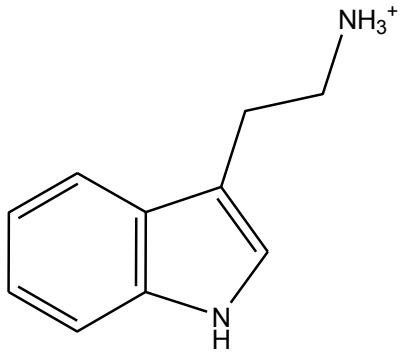

Figure 3.6: Tryptamine at physiological pH

The tryptamine molecule contains only two regions with which it can interact with **HH**Q**K**; the indole ring, and the amino group. Given the paucity of potential interactions with the **HH**Q**K** region, and the lack of results in the gas phase, the calculations were expanded to the EV**HH**Q**K** region as there is potential for interactions with the glutamic acid residue as well. Solution phase optimizations were also performed for all of the systems produced from the gas phase optimizations.

A model of tryptamine as charged for physiological pH was constructed and optimized in MOE after the charges were corrected for the CHARMM22 force field [48,

81]. The optimized energies of the six Aβ conformers are given in Appendix 6 and the energies of tryptamine are summarized in Table 3.46. Energies of the protein conformers were measured with a constrained protein backbone.

Table 3.46: Gas phase energies of tryptamine

	Energies (kcal/mol)		
	E_{tot}	E_{ele}	E_{vdw}
Tryptamine	13.04	6.04	4.70

3.6.1 Gas Phase Interactions Between Tryptamine and β-Amyloid

Gas phase optimizations of tryptamine and Aβ were performed in MOE using the CHARMM22 force field and examined for potential interactions that could occur with the EV**HH**Q**K** region [48, 81].

3.6.1.1 Selection of Initial Orientations for Gas Phase Optimization

Each system was set up such that the indole ring and the amino group of tryptamine were oriented approximately 3.0 Å away from two of the charged amino acid side chains in the EV**HH**Q**K** region. Every possible arrangement was attempted; however, some interactions could not be tested as the amino acid side chains were either too far apart, or were on opposite sides of the protein chain.

3.6.1.2 Optimization of the Gas Phase Systems

For each system being optimized, the protein backbone was constrained to prevent self interactions, and the system was then subjected to minimization. These optimized systems were saved for the solution phase optimizations, the energies were calculated, and they were examined for measureable binding interactions that may have occurred between tryptamine and the β-amyloid protein.

The relative favourability was determined by calculating the binding energy of each system using the following formulas:

$$\Delta E_{tot} = E_{tot} - E_{A\beta} - E_{tpm} \tag{3.13}$$

$$\Delta E_{vdw} = E_{vdw} - E_{vdwA\beta} - E_{vdwtpm} \tag{3.14}$$

$$\Delta E_{ele} = E_{ele} - E_{eleA\beta} - E_{eletpm} \tag{3.15}$$

The total binding energy, ΔE_{tot}, the van der Waal energy, ΔE_{vdw}, and the electrostatic energy, ΔE_{ele}, were each calculated by subtracting the energies of the individually optimized Aβ conformer and tryptamine from the energy of the optimized system.

3.6.2 Gas Phase Results of Tryptamine Interacting with β-Amyloid

The results of the gas phase optimizations are summarized in the following table. The indole and amino groups are represented by In and N, respectively, and the initial and final orientations are given, with the amino acids identified by their single letter abbreviations. The calculated binding energies are also summarized for each interaction. The orange coloured squares represent hydrogen bond formation, and light blue indicates a π-π interaction.

Table 3.47: The gas phase results of tryptamine interacting with β-amyloid

Conformer	Initial Orientation						Final Orientation							ΔE_{tot}	ΔE_{vdv}	ΔE_{ele}
	E11	V12	H13	H14	Q15	K16	E11	V12	H13	H14	Q15	K16	Other	(kcal/mol)	(kcal/mol)	(kcal/mol)
1AMB			In	N					In	N/In*			In	-11.05	-8.18	-7.53
			N	In						In			N	-17.91	-4.67	-16.19
			N			In	-	-	-	-	-	-	-	-28.39	-2.22	-24.82
			In			N			In				In	-17.62	-4.12	-16.23
	N			In			N							-36.19	1.99	-43.87
	In			N			In			N				-9.89	-4.15	-8.58
	N		In				N/In*		In				In	-43.82	-13.42	-29.53
	In		N				In		In				N	-14.02	-8.79	-5.67
1AMC			N	In					In				N	-2.45	-3.14	-1.67
			In	N					In				In	-34.29	-8.55	-28.06
			N			In			In				In	-12.27	-0.44	-15.71
			In			N			In					-16.76	1.34	-20.82
	N			In			N			In				-35.60	-1.48	-34.50
	In			N			In							-2.62	-1.48	-1.30
1AML			In	N									In	4.44	-2.67	3.94
			N	In						In			In	-7.95	-3.37	-6.34
			N			In	-	-	-	-	-	-	-	-5.25	-1.18	-5.41
			In			N	-	-	-	-	-	-	-	-7.96	1.75	-14.15
	N			In			N			In	In		In/N*	-26.95	-10.10	-22.93
	In			N			In			In				-9.66	-7.50	-4.61
1BA4			N	In			-	-	-	-	-	-	-	-0.74	0.02	-1.15
			In	N					In					-1.70	-1.62	-0.64
1IYT			N	In			-	-	-	-	-	-	-	-1.54	0.71	-3.47
			In	N			-	-	-	-	-	-	-	-8.64	-2.36	-5.73
			In			N	-	-	-	-	-	-	-	-1.71	-0.62	-1.19
			N			In	-	-	-	-	-	-	-	-4.35	-1.59	-5.07
	N			In			N			In				-30.87	-3.79	-28.01
	In			N			In			N			N	-24.91	-7.96	-15.83
1Z0Q			In	N									In*	6.64	-4.50	8.91
			N	In						In				12.26	-1.93	12.51
			In			N	-	-	-	-	-	-	-	-5.14	-3.33	-5.98
			N			In	-	-	-	-	-	-	-	0.97	-0.46	-0.01
	N			In			N							-40.26	-3.27	-37.99
	In			N			In						N	-31.11	-1.07	-31.01

* indicates interaction is occurring with the $-CH_2-$ chain of the amino acid

The gas phase results showed only one interaction occurring within **HH**Q**K**, and eight within EV**HH**Q**K**. As there were few discernable trends that would allow for identification of systems that should be optimized in the solution phase, all systems were selected to see the effect of the presence of solvent on these systems.

3.6.3 Solution Phase Results for Tryptamine Interacting with β-Amyloid

Upon completion of the gas phase optimizations all of the gas phase systems were selected for solution phase minimizations. Each system was solvated with a box of water molecules large enough to completely surround the system with an 8.0 Å margin.

Results of the solution phase optimizations of the tryptamine-Aβ systems have been summarized in tables for each conformation of β-amyloid. The initial and final binding orientations are given along with three calculated energies: the total binding energy, electrostatic binding energy and van der Waals binding energy. The amino acids are indicated by their three-letter abbreviations and any interactions that occurred between tryptamine and amino acids outside of EV**HH**Q**K** are also identified. Single letter amino acid abbreviations were used in Table 3.51.

Any measureable binding interactions that occurred are indicated according to the following colour scheme: hydrogen bonds are coloured orange, π-π interactions are light blue and π-H interactions are in pink. Interactions occurring between tryptamine and the $–CH_2-$ region of the amino acid are indicated in indigo, while interactions with C=O of the protein backbone are purple; lime green indicates interactions with the –CH- of the protein backbone and yellow interactions with –NH- of the protein backbone.

The final energies for the binding interactions were calculated using the energies listed in Table 3.48 and Appendix 6 using equations 3.13-3.15. The only difference being that the energies used are those of the solvated systems where the

solvent has been removed and the protein backbone has been constrained for β-amyloid.

Table 3.48: Total energies of tryptamine calculated in a solvated environment

	Energies (kcal/mol)		
	E_{tot}	E_{ele}	E_{vdw}
Tryptamine	17.44	7.22	4.95

The results of the solution phase optimizations are summarized in Tables 3.49-3.54. The data shows only one system where binding at two sites (His13-His14) occurs within the **HH**Q**K** region upon solvation. When looking at binding occurring within EV**HH**Q**K**, only six systems showed binding at two sites, Glu11-His14. Binding energies demonstrate no correlation to the number of measurable binding interactions.

Table 3.49: The solution phase results of tryptamine interacting with the 1AMB conformer of β-amyloid

	Tyr10	Glu11	Val12	His13	His14	Gln15	Lys16	Glu11	Val12	His13	His14	Gln15	Lys16	Leu17
Initial Orientation	In			In	N					In				In
					In									
Final Orientation	In			In	In									In
					In									
Total =	-3.10 kcal/mol							-9.75 kcal/mol						
van der Waals =	41.87 kcal/mol							64.52 kcal/mol						
Electrostatic =	-207.27 kcal/mol							-231.13 kcal/mol						
ΔE_{tot} =	-20.11 kcal/mol							-26.77 kcal/mol						
ΔE_{vdw} =	-12.17 kcal/mol							10.48 kcal/mol						
ΔE_{ele} =	-5.26 kcal/mol							-29.13 kcal/mol						
Initial Orientation	N			In				-	-	-	-	-	-	-
Final Orientation	N			In				-	-	-	-	-	-	-
	In													
Total =	5.04 kcal/mol							-33.49 kcal/mol						
van der Waals =	58.57 kcal/mol							50.28 kcal/mol						
Electrostatic =	-203.96 kcal/mol							-238.97 kcal/mol						
ΔE_{tot} =	-11.98 kcal/mol							-50.51 kcal/mol						
ΔE_{vdw} =	4.53 kcal/mol							-3.76 kcal/mol						
ΔE_{ele} =	-1.96 kcal/mol							-36.97 kcal/mol						
Initial Orientation	N	In			In			In			N			
Final Orientation		In			N			In			N			
					In									
Total =	-1.54 kcal/mol							-0.45 kcal/mol						
van der Waals =	50.48 kcal/mol							44.52 kcal/mol						
Electrostatic =	-206.44 kcal/mol							-207.31 kcal/mol						
ΔE_{tot} =	-18.46 kcal/mol							-17.47 kcal/mol						
ΔE_{vdw} =	-3.56 kcal/mol							-9.52 kcal/mol						
ΔE_{ele} =	-4.44 kcal/mol							-5.31 kcal/mol						
Initial Orientation	In	In		In				N						
		N												
Final Orientation	In	In			In			N						
		N						In						
Total =	-41.12 kcal/mol							-38.34 kcal/mol						
van der Waals =	40.45 kcal/mol							47.99 kcal/mol						
Electrostatic =	-227.05 kcal/mol							-250.21 kcal/mol						
ΔE_{tot} =	-58.13 kcal/mol							-55.35 kcal/mol						
ΔE_{vdw} =	-13.59 kcal/mol							-6.05 kcal/mol						
ΔE_{ele} =	-25.05 kcal/mol							-48.21 kcal/mol						

Table 3.50: The solution phase results of tryptamine interacting with the 1AMC conformer of β-amyloid

	Tyr10	Glu11	Val12	His13	His14	Gln15	Lys16	Tyr10	Glu11	Val12	His13	His14	Gln15	Lys16	Leu17
Initial Orientation	In	In			In			N				In			
Final Orientation					In			N				In			
					In										
Total =	-56.16 kcal/mol							-4.34 kcal/mol							
van der Waals =	29.55 kcal/mol							49.51 kcal/mol							
Electrostatic =	-248.38 kcal/mol							-211.76 kcal/mol							
ΔE_{tot} =	-53.65 kcal/mol							-1.83 kcal/mol							
ΔE_{vdw} =	-30.49 kcal/mol							-10.53 kcal/mol							
ΔE_{ele} =	-27.18 kcal/mol							9.43 kcal/mol							
Initial Orientation	In											In			In
Final Orientation	In											In			In
Total =	-28.07 kcal/mol							-3.74 kcal/mol							
van der Waals =	44.70 kcal/mol							55.06 kcal/mol							
Electrostatic =	-236.89 kcal/mol							-243.20 kcal/mol							
ΔE_{tot} =	-25.56 kcal/mol							-1.23 kcal/mol							
ΔE_{vdw} =	-15.34 kcal/mol							-4.98 kcal/mol							
ΔE_{ele} =	-15.69 kcal/mol							-22.01 kcal/mol							
Initial Orientation	In								N			In			
Final Orientation	In				N				N			In			
Total =	-1.11 kcal/mol							-34.49 kcal/mol							
van der Waals =	53.92 kcal/mol							54.12 kcal/mol							
Electrostatic =	-226.74 kcal/mol							-253.09 kcal/mol							
ΔE_{tot} =	1.41 kcal/mol							-31.98 kcal/mol							
ΔE_{vdw} =	-6.12 kcal/mol							-5.92 kcal/mol							
ΔE_{ele} =	-5.54 kcal/mol							-31.89 kcal/mol							

Table 3.51: The solution phase results of tryptamine interacting with the 1AML conformer of β-amyloid

	R5	S8	Y10	E11	V12	H13	H14	Q15	K16	R5	H6	D7	S8	E11	V12	H13	H14	Q15	K16	L17	V18	I31
Initial Orientation			In														In					In
Final Orientation			In														In			In		In
Total =	153.16 kcal/mol									142.91 kcal/mol												
van der Waals =	81.80 kcal/mol									62.71 kcal/mol												
Electrostatic =	-163.33 kcal/mol									-158.96 kcal/mol												
ΔE_{tot} =	3.53 kcal/mol									-6.18 kcal/mol												
ΔE_{vdw} =	11.49 kcal/mol									-7.60 kcal/mol												
ΔE_{ele} =	-13.28 kcal/mol									-8.91 kcal/mol												
Initial Orientation	-	-	-	-	-	-	-	-	-	-	-	-	-	-	-	-	-	-	-	-	-	-
Final Orientation	-	-	-	-	-	-	-	-	-	-	-	-	-	-	-	-	-	-	-	-	-	-
Total =	137.88 kcal/mol									156.15 kcal/mol												
van der Waals =	72.06 kcal/mol									75.19 kcal/mol												
Electrostatic =	-169.84 kcal/mol									-153.81 kcal/mol												
ΔE_{tot} =	-11.75 kcal/mol									6.52 kcal/mol												
ΔE_{vdw} =	1.75 kcal/mol									4.87 kcal/mol												
ΔE_{ele} =	-19.79 kcal/mol									-3.76 kcal/mol												
Initial Orientation				In			In				N	N	N	N			In	N			In	
Final Orientation	In	In		In						In	N	N	N	In			In				In	
														N								
Total =	142.76 kcal/mol									115.91 kcal/mol												
van der Waals =	70.39 kcal/mol									58.84 kcal/mol												
Electrostatic =	-168.70 kcal/mol									-162.70 kcal/mol												
ΔE_{tot} =	-6.85 kcal/mol									-33.72 kcal/mol												
ΔE_{vdw} =	0.08 kcal/mol									-11.47 kcal/mol												
ΔE_{ele} =	-18.65 kcal/mol									-12.64 kcal/mol												

Table 3.52: The solution phase results of tryptamine interacting with the 1BA4 conformer of β-amyloid

1BA4	Glu11	Val12	His13	His14	Gln15	Lys16	Glu11	Val12	His13	His14	Gln15	Lys16
Initial Orientation			In				-	-	-	-	-	-
Final Orientation			In				-	-	-	-	-	-
Total =	113.32 kcal/mol						87.63 kcal/mol					
van der Waals =	69.64 kcal/mol						81.15 kcal/mol					
Electrostatic =	-184.53 kcal/mol						-206.10 kcal/mol					
ΔE_{tot} =	-16.18 kcal/mol						-41.86 kcal/mol					
ΔE_{vdw} =	-3.88 kcal/mol						7.62 kcal/mol					
ΔE_{ele} =	-7.67 kcal/mol						-29.24 kcal/mol					

Table 3.53: The solution phase results of tryptamine interacting with the 1IYT conformer of β-amyloid

1IYT	Glu11	Val12	His13	His14	Gln15	Lys16	Glu11	Val12	His13	His14	Gln15	Lys16
Initial Orientation	-	-	-	-	-	-	-	-	-	-	-	-
Final Orientation	-	-	-	-	-	-				In		
Total =	119.92 kcal/mol						128.90 kcal/mol					
van der Waals =	96.29 kcal/mol						87.19 kcal/mol					
Electrostatic =	-190.09 kcal/mol						-190.57 kcal/mol					
ΔE_{tot} =	8.22 kcal/mol						17.20 kcal/mol					
ΔE_{vdw} =	23.81 kcal/mol						14.72 kcal/mol					
ΔE_{ele} =	4.00 kcal/mol						3.51 kcal/mol					
Initial Orientation	-	-	-	-	-	-	-	-	-	-	-	-
Final Orientation	-	-	-	-	-	-	-	-	-	-	-	-
Total =	106.61 kcal/mol						110.69 kcal/mol					
van der Waals =	74.87 kcal/mol						84.59 kcal/mol					
Electrostatic =	-190.76 kcal/mol						-205.12 kcal/mol					
ΔE_{tot} =	-5.09 kcal/mol						-1.01 kcal/mol					
ΔE_{vdw} =	2.40 kcal/mol						12.12 kcal/mol					
ΔE_{ele} =	3.32 kcal/mol						-11.04 kcal/mol					
Initial Orientation	In			N			N			In		
Final Orientation	In			N			N			In		
							In					
Total =	88.80 kcal/mol						94.11 kcal/mol					
van der Waals =	80.76 kcal/mol						86.80 kcal/mol					
Electrostatic =	-220.01 kcal/mol						-214.03 kcal/mol					
ΔE_{tot} =	-22.90 kcal/mol						-17.59 kcal/mol					
ΔE_{vdw} =	8.29 kcal/mol						14.33 kcal/mol					
ΔE_{ele} =	-25.93 kcal/mol						-31.89 kcal/mol					

Table 3.54: The solution phase results of tryptamine interacting with the 1IZ0Q conformer of β-amyloid

1Z0Q	Gly9	Ty10	Glu11	Val12	His13	His14	Gln15	Lys16	Glu22	Glu11	Val12	His13	His14	Gln15	Lys16
Initial Orientation	In	In											In		
Final Orientation	In				In					-	-	-	-	-	-
Total =	153.47 kcal/mol									134.09 kcal/mol					
van der Waals =	76.24 kcal/mol									78.16 kcal/mol					
Electrostatic =	-175.42 kcal/mol									-196.36 kcal/mol					
ΔE_{tot} =	-5.48 kcal/mol									-24.86 kcal/mol					
ΔE_{vdw} =	-17.34 kcal/mol									-15.42 kcal/mol					
ΔE_{ele} =	10.62 kcal/mol									-10.32 kcal/mol					
Initial Orientation	-	-	-	-	-	-	-	-	-	-	-	-	-	-	-
Final Orientation	-	-	-	-	-	-	-	-	-	-	-	-	-	-	-
Total =	140.80 kcal/mol									160.64 kcal/mol					
van der Waals =	71.96 kcal/mol									82.49 kcal/mol					
Electrostatic =	-186.10 kcal/mol									-170.43 kcal/mol					
ΔE_{tot} =	-18.15 kcal/mol									1.69 kcal/mol					
ΔE_{vdw} =	-21.62 kcal/mol									-11.09 kcal/mol					
ΔE_{ele} =	-0.06 kcal/mol									15.61 kcal/mol					
Initial Orientation			In						N	N					
Final Orientation			In						N	N					
Total =	128.35 kcal/mol									100.24 kcal/mol					
van der Waals =	82.40 kcal/mol									81.90 kcal/mol					
Electrostatic =	-209.27 kcal/mol									-220.08 kcal/mol					
ΔE_{tot} =	-30.61 kcal/mol									-58.71 kcal/mol					
ΔE_{vdw} =	-11.18 kcal/mol									-11.68 kcal/mol					
ΔE_{ele} =	-23.24 kcal/mol									-34.04 kcal/mol					

3.6.4 Conclusions of Tryptamine Interacting with β-Amyloid

The results of the optimization of tryptamine and β-amyloid in the gas phase and solution phase indicated very few interactions within the region of Aβ associated with misfolding. Roughly one quarter of the systems demonstrated binding at two sites within EV**HH**Q**K**, which when compared to the binding seen with the other molecules studied so far, is not a lot. While tryptamine demonstrates a small potential to interact with β-amyloid to prevent misfolding, it is not as desirable a target as the other endogenous molecules examined thus far. As well, the results of *in vitro* assays further suggest that tryptamine has no effect to prevent Aβ aggregation from progressing.

3.7 3-Hydroxyanthranilic Acid and β-Amyloid

Another tryptophan metabolite identified in the search for an endogenous molecule capable of interacting with **HH**Q**K** is 3-hydroxyanthranilic acid (3HAA).

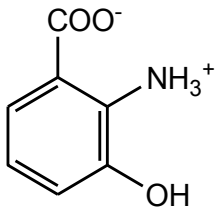

Figure 3.7: 3-hydroxyanthranilic acid at physiological pH

3-hydroxyanthranilic acid has demonstrated activity in suppressing glial cytokine and chemokine expression, resulting in anti-inflammatory effects as well as reducing the amount of neuronal death caused by these cytokines [89]. It was also discovered that 3HAA can stimulate the production of an anti-oxidant enzyme, hemeoxygenase-1, that also has anti-inflammatory and cytoprotective properties [89]. This molecule therefore

presents itself as a molecule of interest in preventing Aβ-aggregation, given it already exhibits other neuroprotective effects on the brain.

3.7.1 GAS PHASE INTERACTIONS BETWEEN 3-HYDROXYANTHRANILIC ACID AND β-AMYLOID

Gas phase optimizations of 3HAA and β-amyloid covered three regions of β-amyloid. First, the potential interactions between the acid and the **HH**Q**K** region of Aβ were examined, which was then expanded to include EV**HH**Q**K**, followed by the LVFF region. The functional groups present on 3-hydroxyanthranilic acid give it the potential to be able to interact with all of these regions of β-amyloid. These optimizations were all performed in MOE using the CHARMM22 force field [48, 87].

3.7.1.1 PREPARATION OF 3-HYDROXYANTHRANILIC ACID FOR OPTIMIZATION

The neutral structure of 3HAA was subjected to a systematic conformational search in MOE, whereupon the lowest energy structure obtained was charged for physiological pH and minimized. The energy of the system is given in Table 3.55 with the Aβ energies for the structures used being the same as those listed in Appendix 6.

Table 3.55: Gas phase energy of 3-hydroxyanthranilic acid

	Total Energy (kcal/mol)
3-hydroxyanthranilic acid	-4.71

3.7.1.2 SELECTION OF INITIAL ORIENTATIONS FOR OPTIMIZATION OF 3HAA AND β-AMYLOID

Every possible orientation of 3HAA interacting with two of the amino acid side chains in **HH**Q**K**, LVFF or EV**HH**Q**K** was attempted. Some interactions were not

possible based on the small size of the acid, as well as the fact that some of the side chains were on opposite sides of the protein. The regions of 3HAA available for interaction are the aromatic ring, the positively charged amino group, the negatively charged carboxylate group, and the hydroxyl group.

3.7.1.3 Optimization of the Gas Phase Systems

Each of the functional groups of 3-hydroxyanthranilic acid was situated in every available combination at a distance of 3.0 Å from the amino acid side chains and optimized with the protein backbone constrained to prevent system collapse. The total binding energy for each system was calculated using the following equation:

$$\Delta E_{bind} = E_{3HAAA\beta} - E_{3HAA} - E_{A\beta} \tag{3.16}$$

The overall binding energy of the system, $\Delta E_{bind,}$ is the result of subtracting the contributions of the individual 3HAA molecule, E_{3HAA}, and Aβ conformer, $E_{A\beta}$, from the overall binding energy of the system, $E_{3HAAA\beta}$. For these calculations, the energies used were calculated with a constrained protein backbone to focus solely on contributions from the interactions between 3HAA and Aβ.

3.7.2 Gas Phase Results of the Optimization of 3-hydroxyanthranilic acid with β-Amyloid

The following tables summarize the gas phase results of 3-hydroxyanthranilic acid interacting with three regions of β-amyloid, first **HH**Q**K**, then EV**HH**Q**K**, and finally LVFF. Each table summarizes the initial orientation of 3HAA and the final binding orientations with Ar representing the aromatic ring, N the positively charged amino group, C the negatively charged carboxylate group, and O the hydroxyl group. The

amino acid residues are given in their single letter abbreviations, and interactions outside the area of interest are listed under the column X. The binding energy of the system, as well as any measureable bonds that formed, are also given.

Table 3.56: The gas phase results of 3-hydroxyanthranilic acid interacting with the HHQK region of the 1AMB conformer of β-amyloid

Initial Orientation				Final Orientation					ΔE_{bind}	Measured
H13	H14	Q15	K16	H13	H14	Q15	K16	X	(kcal/mol)	Bonds
C	N			C	N			N	-48.41	1
N	C			C				C	-50.37	0
N	O			C	Ar			N	-43.29	2
O	N			O/Ar	N			N	-26.34	1
C	O			C	Ar			Ar	-49.23	2
O	C			O/Ar	C/Ar			N	-41.09	0
Ar	C				C			Ar	-26.14	0
C	Ar			C	Ar			Ar	-38.18	0
Ar	O				Ar			Ar	-43.02	0
O	Ar				Ar			O	-15.62	0
Ar	N			C	C/N			Ar	-47.17	0
N	Ar			C	Ar			N	-56.83	0
N			O	-	-	-	-	-	-41.54	0
O			N	-	-	-	-	-	-26.38	0
C			N	C			C		-29.14	1
N			C	N/C			C		-24.94	1
C			O	C					-22.46	0
O			C				C	C/Ar	-39.15	2
C			Ar	C			Ar		-16.96	0
Ar			C	Ar			C	C	-25.29	2
Ar			O	C/Ar					-44.39	0
O			Ar				C	Ar	-44.45	0
N			Ar	C					-38.67	0
Ar			N	C/Ar			C	C/Ar	-48.68	1

Table 3.57: The gas phase results of 3-hydroxyanthranilic acid interacting with the HHQK region of the 1AMC conformer of β-amyloid

Initial Orientation				Final Orientation					ΔE_{bind}	Measured
H13	H14	Q15	K16	H13	H14	Q15	K16	X	(kcal/mol)	Bonds
N	C			C	C			N	-42.19	1
C	N			C	Ar			N	-41.70	1
N	O			C	Ar			N/O	-30.72	0
O	N			N				O	-25.01	0
O	C				C				-20.40	0
C	O			C	Ar			Ar	-39.28	1
Ar	C			C				Ar	-52.68	0
C	Ar				C/N			C/O/Ar	-42.59	0
O	Ar				Ar			O/Ar	-16.91	0
Ar	O							O	-22.23	0
N	Ar				Ar			C/O/N/Ar	-34.50	0
Ar	N				Ar			C/Ar	-39.14	1
C			N	C			C		-28.94	1
N			C	C			C	C	-26.73	1
N			O	-	-	-	-	-	-27.58	0
O			N	-	-	-	-	-	9.52	0
C			O	C					-36.34	0
O			C	O/Ar			C	C	-31.99	2
C			Ar	C					-36.51	0
Ar			C	Ar			C		-24.55	1
Ar			O	C			C		-33.14	1
O			Ar				C		-30.19	1
N			Ar				C/Ar		-27.52	1
Ar			N	C/Ar			C	C/Ar	-31.15	1

Table 3.58: The gas phase results of 3-hydroxyanthranilic acid interacting with the HHQK region of the 1AML conformer of β-amyloid

Initial Orientation				Final Orientation					ΔE_{bind}	Measured
H13	H14	Q15	K16	H13	H14	Q15	K16	X	(kcal/mol)	Bonds
O	N			-	-	-	-	-	-3.63	0
N	O							C/Ar	-10.10	0
N	C			Ar					-45.58	0
C	N			C				Ar	-37.42	0
C	O			C	Ar			C/Ar	-39.23	0
O	C			O	C/Ar			C/Ar	-20.31	0
C	Ar			C					-41.98	0
Ar	C			-	-	-	-	-	-32.83	0
Ar	O				Ar			Ar	-17.02	0
O	Ar			-	-	-	-	-	-7.82	0
N	Ar				Ar			C/Ar	-13.08	0
Ar	N							O/Ar	-0.59	0
O			N				C	O/Ar	-26.16	0
N			O	C				C/N	-35.39	2
N			C	O/N			C		-8.90	0
C			N	C				C/Ar	-36.25	0
O			C				C		-17.15	0
C			O	C			Ar	Ar	-27.26	2
Ar			O					Ar	-16.73	0
O			Ar	O			C		-16.38	0
Ar			N				C		-36.08	0
N			Ar	C					-30.67	0
Ar			C				C		-20.41	1
C			Ar	C					-30.85	0

Table 3.59: The gas phase results of 3-hydroxyanthranilic acid interacting with the HHQK region of the 1BA4 conformer of β-amyloid

Initial Orientation				Final Orientation				ΔE_{bind}	Measured
H13	H14	Q15	K16	H13	H14	Q15	K16	(kcal/mol)	Bonds
O	C			Ar	C			-30.56	0
C	O			C	Ar			-20.70	0
N	C			C/Ar				-30.48	0
C	N			C				-28.75	0
O	N				C			-30.32	0
N	O			-	-	-	-	-21.17	0
Ar	O			-	-	-	-	-27.32	0
O	Ar				C			-23.72	0
Ar	C			C/Ar				-29.97	0
C	Ar			C	Ar			-34.46	0
Ar	N				C			-29.30	0
N	Ar			C	C/Ar			-42.30	0

Table 3.60: The gas phase results of 3-hydroxyanthranilic acid interacting with the HHQK region of the 1IYT conformer of β-amyloid

Initial Orientation				Final Orientation					ΔE_{bind}	Measured
H13	H14	Q15	K16	H13	H14	Q15	K16	X	(kcal/mol)	Bonds
O	N							O	-22.98	0
N	O			C/Ar					-28.42	0
N	C			N					-15.33	1
C	N			C					-40.76	0
O	C			Ar	C			Ar	-26.76	2
C	O			C/Ar	O/Ar			Ar	-33.26	0
O	Ar			-	-	-	-	-	-21.46	0
Ar	O			Ar					-30.41	0
Ar	C			Ar					-22.06	0
C	Ar			C					-30.41	0
Ar	N			Ar				C/O	-33.55	2
N	Ar			Ar	Ar			Ar	-32.51	1
C			N	C					-22.39	0
N			C				C		-26.38	0
N			O	C/Ar			O		-26.83	0
O			N				N	N	-17.11	1
C			O	C					-32.56	0
O			C	Ar			C		-27.42	0
N			Ar	C					-24.64	0
Ar			N	-	-	-	-	-	-29.02	0
Ar			C	Ar			C		-25.89	0
C			Ar	C			Ar		-27.29	0
Ar			O	C					-28.50	0
O			Ar	Ar			C		-24.93	1

Table 3.61: The gas phase results of 3-hydroxyanthranilic acid interacting with the HHQK region of the 1Z0Q conformer of β-amyloid

Initial Orientation				Final Orientation					ΔE_{bind}	Measured
H13	H14	Q15	K16	H13	H14	Q15	K16	X	(kcal/mol)	Bonds
O	N			O	N			O	-9.38	0
N	O			C/N	Ar			N/O	-31.74	0
C	N			C					-29.86	0
N	C			N	C			C	-12.32	0
C	O			C	O/Ar			Ar	-25.91	0
O	C				C			Ar	-29.38	0
Ar	O			Ar					-18.23	0
O	Ar			-	-	-	-	-	-10.60	0
Ar	C			Ar	C			C	-27.26	0
C	Ar			C	Ar			Ar	-25.93	0
Ar	N			Ar	N/C			O	-25.84	0
N	Ar			C/N	Ar			O	-31.66	0
O			N				C		-15.44	0
N			O	C					-24.48	0
N			C				C		-18.69	2
C			N	C					-15.17	1
O			C				C		-15.15	1
C			O	C			Ar		-17.09	1
O			Ar	Ar			C		-14.40	2
Ar			O	C/Ar			Ar		-14.07	2
N			Ar	-	-	-	-	-	-21.74	0
Ar			N				C		-28.56	1
Ar			C				C		-25.26	1
C			Ar	C					-25.54	0

Six conformations were selected for solution phase optimization from the results of the gas phase interactions of 3-hydroxyanthranilic acid with the **HH**Q**K** region of Aβ, summarized in Tables 3.56-3.61. These selections were based on the requirement of having the lowest overall binding energy, as well as binding at two or more sites on the β-amyloid protein. In the case of the 1BA4 conformer of Aβ, only four systems met these

criteria, so only four solution phase optimizations were performed. Overall 3HAA was capable of binding at His13-His14, and His13-Lys16, with the former being slightly more favoured. The selected systems are summarized in Table 3.62

Table 3.62: Selected systems of 3-hydroxyanthranilic acid and the HHQK region of Aβ for solvation

Interaction	Binding Energy (kcal/mol)
1AMB	
HNHAr	-56.83
HNHC	-50.37
HCHO	-49.23
HCHN	-48.41
HArHN	-47.17
HOHQKAr	-44.45
1AMC	
HArHC	-52.68
HCHAr	-42.59
HNHC	-42.20
HCHN	-41.70
HCHO	-39.28
HArHN	-39.14
1AML	
HCHO	-39.23
HCHN	-37.42
HCHQKN	-36.25
HNHQKO	-35.39
HCHQKO	-27.26
HOHQKN	-26.16

Interaction	Binding Energy (kcal/mol)
1BA4	
HNHAr	-42.30
HCHAr	-34.46
HOHC	-30.56
HCHO	-20.70
1IYT	
HArHN	-33.55
HCHO	-33.26
HNHAr	-32.51
HOHQKC	-27.42
HCHQKAr	-27.29
HNHQKO	-26.83
1Z0Q	
HNHO	-31.74
HNHAr	-31.66
HArHC	-27.26
HCHAr	-25.93
HCHO	-25.91
HArHN	-25.84

The gas phase results of 3-hydroxyanthranilic acid interacting with the EV**HH**Q**K** region of Aβ are summarized in Tables 3.63-68.

Table 3.63: The gas phase results of 3-hydroxyanthranilic acid interacting with the EVHHQK region of the 1AMB conformer of β-amyloid

Initial Orientation						Final Orientation						ΔE_{bind}	Measured
E11	V12	H13	H14	Q15	K16	E11	V12	H13	H14	Q15	K16	(kcal/mol)	Bonds
N			C			N/C						-31.73	0
C			N			-	-	-	-	-	-	-17.96	0
N			O			N/O			O			-8.82	0
O			N			-	-	-	-	-	-	-15.43	0
C			O			O/N/Ar			C/Ar			-37.93	2
O			C			O/Ar			C/Ar			-28.17	1
C			Ar			-	-	-	-	-	-	-12.69	0
Ar			C			Ar			C			-23.33	0
N			Ar			N/Ar			C/Ar	O		-26.03	1
Ar			N			Ar			C			-30.65	0
O			Ar			-	-	-	-	-	-	-14.67	0
Ar			O			-	-	-	-	-	-	-22.20	0

Table 3.64: The gas phase results of 3-hydroxyanthranilic acid interacting with the EVHHQK region of the 1AMC conformer of β-amyloid

Initial Orientation						Final Orientation						ΔE_{bind}	Measured
E11	V12	H13	H14	Q15	K16	E11	V12	H13	H14	Q15	K16	(kcal/mol)	Bonds
N			O			N						-17.29	0
O			N			N						-29.87	0
C			N			C/N						-29.60	1
N			C			N			C			-33.82	1
C			O			N/C/Ar						-20.72	0
O			C			N/O/Ar			C			-37.14	0
N			Ar			N/Ar			Ar			-34.55	0
Ar			N			N/Ar						-28.82	0
O			Ar			N/O/Ar			Ar			-34.89	1
Ar			O			O/Ar						-21.77	1
C			Ar			C			C/Ar	O/Ar		-21.37	1
Ar			C			Ar			C			-23.42	1

Table 3.65: The gas phase results of 3-hydroxyanthranilic acid interacting with the EVHHQK region of the 1AML conformer of β-amyloid

Initial Orientation						Final Orientation							ΔE_{bind}	Measured
E11	V12	H13	H14	Q15	K16	E11	V12	H13	H14	Q15	K16	X	(kcal/mol)	Bonds
C			N			C			N			Ar	-22.54	0
N			C			N			C			N/O/Ar	-40.71	0
O			N			O			N				-12.63	1
N			O			N			N/O			C/N/Ar	-16.19	1
N			Ar			N/O/Ar			C/Ar			N/O/Ar	-42.99	3
Ar			N						Ar			Ar	-23.43	2
C			Ar									C/N/Ar	-40.33	1
Ar			C			Ar			C			Ar	-31.95	0
Ar			O			Ar						C/N/Ar	-18.97	0
O			Ar									C/O/N/Ar	-40.26	0
O			C			O/Ar			C/Ar			O	-21.89	2
C			O			C/Ar			O/Ar	C		C/Ar	-20.06	2

Table 3.66: The gas phase results of 3-hydroxyanthranilic acid interacting with the EVHHQK region of the 1BA4 conformer of β-amyloid

Initial Orientation						Final Orientation							ΔE_{bind}	Measured
E11	V12	H13	H14	Q15	K16	E11	V12	H13	H14	Q15	K16	X	(kcal/mol)	Bonds
C					N	C						C/O/N	-33.24	1
N					C	C/N					C	C/N	-17.53	1
O					N							N/O/Ar	-39.63	0
N					O	N						N/O	-47.19	1
O					Ar							N/O/Ar	-29.15	1
Ar					O	-	-	-	-	-	-	-	-47.04	0
Ar					C	C/Ar					C	C/O/N/Ar	-26.92	1
C					Ar	C/Ar					Ar	C/Ar	-35.59	0

Table 3.67: The gas phase results of 3-hydroxyanthranilic acid interacting with the EVHHQK region of the 1IYT conformer of β-amyloid

Initial Orientation						Final Orientation							ΔE_{bind}	Measured
E11	V12	H13	H14	Q15	K16	E11	V12	H13	H14	Q15	K16	X	(kcal/mol)	Bonds
N			O			N/O/Ar			O				-30.23	2
O			N			N							-24.50	0
C			N			C			N/C				-4.41	1
N			C			N							-24.22	0
O			Ar						Ar				-19.22	0
Ar			O			-	-	-	-	-	-	-	-16.91	0
N			Ar			N/Ar			C/Ar				-37.68	1
Ar			N			O/Ar						C	-23.32	0
Ar			C			Ar							-29.18	0
C			Ar						C				-27.03	0

Table 3.68: The gas phase results of 3-hydroxyanthranilic acid interacting with the EVHHQK region of the 1Z0Q conformer of β-amyloid

Initial Orientation						Final Orientation							ΔE_{bind}	Measured
E11	V12	H13	H14	Q15	K16	E11	V12	H13	H14	Q15	K16	X	(kcal/mol)	Bonds
N			O			N							-15.82	0
O			N						C/Ar			Ar	-56.65	1
C			N			C							-1.29	0
N			C			C/N/Ar			C				-57.78	0
O			C			O			C			Ar	-42.01	0
C			O			Ar							-33.36	0
C			Ar			C							-11.39	0
Ar			C			Ar			C				-43.92	0
O			Ar			O/Ar							-25.30	0
Ar			O			-	-	-	-	-	-	-	-18.67	0
N			Ar			N/O							-30.09	1
Ar			N			Ar			Ar				-53.38	0

The results of the gas phase interactions occurring between 3-hydroxyanthranilic acid and the EV**HH**Q**K** region of β-amyloid indicate binding can occur in this region of interest. From each conformer of Aβ four systems were selected for optimization in the solution phase; these had to have the lowest energy and binding interactions at two or more of the amino acid side chains. The systems targeted for solution phase optimizations are summarized in Table 3.69.

Table 3.69: Selected systems of 3-hydroxyanthranilic acid and the EVHHQK region of Aβ for solvation

Interaction	Binding Energy (kcal/mol)	Interaction	Binding Energy (kcal/mol)
1AMB		1BA4	
ECVHHO	-37.93	ENVHHQKO	-47.19
EArVHHN	-30.65	ECVHHQKAr	-35.59
EOVHHC	-28.17	ECVHHQKN	-33.24
EArVHHN	-26.03	EArVHHQKC	-26.92
1AMC		1IYT	
EOVHHC	-37.14	ENVHHAr	-37.68
EOVHHAr	-34.89	ENVHHO	-30.23
ENVHHAr	-34.55	EArVHHN	-23.32
ENVHHC	-33.82	ECVHHN	-4.41
1AML		1Z0Q	
ENVHHAr	-42.99	ENVHHC	-57.78
ENVHHC	-40.71	EOVHHN	-56.65
EArVHHC	-31.95	EArVHHN	-53.38
EArVHHN	-23.43	EArVHHC	-43.92

The results of the gas phase interactions between 3HAA and the LVFF region of β-amyloid are summarized in Table 3.70. As there are very few interactions occurring in this region, it was determined that half of the systems for each conformer of Aβ would undergo solution phase optimization. These systems had to have low energies and binding interactions at two or more sites with Aβ; in the case of the 1BA4 conformer there were no viable systems for solution phase optimization.

The systems selected for optimization in the solution phase are summarized in Table 3.71.

Table 3.70: The gas phase results of 3-hydroxyanthranilic acid interacting with the LVFF region of β-amyloid

Conformer	Initial Orientation				Final Orientation					ΔE_{bind}	Measured
	L17	V18	F19	F20	L17	V18	F19	F20	X	(kcal/mol)	Bonds
1AMB	Ar			N	Ar			C		-13.24	0
	Ar			O	Ar					-6.42	0
			Ar	N			Ar		C	-9.73	0
			N	Ar			N/C/Ar	Ar	C/O/Ar	-73.45	0
			O	Ar			O		Ar	-37.48	0
			Ar	O			Ar	Ar	C/O	-55.42	1
		Ar	N				C		Ar	-23.66	0
		Ar	O			Ar				-27.43	1
1AMC	Ar			N	Ar					-16.51	0
	Ar			O	C/Ar				C	-24.23	0
			Ar	N			Ar		O/Ar	-41.55	0
			N	Ar			N			-18.80	1
			Ar	O	-	-	-	-	-	-13.19	0
			O	Ar			O		Ar	-28.81	0
		Ar	N			Ar	N		C/O/Ar	-28.59	1
		Ar	O		-	-	-	-	-	-15.06	0
1AML	Ar			O				O	Ar	-18.92	0
	Ar			N				C/Ar	O/Ar	-31.34	0
			Ar	O	-	-	-	-	-	-20.49	0
			O	Ar				Ar	O	-30.51	0
			Ar	N	-	-	-	-	-	-21.30	0
			N	Ar				O	N	-28.17	0
1BA4	Ar			N	Ar					-21.27	0
	Ar			O				Ar		-16.97	0
		Ar	O						O	-22.68	1
1IYT	Ar			N	Ar					-11.93	0
	Ar			O					Ar	-18.01	0
			O	Ar					N	-27.72	1
			Ar	O			Ar		C/O/Ar	-29.08	3
		Ar	O				O		Ar	-16.27	0
1Z0Q	Ar			N	Ar			N		-8.03	0
	Ar			O			Ar			-8.76	0
	Ar		N				Ar	O/Ar		-27.37	1
	Ar		O		-	-	-	-	-	-9.31	0
			Ar	N			Ar	O/Ar		-22.80	1
			N	Ar			O	Ar		-27.48	0
			Ar	O			Ar	C/O/N/Ar		-18.01	2
			O	Ar	-	-	-	-	-	-10.22	0

Table 3.71: Selected systems of 3-hydroxyanthranilic acid and the LVFF region of Aβ for solvation

Interaction	Binding Energy (kcal/mol)
1AMB	
FNFAr	-73.45
FArFO	-55.42
FOFAr	-37.48
VArFO	-27.43
1AMC	
FArFN	-41.55
FOFAr	-28.81
VArFN	-28.59
LArVFFO	-24.23
1AML	
LArVFFN	-31.34
FOFAr	-30.51
FNFAr	-28.17
LArVFFO	-18.92

Interaction	Binding Energy (kcal/mol)
1IYT	
FArFO	-29.08
VArFO	-16.27
1Z0Q	
FNFAr	-27.48
FArFN	-22.80
FArFO	-18.01
LArVFFN	-8.03

3.7.3 Solution Phase Results for 3-hydroxyanthranilic acid Interacting with β-Amyloid

Solution phase optimizations were performed for each of the regions of β-amyloid interacting with 3HAA. These optimizations were performed in MOE following the procedure outlined in Section 3.5.4.1. The results of these calculations are summarized according to conformer and each region of Aβ that was the focus for binding. The initial and final binding orientations are given, with 3 letter abbreviations for the amino acid residues. Identification of the functional groups of 3HAA follows the same pattern as outlined in the gas phase optimizations. The binding energies of each system were calculated via the following equations:

$$\Delta E_{tot} = E_{tot} - E_{A\beta} - E_{HAA} \tag{3.17}$$

$$\Delta E_{vdw} = E_{vdw} - E_{vdwA\beta} - E_{vdw3HAA} \quad (3.18)$$

$$\Delta E_{ele} = E_{ele} - E_{eleA\beta} - E_{ele3HAA} \quad (3.19)$$

These equations are identical to those used for previous solution phase optimizations, where the measured energies are calculated with a constrained protein backbone and the solvent removed from the system. The energies of the solvated Aβ conformers are the same as those in Appendix 6 and the energy of the solution phase optimized 3-hydroxyanthranilic acid is given in Table 3.72.

Table 3.72: The solution phase energy of 3-hydroxyanthranilic acid

	Energies (kcal/mol)		
	E_{tot}	E_{ele}	E_{vdw}
3-hydroxyanthranilic acid	-3.16	17.45	-26.72

Binding interactions that occurred in the solution phase are denoted by coloured squares: orange indicates a hydrogen bond, the darker the orange, the more hydrogen bonds have formed; green indicates cation-π interactions, the darker the green, the more cation-π interactions that are occurring at that site; light blue signifies π-π interactions, as the shade becomes more intense, more interactions are occurring. There are also interactions occurring with regions other than the R group of the amino acids: indigo indicates interactions with the $–CH_2$- chain, whereas lime green is used for the –CH- of the protein backbone; light purple is used for interactions with the C=O of the protein backbone; and finally yellow represents the –NH- of the protein backbone.

Tables 3.73-3.78 detail the results of the solution phase optimization of 3HAA and the HHQK region of β-amyloid.

Table 3.73: The solution phase results of 3-hydroxyanthranilic acid interacting with the HHQK region of the 1AMB conformer of β-amyloid

	Tyr10	His13	His14	Gln15	Lys16	Leu17	Val18
Initial Orientation		C	Ar			N	
Final Orientation		C	Ar			C	O
						N	Ar
Total =	-52.85 kcal/mol						
van der Waals =	60.35 kcal/mol						
Electrostatic =	-281.84 kcal/mol						
ΔE_{tot} =	-48.04 kcal/mol						
ΔE_{vdw} =	-3.87 kcal/mol						
ΔE_{ele} =	-57.13 kcal/mol						
Initial Orientation	C	C					
Final Orientation	N	C	Ar			Ar	
Total =	-49.20 kcal/mol						
van der Waals =	73.21 kcal/mol						
Electrostatic =	-272.24 kcal/mol						
ΔE_{tot} =	-44.39 kcal/mol						
ΔE_{vdw} =	9.00 kcal/mol						
ΔE_{ele} =	-47.52 kcal/mol						
Initial Orientation	N	C	N				
Final Orientation	N	C	Ar				
Total =	-55.40 kcal/mol						
van der Waals =	50.55 kcal/mol						
Electrostatic =	-261.01 kcal/mol						
ΔE_{tot} =	-50.59 kcal/mol						
ΔE_{vdw} =	-13.66 kcal/mol						
ΔE_{ele} =	-39.29 kcal/mol						

Table 3.73: The solution phase results of 3-hydroxyanthranilic acid interacting with the HHQK region of the 1AMB conformer of β-amyloid

	Tyr10	His13	His14	Gln15	Lys16	Leu17	Phe20
Initial Orientation		C	N			Ar	
			C				
Final Orientation	C	C	N			Ar	
Total =	-70.93 kcal/mol						
van der Waals =	59.05 kcal/mol						
Electrostatic =	-280.02 kcal/mol						
ΔE_{tot} =	-66.12 kcal/mol						
ΔE_{vdw} =	-5.17 kcal/mol						
ΔE_{ele} =	-55.31 kcal/mol						
Initial Orientation					C		Ar
Final Orientation					C		Ar
Total =	-42.55 kcal/mol						
van der Waals =	70.54 kcal/mol						
Electrostatic =	-270.35 kcal/mol						
ΔE_{tot} =	-37.74 kcal/mol						
ΔE_{vdw} =	6.33 kcal/mol						
ΔE_{ele} =	-45.63 kcal/mol						
Initial Orientation	Ar	C	Ar				
			Ar				
Final Orientation	Ar	C	Ar				
		Ar					
Total =	-15.02 kcal/mol						
van der Waals =	57.04 kcal/mol						
Electrostatic =	-244.67 kcal/mol						
ΔE_{tot} =	-10.21 kcal/mol						
ΔE_{vdw} =	-7.18 kcal/mol						
ΔE_{ele} =	-19.95 kcal/mol						

Table 3.74: The solution phase results of 3-hydroxyanthranilic acid interacting with the HHQK region of the 1AMC conformer of β-amyloid

	Tyr10	His13	His14	Gln15	Lys16	Leu17	Val18
Initial Orientation	Ar		Ar			C	
Final Orientation	Ar		Ar			C	
Total =	-68.29 kcal/mol						
van der Waals =	64.52 kcal/mol						
Electrostatic =	-294.30 kcal/mol						
ΔE_{tot} =	-37.91 kcal/mol						
ΔE_{vdw} =	1.80 kcal/mol						
ΔE_{ele} =	-47.08 kcal/mol						
Initial Orientation	C		C			O	N
			N			Ar	
Final Orientation	C					Ar	
Total =	-70.38 kcal/mol						
van der Waals =	68.06 kcal/mol						
Electrostatic =	-296.80 kcal/mol						
ΔE_{tot} =	-40.01 kcal/mol						
ΔE_{vdw} =	5.33 kcal/mol						
ΔE_{ele} =	-49.58 kcal/mol						
Initial Orientation	Ar	C					
Final Orientation	Ar		Ar				
Total =	-69.43 kcal/mol						
van der Waals =	64.03 kcal/mol						
Electrostatic =	-298.80 kcal/mol						
ΔE_{tot} =	-39.06 kcal/mol						
ΔE_{vdw} =	1.31 kcal/mol						
ΔE_{ele} =	-51.58 kcal/mol						

Table 3.74: The solution phase results of 3-hydroxyanthranilic acid interacting with the HHQK region of the 1AMC conformer of β-amyloid

	Tyr10	His13	His14	Gln15	Lys16	Leu17
Initial Orientation	N	C	C			
Final Orientation	N		C			
Total =	-79.18 kcal/mol					
van der Waals =	63.01 kcal/mol					
Electrostatic =	-298.72 kcal/mol					
ΔE_{tot} =	-48.81 kcal/mol					
ΔE_{vdw} =	0.28 kcal/mol					
ΔE_{ele} =	-51.50 kcal/mol					
Initial Orientation	N	C	Ar			
Final Orientation	N	C	Ar			
Total =	-58.43 kcal/mol					
van der Waals =	70.06 kcal/mol					
Electrostatic =	-277.61 kcal/mol					
ΔE_{tot} =	-28.05 kcal/mol					
ΔE_{vdw} =	7.33 kcal/mol					
ΔE_{ele} =	-30.39 kcal/mol					
Initial Orientation	Ar	C	Ar			
Final Orientation	Ar	C	Ar			C N
Total =	-52.98 kcal/mol					
van der Waals =	60.60 kcal/mol					
Electrostatic =	-267.49 kcal/mol					
ΔE_{tot} =	-22.60 kcal/mol					
ΔE_{vdw} =	-2.12 kcal/mol					
ΔE_{ele} =	-20.27 kcal/mol					

Table 3.75: The solution phase results of 3-hydroxyanthranilic acid interacting with the HHQK region of the 1AML conformer of β-amyloid

	Tyr10	Val12	His13	His14	Gln15	Lys16
Initial Orientation	C		C	Ar		
	Ar					
Final Orientation	C		C	Ar		
Total =	67.90 kcal/mol					
van der Waals =	76.99 kcal/mol					
Electrostatic =	-230.00 kcal/mol					
ΔE_{tot} =	-55.24 kcal/mol					
ΔE_{vdw} =	-8.37 kcal/mol					
ΔE_{ele} =	-44.15 kcal/mol					
Initial Orientation	Ar		C			
Final Orientation	C		C			
	Ar					
Total =	97.87 kcal/mol					
van der Waals =	95.00 kcal/mol					
Electrostatic =	-222.07 kcal/mol					
ΔE_{tot} =	-25.26 kcal/mol					
ΔE_{vdw} =	9.63 kcal/mol					
ΔE_{ele} =	-36.22 kcal/mol					
Initial Orientation		C	C			
		Ar				
Final Orientation		C	C			
Total =	104.27 kcal/mol					
van der Waals =	86.64 kcal/mol					
Electrostatic =	-212.92 kcal/mol					
ΔE_{tot} =	-18.86 kcal/mol					
ΔE_{vdw} =	1.28 kcal/mol					
ΔE_{ele} =	-27.07 kcal/mol					

Table 3.75: The solution phase results of 3-hydroxyanthranilic acid interacting with the HHQK region of the 1AML conformer of β-amyloid

	Val12	His13	His14	Gln15	Lys16
Initial Orientation	C	C			
	N				
Final Orientation	C	C			Ar
	N				
Total =	104.65 kcal/mol				
van der Waals =	99.75 kcal/mol				
Electrostatic =	-221.24 kcal/mol				
ΔE_{tot} =	-18.48 kcal/mol				
ΔE_{vdw} =	14.38 kcal/mol				
ΔE_{ele} =	-35.40 kcal/mol				
Initial Orientation	Ar	C			Ar
Final Orientation		C			Ar
Total =	102.82 kcal/mol				
van der Waals =	84.92 kcal/mol				
Electrostatic =	-214.85 kcal/mol				
ΔE_{tot} =	-20.31 kcal/mol				
ΔE_{vdw} =	-0.45 kcal/mol				
ΔE_{ele} =	-29.00 kcal/mol				
Initial Orientation	O				C
	Ar				
Final Orientation	O				
	Ar				
Total =	117.88 kcal/mol				
van der Waals =	98.02 kcal/mol				
Electrostatic =	-202.45 kcal/mol				
ΔE_{tot} =	-5.25 kcal/mol				
ΔE_{vdw} =	12.66 kcal/mol				
ΔE_{ele} =	-16.60 kcal/mol				

Table 3.76: The solution phase results of 3-hydroxyanthranilic acid interacting with the HHQK region of the 1BA4 conformer of β-amyloid

	His13	His14	Gln15	Lys16
Initial Orientation	C	C		
		Ar		
Final Orientation	C	C		
		Ar		
Total =	55.81 kcal/mol			
van der Waals =	79.47 kcal/mol			
Electrostatic =	-242.03 kcal/mol			
ΔE_{tot} =	-82.45 kcal/mol			
ΔE_{vdw} =	-29.80 kcal/mol			
ΔE_{ele} =	-45.80 kcal/mol			
Initial Orientation	C	Ar		
Final Orientation	C	C		
		Ar		
Total =	88.52 kcal/mol			
van der Waals =	95.75 kcal/mol			
Electrostatic =	-225.32 kcal/mol			
ΔE_{tot} =	-49.73 kcal/mol			
ΔE_{vdw} =	-13.52 kcal/mol			
ΔE_{ele} =	-29.10 kcal/mol			
Initial Orientation	Ar	C		
Final Orientation	Ar	C		
Total =	80.28 kcal/mol			
van der Waals =	94.59 kcal/mol			
Electrostatic =	-229.72 kcal/mol			
ΔE_{tot} =	-57.98 kcal/mol			
ΔE_{vdw} =	-14.68 kcal/mol			
ΔE_{ele} =	-33.49 kcal/mol			
Initial Orientation	C	Ar		
Final Orientation	N	Ar		
	C			
Total =	97.49 kcal/mol			
van der Waals =	89.20 kcal/mol			
Electrostatic =	-202.59 kcal/mol			
ΔE_{tot} =	-40.76 kcal/mol			
ΔE_{vdw} =	-20.06 kcal/mol			
ΔE_{ele} =	-6.36 kcal/mol			

Table 3.77: The solution phase results of 3-hydroxyanthranilic acid interacting with the HHQK region of the 1IYT conformer of β-amyloid

	Gly9	Tyr10	His13	His14	Gln15	Lys16	Leu17
Initial Orientation	O		Ar				C
			Ar				
Final Orientation	O		Ar				
			Ar				
Total =	32.35 kcal/mol						
van der Waals =	88.71 kcal/mol						
Electrostatic =	269.53 kcal/mol						
ΔE_{tot} =	-41.13 kcal/mol						
ΔE_{vdw} =	-16.93 kcal/mol						
ΔE_{ele} =	-26.26 kcal/mol						
Initial Orientation	Ar	Ar	C	O			
			Ar	Ar			
Final Orientation	Ar	Ar	C				
Total =	106.57 kcal/mol						
van der Waals =	97.50 kcal/mol						
Electrostatic =	-273.12 kcal/mol						
ΔE_{tot} =	33.09 kcal/mol						
ΔE_{vdw} =	-8.14 kcal/mol						
ΔE_{ele} =	-29.85 kcal/mol						
Initial Orientation			Ar	Ar			Ar
Final Orientation			N	Ar			Ar
			C				
Total =	39.60 kcal/mol						
van der Waals =	90.27 kcal/mol						
Electrostatic =	-271.68 kcal/mol						
ΔE_{tot} =	-33.89 kcal/mol						
ΔE_{vdw} =	-15.37 kcal/mol						
ΔE_{ele} =	-28.41 kcal/mol						

Table 3.77: The solution phase results of 3-hydroxyanthranilic acid interacting with the HHQK region of the 1IYT conformer of β-amyloid

	His13	His14	Gln15	Lys16
Initial Orientation	Ar			C
Final Orientation	Ar			Ar
				C
Total =	71.16 kcal/mol			
van der Waals =	98.15 kcal/mol			
Electrostatic =	-250.12 kcal/mol			
ΔE_{tot} =	-2.32 kcal/mol			
ΔE_{vdw} =	-7.49 kcal/mol			
ΔE_{ele} =	-6.85 kcal/mol			
Initial Orientation	C			Ar
Final Orientation	C			Ar
Total =	49.04 kcal/mol			
van der Waals =	82.66 kcal/mol			
Electrostatic =	-258.21 kcal/mol			
ΔE_{tot} =	-24.44 kcal/mol			
ΔE_{vdw} =	-22.97 kcal/mol			
ΔE_{ele} =	-14.94 kcal/mol			
Initial Orientation	C			O
	Ar			
Final Orientation	C			Ar
Total =	78.99 kcal/mol			
van der Waals =	86.14 kcal/mol			
Electrostatic =	-273.59 kcal/mol			
ΔE_{tot} =	5.51 kcal/mol			
ΔE_{vdw} =	-19.50 kcal/mol			
ΔE_{ele} =	-30.32 kcal/mol			

Table 3.78: The solution phase results of 3-hydroxyanthranilic acid interacting with the HHQK region of the 1Z0Q conformer of β-amyloid

	Tyr10	His13	His14	Gln15	Lys16
Initial Orientation	N	C	Ar		
	O	N			
Final Orientation	O	C	Ar		
Total =	91.01 kcal/mol				
van der Waals =	87.14 kcal/mol				
Electrostatic =	-249.02 kcal/mol				
ΔE_{tot} =	-27.62 kcal/mol				
ΔE_{vdw} =	-2.79 kcal/mol				
ΔE_{ele} =	-36.93 kcal/mol				
Initial Orientation	O	N	Ar		
		C			
Final Orientation	O	C			
Total =	101.32 kcal/mol				
van der Waals =	93.77 kcal/mol				
Electrostatic =	-244.89 kcal/mol				
ΔE_{tot} =	-17.31 kcal/mol				
ΔE_{vdw} =	3.84 kcal/mol				
ΔE_{ele} =	-32.80 kcal/mol				
Initial Orientation	C	Ar	C		
Final Orientation	C	Ar	C		
Total =	81.04 kcal/mol				
van der Waals =	81.59 kcal/mol				
Electrostatic =	-244.54 kcal/mol				
ΔE_{tot} =	-37.58 kcal/mol				
ΔE_{vdw} =	-8.32 kcal/mol				
ΔE_{ele} =	-32.45 kcal/mol				

Table 3.78: The solution phase results of 3-hydroxyanthranilic acid interacting with the HHQK region of the 1Z0Q conformer of β-amyloid

	Gly9	Tyr10	His13	His14	Gln15	Lys16
Initial Orientation		Ar	C	Ar		
Final Orientation	Ar	Ar	C			
Total =	112.90 kcal/mol					
van der Waals =	106.44 kcal/mol					
Electrostatic =	-243.42 kcal/mol					
ΔE_{tot} =	-5.72 kcal/mol					
ΔE_{vdw} =	16.52 kcal/mol					
ΔE_{ele} =	-31.33 kcal/mol					
Initial Orientation		Ar	C	O Ar		
Final Orientation		Ar	C			
Total =	118.85 kcal/mol					
van der Waals =	94.13 kcal/mol					
Electrostatic =	-236.32 kcal/mol					
ΔE_{tot} =	0.23 kcal/mol					
ΔE_{vdw} =	4.20 kcal/mol					
ΔE_{ele} =	-24.23 kcal/mol					
Initial Orientation		O	Ar	N C		
Final Orientation		O	Ar			
Total =	92.74 kcal/mol					
van der Waals =	88.03 kcal/mol					
Electrostatic =	-239.57 kcal/mol					
ΔE_{tot} =	-25.89 kcal/mol					
ΔE_{vdw} =	-1.89 kcal/mol					
ΔE_{ele} =	-27.47 kcal/mol					

These results indicate that 3HAA is capable of binding to and interacting with the **HH**Q**K** region of β-amyloid. Interactions occurring at His13-His14 are favoured 3:1 over those at His13-Lys16. There is a large variability in the energies of the systems, and the presence of measurable bonds does not always indicate favourable energetics. In general the electrostatic energies make more of a contribution to the overall binding than the van

der Waals energies. Cation-π interactions were more prevalent than hydrogen bonds in these systems.

The results of the solution phase optimizations of 3-hydroxyanthranilic acid and the EV**HH**Q**K** region of β-amyloid are summarized in Tables 3.79-3.84. In general, the results of these calculations show binding at Glu11-His14 to be preferred, with interactions occurring at these two amino acids in over half of the systems; all systems demonstrated at least one interaction occurring at multiple sites within EV**HH**Q**K**. Both cation-π and hydrogen bonds were present, and for most of the systems the electrostatic energies contribute more to the overall energy of the system than the van der Waals energy.

Table 3.79: The solution phase results of 3-hydroxyanthranilic acid interacting with the EVHHQK region of the 1AMB conformer of β-amyloid

	Glu11	Val12	His13	His14	Gln15	Lys16
Initial Orientation	N			Ar		
	Ar			C		
	O					
Final Orientation	N			Ar	O	
	Ar			C	Ar	
Total =	-50.56 kcal/mol					
van der Waals =	57.09 kcal/mol					
Electrostatic =	-258.62 kcal/mol					
ΔE_{tot} =	-45.84 kcal/mol					
ΔE_{vdw} =	-7.12 kcal/mol					
ΔE_{ele} =	-33.90 kcal/mol					
Initial Orientation	Ar			C		
Final Orientation	Ar			C		
				N		
				Ar		
Total =	-7.57 kcal/mol					
van der Waals =	63.07 kcal/mol					
Electrostatic =	-239.80 kcal/mol					
ΔE_{tot} =	-2.76 kcal/mol					
ΔE_{vdw} =	-1.15 kcal/mol					
ΔE_{ele} =	-15.08 kcal/mol					
Initial Orientation	O			Ar		
	Ar			C		
Final Orientation	O			C		
	Ar			Ar		
Total =	-33.13 kcal/mol					
van der Waals =	60.32 kcal/mol					
Electrostatic =	-249.80 kcal/mol					
ΔE_{tot} =	-28.32 kcal/mol					
ΔE_{vdw} =	-3.89 kcal/mol					
ΔE_{ele} =	-25.08 kcal/mol					
Initial Orientation	N			Ar	O	
	Ar			C		
Final Orientation	N			Ar		
	Ar					
Total =	-38.01 kcal/mol					
van der Waals =	64.95 kcal/mol					
Electrostatic =	-266.20 kcal/mol					
ΔE_{tot} =	-33.20 kcal/mol					
ΔE_{vdw} =	0.73 kcal/mol					
ΔE_{ele} =	-41.48 kcal/mol					

Table 3.80: The solution phase results of 3-hydroxyanthranilic acid interacting with the EVHHQK region of the 1AMC conformer of β-amyloid

	Glu11	Val12	His13	His14	Gln15	Lys16
Initial Orientation	N			Ar		
	Ar					
Final Orientation	O			Ar		
	Ar					
Total =	-42.20 kcal/mol					
van der Waals	57.80 kcal/mol					
Electrostatic =	-266.94 kcal/mol					
ΔE_{tot} =	-11.82 kcal/mol					
ΔE_{vdw} =	-4.92 kcal/mol					
ΔE_{ele} =	-19.72 kcal/mol					
Initial Orientation	N			C		
Final Orientation	N					
Total =	-36.80 kcal/mol					
van der Waals	70.15 kcal/mol					
Electrostatic =	-273.57 kcal/mol					
ΔE_{tot} =	-6.42 kcal/mol					
ΔE_{vdw} =	7.42 kcal/mol					
ΔE_{ele} =	-26.35 kcal/mol					
Initial Orientation	N			C		
	O					
	Ar					
Final Orientation				C	C	
					Ar	
Total =	-22.79 kcal/mol					
van der Waals	75.98 kcal/mol					
Electrostatic =	-259.81 kcal/mol					
ΔE_{tot} =	7.59 kcal/mol					
ΔE_{vdw} =	13.25 kcal/mol					
ΔE_{ele} =	-12.59 kcal/mol					
Initial Orientation	N			Ar		
	Ar			C		
	O					
Final Orientation	O			Ar		
	N			C		
Total =	-51.09 kcal/mol					
van der Waals	58.50 kcal/mol					
Electrostatic =	-279.31 kcal/mol					
ΔE_{tot} =	-20.72 kcal/mol					
ΔE_{vdw} =	-4.23 kcal/mol					
ΔE_{ele} =	-32.09 kcal/mol					

Table 3.81: The solution phase results of 3-hydroxyanthranilic acid interacting with the EVHHQK region of the 1AML conformer of β-amyloid

	Asp7	Set8	Tyr10	Glu11	Val12	His13	His14	Gln15	Lys16
Initial Orientation		N	O	N			Ar		
		Ar		O			Ar		
				Ar			C		
Final Orientation		O	O	N			Ar		
		Ar		O			C		
				Ar			N		
Total =	99.59 kcal/mol								
van der Waals =	86.97 kcal/mol								
Electrostatic =	-219.22 kcal/mol								
ΔE_{tot} =	-23.55 kcal/mol								
ΔE_{vdw} =	1.63 kcal/mol								
ΔE_{ele} =	-33.37 kcal/mol								
Initial Orientation	O	O		N			C		
		N							
		Ar							
Final Orientation	O	O		N			C		
		N							
		Ar							
Total =	91.32 kcal/mol								
van der Waals =	79.89 kcal/mol								
Electrostatic =	-214.49 kcal/mol								
ΔE_{tot} =	-31.81 kcal/mol								
ΔE_{vdw} =	-5.47 kcal/mol								
ΔE_{ele} =	-28.65 kcal/mol								
Initial Orientation		Ar		Ar			C		
Final Orientation				Ar			C		
Total =	107.00 kcal/mol								
van der Waals =	95.34 kcal/mol								
Electrostatic =	-205.89 kcal/mol								
ΔE_{tot} =	-16.13 kcal/mol								
ΔE_{vdw} =	9.98 kcal/mol								
ΔE_{ele} =	-20.04 kcal/mol								
Initial Orientation		Ar					Ar		
							Ar		
Final Orientation							Ar		
Total =	113.39 kcal/mol								
van der Waals =	81.06 kcal/mol								
Electrostatic =	-191.61 kcal/mol								
ΔE_{tot} =	-9.74 kcal/mol								
ΔE_{vdw} =	-4.30 kcal/mol								
ΔE_{ele} =	-5.76 kcal/mol								

Table 3.82: The solution phase results of 3-hydroxyanthranilic acid interacting with the EVHHQK region of the 1BA4 conformer of β-amyloid

	Asp1	Glu3	Glu11	Val12	His13	His14	Gln15	Lys16	Phe19
Initial Orientation	O	N	C						C
Final Orientation		N	C						C
		Ar							
Total =	59.91 kcal/mol								
van der Waals	84.22 kcal/mol								
Electrostatic =	-245.63 kcal/mol								
ΔE_{tot} =	-78.34 kcal/mol								
ΔE_{vdw} =	-25.05 kcal/mol								
ΔE_{ele} =	-49.40 kcal/mol								
Initial Orientation			C					C	Ar
			Ar						O
									C
									N
Final Orientation		C	Ar					C	Ar
									C
									O
									N
Total =	107.57 kcal/mol								
van der Waals	88.81 kcal/mol								
Electrostatic =	-215.61 kcal/mol								
ΔE_{tot} =	-30.69 kcal/mol								
ΔE_{vdw} =	-20.45 kcal/mol								
ΔE_{ele} =	-19.39 kcal/mol								
Initial Orientation			N						N
									O
Final Orientation			N						N
									O
Total =	77.40 kcal/mol								
van der Waals	92.28 kcal/mol								
Electrostatic =	-236.07 kcal/mol								
ΔE_{tot} =	-60.85 kcal/mol								
ΔE_{vdw} =	-16.99 kcal/mol								
ΔE_{ele} =	-39.85 kcal/mol								
Initial Orientation		Ar	C					Ar	C
			Ar						Ar
Final Orientation		Ar	C						C
			Ar						Ar
Total =	80.43 kcal/mol								
van der Waals	83.34 kcal/mol								
Electrostatic =	-216.04 kcal/mol								
ΔE_{tot} =	-57.82 kcal/mol								
ΔE_{vdw} =	-25.93 kcal/mol								
ΔE_{ele} =	-19.81 kcal/mol								

Table 3.83: The solution phase results of 3-hydroxyanthranilic acid interacting with the EVHHQK region of the 1IYT conformer of β-amyloid

	Tyr10	Glu11	Val12	His13	His14	Gln15	Lys16
Initial Orientation		N			Ar		
		Ar			C		
Final Orientation		N			Ar		
		Ar			C		
Total =	28.25 kcal/mol						
van der Waals =	97.88 kcal/mol						
Electrostatic =	-289.44 kcal/mol						
ΔE_{tot} =	-45.24 kcal/mol						
ΔE_{vdw} =	-7.76 kcal/mol						
ΔE_{ele} =	-46.17 kcal/mol						
Initial Orientation		N			O		
		O					
		Ar					
Final Orientation		N					
		O					
		Ar					
Total =	71.14 kcal/mol						
van der Waals =	102.88 kcal/mol						
Electrostatic =	-247.90 kcal/mol						
ΔE_{tot} =	-2.35 kcal/mol						
ΔE_{vdw} =	-2.76 kcal/mol						
ΔE_{ele} =	-4.63 kcal/mol						
Initial Orientation	C	O					
		Ar					
Final Orientation	C	Ar			N		
		C					
		N					
Total =	43.34 kcal/mol						
van der Waals =	92.80 kcal/mol						
Electrostatic =	-267.75 kcal/mol						
ΔE_{tot} =	-30.15 kcal/mol						
ΔE_{vdw} =	-12.83 kcal/mol						
ΔE_{ele} =	-24.48 kcal/mol						
Initial Orientation		C			N		
					C		
Final Orientation		C			N		
					C		
Total =	77.46 kcal/mol						
van der Waals =	88.71 kcal/mol						
Electrostatic =	-233.62 kcal/mol						
ΔE_{tot} =	3.97 kcal/mol						
ΔE_{vdw} =	-16.93 kcal/mol						
ΔE_{ele} =	9.65 kcal/mol						

Table 3.84: The solution phase results of 3-hydroxyanthranilic acid interacting with the EVHHQK region of the 1Z0Q conformer of β-amyloid

	Glu11	Val12	His13	His14	Gln15	Lys16	Val18	Glu22
Initial Orientation	N			C				
	Ar							
	C							
Final Orientation	N			C	C			
	Ar							
	C							
Total =	79.15 kcal/mol							
van der Waals =	87.60 kcal/mol							
Electrostatic =	-250.13 kcal/mol							
ΔE_{tot} =	-39.48 kcal/mol							
ΔE_{vdw} =	-2.32 kcal/mol							
ΔE_{ele} =	-38.04 kcal/mol							
Initial Orientation				Ar				Ar
				C				
Final Orientation	O			Ar			Ar	Ar
Total =	83.56 kcal/mol							
van der Waals =	85.90 kcal/mol							
Electrostatic =	-239.63 kcal/mol							
ΔE_{tot} =	-35.06 kcal/mol							
ΔE_{vdw} =	-4.02 kcal/mol							
ΔE_{ele} =	-27.54 kcal/mol							
Initial Orientation	Ar			Ar				
Final Orientation				Ar				
Total =	90.16 kcal/mol							
van der Waals =	88.74 kcal/mol							
Electrostatic =	-249.46 kcal/mol							
ΔE_{tot} =	-28.46 kcal/mol							
ΔE_{vdw} =	-1.18 kcal/mol							
ΔE_{ele} =	-37.37 kcal/mol							
Initial Orientation	Ar			C				
Final Orientation	Ar			C				
Total =	108.20 kcal/mol							
van der Waals =	90.81 kcal/mol							
Electrostatic =	-234.07 kcal/mol							
ΔE_{tot} =	-10.43 kcal/mol							
ΔE_{vdw} =	0.89 kcal/mol							
ΔE_{ele} =	-21.98 kcal/mol							

The results of 3-hydroxyanthranilic acid interacting with the LVFF region of Aβ in a solvated environment are summarized in Tables 3.85-3.89. There are no systems that were optimized in the solution phase for the 1BA4 conformer of Aβ. Very few binding interactions occurred within the LVFF region of β-amyloid, and those that did only occurred with the 1AMB and 1Z0Q conformations, and Phe19-Phe20 was preferred.

Table 3.85: The solution phase results of 3-hydroxyanthranilic acid interacting with the LVFF region of the 1AMB conformer of β-amyloid

	His14	Gln15	Lys16	Leu17	Val18	Phe19	Phe20	Asp23
Initial Orientation			C			N	Ar	O
						C		Ar
						Ar		
Final Orientation			C			N	Ar	O
						C		
						Ar		
Total =	-74.43 kcal/mol							
van der Waals =	58.48 kcal/mol							
Electrostatic =	-298.69 kcal/mol							
ΔE_{tot} =	-69.62 kcal/mol							
ΔE_{vdw} =	-5.74 kcal/mol							
ΔE_{ele} =	-73.97 kcal/mol							
Initial Orientation			C			Ar	Ar	O
Final Orientation			C			Ar	Ar	O
Total =	-69.27 kcal/mol							
van der Waals =	58.40 kcal/mol							
Electrostatic =	-288.29 kcal/mol							
ΔE_{tot} =	-64.46 kcal/mol							
ΔE_{vdw} =	-5.82 kcal/mol							
ΔE_{ele} =	-63.57 kcal/mol							
Initial Orientation			Ar			O		
Final Orientation			Ar			O		
Total =	-34.65 kcal/mol							
van der Waals =	70.18 kcal/mol							
Electrostatic =	-278.71 kcal/mol							
ΔE_{tot} =	-29.84 kcal/mol							
ΔE_{vdw} =	5.97 kcal/mol							
ΔE_{ele} =	-54.00 kcal/mol							
Initial Orientation	Ar				Ar			
Final Orientation	Ar	Ar			Ar	O		
Total =	-14.67 kcal/mol							
van der Waals =	63.03 kcal/mol							
Electrostatic =	-236.93 kcal/mol							
ΔE_{tot} =	-9.87 kcal/mol							
ΔE_{vdw} =	-1.19 kcal/mol							
ΔE_{ele} =	-12.22 kcal/mol							

Table 3.86: The solution phase results of 3-hydroxyanthranilic acid interacting with the LVFF region of the 1AMC conformer of β-amyloid

	His13	Gln15	Lys16	Leu17	Val18	Phe19	Phe20	Glu22	Asp23
Initial Orientation						Ar			O
									Ar
Final Orientation						Ar			O
									Ar
Total =	-69.53 kcal/mol								
van der Waals =	46.53 kcal/mol								
Electrostatic =	-281.81 kcal/mol								
ΔE_{tot} =	-39.15 kcal/mol								
ΔE_{vdw} =	-16.20 kcal/mol								
ΔE_{ele} =	-34.59 kcal/mol								
Initial Orientation			Ar			O			
Final Orientation			Ar						
Total =	-46.49 kcal/mol								
van der Waals =	57.64 kcal/mol								
Electrostatic =	-270.62 kcal/mol								
ΔE_{tot} =	-16.12 kcal/mol								
ΔE_{vdw} =	-5.09 kcal/mol								
ΔE_{ele} =	-23.40 kcal/mol								
Initial Orientation	C		C						
			Ar						
Final Orientation			Ar						
Total =	-71.59 kcal/mol								
van der Waals =	53.40 kcal/mol								
Electrostatic =	-283.59 kcal/mol								
ΔE_{tot} =	-41.21 kcal/mol								
ΔE_{vdw} =	-9.33 kcal/mol								
ΔE_{ele} =	-36.37 kcal/mol								
Initial Orientation		O			Ar	N		O	
		Ar						Ar	
Final Orientation		O			Ar			O	
		Ar						Ar	
Total =	-57.76 kcal/mol								
van der Waals =	66.08 kcal/mol								
Electrostatic =	-272.73 kcal/mol								
ΔE_{tot} =	-27.38 kcal/mol								
ΔE_{vdw} =	3.36 kcal/mol								
ΔE_{ele} =	-25.51 kcal/mol								

Table 3.87: The solution phase results of 3-hydroxyanthranilic acid interacting with the LVFF region of the 1AML conformer of β-amyloid

	Leu17	Val18	Phe19	Phe20	Asp23	Gly29	Ala30
Initial Orientation			O		N		
Final Orientation					N		
Total =	123.73 kcal/mol						
van der Waals =	103.26 kcal/mol						
Electrostatic =	-200.65 kcal/mol						
ΔE_{tot} =	0.60 kcal/mol						
ΔE_{vdw} =	17.89 kcal/mol						
ΔE_{ele} =	-14.80 kcal/mol						
Initial Orientation				Ar		O	Ar
				C			
Final Orientation				N			
				C			
				Ar			
Total =	102.99 kcal/mol						
van der Waals =	79.96 kcal/mol						
Electrostatic =	-204.35 kcal/mol						
ΔE_{tot} =	-20.15 kcal/mol						
ΔE_{vdw} =	-5.41 kcal/mol						
ΔE_{ele} =	-18.51 kcal/mol						
Initial Orientation				Ar	O		
Final Orientation				Ar	O		
Total =	156.39 kcal/mol						
van der Waals =	99.94 kcal/mol						
Electrostatic =	-219.35 kcal/mol						
ΔE_{tot} =	33.26 kcal/mol						
ΔE_{vdw} =	14.57 kcal/mol						
ΔE_{ele} =	-33.50 kcal/mol						

Table 3.88: The solution phase results of 3-hydroxyanthranilic acid interacting with the LVFF region of the 1IYT conformer of β-amyloid

	Gln15	Lys16	Leu17	Val18	Phe19	Phe20	Asp23
Initial Orientation		Ar			Ar		O
		C					
Final Orientation		Ar			Ar		O
		C					Ar
Total =	35.19 kcal/mol						
van der Waals =	90.13 kcal/mol						
Electrostatic =	-278.29 kcal/mol						
ΔE_{tot} =	-38.30 kcal/mol						
ΔE_{vdw} =	-15.51 kcal/mol						
ΔE_{ele} =	-35.03 kcal/mol						
Initial Orientation	Ar				O		
Final Orientation	-	-	-	-	-	-	-
Total =	139.14 kcal/mol						
van der Waals =	98.58 kcal/mol						
Electrostatic =	-242.23 kcal/mol						
ΔE_{tot} =	65.65 kcal/mol						
ΔE_{vdw} =	-7.05 kcal/mol						
ΔE_{ele} =	1.04 kcal/mol						

Table 3.89: The solution phase results of 3-hydroxyanthranilic acid interacting with the LVFF region of the 1Z0Q conformer of β-amyloid

	Leu17	Val18	Phe19	Phe20	Asp23
Initial Orientation			O	Ar	
Final Orientation			O	Ar	
Total =	77.87	kcal/mol			
van der Waals =	84.92	kcal/mol			
Electrostatic =	-247.19	kcal/mol			
ΔE_{tot} =	-40.76	kcal/mol			
ΔE_{vdw} =	-5.00	kcal/mol			
ΔE_{ele} =	-35.10	kcal/mol			
Initial Orientation			Ar	Ar	
				O	
Final Orientation			Ar	N	O
				Ar	
				O	
Total =	86.52	kcal/mol			
van der Waals =	82.26	kcal/mol			
Electrostatic =	-242.68	kcal/mol			
ΔE_{tot} =	-32.11	kcal/mol			
ΔE_{vdw} =	-7.66	kcal/mol			
ΔE_{ele} =	-30.59	kcal/mol			
Initial Orientation			Ar	Ar	
				N	
				O	
				C	
Final Orientation			Ar	Ar	
Total =	112.51	kcal/mol			
van der Waals =	92.53	kcal/mol			
Electrostatic =	-221.60	kcal/mol			
ΔE_{tot} =	-6.11	kcal/mol			
ΔE_{vdw} =	2.60	kcal/mol			
ΔE_{ele} =	-9.51	kcal/mol			
Initial Orientation	Ar			N	
Final Orientation	Ar			O	
Total =	108.56	kcal/mol			
van der Waals =	84.58	kcal/mol			
Electrostatic =	-219.34	kcal/mol			
ΔE_{tot} =	-10.07	kcal/mol			
ΔE_{vdw} =	-5.35	kcal/mol			
ΔE_{ele} =	-7.25	kcal/mol			

3.7.4 CONCLUSIONS OF 3-HYDROXYANTHRANILIC ACID INTERACTING WITH β-AMYLOID IN SILICO

3-Hydroxyanthranilic acid demonstrates a capacity to bind to β-amyloid in both gas and solution phase environments. For the most part, the orientation of 3HAA tended to remain the same upon optimization in a solvated environment. An example of a binding interaction can be seen in Figure 3.8.

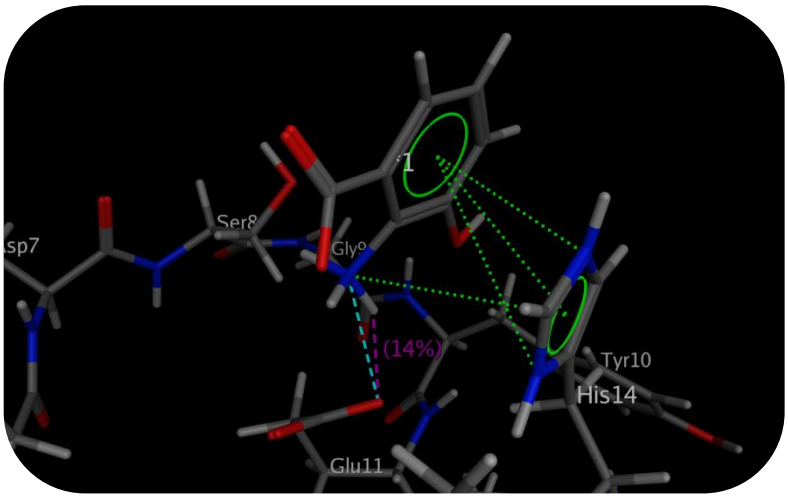

Figure 3.8: Binding interaction between 3HAA and β-amyloid. Dashed green lines indicate cation-π interactions and aromatic-aromatic stacking interactions. The dashed purple line indicates formation of a hydrogen bond.

The LVFF region demonstrated the least potential for binding to the acid. This is likely due in part to the small size of the target molecule. Given that the amino group is so close to the aromatic ring of 3HAA, there was likely not enough distance between the two to interact with two side chains at the same time in this region. The same could be said for the hydroxyl group and the aromatic ring.

EV**HH**Q**K** and **HH**Q**K** combined to form the most favourable target region of Aβ for binding to 3-hydroxyanthranilic acid. The His13-His14 and Glu11-His14 side chains

were the most favoured orientations where binding occurred between the acid and Aβ at multiple sites. Interactions at His13 favoured the carboxylate group, while His14 interacted more so with the aromatic ring; in the case of interactions occurring at His14 and Glu11, His14 bound almost equally to the carboxylate group and the aromatic ring. The Glu11 site was favoured for interactions with both the aromatic ring and the amino group of 3-hydroxyanthranilic acid. 3HAA therefore presents itself as a viable molecule for acting as an anti-aggregant.

3.8 Biological Support of 3-hydroxyanthranilic acid as a Lead Molecule

Given the results of screening the library of endogenous compounds, several compounds were selected for *in vitro* testing to determine whether they could indeed act as anti-aggregants. 3-hydroxyanthranilic acid was subjected to *in vitro* assays, and demonstrated a capacity to inhibit Aβ aggregation. The results of TEM scans of Aβ in presence and absence of 3HAA are shown in Figure 3.9 and were performed by Rose Chen. It can be seen that only diffuse aggregates of Aβ form in the presence of the acid when compared to the control.

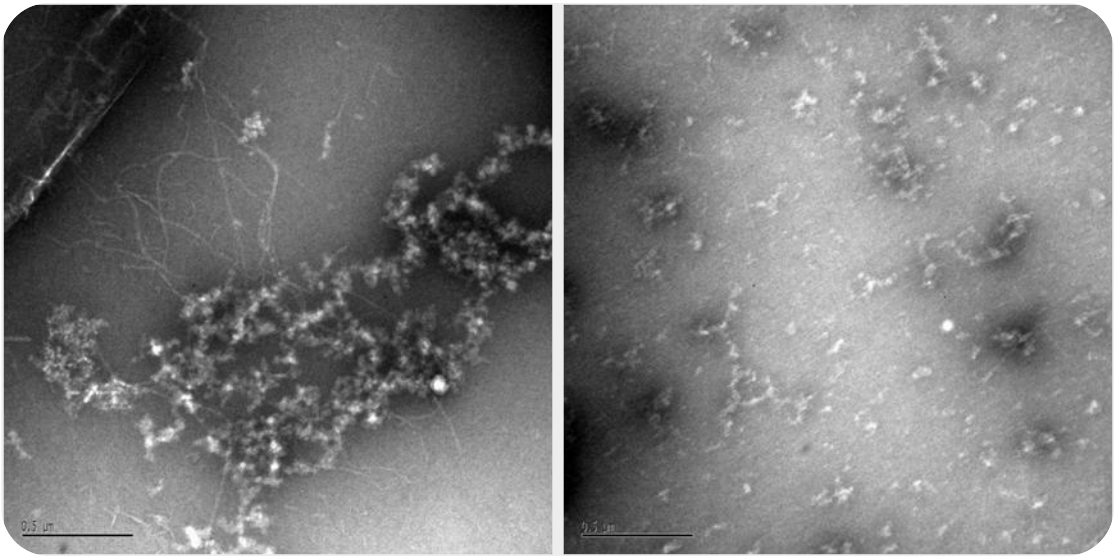

Figure 3.9: Transmission electron microscopy (TEM) of $A\beta_{40}$ (20 μM) in the absence (left) and presence (right) of 3-HAA (100 μM). A mixture of fibrillar and diffuse Aβ aggregates can be seen on the left, while the incubation containing 3-HA contains only diffuse aggregates on the right. For both micrographs, scale bar represents 0.5 μm.

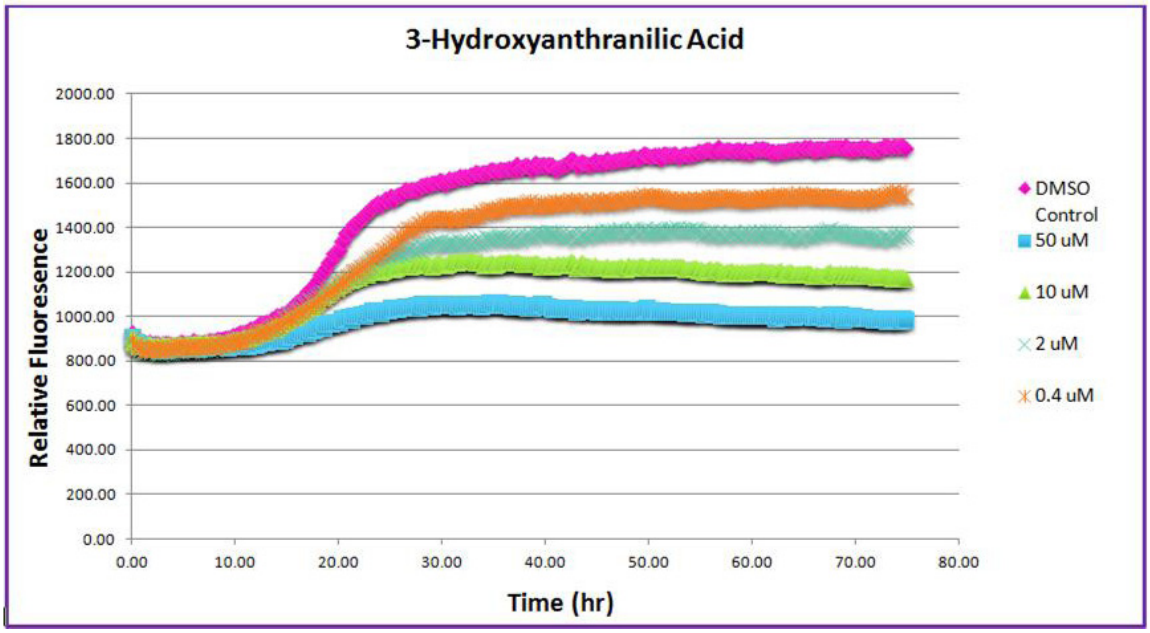

Figure 3.10: Thioflavin-T assay of 3-hydroxyanthranilic acid at various concentrations interacting with Aβ

Figure 3.10 shows the results of a thioflavin T (ThT) assay of 3HAA at various concentrations, and its effect on the amount of aggregated β-amyloid. This method is also

used to calculate the IC_{50}, which is the half maximal inhibitory concentration (the amount of compound needed to inhibit a biological process by half).

The thioflavin T assay measures fluorescence in regards to β-amyloid aggregation. ThT is a dye that fluoresces when it binds to aggregated Aβ, if there is less aggregation occurring, there will be less fluorescence observed. As the concentration of 3HAA increases, the amount of fluorescence occurring decreases; this indicates that binding is occurring to prevent aggregation. Dimethyl sulfoxide (DMSO) is used as a control as it does not affect the aggregation of Aβ. The methodology for this assay is given in Appendix 5. The thioflavin T assays were performed by Gordon Simms.

Thioflavin S is used in a similar fashion to thioflavin T but for examining tau aggregation. As tau is also an important factor in AD, a molecule that can inhibit aggregation in both β-amyloid and tau is desirable. The results of the thioflavin S assay (performed by Rose Chen) of 3-hydroxyanthranilic acid are shown in Figure 3.11.

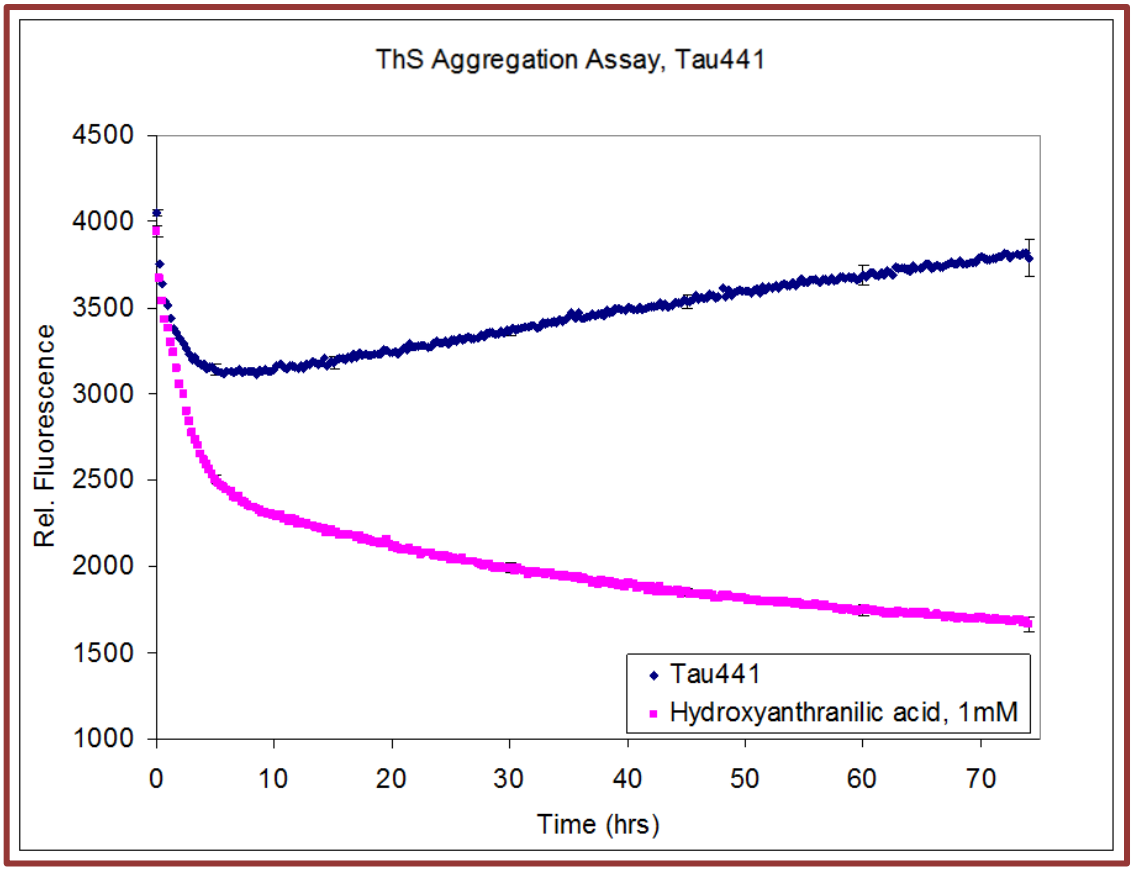

Figure 3.11: Thioflavin S assay of 3-hydroxyanthranilic acid interacting with tau

3HAA also exhibits an inhibitory effect on tau aggregation. The positive results of the *in silico* and *in vitro* binding of 3-hydroxyanthranilic acid with β-amyloid lead to the selection of the compound as a lead molecule for further developing analogues in an attempt to improve its binding efficiency.

3.9 A Quantitative Structure-Activity Relationship Study of 3-hydroxyanthranilic acid and its Analogues

In collaboration with Gordon Simms, research was performed to develop a series of analogues based on 3-hydroxyanthranilic acid using a quantitative structure-activity relationship (QSAR) study. This QSAR was used to predict the activity of molecules to

determine which would be best to synthesize and test for anti-aggregant activity. A QSAR uses a variety of descriptors covering geometry, electronic features, physicochemical properties and topological indices to correlate biological activity [39].

3.9.1 Development of a Series of Analogues Based on 3-hydroxyanthranilic acid

The first step in the QSAR process was to develop a series of analogues of 3HAA to be synthesized for *in vitro* testing to determine their IC_{50}, which is the half maximal inhibitory concentration (the amount of compound needed to inhibit a biological process by half), and therefore the activity of the compounds. In collaboration, a series of fifty compounds was designed based on the use of bioisosteric substitution.

Bioisosteric substitution involves replacing functional groups on the molecule of interest with other groups having either similar charge distributions or size, for example. The purpose is to attempt to improve the biological activity of the compound by replacing certain functional groups with others that mimic the electronegativity, spatial arrangement or lipophilicity of that area [90]. If, for example, the spatial arrangement is maintained by replacing a hydrogen atom with fluorine, the effect of a greater electronegativity on the activity of the molecule can be seen [90, 91]. Some bioisosteric substitutions can be made to improve stability and lipophilicity; replacing a carboxylate group with tetrazole matches the acidity, while allowing for more stability and lipophilicity that would allow penetration of the blood-brain barrier [91].

For these analogues, substitution could occur at any point on the ring, with the carboxylate, amino and hydroxyl groups having the most possibilities for substitution.

The list of analogues developed though these are detailed with their name, structure, and series identifier in Figures 3.12 and 3.13.

The activities measured for these compounds are given in Table 3.90.

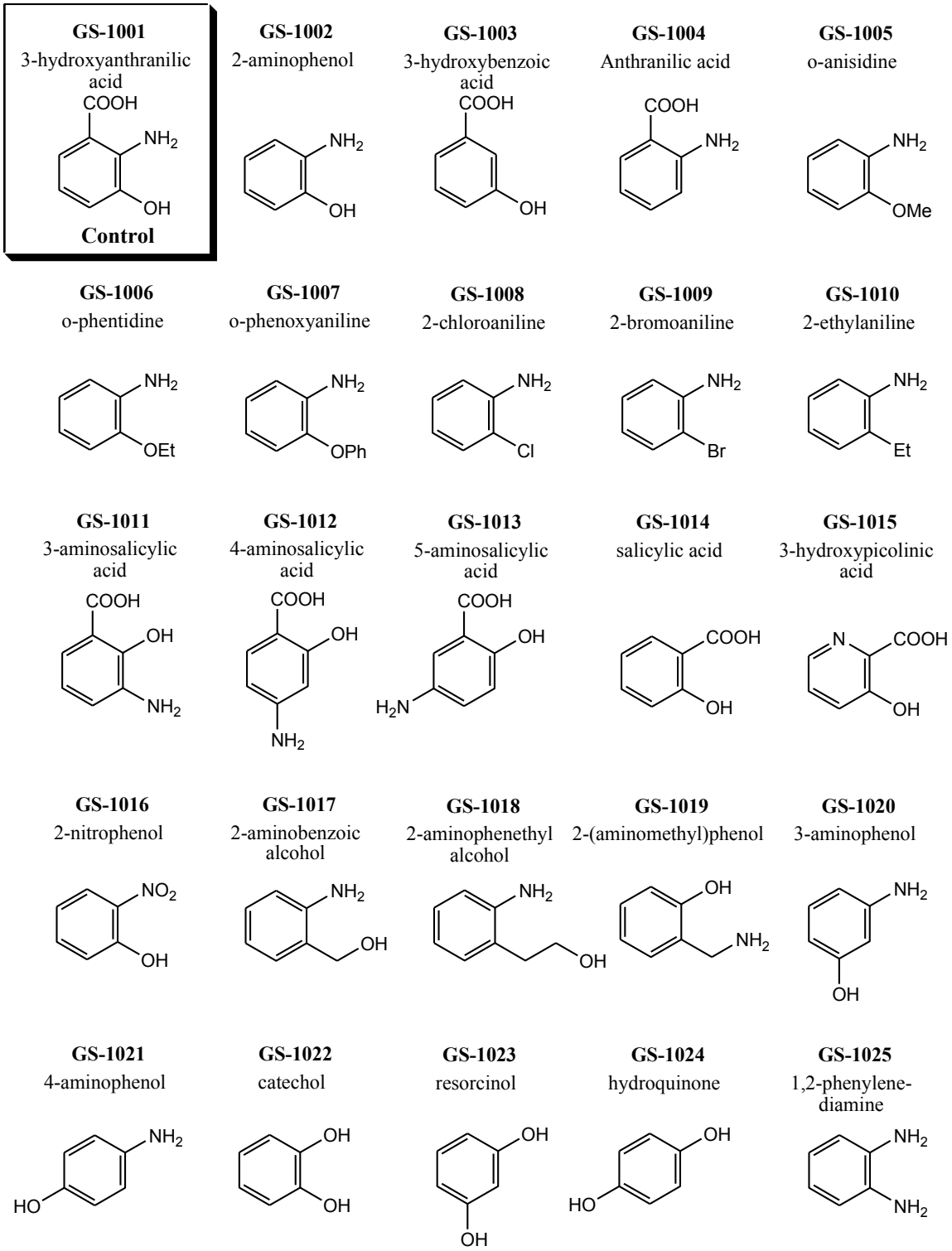

Figure 3.12: 3HAA analogues 1-25

GS-1026
1,3-phenylene-diamine

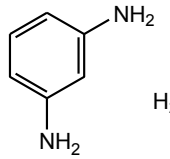

GS-1027
1,4-phenylene-diamine

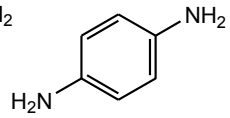

GS-1028
2-hydroxy-6-methylaniline

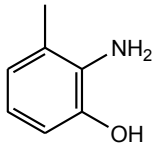

GS-1029
2-amino-p-cresol

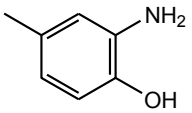

GS-1030
2-amino-5-methylphenol

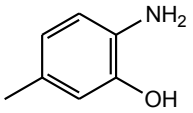

GS-1031
2-methoxyphenol

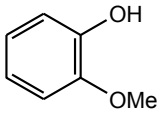

GS-1032
1,2-dimethyoxy-benzene

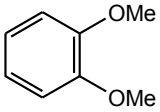

GS-1033
2-(benzyloxy) phenol

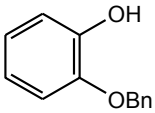

GS-1034
1,2-bis(benzyloxy) phenol

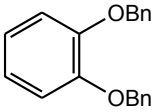

GS-1035
1-(benzyloxy)-2-methoxybenzene

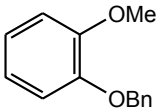

GS-1036
2-methoxy-N-methylaniline HCl

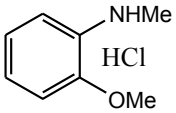

GS-1037
2-methoxy-N,N-dimethylaniline HCl

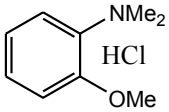

GS-1038
N-benzyl-2-methoxyaniline HCl

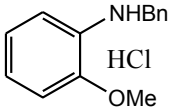

GS-1039
N,N-dibenzyl-2-methoxyaniline HCl

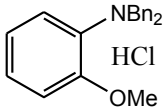

GS-1040
3-methoxy-N-methylaniline HCl

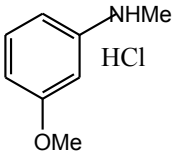

GS-1041
3-methoxy-N,N-dimethylaniline HCl

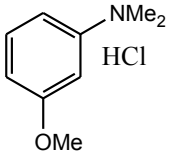

GS-1042
N-benzyl-3-methoxyaniline HCl

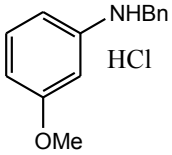

GS-1043
N,N-dibenzyl-3-methoxyaniline HCl

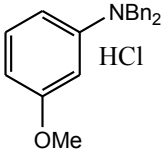

GS-1044
N-(2-hydroxyphenyl) formamide

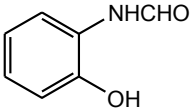

GS-1045
2-(phenylamino) phenol HCl

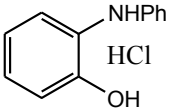

GS-1046
2-methoxy-*N*-phenylaniline HCl

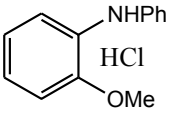

GS-1047
2-(methylamino) phenol

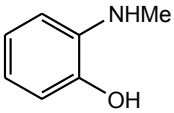

GS-1048
2-(dimethylamino) phenol

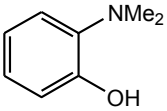

GS-1049
2-(benzylamino) phenol

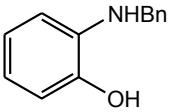

GS-1050
4-(methylamino) phenol

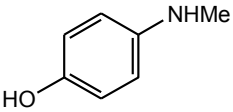

Figure 3.13: 3HAA analogues 26-50

Table 3.90: 3HAA analogues and their calculated IC_{50}s

Compound Identifier	Calculated IC_{50} (μM)
GS-1001	5.05
GS-1002	4.545
GS-1003	> 300
GS-1004	> 300
GS-1005	> 300
GS-1006	> 300
GS-1007	297.95
GS-1008	> 300
GS-1009	> 300
GS-1010	> 300
GS-1011	> 300
GS-1012	> 300
GS-1013	9.999
GS-1014	> 300
GS-1015	> 300
GS-1016	> 300
GS-1017	> 300
GS-1018	> 300
GS-1019	> 300
GS-1020	> 300
GS-1021	2.323
GS-1022	8.2315
GS-1023	> 300
GS-1024	12.8775
GS-1025	> 300
GS-1026	> 300
GS-1027	1.818
GS-1028	2.424
GS-1029	21.816
GS-1030	14.3925
GS-1031	> 300
GS-1032	> 300
GS-1033	> 300
GS-1034	> 300
GS-1035	> 300
GS-1036	> 300
GS-1037	> 300
GS-1038	> 300
GS-1039	> 300
GS-1040	> 300
GS-1041	> 300
GS-1042	> 300
GS-1043	> 300
GS-1044	262.6
GS-1045	2.727
GS-1046	> 300
GS-1047	6.9185
GS-1048	8.888
GS-1049	2.5755
GS-1050	2.02

3.9.2 DEVELOPMENT OF A QSAR FOR ACTIVITY PREDICTION

Using the structural data and biological activities, the 3HAA analogues were divided into two sets: a training set, and a validation set. The training set is used to develop the QSAR equation for predicting activity, and the validation set is used to determine how accurate that equation truly is.

Initial attempts divided the fifty analogues into a training set of 33 compounds and a validation set of 17 compounds. The structures were optimized in MOE, and the pIC_{50} was calculated from each IC_{50} [87]. All descriptors available in MOE were calculated for the training set, and those with zero contribution were eliminated. The partial least squares (PLS) method was first used; however despite changes to the size and components of the training set, as well as the number of descriptors calculated, this method proved to be ineffective at predicting compound activity. It appears that the biological data does not provide enough range for the PLS method, as the compounds were all either highly active or very inactive.

3.9.3 DEVELOPMENT OF A BINARY QSAR TO PREDICT 3HAA ANALOGUE ACTIVITY

A successful QSAR was developed in MOE using a binary method of relating descriptors to activity. For this method, compounds are considered to be either active or inactive, and each descriptor is tested to see if it is valid for both the active and inactive species. This proved to be a more suitable approach to the QSAR as the synthesized compounds exhibited either high activity or complete inactivity. The QSAR used a training set of 34 molecules, containing a mixture of active and inactive species, with attempts to include representations of the different molecular substitutions. The threshold

for activity was set for a pIC_{50} (the negative log of the IC_{50}) of -2.0, and all of the available descriptors in MOE were calculated. These descriptors were narrowed down by first eliminating those with values of zero, or identical values for all species. Once these descriptors were removed, the relative importance of the remaining descriptors as well as their effect on the predictive capacity was used to narrow the field. Descriptors were removed one at time, and their effect on the predictivity of the QSAR was examined, those whose removal resulted in increased predictivity were eliminated, while those whose removal resulted in a decreased predictivity were retained. Furthermore, descriptors having similar functions were also weeded down by seeing which had a more positive impact on the prediction; the MOE system contains a large variety of descriptors, some of which have identical functions but that are calculated by different means (e.g. the heat of formation can be calculated by AM1, PM3 or MNDO). Thus descriptors were gradually eliminated until a reasonable prediction of activity versus inactivity could be obtained using a small amount of descriptors (as the more descriptors present, the greater the risk of overfitting the data, which would result in a QSAR with poor predictivity for molecules outside the training set).

The final system is composed of 9 descriptors and a short summary of their function is summarized in Table 3.91.

Table 3.91: Descriptors used in the QSAR for 3HAA

Descriptor	Function
PM3-HF	The heat of formation calculated using the PM3 Hamiltonian
SlogP_VSA5	Log of the octanol/water coefficient based on the accessible van der Waals surface area
SMR_VSA0 SMR_VSA1 SMR_VSA4 SMR_VSA5	Contributions to the molar refractivity based on the accessible van der Waals surface area falling within a specific range
vdw_vol	Calculates the van der Waals volume
vsa_don	Approximate sum of the van der Waals surface areas of pure hydrogen bond donors
vsurf_W2	Hydrophilic volume

Using these nine descriptors, a total accuracy of 0.97 was obtained for the training set that can be broken down to 0.92 for the active molecules and 1.00 for the inactive analogues. The total accuracy on the actives is considered the sensitivity of the model, that is the measure of the number of actives that were correctly predicted, while the total accuracy on the inactives is considered the specificity, that is the measure of the number of inactives that were correctly predicted. Cross-validation statistics indicate a total accuracy of 0.91 for the model, which can be broken down to 0.83 for the active molecules and 0.95 for the inactive molecules. Cohen's kappa (a statistical measure of agreement for binary systems) was calculated to be 0.93 for the training set, which is an excellent value indicating good agreement between the observed and predicted values. The kappa value also takes into consideration the possibility of this agreement occurring by chance.

When the QSAR model was applied to the validation set, four false positives and one false negative were identified. The predicted activities were given as a scale from 0

(inactive) to 1 (active). Compounds were therefore judged to be active if the predicted value was above 0.5. It should be noted that one of the molecules in the validation set that was incorrectly predicted as active had a prediction value of 0.5012. The Cohen's kappa value for the validation set was 0.23, which is a fair value, but not as good as seen in the training set; this number would increase to 0.35 if the compound with a prediction value of 0.5012 was assigned as inactive. The measured sensitivity and selectivity of the applied model are 0.67 and 0.77, respectively. The results of this QSAR are summarized in Table 3.92.

Table 3.92: Predicted activities for the training and validations sets of 3HAA analogues 1-50

Training Set			Validation Set		
Compound ID	IC_{50} (μM)	Predicted Activity	Compound ID	IC_{50} (μM)	Predicted Activity
GS-1001	5.05	Active	GS-1007	297.95	Inactive
GS-1002	4.545	Active	GS-1008	300	Inactive
GS-1003	300	Inactive	GS-1013	9.999	Active
GS-1004	300	Inactive	GS-1016	300	**Active**
GS-1005	300	Inactive	GS-1017	300	Inactive
GS-1006	300	Inactive	GS-1019	300	**Active**
GS-1009	300	Inactive	GS-1021	2.323	Active
GS-1010	300	Inactive	GS-1023	300	**Active**
GS-1011	300	Inactive	GS-1032	300	Inactive
GS-1012	300	Inactive	GS-1034	300	Inactive
GS-1014	300	Inactive	GS-1037	300	Inactive
GS-1015	300	Inactive	GS-1038	300	Inactive
GS-1018	300	Inactive	GS-1040	300	Inactive
GS-1020	300	Inactive	GS-1042	300	**Active**
GS-1022	8.2315	Active	GS-1046	300	Inactive
GS-1024	12.8775	Active	GS-1048	8.888	**Inactive**
GS-1025	300	Inactive			
GS-1026	300	Inactive			
GS-1027	1.818	**Inactive**			
GS-1028	2.424	Active			
GS-1029	21.816	Active			
GS-1030	14.3925	Active			
GS-1031	300	Inactive			
GS-1033	300	Inactive			
GS-1035	300	Inactive			
GS-1036	300	Inactive			
GS-1039	300	Inactive			
GS-1041	300	Inactive			
GS-1043	300	Inactive			
GS-1044	262.6	Inactive			
GS-1045	2.727	Active			
GS-1047	6.9185	Active			
GS-1049	1.616	Active			
GS-1050	2.02	Active			

3.9.4 PREDICTION OF ACTIVITY OF A SERIES OF ANALOGUES BASED ON 3-HYDROXYANTHRANILIC ACID

The binary QSAR demonstrated its potential to correctly predict the activity of the first series of 3-hydroxyanthranilic acid analogues to a moderate level; therefore, this combination of descriptors was deemed useful and was used to predict the activity of a second set of analogues composed of 86 new molecules. The full list of structures is given in Appendix 7, along with their predicted activity.

From the 86 analogues, 39 were predicted to be active. To date twenty-six analogues have been synthesized from this new series, containing a mixture of active and inactive compounds. Some inactive compounds were included to verify that the prediction was accurate enough for further use. The synthesized analogues are shown in Figure 3.14, and are currently undergoing biological testing to determine the IC_{50} values. Initial data has been provided to determine if the compounds are active or inactive, and the results are compared to the predicted values in Table 3.93.

.

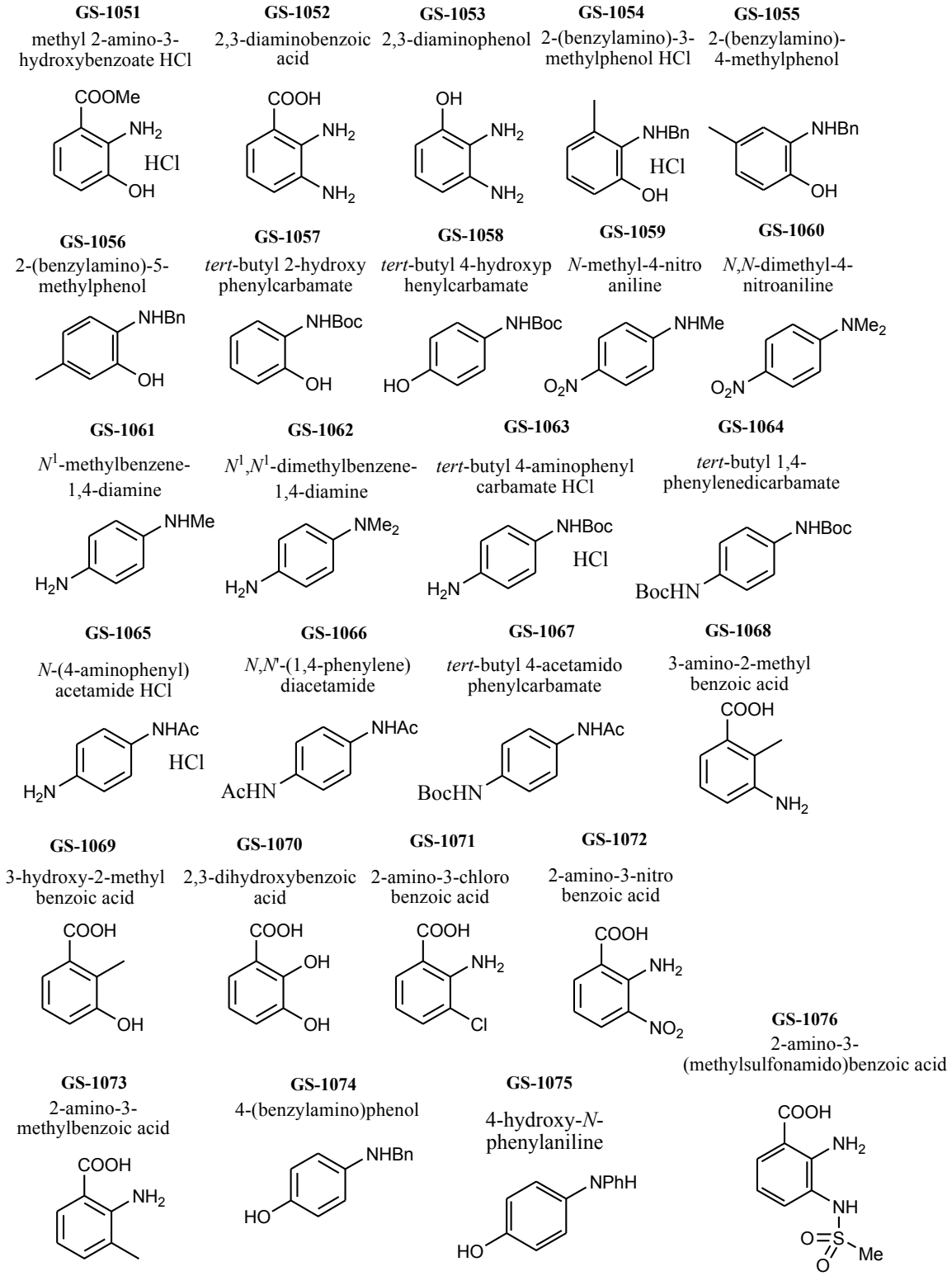

Figure 3.14: 3HAA analogues 51-76

Table 3.93: Predicted and observed activities of analogues 51-76 of 3HAA

Compound ID	Predicted Activity	Biological Activity
GS-1051	**Inactive**	Active
GS-1052	Inactive	Inactive
GS-1053	Active	Active
GS-1054	Active	Active
GS-1055	Active	Active
GS-1056	Active	Active
GS-1057	Active	Active
GS-1058	Active	Active
GS-1059	Active	Active
GS-1060	Active	Active
GS-1061	Active	Active
GS-1062	Active	Active
GS-1063	Active	Active
GS-1064	**Active**	Inactive
GS-1065	**Inactive**	Active
GS-1066	**Active**	Inactive
GS-1067	**Active**	Inactive
GS-1068	Inactive	Inactive
GS-1069	Inactive	Inactive
GS-1070	Inactive	Inactive
GS-1071	Inactive	Inactive
GS-1072	Active	Active
GS-1073	Inactive	Inactive
GS-1074	Active	Active
GS-1075	Active	Active
GS-1076	Active	Active

The results of the QSAR predictions are quite accurate. Of the twenty-six compounds synthesized to date, the biological activity was correctly predicted for twenty-one of the system for an 81 percent accurate prediction. In total, three compounds were incorrectly predicted to be active, and two predicted to be inactive. The specificity is therefore calculated to be 0.75, with a selectivity of 0.83. Cohen's kappa indicates a correlation between the predicted and observed values of 0.56, which can be considered a

moderately good result. Therefore the data can be used to determine if any more of the compounds in the series should be synthesized as well.

Once the IC_{50}s of these newly synthesized analogues are calculated, the data will be incorporated to make a new training set of compounds for the QSAR to better improve its predictive ability. The technique has so far proved useful and quite accurate in selecting novel compounds for synthesis. This is an iterative process, and will be repeated as many times as necessary in order to design the best lead molecule capable of binding to β-amyloid to prevent aggregation

3.10 Novel Bi-aromatic Compounds Targeting the BBXB Region of Proteins Involved in Alzheimer's Disease

As mentioned previously, there exists a common motif among several proteins involved in AD. The motif follows the pattern of **BB**X**B** where B is any basic amino acid, and X represents any other amino acid (and can include basic amino acids as well). Previous research by the Weaver group has identified twenty-seven proteins implicated in the Alzheimer's disease process that contain this **BB**X**B** motif [41].

We postulate that a single molecule can act as a promiscuous drug to target this common motif [41]. A single drug capable of acting on multiple targets involved in AD would allow for better treatment, not only inhibiting β-amyloid aggregation, but diffusing some of the negative effects caused by inflammatory responses in the region of Aβ aggregation.

Four bi-aromatic molecules developed by the Weaver group were selected to test their capacity to act as promiscuous drug molecules targeting the **BB**X**B** region of these

proteins. The four compounds are NCE-0103, NCE-0112, NCE-0216 and NCE-0325 (Figure 3.15), where NCE stands for novel chemical entity.

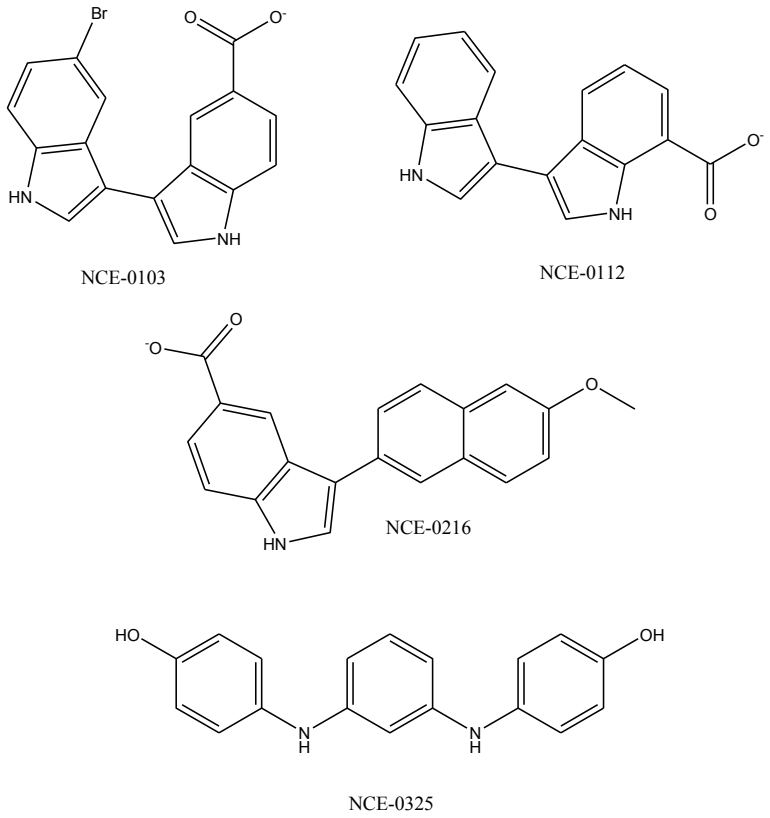

Figure 3.15: NCE-0103, NCE-0112, NCE-0216, and NCE-0325

Of the twenty-seven identified proteins, several were not viable options for this study. Although tau plays a major role in AD, there are currently no structures available of the protein in the RCSB protein data bank and thus it could not be examined for potential interactions with these four compounds. Interleukin-1 receptor 1 and interleukin-10 were not studied, and interleukin-6, hemochromatosis protein and the class II major histocompatibility complex had **BB**X**B** regions that were inaccessible upon optimization in QUANTA [46]. The only structure of interleukin 3 available in the RCSB PDB contained mutations in the **BB**X**B** region and was not a viable option for study.

Gas phase optimizations were performed to determine if these lead compounds could interact with the **BB**X**B** region on each of the remaining proteins: S100β, complement component 1, q subcomponent, A chain, (C1qA), interferon-gamma (IFN-γ), acetylcholinesterase (AChE), apolipoprotein ε4 (Apoε4), interleukin-1 β converting enzyme (IL-1βCE), interleukin 4 (IL-4), interleukin 12 (IL-12), interleukin 13 (IL-13), alpha-1-antichymotrypsin (α_1-ACT), betaine-homocysteine methyl transferase (BHMT), T lymphocyte activation antigen (B7-1), intercellular adhesion molecule 1 (ICAM-1), macrophage inflammatory protein-1α (MIP-1α), macrophage inflammatory protein-1β (MIP-1β), stromal cell-derived factor-1 (SDF-1), neprilysin (NEP), transferrin, and regulated upon activation, normal T-cell expressed, and secreted (RANTES).

The **BB**X**B** motif for each protein is detailed in Table 3.94, and some have more than one **BB**X**B** region available.

Table 3.94: Identification of the amino acids composing the BBXB motif

Protein	BBXB amino acids			
	B	B	X	B
α_1-ACT	Lysine	Arginine	Tryptophan	Arginine
Aβ	Histidine	Histidine	Glutamine	Lysine
AChE	Arginine	Arginine	Phenylalanine	Arginine
Apoε4	Lysine	Arginine	Leucine	Histidine
	Lysine	Arginine	Leucine	Lysine
	Arginine	Lysine	Leucine	Arginine
B7-1	Lysine	Arginine	Glutamic Acid	Histidine
BHMT	Lysine	Arginine	Alanine	Arginine
C1qA	Lysine	Lysine	Glycine	Histidine
ICAM-1	Arginine	Arginine	Aspartic Acid	Histidine
	Histidine	Histidine	Aspartic Acid	Arginine
IFN-γ	Lysine	Lysine	Lysine	Arginine
IL-1βCE	Lysine	Lysine	Alanine	Histidine
IL-4	Histidine	Histidine	Glutamic Acid	Lysine
	Histidine	Arginine	Histidine	Lysine
IL-12	Histidine	Lysine	Leucine	Lysine
IL-13	Lysine	Lysine	Leucine	Histidine
MIP-1α	Lysine	Arginine	Serine	Arginine
MIP-1β	Lysine	Arginine	Serine	Lysine
Neprilysin	Lysine	Arginine	Cysteine	Histidine
	Lysine	Lysine	Leucine	Arginine
RANTES	Arginine	Lysine	Asparagine	Arginine
S100β	Histidine	Lysine	Leucine	Lysine
	Lysine	Lysine	Leucine	Lysine
SDF-1	Lysine	Histidine	Leucine	Lysine
Transferrin	Lysine	Lysine	Glycine	Arginine

3.10.1 PREPARATION OF THE LEAD MOLECULES AND PROTEINS

Gas phase minimizations were performed to find the lowest energy systems for each of the four lead molecules and the proteins. For the four lead compounds, the molecules were constructed in QUANTA and subjected to systematic conformational

searches; each torsional angle was rotated from 0-330° in 30° increments, and the lowest energy structure resulting from this scan was selected [46]. The energies of these systems are given in Table 3.95.

Table 3.95: Energies of the four NCE molecules

	Energy (kcal/mol)		
Compound	E_{tot}	E_{vdw}	E_{ele}
NCE-0103	45.51	5.65	-5.10
NCE-0112	56.04	4.96	23.45
NCE-0216	42.70	12.64	-0.90
NCE-0325	-22.50	3.06	-36.34

The proteins underwent different processing as necessary to prepare them for optimization in the QUANTA environment [46]. The details for interleukins 4, 12 and 13, ICAM-1, S100β and RANTES are given in Chapter 2, Sections 2.7.1.1-2.7.1.6. The remaining proteins were prepared as follows.

3.10.1.1 β-AMYLOID

The β-amyloid protein is believed to be the causative factor in Alzheimer's disease, initiating a cascade of neurotoxic events when it undergoes misfolding [8, 9]. The optimized structure of the 1IYT conformer of β-amyloid used in previous optimization with dopamine and phenylalanine was used for this project.

3.10.1.2 α_1-ACT

Although the precise function of α_1-ACT is unknown, it is believed to play an anti-inflammatory role [92]. This protein is found localized in the amyloid plaques in the brain [81]. The PDB structure, 1QMN, was downloaded into MOE, where hydrogen

atoms were added, the histidine residues protonated, and then the file was formatted for QUANTA [46, 47]. Upon importation, there was a carboxylate group incorrectly constructed as an aldehyde group that was retyped before the protein backbone was constrained and the system was minimized via steepest descents.

3.10.1.3 AChE

Acetylcholinesterase is the enzyme involved in the metabolism of acetylcholine, and levels of the acetylcholine neurotransmitter decline with the progression of AD [6, 7]. The structure of AChE was downloaded from the PDB (as 2J3D) into MOE [47, 93]. Hydrogen atoms were added, solvent and other substances removed, and the histidine residues were protonated before being imported into QUANTA [46]. The structure was minimized using steepest descents with a constrained protein backbone.

3.10.1.4 ApoE4

The apolipoprotein ε4 is an isoform of the protein, which normally plays a role in maintaining and repairing neurons; the ε4 isoform is linked to AD, and its mode of action remains to be determined [94]. The 1G39 entry of the PDB was downloaded, and in MOE actions were taken to remove solvent, add hydrogen atoms and protonate histidine [47, 95]. The structure was imported into QUANTA and underwent gas phase optimization using the steepest descents algorithm with a constrained protein backbone [46].

3.10.1.5 B7-1

The B7-1 protein is located on the surface of antigen-presenting cells, and plays a role in signalling immune response when binding to white blood cells [96]. The PDB structure, 1DR9, was protonated for physiological pH after extraneous molecules were

deleted and hydrogen atoms added to the structure [96]. The protein required some asparagine residues and carboxylate groups to be corrected as well; the system was then optimized with a constrained protein backbone via steepest descents.

3.10.1.6 BHMT

The betaine-homocysteine methyl transferase enzyme exerts a role in cellular and plasma levels of homocysteine [97]. It has been suggested that elevated levels of homocysteine may play a role in AD [97]. For this structure, identified by 1LT8, preparation involved adding hydrogen atoms, removing solvent, zinc, and an identical chain, and finally protonating the His residues before importation in QUANTA, and following the same optimization scheme as the other proteins [46, 97].

3.10.1.7 C1QA

The C1q protein (PDB entry 2JG9) plays a role in clearing apoptotic cells by binding to the surface of these cells to signal phagocytes to engulf them, and plays a role in controlling the inflammatory process [98]. As in the case of the previous proteins, before minimization (with a constrained protein backbone) in QUANTA, the protein first needed hydrogen atoms added to the structure, solvent and extraneous molecules removed and the histidine residues protonated [46].

3.10.1.8. IFN-γ

Interferon-γ is a cytokine that exerts immunomodulatory effects, and exists in a dimeric form [99]. IL-12 can increase the production of this inflammatory protein, which activates natural killer cells that lead to cell death [22, 69]. Solvent molecules were deleted, hydrogen atoms added and histidine residues protonated, with the C terminal

carboxylate corrected for the 1EKU structure of IFN-γ before optimization in QUANTA [46, 99].

3.10.1.9 IL-1βCE

This enzyme plays a role in producing the inflammatory cytokine, interleukin-1β and may play a role in regulating the programmed cell death of neuronal cells [100]. The same process of preparing the protein was followed as in Section 3.2.8.1.3.

3.10.1.10 MIP-1α AND MIP-1β

These macrophage inflammatory proteins play a role as chemoattractants, initiating inflammatory responses [101]. They can play a role in activating white blood cells to bind to other cells for their removal [101]. Both 2X69 and 2X6L (MIP-1α and MIP-1β, respectively) were imported directly into QUANTA, where the protein backbone was constrained and minimization occurred via steepest descents.

3.10.1.11 NEP

Neutral endopeptidase, or neprilysin, is involved in the degradation of a peptide exhibiting vasodilatory and diuretic activities [102]. The structure, 2YB9, was prepared by adding hydrogen atoms, removing solvent and other molecules, and protonating the histidine residues [102]. Optimization in QUANTA followed the same method as the other proteins.

3.10.1.12 SDF-1

SDF-1 is another pro-inflammatory protein that acts as a chemoattractant for various types of white blood cells [103]. Its PDB structure, 2SDF, required only

protonation for physiological pH before it was imported into QUANTA and optimized [5, 103].

3.10.1.13 TRANSFERRIN

Transferrin, as its name implies, binds to iron and transports it throughout the body [104]. The release of iron is in part triggered by lower pH and iron is one of the metal ions found located in Aβ plaques, which tends towards lower pH [81, 104]. The transferrin protein, 3S9N, was prepared by deleting extraneous chains, adding hydrogen atoms, and then correcting numerous side chains that were lacking the R group before ensuring the system was charged for physiological pH and imported into QUANTA [46].

3.10.2 GAS PHASE OPTIMIZATION OF THE NCE COMPOUNDS WITH BBXB

Optimizations of these compounds with the **BB**X**B** region of the various proteins was set up such that the functional groups/aromatic rings of the NCE compounds were approximately 3.0 Å away from two of the basic amino acids in the **BB**X**B** region of the protein being examined. Each system was minimized with a constrained protein backbone via steepest descents.

The binding energies were calculated using the following equations:

$$\Delta E_{tot} = E_{tot} - E_{BBXB} - E_{NCE} \tag{3.20}$$

$$\Delta E_{vdw} = E_{vdw} - E_{vdwBBXB} - E_{vdwNCE} \tag{3.21}$$

$$\Delta E_{ele} = E_{ele} - E_{eleBBXB} - E_{eleNCE} \tag{3.23}$$

The total, van der Waals and electrostatic interactions were calculated for each gas phase system, where the energy of the protein was calculated with a constrained protein backbone. The energies of the proteins are summarized in Appendix 8.

Each of the optimized systems was imported into MOE to better determine what interactions were occurring between the ligand and the protein [47].

3.10.3 Results of the Optimization of the NCE Compounds with BBXB

The results of the optimizations are summarized in Tables 3.96-3.119. Amino acid side chains are represented by their single letter abbreviation followed by their number on the chain. The NCE compounds are represented by the abbreviations shown in Figure 3.16. The initial and final binding orientations are given, and the calculated energies. Different types of binding interactions are represented by different colours, and the darker the shade of the colour, the more that type of interaction is occurring at that site. Cation-π and π-π interactions are represented by blue and green, while hydrogen bonds are orange. Interactions with the $–CH_2$- chain on the amino acids (particularly common with lysine) are coloured indigo, while light purple indicates potential interactions with the C=O of the protein backbone; lime green represents those occurring with the –CH- of the backbone.

For IFN-γ, MIP-1α, MIP-1β and RANTES, there exist two identical **BB**X**B** motifs, either on the same chain, or on an identical chain. For these systems there are also tables summarizing systems optimized with two molecules of the NCE compounds, one at each site; the interactions are broken down in to (A) and (B) to show to which of the two identical motifs the molecule was binding.

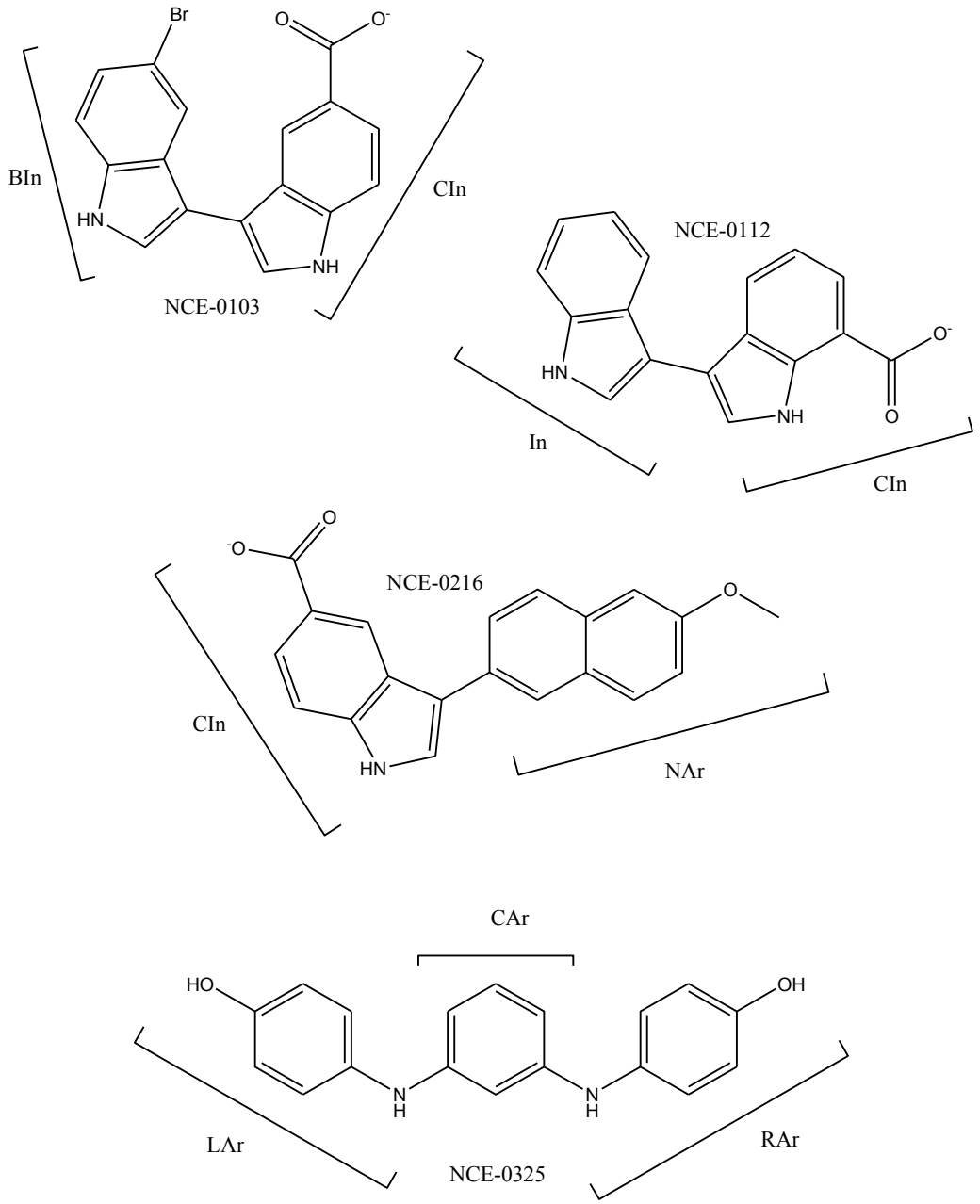

Figure 3.16: Regions of NCE compounds identified for interactions with BBXB

Table 3.96: Results of the optimization of the lead molecules and α_1-ACT

α1-ACT	Initial Orientation				Final Orientation									Binding Energy (kcal/mol)		
	K273	R274	W275	R276	E234	**K273**	**R274**	**W275**	**R276**	D277	S278	T381	Q384	Total	VdW	Ele
NCE 0103	CIn	BIn			BIn	CIn	BIn							-33.00	-11.13	-27.38
	BIn	CIn			CIn	BIn	CIn							-29.35	-14.34	-23.08
	BIn			CIn					CIn			CIn		-7.71	-9.15	-3.60
	CIn			BIn		CIn			BIn	CIn				-19.00	-13.03	-12.72
NCE 0112	CIn	In			-	-	-	-	-	-	-	-	-	-22.98	-5.13	-22.02
	In	CIn				In	CIn							-40.43	-10.97	-34.30
	In			CIn		In			CIn	In				-25.65	-15.56	-17.15
	CIn			In		CIn			In	CIn			In	-21.74	-14.08	-11.03
NCE 0216	NAr	CIn			CIn		CIn							-19.44	-5.56	-20.42
	CIn	NAr				CIn	NAr							-28.52	-6.81	-26.18
	CIn			NAr		CIn/NAr			NAr	NAr			NAr	-29.37	-13.73	-21.38
	NAr			CIn					CIn	NAr				-17.17	-14.61	-6.66
NCE 0325	LAr	RAr				LAr	RAr				RAr			-21.64	-7.33	-17.36
	RAr	LAr			LAr	RAr	LAr							-15.89	-6.50	-11.66
	LAr			RAr					RAr	RAr				-24.80	-7.70	-19.76
	RAr			LAr		RAr			LAr	RAr				-34.76	-13.41	-26.15

Table 3.97: Results of the optimization of the lead molecules and Aβ

Aβ	Initial Orientation				Final Orientation							Binding Energy (kcal/mol)		
	H13	H14	Q15	K16	Y10	**H13**	**H14**	**Q15**	**K16**	L17	F20	Total	VdW	Ele
NCE 0103	CIn	BIn				CIn	BIn			CIn		-19.48	-11.54	-10.60
	BIn	CIn				BIn	CIn			BIn		-19.60	-10.73	-11.95
						BIn	CIn							
	BIn			CIn		BIn			CIn		CIn	-24.40	-8.03	-17.50
	CIn			BIn		CIn			BIn		BIn	-24.68	-9.00	-17.71
NCE 0112	CIn	In				CIn	In			CIn		-7.75	-7.36	-5.02
	In	CIn				In	CIn			CIn		-5.03	-6.23	-3.65
	In			CIn		In			CIn		CIn	-12.76	-4.63	-13.21
	CIn			In		CIn						-3.36	-4.03	-3.53
NCE 0216	NAr	CIn			CIn	NAr	CIn			CIn		-18.55	-11.32	-9.77
	CIn	NAr			NAr	CIn	NAr			NAr		-25.61	-11.97	-16.85
						CIn								
	CIn			NAr		CIn			NAr			-19.66	-9.60	-12.56
	NAr			CIn		NAr			CIn		CIn	-25.57	-9.69	-15.79
									CIn					
NCE 0325	LAr	RAr				LAr	RAr			CAr		-14.76	-8.96	-8.69
										RAr				
	RAr	LAr			LAr	RAr	LAr					-14.86	-6.33	-10.90
	LAr			RAr		LAr			RAr		RAr	-14.38	-6.27	-9.39
	RAr			LAr		RAr			LAr			-6.25	-2.65	-4.64

Table 3.98: Results of the optimization of the lead molecules and AChE

AChE	Initial Orientation				Final Orientation							Binding Energy (kcal/mol)		
	R44	F45	R46	R47	**R44**	**F45**	**R46**	**R47**	E49	Q162	E163	Total	VdW	Ele
NCE			BIn	CIn						CIn		-68.80	-7.81	59.10
0103			CIn	BIn			CIn					-9.39	-10.85	-6.75
NCE			CIn	In	-	-	-	-	-	-	-	-36.31	-2.05	-38.94
0112			In	CIn			In	CIn	In	CIn		63.33	-8.16	81.98
							CIn							
NCE			NAr	CIn			NAr				NAr	-63.19	-3.57	-68.11
0216			CIn	NAr					Cin			-10.06	-6.99	-5.15
NCE			LAr	RAr			LAr	RAr		RAr	LAr	-81.74	1.42	-93.58
0325			RAr	LAr			RAr				RAr	-69.48	1.16	-79.18

Table 3.99: Results of the optimization of the lead molecules and Apoε4

Apoε4	Initial Orientation				Final Orientation							Binding Energy (kcal/mol)		
	H140	L141	R142	K143	S139	**H140**	**L141**	**R142**	**K143**			Total	VdW	Ele
NCE	BIn			CIn		BIn			CIn			-39.00	-13.59	-23.04
0103	CIn			BIn		CIn			BIn			-175.00	-24.64	-138.57
NCE	In			CIn	-	-	-	-	-	-	-	-128.35	-16.34	-103.07
0112	CIn			In	-	-	-	-	-	-	-	-148.72	-16.67	-126.88
NCE	CIn			NAr	NAr				NAr			-149.12	-19.83	-124.52
0216	NAr			CIn		CIn			CIn			-45.61	-16.18	-30.39
						NAr								
NCE	LAr			RAr	-	-	-	-	-	-	-	-26.73	-5.51	-21.42
0325	RAr			LAr	LAr	LAr			LAr			-171.95	-16.46	-150.56
						CAr								
	R142	K143	L144	R145	R38	A138	S139	**R142**	**K143**	**L144**	**R145**			
NCE	BIn			CIn		CIn		BIn			CIn	83.40	-14.06	-70.35
0103	CIn			BIn				CIn				-17.35	-12.36	2.33
NCE	In			CIn	CIn						CIn	-38.05	-14.49	-16.55
0112	CIn			In	-	-	-	-	-	-	-	-253.86	-17.12	-219.42
NCE	NAr	CIn				NAr	NAr				CIn	-43.02	-16.92	-26.85
0216	CIn	NAr			-	-	-	-	-	-	-	-7.55	-7.70	3.31
	CIn			NAr				CIn				-132.40	-14.83	-105.05
	NAr			CIn	-	-	-	-	-	-	-	-59.81	-9.04	-43.21
NCE	LAr	RAr					LAr	LAr	RAr			-36.21	-12.52	-21.66
								LAr						
0325	RAr	LAr				LAr	LAr	RAr	LAr			-45.57	-12.99	-23.76
	LAr			RAr	RAr			LAr			RAr	-50.07	-12.95	-36.17
					RAr									
	RAr			LAr	LAr						LAr	-36.40	-12.28	-21.48
	K143	L144	R145	K146	R38	**K143**	**L144**	**R145**	**K146**	L149	D153			
NCE			CIn	BIn	-	-	-	-	-	-	-	-276.27	-17.07	-246.19
0103			BIn	CIn					CIn	CIn		-93.20	-12.75	-80.20
NCE			CIn	In					In			-88.01	-11.47	-69.08
0112			In	CIn				In		In/CIn		-37.23	-10.94	-3.40
NCE			NAr	CIn	NAr				CIn	CIn		-24.38	-13.61	-12.18
0216			CIn	NAr				CIn		NAr	NAr	-62.78	-13.92	-44.27
NCE			LAr	RAr	LAr				RAr	CAr		-166.51	-19.01	-146.65
0325			RAr	LAr	RAr				LAr	RAr/CAr/LAr		-48.53	-16.26	-33.86

Table 3.100: Results of the optimization of the lead molecules and B7-1

B7-1	Initial Orientation				Final Orientation				Binding Energy (kcal/mol)		
	K93	R94	E95	H96	K93	R94	E95	H96	Total	VdW	Ele
NCE 0103	CIn	BIn			CIn				-11.08	-3.64	-9.02
	BIn	CIn				CIn			-8.75	-4.35	-6.74
		BIn		CIn		BIn	CIn	CIn	-14.46	-4.02	-12.71
		CIn		BIn	-	-	-	-	-16.07	-0.53	-17.12
	BIn			CIn				CIn	-18.74	-5.08	-15.19
	CIn			BIn	-	-	-	-	-16.89	-0.17	-18.76
NCE 0112	CIn	In			-	-	-	-	-5.39	-1.70	-4.95
	In	CIn			-	-	-	-	-1.01	-1.74	-0.77
		In		CIn	-	-	-	-	-8.32	-2.54	-7.43
		CIn		In		CIn			-12.32	-2.24	-14.31
	In			CIn	-	-	-	-	-8.90	-2.20	-7.76
	CIn			In	-	-	-	-	-3.32	-2.26	-1.68
NCE 0216	NAr	CIn				CIn			-9.02	-2.98	-8.31
	CIn	NAr			CIn				-16.26	-3.75	-15.21
		CIn		NAr		CIn			-10.99	-1.29	-13.94
		NAr		CIn					-6.58	-4.29	-4.93
	CIn			NAr	CIn			CIn	-10.80	-4.01	-9.23
	NAr			CIn				CIn	-14.10	-4.34	-12.87
NCE 0325	LAr	RAr				RAr			-9.72	-2.29	-7.37
	RAr	LAr			RAr	LAr			-3.71	-1.54	-2.59
		RAr		LAr		RAr LAr		LAr	-16.99	-3.03	-15.12
		LAr		RAr		LAr		RAr	-17.84	-3.32	-15.92
	LAr			RAr				RAr	-8.05	-3.20	-7.45
	RAr			LAr				LAr	-11.27	-4.13	-9.09

Table 3.101: Results of the optimization of the lead molecules and BHMT

BHMT	Initial Orientation				Final Orientation							Binding Energy (kcal/mol)		
	R346	A347	R348	K349	W331	S333	**R346**	**A347**	**R348**	**K349**	E350	Total	VdW	Ele
NCE 0103			BIn	CIn			CIn			CIn	BIn	-70.80	-3.19	-77.20
			CIn	BIn					CIn	BIn		-45.04	-11.26	-44.37
					CIn				CIn	BIn				
NCE 0216			NAr	CIn					NAr	CIn	NAr	-23.22	-11.46	-27.24
			CIn	NAr					CIn	NAr		-38.81	-3.79	-41.87
NCE 0325			LAr	RAr					LAr	RAr	LAr	-40.74	-8.48	-35.52
						RAr		RAr	RAr	LAr	RAr			
			RAr	LAr					RAr	RAr LAr	CAr	-71.31	-11.24	-65.42

Table 3.102: Results of the optimization of the lead molecules and C1qA

C1qA	Initial Orientation				Final Orientation						Binding Energy (kcal/mol)		
	K200	K201	G202	H203	W147	E148	**K200**	**K201**	**G202**	**H203**	Total	VdW	Ele
NCE 0103	CIn	BIn					CIn				-129.94	-3.18	-134.99
	BIn	CIn					BIn	CIn			-129.77	-9.46	-127.56
		BIn		CIn		BIn				CIn	-100.84	-6.47	-99.64
		CIn		BIn		CIn	CIn	CIn			-114.44	-8.07	-114.67
	BIn			CIn		CIn	BIn			CIn	-112.57	-10.51	-109.83
	CIn			BIn		BIn	CIn				-118.77	-8.78	-116.97
NCE 0112	CIn	In					CIn				-109.91	-4.56	-113.10
	In	CIn						CIn			-142.02	-9.83	-140.07
		In		CIn		In				CIn	-92.21	-10.38	-84.04
		CIn		In		CIn	CIn	CIn		In	-115.23	-10.89	-119.52
							CIn						
	In			CIn	CIn		In			CIn	-76.44	-5.69	-78.29
	CIn			In			CIn				-114.94	-4.09	-117.65
NCE 0216	NAr	CIn						CIn			-103.83	-4.55	-106.84
	CIn	NAr				NAr	CIn				-109.82	-0.62	-117.60
		CIn		NAr			CIn	CIn			-115.25	-6.30	-119.69
		NAr		CIn	CIn					CIn	-76.88	-6.45	-74.52
	CIn			NAr			CIn				-108.66	-3.83	-112.23
	NAr			CIn			NAr			CIn	-72.24	-2.94	-75.86
NCE 0325	LAr	RAr				RAr	LAr	RAr			-54.53	-3.35	-53.48
	RAr	LAr				LAr	RAr	LAr			-54.09	-3.65	-55.02
		RAr		LAr	LAr	RAr	RAr				-52.28	-8.04	-45.19
							RAr						
		LAr		RAr		LAr	LAr			RAr	-38.92	-5.26	-35.69
	LAr			RAr			LAr				-52.06	-8.76	-50.83
	RAr			LAr			RAr				-45.23	-1.60	-46.56

Table 3.103: Results of the optimization of the lead molecules and ICAM-1

ICAM-1	Initial Orientation				Final Orientation											Binding Energy (kcal/mol)		
	R149	R150	D151	H152	R125	L130	T144	T145	V146	L147	**R149**	**R150**	**D151**	**H152**	H153	Total	VdW	Ele
NCE 0103	CIn	BIn									CIn	BIn	CIn			-20.13	-7.59	-13.37
	BIn	CIn									BIn	CIn				-18.76	-5.42	-13.64
	BIn			CIn	CIn						BIn			CIn		-18.85	-6.43	-13.80
	CIn			BIn			BIn		BIn	CIn	CIn					-35.16	-16.94	-18.39
NCE 0112	CIn	In			-	-	-	-	-	-	-	-	-	-	-	-15.53	-3.27	-12.14
	In	CIn									In					-16.18	-2.81	-12.54
	In			CIn	CIn				CIn	CIn	CIn			CIn		-20.45	-11.83	-15.25
											In							
	CIn			In						CIn	CIn					-24.08	-10.32	-20.55
NCE 0216	NAr	CIn										CIn				-14.10	-4.15	-13.03
	CIn	NAr									CIn					-11.43	-4.82	-8.24
	CIn			NAr	NAr	NAr			NAr	CIn	CIn					-33.62	-13.66	-21.66
	NAr			CIn					CIn	CIn	NAr					-27.44	-13.14	-18.72
NCE 0325	LAr	RAr									LAr	RAr				-10.87	-3.97	-7.73
	RAr	LAr									RAr		RAr		LAr	-15.90	-8.17	-11.13
	LAr			RAr				RAr	RAr	LAr						-23.70	-13.20	-13.23
	RAr			LAr	LAr	LAr			LAr		RAr					-21.48	-14.62	-11.68
	R150	D151	H152	H153	R125	R149	**R150**	**D151**	**H152**	**H153**								
NCE 0103	CIn	BIn			CIn		CIn		CIn							-41.09	-14.69	-29.19
	BIn	CIn					BIn									-31.91	-7.97	-26.14
	BIn			CIn			BIn			CIn						-28.32	-7.30	-22.23
	CIn			BIn			CIn			BIn						-17.03	-6.90	-11.56
NCE 0112	CIn	In			CIn	CIn		In								-23.48	-12.04	-17.47
	In	CIn			In	In		CIn								-25.45	-10.37	-21.97
	In			CIn			In			CIn						-8.42	-4.59	-9.41
	CIn			In				CIn								-9.60	-5.26	-9.23
NCE 0216	NAr	CIn						NAr	NAr	CIn						-37.19	-11.15	-28.12
	CIn	NAr			CIn				CIn							-28.84	-9.69	-21.21
	CIn			NAr			CIn	NAr		NAr						-21.75	-10.10	-12.76
	NAr			CIn			NAr									-16.56	-4.13	-14.32
NCE 0325	LAr	RAr			LAr	LAr		CAr	LAr	RAr						-21.94	-10.60	-12.98
	RAr	LAr			RAr	CAr		LAr	RAr	LAr						-19.65	-11.89	-8.10
	LAr			RAr	-	-	-	-	-	-						-8.20	-3.43	-6.86
	RAr			LAr			RAr									-7.80	-3.62	-5.15

Table 3.104: Results of the optimization of the lead molecules and IFN-γ

IFN-γ	Initial Orientation				Final Orientation										Binding Energy (kcal/mol)		
	K86	K87	K88	R89	K74	E75	N78	N85	**K86**	**K87**	**K88**	**R89**	D90	E93	Total	VdW	Ele
NCE 0103	CIn	BIn									CIn				-17.21	-4.41	-12.17
	BIn	CIn									BIn				-21.39	-4.60	-15.48
		BIn		CIn									BIn		-19.31	-3.81	-13.48
		CIn		BIn						CIn		BIn	CIn/BIn		-18.09	-8.86	-7.30
	BIn			CIn		CIn		CIn	BIn			CIn			-44.57	-15.33	-27.84
	CIn			BIn	BIn		BIn		CIn			BIn	BIn		-26.80	-12.78	-13.00
NCE 0112	CIn	In							CIn						-18.99	-8.48	-9.15
	In	CIn							In	CIn					-20.53	-8.03	-10.19
		In		CIn									CIn		-13.99	-8.41	-3.86
		CIn		In					In			In	In		-24.29	-7.25	-14.61
	In			CIn					In			CIn		CIn	-16.41	-6.52	-9.04
	CIn			In					CIn			CIn			-20.12	-6.44	-11.93
NCE 0216	NAr	CIn								CIn					-11.69	-4.06	-6.22
	CIn	NAr							CIn						-22.62	-7.34	-13.44
		CIn		NAr	-	-	-	-	-	-	-	-	-	-	-11.27	-4.77	-6.50
		NAr		CIn					CIn	NAr		CIn			-22.41	-7.31	-13.91
	CIn			NAr					CIn						-26.02	-9.75	-14.31
	NAr			CIn					NAr			CIn			-21.62	-9.38	-11.33
												CIn					
NCE 0325	LAr	RAr								RAr					-17.40	-4.78	-11.11
	RAr	LAr							RAr						-13.68	-4.23	-9.27
		RAr		LAr								LAr			-17.44	-4.05	-12.18
		LAr		RAr					RAr			RAr	LAr		-15.12	-6.56	-7.23
	LAr			RAr					LAr			RAr		RAr	-17.38	-7.46	-8.85
	RAr			LAr					RAr						-17.39	-7.27	-8.62

Table 3.105: Results of the optimization of the lead molecules and IFN-γ at two binding sites

IFN-γ		Initial Orientation				Final Orientation									Binding Energy (kcal/mol)		
	(A)	K86	K87	K88	R89	K74	N78	**K86**	**K87**	**K88**	**R89**	D90	E93	K94			
	(B)	K206	K207	K208	R209	K194	N198	**K206**	**K207**	**K208**	**R209**	D210	E213		Total	VdW	Ele
NCE 0103	(A)	CIn	BIn					CIn							-42.06	-8.24	-28.82
	(B)							CIn									
	(A)	BIn	CIn					BIn							-33.61	-10.54	-23.48
	(B)							BIn									
	(A)		BIn		CIn			CIn			CIn	BIn		BIn	-39.35	-12.34	-24.97
	(B)								BIn		CIn	BIn/CIn					
	(A)		CIn		BIn			BIn	CIn		BIn	BIn		CIn	-30.11	-16.16	-12.32
	(B)										BIn						
	(A)	BIn			CIn			BIn			CIn				-28.77	-7.88	-17.40
	(B)							BIn			CIn						
	(A)	CIn			BIn			CIn							-27.10	-7.55	-14.67
	(B)							CIn									
NCE 0112	(A)	CIn	In					CIn							-26.67	-9.10	-12.72
	(B)							CIn									
	(A)	In	CIn					In							-33.70	-8.13	-23.51
	(B)								CIn								
	(A)		In		CIn			CIn			CIn	In/CIn			-47.91	-19.26	-25.09
	(B)							CIn			CIn	In/CIn					
	(A)		CIn		In			In			CIn	In/CIn			-40.86	-16.40	-23.06
	(B)							In			In	In					
	(A)	In			CIn	CIn	CIn	In			CIn	CIn	CIn		-66.75	-29.41	-34.70
	(B)					CIn	CIn	In			CIn		CIn				
	(A)							In			In						
		CIn			In			CIn							-35.00	-10.90	-20.33
	(B)							In			In						
								CIn									
NCE 0216	(A)	NAr	CIn			-	-	-	-	-	-	-	-	-	-38.02	-9.60	-26.02
	(B)					-	-	-	-	-	-	-	-	-			
	(A)	CIn	NAr					CIn							-21.32	-3.79	-17.63
	(B)							CIn									
	(A)		NAr		CIn			CIn	Nar		CIn				-22.64	-11.17	-11.74
	(B)							CIn	Nar		CIn						
	(A)		CIn		NAr			NAr				NAr			-30.91	-10.16	-19.68
	(B)					-	-	-	-	-	-	-	-	-			
	(A)	NAr			CIn			NAr			CIn				-31.26	-10.91	-19.29
	(B)							NAr			CIn						
	(A)	CIn			NAr			CIn							-43.37	-9.43	-34.08
	(B)							CIn									
NCE 0325	(A)	LAr	RAr						RAr						-26.70	-4.92	-20.56
	(B)								RAr								
	(A)	RAr	LAr			-	-	-	-	-	-	-	-	-	-21.75	-5.01	-16.78
	(B)					-	-	-	-	-	-	-	-	-			
	(A)		LAr		RAr						RAr				-41.77	-9.31	-32.62
	(B)							RAr			RAr	RAr					
	(A)		RAr		LAr						LAr	LAr/RAr			-25.10	-11.73	-14.01
	(B)										LAr						
	(A)							LAr/CAr			CAr		RAr				
		LAr			RAr						RAr				-37.85	-8.62	-27.07
	(B)					-	-	-	-	-	-	-	-	-			
	(A)							RAr			LAr		LAr				
		RAr			LAr						RAr				-29.21	-14.94	-13.94
	(B)							RAr			LAr		LAr				

Table 3.106: Results of the optimization of the lead molecules and IL-1βCE

IL-1βCE	Initial Orientation				Final Orientation					Binding Energy (kcal/mol)		
	K319	K320	A321	H322	D275	**K319**	**K320**	**A321**	**H322**	Total	VdW	Ele
NCE 0103	CIn	BIn				CIn			BIn	-125.34	-5.25	-122.97
	BIn	CIn					CIn			-98.30	-4.77	-92.99
		BIn		CIn	-	-	-	-	-	-88.37	-2.12	-88.96
		CIn		BIn	-	-	-	-	-	-78.95	2.95	-89.43
	BIn			CIn		BIn				-98.37	-4.66	-94.85
	CIn			BIn		CIn			BIn	-131.80	-11.06	-123.32
NCE 0112	CIn	In				CIn	In		In	-95.20	-5.39	-92.20
	In	CIn				In				-93.69	-4.78	-87.96
		In		CIn					CIn	-104.10	-2.49	-101.43
		CIn		In			CIn		In	-56.05	-5.09	-52.59
	In			CIn		In				-102.62	-6.63	-95.22
	CIn			In		CIn	CIn		In/CIn	-112.06	-4.31	-108.72
NCE 0216	NAr	CIn					CIn			-73.30	-1.95	-75.13
	CIn	NAr				CIn			CIn	-124.98	-4.46	-120.05
		CIn		NAr			CIn		NAr	-77.23	-5.84	-79.41
		NAr		CIn	-	-	-	-	-	-86.93	-0.99	-87.70
NCE 0325	LAr	RAr				LAr	RAr			-41.01	-5.45	-40.45
	RAr	LAr			RAr		LAr		LAr RAr	-95.52	-7.47	-94.71
		RAr		LAr			RAr			-70.66	-2.09	-79.70
		LAr		RAr			LAr			-41.59	-0.70	-36.51
	LAr			RAr		LAr			RAr	-32.53	-4.10	-40.61
	RAr			LAr	RAr	RAr				-47.34	-7.34	-41.27
	R371	K372	V373	R374	**R371**	**K372**	**V373**	**R374**	M386			
NCE 0103	BIn			CIn	BIn					137.21	-7.00	145.52
	CIn			BIn	CIn					80.68	-3.34	83.36
NCE 0112	In			CIn	-	-	-	-	-	-64.88	-1.52	-70.77
	CIn			In	-	-	-	-	-	44.03	-8.37	52.51
NCE 0216	CIn			NAr	-	-	-	-	-	-66.52	-1.16	-73.25
	NAr			Cin	-	-	-	-	-	-35.97	-2.99	-40.69
NCE 0325	LAr			RAr	LAr					-49.79	-3.68	-50.17
	RAr			LAr					LAr	-40.22	-6.30	-36.55

Table 3.107: Results of the optimization of the lead molecules and IL-4

IL-4	Initial Orientation				Final Orientation										Binding Energy (kcal/mol)		
	K86	K87	K88	R89	L27	T28	S57	**H58**	**H59**	**E60**	**K61**	D62	R64	Q106	Total	VdW	Ele
NCE 0103	CIn	BIn				BIn		CIn	BIn					BIn	-17.45	-13.54	-6.26
	BIn	CIn											CIn		-24.72	-4.92	-22.80
		BIn		CIn				BIn	BIn		CIn	BIn	BIn		-22.24	-11.28	-13.38
		CIn		BIn				CIn	CIn		BIn	CIn	CIn		-29.99	-11.26	-23.38
								CIn									
	BIn			CIn							CIn				-26.18	-3.48	-26.46
	CIn			BIn				CIn			BIn				-21.47	-6.89	-16.76
NCE 0112	CIn	In				In		CIn	In						-14.70	-10.50	-5.38
	In	CIn			CIn	CIn		In	CIn				CIn		-33.24	-6.38	-32.07
		In		CIn				In			CIn	In			-30.13	-13.11	-23.05
		CIn		In			In	CIn	CIn		CIn	CIn			-31.55	-13.23	-22.12
	In			CIn							CIn				-23.65	-5.01	-20.89
	CIn			In	-	-	-	-	-	-	-	-	-	-	-18.45	-0.05	-20.91
NCE 0216		CIn		NAr				CIn	CIn			CIn	CIn		-20.06	-10.56	-14.88
								CIn									
		NAr		CIn				NAr			CIn		NAr		-25.87	-9.34	-19.97
	CIn			NAr				CIn			NAr				-22.60	-8.61	-20.86
	NAr			CIn							CIn				-12.85	-5.37	-11.85
NCE 0325	LAr	RAr							RAr						-16.89	-5.15	-13.78
	RAr	LAr				LAr			LAr						-19.00	-7.52	-13.24
		RAr		LAr				RAr	RAr		LAr	RAr			-18.87	-7.78	-12.53
		LAr		RAr			RAr	LAr	LAr		RAr	LAr	LAr		-23.81	-12.48	-15.09
	LAr			RAr							RAr				-15.34	-3.09	-15.75
	RAr			LAr							LAr				-14.78	-1.73	-15.82
	H74	R75	H76	K77	Q71	**H74**	**R75**	**H76**	**K77**	Q78							
NCE 0103	CIn	BIn				CIn	BIn								-29.28	-2.97	-29.22
	BIn	CIn				BIn				BIn					-13.66	-5.78	-11.10
	BIn			CIn		BIn			CIn						-21.98	-6.51	-18.46
	CIn			BIn	-	-	-	-	-	-					-15.07	-1.08	-15.71
NCE 0112	CIn	In			In	CIn				CIn					-23.39	-5.49	-21.73
	In	CIn			-	-	-	-	-	-					-19.03	-1.12	-19.83
	In			CIn		In									-22.90	-4.04	-19.89
	CIn			In		CIn									-18.68	-2.92	-17.30
NCE 0216	CIn	NAr			NAr	CIn	NAr			CIn					-25.91	-5.86	-22.33
	NAr	CIn			CIn	NAr	CIn								-28.18	-5.97	-25.26
	CIn			NAr		CIn			NAr						-26.59	-3.82	-27.15
	NAr			CIn		NAr			CIn						-21.67	-7.55	-17.17
NCE 0325	LAr	RAr					RAr								-5.30	-1.96	-4.57
	RAr	LAr				RAr	LAr			RAr					-15.07	-3.44	-14.22
	LAr			RAr		LAr			RAr						-7.79	-2.09	-8.21
	RAr			LAr					LAr						-13.02	-3.52	-11.68

Table 3.108: Results of the optimization of the lead molecules and IL-12

IL-12	Initial Orientation				Final Orientation							Binding Energy (kcal/mol)		
	H194	K195	L196	K197	K84	D93	I126	**H194**	**K195**	**L196**	**K197**	Total	VdW	Ele
NCE 0103	CIn	BIn						CIn	BIn			-36.47	-6.28	-31.43
								BIn	BIn					
	BIn	CIn					BIn	BIn	CIn			-44.14	-8.41	-40.94
		BIn		CIn				BIn				-35.02	-2.89	-35.23
		CIn		BIn							BIn	-42.04	-0.89	-39.65
	BIn			CIn		CIn		BIn			CIn	-33.39	-7.73	-25.77
	CIn			BIn	BIn	BIn	CIn	CIn			BIn	-52.16	-13.06	-39.30
NCE 0112	CIn	In							In			-23.57	-3.42	-26.69
	In	CIn						In	CIn			-31.54	-3.13	-36.45
		In		CIn				CIn			CIn	-41.33	-4.98	-40.20
		CIn		In	-	-	-	-	-	-	-	-33.15	-3.27	-35.79
	In			CIn				In				-18.68	-2.23	-21.41
	CIn			In				CIn				-33.23	-2.34	-34.67
NCE 0216	NAr	CIn							CIn			-33.82	-3.10	-33.07
	CIn	NAr						CIn				-30.16	-3.05	-29.52
		CIn		NAr					CIn			-29.00	-2.78	-28.52
		NAr		CIn							CIn	-26.67	-6.18	-26.23
	CIn			NAr	-	-	-	-	-	-	-	-18.29	-3.25	-17.68
	NAr			CIn				NAr			CIn	-16.05	-5.23	-13.60
NCE 0325	LAr	RAr							RAr			-10.60	-2.14	-8.85
	RAr	LAr					RAr	RAr	LAr			-13.56	-5.38	-10.39
		RAr		LAr	-	-	-	-	-	-	-	-10.90	-0.23	-11.17
		LAr		RAr							RAr	-13.11	-2.24	-12.93

Table 3.109: Results of the optimization of the lead molecules and IL-13

IL-13	Initial Orientation				Final Orientation					Binding Energy (kcal/mol)		
	H102	L103	K104	K105	A41	**H102**	**L103**	**K104**	**K105**	Total	VdW	Ele
NCE 0103	BIn			CIn	-	-	-	-	-	-9.28	-2.32	-7.82
	CIn			BIn					BIn	-9.75	-4.35	-6.48
NCE 0112	CIn			In	-	-	-	-	-	-6.14	-1.96	-4.23
	In			CIn	-	-	-	-	-	-8.83	-2.37	-7.36
NCE 0216	NAr			CIn					CIn	-7.11	-4.02	-3.78
									CIn			
	CIn			NAr		CIn				11.92	-3.81	-10.60
NCE 0325	LAr			RAr	LAr	LAr			RAr	-7.54	-5.54	-3.30
	RAr			LAr		RAr			LAr	-10.15	-5.22	-6.43

Table 3.110: Results of the optimization of the lead molecules and MIP-1α

MIP-1α	Initial Orientation				Final Orientation							Binding Energy (kcal/mol)		
	K45	R46	S47	R48	R18	N23	F24	**K45**	**R46**	**S47**	**R48**	Total	VdW	Ele
NCE 0103	CIn	BIn				CIn			BIn			-30.44	-6.10	-22.63
	BIn	CIn				BIn		BIn	CIn			-26.17	-6.24	-19.64
		BIn		CIn	CIn				BIn		CIn	-28.40	-7.70	-21.10
		CIn		BIn					CIn		BIn	-20.65	-6.95	-12.53
	BIn			CIn		BIn		BIn	CIn		CIn	-38.51	-15.72	-21.66
	CIn			BIn			BIn	CIn				-21.73	-10.10	-11.17
NCE 0112	CIn	In			-	-	-	-	-	-	-	-15.61	-2.23	-11.95
	In	CIn			-	-	-	-	-	-	-	-16.16	-2.82	-11.69
		In		CIn	CIn				In		CIn	-29.19	-7.39	-20.95
		CIn		In					CIn		In	-27.67	-6.93	-18.96
	In			CIn			CIn	In			CIn	-27.29	-12.07	-14.06
	CIn			In		CIn	CIn	CIn	In			-27.55	-13.53	-13.19
NCE 0216	NAr	CIn							CIn			-16.50	-3.04	-14.02
	CIn	NAr			-	-	-	-	-	-	-	-20.61	2.56	-18.88
		CIn		NAr					CIn		NAr	-17.11	-5.93	-11.18
		NAr		CIn	CIn				NAr		CIn	-33.55	-8.23	-25.36
	CIn			NAr					NAr		NAr	-32.29	-10.56	-21.20
	NAr			CIn		NAr	NAr/CIn	NAr			CIn	-27.45	-12.82	-15.74
NCE 0325	LAr	RAr							RAr			-12.47	-2.45	-9.90
	RAr	LAr							LAr			-10.80	-3.65	-7.21
		RAr		LAr							LAr	13.87	-5.36	-9.31
		LAr		RAr					LAr		RAr	-12.16	-4.43	-7.92
	RAr			LAr				RAr			LAr	-11.81	-7.50	-5.18
	LAr			RAr				LAr	RAr		RAr	-20.85	-10.64	-9.04

Table 3.111: Results of the optimization of the lead molecules and MIP-1α at two binding sites

MIP-1α		Initial Orientation				Final Orientation							Binding Energy (kcal/mol)		
	(A)	K45	R46	S47	R48	R18	N23	F24	**K45**	**R46**	**S47**	**R48**			
	(B)	K45	R46	S47	R48	R18	N23	F24	**K45**	**R46**	**S47**	**R48**	Total	VdW	Ele
NCE 0103	(A)	CIn	BIn						CIn				-31.60	-9.29	-21.08
	(B)								CIn	BIn					
	(A)	BIn	CIn				BIn			CIn			-45.98	-11.05	-33.55
	(B)									CIn					
	(A)		BIn		CIn							CIn	-46.14	-9.49	-34.63
	(B)									BIn		CIn			
	(A)		CIn		BIn					CIn		BIn	-39.64	-10.40	-24.75
	(B)											BIn			
	(A)	BIn			CIn			BIn/CIn	BIn			CIn	-68.83	-27.67	-39.21
	(B)						BIn	BIn/CIn	BIn	CIn		CIn			
	(A)	CIn			BIn			BIn/CIn	CIn			BIn	-61.09	-28.25	-30.64
	(B)						CIn	BIn/CIn	CIn	BIn					
NCE 0112	(A)	CIn	In			-	-	-	-	-	-	-	-43.55	-6.87	-34.70
	(B)								CIn						
	(A)	In	CIn			-	-	-	-	-	-	-	-26.61	-4.87	-20.90
	(B)					-	-	-	-	-	-	-			
	(A)		In		Cin							Cin	-51.45	-9.32	-39.15
	(B)									In					
	(A)		CIn		In					Cin		In	-24.88	-9.73	-13.04
	(B)											In			
NCE 0216	(A)	NAr	CIn						NAr	CIn			-27.10	-6.82	-21.96
	(B)									CIn					
	(A)	CIn	NAr			-	-	-	-	-	-	-	-38.41	-5.89	-33.91
	(B)						CIn								
	(A)		NAr		CIn	CIn				NAr		CIn	-54.81	-12.06	-42.51
	(B)									NAr		CIn			
	(A)		CIn		NAr					CIn		NAr	-18.33	-10.63	-9.05
	(B)									CIn		NAr			
	(A)	NAr			CIn		NAr	NAr/CIn	NAr				-51.94	-20.97	-33.36
	(B)							NAr		CIn		CIn			
	(A)	CIn			NAr				CIn	NAr		NAr	-62.86	-26.55	-37.16
	(B)						CIn	NAr/CIn	CIn	NAr		NAr			
NCE 0325	(A)	LAr	RAr							RAr			-15.88	-5.20	-10.83
	(B)								LAr	RAr					
	(A)	RAr	LAr							LAr			-19.05	-6.54	-13.78
	(B)								RAr	LAr					
	(A)		LAr		RAr					LAr		RAr	-24.99	-9.23	-15.65
	(B)									LAr		RAr			
										LAr					
	(A)		RAr		LAr					RAr		LAr	-40.62	-12.53	-28.22
	(B)									RAr		LAr			
	(A)	LAr			RAr			RAr	LAr	RAr		RAr	-38.08	-23.05	-14.59
	(B)						LAr	LAr	LAr	RAr					
	(A)	RAr			LAr		RAr	RAr	RAr	LAr		LAr	-41.50	-23.78	-19.36
	(B)						RAr	RAr	RAr						

Table 3.112: Results of the optimization of the lead molecules and MIP-1β

MIP-1β	Initial Orientation				Final Orientation				Binding Energy (kcal/mol)		
	K45	R46	S47	K58	K45	R46	S47	K58	Total	VdW	Ele
NCE 0103	CIn	BIn			CIn	BIn			-8.95	-5.77	-4.46
	BIn	CIn			-	-	-	-	-1.35	-2.32	1.16
		BIn		CIn				CIn	-10.20	-6.31	-5.28
		CIn		BIn		CIn		BIn	-10.30	-5.01	-5.82
						CIn		CIn			
	BIn			CIn		CIn			-8.96	-8.06	-0.97
						BIn					
	CIn			BIn		BIn		BIn	-18.87	-11.12	-7.80
						BIn					
NCE 0112	CIn	In			-	-	-	-	-0.64	-3.04	3.52
	In	CIn			-	-	-	-	-1.94	-2.05	0.33
		In		CIn	-	-	-	-	-7.28	-2.74	-4.05
		CIn		In		CIn			-5.54	-3.69	-1.79
	In			CIn		CIn		CIn	-10.51	-10.80	0.40
						In					
	CIn			In	CIn	In			-15.35	-10.16	-5.25
NCE 0216	NAr	CIn				CIn			-1.36	-2.32	0.15
	CIn	NAr			-	-	-	-	-3.45	-3.00	-1.04
		CIn		NAr	-	-	-	-	-3.37	-2.94	-1.58
		NAr		CIn		NAr		CIn	-7.63	-4.92	-3.88
	CIn			NAr	CIn	NAr			-6.77	-9.20	1.02
	NAr			CIn	NAr	CIn		CIn	-21.51	-11.21	-13.54
						NAr					
NCE 0325	LAr	RAr				RAr			-5.16	-2.35	-3.13
	RAr	LAr			-	-	-	-	-4.43	-2.36	-3.72
		RAr		LAr		RAr		LAr	-5.89	-3.76	-2.54
		LAr		RAr				RAr	-5.95	-4.08	-3.12
	LAr			RAr	LAr	RAr		RAr	-9.04	-6.02	-3.57
	RAr			LAr	RAr	RAr			-13.81	-6.51	-7.16

Table 3.113: Results of the optimization of the lead molecules and MIP-1β at two binding sites

MIP-1β		Initial Orientation				Final Orientation				Binding Energy (kcal/mol)		
	(A)	K45	R46	S47	K48	**K45**	**R46**	**S47**	**K48**			
	(B)	K45	R46	S47	K48	**K45**	**R46**	**S47**	**K48**	Total	VdW	Ele
NCE 0103	(A)	CIn	BIn			CIn				-30.05	-10.70	-20.37
	(B)					CIn	BIn					
	(A)	BIn	CIn			BIn	CIn			-21.85	-11.82	-8.23
	(B)						CIn					
	(A)		BIn		CIn		BIn		CIn	-36.75	-10.38	-28.32
	(B)						BIn					
	(A)		CIn		BIn		BIn		BIn	-21.90	-9.87	-14.48
	(B)						CIn					
NCE 0112	(A)	CIn	In			-	-	-	-	-14.17	-5.74	-10.14
	(B)					CIn	In					
	(A)	In	CIn			-	-	-	-	-7.83	-3.40	-4.24
	(B)					-	-	-	-			
	(A)		In		Cin	-	-	-	-	-17.88	-5.27	-12.51
	(B)						In					
	(A)		CIn		In		CIn			-7.30	-6.12	-2.18
	(B)					-	-	-	-			
NCE 0216	(A)	NAr	CIn			NAr	CIn			-19.51	-11.98	-11.37
	(B)					NAr	CIn					
	(A)	CIn	NAr			-	-	-	-	-11.41	-4.10	-12.24
	(B)					-	-	-	-			
	(A)		NAr		CIn	-	-	-	-	-21.99	-7.62	-16.96
	(B)						NAr		CIn			
	(A)		CIn		NAr		CIn		NAr	-17.65	-12.61	-8.48
	(B)						CIn		NAr			
							NAr					
NCE 0325	(A)	LAr	RAr			LAr				-12.94	-7.04	-8.69
	(B)					LAr	RAr					
	(A)	RAr	LAr			RAr				-13.49	-5.13	-10.24
	(B)						LAr					
	(A)		LAr		RAr		RAr		RAr	-16.69	-8.33	-11.02
									LAr			
	(B)								RAr			
	(A)		RAr		LAr	-	-	-	-	-13.38	-4.44	-8.79
	(B)						RAr					
	(A)	LAr			RAr		RAr	RAr	RAr	-38.89	-23.30	-17.98
	(B)					LAr	RAr	RAr	RAr			
	(A)					RAr	LAr		LAr	-28.25	-18.20	-11.70
	(B)	RAr			LAr	RAr	LAr	LAr	LAr			
							LAr					

Table 3.114: Results of the optimization of the lead molecules and NEP

NEP	Initial Orientation				Final Orientation									Binding Energy (kcal/mol)		
	K523	K524	L525	R526	E498	K520	**K523**	**K524**	**L525**	**R526**	E527	D530	R533	Total	VdW	Ele
NCE	BIn	CIn			BIn	CIn		CIn						106.68	-16.61	117.04
0103	CIn	BIn			-	-	-	-	-	-	-	-	-	72.18	-15.05	79.05
NCE	In	CIn						CIn						103.12	-17.33	112.21
0112	CIn	In			-	-	-	-	-	-	-	-	-	2.75	-14.27	17.09
NCE	LAr	RAr						RAr					RAr	-92.54	-9.94	-89.90
0325	RAr	LAr			RAr			LAr			LAr	LAr	LAr	-90.52	-14.87	-86.12
	H733	C734	R735	K736	E77	E730	**H733**	**C734**	**R735**	**K736**						
NCE	BIn			CIn	-	-	-	-	-	-				-7.22	-12.78	5.48
0103	CIn			BIn				BIn						-36.47	-17.65	-20.91
	BIn		CIn						CIn					-35.28	-5.28	-30.82
	CIn		BIn						BIn					-42.47	-11.58	-32.35
NCE	In			CIn				CIn		CIn				73.12	-11.12	88.03
0112	CIn			In						In				-56.46	-10.96	-47.10
	In		CIn		-	-	-	-	-	-				-29.35	-2.41	-29.06
	CIn		In		-	-	-	-	-	-				-121.30	2.00	-119.85
NCE	NAr		CIn		-	-	-	-	-	-				-39.80	-6.95	-29.63
0216	CIn		NAr		NAr									-67.06	-8.24	-64.23
	CIn			NAr				NAr		NAr				44.20	-20.46	-25.46
	NAr			CIn	-	-	-	-	-	-				-53.06	11.14	-47.19
NCE	LAr		RAr		RAr				RAr					-75.97	-4.33	-73.00
0325	RAr		LAr		LAr				LAr					-79.12	-3.00	-79.88
	LAr			RAr				RAr		RAr				-88.52	-18.18	-76.83
	RAr			LAr		LAr				LAr				-79.34	-9.00	-69.21

Table 3.115: Results of the optimization of the lead molecules and RANTES

RANTES	Initial Orientation				Final Orientation								Binding Energy (kcal/mol)		
	R44	K45	N46	R47	S1	P2	Y3	H23	**R44**	**K45**	**N46**	**R47**	Total	VdW	Ele
NCE	CIn	BIn							CIn	BIn			-151.85	-6.26	-150.58
0103	BIn	CIn							BIn	CIn			-151.78	-6.22	-145.06
		BIn		CIn	CIn					BIn		CIn	-154.14	-7.53	-144.88
		CIn		BIn			BIn			CIn			-122.72	1.49	-129.42
	BIn			CIn					BIn			CIn	-175.22	-1.80	-177.97
	CIn			BIn					CIn				-168.01	0.09	-173.84
NCE	CIn	In							CIn	In			-157.66	-4.73	-165.31
0112	In	CIn							In	CIn			-150.46	-4.92	-147.12
		In		CIn	CIn					CIn		CIn	-143.15	-15.20	-123.84
										In					
		CIn		In						CIn		In	-104.07	-7.34	-98.31
										In					
	In			CIn					In			CIn	-148.61	-6.36	-154.50
	CIn			In				CIn	CIn			In	-156.26	-2.37	-157.16
NCE	NAr	CIn							NAr	CIn			-132.63	-5.24	-125.29
0216	CIn	NAr							CIn	NAr			-128.56	0.83	-130.67
		CIn		NAr		NAr				CIn			-160.60	-4.45	-150.77
		NAr		CIn						NAr		CIn	-151.20	-7.22	-151.39
	CIn			NAr		NAr			CIn			NAr	-158.21	-4.13	-155.61
	NAr			CIn					NAr			CIn	-143.27	-2.09	-143.24
NCE	LAr	RAr							LAr	RAr			-45.63	-2.11	-44.28
0325	RAr	LAr							RAr	LAr			-63.84	-3.47	-62.85
		RAr		LAr						RAr		LAr	-50.35	-8.84	-42.35
		LAr		RAr		RAr				LAr		RAr	-56.64	-2.23	-62.88
	RAr			LAr					RAr			LAr	-55.33	-2.60	-55.50
	LAr			RAr					LAr				-51.69	-0.94	-54.48

Table 3.116: Results of the optimization of the lead molecules and RANTES at two binding sites

RANTES		Initial Orientation				Final Orientation						Binding Energy (kcal/mol)		
	(A)	R44	K45	N46	R47	S1	P2	**R44**	**K45**	**N46**	**R47**			
	(B)	R44	K45	N46	R47	S1	P2	**R44**	**K45**	**N46**	**R47**	Total	VdW	Ele
NCE 0103	(A)	CIn	BIn					CIn	BIn			-329.10	-4.69	-334.91
	(B)							CIn	BIn					
	(A)	BIn	CIn					BIn	CIn			-298.41	-14.21	-277.38
	(B)							BIn	CIn					
	(A)		BIn		CIn				BIn		CIn	-316.70	-14.75	-296.00
	(B)					CIn			BIn		CIn			
	(A)					CIn			CIn		CIn	-303.75	-22.29	-280.23
			CIn		BIn						BIn			
	(B)					CIn			CIn		BIn			
											CIn			
	(A)	BIn			CIn			BIn			CIn	-359.65	-0.95	-358.53
	(B)							BIn			CIn			
	(A)	CIn			BIn			CIn			BIn	-324.31	-12.87	-314.95
	(B)							CIn			BIn			
NCE 0112	(A)	CIn	In					CIn	In			-355.27	-1.02	-353.24
	(B)							CIn	In					
	(A)	In	CIn					In	CIn			-326.63	-9.23	-311.42
	(B)							In	CIn					
	(A)		In		Cin	-	-	-	-	-	-	-205.54	-7.72	-184.73
	(B)					-	-	-	-	-	-			
	(A)					In			CIn		In	-297.56	-20.38	-263.53
			CIn		In				CIn					
	(B)					CIn	In		CIn		CIn			
	(A)							In			CIn	-329.66	-15.09	-325.87
	(B)	In			Cin			In			CIn			
								CIn						
	(A)	CIn			In		In	CIn			In	-353.06	-8.58	-358.07
	(B)						In	CIn			In			
NCE 0216	(A)							NAr	CIn			-279.57	-3.67	-268.49
		NAr	CIn					NAr	CIn					
	(B)							NAr						
	(A)	CIn	NAr					CIn	NAr			-275.04	5.74	-293.12
	(B)							CIn	NAr					
	(A)		NAr		CIn	CIn					CIn	-252.52	-6.03	-238.46
	(B)					CIn					CIn			
	(A)		CIn		NAr		NAr		CIn			-290.61	-9.00	-288.70
	(B)						NAr		CIn		NAr			
	(A)	NAr			CIn			NAr			CIn	-277.26	-19.56	-262.96
	(B)							NAr			CIn			
	(A)	CIn			NAr		NAr	CIn				-310.57	-7.30	-308.55
	(B)							CIn			NAr			
NCE 0325	(A)	LAr	RAr					LAr	RAr			-122.86	0.63	-129.96
	(B)							LAr	RAr					
	(A)	RAr	LAr					RAr	LAr			-126.14	-7.66	-123.80
	(B)							RAr	LAr					
	(A)					RAr			LAr		RAr	-84.66	-11.73	-81.10
	(B)		LAr		RAr	RAr			CAr		RAr			
									LAr					
	(A)		RAr		LAr	LAr			RAr		LAr	-79.09	-12.13	-69.88
	(B)					LAr			RAr		LAr			
	(A)	LAr			RAr			LAr			RAr	-102.74	-4.21	-106.45
	(B)							LAr						
	(A)	RAr			LAr			RAr			LAr	-101.85	-3.05	-103.54
	(B)							RAr			LAr			

Table 3.117: Results of the optimization of the lead molecules and S100β

S100β	Initial Orientation				Final Orientation											Binding Energy (kcal/mol)		
	H25	K26	L27	K28	E21	G22	D23	K24	**H25**	**K26**	**L27**	**K28**	E67	E86	E89	Total	VdW	Ele
NCE	CIn	BIn						CIn	CIn	BIn						-21.86	-8.88	-13.09
0103	BIn	CIn						BIn	BIn	CIn					BIn	-27.77	-13.38	-17.52
		BIn		CIn	BIn					BIn		CIn	BIn			-39.35	-14.08	-25.72
		CIn		BIn	CIn		CIn			CIn		BIn	CIn			-48.80	-17.36	-30.51
NCE	CIn	In							CIn	In				CIn	CIn	-18.34	-7.64	-13.93
0112	In	CIn							In	CIn					In	-9.37	-4.55	-7.69
		In		CIn	In		In			In		CIn				-41.04	-14.37	-27.78
		CIn		In	CIn	CIn	CIn					In				-34.66	-12.42	-25.58
NCE	NAr	CIn			-	-	-	-	-	-	-	-	-	-	-	-14.54	-3.81	-8.35
0216	CIn	NAr							CIn	NAr						-14.54	-5.80	-9.81
		CIn		NAr	-	-	-	-	-	-	-	-	-	-	-	-15.75	-6.09	-8.34
		NAr		CIn								CIn	NAr			-36.79	-6.13	-27.76
NCE	LAr	RAr			-	-	-	-	-	-	-	-	-	-	-	-23.08	-7.27	-15.36
0325	RAr	LAr					CAr	RAr	RAr	LAr						-26.30	-9.48	-17.01
		RAr		LAr	-	-	-	-	-	-	-	-	-	-	-	-25.86	-5.85	-18.41
		LAr		RAr	-	-	-	-	-	-	-	-	-	-	-	-20.77	-5.64	-13.51
	K26	L27	K28	K29	K26	L27	K28	K29										
NCE			BIn	CIn			BIn	CIn								-48.81	-12.67	-33.21
0103			CIn	BIn			CIn	BIn								-28.80	-6.32	-21.39
NCE			In	CIn			In	CIn								-24.86	-7.11	-16.85
0112			CIn	In			CIn	In								-23.70	-5.32	-18.35
NCE			CIn	NAr			CIn	NAr								-31.50	-6.23	-23.61
0216			NAr	Cin			NAr	CIn CIn								-28.21	-7.80	-16.36
NCE			LAr	RAr	-	-	-	-								-16.58	-3.16	-10.96
0325			RAr	LAr	-	-	-	-								-34.22	-7.84	-22.25

Table 3.118: Results of the optimization of the lead molecules and SDF-1

SDF-1	Initial Orientation				Final Orientation				Binding Energy (kcal/mol)		
	K24	H25	L26	K27	K24	H25	L26	K27	Total	VdW	Ele
NCE	BIn	CIn			BIn	CIn			-70.30	-8.73	-59.62
0103	CIn	BIn			CIn	BIn			-77.06	-9.90	-66.64
NCE	CIn	In			In	In			-96.07	-7.80	-86.53
0112					CIn						
	In	CIn				CIn			-57.05	-7.43	-45.14
NCE	NAr	CIn			NAr	CIn			-57.15	-7.89	-46.67
0216	CIn	NAr			CIn	NAr			-75.83	-8.33	-65.56
					NAr						
NCE	LAr	RAr			LAr	RAr			-39.42	-7.31	-33.49
0325	RAr	LAr			RAr	RAr			-42.63	-7.82	-37.58
						LAr					

Table 3.119: Results of the optimization of the lead molecules and Transferrin

Trans-ferrin	Initial Orientation				Final Orientation					Binding Energy (kcal/mol)		
	R113	G114	K115	K116	F107	**R113**	**G114**	**K115**	**K116**	Total	VdW	Ele
NCE 0103	BIn		CIn		-	-	-	-	-	-22.77	-6.01	-23.41
	CIn		BIn			CIn BIn		BIn		-19.43	-9.09	-17.25
			BIn	CIn					CIn	-13.49	-6.04	-13.90
			CIn	BIn			CIn		BIn	-9.48	-6.69	-5.14
NCE 0112	CIn		In			CIn				-25.53	-7.54	-22.81
	In		CIn			In		CIn		-26.29	-9.13	-22.89
			CIn	In	-	-	-	-	-	-20.33	-5.52	-24.57
			In	CIn	-	-	-	-	-	-9.95	-7.62	-12.09
NCE 0216	NAr		CIn			NAr		CIn		-13.54	-7.50	-12.12
	CIn		NAr			CIn				-25.79	-7.52	-24.85
			NAr	CIn				NAr	CIn	-22.98	-9.32	-20.89
			CIn	NAr	CIn			CIn	NAr	-9.45	-7.56	-9.45
NCE 0325			LAr	RAr				LAr		-27.12	-5.56	-27.46
			RAr	LAr					LAr	-28.25	-4.91	-28.12
	LAr		RAr			LAr		RAr		-22.30	-7.75	-20.10
	RAr		LAr			RAr		LAr		-24.76	-8.87	-22.65

Assigning the basic amino acids numbers from left to right as B^1-B^2-X-B^3, the number of interactions occurring at B^1B^2, B^1B^3, and B^2B^3 were examined for each of the above systems.

The NCEs were capable of interacting with multiple configurations of B^1B^2, B^1B^3, and B^2B^3 equally for some of the proteins: These included Aβ, C1qA, ICAM-1, IL-1βCE, IL-4, IL-12, MIP-1α (when binding at two sites), MIP-1β and RANTES. Figure 3.17 shows an example of binding between NCE-0325 and IL-1βCE.

The remaining proteins, AChE, BHMT, S100β and SDF-1 favoured interactions with the NCE molecules at B^1B^2, while $B^1B^3$was the favoured orientation for Apoε4, IFN-γ, and IL-13 with B7-1 and transferrin preferring B^2B^3. None of the NCEs formed interactions at two sites within the **BB**X**B** region of neprilysin. The preferential binding at these sites was due to the spatial orientation of the amino acid side chains within the **BB**X**B** motif for each protein.

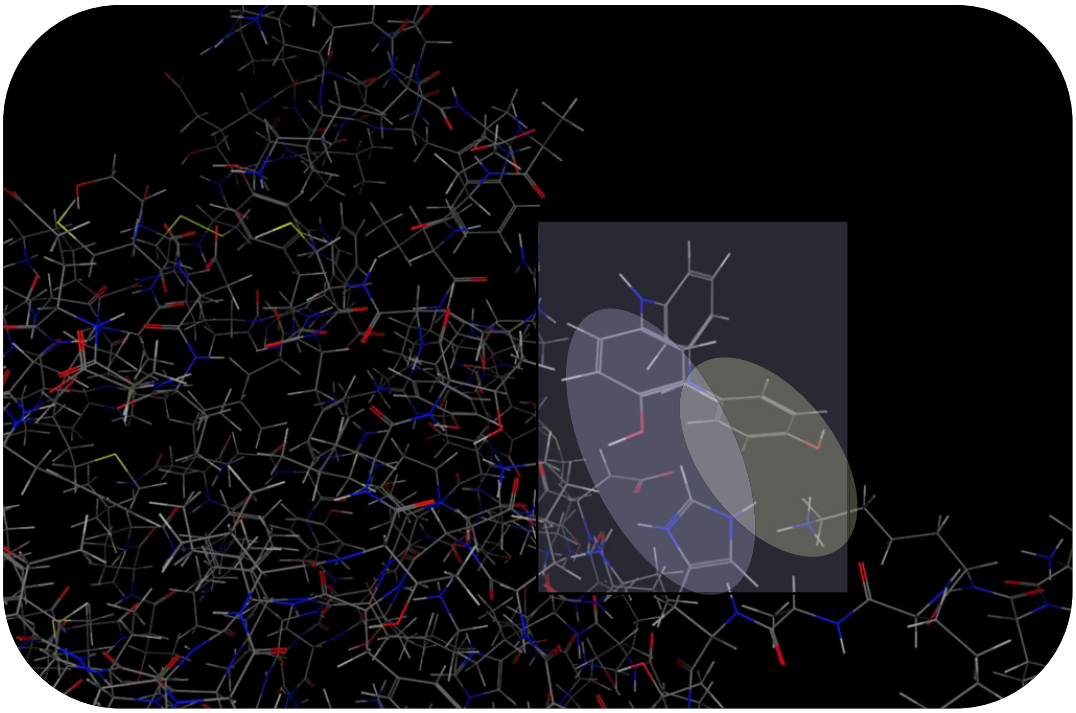

Figure 3.17: Example of NCE-0325 binding to IL-1βCE. Interactions between the compound and the BBXB region are highlighted.

3.10.4 Conclusions on the NCE Molecules Interacting with Proteins Containing BBXB

The results of the gas phase optimizations of NCE-0103, NCE-0112, NCE-0216 and NCE-0325 indicate that all four compounds are capable of binding to and interacting with the **BB**X**B** region of multiple proteins involved in AD. Hydrogen bonds and cation-π interactions were the most commonly observed measureable interactions.

All four NCEs are capable of binding to the **BB**X**B** region of Aβ, C1qA, IFN-γ, IL-12, MIP-1α, MIP-1β, RANTES, SDF-1 and transferrin. For all of these systems, each NCE is capable of forming at least one binding interaction with two of the basic amino acids in the **BB**X**B** motif of that protein.

For a few of the proteins where multiple **BB**X**B** regions were accessible, some of the NCEs were capable of binding to one or two of those receptors but not all of them; this occurred for Apoε4, ICAM-1, IL-4 and S100β. Similar situations arose when binding was occurring at two **BB**X**B** regions simultaneously on MIP-1α and MIP-1β.

In some optimized systems, not all of the NCE molecules were capable of binding at two sites; these included AChE, B7-1 and IL-13, with which only the longer NCE-0325 was capable of forming multiple interactions.

In the case of the BHMT protein, NCE-0112 was not capable of interacting with the side chains given their spatial orientation. In general NCE-0112 appeared to be the least successful at forming binding interactions with the **BB**X**B** region of multiple proteins. NCE-0216 was also slightly less favoured on occasion.

Overall, it appears that NCE-0325 and NCE-0103 are the most capable of binding to the **BB**X**B** region on multiple proteins affiliated with AD. The results of these optimizations are quite favourable for promoting the concept of a promiscuous drug. These synthetic entities are capable of interacting with multiple proteins, at a motif specific to those involved in AD pathology, as was also seen with phosphoserine. Given these positive results, a more promising NCE was also examined.

3.11 NCE-217 as a Drug Molecule Capable of Targeting BBXB

One of the most promising compounds developed by the Weaver group is NCE-217 (Figure 3.18). This compound is currently being further advanced by the Weaver group to improve its efficacy. Given its promise, and knowing that it is capable of

inhibiting β-amyloid aggregation *in vitro*, the compound was selected for gas phase optimizations with some of the proteins examined in section 3.2.8.

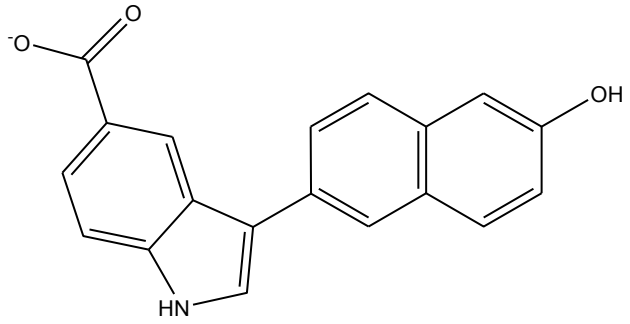

Figure 3.18: NCE-0217

Gas phase optimizations were performed in QUANTA using the CHARMM22 force field [46, 48].

3.11.1 GAS PHASE OPTIMIZATION OF NCE-0217 AND PROTEINS BEARING BBXB

The NCE-0217 molecule was constructed in QUANTA and a systematic grid search was performed to find the lowest energy conformation to be used for the gas phase minimizations. The energy of the selected structure is given in Table 3.120.

Table 3.120: Gas phase energy of NCE-0217

	Energy (kcal/mol)		
	E_{tot}	E_{vdw}	E_{ele}
NCE-0217	34.64	11.84	-6.94

The proteins selected for study are Aβ, C1qA, ICAM-1, IFN-γ, IL-4, IL-12-, IL-13, MIP-1α, MIP-1β, and RANTES. The energies of these proteins can be found in Appendix 8.

Each system was set up such that one of the aromatic rings (or its attached functional groups) was located roughly 3.0 Å away from two of the basic amino acids in the **BB**X**B** motif for each protein. The same set up was used for proteins with two identical **BB**X**B** motifs. Before minimization, the protein backbone was constrained, and the steepest descents algorithm was used. The final systems were imported into MOE to determine what type of binding interactions may have occurred [47].

3.11.2 Gas Phase Results of the Optimization of NCE-0217 with Proteins Bearing BBXB

The results of the gas phase minimizations are summarized in the following tables. Binding interactions are coloured green for cation-π, light blue for π-π and orange for hydrogen bonds: the darker the colour, the more interactions occurring. Binding with the $–CH_2$- chain is indicated in indigo, and with the C=O of the protein backbone in light purple.

Table 3.121: The gas phase results of the optimization of NCE-0217 with Aβ, C1qA, ICAM-1, IFN-γ, IL-4, Il-12 and IL-13

Protein		Initial Orientation				Final Orientation							Binding Energy (kcal/mol)		
		H13	H14	Q15	K16	Y10	V12	**H13**	**H14**	**Q15**	**K16**		Total	VdW	Ele
Aβ		NAr	CIn			CIn		NAr	CIn				-14.78	-9.29	-6.44
								NAr							
		CIn	NAr					CIn	NAr				-15.51	-7.15	-9.46
		CIn			NAr		CIn	CIn			NAr		-20.85	-7.39	-15.09
		NAr			CIn		NAr	NAr			CIn		-22.28	-9.32	-14.24
		K200	K201	G202	H203	E148	**K200**	**K201**	**G202**	**H203**					
C1qA		NAr	CIn				NAr	CIn					-111.63	-5.60	-113.67
		CIn	NAr				CIn						-109.31	-4.75	-108.90
			CIn		NAr	CIn	CIn	CIn		NAr			-111.48	-7.46	-111.13
			NAr		CIn	NAr		NAr		CIn			-94.97	-8.79	-92.83
		CIn			NAr		CIn						-115.01	-0.94	-122.01
		NAr			CIn		NAr			CIn			-124.18	-10.47	-120.39
		R149	R150	D151	H152	R125	L130	L147	**R149**	**R150**	**D151**	**H152**			
ICAM-1		NAr	CIn						NAr	CIn			-14.41	-6.04	-9.54
		CIn	NAr						CIn	NAr			-18.84	-5.83	-14.65
		CIn			NAr	NAr		NAr	NAr			NAr	-30.00	-12.64	-19.85
									CIn						
		NAr			CIn	CIn	CIn		NAr			CIn	-37.17	-13.11	-28.88
		R150	D151	H152	H153	R125	R149	**R150**	**D151**	**H152**	**H153**				
				NAr	CIn	NAr	NAr		NAr	NAr			-27.26	-13.80	-19.41
				CIn	NAr	CIn	CIn		NAr	CIn			-37.16	-13.19	-28.04
		CIn			NAr			CIn					-10.75	-5.48	-7.67
		NAr			CIn			NAr			CIn		-21.50	-5.41	-18.63
		K86	K87	K88	R89	**K86**	**K87**	**K88**	**R89**	D90					
IFN-γ		NAr	CIn			NAr							-19.75	-3.50	-14.17
		CIn	NAr			CIn							-20.88	-3.55	-14.39
			CIn		NAr		CIn						3.43	-7.08	9.09
			NAr		CIn				CIn	CIn			-16.03	-6.98	-8.55
		CIn			NAr	-	-	-	-	-			-14.79	-4.96	-9.84
		NAr			CIn	NAr							-18.79	-5.62	-12.50
	(A)	K86	K87	K88	R89	K74	**K86**	**K87**	**K88**	**R89**	D90				
	(B)	K206	K207	K208	R209	K194	**K206**	**K207**	**K208**	**R209**	E213				
	(A)	NAr	CIn				NAr						-41.45	-7.82	-32.99
	(B)						NAr								
	(A)	CIn	NAr				CIn						-29.81	-4.08	-24.80
	(B)						CIn								
	(A)		NAr		CIn		CIn			CIn	NAr		-42.43	-9.99	-32.42
	(B)						CIn			CIn					
	(A)		CIn		NAr			CIn		NAr	NAr		-18.23	-12.17	-5.32
	(B)					-	-	-	-	-	-				
	(A)	NAr			CIn	-	-	-	-	-	-		-34.76	-7.01	-28.61
	(B)						CIn/NAr			CIn					
	(A)	CIn			NAr	NAr	CIn			NAr			-41.04	-14.42	-24.79
	(B)					NAr	CIn			NAr	NAr				
		H58	H59	E60	K61	S57	**H58**	**H59**	**E60**	**K61**	D62	R64			
IL-4		NAr	CIn				NAr/CIn	CIn					-20.62	-6.56	-16.46
		CIn	NAr					NAr				NAr	-17.26	-5.19	-15.21
			CIn		NAr	NAr	CIn	CIn		NAr	CIn	CIn	-25.40	-11.69	-19.61
			NAr		CIn		NAr	NAr		CIn	NAr		-28.90	-11.64	-21.78
		CIn			NAr					CIn			-19.10	-4.18	-17.57
		NAr			CIn	CIn	CIn			NAr			-24.77	-10.23	-20.21
		H74	R75	H76	K77	Q71	**H74**	**R75**	**H76**	**K77**					
		NAr	CIn			NAr	NAr						-24.83	-3.94	-23.72
		CIn	NAr			NAr	CIn	NAr					-25.36	-4.05	-23.87
		CIn			NAr		CIn						-17.51	-0.84	-18.26
		NAr			CIn					CIn			-17.54	-3.36	-18.25
		H194	K195	L196	K197	H194	K195	L196	K197						
Il-12		NAr	CIn			NAr	CIn						-36.00	-6.38	-31.00
		CIn	NAr			CIn	NAr						-32.85	-5.82	-31.47
			CIn		NAr		CIn		NAr				-38.28	-5.63	-35.59
			NAr		CIn				CIn				-46.15	-1.69	-43.78
		CIn			NAr	CIn							-26.56	-6.13	-24.52
		NAr			CIn	-	-	-	-				-20.72	-3.47	-20.04
		H102	L103	K104	K105	I37	L101	**H102**	**L103**	**K104**	**K105**				
IL-13		CIn			NAr		CIn	CIn					-10.35	-4.27	-6.89
		NAr			CIn	NAr		NAr			CIn		-8.27	-9.53	-0.83

Table 3.122: The gas phase results of the optimization of NCE-0217 with MIP-1α, MIP-1β, and RANTES

Protein		Initial Orientation				Final Orientation							Binding Energy (kcal/mol)		
		K45	R46	S47	R48	R18	N23	F24	**K45**	**R46**	**S47**	**R48**	Total	VdW	Ele
MIP-1α		NAr	CIn							CIn			-13.73	-4.00	-10.30
		CIn	NAr						CIn				-15.82	-2.87	-12.86
			CIn		NAr					CIn		NAr	-11.85	-4.86	-7.56
			NAr		CIn	CIn						CIn	-24.54	-3.78	-19.61
		CIn			NAr		CIn	NAr	CIn			NAr	-30.99	-14.49	-16.60
		NAr			CIn			NAr	NAr			CIn	-18.34	-11.28	-8.98
	(A)	K45	R46	S47	R48	R18	N23	F24	**K45**	**R46**	**S47**	**R48**			
	(B)	K45	R46	S47	R48	R18	N23	F24	**K45**	**R46**	**S47**	**R48**			
	(A)	NAr	CIn							CIn			-32.75	-6.14	-28.31
	(B)									CIn					
	(A)	CIn	NAr			-	-	-	-	-	-	-	-40.85	-4.16	-36.86
	(B)								CIn						
	(A)		NAr		CIn	CIn				NAr		CIn	-44.64	-10.45	-34.30
	(B)									NAr		CIn			
	(A)		CIn		NAr	NAr				CIn		NAr	-31.13	-11.38	-20.00
	(B)									CIn		NAr			
	(A)	NAr			CIn			NAr/CIn	NAr			CIn	-48.73	-21.04	-30.50
	(B)							NAr		CIn		CIn			
	(A)						CIn					NAr			
	(B)	CIn			NAr		CIn	NAr	CIn				-55.98	-23.74	-32.57
								CIn							
		K45	R46	S47	K58	K45	R46	S47	K58						
MIP-1β		NAr	CIn			-	-	-	-				-3.43	-1.65	-3.40
		CIn	NAr			CIn							-4.47	-3.65	-2.68
			CIn		NAr	-	-	-	-				-10.37	-3.73	-8.15
			NAr		CIn		NAr		CIn				-10.62	-4.82	-7.54
		CIn			NAr	CIn	NAr						-9.70	-6.87	-2.86
		NAr			CIn		CIn/NAr		CIn				-16.97	-10.34	-8.77
	(A)	K45	R46	S47	K48	K45	R46	S47	K48						
	(B)	K45	R46	S47	K48	K45	R46	S47	K48						
	(A)	NAr	CIn			NAr	CIn						-20.09	-5.90	-15.83
	(B)						CIn								
	(A)	CIn	NAr				CIn						-14.52	-5.85	-11.96
	(B)						CIn								
	(A)		NAr		CIn	-	-	-	-				-28.65	-5.35	-24.47
	(B)								CIn						
	(A)						CIn		NAr						
	(B)		CIn		NAr		CIn						-11.17	-9.75	-3.51
							NAr		NAr						
		R44	K45	N46	R47	S1	P2	**R44**	**K45**	**N46**	**R47**				
RANTES		NAr	CIn					NAr	CIn				-151.47	-4.65	-147.29
		CIn	NAr					CIn	NAr				-149.21	1.43	-158.31
			CIn		NAr	NAr	NAr		CIn		NAr		-143.92	-5.80	-140.14
			NAr		CIn	CIn					CIn		-113.82	-5.77	-103.87
		CIn			NAr			CIn			NAr		-190.70	2.02	-196.39
		NAr			CIn			NAr			CIn		-145.33	-6.24	-139.53
	(A)	R44	K45	N46	R47	S1	P2	**R44**	**K45**	**N46**	**R47**				
	(B)	R44	K45	N46	R47	S1	P2	**R44**	**K45**	**N46**	**R47**				
	(A)	NAr	CIn					NAr	CIn				-313.90	-11.43	-296.37
	(B)							NAr	CIn						
	(A)	CIn	NAr					CIn	NAr				-306.47	6.38	-334.10
	(B)							CIn	NAr						
	(A)		NAr		CIn				CIn		CIn		-264.20	-10.20	-241.44
	(B)								NAr/CIn		CIn				
	(A)		CIn		NAr	NAr	NAr		CIn		NAr		-241.09	-14.73	-234.91
	(B)								CIn		NAr				
	(A)	NAr			CIn			NAr			CIn		-314.20	-10.40	-316.84
	(B)							NAr			CIn				
	(A)	CIn			NAr		NAr	CIn			NAr		-345.17	-3.81	-341.04
	(B)						NAr	CIn			NAr				

The results of the optimization of NCE-0217 with the **BBXB** region are quite favourable. For all of the proteins, with the exception of IFN-γ, the compound was

capable of binding to **BB**X**B** at multiple sites. Overall, hydrogen bonds were the preferred type of interaction, followed by cation-π interactions; very few π-π systems were observed.

For the interactions with β-amyloid, NCE-0217 bound equally at B^1B^2 and B^1B^3, with numerous cation-π interactions occurring. The electrostatic energy contributions are slightly more favourable than the van der Waals contributions.

In the optimizations with C1qA, only hydrogen bonds formed, with all possible combinations of **BB**X**B** interactions forming equally. The electrostatic energies are significantly lower than the van der Waals energies.

NCE-0217 was capable of binding to ICAM-1 at B^1B^2 and B^1B^3; however multiple binding orientations occurred at one of the **BB**X**B** regions preferentially. In general the electrostatic energies contributed more so to the overall binding energies. Both hydrogen bonds and cation-π interactions were observed in almost equal numbers for these systems.

The results of the gas phase minimization of NCE-0217 with IFN-γ demonstrated a lack of binding to multiple sites of **BB**X**B** when only one region was targeted. When two sites were interacting with the compound, binding favoured B^1B^3, and there were more hydrogen bonds present in these systems. The overall energies were quite variable.

Binding interactions at B^1B^2 were slightly more favoured than the other two arrangements for the optimization of IL-4 and NCE-0217. One **BB**X**B** target was capable of forming more bonds than the other, although there were no significant differences

between the energies observed at these different sites; both cation-π and hydrogen bonds formed.

Interactions at multiple sites within the **BB**X**B** region of IL-12 were observed. The electrostatic energies were lower, and only hydrogen bonds formed in these systems.

In the case of the IL-13 protein, the energies were the least favourable of all the minimizations, although binding still occurred at two sites within the **BB**X**B** region.

When both the single site and multiple site results of NCE-0217 optimized with MIP-1α are examined, it can be observed that mostly hydrogen bonds have formed, B^1B^3 and B^2B^3 are the favoured binding orientations at multiple sites, and the electrostatic energies tend to be more favourable.

The B^2B^3 orientation is slightly more preferred for NCE-0217 binding to MIP-1β. Measured bonds consist of both hydrogen bonds and cation-π interactions, and energies are variable.

The gas phase minimizations of NCE-0217 with RANTES are quite favourable; interactions occurred at multiple sites within **BB**X**B**, almost all of the systems had formed hydrogen bonds, and the energies are very low, with the electrostatic contributions outweighing the van der Waals energies. An example of one of these favourable interactions can be seen in Figure 3.19.

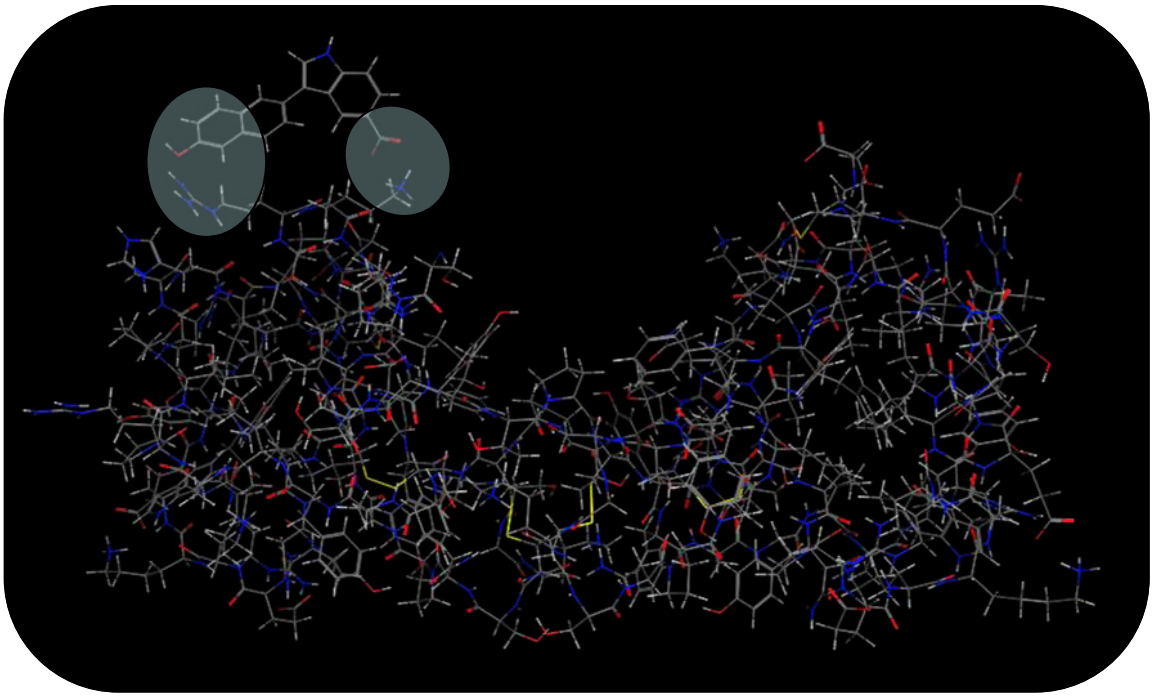

Figure 3.19: Interaction between NCE-0217 and RANTES. Binding sites between the molecule and the BBXB region are highlighted.

3.11.3 CONCLUSIONS OF NCE-0217 OPTIMIZED WITH PROTEINS BEARING BBXB

The results of the minimizations of NCE-0217 and multiple proteins indicated in Alzheimer's disease suggest this is a potential lead molecule. The compound was capable of binding to multiple sites within the **BB**X**B** region for all of the proteins examined and the energies are favourable.

Overall the energy contributions were more strongly affected by the electrostatic contributions, with hydrogen bonds and cation-π interactions being the most prevalent of the measured interactions.

This molecule has also been tested *in vitro* and has shown itself capable of preventing Aβ aggregation. A series of analogues of NCE-0217 was thus developed by

the Weaver group for furthering the advancement of the active properties of this molecule.

3.11.4 Development of a QSAR for Analogues of NCE-0217

Recognizing the potential of NCE-0217 as an anti-aggregant for AD and as a potential "promiscuous" drug has led to the design of a series of analogues of this compound. These analogues were used to develop a QSAR to determine which compounds would be suitable for synthesis. A series of 77 analogues was used to develop a suitable model.

3.11.4.1 Development of the QSAR model of NCE-0217

There were 77 analogues of NCE-0217 that were suitable for use in developing a QSAR. Only a few of the compounds had measured IC_{50} values, so the rest of the compounds were assigned values based on their relative activity. Several attempts were made before a suitable model could be developed.

Initial attempts to use the PLS method for the QSAR were unsuccessful despite manipulation of the training and validation set sizes and compositions. Given the presence of boron in some of the analogues it was determined that the MMFF94x force field would best be able to model all of the series. Finally the binary method was used to determine whether compounds were active or inactive.

The training set was composed of 56 molecules, and attempts were made to ensure every type of molecule was included and that a range of activities was covered. The remaining 21 molecules formed the validation set. The pIC_{50} value was calculated

from the IC_{50}s and used as the activity for determining which descriptors would be relevant. The threshold for activity was set at -2.65.

All of the available descriptors in MOE were calculated for this QSAR, and were eliminated one by one based on their relative importance to the prediction [88]. This followed the same procedure as in Section 3.9. Thirteen descriptors were selected as the final amount necessary to predict activity or inactivity to a reasonable level and they are defined in Table 3.123.

The overall accuracy of the model for the training set was 0.95 (with a sensitivity of 0.95 and a selectivity of 0.95) with a cross-validated accuracy of 0.89 (0.86 for the sensitivity and 0.95 for the selectivity). This model predicted one false positive and three false negatives in the training set. The Cohen's kappa value for the model was calculated to be 0.84, which indicates excellent agreement between the observed and predicted activities. Two false positives and four false negatives were predicted in the validation set, resulting in a sensitivity of 0.78 and a selectivity of 0.57. The calculated Cohen's kappa is 0.36, which is a fair value but could be improved upon. The predictions are summarized in Table 3.124, and full structures of the analogues are listed in Appendix 9.

Table 3.123: Descriptors used for the QSAR of NCE-0217 analogues

Descriptor	Function
ASA+	The water accessible surface area for atoms with a positive partial charge
b_triple	Number of triple bonds
CASA-	Negative charge weighted surface area
E	The potential energy
E_nb	The value of the potential energy with all bonded terms disabled
PEOE_VSA-3 PEOE_VSA+1 PEOE_VSA_HYD	Partial equilization of orbital electronegativities used to calculate atomic partial charges over the van der Waals surface area and the hydrophobic van der Waals surface area
SlogP_VSA3 SlogP_VSA9	Log of the octanol/water coefficient based on the accessible van der Waals surface area
SMR_VSA0	Contributions to the molar refractivity based on the accessible van der Waals surface area falling within a specific range
vsurf_HB7	Hydrogen bond donor capacity
vsurf_W6	Hydrophilic volume

Table 3.124: Predicted activities for the training and validation sets of the NCE-0217 analogues

Compound ID	IC_{50}	Predicted Activity	Compound ID	IC_{50}	Predicted Activity
Training set			Training set		
103	15.6	Active	238	20.9	Active
104	500	**Active**	239	1000	Inactive
105	50.4	Active	240	12	Active
108	60	Active	241	1000	Inactive
109	6.5	Active	252	100	Active
110	10	Active	253	11.8	Active
111	60	Active	254	60	Active
112	34.4	Active	289	500	Inactive
116	1000	Inactive	295	10	Active
117	10	Active	309	60	**Inactive**
120	60	Active	332	60	Active
122	60	Active	335	18.7	Active
123	500	Inactive	336	2.9	Active
125	1000	Inactive	342	6.7	Active
133	60	Active	343	6.9	Active
135	60	**Inactive**	353	6.2	Active
137	500	Inactive	354	20	Active
155	60	**Inactive**	Validation set		
156	500	Inactive	106	24.7	Active
157	500	Inactive	107	500	Inactive
161	60	Active	115	500	Inactive
169	500	Inactive	121	60	Active
170	500	Inactive	124	500	**Active**
172	10	Active	132	60	Active
173	1000	Inactive	134	60	Active
175	100	Active	136	500	Inactive
176	1.99	Active	163	500	**Active**
177	1000	Inactive	168	500	**Active**
179	60	Active	171	5.8	Active
182	1000	Inactive	174	1000	Inactive
185	12.5	Active	181	100	Active
190	60	Active	236	60	**Inactive**
191	500	Inactive	251	10	Active
200	500	Inactive	276	16.5	**Inactive**
201	500	Inactive	300	1.7	Active
213	100	Active	303	21	Active
218	100	Active	327	10.3	Active
230	60	Active	329	13	Active
235	1000	Inactive	334	8.3	**Inactive**

3.11.4.2 Results of the NCE-0217 QSAR

The model QSAR that was developed was used to predict the activity of a series of 63 new analogues of NCE-0217 with unknown activities. These predictions were used to determine which molecules would be best suited for synthesis and *in vitro* testing. The results of the predictions are detailed in Appendix 9.

From the series, forty-one of the molecules were predicted to be active, with one more compound that was borderline inactive. The downside to the binary QSAR is that it only predicts active or inactive; it is difficult to tell which of these compounds would be most active. It is hoped that once more analogues are synthesized and IC_{50} values are obtained that the QSAR model can be improved to better predict activity.

3.12 Conclusions

The results of the optimizations of various small molecules endogenous to the brain with the **HH**Q**K** region of β-amyloid with Alzheimer's disease indicate their potential as amyloid-antiaggregants. Both active and inactive molecules are found within the endogenous species examined, allowing for identification of the more viable routes to pursue.

Synthetic bi-aromatic molecules have also exhibited potential to act as promiscuous drug molecules by binding to the **BB**X**B** motif present on many proteins implicated in AD. Furthermore, the use of QSAR studies can help develop these molecules into even better targets.

Examination of the data has revealed that "physinformatics" may be a useful tool in the drug design process. While cheminformatics deals with large scale data mining such as screening virtual libraries, and docking simulations, there are details at the submolecular level that are also relevant. The atomic features that allow for bond formation and various types of interactions to occur are useful in designing drugs when the target region is known. In the case of this study, ideally the drug molecule should be capable of forming aromatic-aromatic interactions, aromatic-cationic interactions or hydrogen bonds. Physinformatics deals with searching libraries of data for specific functional groups and specific electronic arrangements of these functional groups such that molecules could be identified that bear these desired features. If the relative spatial arrangement and chemical features of the target are known (such as the **BB**X**B** region), the use of physinformatics allows for identification of lead molecules that will interact with more specificity. The positive results of the use of physinformatics can be seen in this chapter, as the screening of endogenous molecules looked at specific charged and aromatic regions at certain distances; most of the identified species were very capable of binding to the charged region of interest and lend themselves to further development.

3.13 INTERPRETATION

The results of the *in silico* optimizations of phenylalanine, dopamine, D- and L-tryptophan, tryptamine and 3-hydroxyanthranilic acid demonstrate that not all endogenous small molecules are capable of binding to β-amyloid to prevent its aggregation.

Of the molecules systematically examined from the indoleamine metabolic pathway, only one demonstrated noticeable activity towards β-amyloid. Both tryptophan and tryptamine demonstrated only a few interactions with the **HH**Q**K** region of Aβ. When the measured binding energies of these systems were compared to the other species presented in this chapter, they were much less favourable. Combining both the number of interactions with the measured binding energies, it can be concluded that both D- and L-tryptophan and tryptamine are inactive molecules; this is further supported by *in vitro* results indicating a lack of effect in Aβ aggregation inhibition. Relative to these two species, 3HAA demonstrates considerably more activity, both *in silico* and *in vitro*. The *in silico* studies on 3HAA demonstrate a capacity to bind to both the **HH**Q**K** and EV**HH**Q**K** regions of Aβ.

Phenylalanine and dopamine bind to β-amyloid in the **HH**Q**K** and LVFF regions of the protein. The binding energies of these two molecules are more favourable than those of 3-hydroxyanthranilic acid, but the numbers of measureable binding interactions are more similar. These three molecules all represent viable targets for further development, and indeed the QSAR on 3HAA has shown that further active molecules can be designed through bioisosteric substitution and their binding sensitivity and selectivity can be improved accordingly.

The results of comparing the binding capacity of the novel chemical entities with a common **BB**X**B** receptor show the usefulness of designing molecules for a specific target located on multiple proteins. Given the implication of multiples factors in the progression of AD, there are a significant number of druggable targets; however, the more drugs an individual takes, the greater the risk of adverse drug-drug interactions.

The results of the NCEs demonstrate the viability of a single molecule, such as NCE-0103 or NCE-0325, binding to a specific **BB**X**B** receptor motif which is located only on proteins involved in AD. This presents the opportunity to design a single drug molecule to target a disease from multiple angles. For almost all of the proteins studies, the molecules bound within the **BB**X**B** region, with only a few interactions occurring with the amino acids of the surrounding side chains. This demonstrates a specificity of the compounds for the targeted region, which would further minimize adverse reactions.

The NCE compounds also demonstrate how analogues can be designed to increase the specificity and efficacy of potential therapeutic molecules. Of the NCEs examined, NCE-0112 demonstrates the lease amount of binding and when compared to the other analogues, is the smallest and least substituted species. This information indicates that the size of the molecule plays a role in its capacity to interact with the **BB**X**B** target, and the substitution may play a role in how well those interactions occur.

The QSAR of NCE-0217 demonstrates that *in silico* methods can be used to reduce synthetic cost by identifying which species would be the most ideal options to synthesize in order to maximize activity, and to avoid wasting time and resources developing inactive analogues.

CHAPTER 4: THE SEARCH FOR AN ENDOGENOUS ANTI-ALZHEIMER'S DRUG TARGETING EVHHQK

The **HH**Q**K** region of β-amyloid is of interest in the development of anti-aggregants due to the role it plays in the protein misfolding. This highly positively charged region can interact with negatively charged macromolecules on cell membranes, such as with glycosaminoglycans; allowing for the misfolding process to occur and a seeding process to begin [16, 17]. If a molecule could bind to that region, it could prevent these interactions from occurring.

The focus on **HH**Q**K** can be expanded to EV**HH**Q**K**. The presence of a negatively charged glutamic acid residue located immediately next to **HH**Q**K** allows for different species of molecules to be examined as potential targets. A molecule binding across this expanded region could likewise prevent unwanted binding with membrane surfaces. Some of the species examined in the previous chapter looked at their capacity to bind to EV**HH**Q**K** as well as the other regions of interest, **HH**Q**K** and LVFF.

This chapter will study the potential interactions of two endogenous molecules and two synthetic compounds, to determine how they could bind to the EV**HH**Q**K** region of Aβ, and if the negatively charged functional group present plays a role in their binding strength.

4.1 γ-AMINOBUTYRIC ACID

γ-Aminobutyric acid (GABA) is an endogenous molecule of the brain that plays a role as an inhibitory neurotransmitter [39]. GABA is a γ amino acid, and exists as a zwitterion at physiological pH (Figure 4.1). The presence of both a negatively charged carboxylate group and a positively charged amino group should allow the molecule to interact with the EV**HH**Q**K** region of β-amyloid.

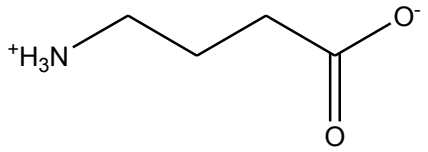

Figure 4.1: GABA at physiological pH

4.1.1 GAS PHASE OPTIMIZATIONS OF GABA AND β-AMYLOID

Gas phase optimizations were performed to examine the potential for GABA to bind to the EV**HH**Q**K** region of Aβ. These studies were performed in MOE using the CHARMM22 force field [48, 88].

4.1.1.1 PREPARATION OF SYSTEMS FOR OPTIMIZATIONS

For the gas phase energy minimizations, the six conformers of β-amyloid (1AMB, 1AMC, 1AMl, 1BA4, 1IYT, 1Z0Q) were modified for physiological pH conditions [68-72, 83, 88]. As necessary, hydrogen atoms were added, and side chains were charged appropriately before optimization with a constrained protein backbone. The energies of these geometry optimized structures are listed in Appendix 6.

A model of GABA was constructed in an extended conformation and subjected to energy minimization (the results of a conformational search generated structures that were too collapsed for use). The optimized energies of GABA are given in Table 4.1.

Table 4.1: Gas phase energies of GABA

	Energies (kcal/mol)		
	E_{tot}	E_{vdw}	E_{ele}
GABA	-10.51	1.11	-12.18

4.1.1.2 Selection of Systems for Optimization

For the gas phase minimizations, each system was set up such that either the carboxylate group or the amino group of GABA was oriented approximately 3.0 Å away from two of the charged amino acids in the EV**HH**Q**K** region of β-amyloid. This was performed for each of the six different conformations of Aβ. Although interactions were expected to be unfavourable when the amino group was oriented towards the lysine side chain, they were still included to see what kind of binding interactions could occur in these situations.

4.1.1.3 Optimization of the Gas Phase Systems

For each of the minimizations the charges of the system were optimized for the CHARMM22 force field, and the protein backbone was constrained [48]. Each system was examined for potential binding interactions, and the energies of the geometry optimized systems were calculated via the following equations:

$$\Delta E_{tot} = E_{tot} - E_{A\beta} - E_{GABA} \tag{4.1}$$

$$\Delta E_{vdw} = E_{vdw} - E_{vdwA\beta} - E_{vdwGABA} \tag{4.2}$$

$$\Delta E_{ele} = E_{ele} - E_{eleA\beta} - E_{eleGABA} \quad (4.3)$$

The energies of the individually optimized protein conformation and GABA molecule were subtracted from the energy of the optimized system.

4.1.2 Results of the Gas Phase Optimizations of GABA and β-Amyloid

The results of the gas phase minimized systems of Aβ and GABA are summarized in the following table, and divided by conformer. The initial orientation of the system, and the resulting orientation upon optimization are summarized with the amino acid side chains represented by single letter abbreviations; X indicates an amino acid outside of the EV**HH**Q**K** region of interest. The amino group of GABA is represented by N, while the carboxylate group is represented by C.

The calculated binding energies are also given, along with the number of measurable bonds that formed in each system.

Table 4.2: The gas phase results of GABA interacting with β-amyloid

Conformer	Initial Orientation						Final Orientation							ΔE_{tot}	ΔE_{vdv}	ΔE_{ele}	Measured
	E11	V12	H13	H14	Q15	K16	E11	V12	H13	H14	Q15	K16	X	(kcal/mol)	(kcal/mol)	(kcal/mol)	Bonds
1AMB	C			N						C				-36.35	-0.29	-37.83	0
	N			C			N			C				-29.96	-1.59	-28.56	1
			N	C						C			N	-21.77	-2.83	-19.83	1
			C	N					C	C				-31.09	-4.44	-29.98	0
			C			N			C			C		-35.92	-1.91	-35.33	1
			N			C						C		-36.12	-1.86	-34.77	1
1AMC	C			N			-	-	-	-	-	-	-	-4.40	0.28	-4.77	0
	N			C			N			C				-48.19	-0.75	-47.91	0
			C	N					C	N			C	-31.53	-4.94	-29.38	0
			N	C						C			N	-42.19	-0.37	-43.76	0
			C			N			C			C		-37.58	-2.22	-36.33	1
			N			C							C	-39.43	-1.39	-39.02	0
1AML	N			C			N			C	N		C	-29.57	-3.50	-27.29	0
	C			N						C				-18.14	-3.45	-15.89	0
			N	C									C	-41.01	0.84	-49.17	0
			C	N					C				C	-56.26	-8.47	-51.11	0
			C			N		C	C					-43.94	-2.99	-41.56	1
			N			C						C		-29.67	-1.13	-29.98	0
1BA4	N					C	C					C	N/C	-18.91	-8.15	-19.59	0
	C					N	N					N	N/C	-48.97	-3.57	-46.26	0
			N	C					C	C				-48.09	-3.55	-44.32	0
			C	N					C					-36.09	-1.41	-34.03	0
1IYT	N			C			N			C				-41.41	-5.56	-35.33	0
	C			N						N			N	-16.64	-5.12	-10.53	0
			C	N					C	C			C	-41.27	-5.13	-34.72	0
			N	C					N/C	C				-20.66	-2.05	-17.05	1
			N			C						C		-36.80	-0.43	-34.44	0
			C			N						C	N	-38.91	-3.58	-36.07	0
1Z0Q	N			C			N			C				-46.87	-2.60	-44.77	1
	C			N			C				C			-10.73	-2.40	-11.50	0
			N	C						C				-24.11	-3.05	-23.24	0
			C	N					C				C	-37.26	-3.64	-35.23	0
			C			N						C		-31.49	-0.50	-31.40	1
			N			C						C		-27.38	-0.41	-27.37	1

The gas phase results indicate that GABA is capable of binding to the EV**HH**Q**K** region of Aβ. Interactions at Glu11-His14 and His13-His14 are the favoured orientations in the minimized systems.

4.1.3 THE SOLUTION PHASE OPTIMIZATION OF GABA AND β-AMYLOID

Solution phase geometry optimizations were performed for each of the gas phase optimized systems of GABA and β-amyloid. Systems were solvated with a box of water molecules large enough to surround the system with an 8.0 Å margin. Energy

minimization was performed with unconstrained protein backbones and periodic boundary conditions, and the optimized systems were examined for potential binding interactions. The energies of the systems were measured in the absence of solvent with constrained protein backbones to better determine the strength of interactions.

The binding energies were calculated using the following equations:

$$\Delta E_{tot} = E_{tot} - E_{A\beta} - E_{GABA} \quad (4.4)$$

$$\Delta E_{ele} = E_{ele} - E_{eleA\beta} - E_{eleGABA} \quad (4.5)$$

$$\Delta E_{vdw} = E_{vdw} - E_{vdwA\beta} - E_{vdwGABA} \quad (4.6)$$

The energies of Aβ and GABA optimized individually in solvated environments were subtracted from the energies of the optimized systems to calculate the binding energies. The energies of the β-amyloid conformers are given in Appendix 6 and the energies of the optimized GABA molecule are given in Table 4.3.

Table 4.3: Solution phase energies of GABA

	Energies (kcal/mol)		
	E_{tot}	E_{vdw}	E_{ele}
GABA	-4.73	0.85	-11.72

4.1.4 The Results of the Solution Phase Optimization of GABA and β-Amyloid

The results of the energy minimization of solvated systems of GABA and six different conformers of β-amyloid are summarized in the following tables. The initial and final orientations of the system are given with the three letter abbreviations of the amino acids. The measured energies and the binding energies are given, and binding interactions are noted according to colour. Hydrogen bonds are coloured orange, and interactions with

the –CH_2- chain are indigo, the –CH- of the backbone are lime green, and the C=O of the backbone are purple.

Table 4.4: The solution phase results of GABA interacting with the 1AMB conformer of β-amyloid

	Glu11	Val12	His13	His14	Gln15	Lys16	Tyr10	Glu11	Val12	His13	His14	Gln15	Lys16	Leu17
Initial Orientation				C			N				C			
Final Orientation				C			N				C			
Total =	-54.71 kcal/mol						-57.67 kcal/mol							
van der Waals =	38.81 kcal/mol						44.48 kcal/mol							
Electrostatic =	-261.81 kcal/mol						-253.80 kcal/mol							
ΔE_{tot} =	-64.37 kcal/mol						-67.32 kcal/mol							
ΔE_{vdw} =	-10.19 kcal/mol						-4.51 kcal/mol							
ΔE_{ele} =	-55.86 kcal/mol						-47.85 kcal/mol							
Initial Orientation	N			C						C			C	
Final Orientation	N									C				
Total =	-49.81 kcal/mol						-45.92 kcal/mol							
van der Waals =	42.06 kcal/mol						51.70 kcal/mol							
Electrostatic =	-256.77 kcal/mol						-254.23 kcal/mol							
ΔE_{tot} =	-59.47 kcal/mol						-55.58 kcal/mol							
ΔE_{vdw} =	-6.94 kcal/mol						2.70 kcal/mol							
ΔE_{ele} =	-50.83 kcal/mol						-48.28 kcal/mol							
Initial Orientation			C	C									C	
Final Orientation			C	C						C			C	C
Total =	-61.02 kcal/mol						-53.28 kcal/mol							
van der Waals =	43.62 kcal/mol						42.83 kcal/mol							
Electrostatic =	-252.97 kcal/mol						-244.36 kcal/mol							
ΔE_{tot} =	-70.68 kcal/mol						-62.94 kcal/mol							
ΔE_{vdw} =	-5.38 kcal/mol						-6.17 kcal/mol							
ΔE_{ele} =	-47.02 kcal/mol						-38.41 kcal/mol							

Table 4.5: The solution phase results of GABA interacting with the 1AMC conformer of β-amyloid

	Glu11	Val12	His13	His14	Gln15	Lys16	Tyr10	Glu11	Val12	His13	His14	Gln15	Lys16	Leu17
Initial Orientation	-	-	-	-	-	-					C			N
Final Orientation				N							C			N
Total =	-18.48 kcal/mol						-78.66 kcal/mol							
van der Waals =	52.93 kcal/mol						45.81 kcal/mol							
Electrostatic =	-244.22 kcal/mol						-275.78 kcal/mol							
ΔE_{tot} =	16.68 kcal/mol						-43.49 kcal/mol							
ΔE_{vdw} =	16.11 kcal/mol						8.99 kcal/mol							
ΔE_{ele} =	-2.86 kcal/mol						-34.42 kcal/mol							
Initial Orientation	N			C						C	N			C
Final Orientation	N			C			C			C	N			C
											C			
Total =	-99.65 kcal/mol						-81.76 kcal/mol							
van der Waals =	33.15 kcal/mol						38.61 kcal/mol							
Electrostatic =	-282.68 kcal/mol						-276.81 kcal/mol							
ΔE_{tot} =	-64.48 kcal/mol						-46.59 kcal/mol							
ΔE_{vdw} =	-3.67 kcal/mol						1.79 kcal/mol							
ΔE_{ele} =	-41.32 kcal/mol						-35.45 kcal/mol							
Initial Orientation			C			C								C
Final Orientation			C			C	-	-	-	-	-	-	-	-
Total =	-70.99 kcal/mol						-79.45 kcal/mol							
van der Waals =	46.49 kcal/mol						50.17 kcal/mol							
Electrostatic =	-278.28 kcal/mol						-285.23 kcal/mol							
ΔE_{tot} =	-35.83 kcal/mol						-44.28 kcal/mol							
ΔE_{vdw} =	9.67 kcal/mol						13.35 kcal/mol							
ΔE_{ele} =	-36.92 kcal/mol						-43.87 kcal/mol							

Table 4.6: The solution phase results of GABA interacting with the 1AML conformer of β-amyloid

	Arg5	Glu11	Val12	His13	His14	Gln15	Lys16	Val18	Tyr10	Glu11	Val12	His13	His14	Gln15	Lys16
Initial Orientation					C				C			C			
Final Orientation	C								C			C			
Total =	91.90 kcal/mol								47.94 kcal/mol						
van der Waals =	60.19 kcal/mol								63.23 kcal/mol						
Electrostatic =	-192.81 kcal/mol								-228.06 kcal/mol						
ΔE_{tot} =	-22.68 kcal/mol								-66.64 kcal/mol						
ΔE_{vdw} =	-10.11 kcal/mol								-7.07 kcal/mol						
ΔE_{ele} =	-9.99 kcal/mol								-45.24 kcal/mol						
Initial Orientation	C	N			C	N			C						
Final Orientation	C	N				N		N					C		
Total =	77.48 kcal/mol								42.43 kcal/mol						
van der Waals =	66.61 kcal/mol								72.37 kcal/mol						
Electrostatic =	-196.75 kcal/mol								-238.93 kcal/mol						
ΔE_{tot} =	-37.10 kcal/mol								-72.15 kcal/mol						
ΔE_{vdw} =	-3.69 kcal/mol								2.07 kcal/mol						
ΔE_{ele} =	-13.93 kcal/mol								-56.11 kcal/mol						
Initial Orientation			C	C											C
Final Orientation			C	C			C								C
Total =	63.09 kcal/mol								93.41 kcal/mol						
van der Waals =	68.02 kcal/mol								70.90 kcal/mol						
Electrostatic =	-226.49 kcal/mol								-214.71 kcal/mol						
ΔE_{tot} =	-51.49 kcal/mol								-21.17 kcal/mol						
ΔE_{vdw} =	-2.28 kcal/mol								0.60 kcal/mol						
ΔE_{ele} =	-43.67 kcal/mol								-31.89 kcal/mol						

Table 4.7: The solution phase results of GABA interacting with the 1BA4 conformer of β-amyloid

	Glu3	Glu11	Val12	His13	His14	Gln15	Lys16	Phe19
Initial Orientation	N	N					N	C
Final Orientation	N						N	N
								C
Total =	75.27 kcal/mol							
van der Waals =	73.11 kcal/mol							
Electrostatic =	-217.83 kcal/mol							
ΔE_{tot} =	-46.84 kcal/mol							
ΔE_{vdw} =	1.14 kcal/mol							
ΔE_{ele} =	-42.89 kcal/mol							
Initial Orientation	N	C					C	C
	C							
Final Orientation	N	N					C	C
Total =	72.94 kcal/mol							
van der Waals =	80.46 kcal/mol							
Electrostatic =	-217.83 kcal/mol							
ΔE_{tot} =	-49.17 kcal/mol							
ΔE_{vdw} =	8.49 kcal/mol							
ΔE_{ele} =	-42.79 kcal/mol							
Initial Orientation				C				
Final Orientation				C				
Total =	66.95 kcal/mol							
van der Waals =	72.17 kcal/mol							
Electrostatic =	-216.33 kcal/mol							
ΔE_{tot} =	-55.16 kcal/mol							
ΔE_{vdw} =	0.19 kcal/mol							
ΔE_{ele} =	-41.29 kcal/mol							
Initial Orientation				C	C			
Final Orientation				C	C			
Total =	28.59 kcal/mol							
van der Waals =	69.93 kcal/mol							
Electrostatic =	-250.16 kcal/mol							
ΔE_{tot} =	-93.52 kcal/mol							
ΔE_{vdw} =	-2.05 kcal/mol							
ΔE_{ele} =	-75.12 kcal/mol							

Table 4.8: The solution phase results of GABA interacting with the 1IYT conformer of β-amyloid

	Glu11	Val12	His13	His14	Gln15	Lys16	Phe20	Tyr10	Glu11	Val12	His13	His14	Gln15	Lys16	Leu17
Initial Orientation			N	C				N				N			
			C												
Final Orientation			N	C				N	N			N			
			C												
Total =	78.59 kcal/mol							68.99 kcal/mol							
van der Waals =	59.40 kcal/mol							64.70 kcal/mol							
Electrostatic =	-214.32 kcal/mol							-214.83 kcal/mol							
ΔE_{tot} =	-66.51 kcal/mol							-76.11 kcal/mol							
ΔE_{vdw} =	-17.56 kcal/mol							-12.26 kcal/mol							
ΔE_{ele} =	4.45 kcal/mol							3.93 kcal/mol							
Initial Orientation						C	N		N			C			
Final Orientation						C	N		N			C			
Total =	38.36 kcal/mol							47.02 kcal/mol							
van der Waals =	70.07 kcal/mol							71.76 kcal/mol							
Electrostatic =	-257.00 kcal/mol							-247.41 kcal/mol							
ΔE_{tot} =	-106.74 kcal/mol							-98.08 kcal/mol							
ΔE_{vdw} =	-6.90 kcal/mol							-5.20 kcal/mol							
ΔE_{ele} =	-38.24 kcal/mol							-28.65 kcal/mol							
Initial Orientation						C					C	C			C
Final Orientation			C								C	C			C
Total =	62.09 kcal/mol							49.40 kcal/mol							
van der Waals =	64.66 kcal/mol							74.62 kcal/mol							
Electrostatic =	-233.50 kcal/mol							-263.68 kcal/mol							
ΔE_{tot} =	-83.01 kcal/mol							-95.70 kcal/mol							
ΔE_{vdw} =	-12.30 kcal/mol							-2.34 kcal/mol							
ΔE_{ele} =	-14.74 kcal/mol							-44.92 kcal/mol							

Table 4.9: The solution phase results of GABA interacting with the 1Z0Q conformer of β-amyloid

	Glu11	Val12	His13	His14	Gln15	Lys16	Tyr10	Glu11	Val12	His13	His14	Gln15	Lys16
Initial Orientation	C				C		C			C			
Final Orientation	C				C		C			C			
Total =	86.70 kcal/mol						66.11 kcal/mol						
van der Waals =	62.28 kcal/mol						70.70 kcal/mol						
Electrostatic =	-215.62 kcal/mol						-238.28 kcal/mol						
ΔE_{tot} =	-45.30 kcal/mol						-65.98 kcal/mol						
ΔE_{vdw} =	-19.78 kcal/mol						-11.36 kcal/mol						
ΔE_{ele} =	-22.27 kcal/mol						-44.93 kcal/mol						
Initial Orientation	N			C							C		
Final Orientation	N			C			C			C	C		
Total =	68.29 kcal/mol						116.70 kcal/mol						
van der Waals =	83.65 kcal/mol						77.94 kcal/mol						
Electrostatic =	-251.24 kcal/mol						-208.98 kcal/mol						
ΔE_{tot} =	-63.71 kcal/mol						-15.29 kcal/mol						
ΔE_{vdw} =	1.60 kcal/mol						-4.11 kcal/mol						
ΔE_{ele} =	-57.89 kcal/mol						-15.63 kcal/mol						
Initial Orientation						C							C
Final Orientation						C							C
Total =	112.94 kcal/mol						61.90 kcal/mol						
van der Waals =	80.70 kcal/mol						71.70 kcal/mol						
Electrostatic =	-217.54 kcal/mol						-249.29 kcal/mol						
ΔE_{tot} =	-19.06 kcal/mol						-70.10 kcal/mol						
ΔE_{vdw} =	-1.35 kcal/mol						-10.36 kcal/mol						
ΔE_{ele} =	-24.19 kcal/mol						-55.94 kcal/mol						

The results of the solution phase optimization of GABA with β-amyloid indicate the neurotransmitter is capable of binding to the protein at two or more sites simultaneously within the EV**HH**Q**K** region of interest. Interactions at His13-His14 are favoured, followed by Glu11-His14, then His13-Lys16. Only hydrogen bond interactions were formed in the optimized systems.

The electrostatic energies are much more favourable than the van der Waals energies of the systems, and there is no correlation between the favourability of the energies and the amount of binding occurring in the system. There are likely repulsive factors at play that cannot be visualized.

4.2 β-ALANINE

β-Alanine (Figure 4.2) is another small molecule endogenous to the brain that exhibits neuromodulatory effects [39]. It can exhibit effects on both GABAergic and glutamatergic processes in the brain [39]. It is similar in structure to GABA, being only one carbon unit shorter.

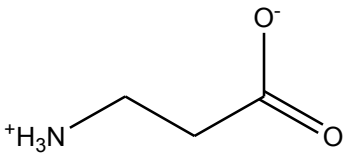

Figure 4.2: β-alanine at physiological pH

While the molecule exhibits the same functional groups as GABA, the shorter length will help to determine if the size of the amino acid is factor in its potential to form interactions within the EV**HH**Q**K** region of β-amyloid.

4.2.1 THE GAS PHASE OPTIMIZATION OF β-ALANINE AND β-AMYLOID

An extended conformation of β-alanine was constructed and geometry optimized in the gas phase using the CHARMM22 force field [48, 88]. The energies of the optimized structure are given in Table 4.10.

Table 4.10: The gas phase energies of β-alanine

	Energies (kcal/mol)		
	E_{tot}	E_{vdw}	E_{ele}
β-alanine	-22.66	0.82	-23.78

Gas phase optimizations were performed following the procedure outlined in section 4.1.1.2-4.1.1.3. The energies were calculated using the same equations 4.1-4.3 with the energy of the optimized β-alanine molecule replacing the energy of GABA. The

protein energies are those calculated with a constrained backbone and listed in Appendix 6.

4.2.2 The Gas Phase Results of β-Alanine Interacting with β-Amyloid

The gas phase results are summarized in the following table. The initial orientation of β-alanine and the final orientation upon minimization are given with the amino acids represented by single letters. The amino and carboxylate groups of β-alanine are represented by N and C, respectively. Interactions occurring with amino acids outside the EV**HH**Q**K** region of interest are listed under the column X. The calculated binding energies are listed for each system, as well as the number of measurable bonds that formed.

The gas phase optimizations of β-alanine and the different conformers of Aβ indicate that binding interactions can form at multiple sites within EV**HH**Q**K**. Glu11-His14, His13-His14, and His13-Lys16 are the order of preferred binding interactions.

Table 4.11: The gas phase results of β-alanine interacting with β-amyloid

Conformer	Initial Orientation						Final Orientation							ΔE_{tot}	ΔE_{vdv}	ΔE_{ele}	Measured
	E11	V12	H13	H14	Q15	K16	E11	V12	H13	H14	Q15	K16	X	(kcal/mol)	(kcal/mol)	(kcal/mol)	Bonds
1AMB	C			N						C				-24.49	-1.16	-26.85	0
	N			C			N			C				-27.01	-2.59	-24.46	0
			N	C									C	-36.33	-3.33	-32.71	0
			C	N					C	C			N	-36.79	-4.50	-35.20	0
			C			N			C			C		-31.09	-1.20	-30.61	1
			N			C			C					-33.62	-1.47	-34.05	0
1AMC	C			N			N							-33.13	-0.98	-32.66	1
	N			C			N			C				-34.61	-0.30	-34.82	1
			C	N					C	C/N			N	-37.10	-3.93	-35.05	0
			N	C						C			N/C	-10.73	-4.28	-7.29	0
			C			N			C			C		-37.01	-3.05	-35.12	1
			N			C			C				C	-34.58	0.23	-36.59	0
1AML	C			N						C				-36.54	-1.79	-34.83	0
	N			C			N			C			N	-33.44	-4.57	-29.50	0
			C	N					C				C	-59.92	-7.15	-56.11	1
			N	C									C	-31.77	0.22	-33.95	0
			C			N	-	-	-	-	-	-	-	-32.86	-1.89	-32.15	0
			N			C						C		-26.79	-1.38	-25.96	0
1BA4	C					N	C						N/C	-43.99	-3.79	-45.74	0
	N					C	N						N	-30.07	-4.97	-27.16	1
			N	C						C				-40.08	-2.04	-38.07	0
			C	N					C	C				-32.94	-1.89	-30.53	0
1IYT	C			N			-	-	-	-	-	-	-	-2.52	-1.66	-3.06	0
	N			C			N			C				-28.87	-4.00	-24.69	1
			N	C					C	C				-25.89	-1.38	-23.21	0
			C	N					C					-22.02	-2.25	-20.47	0
			C			N			C			C		-26.01	-1.97	-24.13	0
			N			C						C		-31.49	-2.91	-28.57	1
1Z0Q	C			N			C			N				3.68	-0.85	2.49	0
	N			C						C				-43.36	-2.58	-39.68	0
			N	C						C				-24.15	-0.90	-24.89	0
			C	N					C					-30.39	-3.01	-27.20	0
			C			N			C					-26.16	-0.87	-26.04	0
			N			C						C		-26.07	-0.23	-26.03	0

4.2.3 THE SOLUTION PHASE OPTIMIZATION OF β-ALANINE AND β-AMYLOID

Each of the gas phase systems was optimized in a solution phase environment. Explicit water molecules were used to solvate the system in a box surrounding the systems, with an 8.0 Å margin selected. Periodic boundary conditions were in place during the energy minimization.

The energies of the optimized systems were measured with a constrained protein backbone and the solvent molecules excluded. The energies could therefore be compared to better understand the contributions due to the binding or non-binding interactions

occurring. The same equations of 4.4-4.6 were used with the solution phase optimized β-alanine energy replaced the solvated GABA energy. The energies of the solution phase minimized β-alanine are given in Table 4.12.

Table 4.12: Solution phase energies of β-alanine

	Energies (kcal/mol)		
	E_{tot}	E_{vdw}	E_{ele}
β-alanine	-18.32	2.67	-23.64

4.2.4 THE RESULTS OF THE SOLUTION PHASE OPTIMIZATION OF β-ALANINE AND β-AMYLOID

The results of the solvation energy minimized systems of β-alanine and β-amyloid are summarized in Tables 4.13-4.18. Initial and final orientations of the interactions of β-alanine with the protein are represented by 3 letter amino acid abbreviations, and N and C for the charged amino and carboxylate groups of β-alanine. The measured energies of the systems are given, and the resulting binding energies that were calculated.

Hydrogen bonds are represented by orange coloured cells, and a cation-π interaction is in green. Interactions with the $–CH_2$- chain of the amino acid are in indigo, while backbone interactions are coloured purple for C=O and lime green for –CH-.

Table 4.13: The solution phase results of β-alanine interacting with the 1AMB conformer of β-amyloid

	Glu11	Val12	His13	His14	Gln15	Lys16	Tyr10	Glu11	Val12	His13	His14	Gln15	Lys16
Initial Orientation				C			N			C	C		
Final Orientation				N			N			C			
				C									
Total =	-60.34 kcal/mol						-70.01 kcal/mol						
van der Waals =	40.23 kcal/mol						37.72 kcal/mol						
Electrostatic =	-255.43 kcal/mol						-266.91 kcal/mol						
ΔE_{tot} =	-56.41 kcal/mol						-66.08 kcal/mol						
ΔE_{vdw} =	-10.60 kcal/mol						-13.10 kcal/mol						
ΔE_{ele} =	-37.57 kcal/mol						-49.05 kcal/mol						
Initial Orientation	N			C			C						
Final Orientation	N			C			C				C		
Total =	-65.24 kcal/mol						-72.06 kcal/mol						
van der Waals =	48.37 kcal/mol						38.17 kcal/mol						
Electrostatic =	-264.55 kcal/mol						-277.98 kcal/mol						
ΔE_{tot} =	-61.31 kcal/mol						-68.13 kcal/mol						
ΔE_{vdw} =	-2.45 kcal/mol						-12.65 kcal/mol						
ΔE_{ele} =	-46.69 kcal/mol						-60.12 kcal/mol						
Initial Orientation			C							C			C
Final Orientation			C							C			C
Total =	-68.76 kcal/mol						-55.54 kcal/mol						
van der Waals =	50.30 kcal/mol						50.72 kcal/mol						
Electrostatic =	-275.90 kcal/mol						-264.28 kcal/mol						
ΔE_{tot} =	-64.83 kcal/mol						-51.61 kcal/mol						
ΔE_{vdw} =	-0.52 kcal/mol						-0.10 kcal/mol						
ΔE_{ele} =	-58.03 kcal/mol						-46.42 kcal/mol						

Table 4.14: The solution phase results of β-alanine interacting with the 1AMC conformer of β-amyloid

	Glu11	Val12	His13	His14	Gln15	Lys16	Tyr10	Glu11	Val12	His13	His14	Gln15	Lys16	Leu17
Initial Orientation	N						N			C	C			
											N			
Final Orientation	N						N			C				
							C							
Total =	-70.56 kcal/mol						-78.89 kcal/mol							
van der Waals =	40.10 kcal/mol						41.43 kcal/mol							
Electrostatic =	-271.20 kcal/mol						-290.84 kcal/mol							
ΔE_{tot} =	-21.81 kcal/mol						-30.14 kcal/mol							
ΔE_{vdw} =	1.45 kcal/mol						2.78 kcal/mol							
ΔE_{ele} =	-17.92 kcal/mol						-37.57 kcal/mol							
Initial Orientation	N			C						C				C
Final Orientation	N													C
Total =	-89.61 kcal/mol						-85.29 kcal/mol							
van der Waals =	43.36 kcal/mol						36.10 kcal/mol							
Electrostatic =	-291.71 kcal/mol						-281.39 kcal/mol							
ΔE_{tot} =	-40.86 kcal/mol						-36.54 kcal/mol							
ΔE_{vdw} =	4.71 kcal/mol						-2.55 kcal/mol							
ΔE_{ele} =	-38.43 kcal/mol						-28.12 kcal/mol							
Initial Orientation			C			C	N				C			
							C							
Final Orientation			C			C	N				C			
							C							
Total =	-70.52 kcal/mol						-45.86 kcal/mol							
van der Waals =	47.77 kcal/mol						46.62 kcal/mol							
Electrostatic =	-276.41 kcal/mol						-249.21 kcal/mol							
ΔE_{tot} =	-21.77 kcal/mol						2.89 kcal/mol							
ΔE_{vdw} =	9.12 kcal/mol						7.97 kcal/mol							
ΔE_{ele} =	-23.14 kcal/mol						4.07 kcal/mol							

Table 4.15: The solution phase results of β-alanine interacting with the 1AML conformer of β-amyloid

	Ser8	Glu11	Val12	His13	His14	Gln15	Lys16	Tyr10	Glu11	Val12	His13	His14	Gln15	Lys16	Leu17
Initial Orientation					C			C			C				
Final Orientation	C				C			C			C				C
Total =	66.72 kcal/mol							48.74 kcal/mol							
van der Waals =	72.70 kcal/mol							49.97 kcal/mol							
Electrostatic =	-213.88 kcal/mol							-242.86 kcal/mol							
ΔE_{tot} =	-34.27 kcal/mol							-52.25 kcal/mol							
ΔE_{vdw} =	0.58 kcal/mol							-22.15 kcal/mol							
ΔE_{ele} =	-19.14 kcal/mol							-48.12 kcal/mol							
Initial Orientation	N	N			C			C							
Final Orientation	N	N			C			-	-	-	-	-	-	-	-
Total =	80.73 kcal/mol							62.46 kcal/mol							
van der Waals =	76.62 kcal/mol							74.45 kcal/mol							
Electrostatic =	-221.04 kcal/mol							-223.24 kcal/mol							
ΔE_{tot} =	-20.26 kcal/mol							-38.53 kcal/mol							
ΔE_{vdw} =	4.49 kcal/mol							2.32 kcal/mol							
ΔE_{ele} =	-26.30 kcal/mol							-28.51 kcal/mol							
Initial Orientation							C	-	-	-	-	-	-	-	-
Final Orientation							C				C				
Total =	71.60 kcal/mol							82.05 kcal/mol							
van der Waals =	68.87 kcal/mol							80.59 kcal/mol							
Electrostatic =	-209.45 kcal/mol							-220.96 kcal/mol							
ΔE_{tot} =	-29.40 kcal/mol							-18.94 kcal/mol							
ΔE_{vdw} =	-3.26 kcal/mol							8.47 kcal/mol							
ΔE_{ele} =	-14.71 kcal/mol							-26.23 kcal/mol							

Table 4.16: The solution phase results of β-alanine interacting with the 1BA4 conformer of β-amyloid

	Glu3	Glu11	Val12	His13	His14	Gln15	Lys16	Phe19
Initial Orientation	N	C						C
Final Orientation	N	C					N	C
Total =	38.41 kcal/mol							
van der Waals =	67.50 kcal/mol							
Electrostatic =	-231.71 kcal/mol							
ΔE_{tot} =	-70.12 kcal/mol							
ΔE_{vdw} =	-6.30 kcal/mol							
ΔE_{ele} =	-4.76 kcal/mol							
Initial Orientation		N						N
Final Orientation		N						N
Total =	84.27 kcal/mol							
van der Waals =	70.82 kcal/mol							
Electrostatic =	-202.33 kcal/mol							
ΔE_{tot} =	-24.25 kcal/mol							
ΔE_{vdw} =	-2.98 kcal/mol							
ΔE_{ele} =	-15.38 kcal/mol							
Initial Orientation				C	C			
Final Orientation					C			
Total =	78.45 kcal/mol							
van der Waals =	75.02 kcal/mol							
Electrostatic =	-214.41 kcal/mol							
ΔE_{tot} =	-30.08 kcal/mol							
ΔE_{vdw} =	1.22 kcal/mol							
ΔE_{ele} =	-27.46 kcal/mol							
Initial Orientation					C			
Final Orientation					C			
Total =	53.81 kcal/mol							
van der Waals =	71.35 kcal/mol							
Electrostatic =	-228.96 kcal/mol							
ΔE_{tot} =	-54.72 kcal/mol							
ΔE_{vdw} =	-2.45 kcal/mol							
ΔE_{ele} =	-42.00 kcal/mol							

Table 4.17: The solution phase results of β-alanine interacting with the 1IYT conformer of β-amyloid

	Glu11	Val12	His13	His14	Gln15	Lys16		Tyr10	Glu11	Val12	His13	His14	Gln15	Lys16	Leu17
Initial Orientation			C	C					N			C			
Final Orientation				C				C	N			C			
								N							
Total =	43.27 kcal/mol							30.81 kcal/mol							
van der Waals =	70.54 kcal/mol							54.89 kcal/mol							
Electrostatic =	-249.65 kcal/mol							-243.80 kcal/mol							
ΔE_{tot} =	-88.24 kcal/mol							-100.70 kcal/mol							
ΔE_{vdw} =	-8.25 kcal/mol							-23.90 kcal/mol							
ΔE_{ele} =	-18.98 kcal/mol							-13.13 kcal/mol							
Initial Orientation			C			C		-	-	-	-	-	-	-	-
Final Orientation						C			N						
Total =	35.49 kcal/mol							68.55 kcal/mol							
van der Waals =	69.32 kcal/mol							66.17 kcal/mol							
Electrostatic =	-260.79 kcal/mol							-226.16 kcal/mol							
ΔE_{tot} =	-96.02 kcal/mol							-62.96 kcal/mol							
ΔE_{vdw} =	-9.47 kcal/mol							-12.62 kcal/mol							
ΔE_{ele} =	-30.12 kcal/mol							4.52 kcal/mol							
Initial Orientation						C					C				
Final Orientation						C					C	N			C
Total =	40.08 kcal/mol							49.03 kcal/mol							
van der Waals =	71.50 kcal/mol							72.21 kcal/mol							
Electrostatic =	-252.93 kcal/mol							-248.12 kcal/mol							
ΔE_{tot} =	-91.43 kcal/mol							-82.48 kcal/mol							
ΔE_{vdw} =	-7.29 kcal/mol							-6.58 kcal/mol							
ΔE_{ele} =	-22.25 kcal/mol							-17.44 kcal/mol							

Table 4.18: The solution phase results of β-alanine interacting with the 1Z0Q conformer of β-amyloid

	Glu11	Val12	His13	His14	Gln15	Lys16	Gly9	Tyr10	Glu11	Val12	His13	His14	Gln15	Lys16
Initial Orientation	C			N							C			
Final Orientation	C			N			C	C			C			
Total =	95.81 kcal/mol						46.56 kcal/mol							
van der Waals =	69.36 kcal/mol						68.30 kcal/mol							
Electrostatic =	-227.24 kcal/mol						-262.33 kcal/mol							
ΔE_{tot} =	-22.61 kcal/mol						-71.85 kcal/mol							
ΔE_{vdw} =	-14.52 kcal/mol						-15.59 kcal/mol							
ΔE_{ele} =	-21.97 kcal/mol						-57.06 kcal/mol							
Initial Orientation				C								C		
Final Orientation				C								C		
Total =	69.15 kcal/mol						78.34 kcal/mol							
van der Waals =	86.08 kcal/mol						72.31 kcal/mol							
Electrostatic =	-268.04 kcal/mol						-232.76 kcal/mol							
ΔE_{tot} =	-49.27 kcal/mol						-40.07 kcal/mol							
ΔE_{vdw} =	2.20 kcal/mol						-11.57 kcal/mol							
ΔE_{ele} =	-62.77 kcal/mol						-27.50 kcal/mol							
Initial Orientation						C					C			
Final Orientation						C					C			
Total =	72.87 kcal/mol						63.52 kcal/mol							
van der Waals =	67.60 kcal/mol						67.40 kcal/mol							
Electrostatic =	-244.30 kcal/mol						-251.69 kcal/mol							
ΔE_{tot} =	-45.55 kcal/mol						-54.89 kcal/mol							
ΔE_{vdw} =	-16.28 kcal/mol						-16.48 kcal/mol							
ΔE_{ele} =	-39.03 kcal/mol						-46.42 kcal/mol							

The solution phase results indicate that fewer interactions occur between β-alanine and β-amyloid in the presence of water. Interactions were favoured at Glu11-His14, although a few others formed as well. The systems formed only two measureable bonds in the presence of solvent compared to the eight in the gas phase results. Systems did tend to retain the initial orientations of interactions, but not as well as GABA.

Electrostatic energies were more negative than the van der Waals energies of the systems, indicating that they play a greater role in the overall energetic favourability of a system. The amount of binding interactions occurring had no correlation with the energies of the systems.

4.3 HOMOTAURINE

Homotaurine (Figure 4.3) is a small molecule with an analogous structure to GABA, having a sulfonate group instead of a carboxylate group. This compound is capable of crossing the blood-brain barrier by active transport, and *in vitro* studies demonstrate a capacity to bind to β-amyloid [105].

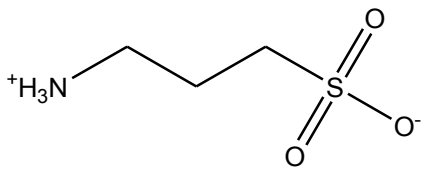

Figure 4.3: Homotaurine at physiological pH

At physiological pH, homotaurine exists in a zwitterionic form and should be capable of interacting with the EV**HH**Q**K** region of β-amyloid.

4.3.1 GAS PHASE OPTIMIZATIONS OF HOMOTAURINE AND β-AMYLOID

The structure of homotaurine was constructed in an extended form before undergoing minimization. The energies of the optimized molecule are summarized in Table 4.19.

Table 4.19: The gas phase energies of homotaurine

	Energies (kcal/mol)		
	E_{tot}	E_{vdw}	E_{ele}
Homotaurine	-12.58	-0.22	-12.86

The minimizations of the gas phase systems were performed following the procedure outlined in section 4.1.1.2-4.1.1.3. The binding energies were calculated using equations 4.1-4.3, where the energy of optimized homotaurine is replacing the energy of GABA. The protein energies are listed in Appendix 6.

4.3.2 THE GAS PHASE RESULTS OF HOMOTAURINE INTERACTING WITH β-AMYLOID

The results of the gas phase energy minimized systems of homotaurine and Aβ are given in Table 4.20. The initial orientation that homotaurine was arranged in is given, along with the orientation that resulted after minimization. The amino acid residues are represented by single letters and the amino and sulfonate groups of homotaurine are represent by N, and S, respectively. The calculated binding energies for each system are included, as well as the number of measureable bonds that formed.

Table 4.20: The gas phase results of homotaurine interacting with β-amyloid

Conformer	Initial Orientation						Final Orientation							ΔE_{tot}	ΔE_{vdv}	ΔE_{ele}	Measured
	E11	V12	H13	H14	Q15	K16	E11	V12	H13	H14	Q15	K16	X	(kcal/mol)	(kcal/mol)	(kcal/mol)	Bonds
1AMB	S			N						S				-35.88	-2.73	-37.02	0
	N			S			N			S				-24.92	-2.14	-23.17	1
			S	N					S	S			S/N	-46.44	-11.20	-35.39	0
			N	S						S			S	-27.61	-7.07	-21.03	0
			S			N			S			S	S	-32.25	-2.99	-30.03	1
			N			S			S			S		-37.17	-3.64	-34.02	1
1AMC	S			N			N							-44.18	-1.49	-41.72	1
	N			S			N			S				-40.50	-0.97	-39.41	1
			N	S						S			S	-50.40	-2.07	-49.99	1
			S	N					S	N/S			N/S	-50.25	-9.63	-43.30	0
			S			N			S			S	S	-35.31	-3.94	-32.09	1
			N			S			S			S	S	-35.66	-4.02	-33.99	1
1AML	S			N						S				-31.14	-2.39	-28.09	0
	N			S			N			S			N	-29.61	-5.09	-24.14	0
			S	N					S	S			S	-49.99	-9.04	-40.56	0
			N	S					S				S	-50.08	-4.49	-46.53	0
			S			N		S	S					-42.20	-5.23	-37.28	2
			N			S		S	S				S	-41.29	-5.20	-36.29	1
1BA4	N					S	N						N	-25.18	-3.87	-21.96	0
	S					N	S						N/S	-43.12	-4.93	-39.23	0
			N	S					S	S				-40.99	-4.13	-37.58	0
			S	N					S	S				-44.54	-4.15	-40.72	1
1IYT	S			N			N							-33.54	-4.92	-27.60	1
	N			S			N			S				-29.92	-5.97	-23.81	1
			S	N					S				S	-36.64	-6.80	-28.71	0
			N	S					S	S			S	-31.79	-4.90	-26.38	0
			S			N			S					-32.03	-2.21	-30.80	0
			N			S			S			S		-34.71	-3.90	-30.78	0
1Z0Q	S			N			N						S	-49.21	-4.51	-43.24	1
	N			S			N			S			S	-47.69	-6.25	-43.03	1
			N	S					S	S			S	-34.76	-5.73	-29.95	0
			S	N					S	S			S	-28.71	-5.69	-23.47	0
			N			S			S			S		-28.92	-3.81	-24.90	0
			S			N						S		-30.56	-1.64	-29.10	1

The gas phase results of homotaurine interacting with different conformers of β-amyloid indicate its potential to bind to the EV**HH**Q**K** region of interest at multiple sites. Interactions favour His13-His14 and His13-Lys16 over Glu11-His14.

4.3.3 THE SOLUTION PHASE OPTIMIZATION OF HOMOTAURINE AND β-AMYLOID

Solution phase optimizations were performed for each of the resulting gas phase optimized systems. Water molecules were placed on the system in a box large enough to surround the protein-homotaurine complex completely.

The systems were energy minimized without constrained protein backbones, and with periodic boundary conditions in place. The energies of the optimized systems were measured with the solvent molecules excluded and a constrained protein backbone. Equations of 4.4-4.6 were used to calculate the binding energies with the solution phase optimized energy of homotaurine (Table 4.21) replacing the solvated GABA energy.

Table 4.21: Solution phase energies of homotaurine

	Energies (kcal/mol)		
	E_{tot}	E_{vdw}	E_{ele}
Homotaurine	-9.96	-0.15	-12.36

4.3.4 THE RESULTS OF THE SOLUTION PHASE OPTIMIZATION OF HOMOTAURINE AND β-AMYLOID

The solution phase minimized systems of homotaurine and β-amyloid are summarized in the following tables according to Aβ conformer. Three letter abbreviations are used to indicate the amino acids for the initial and final orientations that homotaurine is located in. The amino group of homotaurine is represented by N, while the sulfonate group is represented by S. The measured energies of the system (with a constrained

protein backbone, and ignoring solvent contributions) and the calculated binding energies are given.

Orange coloured cells indicate where hydrogen bonds have formed and the darker the orange, the greater the number of bonds. Interactions with the $–CH_2$- chain of the amino acid are coloured in indigo. Backbone interactions are coloured purple for C=O, lime green for –CH-, and yellow for -NH-.

Table 4.22: The solution phase results of homotaurine interacting with the 1AMB conformer of β-amyloid

	Glu11	Val12	His13	His14	Gln15	Lys16	Tyr10	Glu11	Val12	His13	His14	Gln15	Lys16	Leu17	Val18
Initial Orientation	N			S						S			S	S	
Final Orientation	N			S						S			S	S	
Total =	-58.86 kcal/mol						-56.13 kcal/mol								
van der Waals =	35.20 kcal/mol						49.98 kcal/mol								
Electrostatic =	-252.38 kcal/mol						-256.55 kcal/mol								
ΔE_{tot} =	-63.29 kcal/mol						-60.55 kcal/mol								
ΔE_{vdw} =	-12.80 kcal/mol						1.98 kcal/mol								
ΔE_{ele} =	-45.80 kcal/mol						-49.97 kcal/mol								
Initial Orientation				S							S			S	S
Final Orientation	-	-	-	-	-	-					S			S	S
Total =	-80.56 kcal/mol						-54.50 kcal/mol								
van der Waals =	38.11 kcal/mol						43.23 kcal/mol								
Electrostatic =	-272.22 kcal/mol						-250.36 kcal/mol								
ΔE_{tot} =	-84.98 kcal/mol						-58.93 kcal/mol								
ΔE_{vdw} =	-9.89 kcal/mol						-4.77 kcal/mol								
ΔE_{ele} =	-65.64 kcal/mol						-43.78 kcal/mol								
Initial Orientation			S			S	S			S	S				
							N								
Final Orientation			S			S	S			S	S				
							N				N				
Total =	-62.72 kcal/mol						-77.83 kcal/mol								
van der Waals =	53.10 kcal/mol						29.35 kcal/mol								
Electrostatic =	-276.97 kcal/mol						-252.78 kcal/mol								
ΔE_{tot} =	-67.15 kcal/mol						-82.25 kcal/mol								
ΔE_{vdw} =	5.10 kcal/mol						-18.66 kcal/mol								
ΔE_{ele} =	-70.39 kcal/mol						-46.20 kcal/mol								

Table 4.23: The solution phase results of homotaurine interacting with the 1AMC conformer of β-amyloid

	Asp7	Glu11	Val12	His13	His14	Gln15	Lys16	Leu17	Tyr10	Glu11	Val12	His13	His14	Gln15	Lys16	Leu17
Initial Orientation		N			S							S			S	S
Final Orientation		N			S	S						S			S	S
Total =	72.39 kcal/mol								-84.84 kcal/mol							
van der Waals =	41.11 kcal/mol								25.00 kcal/mol							
Electrostatic =	-274.90 kcal/mol								-264.89 kcal/mol							
ΔE_{tot} =	-32.00 kcal/mol								-44.45 kcal/mol							
ΔE_{vdw} =	5.29 kcal/mol								-10.83 kcal/mol							
ΔE_{ele} =	-32.91 kcal/mol								-22.90 kcal/mol							
Initial Orientation		N							S				S			
Final Orientation	N	N							S				S			
Total =	-73.06 kcal/mol								-59.21 kcal/mol							
van der Waals =	43.80 kcal/mol								49.95 kcal/mol							
Electrostatic =	-271.25 kcal/mol								-268.15 kcal/mol							
ΔE_{tot} =	-32.67 kcal/mol								-18.82 kcal/mol							
ΔE_{vdw} =	7.97 kcal/mol								14.12 kcal/mol							
ΔE_{ele} =	-29.26 kcal/mol								-26.16 kcal/mol							
Initial Orientation				S			S	S	N			S	N			
									S				S			
Final Orientation				S					N			S	N			S
									S				S			
Total =	-74.88 kcal/mol								-72.28 kcal/mol							
van der Waals =	38.45 kcal/mol								40.54 kcal/mol							
Electrostatic =	-275.80 kcal/mol								-284.35 kcal/mol							
ΔE_{tot} =	-34.49 kcal/mol								-31.89 kcal/mol							
ΔE_{vdw} =	2.62 kcal/mol								4.72 kcal/mol							
ΔE_{ele} =	-33.81 kcal/mol								-42.36 kcal/mol							

Table 4.24: The solution phase results of homotaurine interacting with the 1AML conformer of β-amyloid

	Ser8	Glu11	Val12	His13	His14	Gln15	Lys16	Val18	Tyr10	Glu11	Val12	His13	His14	Gln15	Lys16	Leu17
Initial Orientation	N	N			S						S	S			S	
Final Orientation	N	N			S			S			S	S			S	
Total =	79.42 kcal/mol								59.34 kcal/mol							
van der Waals =	65.55 kcal/mol								68.99 kcal/mol							
Electrostatic =	-205.42 kcal/mol								-219.49 kcal/mol							
ΔE_{tot} =	-29.93 kcal/mol								-50.01 kcal/mol							
ΔE_{vdw} =	-3.75 kcal/mol								-0.32 kcal/mol							
ΔE_{ele} =	-21.97 kcal/mol								-36.03 kcal/mol							
Initial Orientation					S				S			S				S
Final Orientation		S			S				S			S				S
Total =	93.64 kcal/mol								64.72 kcal/mol							
van der Waals =	63.06 kcal/mol								70.47 kcal/mol							
Electrostatic =	-183.71 kcal/mol								-220.18 kcal/mol							
ΔE_{tot} =	-15.71 kcal/mol								-44.63 kcal/mol							
ΔE_{vdw} =	-6.24 kcal/mol								1.17 kcal/mol							
ΔE_{ele} =	-0.26 kcal/mol								-36.72 kcal/mol							
Initial Orientation			S	S					S			S	S			S
Final Orientation			S	S			S		S			S	S			S
Total =	56.39 kcal/mol								47.65 kcal/mol							
van der Waals =	63.50 kcal/mol								66.02 kcal/mol							
Electrostatic =	-226.29 kcal/mol								-235.63 kcal/mol							
ΔE_{tot} =	-52.96 kcal/mol								-61.70 kcal/mol							
ΔE_{vdw} =	-5.80 kcal/mol								-3.29 kcal/mol							
ΔE_{ele} =	-42.84 kcal/mol								-52.18 kcal/mol							

Table 4.25: The solution phase results of homotaurine interacting with the 1BA4 conformer of β-amyloid

	Asp1	Glu3	Glu11	Val12	His13	His14	Gln15	Lys16	Phe19
Initial Orientation		N	N						
Final Orientation		N	N						
Total =	116.30 kcal/mol								
van der Waals =	69.24 kcal/mol								
Electrostatic =	-175.01 kcal/mol								
ΔE_{tot} =	-0.58 kcal/mol								
ΔE_{vdw} =	-1.74 kcal/mol								
ΔE_{ele} =	0.66 kcal/mol								
Initial Orientation		N	S						S
Final Orientation	N	N						N	S
Total =	83.95 kcal/mol								
van der Waals =	68.20 kcal/mol								
Electrostatic =	-196.75 kcal/mol								
ΔE_{tot} =	-32.94 kcal/mol								
ΔE_{vdw} =	-2.78 kcal/mol								
ΔE_{ele} =	-21.08 kcal/mol								
Initial Orientation					S	S			
Final Orientation					S				
Total =	65.72 kcal/mol								
van der Waals =	68.50 kcal/mol								
Electrostatic =	-223.82 kcal/mol								
ΔE_{tot} =	-51.16 kcal/mol								
ΔE_{vdw} =	-2.48 kcal/mol								
ΔE_{ele} =	-48.15 kcal/mol								
Initial Orientation					S	S			
Final Orientation					S	S			
Total =	55.56 kcal/mol								
van der Waals =	62.29 kcal/mol								
Electrostatic =	-231.22 kcal/mol								
ΔE_{tot} =	-61.32 kcal/mol								
ΔE_{vdw} =	-8.69 kcal/mol								
ΔE_{ele} =	-55.55 kcal/mol								

Table 4.26: The solution phase results of homotaurine interacting with the 1IYT conformer of β-amyloid

	Tyr10	Glu11	Val12	His13	His14	Gln15	Lys16	Glu11	Val12	His13	His14	Gln15	Lys16	Leu17
Initial Orientation		N			S					S				
Final Orientation	S	N			S					S				
Total =	47.31 kcal/mol							44.75 kcal/mol						
van der Waals =	67.15 kcal/mol							69.93 kcal/mol						
Electrostatic =	-243.31 kcal/mol							-259.79 kcal/mol						
ΔE_{tot} =	-92.56 kcal/mol							-95.12 kcal/mol						
ΔE_{vdw} =	-8.82 kcal/mol							-6.03 kcal/mol						
ΔE_{ele} =	-23.92 kcal/mol							-40.40 kcal/mol						
Initial Orientation		N								S	S			S
Final Orientation		N								S	S			S
Total =	53.64 kcal/mol							54.00 kcal/mol						
van der Waals =	73.71 kcal/mol							61.75 kcal/mol						
Electrostatic =	-238.73 kcal/mol							-233.03 kcal/mol						
ΔE_{tot} =	-86.23 kcal/mol							-85.87 kcal/mol						
ΔE_{vdw} =	-2.26 kcal/mol							-14.21 kcal/mol						
ΔE_{ele} =	-19.34 kcal/mol							-13.64 kcal/mol						
Initial Orientation				S			S			S				S
Final Orientation				S			S			S	S			S
Total =	104.02 kcal/mol							30.96 kcal/mol						
van der Waals =	68.79 kcal/mol							61.35 kcal/mol						
Electrostatic =	-257.44 kcal/mol							-242.19 kcal/mol						
ΔE_{tot} =	-35.85 kcal/mol							-108.91 kcal/mol						
ΔE_{vdw} =	-7.17 kcal/mol							-14.62 kcal/mol						
ΔE_{ele} =	-38.05 kcal/mol							-22.79 kcal/mol						

Table 4.27: The solution phase results of homotaurine interacting with the 1Z0Q conformer of β-amyloid

	Phe4	Glu11	Val12	His13	His14	Gln15	Lys16	Val18	Gly9	Tyr10	Glu11	Val12	His13	His14	Gln15	Lys16
Initial Orientation		N			S			S								S
Final Orientation		N			S			S								S
Total =	81.50 kcal/mol								96.18 kcal/mol							
van der Waals =	71.69 kcal/mol								68.74 kcal/mol							
Electrostatic =	-236.46 kcal/mol								-222.11 kcal/mol							
ΔE_{tot} =	-45.27 kcal/mol								-30.59 kcal/mol							
ΔE_{vdw} =	-9.37 kcal/mol								-12.32 kcal/mol							
ΔE_{ele} =	-42.48 kcal/mol								-28.13 kcal/mol							
Initial Orientation	S	N								S			S	S		S
Final Orientation	S	N								S			S	S		
Total =	71.19 kcal/mol								89.01 kcal/mol							
van der Waals =	67.45 kcal/mol								87.76 kcal/mol							
Electrostatic =	-238.48 kcal/mol								-241.61 kcal/mol							
ΔE_{tot} =	-55.58 kcal/mol								-37.76 kcal/mol							
ΔE_{vdw} =	-13.61 kcal/mol								6.70 kcal/mol							
ΔE_{ele} =	-44.50 kcal/mol								-47.63 kcal/mol							
Initial Orientation				S			S		S	S			S	S		
Final Orientation				S			S		S	S			S			
Total =	113.10 kcal/mol								89.03 kcal/mol							
van der Waals =	78.03 kcal/mol								68.91 kcal/mol							
Electrostatic =	-212.24 kcal/mol								-223.87 kcal/mol							
ΔE_{tot} =	-13.67 kcal/mol								-37.73 kcal/mol							
ΔE_{vdw} =	-3.03 kcal/mol								-12.15 kcal/mol							
ΔE_{ele} =	-18.26 kcal/mol								-29.89 kcal/mol							

The solution phase optimizations of homotaurine and Aβ indicate that binding can occur at multiple sites within the EV**HH**Q**K** region of interest. His13-His14 and His13-Lys16 were the most favoured orientations for interactions, followed immediately by Glu11-His14. Homotaurine bound quite well within the EV**HH**Q**K** region of Aβ, and tended to retain the same orientation as in the gas phase despite the presence of water molecules.

Hydrogen bonds were the only measureable type of bonds that were observed in the optimized systems. The energies tended to be favourable, especially the electrostatic energy contributions.

4.4 3-AMINOPROPYL DIHYDROGEN PHOSPHATE

A synthetic molecule, 3-aminopropyl dihydrogen phosphate (Figure 4.4), was selected for study to compare the effect of a phosphate group on the potential binding interactions with the EV**HH**Q**K** region of β-amyloid, relative to carboxylate or sulfonate.

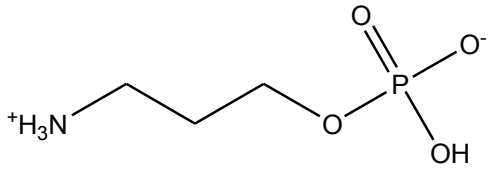

Figure 4.4: 3-Aminopropyl dihydrogen phosphate at physiological pH

The functional groups on 3-aminopropyl dihydrogen phosphate exist in a zwitterionic state at physiological pH.

4.4.1 GAS PHASE OPTIMIZATIONS OF 3-AMINOPROPYL DIHYDROGEN PHOSPHATE AND β-AMYLOID

A model of 3-aminopropyl dihydrogen phosphate was constructed in an extended structure and geometry optimized; the energies are given in Table 4.28.

Table 4.28: The gas phase energies of 3-aminopropyl dihydrogen phosphate

	Energies (kcal/mol)		
	E_{tot}	E_{vdw}	E_{ele}
3-aminopropyl dihydrogen phosphate	-21.69	1.31	-29.25

Each system was prepared such that the amino and phosphate group of 3-aminopropyl dihydrogen phosphate were oriented approximately 3.0 Å away from two of the charged amino acid side chains in the EV**HH**Q**K** region of Aβ. The optimizations were performed following the procedure outlined in Section 4.1.1.3. The calculated

energies used equations 4.1-4.3 with the energy of the optimized 3-aminopropyl dihydrogen phosphate replacing the energy of optimized GABA.

4.4.2 Results of the Gas Phase Optimizations of 3-Aminopropyl Dihydrogen Phosphate and β-Amyloid

The results of the gas phase optimizations of 3-aminopropyl dihydrogen phosphate with Aβ in different conformations are summarized in the following table. The initial and finial orientations of the optimized systems are given with the amino and phosphate groups of 3-aminopropyl dihydrogen phosphate represented by N and P, and the amino acids by single letters. The numbers of measured bonding interactions for each system are given along with the calculated binding energies for each system.

Table 4.29: The gas phase results of 3-aminopropyl dihydrogen phosphate interacting with β-amyloid

Conformer	Initial Orientation						Final Orientation							ΔE_{tot}	ΔE_{vdv}	ΔE_{ele}	Measured
	E11	V12	H13	H14	Q15	K16	E11	V12	H13	H14	Q15	K16	X	(kcal/mol)	(kcal/mol)	(kcal/mol)	Bonds
1AMB	P			N			P							-23.17	-0.79	-25.92	0
	N			P			N			P				-48.14	-4.82	-40.69	1
			P	N					P	P				-46.02	-9.32	-40.15	0
			N	P						P			P	-61.73	-0.44	-56.42	0
			P			N			P			P		-40.19	-2.07	-39.48	1
			N			P	-	-	-	-	-	-	-	-33.32	-1.98	-34.01	0
1AMC	P			N			P							-30.11	-1.12	-28.57	0
	N			P			N			P	P			-47.68	-3.95	-46.28	2
			N	P						P				-42.68	-0.31	-45.74	0
			P	N			N		P	N/P			N/P	-52.44	-9.32	-46.04	0
			P			N			P			P		-43.87	-2.02	-42.98	1
			N			P			P				P	-35.09	-3.29	-34.97	0
1AML	P			N			P			P			P	-42.82	-4.81	-39.88	1
	N			P			N			P			N/P	-50.32	-5.83	-39.57	1
			P	N					P				P	-82.49	-10.97	-71.69	1
			N	P						P			P	-59.91	-3.98	-61.92	0
			P			N			P					-21.44	-0.48	-23.00	0
			N			P						P		-22.89	-1.24	-23.72	0
1BA4	N					P	N					P	P	-26.29	-4.07	-26.18	1
	P					N	P						N/P	-66.40	-11.25	-54.24	0
			P	N					P					-26.45	-0.91	-25.84	0
			N	P						P				-45.55	-1.53	-45.26	1
1IYT	P			N			-	-	-	-	-	-	-	-17.24	-4.85	-13.15	0
	N			P			N			P				-38.18	-8.07	-31.12	0
			P	N					P					-36.89	-3.83	-32.74	0
			N	P						P				-20.73	-2.19	-18.79	0
			P			N			P					-30.19	-0.47	-31.02	0
			N			P						P		-25.81	-1.52	-25.48	0
1Z0Q	P			N			P						N/P	-56.04	-3.18	-58.78	0
	N			P			N			P			P	-61.99	-9.37	-52.88	0
			N	P						P				-29.40	-3.87	-27.45	0
			P	N					P				P	-41.30	-6.18	-36.98	0
			P			N			P					-33.22	-0.90	-32.40	1
			N			P						P		-35.04	-2.92	-31.44	1
				N		P						P		-27.13	-5.10	-23.00	0
				P		N				P		P		-46.01	-7.84	-41.06	0

The results of the gas phase minimizations of 3-aminopropyl dihydrogen phosphate with the different conformers of Aβ suggest that the molecule is capable of binding to the EV**HH**Q**K** region of the protein. Interactions at Glu11-His14 were the preferred orientation of binding.

4.4.3 THE SOLUTION PHASE OPTIMIZATION OF 3-AMINOPROPYL DIHYDROGEN PHOSPHATE AND β-AMYLOID

Each of the systems resulting from the gas phase minimization of 3-aminopropyl dihydrogen phosphate with β-amyloid was subjected to solution phase optimization.

Each system was solvated using a box of explicit water molecules with periodic boundary conditions in place during the minimization and having an unconstrained protein backbone. Energies were measured with the protein backbone constrained and solvent contributions were ignored. Equations 4.4-4.6 were used to calculate the binding energies with the energy of the solution phase optimized 3-aminopropyl dihydrogen phosphate substituted for the GABA energy. Appendix 6 contains the energies of the proteins and Table 4.30 lists the energies of the optimized 3-aminopropyl dihydrogen phosphate, ignoring solvent contributions.

Table 4.30: Solution phase energies of 3-aminopropyl dihydrogen phosphate

	Energies (kcal/mol)		
	E_{tot}	E_{vdw}	E_{ele}
3-aminopropyl dihydrogen phosphate	-16.52	0.76	-29.65

4.3.4 THE RESULTS OF THE SOLUTION PHASE OPTIMIZATION OF 3-AMINOPROPYL DIHYDROGEN PHOSPHATE AND β-AMYLOID

The results of the solution phase minimization of 3-aminopropyl dihydrogen phosphate with β-amyloid are given in Tables 4.31-4.36 according to β-amyloid conformer. The amino and phosphate group of 3-aminopropyl dihydrogen phosphate are represented by N and P and are shown in the initial orientation before minimization in a solvated environment and the resulting final orientation after. The amino acids involved

are listed by their three-letter abbreviations, and both the measured and calculated energies for each system are given.

Instances where hydrogen bonds have formed are coloured in orange, and interactions with the $–CH_2$- chain of the amino acid are shown in indigo. Where interactions occur with the –CH-, -NH- or C=O of the protein backbone, cells are coloured lime green, yellow, and purple, respectively.

Table 4.31: The solution phase results of 3-aminopropyl dihydrogen phosphate interacting with the 1AMB conformer of β-amyloid

	Glu11	Val12	His13	His14	Gln15	Lys16	Val18	Glu11	Val12	His13	His14	Gln15	Lys16
Initial Orientation				P			P			P			P
Final Orientation				P			P			P			P
Total =	-83.77 kcal/mol							-42.55 kcal/mol					
van der Waals =	44.76 kcal/mol							48.92 kcal/mol					
Electrostatic =	-290.16 kcal/mol							-257.12 kcal/mol					
ΔE_{tot} =	-81.64 kcal/mol							-40.42 kcal/mol					
ΔE_{vdw} =	-4.14 kcal/mol							0.01 kcal/mol					
ΔE_{ele} =	-66.28 kcal/mol							-33.24 kcal/mol					
Initial Orientation			P	P				N			P		
Final Orientation	N		P	N				N					
Total =	-89.70 kcal/mol							-60.75 kcal/mol					
van der Waals =	35.27 kcal/mol							52.20 kcal/mol					
Electrostatic =	-286.06 kcal/mol							-277.94 kcal/mol					
ΔE_{tot} =	-87.56 kcal/mol							-58.62 kcal/mol					
ΔE_{vdw} =	-13.63 kcal/mol							3.30 kcal/mol					
ΔE_{ele} =	-62.18 kcal/mol							-54.06 kcal/mol					
Initial Orientation	-	-	-	-	-	-	-	P					
Final Orientation	-	-	-	-	-	-	-	P					
Total =	-56.46 kcal/mol							-54.88 kcal/mol					
van der Waals =	55.44 kcal/mol							41.59 kcal/mol					
Electrostatic =	-275.92 kcal/mol							-258.70 kcal/mol					
ΔE_{tot} =	-54.33 kcal/mol							-52.75 kcal/mol					
ΔE_{vdw} =	6.54 kcal/mol							-7.32 kcal/mol					
ΔE_{ele} =	-52.04 kcal/mol							-34.83 kcal/mol					

Table 4.32: The solution phase results of 3-aminopropyl dihydrogen phosphate interacting with the 1AMC conformer of β-amyloid

	Glu11	Val12	His13	His14	Gln15	Lys16	Tyr10	Glu11	Val12	His13	His14	Gln15	Lys16	Leu17
Initial Orientation	N			P	P		P	N		P	P			
							N				N			
Final Orientation	N			P			P	P			P			
							N	N			N			
Total =	-89.22 kcal/mol						-106.21 kcal/mol							
van der Waals =	52.86 kcal/mol						35.47 kcal/mol							
Electrostatic =	-314.11 kcal/mol						-311.32 kcal/mol							
ΔE_{tot} =	-42.27 kcal/mol						-59.26 kcal/mol							
ΔE_{vdw} =	16.13 kcal/mol						-1.26 kcal/mol							
ΔE_{ele} =	-54.82 kcal/mol						-52.03 kcal/mol							
Initial Orientation	P													P
Final Orientation	-	-	-	-	-	-								P
Total =	-87.23 kcal/mol						-63.82 kcal/mol							
van der Waals =	39.24 kcal/mol						44.95 kcal/mol							
Electrostatic =	-278.08 kcal/mol						-277.87 kcal/mol							
ΔE_{tot} =	-40.28 kcal/mol						-16.87 kcal/mol							
ΔE_{vdw} =	2.51 kcal/mol						8.22 kcal/mol							
ΔE_{ele} =	-18.79 kcal/mol						-18.59 kcal/mol							
Initial Orientation				P									P	
Final Orientation				P									P	
Total =	-65.34 kcal/mol						-49.05 kcal/mol							
van der Waals =	43.37 kcal/mol						46.64 kcal/mol							
Electrostatic =	-218.94 kcal/mol						-267.60 kcal/mol							
ΔE_{tot} =	-18.39 kcal/mol						-2.10 kcal/mol							
ΔE_{vdw} =	6.64 kcal/mol						9.91 kcal/mol							
ΔE_{ele} =	-22.65 kcal/mol						-8.31 kcal/mol							

Table 4.33: The solution phase results of 3-aminopropyl dihydrogen phosphate interacting with the 1AML conformer of β-amyloid

	His6	Asp7	Ser8	Glu11	Val12	His13	His14	Gln15	Lys16	Tyr10	Glu11	Val12	His13	His14	Gln15	Lys16	Leu17
Initial Orientation	N	N	N	N			P			P				P			
Final Orientation	N	N	N				P			P							
Total =	55.93 kcal/mol									35.33 kcal/mol							
van der Waals =	68.82 kcal/mol									71.35 kcal/mol							
Electrostatic =	-234.38 kcal/mol									-278.25 kcal/mol							
ΔE_{tot} =	-46.86 kcal/mol									-67.46 kcal/mol							
ΔE_{vdw} =	-1.39 kcal/mol									1.14 kcal/mol							
ΔE_{ele} =	-33.63 kcal/mol									-77.50 kcal/mol							
Initial Orientation			P	P			P			P			P				P
Final Orientation			P	P			P			P			P				
Total =	98.74 kcal/mol									82.52 kcal/mol							
van der Waals =	78.45 kcal/mol									69.97 kcal/mol							
Electrostatic =	-222.15 kcal/mol									-256.88 kcal/mol							
ΔE_{tot} =	-4.05 kcal/mol									-20.27 kcal/mol							
ΔE_{vdw} =	8.24 kcal/mol									-0.23 kcal/mol							
ΔE_{ele} =	-21.40 kcal/mol									-56.13 kcal/mol							
Initial Orientation									P				P				
Final Orientation									P				P				
Total =	77.87 kcal/mol									83.58 kcal/mol							
van der Waals =	72.57 kcal/mol									78.77 kcal/mol							
Electrostatic =	-218.30 kcal/mol									-209.99 kcal/mol							
ΔE_{tot} =	-24.92 kcal/mol									-19.21 kcal/mol							
ΔE_{vdw} =	2.36 kcal/mol									8.57 kcal/mol							
ΔE_{ele} =	-17.55 kcal/mol									-9.24 kcal/mol							

Table 4.34: The solution phase results of 3-aminopropyl dihydrogen phosphate interacting with the 1BA4 conformer of β-amyloid

	Asp1	Glu3	Glu11	Val12	His13	His14	Gln15	Lys16	Phe19	Phe20	Asp23
Initial Orientation		P	N					P	P		P
Final Orientation	P	N	N					P	P	P	P
Total =	76.66 kcal/mol										
van der Waals =	76.24 kcal/mol										
Electrostatic =	-227.89 kcal/mol										
ΔE_{tot} =	-33.67 kcal/mol										
ΔE_{vdw} =	4.36 kcal/mol										
ΔE_{ele} =	-34.92 kcal/mol										
Initial Orientation	N		P						P		N
									N		
Final Orientation	N		P						P	N	N
									N		
Total =	17.79 kcal/mol										
van der Waals =	66.83 kcal/mol										
Electrostatic =	-264.35 kcal/mol										
ΔE_{tot} =	-92.54 kcal/mol										
ΔE_{vdw} =	-5.06 kcal/mol										
ΔE_{ele} =	-71.38 kcal/mol										
Initial Orientation						P					
Final Orientation						P					
Total =	72.75 kcal/mol										
van der Waals =	82.23 kcal/mol										
Electrostatic =	-218.78 kcal/mol										
ΔE_{tot} =	-37.57 kcal/mol										
ΔE_{vdw} =	10.34 kcal/mol										
ΔE_{ele} =	-25.80 kcal/mol										
Initial Orientation					P						
Final Orientation	-	-	-	-	-	-	-	-	-	-	-
Total =	75.27 kcal/mol										
van der Waals =	79.11 kcal/mol										
Electrostatic =	-224.20 kcal/mol										
ΔE_{tot} =	-35.05 kcal/mol										
ΔE_{vdw} =	7.23 kcal/mol										
ΔE_{ele} =	-31.22 kcal/mol										

Table 4.35: The solution phase results of 3-aminopropyl dihydrogen phosphate interacting with the 1IYT conformer of β-amyloid

	Glu11	Val12	His13	His14	Gln15	Lys16		Glu11	Val12	His13	His14	Gln15	Lys16	Leu17
Initial Orientation	N			P						P				
Final Orientation	N			P						P				P
Total =	56.67 kcal/mol							51.27 kcal/mol						
van der Waals =	72.75 kcal/mol							75.34 kcal/mol						
Electrostatic =	-251.36 kcal/mol							-257.89 kcal/mol						
ΔE_{tot} =	-76.64 kcal/mol							-82.04 kcal/mol						
ΔE_{vdw} =	-4.12 kcal/mol							-1.53 kcal/mol						
ΔE_{ele} =	-14.67 kcal/mol							-21.20 kcal/mol						
Initial Orientation	-	-	-	-	-	-							P	
Final Orientation	P												P	
Total =	63.97 kcal/mol							58.79 kcal/mol						
van der Waals =	74.24 kcal/mol							81.43 kcal/mol						
Electrostatic =	-237.73 kcal/mol							-261.26 kcal/mol						
ΔE_{tot} =	-69.34 kcal/mol							-74.52 kcal/mol						
ΔE_{vdw} =	-2.63 kcal/mol							4.56 kcal/mol						
ΔE_{ele} =	-1.04 kcal/mol							-24.57 kcal/mol						
Initial Orientation				P						P				
Final Orientation			N	P						P				
Total =	36.02 kcal/mol							116.91 kcal/mol						
van der Waals =	68.56 kcal/mol							68.15 kcal/mol						
Electrostatic =	-254.83 kcal/mol							-261.92 kcal/mol						
ΔE_{tot} =	-97.29 kcal/mol							-16.40 kcal/mol						
ΔE_{vdw} =	-8.31 kcal/mol							-8.72 kcal/mol						
ΔE_{ele} =	-18.14 kcal/mol							-25.23 kcal/mol						

Table 4.36: The solution phase results of 3-aminopropyl dihydrogen phosphate interacting with the 1Z0Q conformer of β-amyloid

	Gly9	Tyr10	Glu11	Val12	His13	His14	Gln15	Lys16	Val18	Glu22	Glu11	Val12	His13	His14	Gln15	Lys16	Leu17
Initial Orientation			N			P			P	P						P	
Final Orientation			N			P			P	P						P	
Total =	34.94 kcal/mol										81.59 kcal/mol						
van der Waals =	70.19 kcal/mol										59.16 kcal/mol						
Electrostatic =	-288.71 kcal/mol										-235.18 kcal/mol						
ΔE_{tot} =	-85.27 kcal/mol										-38.62 kcal/mol						
ΔE_{vdw} =	-11.77 kcal/mol										-22.81 kcal/mol						
ΔE_{ele} =	-77.43 kcal/mol										-23.90 kcal/mol						
			P							N							
Initial Orientation			P							N			P				
Final Orientation											-	-	-	-	-	-	-
Total =	53.54 kcal/mol										78.53 kcal/mol						
van der Waals =	59.59 kcal/mol										65.00 kcal/mol						
Electrostatic =	-273.42 kcal/mol										-236.83 kcal/mol						
ΔE_{tot} =	-66.67 kcal/mol										-41.67 kcal/mol						
ΔE_{vdw} =	-12.27 kcal/mol										-16.96 kcal/mol						
ΔE_{ele} =	-62.14 kcal/mol										-25.55 kcal/mol						
Initial Orientation						P										P	
Final Orientation					N	P							P			P	
Total =	73.30 kcal/mol										72.41 kcal/mol						
van der Waals =	70.21 kcal/mol										81.75 kcal/mol						
Electrostatic =	-247.11 kcal/mol										-250.43 kcal/mol						
ΔE_{tot} =	-46.91 kcal/mol										-47.80 kcal/mol						
ΔE_{vdw} =	-11.75 kcal/mol										-0.21 kcal/mol						
ΔE_{ele} =	-35.83 kcal/mol										-39.15 kcal/mol						
Initial Orientation	P	P			P									P		P	
Final Orientation	P	P			P								P	P			P
Total =	71.31 kcal/mol										82.86 kcal/mol						
van der Waals =	61.68 kcal/mol										80.82 kcal/mol						
Electrostatic =	-247.15 kcal/mol										-245.90 kcal/mol						
ΔE_{tot} =	-48.90 kcal/mol										-37.35 kcal/mol						
ΔE_{vdw} =	-20.28 kcal/mol										-1.14 kcal/mol						
ΔE_{ele} =	-35.87 kcal/mol										-34.62 kcal/mol						

The solution phase energy minimizations of 3-aminopropyl dihydrogen phosphate with the different conformers of β-amyloid result in multiple binding interactions in the EV**HH**Q**K** region. Interactions at Glu11-His14 are favoured, followed by His13-His14. Only five hydrogen bonds were measured in the optimized systems; fewer measureable interactions occurred than in the gas phase minimized systems, however, there was not much difference in the orientations of the interactions.

The energies of the optimized systems were mostly favourable, and the electrostatic energies were much lower than the van der Waals energies. Comparing

systems with multiple interactions to those with few or none indicates that the energies vary and that having more potential binding interactions does not equate to energetic favourability. It is likely that repulsive factors are also a contributing factor in these systems.

4.5 Semi-Empirical Energy Calculations of GABA, β-Alanine, Homotaurine and 3-Aminopropyl Dihydrogen Phosphate with β-Amyloid

To further compare the results of the gas and solution phase minimizations of the four compounds covered in this chapter, semi-empirical calculations were performed. The Austin Model 1 (AM1) model was selected for use [42, 106].

4.5.1 Selection of Systems for Semi-Empirical Calculations

Selected systems from the gas phase energy minimized results of each of GABA, β-alanine, homotaurine and 3-aminopropyl dihydrogen phosphate with β-amyloid, were used for semi-empirical calculations using the AM1 Hamiltonian as implemented in the Gaussian 09W suite of programs [107].

For each of the four compounds, one system with each of the six β-amyloid conformers was selected for modelling at the semi-empirical level. These systems needed to have binding interactions occurring with at least two different amino acid residues. The individual molecules and each Aβ conformer were also submitted for energy calculations.

4.5.2 SEMI-EMPIRICAL ENERGY CALCULATION SET-UP

Each of the selected systems was submitted for energy calculations. These energies were calculated in the ground state with a singlet spin. The quadratically convergent SCF function was selected, as convergence of the system was not obtained otherwise. The units of measurement of Gaussian calculations are in hartrees; the energies were converted to kcal/mol for comparison.

The energy of interaction of each system was calculated by subtracting the individual energies of each molecule and the specific β-amyloid conformer from the energy of the modelled system via the following equation:

$$\Delta E_{bind} = E_{A\beta mol} - E_{A\beta} - E_{mol} \tag{4.7}$$

Where E_{mol} is the energy of the target molecule, $E_{A\beta}$ is the energy of the β-amyloid conformer and $E_{A\beta mol}$ is the energy of the interacting Aβ-molecule system. The energies of the Aβ conformers are listed in Appendix 6.

4.5.3 RESULTS OF THE SEMI-EMPIRICAL ENERGY CALCULATIONS

The energies of each of the four molecules were calculated using the AM1 model and are summarized in the following table.

Table 4.37: Energies of GABA, β-alanine, homotaurine and 3-aminopropyl dihydrogen phosphate calculated at the AM1 level of theory

	Energy
GABA	-0.053803541 hartrees
	-33.762 kcal/mol
β-alanine	-0.064715664 hartrees
	-40.61 kcal/mol
homotaurine	-0.110178939 hartrees
	-69.138 kcal/mol
3-aminopropyl dihydrogen phosphate	-0.319778234 hartrees
	-200.664 kcal/mol

The results of the energy calculations for each of GABA, β-alanine, homotaurine and 3-aminopropyl dihydrogen phosphate with Aβ using the AM1 level of theory are summarized in Tables 4.38-4.41. The orientation of the interaction is given with the single letter amino acid abbreviation, and the functional groups of each of the molecules are represented by N, C, S and P for the amino, carboxylate, sulfonate and phosphate groups. The measured energy of each system is given, along with the calculated binding energy.

Table 4.38: AM1 energies of GABA interacting with β-amyloid

	R5	E11	V12	H13	H14	Q15	K16	L17
Orientation				C	C			
Energy =	-749.464	kcal/mol						
ΔE_{bind} =	-41.711	kcal/mol						
Orientation				C	N			C
Energy =	-748.947	kcal/mol						
ΔE_{bind} =	-35.713	kcal/mol						
Orientation	C	N			C	N		
Energy =	-992.926	kcal/mol						
ΔE_{bind} =	-57.669	kcal/mol						

	E3	E11	V12	H13	H14	Q15	K16	F19
Orientation	N C	C					C	C
Energy =	-1078.737	kcal/mol						
ΔE_{bind} =	-11.122	kcal/mol						
Orientation				N C	C			
Energy =	-1398.660	kcal/mol						
ΔE_{bind} =	-0.193	kcal/mol						
Orientation		N			C			
Energy =	-917.623	kcal/mol						
ΔE_{bind} =	-76.516	kcal/mol						

Table 4.39: AM1 energies of β-alanine interacting with β-amyloid

	S8	E11	V12	H13	H14	Q15	K16
Orientation		N			C		
Energy =	-735.381	kcal/mol					
ΔE_{bind} =	-20.782	kcal/mol					
Orientation				C			C
Energy =	-777.692	kcal/mol					
ΔE_{bind} =	-57.610	kcal/mol					
Orientation	N	N			C		
Energy =	-1006.058	kcal/mol					
ΔE_{bind} =	-63.954	kcal/mol					

	E3	E11	V12	H13	H14	Q15	K16	F19
Orientation	N	C						C
Energy =	-1097.851	kcal/mol						
ΔE_{bind} =	-23.389	kcal/mol						
Orientation	N				C			
Energy =	-1468.757	kcal/mol						
ΔE_{bind} =	-63.444	kcal/mol						
Orientation	C				N			
Energy =	-814.268	kcal/mol						
ΔE_{bind} =	33.686	kcal/mol						

Table 4.40: AM1 energies of homotaurine interacting with β-amyloid

	S8	Y10	E11	V12	H13	H14	Q15	K16
Orientation			N			S		
Energy =	-795.621	kcal/mol						
ΔE_{bind} =	-52.493	kcal/mol						
Orientation		S			S	N		
		N				S		
Energy =	-787.256	kcal/mol						
ΔE_{bind} =	-38.646	kcal/mol						
Orientation	N		N			S		
Energy =	-1042.940	kcal/mol						
ΔE_{bind} =	-72.307	kcal/mol						

	E11	V12	H13	H14	Q15	K16	V18
Orientation			S	S			
Energy =	-1160.430	kcal/mol					
ΔE_{bind} =	-57.440	kcal/mol					
Orientation	N			S			
Energy =	-1494.552	kcal/mol					
ΔE_{bind} =	-60.710	kcal/mol					
Orientation	N			S			S
Energy =	-943.679	kcal/mol					
ΔE_{bind} =	-67.197	kcal/mol					

Table 4.41: AM1 energies of 3-aminopropyl dihydrogen phosphate interacting with β-amyloid

	S8	E11	V12	H13	H14	Q15	K16
Orientation				P			P
Energy =	-944.378	kcal/mol					
ΔE_{bind} =	-69.725	kcal/mol					
Orientation		N			P	P	
Energy =	-948.158	kcal/mol					
ΔE_{bind} =	-68.023	kcal/mol					
Orientation	P	P			P		
Energy =	-1111.677	kcal/mol					
ΔE_{bind} =	-9.519	kcal/mol					

	E3	E11	V12	H13	H14	Q15	K16	V18	F19	E22	D23
Orientation	P	N					P		P		P
Energy =	-1234.782	kcal/mol									
ΔE_{bind} =	-0.266	kcal/mol									
Orientation		N			P						
Energy =	-1619.361	kcal/mol									
ΔE_{bind} =	-53.993	kcal/mol									
Orientation		N			P			P		P	
Energy =	-1072.663	kcal/mol									
ΔE_{bind} =	-64.655	kcal/mol									

The energies of each system can be compared to determine whether the negatively charged functional group plays a role in the strength of the interactions that occur.

Homotaurine interacting with β-amyloid resulted in the most consistently favourable energies. All of the systems selected demonstrated binding within the EV**HH**Q**K** region of Aβ.

Energies of 3-aminopropyl dihydrogen phosphate binding to β-amyloid in different conformations were the next most favourable relative to homotaurine. With the exception of two systems, the energies were all very low, and interactions occurred at two or more sites within EV**HH**Q**K**. Interestingly, the systems with the highest energies had hydrogen bonds present and multiple binding sites between the molecule and protein.

The energies calculated for GABA interacting with Aβ demonstrated slightly less favourability compared to 3-aminopropyl dihydrogen phosphate. The energies of these systems were a bit more variable.

While the calculated binding energies of β-alanine were more consistent than 3-aminopropyl dihydrogen phosphate and GABA, they tended to be slightly higher. One system did not have interactions occurring at two sites within EV**HH**Q**K**, and one occurring in that region was extremely unfavourable.

4.6 Conclusions on GABA, β-Alanine, Homotaurine and 3-Aminopropyl Dihydrogen Phosphate Interacting with the EVHHQK Region of β-Amyloid

Overall comparing the interactions occurring between GABA, β-alanine, homotaurine and 3-aminopropyl dihydrogen phosphate with β-amyloid allows for some conclusions to be drawn based on their nature.

First, both the endogenous and synthetic compounds demonstrated a capacity to bind to the EV**HH**Q**K** region of β-amyloid *in silico*. This indicates that these small molecules may be used to target this region to prevent amyloid aggregation from occurring. Furthermore they could be used as lead molecules to design even more effective binding agents, or drugs that would increase the levels of the endogenous compounds could be developed.

Second, the nature of the negatively charged group on the zwitterions plays a role in the strength of binding interactions. Comparing the energies of the four molecules showed that the order of favourability ranked $SO_3^- > PO_3^- > CO_2^-$. Also, the length of the $–CH_2$- chain played a factor. GABA was capable of forming more measureable binding interactions than β-alanine.

Homotaurine presents itself as the most viable option of the four molecules for binding to the EV**HH**Q**K** region of β-amyloid. Indeed, this may be the mechanism by which the molecule keeps the protein in its monomeric form *in vivo* [105].

4.7 INTERPRETATION

The results of the *in silico* optimizations of GABA, β-alanine, homotaurine and 3-aminopropyl dihydrogen phosphate demonstrate how both the size of the molecule and the anionic group are important in forming binding interactions with the EV**HH**Q**K** region of β-amyloid.

Of the systems studied, the synthetic compound homotaurine demonstrated the most favourable binding energies (calculated at a semi-empirical level of theory) and the greatest capacity to form binding interactions within the EV**HH**Q**K** region of interest. Homotaurine was especially capable of forming binding interactions with the **BB**X**B** motif of Aβ, **HH**Q**K**.

The next most favourable interactions occurred between GABA and β-amyloid. More binding interactions formed in both the **HH**Q**K** and expanded EV**HH**Q**K** regions than 3-aminopropyl dihydrogen phosphate. The semi-empirical binding energies of GABA were more variable than those of the phosphate species, and slightly less favourable. 3-Aminopropyl dihydrogen phosphate formed fewer binding interaction than GABA in the EV**HH**Q**K** systems studied. Though it is difficult to rank these species in terms of favourability, the binding energies suggest that 3-aminopropyl dihydrogen phosphate can interact more strongly with β-amyloid.

The interactions between β-alanine and β-amyloid are the least favourable of the four molecules examined in this chapter. The number of binding interactions occurring with the protein is less than those observed for 3-aminopropyl dihydrogen phosphate, as well the binding energies (measured by semi-empirical calculations) were the least favourable of the four; one system demonstrated highly unfavourable energetics. The molecular mechanics binding energies further support the notion that the β-alanine systems are less favourable than those of the other three molecules.

Overall these results can be interpreted to suggest that the anionic group present on these endogenous and synthetic species plays an important role in determining the strength of binding interactions that can occur. The three anionic groups can all be considered acidic species with the order of relative acidity sulfonic acid > phosphonic acid > carboxylic acid for the functional groups. It is more likely that this feature affects the strength of interaction, which may potentially be affected by the size of the anionic group as well: phosphonate and sulfonate are both larger than carboxylate. The larger, more acidic species can interact more strongly with the positively charged amino acids to form more energetically favourable interactions.

Furthermore, the length of the carbon chain also plays a role in the effective binding of molecules to the EV**HH**Q**K** region of Aβ. Although β-alanine and GABA are functionally identical, the difference of one carbon unit in the chain length between charged functional groups clearly impacts the amount of binding interactions that can occur. The number of binding interactions between β-alanine and Aβ are only about half of those formed between GABA and Aβ. It appears that the size of the molecule is also important for the binding interactions to form between itself and β-amyloid.

These results indicate that molecules can be developed to target the EV**HH**Q**K** region of β-amyloid with greater specificity by tuning the anionic functional groups present to form stronger binding interactions with the positively charged amino acids. Adjusting the length/size of the molecule can also play a role in increasing the strength of interactions within the EV**HH**Q**K** region of interest.

CHAPTER 5: THE SEARCH FOR AN ENDOGENOUS ANTI-ALZHEIMER'S DRUG TARGETING LVFF

Located immediately next to the **HH**Q**K** region of β-amyloid is the LVFF region. The highly positively charged **HH**Q**K** segment plays a role in the misfolding process of the protein by binding to negatively charged glycosaminoglycans on the surface of membranes. Similarly, the LVFF region of Aβ is a hydrophobic region that can interact with cholesterol rafts on the surface of membranes to further facilitate the conformational change.

The LVFF region follows a pattern that can be identified as AAXA, where A is an aliphatic or aromatic amino acid. As this motif is similar to **BB**X**B**, there arose the question as to whether or not a single drug molecule could bind to both **HH**Q**K** and LVFF with the same strength and efficacy, if so this would provide further evidence to support the concept of a "promiscuous drug" targeting β-amyloid to prevent aggregation.

5.1 Interactions Between an Indole and the HHQK and LVFF Regions of β-Amyloid

A simple indole (Figure 5.1) was selected for this study to determine its capacity to bind to the LVVF region of Aβ, relative to **HH**Q**K**. An indole is a small aromatic molecule that should, in essence, be able to interact with both regions by forming cation-π and π-π type interactions. The indole is also representative of biological molecules

endogenous to the brain. Indole constitutes the aromatic moiety within tryptophan (examined in Chapter 4) and is present in some of tryptophan's metabolites.

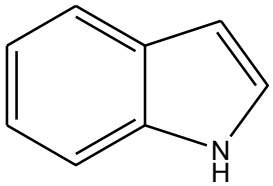

Figure 5.1: Indole

5.1.1 Isolation of the HHQK and LVFF Regions of β-Amyloid

To better compare the binding of indole, the LVFF and **HH**Q**K** regions were isolated from β-amyloid. For the LVFF region, residues 13-24 were isolated. This provided a four amino acid cap on either side of the region that would be more reflective of the area as it exists in a natural state; isolating only the LVFF region is too exposed to empty space and is less reflective of the interactions that could form. The ends of the 13-24 residue segment were capped with amide groups. Six different conformers of Aβ were used for this study and each was optimized with a constrained protein backbone *in vacuo* using the CHARMM22 force field in MOE [47, 48].

Similarly, the **HH**Q**K** region was isolated in residues 9-20 of Aβ. Each terminal end was capped with an amide group before optimization (with a constrained protein backbone) in the gas phase. The energies observed for both the isolated **HH**Q**K** and LVFF regions of Aβ used in this chapter are summarized in Appendix 5.

The indole structure was built in MOE and optimized to obtain the following energies:

Table 5.1: The gas phase energies of an indole

	Energies (kcal/mol)		
	E_{tot}	E_{vdw}	E_{ele}
Indole	16.40	6.39	-0.15

5.1.2 THE GAS PHASE OPTIMIZATION OF AN INDOLE WITH HHQK AND LVFF

Gas phase systems were set up such that the indole ring could interact with two of the basic amino acids in **HH**Q**K** or two of the aliphatic/aromatic amino acids in LVFF. These orientations were set up such that the indole was situated approximately 3.0Å away from the two side chains. As indole is composed of a benzyl ring connected to a pyrrole ring, the systems were differentiated by denoting which ring was oriented towards the amino acids.

Each energy minimization was performed with the protein backbone constrained to prevent structural collapse, and the binding energies were calculated using the following equations:

$$\Delta E_{tot} = E_{tot} - E_{A\beta} - E_{Indole} \tag{5.1}$$

$$\Delta E_{vdw} = E_{vdw} - E_{vdwA\beta} - E_{vdwIndole} \tag{5.2}$$

$$\Delta E_{ele} = E_{ele} - E_{eleA\beta} - E_{eleIndole} \tag{5.3}$$

The total, van der Waals, and electrostatic energies of each of the optimized indole and Aβ segment were subtracted from the energies of the optimized systems to determine the relative strength of binding for each of the three energies.

5.1.3 THE RESULTS OF THE GAS PHASE OPTIMIZATIONS OF AN INDOLE AND THE HHQK AND LVFF REGIONS OF β-AMYLOID

The gas phase results of the minimization of the indole with each of the isolated **HH**Q**K** and LVFF segments of Aβ in six different conformations are summarized in the following two tables. The calculated energies are given for each system, along with the initial orientation the indole was arranged in and the final orientation upon optimization. The indole ring is represented by InB to represent the benzyl ring of the indole, InP to represent the pyrrole ring, and In is used for interactions occurring with both rings. The bonding interactions that formed are coloured accordingly: orange for hydrogen bonds, light blue for π-π interactions, and green for cation-π interactions. Darker shades of the colours indicate the presence of more of that type of interaction.

Table 5.2: The gas phase results of an indole interacting with the HHQK region of β-amyloid

Conformer	Initial Orientation				Final Orientation					ΔE_{tot}	ΔE_{vdv}	ΔE_{ele}
	H13	H14	Q15	K16	H13	H14	Q15	K16	Other	(kcal/mol)	(kcal/mol)	(kcal/mol)
1AMB	InB	InP			InB	InP			InB	-16.04	-6.53	-12.22
	InP	InB			InP	InB			In	-15.43	-8.68	-7.00
	InB			InP				InB	In	-14.40	-8.37	-6.46
	InP			InB				InB	In	-15.02	-8.37	-6.93
1AMC	InB	InP				InP				-10.99	-6.96	-4.33
	InP	InB			InP	InB			InP	-13.05	-7.93	-5.75
	InB			InP	InB				In	-12.98	-8.67	-4.46
	InP			InB					In	-13.48	-7.15	-6.39
1AML	InB	InP							In	-8.69	-4.08	-5.19
	InP	InB							InB	-9.61	-4.10	-5.91
	InB			InP	InB			InP		-8.46	-3.50	-6.22
	InP			InB				InB		-10.02	-4.50	-6.22
1BA4	InB	InP			InB	InP				-7.46	-4.90	-2.96
						InB				.		
	InP	InB			InP	InB				-8.26	-4.64	-4.07
						InP						
1IYT	InB	InP			InB	InP				-16.82	-5.35	-13.29
	InP	InB			InP	InB				-13.78	-7.37	-7.68
	InB			InP	InB			InP		-11.14	-5.47	-5.66
	InP			InB	InP			InB		-12.15	-5.39	-6.12
1Z0Q	InB	InP				InP				-14.82	-7.97	-8.21
	InP	InB			InP					-7.57	-5.75	-2.08
	InB			InP	InB			InP		-6.10	-3.40	-3.82
	InP			InB	In				InB	-13.29	-6.67	-7.57

Table 5.3: The gas phase results of an indole interacting with the LVFF region of β-amyloid

Conformer	Initial Orientation				Final Orientation					ΔE_{tot}	ΔE_{vdv}	ΔE_{ele}
	L17	V18	F19	F20	L17	V18	F19	F20	Other	(kcal/mol)	(kcal/mol)	(kcal/mol)
1AMB			InB	InP					InB	-5.26	-3.35	-2.62
			InP	InB				InB	In	-17.20	-6.49	-11.46
	InB			InP	InB			InP		-10.06	-4.21	-5.87
	InP			InB	InP			InB		-8.12	-3.00	-5.33
1AMC			InB	InP				InP	In	-18.23	-6.27	-12.91
			InP	InB			InP			-15.07	-5.67	-8.05
	InB			InP	InB			In		-8.06	-4.22	-3.64
	InP			InB	InP			InB		-8.22	-4.82	-2.70
1AML			InB	InP				InP	InB	-10.69	-4.31	-7.24
			InP	InB			InP	InB	InB	-11.16	-7.65	-4.23
	InB			InP	-	-	-	-	-	-4.41	-2.97	-1.12
	InP			InB	InP			InB		-4.25	-3.32	-0.90
1BA4	InB			InP	InB			InP		-14.27	-4.61	-6.23
	InP			InB	InP			InB		-8.35	-4.18	-4.25
1IYT			InB	InP			InB		InB	-5.54	-3.09	-2.51
			InP	InB			InP		InP	-9.88	-2.72	-6.90
	InB			InP	InB			InP		-5.71	-3.49	-2.63
	InP			InB	InP			InB		-7.40	-3.84	-3.81
1Z0Q			InB	InP				InP		-9.20	-5.23	-5.21
			InP	InB			InP	InB		-7.23	-3.70	-5.54
	InB		InP		InB		InP			-6.52	-3.27	-3.30
	InP		InB		In		InB	InB		-13.57	-8.54	-9.99
	InB			InP	InB			InP		-6.95	-5.17	-6.22
	InP			InB	InP			InB		-4.73	-4.24	-2.73

More measureable interactions form between the indole and the **HH**Q**K** region of β-amyloid compared to the LVFF region. Interactions in the **HH**Q**K** region favour binding at His13-His14 and His13-Lys16. In the LVFF region, binding at Leu17-Phe20 is favoured over any other possible orientations.

For both regions, the electrostatic energies and van der Waals energies are comparable; the **HH**Q**K** total binding energies are slightly more favourable than those of LVFF (although there are a few that are on par).

5.1.4 THE SOLUTION PHASE OPTIMIZATION OF AN INDOLE WITH HHQK AND LVFF

Each of the systems resulting from the gas phase minimizations of an indole with the **HH**Q**K** and LVFF regions of Aβ was subjected to solution phase optimizations to determine whether binding would still occur in an aqueous environment.

A box of explicit water molecules was placed on each peptide-indole system, with periodic boundary conditions in place. The systems were optimized without constrained protein backbones. The energies for each interaction were calculated in the absence of solvent, and with a constrained protein backbone using equations 5.1-5.3. The energies of the solution phase optimized protein segments are listed in Appendix 5 and the indole is given in Table 5.4.

Table 5.4: The solution phase energies of an indole

	Energies (kcal/mol)		
	E_{tot}	E_{vdw}	E_{ele}
Indole	17.23	6.62	-0.17

5.1.5 THE RESULTS OF THE SOLUTION PHASE OPTIMIZATIONS OF AN INDOLE AND THE HHQK AND LVFF REGIONS OF β-AMYLOID

The results of the minimization of an indole with the **HH**Q**K** and LVFF regions of β-amyloid in a solution phase environment are summarized in the following table according to Aβ conformer. Each table lists the interactions in the **HH**Q**K** region on the left-hand side, and the LVFF region on the right-hand side; initial and final orientations are given. The amino acid side chains are given in their three letter abbreviations, and the indole interactions can be represented one of three ways: interactions with both rings are represented by In, those with the benzyl ring by InB, and those with the pyrrole by InP.

Coloured cells are used to indicate binding interactions: hydrogen bonds, cation-π and π-π interactions are in orange, green and light blue. Darker shaded cells indicate a greater number of bonds formed. Indigo cells represent interactions occurring with the –CH_2- chain of the amino acid. Interactions with the protein backbone are signified by purple (C=O), and lime green (-CH-).

Table 5.5: The solution phase results of an indole interacting with HHQK and LVFF on the 1AMB conformer of β-amyloid

	Tyr10	His13	His14	Gln15	Lys16	Leu17	Phe20	Lys16	Leu17	Val18	Phe19	Phe20
Initial Orientation	InB	InB	InP						InB			InP
Final Orientation	InB	InB			In				InB			InP
Total =	89.81 kcal/mol							279.72 kcal/mol				
van der Waals =	41.17 kcal/mol							40.96 kcal/mol				
Electrostatic =	-42.30 kcal/mol							4.66 kcal/mol				
ΔE_{tot} =	-3.81 kcal/mol							146.06 kcal/mol				
ΔE_{vdw} =	-6.73 kcal/mol							6.64 kcal/mol				
ΔE_{ele} =	-5.51 kcal/mol							-6.06 kcal/mol				
Initial Orientation					InB	InB	InP		InP			InB
Final Orientation		InB			InB	InB	InP					InB
							InB					
Total =	74.21 kcal/mol							118.17 kcal/mol				
van der Waals =	32.90 kcal/mol							24.49 kcal/mol				
Electrostatic =	-43.94 kcal/mol							7.32 kcal/mol				
ΔE_{tot} =	-19.40 kcal/mol							-15.50 kcal/mol				
ΔE_{vdw} =	-15.00 kcal/mol							-9.83 kcal/mol				
ΔE_{ele} =	-7.15 kcal/mol							-3.40 kcal/mol				
Initial Orientation	In	InP	InB					InB				
Final Orientation			InB					In				
Total =	83.11 kcal/mol							289.23 kcal/mol				
van der Waals =	43.87 kcal/mol							37.25 kcal/mol				
Electrostatic =	-44.67 kcal/mol							7.60 kcal/mol				
ΔE_{tot} =	-10.50 kcal/mol							155.57 kcal/mol				
ΔE_{vdw} =	-4.03 kcal/mol							2.94 kcal/mol				
ΔE_{ele} =	-7.88 kcal/mol							-3.11 kcal/mol				
Initial Orientation					InB	InB	InB	In				InB
Final Orientation					InB	InB	InB	In			InB	
Total =	83.41 kcal/mol							120.80 kcal/mol				
van der Waals =	39.43 kcal/mol							26.00 kcal/mol				
Electrostatic =	-36.79 kcal/mol							2.70 kcal/mol				
ΔE_{tot} =	-10.20 kcal/mol							-12.87 kcal/mol				
ΔE_{vdw} =	-8.47 kcal/mol							-8.32 kcal/mol				
ΔE_{ele} =	-0.01 kcal/mol							-8.02 kcal/mol				

Table 5.6: The solution phase results of an indole interacting with HHQK and LVFF on the 1AMC conformer of β-amyloid

	His13	His14	Gln15	Lys16	Leu17	Val18	Phe20	Lys16	Leu17	Val18	Phe19	Phe20
Initial Orientation		InP						In				InP
Final Orientation		InP				In		In			InB	In
		InP										
		InB										
Total =	63.75 kcal/mol							112.37 kcal/mol				
van der Waals =	39.20 kcal/mol							24.99 kcal/mol				
Electrostatic =	-58.16 kcal/mol							4.28 kcal/mol				
ΔE_{tot} =	-11.93 kcal/mol							-9.24 kcal/mol				
ΔE_{vdw} =	-3.68 kcal/mol							-6.12 kcal/mol				
ΔE_{ele} =	-4.20 kcal/mol							-5.27 kcal/mol				
Initial Orientation	InP	InB			InP						InP	
Final Orientation		In				InB		InB			InB	InB
Total =	71.85 kcal/mol							118.76 kcal/mol				
van der Waals =	36.69 kcal/mol							27.09 kcal/mol				
Electrostatic =	-51.55 kcal/mol							15.85 kcal/mol				
ΔE_{tot} =	-3.83 kcal/mol							-2.84 kcal/mol				
ΔE_{vdw} =	-6.19 kcal/mol							-4.02 kcal/mol				
ΔE_{ele} =	2.41 kcal/mol							6.30 kcal/mol				
Initial Orientation	InB				In		InP		InB			In
Final Orientation	InB			InB	In		InP		InB			In
Total =	81.34 kcal/mol							115.47 kcal/mol				
van der Waals =	35.66 kcal/mol							28.13 kcal/mol				
Electrostatic =	-40.71 kcal/mol							1.25 kcal/mol				
ΔE_{tot} =	5.66 kcal/mol							-6.14 kcal/mol				
ΔE_{vdw} =	-7.22 kcal/mol							-2.98 kcal/mol				
ΔE_{ele} =	13.25 kcal/mol							-8.30 kcal/mol				
Initial Orientation					InP		InB		InP			InB
Final Orientation					InP		InB		InP			InP
												InB
Total =	91.09 kcal/mol							117.25 kcal/mol				
van der Waals =	38.12 kcal/mol							31.69 kcal/mol				
Electrostatic =	-46.31 kcal/mol							-5.22 kcal/mol				
ΔE_{tot} =	15.41 kcal/mol							-4.36 kcal/mol				
ΔE_{vdw} =	-4.76 kcal/mol							0.59 kcal/mol				
ΔE_{ele} =	7.66 kcal/mol							-14.78 kcal/mol				

Table 5.7: The solution phase results of an indole interacting with HHQK and LVFF on the 1AML conformer of β-amyloid

	His13	His14	Gln15	Lys16	Leu17		Leu17	Val18	Phe19	Phe20	Asp23
Initial Orientation					In					InP	InB
Final Orientation					In					InB	InB
Total =	122.09 kcal/mol						112.65 kcal/mol				
van der Waals =	40.08 kcal/mol						28.39 kcal/mol				
Electrostatic =	-2.15 kcal/mol						1.95 kcal/mol				
ΔE_{tot} =	-2.59 kcal/mol						-2.93 kcal/mol				
ΔE_{vdw} =	-8.96 kcal/mol						-5.44 kcal/mol				
ΔE_{ele} =	8.96 kcal/mol						1.46 kcal/mol				
Initial Orientation					InB				InP	InB	InB
Final Orientation					In				InB	InB	InB
Total =	103.47 kcal/mol						107.88 kcal/mol				
van der Waals =	43.63 kcal/mol						25.62 kcal/mol				
Electrostatic =	-18.85 kcal/mol						-2.34 kcal/mol				
ΔE_{tot} =	-21.21 kcal/mol						-10.70 kcal/mol				
ΔE_{vdw} =	-5.42 kcal/mol						-8.20 kcal/mol				
ΔE_{ele} =	-7.75 kcal/mol						-2.83 kcal/mol				
Initial Orientation	InB			InP			-	-	-	-	-
Final Orientation	InB			InP			-	-	-	-	-
Total =	124.13 kcal/mol						127.97 kcal/mol				
van der Waals =	43.70 kcal/mol						36.49 kcal/mol				
Electrostatic =	-6.82 kcal/mol						1.68 kcal/mol				
ΔE_{tot} =	-0.55 kcal/mol						12.40 kcal/mol				
ΔE_{vdw} =	-5.35 kcal/mol						2.67 kcal/mol				
ΔE_{ele} =	4.28 kcal/mol						1.19 kcal/mol				
Initial Orientation				InB			InP			InB	
Final Orientation				In						InB	
Total =	111.66 kcal/mol						118.23 kcal/mol				
van der Waals =	44.31 kcal/mol						32.62 kcal/mol				
Electrostatic =	-11.97 kcal/mol						8.60 kcal/mol				
ΔE_{tot} =	-13.02 kcal/mol						2.65 kcal/mol				
ΔE_{vdw} =	-4.73 kcal/mol						-1.20 kcal/mol				
ΔE_{ele} =	-0.86 kcal/mol						8.11 kcal/mol				

Table 5.8: The solution phase results of an indole interacting with HHQK and LVFF on the 1BA4 conformer of β-amyloid

	His13	His14	Gln15	Lys16		Leu17	Val18	Phe19	Phe20
Initial Orientation	InB	InP				InB			InP
		InB							
Final Orientation	InB	InB				In			InP
		In							
Total =	116.49 kcal/mol					89.01 kcal/mol			
van der Waals =	46.49 kcal/mol					26.12 kcal/mol			
Electrostatic =	-33.39 kcal/mol					-19.18 kcal/mol			
ΔE_{tot} =	1.98 kcal/mol					-32.59 kcal/mol			
ΔE_{vdw} =	2.50 kcal/mol					-12.71 kcal/mol			
ΔE_{ele} =	-13.06 kcal/mol					-8.45 kcal/mol			
Initial Orientation	InP	InB				InP			InB
		InP							
Final Orientation		In				InP			In
Total =	112.21 kcal/mol					107.25 kcal/mol			
van der Waals =	48.46 kcal/mol					33.35 kcal/mol			
Electrostatic =	-27.81 kcal/mol					-10.16 kcal/mol			
ΔE_{tot} =	-2.30 kcal/mol					-14.35 kcal/mol			
ΔE_{vdw} =	4.47 kcal/mol					-5.49 kcal/mol			
ΔE_{ele} =	-7.48 kcal/mol					0.57 kcal/mol			

Table 5.9: The solution phase results of an indole interacting with HHQK and LVFF on the 1IYT conformer of β-amyloid

	Gly9	Tyr10	His13	His14	Gln15	Lys16	Leu17	Lys16	Leu17	Val18	Phe19	Phe20	Asp23
Initial Orientation			InB	InP							InP		InP
Final Orientation	InP	InP	InB	InP							InP		In
			InB										
			InP										
Total =	84.81 kcal/mol							108.02 kcal/mol					
van der Waals =	39.37 kcal/mol							31.58 kcal/mol					
Electrostatic =	-37.89 kcal/mol							-4.49 kcal/mol					
ΔE_{tot} =	-21.21 kcal/mol							-6.75 kcal/mol					
ΔE_{vdw} =	-14.38 kcal/mol							-5.89 kcal/mol					
ΔE_{ele} =	-7.01 kcal/mol							0.54 kcal/mol					
Initial Orientation			InP	InB							InB		InB
Final Orientation		InB	InP				InB	InP			InB		InB
			InP										
			InB										
Total =	77.39 kcal/mol							112.19 kcal/mol					
van der Waals =	40.25 kcal/mol							32.54 kcal/mol					
Electrostatic =	-43.76 kcal/mol							4.80 kcal/mol					
ΔE_{tot} =	-28.63 kcal/mol							-2.58 kcal/mol					
ΔE_{vdw} =	-13.49 kcal/mol							-4.93 kcal/mol					
ΔE_{ele} =	-12.87 kcal/mol							9.83 kcal/mol					
Initial Orientation			InB			InP			InB			InP	
Final Orientation			InB			InP			InB			InP	
						InB							
Total =	80.49 kcal/mol							114.07 kcal/mol					
van der Waals =	42.85 kcal/mol							30.47 kcal/mol					
Electrostatic =	-34.62 kcal/mol							0.69 kcal/mol					
ΔE_{tot} =	-27.10 kcal/mol							-0.70 kcal/mol					
ΔE_{vdw} =	-13.12 kcal/mol							-7.00 kcal/mol					
ΔE_{ele} =	-3.16 kcal/mol							5.72 kcal/mol					
Initial Orientation			InP			InB			InP			InB	
Final Orientation			InP			InB			InP			InB	
			InB										
Total =	89.39 kcal/mol							121.98 kcal/mol					
van der Waals =	41.66 kcal/mol							36.15 kcal/mol					
Electrostatic =	-34.68 kcal/mol							-2.21 kcal/mol					
ΔE_{tot} =	-16.63 kcal/mol							7.22 kcal/mol					
ΔE_{vdw} =	-12.08 kcal/mol							-1.33 kcal/mol					
ΔE_{ele} =	-3.80 kcal/mol							2.81 kcal/mol					

Table 5.10: The solution phase results of an indole interacting with HHQK and LVFF on the 1Z0Q conformer of β-amyloid

	Gly9	Tyr10	Val12	His13	His14	Gln15	Lys16	Lys16	Leu17	Val18	Phe19	Phe20
Initial Orientation					InP							InP
Final Orientation	InB	In		InB	InP						InB	
											InP	
Total =	96.19 kcal/mol							139.91 kcal/mol				
van der Waals =	36.22 kcal/mol							32.67 kcal/mol				
Electrostatic =	-36.60 kcal/mol							5.52 kcal/mol				
ΔE_{tot} =	-15.91 kcal/mol							-5.32 kcal/mol				
ΔE_{vdw} =	-10.19 kcal/mol							-3.21 kcal/mol				
ΔE_{ele} =	-6.62 kcal/mol							-11.56 kcal/mol				
Initial Orientation				InP							InP	InB
Final Orientation	InB	InB		InB	InB						InP	In
Total =	99.64 kcal/mol							153.18 kcal/mol				
van der Waals =	48.75 kcal/mol							35.46 kcal/mol				
Electrostatic =	-28.34 kcal/mol							27.08 kcal/mol				
ΔE_{tot} =	-12.45 kcal/mol							7.95 kcal/mol				
ΔE_{vdw} =	2.33 kcal/mol							-0.42 kcal/mol				
ΔE_{ele} =	1.63 kcal/mol							10.00 kcal/mol				
Initial Orientation				InB			InP		InB			InP
Final Orientation				InB					In			InP
Total =	108.49 kcal/mol							142.57 kcal/mol				
van der Waals =	36.56 kcal/mol							29.49 kcal/mol				
Electrostatic =	-19.13 kcal/mol							21.38 kcal/mol				
ΔE_{tot} =	-3.60 kcal/mol							-2.66 kcal/mol				
ΔE_{vdw} =	-9.86 kcal/mol							-6.39 kcal/mol				
ΔE_{ele} =	10.84 kcal/mol							4.30 kcal/mol				
Initial Orientation			InB	In					InP			InB
Final Orientation			In	In					In			InB
Total =	108.08 kcal/mol							142.26 kcal/mol				
van der Waals =	40.88 kcal/mol							34.78 kcal/mol				
Electrostatic =	-16.52 kcal/mol							15.58 kcal/mol				
ΔE_{tot} =	-4.02 kcal/mol							-2.98 kcal/mol				
ΔE_{vdw} =	-5.54 kcal/mol							-1.10 kcal/mol				
ΔE_{ele} =	13.45 kcal/mol							-1.50 kcal/mol				
Initial Orientation									InB		InP	
Final Orientation									InB		In	
Total =								137.51 kcal/mol				
van der Waals =								35.69 kcal/mol				
Electrostatic =								21.67 kcal/mol				
ΔE_{tot} =								-7.73 kcal/mol				
ΔE_{vdw} =								-0.19 kcal/mol				
ΔE_{ele} =								4.59 kcal/mol				
Initial Orientation									In		InB	InB
Final Orientation								InB	In			InB
Total =								138.01 kcal/mol				
van der Waals =								35.77 kcal/mol				
Electrostatic =								7.02 kcal/mol				
ΔE_{tot} =								-7.23 kcal/mol				
ΔE_{vdw} =								-0.11 kcal/mol				
ΔE_{ele} =								-10.06 kcal/mol				

The results of the solution phase optimizations of an indole interacting with the **HH**Q**K** and LVFF region of Aβ show a capacity to bind to both regions. The indole favours binding at His13-Lys16 and His13-His14 in the **HH**Q**K** region, while Leu17-Phe20, and Phe19-Phe20 are the favoured sites for multiple interactions in LVFF.

The binding energies are somewhat variable, with binding at **HH**Q**K** being perhaps slightly more favourable than at LVFF. In general, the van der Waals energy contributions were more significant than those of the electrostatic energy; this is expected as the interactions occurring are primarily between aromatic ring systems.

5.2 Interactions Between a Biindole and the HHQK and LVFF Regions of β-Amyloid

Given that a simple indole demonstrates a capacity to bind to both the BBXB and AAXA regions of β-amyloid with nearly equal strength, the question arises if a larger molecule will be able to act with the same efficacy. To this purpose, an unsubstituted biindole molecule (Figure 5.2) was constructed to determine how well it could bind to the **HH**Q**K** and LVFF areas of interest.

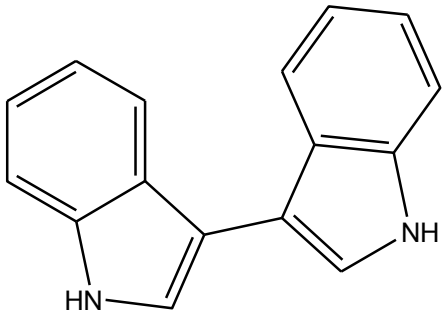

Figure 5.2: Biindole

The biindole molecule was constructed and subjected to a conformational search, with the resulting lowest energy conformation selected for use. The same isolated **HH**Q**K** and LVFF regions of β-amyloid were used as for the single indole calculations, and the energies are given in Appendix 5. The optimized energies of the biindole are given in Table 5.11.

Table 5.11: The gas phase energies of a biindole

	Energies (kcal/mol)		
	E_{tot}	E_{vdw}	E_{ele}
Biindole	21.52	11.65	0.47

5.2.1 THE GAS PHASE OPTIMIZATION OF A BIINDOLE WITH HHQK AND LVFF

Gas phase minimizations were performed to determine if the biindole could interact with both the **HH**Q**K** and LVFF regions of β-amyloid with the same efficacy. Systems were set up such that each of the indole groups was situated ~3.0 Å away from the basic amino acids in **HH**Q**K** or ~3.0 Å away from the aliphatic or aromatic groups in LVFF. Where feasible, orientations were attempted with the indole in two possible positions: the benzyl groups oriented towards the side chains, or the pyrrole groups oriented towards the side chains.

Energy minimizations were performed with constrained protein backbones to prevent structural collapse. The following equations were used:

$$\Delta E_{tot} = E_{tot} - E_{A\beta} - E_{Biindole} \quad (5.4)$$

$$\Delta E_{vdw} = E_{vdw} - E_{vdwA\beta} - E_{vdwBiindole} \quad (5.5)$$

$$\Delta E_{ele} = E_{ele} - E_{eleA\beta} - E_{eleBiindole} \quad (5.6)$$

The binding energies were calculated by subtracting the total, van der Waals and electrostatic energies of each of the optimized biindole and Aβ segment from the energies of the optimized systems.

5.2.2 THE RESULTS OF THE GAS PHASE OPTIMIZATIONS OF A BIINDOLE AND THE HHQK AND LVFF REGIONS OF β-AMYLOID

The results of the gas phase minimization of the biindole with the isolated **HH**Q**K** and LVFF segments of Aβ are summarized in the Tables 5.12-5.13. The indole rings of the biindole are represented by InB and InP for the benzyl ring and the pyrrole ring; interactions occurring with both rings and the amino acid are represented by In. Binding with the two different indole rings at the same amino acid residue are separated by a "/". Calculated energies are given for each system, and bonds are indicated by pink for π-H, and blue for π-π. The darker shades indicate the presence of more bonds. Indigo is used to denote interactions with the $–CH_2$- chain of the amino acid. The initial orientation of the two indoles is given, along with the final orientation upon optimization, and the amino acids are represented by single letters with their position on the protein.

Table 5.12: The gas phase results of a biindole interacting with the HHQK region of β-amyloid

Conformer	Initial Orientation				Final Orientation					ΔE_{tot}	ΔE_{vdv}	ΔE_{ele}
	H13	H14	Q15	K16	H13	H14	Q15	K16	Other	(kcal/mol)	(kcal/mol)	(kcal/mol)
1AMB	InB	InB			InB	In/InB			In/InP	-22.76	-12.67	-11.14
	InB			InB	InB			InB	InB	-14.28	-6.67	-7.84
1AMC	InB	InB				InB			In*/InB	-15.53	-7.55	-8.65
	InB			InB				InB	InB*/In	-14.20	-7.71	-6.81
1AML	InB	InB			In	InB			InB	-13.75	-6.75	-10.01
	InP	InP			In	In			InB*/InP	-20.04	-9.53	-13.14
	InB			InB					InB	-9.30	-2.84	-6.81
1BA4	InB	InB			In					-7.89	-1.85	-6.20
	InP	InP			In/InP	In				-10.19	-3.84	-6.21
1IYT	InB	InB			In				InP	-13.02	-4.35	-9.74
	InP	InP			InP	InP				-10.44	-1.77	-8.67
	InB			InB	In			InB		-13.63	-4.75	-7.69
	InP			InP	In			InB	InB	-18.85	-9.76	-11.76
1Z0Q	InB	InB			InB			In		-13.38	-4.30	-9.43
	InP	InP			-	-	-	-	-	-10.59	-4.88	-7.29
	InB			InB				In		-12.43	-3.13	-9.54
	InP			InP	InP			In		-10.60	-2.69	-9.26

*indicates which indole the bond is occurring with

Table 5.13: The gas phase results of a biindole interacting with the LVFF region of β-amyloid

Conformer	Initial Orientation				Final Orientation					ΔE_{tot}	ΔE_{vdv}	ΔE_{ele}
	L17	V18	F19	F20	L17	V18	F19	F20	Other	(kcal/mol)	(kcal/mol)	(kcal/mol)
1AMB	InB	InB			InB	In			InP	-10.81	-5.65	-6.25
	InP	InP			In/InB*	In			InP	-21.96	-7.76	-10.43
		InB	InB				InB		InB	-15.81	-3.14	-8.62
		InP	InP		-	-	-	-	-	-9.64	-2.96	-9.52
			InB	InB			InB	InB	In/InB	-18.76	-7.46	-12.10
			InP	InP			InB		In/InP	-17.66	-5.08	-13.95
	InB			InB	InB			InB		-5.80	-3.01	-2.79
	InP			InP	InP					-11.61	-1.17	-11.10
1AMC	InB	InB			-	-	-	-	-	-6.17	-1.27	-5.13
	InP	InP			In					-8.39	-2.59	-8.88
		InB	InB				InB			-6.45	-1.63	-4.74
		InP	InP		-	-	-	-	-	-7.63	-3.08	-4.59
			InB	InB			InB	InB		-15.02	-5.61	-9.42
			InP	InP			InB*/InP	InP	In/InP	-24.11	-13.51	-12.90
	InB			InB	InB					-6.48	-2.36	-6.32
	InP			InP	InP			InP		-7.71	-2.70	-5.37
1AML	InB	InB			-	-	-	-	-	-8.18	-2.54	-6.67
	InP	InP				InP			InP	-14.05	-8.33	-9.08
		InB	InB			InB	InB		InB	-24.43	-4.39	-24.83
		InP	InP						In/InP	-18.99	-2.32	-20.70
			InB	InB				InB	InB	-12.73	-1.07	-14.91
			InP	InP			In		InP	-27.51	-2.78	-29.87
	InB			InB				InP*/InB		-8.45	-5.12	-3.58
	InP			InP	-	-	-	-	-	-3.58	-1.47	-1.84
		InB		InB				InB	InB	-7.72	-3.79	-4.44
1BA4	InB			InB				InB		-4.59	-1.65	-3.27
	InP			InP	InB*/InP			In	InB	-21.00	-10.70	-15.77
	InB	InB			InB					-12.12	-2.34	-8.10
	InP	InP				InP				-13.26	-2.19	-8.21
		InB	InB			InB			In/InB	-10.08	-5.19	-6.26
		InP	InP			InP	InP		In/InP	-8.31	-7.22	-2.17
1IYT	InB	InB				InB				-6.30	-1.85	-7.49
	InP	InP			-	-	-	-	-	-7.86	-1.76	-7.70
		InB	InB			InB			InB	-9.54	-4.30	-7.62
		InP	InP			InP			InB/InP	-14.34	-6.61	-9.82
			InB	InB			InB		InB	-10.79	-4.02	-8.38
			InP	InP			InP	In	In/InP	-13.25	-6.55	-6.22
	InB			InB				InB		-5.19	-1.55	-3.40
	InP			InP	-	-	-	-	-	-5.67	-0.86	-4.25
1Z0Q	InB	InB			InB	InB			InB	-12.01	-5.33	-9.85
	InP	InP			InP	In			In/InP	-16.91	-5.76	-14.01
	InB		InB		InB		InB			-4.55	-1.43	-4.46
	InP		InP		InP		InP		InB	-9.43	-3.83	-7.02
			InB	InB			InB			-4.94	-1.28	-4.55
			InP	InP			InP	InP		-6.45	-2.43	-5.22
	InB			InB	InB			InB		-4.91	-2.84	-1.97
	InP			InP	InP			InP		-7.63	-3.50	-3.94

*indicates which indole the bond is occurring with

For the minimization of the biindole with the **HHQK** region of Aβ, there were fewer orientations available where the molecule could interact with two of the charged amino acids. The results of the optimizations indicate binding interactions can occur at

multiple sites in the region, preferring His13-His14 and His13-Lys16. Binding also occurred at multiple sites within LVFF, favouring Phe19-Phe20, Leu17-Phe20 and Leu17-Val18. For both Aβ regions, the electrostatic energies were more favourable than the van der Waals energies.

5.2.3 THE SOLUTION PHASE OPTIMIZATION OF A BIINDOLE WITH HHQK AND LVFF

Solution phase optimizations were performed for each of the systems resulting from the gas phase minimizations of the biindole with the **HH**Q**K** and LVFF regions of Aβ. The results of these calculations will demonstrate whether the biindole is still capable of forming binding interactions when water molecules are present.

Explicit solvation was used for these minimizations. A box of water molecules of sufficient size to surround each protein-indole system was put into place, along with periodic boundary conditions. Systems were optimized without constrained protein backbones; however, the energies for each interaction were calculated with a constrained protein backbone in the absence of water and using equations 5.4-5.6. Appendix 5 contains the energies of the solution phase optimized Aβ segments, and the energy of the optimized biindole is given in Table 5.14.

Table 5.14: The solution phase energies of a biindole

	Energies (kcal/mol)		
	E_{tot}	E_{vdw}	E_{ele}
Biindole	26.11	12.73	0.96

5.2.4 THE RESULTS OF THE SOLUTION PHASE OPTIMIZATIONS OF A BIINDOLE AND THE HHQK AND LVFF REGIONS OF β-AMYLOID

The solution phase results are summarized in the following tables according to the region of β-amyloid. The initial and final orientations of the biindole are given, with each of the two indoles arbitrarily assigned as 1 or 2 to distinguish between them. The measured energies and the calculated binding energies are given, and bonds are indicated according to colour; blue for π-π, pink for π-H, and green for cation-π. Interactions with the backbone of the protein are purple for C=O interactions. The indigo coloured cells indicate that the $–CH_2$- chain of the amino acid is involved in the binding.

Table 5.15: The solution phase results of a biindole interacting with the HHQK region on the 1AMB conformer of β-amyloid

	Tyr10	His13	His14	Gln15	Lys16	Val18	Phe20
Initial Orientation	In^2/InP^1	InB^2	In^1/InB^2				
Final Orientation	InP^1/InP^2	InB^2	In^1/InB^2			InB^1	
	InB^2						
Total =	72.50 kcal/mol						
van der Waals =	25.06 kcal/mol						
Electrostatic =	-50.28 kcal/mol						
ΔE_{tot} =	-29.99 kcal/mol						
ΔE_{vdw} =	-28.95 kcal/mol						
ΔE_{ele} =	-14.61 kcal/mol						
Initial Orientation		InB^2			InB^2		InB^1
Final Orientation		InB^2			InB^2		InB^1
Total =	80.75 kcal/mol						
van der Waals =	43.38 kcal/mol						
Electrostatic =	-47.63 kcal/mol						
ΔE_{tot} =	-21.74 kcal/mol						
ΔE_{vdw} =	-10.63 kcal/mol						
ΔE_{ele} =	-11.97 kcal/mol						

Table 5.16: The solution phase results of a biindole interacting with the HHQK region on the 1AMC conformer of β-amyloid

	Tyr10	Glu11	His13	His14	Gln15	Lys16	Leu17	Phe20
Initial Orientation	In	InB^1		InB^1				
	InB^2							
Final Orientation	In	InB^1		InB^1				
	InB^2							
Total =	77.80 kcal/mol							
van der Waals =	39.47 kcal/mol							
Electrostatic =	-48.43 kcal/mol							
ΔE_{tot} =	-6.77 kcal/mol							
ΔE_{vdw} =	-9.52 kcal/mol							
ΔE_{ele} =	4.41 kcal/mol							
Initial Orientation						InB^2	InB^1	InB^1
								In^2
Final Orientation						InB^2	InB^1	In^2
								In^1
Total =	83.01 kcal/mol							
van der Waals =	41.91 kcal/mol							
Electrostatic =	-48.33 kcal/mol							
ΔE_{tot} =	-1.56 kcal/mol							
ΔE_{vdw} =	-7.08 kcal/mol							
ΔE_{ele} =	4.51 kcal/mol							

Table 5.17: The solution phase results of a biindole interacting with the HHQK region on the 1AML conformer of β-amyloid

	Tyr10	Val12	His13	His14	Gln15	Lys16	Leu17
Initial Orientation	InB^1		In^1	InB^2			
Final Orientation	InB^1		InP^1	InB^2			InB^2
			InB^1				
Total =	121.69 kcal/mol						
van der Waals =	45.97 kcal/mol						
Electrostatic =	-13.47 kcal/mol						
ΔE_{tot} =	-11.87 kcal/mol						
ΔE_{vdw} =	-9.19 kcal/mol						
ΔE_{ele} =	-3.50 kcal/mol						
Initial Orientation		InB^1					
Final Orientation		InB^1					
Total =	122.16 kcal/mol						
van der Waals =	48.90 kcal/mol						
Electrostatic =	-2.44 kcal/mol						
ΔE_{tot} =	-11.40 kcal/mol						
ΔE_{vdw} =	-6.25 kcal/mol						
ΔE_{ele} =	7.53 kcal/mol						
Initial Orientation	InP^2		In^1	In^2			InP^1
							InB^1
Final Orientation	InP^2		InP^1	In^2			InP^1
			InP^2/InB^1				InB^1
Total =	110.71 kcal/mol						
van der Waals =	40.94 kcal/mol						
Electrostatic =	-12.01 kcal/mol						
ΔE_{tot} =	-22.85 kcal/mol						
ΔE_{vdw} =	-14.21 kcal/mol						
ΔE_{ele} =	-2.03 kcal/mol						

Table 5.18: The solution phase results of a biindole interacting with the HHQK region on the 1BA4 conformer of β-amyloid

	His13	His14	Gln15	Lys16
Initial Orientation	In^1			
Final Orientation	In^1			
Total =	100.97 kcal/mol			
van der Waals =	39.79 kcal/mol			
Electrostatic =	-32.55 kcal/mol			
ΔE_{tot} =	-22.43 kcal/mol			
ΔE_{vdw} =	-10.31 kcal/mol			
ΔE_{ele} =	-13.35 kcal/mol			
Initial Orientation	In^1/InP^2	In^2		
Final Orientation	In^1	In^2		
Total =	100.76 kcal/mol			
van der Waals =	40.43 kcal/mol			
Electrostatic =	-36.37 kcal/mol			
ΔE_{tot} =	-22.63 kcal/mol			
ΔE_{vdw} =	-9.68 kcal/mol			
ΔE_{ele} =	-17.17 kcal/mol			

Table 5.19: The solution phase results of a biindole interacting with the HHQK region on the 1IYT conformer of β-amyloid

	Val12	His13	His14	Gln15	Lys16	Leu17
Initial Orientation		In^1				InP^1
Final Orientation		In^1	InB^2			InP^1
Total =	96.72 kcal/mol					
van der Waals =	52.85 kcal/mol					
Electrostatic =	-37.09 kcal/mol					
ΔE_{tot} =	-18.18 kcal/mol					
ΔE_{vdw} =	-7.00 kcal/mol					
ΔE_{ele} =	-7.33 kcal/mol					
Initial Orientation		InP^1	InP^2			
Final Orientation		InP^1	InP^2			
Total =	88.05 kcal/mol					
van der Waals =	49.22 kcal/mol					
Electrostatic =	-45.32 kcal/mol					
ΔE_{tot} =	-26.86 kcal/mol					
ΔE_{vdw} =	-10.63 kcal/mol					
ΔE_{ele} =	-15.56 kcal/mol					
Initial Orientation		In^1			InB^2	
Final Orientation		InB^1			InB^2	
Total =	93.00 kcal/mol					
van der Waals =	45.16 kcal/mol					
Electrostatic =	-31.29 kcal/mol					
ΔE_{tot} =	-21.91 kcal/mol					
ΔE_{vdw} =	-14.69 kcal/mol					
ΔE_{ele} =	-1.53 kcal/mol					
Initial Orientation	InB^2	In^2			In^1	
Final Orientation	InB^2	InP^2			InB^1	
		InB^2			InP^1	
Total =	80.75 kcal/mol					
van der Waals =	38.81 kcal/mol					
Electrostatic =	-40.28 kcal/mol					
ΔE_{tot} =	-34.16 kcal/mol					
ΔE_{vdw} =	-21.04 kcal/mol					
ΔE_{ele} =	-10.52 kcal/mol					

Table 5.20: The solution phase results of a biindole interacting with the HHQK region on the 1Z0Q conformer of β-amyloid

	His13	His14	Gln15	Lys16
Initial Orientation	InB[1]			In[1]
Final Orientation	InB[1]			In[1]
	InP[1]			
Total =	110.51 kcal/mol			
van der Waals =	44.22 kcal/mol			
Electrostatic =	-25.25 kcal/mol			
ΔE_{tot} =	-10.47 kcal/mol			
ΔE_{vdw} =	-8.30 kcal/mol			
ΔE_{ele} =	3.60 kcal/mol			
Initial Orientation	-	-	-	-
Final Orientation	InP[1]	InP[1]		
Total =	109.05 kcal/mol			
van der Waals =	52.50 kcal/mol			
Electrostatic =	-29.73 kcal/mol			
ΔE_{tot} =	-11.92 kcal/mol			
ΔE_{vdw} =	-0.03 kcal/mol			
ΔE_{ele} =	-0.88 kcal/mol			
Initial Orientation				In[1]
Final Orientation				InB[1]
Total =	107.84 kcal/mol			
van der Waals =	48.70 kcal/mol			
Electrostatic =	-34.63 kcal/mol			
ΔE_{tot} =	-13.14 kcal/mol			
ΔE_{vdw} =	-3.82 kcal/mol			
ΔE_{ele} =	-5.78 kcal/mol			
Initial Orientation	InP[1]			In[2]
Final Orientation	InP[1]			In[2]
Total =	97.31 kcal/mol			
van der Waals =	44.31 kcal/mol			
Electrostatic =	-39.60 kcal/mol			
ΔE_{tot} =	-23.67 kcal/mol			
ΔE_{vdw} =	-8.22 kcal/mol			
ΔE_{ele} =	-10.75 kcal/mol			

Table 5.21: The solution phase results of a biindole interacting with the LVFF region on the 1AMB conformer of β-amyloid

	Lys16	Leu17	Val18	Phe19	Phe20	Asp23	Val24	His14	Leu17	Val18	Phe19	Phe20	Ala21	Glu22
Initial Orientation				InB^1	InB^2	In^2	InB^2	InP^2	InB^1	In^2				
Final Orientation				InB^1	InB^2	In^2/InP^1		In^2	InB^1	In^2				
Total =	109.02 kcal/mol							110.34 kcal/mol						
van der Waals =	27.59 kcal/mol							32.25 kcal/mol						
Electrostatic =	4.78 kcal/mol							-1.21 kcal/mol						
ΔE_{tot} =	-33.53 kcal/mol							-32.21 kcal/mol						
ΔE_{vdw} =	-12.84 kcal/mol							-8.18 kcal/mol						
ΔE_{ele} =	-16.20 kcal/mol							-13.05 kcal/mol						
Initial Orientation	In^2/InP^1			In^1					InB^1	In^2			InP^2/InP^1	
									InP^1/In^2					
Final Orientation	InB^2/InP^1			In^1					InP^1/In^2	In^2			InP^2/InP^1	
	InP^2								InB^1					
Total =	108.71 kcal/mol							118.19 kcal/mol						
van der Waals =	33.16 kcal/mol							28.27 kcal/mol						
Electrostatic =	-7.12 kcal/mol							7.93 kcal/mol						
ΔE_{tot} =	-33.84 kcal/mol							-24.36 kcal/mol						
ΔE_{vdw} =	-7.27 kcal/mol							-12.16 kcal/mol						
ΔE_{ele} =	-18.96 kcal/mol							-3.91 kcal/mol						
Initial Orientation	-	-	-	-	-	-	-		InB^1			InB^2		
Final Orientation	-	-	-	-	-	-	-		InB^1			InB^2		
Total =	120.72 kcal/mol							131.51 kcal/mol						
van der Waals =	31.64 kcal/mol							36.94 kcal/mol						
Electrostatic =	9.05 kcal/mol							9.10 kcal/mol						
ΔE_{tot} =	-21.83 kcal/mol							-11.04 kcal/mol						
ΔE_{vdw} =	-8.79 kcal/mol							-3.49 kcal/mol						
ΔE_{ele} =	-2.79 kcal/mol							-2.74 kcal/mol						
Initial Orientation		InP^1									InB^1			InB^2
Final Orientation		InP^1									InB^1			InB^2
Total =	118.18 kcal/mol							118.11 kcal/mol						
van der Waals =	36.49 kcal/mol							34.44 kcal/mol						
Electrostatic =	2.52 kcal/mol							2.04 kcal/mol						
ΔE_{tot} =	-24.38 kcal/mol							-24.45 kcal/mol						
ΔE_{vdw} =	-3.94 kcal/mol							-5.99 kcal/mol						
ΔE_{ele} =	-9.32 kcal/mol							-9.80 kcal/mol						

Table 5.22: The solution phase results of a biindole interacting with the LVFF region on the 1AMC conformer of β-amyloid

	Lys16	Leu17	Val18	Phe19	Phe20	Asp23	Leu17	Val18	Phe19	Phe20
Initial Orientation				InB^2	InB^1		InP^2			InP^1
Final Orientation					InB^1		InP^2			In^1
Total =	117.95 kcal/mol						122.44 kcal/mol			
van der Waals =	29.72 kcal/mol						30.51 kcal/mol			
Electrostatic =	-1.08 kcal/mol						9.60 kcal/mol			
ΔE_{tot} =	-12.54 kcal/mol						-8.05 kcal/mol			
ΔE_{vdw} =	-7.50 kcal/mol						-6.71 kcal/mol			
ΔE_{ele} =	-11.75 kcal/mol						-1.07 kcal/mol			
Initial Orientation	InP^2/InP^1			InB^1 InP^2/InP^1	InP^2	InB^2	In^1			
Final Orientation	In^2			InB^1 In^2/InP^1	In^2	InB^2	In^1			
Total =	103.49 kcal/mol						131.43 kcal/mol			
van der Waals =	24.24 kcal/mol						36.70 kcal/mol			
Electrostatic =	-6.97 kcal/mol						12.25 kcal/mol			
ΔE_{tot} =	-27.00 kcal/mol						0.94 kcal/mol			
ΔE_{vdw} =	-12.98 kcal/mol						-0.52 kcal/mol			
ΔE_{ele} =	-17.64 kcal/mol						1.57 kcal/mol			
Initial Orientation	-	-	-	-	-	-			InB^1	
Final Orientation	-	-	-	-	-	-			InB^1	
Total =	123.43 kcal/mol						111.68 kcal/mol			
van der Waals =	40.64 kcal/mol						33.88 kcal/mol			
Electrostatic =	-5.29 kcal/mol						-6.19 kcal/mol			
ΔE_{tot} =	-7.07 kcal/mol						-18.81 kcal/mol			
ΔE_{vdw} =	3.42 kcal/mol						-3.34 kcal/mol			
ΔE_{ele} =	-15.96 kcal/mol						-16.87 kcal/mol			
Initial Orientation		InP^1					-	-	-	-
Final Orientation		InP^1					-	-	-	-
Total =	136.20 kcal/mol						146.73 kcal/mol			
van der Waals =	39.13 kcal/mol						43.19 kcal/mol			
Electrostatic =	6.81 kcal/mol						12.55 kcal/mol			
ΔE_{tot} =	5.71 kcal/mol						16.24 kcal/mol			
ΔE_{vdw} =	1.91 kcal/mol						5.97 kcal/mol			
ΔE_{ele} =	-3.86 kcal/mol						1.87 kcal/mol			

Table 5.23: The solution phase results of a biindole interacting with the LVFF region on the 1AML conformer of β-amyloid

	Leu17	Val18	Phe19	Phe20	Ala21	Asp23	Gln15	Leu17	Val18	Phe19	Phe20	Glu22
Initial Orientation				InB^1		InB^2	-	-	-	-	-	-
Final Orientation				InB^1			-	-	-	-	-	-
Total =	118.91 kcal/mol						125.62 kcal/mol					
van der Waals =	34.43 kcal/mol						34.16 kcal/mol					
Electrostatic =	-1.12 kcal/mol						8.31 kcal/mol					
ΔE_{tot} =	-5.56 kcal/mol						1.16 kcal/mol					
ΔE_{vdw} =	-5.51 kcal/mol						-5.77 kcal/mol					
ΔE_{ele} =	-2.73 kcal/mol						6.70 kcal/mol					
Initial Orientation			In^1			InP^1/InP^2			InB^2	InB^1		InB^1/InB^2
Final Orientation			In^1			InP^1/InP^2	In^1		InB^2			InB^1/InB^2
Total =	90.80 kcal/mol						102.30 kcal/mol					
van der Waals =	34.19 kcal/mol						31.49 kcal/mol					
Electrostatic =	-16.31 kcal/mol						-9.31 kcal/mol					
ΔE_{tot} =	-33.66 kcal/mol						-22.16 kcal/mol					
ΔE_{vdw} =	-5.75 kcal/mol						-8.44 kcal/mol					
ΔE_{ele} =	-17.93 kcal/mol						-10.92 kcal/mol					
Initial Orientation		InP^1			InP^1						InP^1	
											InB^1/InB^2	
Final Orientation	InP^2	InP^1			InP^1				InB^1		InP^1	
	InP^1	InB^1									InB^1	
Total =	107.69 kcal/mol						125.30 kcal/mol					
van der Waals =	28.32 kcal/mol						35.67 kcal/mol					
Electrostatic =	-0.04 kcal/mol						11.15 kcal/mol					
ΔE_{tot} =	-16.78 kcal/mol						0.84 kcal/mol					
ΔE_{vdw} =	-11.62 kcal/mol						-4.27 kcal/mol					
ΔE_{ele} =	-1.65 kcal/mol						9.54 kcal/mol					
Initial Orientation				InB^2	InB^1		In^1					InP^1
Final Orientation				InB^2			In^1		InP^1			InP^1
Total =	118.36 kcal/mol						97.91 kcal/mol					
van der Waals =	36.92 kcal/mol						33.29 kcal/mol					
Electrostatic =	9.13 kcal/mol						-8.89 kcal/mol					
ΔE_{tot} =	-6.11 kcal/mol						-26.55 kcal/mol					
ΔE_{vdw} =	-3.01 kcal/mol						-6.64 kcal/mol					
ΔE_{ele} =	7.52 kcal/mol						-10.51 kcal/mol					
Initial Orientation	-	-	-	-	-	-						
Final Orientation	-	-	-	-	-	-						
Total =	134.03 kcal/mol											
van der Waals =	35.05 kcal/mol											
Electrostatic =	15.54 kcal/mol											
ΔE_{tot} =	9.57 kcal/mol											
ΔE_{vdw} =	-4.88 kcal/mol											
ΔE_{ele} =	13.93 kcal/mol											

Table 5.24: The solution phase results of a biindole interacting with the LVFF region on the 1BA4 conformer of β-amyloid

	Gln15	Leu17	Val18	Phe19	Phe20	Glu22		His13	His14	Lys16	Leu17	Val18	Phe19	Phe20
Initial Orientation					InB[1]			InB[1]	InB[1]	InB[1]	InB[1]			In[2]
											InP[1]			
Final Orientation					In[1]				In[1]	InB[1]	In[1]/InP[2]			In[2]
Total =	117.53 kcal/mol							99.57 kcal/mol						
van der Waals =	34.51 kcal/mol							30.67 kcal/mol						
Electrostatic =	-8.15 kcal/mol							-25.98 kcal/mol						
ΔE_{tot} =	-12.96 kcal/mol							-30.91 kcal/mol						
ΔE_{vdw} =	-10.44 kcal/mol							-14.28 kcal/mol						
ΔE_{ele} =	1.46 kcal/mol							-16.38 kcal/mol						
Initial Orientation	InB[1]		InB[1]			In[1]					InB[1]			
Final Orientation	InB[1]		InB[1]	InB[1]		In[1]					InB[1]	InB[1]		
Total =	114.48 kcal/mol							137.69 kcal/mol						
van der Waals =	35.45 kcal/mol							43.48 kcal/mol						
Electrostatic =	-13.64 kcal/mol							4.16 kcal/mol						
ΔE_{tot} =	-16.01 kcal/mol							7.20 kcal/mol						
ΔE_{vdw} =	-9.50 kcal/mol							-1.47 kcal/mol						
ΔE_{ele} =	-4.03 kcal/mol							13.76 kcal/mol						
Initial Orientation	InP[2]		InP[1]	InP[2]		In[1]/InP[2]						InP[1]		
Final Orientation	InP[2]		InP[1]	InP[2]		In[1]/InP[2]		-	-	-	-	-	-	-
Total =	113.28 kcal/mol							110.53 kcal/mol						
van der Waals =	30.46 kcal/mol							30.23 kcal/mol						
Electrostatic =	-5.52 kcal/mol							-8.61 kcal/mol						
ΔE_{tot} =	-17.21 kcal/mol							-19.95 kcal/mol						
ΔE_{vdw} =	-14.49 kcal/mol							-14.71 kcal/mol						
ΔE_{ele} =	4.09 kcal/mol							0.99 kcal/mol						

Table 5.25: The solution phase results of a biindole interacting with the LVFF region on the 1IYT conformer of β-amyloid

	Gln15	Leu17	Val18	Phe19	Phe20	Glu22	Lys16	Leu17	Val18	Phe19	Phe20	Asp23
Initial Orientation					InB^1		-	-	-	-	-	-
Final Orientation	-	-	-	-	-	-	-	-	-	-	-	-
Total =	127.86 kcal/mol						132.13 kcal/mol					
van der Waals =	37.39 kcal/mol						34.61 kcal/mol					
Electrostatic =	4.87 kcal/mol						3.63 kcal/mol					
ΔE_{tot} =	4.21 kcal/mol						8.48 kcal/mol					
ΔE_{vdw} =	-6.20 kcal/mol						-8.97 kcal/mol					
ΔE_{ele} =	8.77 kcal/mol						7.53 kcal/mol					
Initial Orientation			InB^1				-	-	-	-	-	-
Final Orientation			InB^1				-	-	-	-	-	-
Total =	123.05 kcal/mol						125.10 kcal/mol					
van der Waals =	30.70 kcal/mol						33.23 kcal/mol					
Electrostatic =	1.27 kcal/mol						8.22 kcal/mol					
ΔE_{tot} =	-0.61 kcal/mol						1.45 kcal/mol					
ΔE_{vdw} =	-12.89 kcal/mol						-10.35 kcal/mol					
ΔE_{ele} =	5.17 kcal/mol						12.18 kcal/mol					
Initial Orientation			InB^1			InB^1				InB^1		InB^1
Final Orientation			InB^1	InB^2		In^1				InB^1	InB^2	In^1
Total =	127.50 kcal/mol						126.14 kcal/mol					
van der Waals =	36.33 kcal/mol						30.47 kcal/mol					
Electrostatic =	9.38 kcal/mol						7.63 kcal/mol					
ΔE_{tot} =	3.85 kcal/mol						2.49 kcal/mol					
ΔE_{vdw} =	-7.25 kcal/mol						-13.12 kcal/mol					
ΔE_{ele} =	13.28 kcal/mol						11.53 kcal/mol					
Initial Orientation	InB^1		InP^2			InP^2	InP^1/In^2			InP^1	In^2	
Final Orientation	In^1		In^2	InP^1		InP^2	InB^1/InB^2				In^2	
				InB^1			InB^2					
Total =	106.12 kcal/mol						119.02 kcal/mol					
van der Waals =	33.76 kcal/mol						38.04 kcal/mol					
Electrostatic =	-7.19 kcal/mol						-2.22 kcal/mol					
ΔE_{tot} =	-17.53 kcal/mol						-4.64 kcal/mol					
ΔE_{vdw} =	-9.82 kcal/mol						-5.54 kcal/mol					
ΔE_{ele} =	-3.29 kcal/mol						1.68 kcal/mol					

Table 5.26: The solution phase results of a biindole interacting with the LVFF region on the 1Z0Q conformer of β-amyloid

	His14	Leu17	Val18	Phe19	Phe20	Ala21	Lys16	Leu17	Val18	Phe19	Phe20
Initial Orientation		InB[1]			InB[2]			InB[1]		InB[2]	
Final Orientation		InB[1]			InB[2]		InB[1]	InB[1]		InB[2]	
Total =	164.88 kcal/mol						158.50 kcal/mol				
van der Waals =	44.40 kcal/mol						39.29 kcal/mol				
Electrostatic =	32.71 kcal/mol						24.99 kcal/mol				
ΔE_{tot} =	10.76 kcal/mol						4.38 kcal/mol				
ΔE_{vdw} =	2.42 kcal/mol						-2.69 kcal/mol				
ΔE_{ele} =	14.50 kcal/mol						6.78 kcal/mol				
Initial Orientation	In[1]	InP[1]	In[1]			InP[1]		InP[1]			InP[1]/InP[2]
Final Orientation	In[1]		In[1]			InP[1]		InP[1]			In[2]
Total =	133.87 kcal/mol						155.35 kcal/mol				
van der Waals =	35.70 kcal/mol						45.44 kcal/mol				
Electrostatic =	6.19 kcal/mol						16.49 kcal/mol				
ΔE_{tot} =	-20.25 kcal/mol						1.23 kcal/mol				
ΔE_{vdw} =	-6.29 kcal/mol						3.45 kcal/mol				
ΔE_{ele} =	-12.01 kcal/mol						-1.72 kcal/mol				
Initial Orientation		InB[1]	InB[2]			InB[2]	InB[1]	InP[1]		InP[1]	
Final Orientation		InB[1]	InB[2]			InB[2]	InB[1]			InP[1]	
Total =	139.34 kcal/mol						154.99 kcal/mol				
van der Waals =	40.71 kcal/mol						42.82 kcal/mol				
Electrostatic =	17.10 kcal/mol						17.45 kcal/mol				
ΔE_{tot} =	-14.78 kcal/mol						0.87 kcal/mol				
ΔE_{vdw} =	-1.28 kcal/mol						0.83 kcal/mol				
ΔE_{ele} =	-1.10 kcal/mol						-0.75 kcal/mol				
Initial Orientation				InB[1]						InP[1]	InP[2]
Final Orientation				InB[1]						InP[1]	InP[2]
Total =	159.15 kcal/mol						136.43 kcal/mol				
van der Waals =	43.46 kcal/mol						39.39 kcal/mol				
Electrostatic =	33.37 kcal/mol						13.58 kcal/mol				
ΔE_{tot} =	5.03 kcal/mol						-17.69 kcal/mol				
ΔE_{vdw} =	1.47 kcal/mol						-2.60 kcal/mol				
ΔE_{ele} =	15.17 kcal/mol						-4.63 kcal/mol				

The solution phase results show that even when water molecules are present, the biindole is capable of binding to both the **HH**Q**K** and LVFF regions of β-amyloid. The biindole binds to **HH**Q**K** at His13-His14 and His13-Lys16. In the LVFF region, interactions are favoured almost equally at Leu17-Phe20, Leu17-Val18, Phe19-Phe20, and Val18-Phe19. For both regions the van der Waals energies tend to be more

favourable than the electrostatic energies when contributing to the overall binding of the system. Comparing the energies of binding at **HH**Q**K** and LVFF, interactions at LVFF tend to be lower, and thus more favourable.

5.3 Interactions Between a Bi-aromatic Molecule and the HH and FF Regions of β-Amyloid

To better compare the binding strength of aromatic molecules to the **HH**Q**K** and LVFF regions of Aβ, semi-empirical calculations were performed to measure the binding energies of a bi-aromatic molecule to His13-His14 (HH) and Phe19-Phe20 (FF). For these calculations, gas phase minimizations were performed to find the optimized interacting systems, and these optimized systems were then used for semi-empirical modelling.

5.3.1 Preparation of the Bi-aromatic Systems for Optimization

A simple bi-aromatic molecule, 1,2-diphenylethene (Figure 5.3), was constructed for optimization with the HH and FF regions of β-amyloid. This molecule was constructed to best interact with the geometric arrangements of HH and FF on six different Aβ conformers; the distance between His13 and His14, and Phe19 and Phe20 was measured for each conformer and averaged to suggest that a molecule capable of spanning 10-13 Å would be ideal. As a molecule with two aromatic species was desired for interaction, several molecules were constructed before 1,2-diphenylethene was selected to fit these distances.

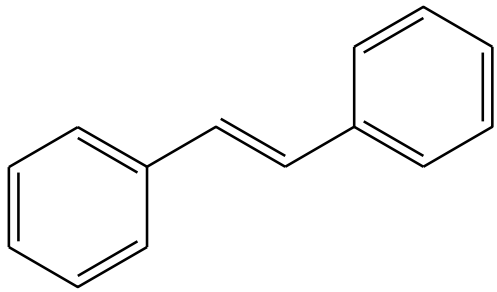

Figure 5.3: 1,2-diphenylethene

Gas phase systems were set up such that each ring of the bi-aromatic molecule was oriented approximately 3.0 Å away from each of the histidine, or phenylalanine residues. In the case of the 1BA4 conformer, the FF region was inaccessible and was not included in these calculations.

Each of the resulting systems was energy minimized at the semi-empirical molecular orbital level of theory using the AM1 Hamiltonian as implemented in the Gaussian 09W suite of programs [107]. Energies were calculated for the singlet state and ground state system, using quadratically convergent SCF. The energies of the β-amyloid conformers are given in Appendix 5, and that of 1,2-diphenylethene in the following table, for both the gas phase minimized system and its optimized energy at the AM1 level.

Table 5.27: The gas phase and semi-empirical energies of 1,2-diphenylethene

	Energies (kcal/mol)		
	E_{tot}	E_{vdw}	E_{ele}
1,2-diphenylethene	31.36	24.85	-0.15
	0.10126097713		hartrees
	63.542		kcal/mol

The binding energies were calculated using the following equations for the gas phase minimized systems:

$$\Delta E_{tot} = E_{tot} - E_{A\beta} - E_{Biaromatic} \quad (5.7)$$

$$\Delta E_{vdw} = E_{vdw} - E_{vdwA\beta} - E_{vdwBiaromatic} \quad (5.8)$$

$$\Delta E_{ele} = E_{ele} - E_{eleA\beta} - E_{eleBiaromatic} \quad (5.9)$$

The binding energies are calculated by subtracting the energies of the optimized bi-aromatic molecule and the Aβ conformers (with constrained protein backbone) from the geometry optimized systems. For the semi-empirical calculations, equation 5.10 was used to calculate the binding energy for each system.

$$\Delta E_{bind} = E_{A\beta Biaromatic} - E_{A\beta} - E_{Biaromatic} \quad (5.10)$$

5.3.2 Gas Phase Results of the Optimization of a Bi-aromatic Molecule with HH and FF of β-Amyloid

The gas phase optimized systems of 1,2-diphenylethene with the HH and FF regions of Aβ are summarized in the following table. The measured and calculated binding energies of the systems are given, also the initial and final orientations of the bi-aromatic molecule. Each ring was arbitrarily assigned as Ar^1 or Ar^2 for the summary. Measureable bonds are coloured pink for π-H and blue for π-π. Interactions with the $-CH_2-$ chain of the amino acid are in indigo, while purple indicates that the C=O of the protein backbone is involved and lime green, the -CH- of the backbone.

Table 5.28: The gas phase results of 1,2-diphenylethene interacting with HH and FF on β-amyloid

Conformer		Gly9	Tyr10	Glu11	His13	His14	Leu17	Val18	Ile31	Lys16	Phe19	Phe20	Asp23	Val24
1AMB	Initial Orientation				Ar^1	Ar^2					Ar^1	Ar^2		
	Final Orientation		Ar^1/Ar^2	Ar^2	Ar^1	Ar^2				Ar^1	Ar^1	Ar^2	Ar^2	Ar^2
	Total =	-0.96 kcal/mol								-6.86 kcal/mol				
	van der Waals =	63.16 kcal/mol								61.45 kcal/mol				
	Electrostatic =	-225.53 kcal/mol								-231.14 kcal/mol				
	ΔE_{tot} =	-20.40 kcal/mol								-26.30 kcal/mol				
	ΔE_{vdw} =	-13.09 kcal/mol								-14.80 kcal/mol				
	ΔE_{ele} =	-8.36 kcal/mol								-13.98 kcal/mol				
1AMC	Initial Orientation				Ar^1	Ar^2					Ar^1	Ar^2		
	Final Orientation		Ar^1		Ar^1	Ar^2		Ar^2		Ar^1	Ar^1	Ar^2		
						Ar^1				Ar^2				
	Total =	1.00 kcal/mol								-14.09 kcal/mol				
	van der Waals =	68.45 kcal/mol								69.14 kcal/mol				
	Electrostatic =	-242.51 kcal/mol								-259.14 kcal/mol				
	ΔE_{tot} =	-18.44 kcal/mol								-33.53 kcal/mol				
	ΔE_{vdw} =	-11.53 kcal/mol								-10.84 kcal/mol				
	ΔE_{ele} =	-8.37 kcal/mol								-25.00 kcal/mol				
1AML	Initial Orientation				Ar^1	Ar^2					Ar^1	Ar^2		
	Final Orientation		Ar^1		Ar^1	Ar^2	Ar^2		Ar^2		Ar^1	Ar^2	Ar^1	
	Total =	159.69 kcal/mol								163.62 kcal/mol				
	van der Waals =	108.68 kcal/mol								112.01 kcal/mol				
	Electrostatic =	-179.47 kcal/mol								-178.51 kcal/mol				
	ΔE_{tot} =	-14.39 kcal/mol								-10.46 kcal/mol				
	ΔE_{vdw} =	-8.84 kcal/mol								-5.51 kcal/mol				
	ΔE_{ele} =	-6.53 kcal/mol								-5.57 kcal/mol				
1IYT	Initial Orientation				Ar^1	Ar^2					Ar^1	Ar^2		
	Final Orientation				Ar^1	Ar^2					Ar^1	Ar^2	Ar^2	
	Total =	72.13 kcal/mol								73.54 kcal/mol				
	van der Waals =	71.83 kcal/mol								73.82 kcal/mol				
	Electrostatic =	-204.59 kcal/mol								-205.19 kcal/mol				
	ΔE_{tot} =	-12.14 kcal/mol								-10.74 kcal/mol				
	ΔE_{vdw} =	-8.67 kcal/mol								-6.68 kcal/mol				
	ΔE_{ele} =	-4.23 kcal/mol								-4.83 kcal/mol				
1Z0Q	Initial Orientation				Ar^1	Ar^2					Ar^1	Ar^2		
	Final Orientation	Ar^1	Ar^1		Ar^1	Ar^2					Ar^1	Ar^2		
			Ar^2											
	Total =	181.65 kcal/mol								193.252 kcal/mol				
	van der Waals =	99.36 kcal/mol								106.749 kcal/mol				
	Electrostatic =	-195.26 kcal/mol								-190.229 kcal/mol				
	ΔE_{tot} =	-17.59 kcal/mol								-5.98 kcal/mol				
	ΔE_{vdw} =	-11.69 kcal/mol								-4.30 kcal/mol				
	ΔE_{ele} =	-7.14 kcal/mol								-2.11 kcal/mol				

The bi-aromatic molecule was capable of binding to HH and FF for all systems. For two of the conformers, the binding energies for FF are more favourable, while the other three indicate that binding to HH is slightly more preferable than FF.

5.3.3 Results of the Semi-empirical Optimization of a Bi-aromatic Molecule with HH and FF on β-Amyloid

The energies calculated from the semi-empirical optimizations of 1,2-diphenylethene with the HH and FF regions of Aβ are summarized in Table 5.29. The measured energies are in Hartrees, while the calculated binding energies have been converted to kcal/mol for easier comparison. Interactions that formed at HH or FF are included – these were taken into consideration when examining the binding energies in order to determine the favoured region of binding for the bi-aromatic molecule.

Table 5.29: Results of the semi-empirical calculations of a bi-aromatic molecule with HH and FF on β-amyloid

Conformer	Orientation	Interactions	Measured Energy (hartrees)	Binding Energy (kcal/mol)	Favoured Orientation
1AMB	H-H	-	-0.98112151594	-5.215	F-F
	F-F	Phe20	-1.01462932116	-26.241	
1AMC	H-H	His14	-0.98447816175	-1.932	F-F
	F-F	Phe19	-1.03521548273	-33.770	
1AML	H-H	-	-1.34255000338	-4.510	F-F
	F-F	Phe19	-1.35412604015	-11.774	
1IYT	H-H	His13	-2.08041616515	-4.318	F-F
	F-F	Phe19/Phe20	-2.09137849898	-11.197	
1Z0Q	H-H	-	-1.18594891661	-0.392	H-H
	F-F	Phe19	-1.18463462204	0.433	

More binding interactions formed with the FF region of Aβ than the HH region. Even taking these bonds into account, the bi-aromatic tended to bind more strongly to Phe19-Phe20.

5.4 Conclusions on Aromatic Compounds Binding to HHQK and LVFF of β-Amyloid

The results of both the gas phase optimizations and the semi-empirical calculations suggest that within β-amyloid, LVFF is also a viable target for endogenous molecules to bind to in addition to **HH**Q**K**. It appears that aromatic molecules such as indoles may bind even more strongly to the LVFF region of Aβ. Therefore endogenous molecules capable of forming aromatic type interactions, such as those examined in Chapter 3, may bind to both regions of β-amyloid to prevent amyloid aggregation from occurring.

5.5 Interpretation

The binding interactions between β-amyloid and indole compared to an unsubstituted biindole suggest that both aromatic species bind to the **BB**X**B** region of Aβ with comparable frequency. Biindole formed more binding interactions with the AAXA motif relative to indole; as the species are chemically similar, this is most likely a difference between the size of the biindole molecule relative to the indole.

The binding energies of biindole are more favourable than those of indole for both interactions at **HH**Q**K** and at LVFF. This indicates that the binding interactions with the biindole molecule are likely stronger than those with indole. Again, this is most likely due to the relative size of the species examined. The biindole presents two identical indole molecules that can each bind to a separate amino acid side chain, whereas for indole, it must interact with two different side chains simultaneously. Thus the size of the

molecule is important in identifying species to interact with the **HH**Q**K** and LVFF regions of Aβ.

The energies of interactions occurring at the AAXA motif are less for most conformations of Aβ relative to those occurring at **BB**X**B**. For indole, the energies of interactions at LVFF are less than those at **HH**Q**K**, despite the fact that more binding interactions can occur at LVFF versus **HH**Q**K**. Thus the interactions occurring at LVFF are likely of a weaker type than those at **HH**Q**K**. For biindole, more interactions have also formed at LVFF relative to **HH**Q**K**; the measured binding energies are more comparable than seen for the indole. Although there are differences in the energetics of interaction, both indole and biindole demonstrate a capacity to bind to the AAXA motif in more systems than observed for the **BB**X**B** motif. This indicates that aromatic species could be designed to target both the **BB**X**B** and AAXA motifs of Aβ to block both these regions from interactions with the negatively charged regions and the cholesterol rafts present on membrane surfaces. This would prevent unwanted conformational changes from occurring.

The semi-empirical studies further confirm that aromatic species can bind to both HH and FF on Aβ, and that interactions with FF tend to be more energetically favourable, at least where unsubstituted molecules are concerned. The presence of electron withdrawing or electron donating groups on the aromatic rings would affect the strength of the binding interactions observed. The conformation of Aβ also appears to play a role in how strongly the bi-aromatic molecule can bind to HH and FF. The different spatial orientations may allow for stronger stacking interactions to occur for some

conformations, and the surrounding amino acid side chains may also influence how energetically favourable these optimized systems are.

It can be concluded that aromatic features may be important in indentifying endogenous molecules that can target the AAXA motif of β-amyloid alongside the **BB**X**B** motif.

CHAPTER 6: THE SEARCH FOR A DIAGNOSTIC AGENT FOR ALZHEIMER'S DISEASE

Currently, there are no definitive methods for diagnosing Alzheimer's disease during the life of a patient; it can only be diagnosed with certainty at autopsy. In living patients, methods such as the Mini-Mental State Examination are combined with structural tools such as positron emission tomography (PET) or magnetic resonance imaging (MRI) to diagnose possible AD [20].

MRI imaging agents can be used to produce contrasting images through the use of paramagnetic species such as gadolinium. Chelated gadolinium has significantly reduced toxicity relative to gadolinium salts, and its paramagnetic nature results in a decrease of the T_1 and T_2 relaxation times in the MRI [108]. The chelated compound can be used to show leaky blood vessels as locations with higher concentrations of complex will show up differently; the gadolinium affects the protons in the vicinity of its chelation allowing for a contrasting image to be visualized [108]. MRI imaging agents for Alzheimer's disease are desirable as this technique is most widely available in hospitals, relative to PET and SPECT.

6.1 SOLAPSONE AS AN IMAGING AGENT FOR ALZHEIMER'S DISEASE

There is a crucial need for new imaging agents with which to visualize aggregating β-amyloid in the brain of a living person. An ideal imaging agent should be safe, capable of binding to Aβ and capable of concomitantly binding to an MRI-active

agent such as gadolinium cations. Based upon previous work by the Weaver group, polyvinylsulfonate (PVS) has been identified as a glycosaminoglycan mimic capable of binding to the **HH**Q**K** region of β-amyloid. PVS is a polyanionic substance that is capable of binding to **HH**Q**K**, but with multiple remaining anionic functional groups capable of also binding to Gd^{3+}; however, PVS is not a safe drug-like molecule. Accordingly, a known drug with molecular properties similar to PVS was sought.

Using standard textbooks of pharmacology and medicinal chemistry, coupled with an extensive literature review, the Weaver group assembled a library of 956 compounds as known drugs (Appendix 10). A search of the library revealed that solapsone (Figure 6.1) was a known drug with striking similarities to PVS. As a result, solapsone was studied as a potential imaging agent.

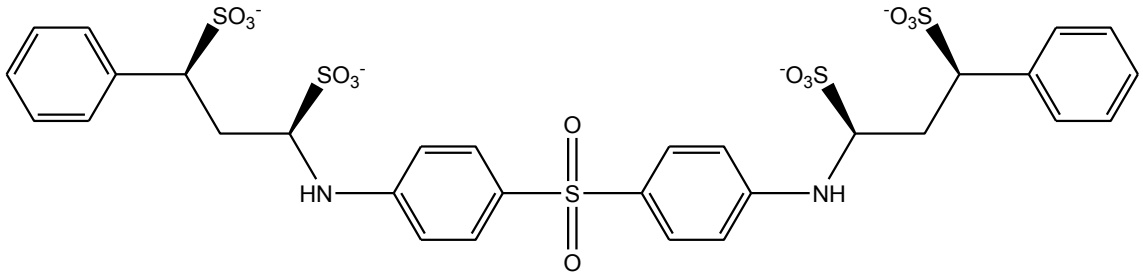

Figure 6.1: Solapsone as charged for physiological pH

Solapsone is a "moderate sized" drug molecule that was used in the early 1960s to treat leprosy [109]. Solapsone is well tolerated with low toxicity and minimal side effects; the LD50 (which is the amount of drug needed to cause death in half of the studied population) was measured as 2.7 g per kilogram [110]. It also appears that solapsone is capable of crossing the blood-brain barrier as concentrations were measured

to be between 1.3-3.7 mg per 100 mL of cerebrospinal fluid, and 2.0-6.1 mg per 100 mg of brain [111].

As it has a high concentration of aromatic rings and negatively charged sulfonate groups, solapsone could potentially interact with both β-amyloid and a cation available for MRI-contrast imaging. It is also structurally similar to glycosaminoglycans, such as heparin sulfate (Figure 6.2), with which Aβ binds to undergo conformational changes: this suggests a capacity for solapsone to bind to the protein.

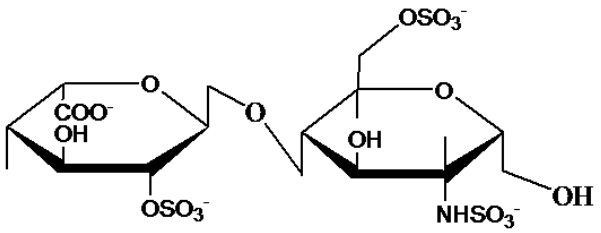

Figure 6.2: Heparin sulfate

Solapsone presents itself as a potential indicator for identifying Alzheimer's disease. Given that it has a flexible structure, it should be capable of chelating to a positively charged metal ion, such as gadolinium or manganese cations, which are commonly used in MRIs, as their paramagnetic properties allow them to be used as contrast agents [112]. The aromatic rings and sulfonate groups should be capable of interacting with the β-amyloid peptide in the **HH**Q**K** and **L**V**FF** regions while chelating the metal ion. Therefore, this could be used as a method of identifying the amount of β-amyloid present in the brain and whether a patient has AD or not; the fact that solapsone has been measured in brain bodes well for its potential use as a contrast imaging agent that must cross the blood-brain barrier.

The strength of solapsone as a chelating agent for Gd^{3+} and Mn^{2+} was compared to that of EDTA and DPDP (Figure 6.3). EDTA and DPDP are frequently used as chelating agents; EDTA is commonly used as a chelating agent for heavy metals, while DPDP is already used as an organ specific contrast agent for MRI, when chelated to manganese [113].

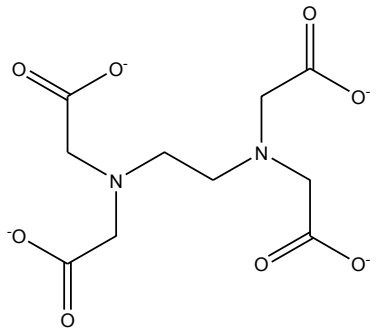

EDTA

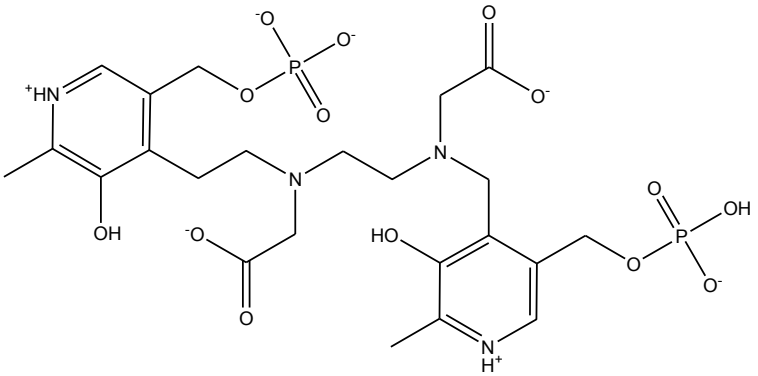

DPDP

Figure 6.3: EDTA and DPDP charged for physiological pH

6.1.1 Preparation of Solapsone, EDTA, and DPDP

Solapsone is a "moderate-sized" organic molecule with numerous aromatic rings and sulfonate groups. A conformational search was performed to determine the lowest energy structure of the molecule [47]. A neutral solapsone molecule was constructed and twelve torsional angles were used to run a systematic conformational search in the gas

phase. From this search the lowest energy conformation was selected and then charged for physiological pH before being optimized in the gas phase. The lowest energy structure of solapsone is relatively symmetric, therefore one half was arbitrarily denoted as the left side and coloured blue to distinguish it from the right half of the molecule.

The same procedure was followed for both EDTA and DPDP, where the molecules were constructed in neutral forms and subjected to systematic conformational searches. There were seven torsional angles examined for EDTA and thirteen for DPDP. The lowest energy conformation from each search was then charged and minimized in the gas phase.

6.1.2 Gas Phase Optimization of Solapsone, EDTA, and DPDP Chelating Gd^{3+} and Mn^{2+}

For each of solapsone, EDTA, and DPDP, initial gas phase geometry optimizations were performed with one ion of either Gd^{3+} or Mn^{2+} placed at distance of 10 Å from the molecule being examined. These were used to calculate the energy of a non-interactive system. Following these calculations, the ions being examined were separated from the various functional groups on each of the three molecules by approximately 3 Å. For each molecule, the interaction that resulted in the lowest overall energy was selected for solution phase optimization.

The results of the gas phase minimizations with Gd^{3+} are given in Table 6.1 where the calculated total, ΔE_{tot}, van der Waals, ΔE_{vdw}, and electrostatic energies, ΔE_{ele}, for each of the gas phase systems selected are given in kcal/mol. The table also identifies functional groups where chelation was occurring.

Table 6.1: Gas phase results of solapsone, EDTA and DPDP chelating Gd^{3+}

	ΔE_{tot}	ΔE_{vdw}	ΔE_{ele}	Chelation sites
Solapsone	-231.28	6.92	-244.50	2 SO_3^-
EDTA	-234.16	13.85	-247.07	2 CO_2^- and 1 N
DPDP	-236.53	9.01	-252.26	2 CO_2^-

The results of the gas phase optimization of the three molecules with Mn^{2+} are given in Table 6.2 for each of the lowest energy systems.

Table 6.2: Gas phase results of solapsone, EDTA and DPDP chelating Mn^{2+}

	ΔE_{tot}	ΔE_{vdw}	ΔE_{ele}	Chelation sites
Solapsone	-134.67	4.27	-142.39	2 SO_3^-
EDTA	-157.36	8.88	-165.20	2 CO_2^- and 1 N
DPDP	-155.24	8.05	-173.89	PO_3^{2-} and 1 CO_2^-

6.1.3 Solution Phase Optimization of Solapsone, EDTA, and DPDP Chelating Gd^{3+} and Mn^{2+}

Each of the selected energetically favourable systems from the gas phase interactions was minimized in a solvated environment . The systems in which the chelating agents were separated by 10 Å were also optimized in the solution phase in order to determine the energies of interaction.

Each system was placed in a 30.28 Å x 30.28 Å x 30.28 Å box of water molecules and minimized. The energies for each system were calculated upon removal of the solvent (as the number of water molecules present will vary with each system) and the chelation sites were identified for solapsone, EDTA and DPDP.

The results of the solution phase optimized interactions between each of the chelating agents and Gd^{3+} are given in Table 6.3, while the interactions with Mn^{2+} are given in Table 6.4. The measured energies are in kcal/mol.

Table 6.3: Solution phase results of solapsone, EDTA and DPDP chelating Gd^{3+}

	ΔE_{tot}	ΔE_{vdw}	ΔE_{ele}	Chelation sites
Solapsone	-221.84	2.91	-220.86	2 SO_3^- and 2 H_2O
EDTA	-232.79	13.33	-240.90	2 CO_2^- and 1 N and 2 H_2O
DPDP	-228.86	4.26	-227.98	2 CO_2^- and 1 H_2O

Table 6.4: Solution phase results of solapsone, EDTA and DPDP chelating Mn^{2+}

	ΔE_{tot}	ΔE_{vdw}	ΔE_{ele}	Chelation sites
Solapsone	-128.13	4.45	-134.11	2 SO_3^-
EDTA	-151.65	5.54	-154.15	2 CO_2^- and 1 N and 2 H_2O
DPDP	-144.65	9.94	-164.76	1 PO_3^{2-} and 1 CO_2^- and 1 H_2O

6.1.4 Conclusions on Solapsone, EDTA and DPDP Chelating Gd^{3+} and Mn^{2+}

Gas phase minimizations indicated that solapsone was capable of chelating both Gd^{3+} and Mn^{2+}. The total binding energy of solapsone relative to EDTA and DPDP for chelating Gd^{3+} is very similar, it is also the case for the electrostatic energies. In terms of the van der Waals energies, solapsone is most favoured, followed by DPDP and then EDTA, this can be explained by the number of aromatic rings present in each molecule.

In the gas phase minimization of the three molecules with Mn^{2+}, solapsone was less favourable in terms of binding energies, with the exception of having the best van der Waals energy of the three. Manganese is a much smaller ion than gadolinium, so it would

seem that the large structure of solapsone is not as capable as the smaller EDTA and DPDP structures in terms of chelating the ion.

The solution phase results of the minimization of solapsone, EDTA and DPDP with Gd^{3+} indicate an order of overall energetic favourability of EDTA ≥ DPDP > solapsone, although solapsone is still quite capable of chelating the ion. Solapsone is still preferred in terms of the van der Waals energy over the other two chelating agents. All three systems have the gadolinium ion chelating with water, as well as the molecule of interest. In the case of solapsone in particular, this indicates that the chelated system could also interact with the β-amyloid peptide. Figure 6.4 demonstrates the orientation of the most favourable chelated complex of solapsone and gadolinium.

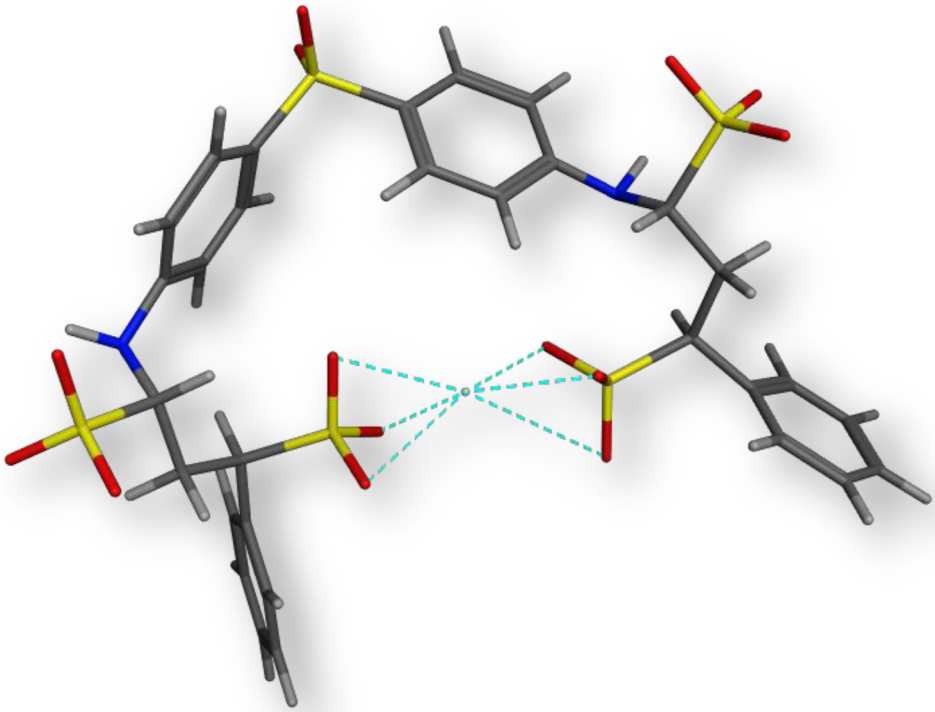

Figure 6.4: Solapsone chelating gadolinium (III).

The results of the solution phase optimization of the systems involving the manganese ion indicate a distinct pattern of EDTA > DPDP > solapsone in terms of the overall binding energy. Contrary to what is seen for the gadolinium systems, DPDP chelated to Mn^{2+} has a lower electrostatic energy than EDTA, which is still much lower than the same energy for solapsone. Similarly, while solapsone is still the most favoured for van der Waals energies, EDTA exhibits a lower energy than DPDP (despite a lack of aromatic rings). One possible explanation for the less favourable solapsone energies may be due to the fact that manganese (II) is chelating in such a position that it is not interacting with any water molecules; this results in few chelation sites for the ion and may indicate that the structure of the system is less favourable as a whole.

6.2 The Optimization of a Solapsone-Gd^{3+} Complex with β-Amyloid

As solapsone presented itself as a viable molecule for chelating paramagnetic cations, the next phase was to determine if a complex of solapsone and gadolinium would be capable of binding to β-amyloid. Molecular mechanics simulations were performed in gas and solution phase environments to determine if binding could occur with the **HH**Q**K** and LVFF regions of Aβ.

6.2.1 Preparation of β-Amyloid-Solapsone-Gd^{3+} Systems for Gas Phase Optimization

The best chelated solapsone-Gd^{3+} complex identified in Section 6.1.1 was selected for optimization with six different conformations of β-amyloid: 1AMB, 1AMC, 1AML, 1BA4, 1IYT and 1Z0Q (as identified by their PDB codes). The gas phase

optimized energies of the Aβ conformers are given in Appendix 6, and that of the solapsone-Gd^{3+} complex is given in Table 6.5.

Table 6.5: The gas phase energies of solapsone chelating gadolinium

	Energies (kcal/mol)		
	E_{tot}	E_{vdw}	E_{ele}
Solapsone -Gd^{3+}	-150.16	47.42	-223.73

As the chelated solapsone-Gd^{3+} complex is more fixed in its structure, there were only a few orientations that could be set up for optimization. Systems were prepared such that two of the functional groups on solapsone were situated ~3.0 Å away from two of the amino acid side chains of interest in the **HH**Q**K** or LVFF region of β-amyloid. For the optimized results, the energies were calculated to determine the binding strength via the following equations:

$$\Delta E_{tot} = E_{tot} - E_{A\beta} - E_{SolapGd} \quad (6.1)$$

$$\Delta E_{vdw} = E_{vdw} - E_{vdwA\beta} - E_{vdwSolapGd} \quad (6.2)$$

$$\Delta E_{ele} = E_{ele} - E_{eleA\beta} - E_{eleSolapGd} \quad (6.3)$$

The total, van der Waals, and electrostatic binding energies were calculated by subtracting the energy of the optimized solapsone-Gd^{3+} complex and the energy of the Aβ conformer from the energy of the gas phase minimized system.

The energy minimizations were performed with constrained protein backbones to prevent structural collapse.

6.2.2 The Gas Phase Results of Solapsone-Gd^{3+} Optimized with β-Amyloid

A significant number of optimized Aβ-solapsone-Gd^{3+} systems were generated from the gas phase minimizations. The complete results are given in Appendix 11. From

the gas phase results, six systems were selected for each of the **HH**Q**K** and LVFF regions of each conformer of β-amyloid for solution phase optimization. The systems that were selected are listed in the following tables according to Aβ conformer. The functional groups on solapsone are identified according to Figure 6.5.

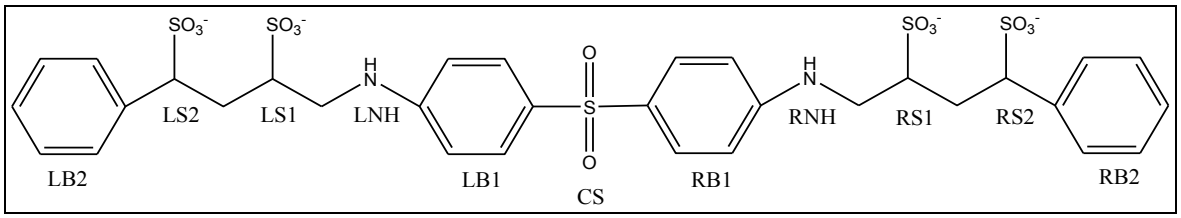

Figure 6.5: Abbreviations of the functional groups on solapsone

The amino acid side chains are represented by their three letter notation, and both the initial orientation of solapsone-Gd^{3+} and its final orientation upon minimization are given. Measured bonds that formed are coloured blue for π-π, green for cation-π, and orange for hydrogen bonds. When more than one hydrogen bond formed with an amino acid, a darker shade of orange was used. Interactions with the $–CH_2$- of the amino acid side chain are shown in indigo, while interactions with the C=O, -NH- or –CH- of the protein backbone are coloured purple, yellow and lime green, respectively. The chelation occurring with Gd^{3+} was also included for reference.

Table 6.6: Selected results of the gas phase minimization of solapsone-Gd^{3+} with the 1AMB conformer of β-amyloid

	Tyr10	His13	His14	Gln15	Lys16	Leu17	Val18	Phe20
Initial Orientation		RS1			LS1			
Final Orientation		RB1			LS1	RS1		LS1
Gd^{3+} chelates 2 SO_3^- @ 5 sites								
Total =	-241.32 kcal/mol			ΔE_{Tot}	-82.49 kcal/mol			
Van der Waals =	78.07 kcal/mol			ΔE_{Vdw}	-21.05 kcal/mol			
Electrostatic =	-506.18 kcal/mol			ΔE_{Ele} =	-70.90 kcal/mol			
Initial Orientation		LS1	RS1					
Final Orientation	CS	RB1	RS1			LS1	RS2	
		LB1					RB2	
		LS1						
Gd^{3+} chelates 2 SO_3^- @ 5 sites								
Total =	-233.53 kcal/mol			ΔE_{Tot}	-74.69 kcal/mol			
Van der Waals =	82.13 kcal/mol			ΔE_{Vdw}	-16.99 kcal/mol			
Electrostatic =	-497.80 kcal/mol			ΔE_{Ele} =	-62.52 kcal/mol			
Initial Orientation		RS2	LS1					
Final Orientation	LB2	RS2	LS1		RS1	RS1	LS1	
		RB2	LB2			LB1		
		RS1	LS2					
Gd^{3+} chelates 2 SO_3^- @ 4 sites								
Total =	-248.40 kcal/mol			ΔE_{Tot}	-89.57 kcal/mol			
Van der Waals =	77.42 kcal/mol			ΔE_{Vdw}	-21.70 kcal/mol			
Electrostatic =	-506.11 kcal/mol			ΔE_{Ele} =	-70.83 kcal/mol			

	Tyr10	His13	His14	Gln15	Lys16	Leu17	Val18	Phe20	Glu22
Initial Orientation		RB1	LB1						
Final Orientation	CS		LB2				LB2		LB2
	RB1								
Gd^{3+} chelates 2 SO_3^- @ 4 sites									
Total =	-238.03 kcal/mol			ΔE_{Tot} =	-79.20 kcal/mol				
Van der Waals =	86.99 kcal/mol			ΔE_{Vdw} =	-12.14 kcal/mol				
Electrostatic =	-502.93 kcal/mol			ΔE_{Ele} =	-67.65 kcal/mol				
Initial Orientation		LB1			RB1				
Final Orientation		LB1			RB1			RS1	
					RS1				
Gd^{3+} chelates 2 SO_3^- @ 4 sites									
Total =	-223.19 kcal/mol			ΔE_{Tot} =	-64.36 kcal/mol				
Van der Waals =	89.18 kcal/mol			ΔE_{Vdw} =	-9.95 kcal/mol				
Electrostatic =	-497.51 kcal/mol			ΔE_{Ele} =	-62.23 kcal/mol				
Initial Orientation		LS1	RS2						
Final Orientation	LS1	LS1	Gd^{3+}			LB2			
			RS2						
			LS1						
Gd^{3+} chelates 2 SO_3^- @ 3 sites									
Total =	-235.17 kcal/mol			ΔE_{Tot} =	-76.33 kcal/mol				
Van der Waals =	84.99 kcal/mol			ΔE_{Vdw} =	-14.13 kcal/mol				
Electrostatic =	-505.24 kcal/mol			ΔE_{Ele} =	-69.96 kcal/mol				

	His13	Lys16	Leu17	Val18	Phe19	Phe20	Asp23	Lys28
Initial Orientation					RB1	LB1		
Final Orientation		LB1			CS		LB2	
		LNH					CS	
Gd^{3+} chelates 3 SO_3^- @ 6 sites								
Total =	-237.86 kcal/mol			ΔE_{Tot}	-79.02 kcal/mol			
Van der Waals =	86.54 kcal/mol			ΔE_{Vdw}	-12.59 kcal/mol			
Electrostatic =	-513.32 kcal/mol			ΔE_{Ele} =	-78.04 kcal/mol			
Initial Orientation			RB1			LB1		
Final Orientation	RS1		RB1					LS1
			RNH					LNH
Gd^{3+} chelates 2 SO_3^- @ 6 sites								
Total =	-225.03 kcal/mol			ΔE_{Tot}	-66.20 kcal/mol			
Van der Waals =	87.41 kcal/mol			ΔE_{Vdw}	-11.71 kcal/mol			
Electrostatic =	-497.62 kcal/mol			ΔE_{Ele} =	-62.34 kcal/mol			
Initial Orientation				RB2	LB2			
Final Orientation				RB2	LB2			
Gd^{3+} chelates 2 SO_3^- @ 5 sites								
Total =	-214.70 kcal/mol			ΔE_{Tot}	-55.87 kcal/mol			
Van der Waals =	89.40 kcal/mol			ΔE_{Vdw}	-9.73 kcal/mol			
Electrostatic =	-480.93 kcal/mol			ΔE_{Ele} =	-45.65 kcal/mol			

	His13	Leu17	Val18	Phe19	Phe20	Ala21	Glu22	Gly25	Lys28
Initial Orientation		LB1			RB1				
Final Orientation	LS1	LB1			RB1				RS1
Gd^{3+} chelates 2 SO_3^- @ 5 sites					4 sites (2L & 2R) + 3 H2O				
Total =	-232.85 kcal/mol			ΔE_{Tot} =	-74.01 kcal/mol				
Van der Waals =	88.43 kcal/mol			ΔE_{Vdw} =	-10.69 kcal/mol				
Electrostatic =	-503.13 kcal/mol			ΔE_{Ele} =	-67.85 kcal/mol				
Initial Orientation			RB2		LB2				
Final Orientation			RB2		LB2	LB2			LS1
Gd^{3+} chelates 2 SO_3^- @ 4 sites									
Total =	-216.82 kcal/mol			ΔE_{Tot} =	-57.98 kcal/mol				
Van der Waals =	82.74 kcal/mol			ΔE_{Vdw} =	-16.38 kcal/mol				
Electrostatic =	-482.74 kcal/mol			ΔE_{Ele} =	-47.46 kcal/mol				
Initial Orientation			LB2	RB2					
Final Orientation	RB2	RB2							
		RS2							
Gd^{3+} chelates 2 SO_3^- @ 5 sites									
Total =	-212.11 kcal/mol			ΔE_{Tot} =	-53.27 kcal/mol				
Van der Waals =	92.23 kcal/mol			ΔE_{Vdw} =	-6.89 kcal/mol				
Electrostatic =	-479.73 kcal/mol			ΔE_{Ele} =	-44.45 kcal/mol				

Table 6.7: Selected results of the gas phase minimization of solapsone-Gd^{3+} with the 1AMC conformer of β-amyloid

	Tyr10	His13	His14	Gln15	Lys16	Leu17	Phe20
Initial Orientation		LB1	RB1				
Final Orientation	CS	LS1	RB1			LS1	
	LB1		CS				
Gd^{3+} chelates 2 SO_3^- @ 6 sites							
Total =	-218.35 kcal/mol			ΔE_{Tot}	-70.68 kcal/mol		
Van der Waals =	97.45 kcal/mol			ΔE_{Vdw}	-12.38 kcal/mol		
Electrostatic =	-506.37 kcal/mol			ΔE_{Ele} =	-57.44 kcal/mol		
Initial Orientation		RS2			LS2		
Final Orientation		RB2			LS1	RB2	LB2
		RS1					
Gd^{3+} chelates 2 SO_3^- @ 6 sites							
Total =	-207.89 kcal/mol			ΔE_{Tot}	-60.22 kcal/mol		
Van der Waals =	104.26 kcal/mol			ΔE_{Vdw}	-5.57 kcal/mol		
Electrostatic =	-504.15 kcal/mol			ΔE_{Ele} =	-55.21 kcal/mol		
Initial Orientation		RS2			LS1		
Final Orientation	RS1	RB1	RS1		LS1	LS1	LS1
					LB1		
Gd^{3+} chelates 2 SO_3^- @ 6 sites							
Total =	-223.14 kcal/mol			ΔE_{Tot}	-75.48 kcal/mol		
Van der Waals =	97.64 kcal/mol			ΔE_{Vdw}	-12.19 kcal/mol		
Electrostatic =	-514.30 kcal/mol			ΔE_{Ele} =	-65.37 kcal/mol		

	Tyr10	His13	His14	Gln15	Lys16	Leu17	Phe20
Initial Orientation		RB2			LB2		
Final Orientation		RB2			LB2		LB1
		RB2			LS2		
					RS2		
Gd^{3+} chelates 3 SO_3^- @ 6 sites							
Total =	-208.95 kcal/mol			ΔE_{Tot} =	-61.29 kcal/mol		
Van der Waals =	95.96 kcal/mol			ΔE_{Vdw} =	-13.88 kcal/mol		
Electrostatic =	-496.19 kcal/mol			ΔE_{Ele} =	-47.26 kcal/mol		
Initial Orientation			LB2		RB2		
Final Orientation	LB2	RB2	LS2				RS2
		RS2	LB2				LS2
		LS2					
Gd^{3+} chelates 3 SO_3^- @ 5 sites							
Total =	-229.7 kcal/mol			ΔE_{Tot} =	-82.07 kcal/mol		
Van der Waals =	94.3 kcal/mol			ΔE_{Vdw} =	-15.51 kcal/mol		
Electrostatic =	-518.8 kcal/mol			ΔE_{Ele} =	-69.87 kcal/mol		
Initial Orientation			RB2		LB2		
Final Orientation	RS2	LS2	RB2				
	RS1	LB2					
	LS2						
	RB2						
Gd^{3+} chelates 2 SO_3^- @ 3 sites							
Total =	-218.05 kcal/mol			ΔE_{Tot} =	-70.38 kcal/mol		
Van der Waals =	86.52 kcal/mol			ΔE_{Vdw} =	-23.31 kcal/mol		
Electrostatic =	-498.94 kcal/mol			ΔE_{Ele} =	-50.00 kcal/mol		

	Gln15	Lys16	Leu17	Val18	Phe19	Phe20	Glu22
Initial Orientation			RB2		LB2		
Final Orientation				RS2	LB2		
				RB2			
Gd^{3+} chelates 2 SO_3^- @ 5 sites							
Total =	-234.22 kcal/mol			ΔE_{Tot}	-86.56 kcal/mol		
Van der Waals =	102.27 kcal/mol			ΔE_{Vdw}	-7.56 kcal/mol		
Electrostatic =	-531.47 kcal/mol			ΔE_{Ele} =	-82.54 kcal/mol		
Initial Orientation				LB1	RB1		
Final Orientation	LB1			LB1	RB1		RB1
	CS				CS		
Gd^{3+} chelates 2 SO_3^- @ 4 sites							
Total =	-221.78 kcal/mol			ΔE_{Tot}	-74.11 kcal/mol		
Van der Waals =	96.54 kcal/mol			ΔE_{Vdw}	-13.30 kcal/mol		
Electrostatic =	-527.11 kcal/mol			ΔE_{Ele} =	-78.17 kcal/mol		
Initial Orientation					LB1	RB1	
Final Orientation		RS1			LB1	RS1	
					RB1		
Gd^{3+} chelates 2 SO_3^- @ 5 sites							
Total =	-213.93 kcal/mol			ΔE_{Tot}	-66.26 kcal/mol		
Van der Waals =	92.89 kcal/mol			ΔE_{Vdw}	-16.94 kcal/mol		
Electrostatic =	-500.23 kcal/mol			ΔE_{Ele} =	-51.30 kcal/mol		

	His13	Lys16	Leu17	Val18	Phe19	Phe20
Initial Orientation			LB2			RB2
Final Orientation	LB2	RS2	LB2			RB2
	RS2	RB2	RS2			
Gd^{3+} chelates 3 SO_3^- @ 6 sites						
Total =	-230.05 kcal/mol			ΔE_{Tot} =	-82.39 kcal/mol	
Van der Waals =	97.69 kcal/mol			ΔE_{Vdw} =	-12.14 kcal/mol	
Electrostatic =	-522.93 kcal/mol			ΔE_{Ele} =	-73.99 kcal/mol	
Initial Orientation			LB1			RB1
Final Orientation	LS1	LS1	LB2			RB1
		LNH	LNH			CS
						LB1
Gd^{3+} chelates 2 SO_3^- @ 5 sites						
Total =	-221.58 kcal/mol			ΔE_{Tot} =	-73.92 kcal/mol	
Van der Waals =	97.62 kcal/mol			ΔE_{Vdw} =	-12.21 kcal/mol	
Electrostatic =	-516.36 kcal/mol			ΔE_{Ele} =	-67.42 kcal/mol	
Initial Orientation			RB1			LB1
Final Orientation	RS1	RS1	RB1			LB2
			RS1			
Gd^{3+} chelates 2 SO_3^- @ 5 sites						
Total =	-211.67 kcal/mol			ΔE_{Tot} =	-64.01 kcal/mol	
Van der Waals =	94.83 kcal/mol			ΔE_{Vdw} =	-15.00 kcal/mol	
Electrostatic =	-502.58 kcal/mol			ΔE_{Ele} =	-53.65 kcal/mol	

Table 6.8: Selected results of the gas phase minimization of solapsone-Gd^{3+} with the 1AML conformer of β-amyloid

	Tyr10	His13	His14	Gln15	Lys16	Leu17	Phe20
Initial Orientation		LB1	RB1				
Final Orientation	LB1	LB1 LS1 LNH	CS			LB1	
Gd^{3+} chelates 3 SO_3^- @ 7 sites							
Total =	-79.29 kcal/mol			ΔE_{Tot}	-114.79 kcal/mol		
Van der Waals =	131.81 kcal/mol			ΔE_{Vdw}	-6.92 kcal/mol		
Electrostatic =	-467.13 kcal/mol			ΔE_{Ele} =	-112.86 kcal/mol		
Initial Orientation		LS1			RS1		
Final Orientation		LS1			RS1		
Gd^{3+} chelates 2 SO_3^- @ 6 sites							
Total =	-74.53 kcal/mol			ΔE_{Tot}	-110.02 kcal/mol		
Van der Waals =	135.24 kcal/mol			ΔE_{Vdw}	-3.49 kcal/mol		
Electrostatic =	-465.66 kcal/mol			ΔE_{Ele} =	-111.39 kcal/mol		
Initial Orientation		RB1			LB1		
Final Orientation					LB1 LNH		CS LB1
Gd^{3+} chelates 2 SO_3^- @ 6 sites							
Total =	-60.49 kcal/mol			ΔE_{Tot}	-95.98 kcal/mol		
Van der Waals =	126.23 kcal/mol			ΔE_{Vdw}	-12.50 kcal/mol		
Electrostatic =	-441.39 kcal/mol			ΔE_{Ele} =	-87.12 kcal/mol		

	Val12	His13	His14	Gln15	Lys16
Initial Orientation		LS2			RS1
Final Orientation	LS2 RS2	LS1			RS1
Gd^{3+} chelates 2 SO_3^- @ 5 sites					
Total =	-89.72 kcal/mol		ΔE_{Tot} =	-125.21 kcal/mol	
Van der Waals =	129.60 kcal/mol		ΔE_{Vdw} =	-9.13 kcal/mol	
Electrostatic =	-471.85 kcal/mol		ΔE_{Ele} =	-117.59 kcal/mol	
Initial Orientation		LS1			RS2
Final Orientation	LS1	LS1			RB1 LS1 LB1 RS1
Gd^{3+} chelates 2 SO_3^- @ 6 sites					
Total =	-68.9 kcal/mol		ΔE_{Tot} =	-104.35 kcal/mol	
Van der Waals =	130.1 kcal/mol		ΔE_{Vdw} =	-8.63 kcal/mol	
Electrostatic =	-465.4 kcal/mol		ΔE_{Ele} =	-111.12 kcal/mol	
Initial Orientation		RS1			LS2
Final Orientation	RS1	RS1			LS2 RS1
Gd^{3+} chelates 2 SO_3^- @ 4 sites					
Total =	-60.35 kcal/mol		ΔE_{Tot} =	-95.85 kcal/mol	
Van der Waals =	129.74 kcal/mol		ΔE_{Vdw} =	-8.99 kcal/mol	
Electrostatic =	-440.58 kcal/mol		ΔE_{Ele} =	-86.31 kcal/mol	

	His13	Lys16	Leu17	Val18	Phe19	Phe20	Asp23	Ala30
Initial Orientation					LB2	RB2		
Final Orientation		LS1			LS1 LB2		LB2	
Gd^{3+} chelates 2 SO_3^- @ 6 sites								
Total =	-70.15 kcal/mol			ΔE_{Tot}	-105.64 kcal/mol			
Van der Waals =	132.06 kcal/mol			ΔE_{Vdw}	-6.67 kcal/mol			
Electrostatic =	-456.32 kcal/mol			ΔE_{Ele} =	-102.06 kcal/mol			
Initial Orientation			RB2		LB2			
Final Orientation	RB2	RB2	RB2			RS2 LS2 LB2		RB2
Gd^{3+} chelates 2 SO_3^- @ 4 sites								
Total =	-60.29 kcal/mol			ΔE_{Tot}	-95.78 kcal/mol			
Van der Waals =	123.81 kcal/mol			ΔE_{Vdw}	-14.92 kcal/mol			
Electrostatic =	-440.73 kcal/mol			ΔE_{Ele} =	-86.47 kcal/mol			
Initial Orientation					RB1	LB1		
Final Orientation		RS1 RB1			RB1 CS	CS LB1	CS	
Gd^{3+} chelates 2 SO_3^- @ 6 sites								
Total =	-55.20 kcal/mol			ΔE_{Tot}	-90.70 kcal/mol			
Van der Waals =	126.54 kcal/mol			ΔE_{Vdw}	-12.19 kcal/mol			
Electrostatic =	-454.14 kcal/mol			ΔE_{Ele} =	-99.88 kcal/mol			

Table 6.9: Selected results of the gas phase minimization of solapsone-Gd^{3+} with the 1BA4 conformer of β-amyloid

	Asp1	Glu3	His6	Asp7	Gly9	Tyr10	His13	His14	Gln15	Lys16
Initial Orientation								RB2		LB2
Final Orientation	LB2	LB2	LS1	LB2	LB2	RB2	RB2			LB2
						RS2				

Gd^{3+} chelates 2 SO_3^- @ 5 sites

Total =	-144.66 kcal/mol	ΔE_{Tot}	-86.21 kcal/mol
Van der Waals =	92.84 kcal/mol	ΔE_{Vdw}	-15.71 kcal/mol
Electrostatic =	-469.32 kcal/mol	ΔE_{Ele} =	-76.05 kcal/mol

Initial Orientation							RB2			LB2
Final Orientation						RB2	RB2	RS1		LB2
						RS2				

Gd^{3+} chelates 2 SO_3^- @ 5 sites

Total =	-139.15 kcal/mol	ΔE_{Tot}	-80.70 kcal/mol
Van der Waals =	93.59 kcal/mol	ΔE_{Vdw}	-14.96 kcal/mol
Electrostatic =	-469.70 kcal/mol	ΔE_{Ele} =	-76.43 kcal/mol

Initial Orientation							LS2	RS1		
Final Orientation							LS1	RS1		
								RB1		

Gd^{3+} chelates 2 SO_3^- @ 5 si3 sites (2L & 1R) + 2 H2O

Total =	-130.15 kcal/mol	ΔE_{Tot}	-71.70 kcal/mol
Van der Waals =	102.55 kcal/mol	ΔE_{Vdw}	-6.01 kcal/mol
Electrostatic =	-460.94 kcal/mol	ΔE_{Ele} =	-67.66 kcal/mol

	Gly9	Tyr10	His13	His14	Gln15	Lys16
Initial Orientation			LB2			RB2
Final Orientation	RB2	LB2	LB2	LS1		
		RS2				
		RB2				

Gd^{3+} chelates 2 SO_3^- @ 4 sites

Total =	-143.45 kcal/mol	ΔE_{Tot} =	-85.00 kcal/mol
Van der Waals =	91.58 kcal/mol	ΔE_{Vdw} =	-16.98 kcal/mol
Electrostatic =	-469.77 kcal/mol	ΔE_{Ele} =	-76.49 kcal/mol

Initial Orientation			LB1	RB1		
Final Orientation			LS1	RS1		

Gd^{3+} chelates 2 SO_3^- @ 6 sites

Total =	-127.60 kcal/mol	ΔE_{Tot} =	-69.14 kcal/mol
Van der Waals =	101.57 kcal/mol	ΔE_{Vdw} =	-6.99 kcal/mol
Electrostatic =	-454.87 kcal/mol	ΔE_{Ele} =	-61.59 kcal/mol

Initial Orientation			RS2	LS1		
Final Orientation			RS1	LS1		
			LS1			

Gd^{3+} chelates 2 SO_3^- @ 5 sites

Total =	-124.56 kcal/mol	ΔE_{Tot} =	-66.10 kcal/mol
Van der Waals =	102.65 kcal/mol	ΔE_{Vdw} =	-5.91 kcal/mol
Electrostatic =	-452.96 kcal/mol	ΔE_{Ele} =	-59.69 kcal/mol

	His14	Gln15	Leu17	Val18	Phe19	Phe20	Glu22
Initial Orientation			RB2	LB2			
Final Orientation			RB2	LB2			

Gd^{3+} chelates 3 SO_3^- @ 7 sites

Total =	-128.90 kcal/mol	ΔE_{Tot}	-70.45 kcal/mol
Van der Waals =	100.41 kcal/mol	ΔE_{Vdw}	-8.15 kcal/mol
Electrostatic =	-445.86 kcal/mol	ΔE_{Ele} =	-52.58 kcal/mol

Initial Orientation			LB2		RB2		
Final Orientation	LS1		LB2	LS2			RB2

Gd^{3+} chelates 2 SO_3^- @ 6 sites

Total =	-141.47 kcal/mol	ΔE_{Tot}	-83.02 kcal/mol
Van der Waals =	99.11 kcal/mol	ΔE_{Vdw}	-9.45 kcal/mol
Electrostatic =	-469.08 kcal/mol	ΔE_{Ele} =	-75.81 kcal/mol

Initial Orientation				RB1	LB1		
Final Orientation		CS			LB1		LS2
					CS		RS1

Gd^{3+} chelates 2 SO_3^- @ 6 sites

Total =	-133.48 kcal/mol	ΔE_{Tot}	-75.03 kcal/mol
Van der Waals =	101.99 kcal/mol	ΔE_{Vdw}	-6.56 kcal/mol
Electrostatic =	-470.46 kcal/mol	ΔE_{Ele} =	-77.18 kcal/mol

	His14	Gln15	Leu17	Val18	Phe19	Phe20	Glu22
Initial Orientation			LB1			RB1	
Final Orientation	LS1		LB1				
	LB1		CS				
	LNH						

Gd^{3+} chelates 2 SO_3^- @ 6 sites

Total =	-102.77 kcal/mol	ΔE_{Tot} =	-44.32 kcal/mol
Van der Waals =	99.13 kcal/mol	ΔE_{Vdw} =	-9.42 kcal/mol
Electrostatic =	-425.45 kcal/mol	ΔE_{Ele} =	-32.18 kcal/mol

Initial Orientation			RB1	LB1			
Final Orientation	LS1		RB1	LB1			
			RS1				

Gd^{3+} chelates 2 SO_3^- @ 6 sites

Total =	-141.52 kcal/mol	ΔE_{Tot} =	-83.07 kcal/mol
Van der Waals =	97.76 kcal/mol	ΔE_{Vdw} =	-10.80 kcal/mol
Electrostatic =	-458.76 kcal/mol	ΔE_{Ele} =	-65.49 kcal/mol

Initial Orientation			RB2		LB2		
Final Orientation		LB2	RB2	RS2			LB2
				LS2			

Gd^{3+} chelates 2 SO_3^- @ 5 sites

Total =	-112.93 kcal/mol	ΔE_{Tot} =	-54.47 kcal/mol
Van der Waals =	98.71 kcal/mol	ΔE_{Vdw} =	-9.84 kcal/mol
Electrostatic =	-434.90 kcal/mol	ΔE_{Ele} =	-41.62 kcal/mol

Table 6.10: Selected results of the gas phase minimization of solapsone-Gd^{3+} with the HHQK region of the 1IYT conformer of β-amyloid

	Gly9	His13	His14	Gln15	Lys16	Leu17	Tyr10	His13	His14	Gln15	Lys16	Leu17
Initial Orientation		LB1	RB1					LS2	RS1			
Initial Orientation	LB2	LB2	RB1				RS1	RB1	RS1			RB2
		LB2	CS					LS1				
		LB1						LS2				
								RS2				
Gd^{3+} chelates 3 SO_3^- @ 7 sites							Gd^{3+} chelates 2 SO_3^- @ 5 sites					
Total =	-174.37	kcal/mol					-168.28	kcal/mol				
Van der Waals =	88.30	kcal/mol					88.10	kcal/mol				
Electrostatic =	-487.17	kcal/mol					-482.30	kcal/mol				
ΔE_{Tot} =	-77.13	kcal/mol					-71.04	kcal/mol				
ΔE_{Vdw} =	-14.83	kcal/mol					-15.03	kcal/mol				
ΔE_{Ele} =	-63.19	kcal/mol					-58.31	kcal/mol				
Initial Orientation		RS2	LS1					RS1	LS2			
Initial Orientation		RS1	LS1			RB1	LB2	RS1	LS1			RB1
		RS2				LB1						LB1
Gd^{3+} chelates 2 SO_3^- @ 5 sites							Gd^{3+} chelates 2 SO_3^- @ 6 sites					
Total =	-164.57	kcal/mol					-163.1	kcal/mol				
Van der Waals =	90.55	kcal/mol					96.3	kcal/mol				
Electrostatic =	-479.42	kcal/mol					-487.4	kcal/mol				
ΔE_{Tot} =	-67.33	kcal/mol					-65.83	kcal/mol				
ΔE_{Vdw} =	-12.58	kcal/mol					-6.80	kcal/mol				
ΔE_{Ele} =	-55.43	kcal/mol					-63.42	kcal/mol				
Initial Orientation		LS1	RS1					RS1			LS1	
Initial Orientation		LS1	RS1			RB2		RS1			LS1	
		LS2										
Gd^{3+} chelates 2 SO_3^- @ 5 sites							Gd^{3+} chelates 2 SO_3^- @ 6 sites					
Total =	-162.67	kcal/mol					-161.53	kcal/mol				
Van der Waals =	90.55	kcal/mol					99.37	kcal/mol				
Electrostatic =	-478.55	kcal/mol					-484.59	kcal/mol				
ΔE_{Tot} =	-65.42	kcal/mol					-64.28	kcal/mol				
ΔE_{Vdw} =	-12.59	kcal/mol					-3.77	kcal/mol				
ΔE_{Ele} =	-54.57	kcal/mol					-60.61	kcal/mol				

Table 6.11: Selected results of the gas phase minimization of solapsone-Gd^{3+} with the LVFF region of the 1IYT conformer of β-amyloid

	His14	Gln15	Lys16	Leu17	Val18	Phe19	Phe20	Asp23
Initial Orientation					RB1	LB1		
Final Orientation	RS1	RS1	LS1		RS1	LB1		
		LS1			RB1	LS1		
Gd^{3+} chelates 2 SO_3^- @ 5 sites and Gln15 @ 1 site								
Total =	-200.37 kcal/mol			ΔE_{Tot}	-103.13 kcal/mol			
Van der Waals =	84.01 kcal/mol			ΔE_{Vdw}	-19.12 kcal/mol			
Electrostatic =	-504.17 kcal/mol			ΔE_{Ele} =	-80.18 kcal/mol			
Initial Orientation						LB1	RB1	
Final Orientation			RB1				RB1	CS
Gd^{3+} chelates 3 SO_3^- @ 7 sites								
Total =	-139.11 kcal/mol			ΔE_{Tot}	-41.87 kcal/mol			
Van der Waals =	94.48 kcal/mol			ΔE_{Vdw}	-8.66 kcal/mol			
Electrostatic =	-461.08 kcal/mol			ΔE_{Ele} =	-37.10 kcal/mol			
Initial Orientation						RB1	LB1	
Final Orientation			RB1			CS	LB1	CS
			LB1			RB1	CS	
			CS					
			RS1					
Gd^{3+} chelates 2 SO_3^- @ 6 sites								
Total =	-136.63 kcal/mol			ΔE_{Tot}	-39.39 kcal/mol			
Van der Waals =	90.85 kcal/mol			ΔE_{Vdw}	-12.29 kcal/mol			
Electrostatic =	-451.45 kcal/mol			ΔE_{Ele} =	-27.47 kcal/mol			

	His13	Lys16	Leu17	Val18	Phe19	Phe20	Ala21	Asp23
Initial Orientation			RB2		LB2			
Final Orientation	RB2	RS2	RB2			RB2		LB2
		LS2				RS2		
Gd^{3+} chelates 2 SO_3^- @ 5 sites								
Total =	-147.55 kcal/mol			ΔE_{Tot} =	-50.30 kcal/mol			
Van der Waals =	92.24 kcal/mol			ΔE_{Vdw} =	-10.90 kcal/mol			
Electrostatic =	-471.44 kcal/mol			ΔE_{Ele} =	-47.45 kcal/mol			
Initial Orientation			RB1			LB1		
Final Orientation	RB1		RB1			LB1		
	RB2					CS		
Gd^{3+} chelates 2 SO_3^- @ 5 sites								
Total =	-136.96 kcal/mol			ΔE_{Tot} =	-39.72 kcal/mol			
Van der Waals =	88.44 kcal/mol			ΔE_{Vdw} =	-14.69 kcal/mol			
Electrostatic =	-455.31 kcal/mol			ΔE_{Ele} =	-31.33 kcal/mol			
Initial Orientation			LB1			RB1		
Final Orientation			CS			RB1	CS	
			LB1			RS1		
Gd^{3+} chelates 2 SO_3^- @ 6 sites								
Total =	-134.72 kcal/mol			ΔE_{Tot} =	-37.48 kcal/mol			
Van der Waals =	92.94 kcal/mol			ΔE_{Vdw} =	-10.20 kcal/mol			
Electrostatic =	-452.02 kcal/mol			ΔE_{Ele} =	-28.04 kcal/mol			

Table 6.12: Selected results of the gas phase minimization of solapsone-Gd^{3+} with the HHQK region of the 1Z0Q conformer of β-amyloid

	Gly9	Tyr10	His13	His14	Gln15	Lys16	Leu17
Initial Orientation				RS1		LS1	
Final Orientation	CS	CS	LB1	RS1		LS1	
Gd^{3+} chelates 2 SO_3^- @ 6 sites							
Total =	-72.10 kcal/mol			ΔE_{Tot} =	-85.39 kcal/mol		
Van der Waals =	121.54 kcal/mol			ΔE_{Vdw} =	-7.03 kcal/mol		
Electrostatic =	-484.65 kcal/mol			ΔE_{Ele} =	-79.87 kcal/mol		
Initial Orientation			RS1	LS1			
Final Orientation			RS1	LS1 LB1			CS
Gd^{3+} chelates 2 SO_3^- @ 6 sites							
Total =	-62.75 kcal/mol			ΔE_{Tot} =	-76.04 kcal/mol		
Van der Waals =	118.78 kcal/mol			ΔE_{Vdw} =	-9.79 kcal/mol		
Electrostatic =	-475.26 kcal/mol			ΔE_{Ele} =	-70.49 kcal/mol		
Initial Orientation			RS2	LS1			
Final Orientation	RS2	LS1	RS1 RB2 RS2	LS1		RS1	
Gd^{3+} chelates 2 SO_3^- @ 6 sites							
Total =	-59.70 kcal/mol			ΔE_{Tot} =	-72.98 kcal/mol		
Van der Waals =	116.27 kcal/mol			ΔE_{Vdw} =	-12.30 kcal/mol		
Electrostatic =	-473.41 kcal/mol			ΔE_{Ele} =	-68.63 kcal/mol		

	Gly9	Tyr10	His13	His14	Gln15	Lys16
Initial Orientation			LS1	RS1		
Final Orientation	LS1	LB1	LS1	RS1		
Gd^{3+} chelates 2 SO_3^- @ 4 sites						
Total =	-64.81 kcal/mol			ΔE_{Tot} =	-78.09 kcal/mol	
Van der Waals =	121.90 kcal/mol			ΔE_{Vdw} =	-6.67 kcal/mol	
Electrostatic =	-480.66 kcal/mol			ΔE_{Ele} =	-75.88 kcal/mol	
Initial Orientation				LS1		RS1
Final Orientation		LS1	RB2	LS1		RS1
Gd^{3+} chelates 2 SO_3^- @ 5 sites						
Total =	-62.6 kcal/mol			ΔE_{Tot} =	-75.84 kcal/mol	
Van der Waals =	119.0 kcal/mol			ΔE_{Vdw} =	-9.53 kcal/mol	
Electrostatic =	-474.4 kcal/mol			ΔE_{Ele} =	-69.63 kcal/mol	
Initial Orientation			LB1			RB1
Final Orientation			LS1 CS			RB1 RS1
Gd^{3+} chelates 2 SO_3^- @ 6 sites						
Total =	-47.76 kcal/mol			ΔE_{Tot} =	-61.04 kcal/mol	
Van der Waals =	121.27 kcal/mol			ΔE_{Vdw} =	-7.30 kcal/mol	
Electrostatic =	-462.81 kcal/mol			ΔE_{Ele} =	-58.03 kcal/mol	

Table 6.13: Selected results of the gas phase minimization of solapsone-Gd^{3+} with the LVFF region of the 1Z0Q conformer of β-amyloid

	Lys16	Leu17	Val18	Phe19	Phe20	His14	Lys16	Leu17	Val18	Phe19	Phe20	Ala21	Glu22
Initial Orientation		LB1		RB1				RB1	LB1				
Final Orientation	LS1	LB1		CS	CS	LS1	RS1	CS	LB1			CS	
	LB1				RB1			RB1					
	LNH												
Gd^{3+} chelates 3 SO_3^- @ 7 sites						Gd^{3+} chelates 2 SO_3^- @ 6 sites							
Total =	-62.93	kcal/mol				-47.10	kcal/mol						
Van der Waals =	115.15	kcal/mol				114.66	kcal/mol						
Electrostatic =	-476.38	kcal/mol				-452.59	kcal/mol						
ΔE_{Tot} =	-76.22	kcal/mol				-60.39	kcal/mol						
ΔE_{Vdw} =	-13.42	kcal/mol				-13.91	kcal/mol						
ΔE_{Ele} =	-71.61	kcal/mol				-47.82	kcal/mol						
Initial Orientation				LB1	RB1			LB2		RB2			
Final Orientation		RS2		RB1	RB1			LB2		RB2			
		RB2			RB2								
Gd^{3+} chelates 3 SO_3^- @ 7 sites						Gd^{3+} chelates 3 SO_3^- @ 7 sites							
Total =	-36.08	kcal/mol				-33.05	kcal/mol						
Van der Waals =	118.41	kcal/mol				122.21	kcal/mol						
Electrostatic =	-443.94	kcal/mol				-450.01	kcal/mol						
ΔE_{Tot} =	-49.36	kcal/mol				-46.33	kcal/mol						
ΔE_{Vdw} =	-10.16	kcal/mol				-6.36	kcal/mol						
ΔE_{Ele} =	-39.16	kcal/mol				-45.23	kcal/mol						
Initial Orientation				RB1	LB1			LB1	RB1				
Final Orientation		CS			LB1	RB1		LB1	CS			CS	CS
		RB1			CS							LB1	
Gd^{3+} chelates 2 SO_3^- @ 5 sites						Gd^{3+} chelates 2 SO_3^- @ 6 sites							
Total =	-29.97	kcal/mol				-23.73	kcal/mol						
Van der Waals =	119.23	kcal/mol				111.48	kcal/mol						
Electrostatic =	-442.94	kcal/mol				-427.48	kcal/mol						
ΔE_{Tot} =	-43.26	kcal/mol				-37.01	kcal/mol						
ΔE_{Vdw} =	-9.34	kcal/mol				-17.09	kcal/mol						
ΔE_{Ele} =	-38.16	kcal/mol				-22.70	kcal/mol						

Where possible, the gas phase systems selected for optimization in the solution phase had low energies, and binding interactions occurring at multiple sites within the Aβ region of interest. It can be seen that the complex can bind to β-amyloid at multiple sites within the **HH**Q**K** and LVFF regions and gadolinium can chelate solapsone at multiple sites while these interactions are occurring.

6.2.3 THE SOLUTION PHASE OPTIMIZATION OF SOLAPSONE-GD^{3+} WITH β-AMYLOID

The solution phase optimizations were performed by surrounding the gas phase system with a box of explicit water molecules. Minimization was performed with unconstrained protein backbones and periodic boundary conditions in place. Each of the optimized systems was examined for potential binding interactions, the energies were measured ignoring solvent contributions, and with a constrained protein backbone. The binding energies were calculated using equations 6.1-6.3; the energies of the solution phase optimized proteins are given in Appendix 6, and the energy of the solapsone-Gd^{3+} complex is given in the following table.

Table 6.14: The solution phase energies of solapsone-Gd^{3+}

	Energies (kcal/mol)		
	E_{tot}	E_{vdw}	E_{ele}
Solapsone -Gd^{3+}	-130.46	51.01	-210.73

6.2.4 RESULTS OF THE SOLUTION PHASE OPTIMIZATION OF SOLAPSONE-GD^{3+} WITH β-AMYLOID

The results of the Aβ-solapsone-Gd^{3+} systems geometry optimized in an aqueous environment are summarized in the following tables according to β-amyloid conformer and region of interest (**HH**Q**K** or LVFF). The measured and calculated energies for each system are given, along with the initial and final orientations of binding (amino acids are noted by their three letter abbreviations). The chelation occurring with gadolinium is also given, and the measured bonds that formed in the systems are indicated according to the following colours: orange for hydrogen bonds, green for cation-π, and blue for π-π. Darker shades indicate the formation of multiple bonds of that type. Indigo is used for

interactions occurring with the $–CH_2$- chain of the amino acid, lime green is used for the –CH- of the backbone, and yellow and purple are used for the –NH- and C=O of the backbone.

Table 6.15: The solution phase results of solapsone-Gd^{3+} interacting with the HHQK region of the 1AMB conformer of β-amyloid

	Tyr10	His13	His14	Gln15	Lys16	Leu17	Val18	Phe20
Initial Orientation		RB1			LS1	RS1		LS1
Final Orientation		RB1 LB1 RNH			LS1 LB1	RS1		LS1
Gd^{3+} chelates 2 SO_3^- @ 5 sites + 2 H_2O								
Total =	-218.65	kcal/mol						
Van der Waals =	93.07	kcal/mol						
Electrostatic =	-489.39	kcal/mol						
ΔE_{Tot} =	-96.13	kcal/mol						
ΔE_{Vdw} =	-9.82	kcal/mol						
ΔE_{Ele} =	-66.74	kcal/mol						
Initial Orientation	CS	RB1 LB1 LS1	RS1			LS1	RS2 RB2	
Final Orientation	CS	LS1	RB1			LS1		
Gd^{3+} chelates 2 SO_3^- @ 4 sites								
Total =	-234.93	kcal/mol						
Van der Waals =	85.20	kcal/mol						
Electrostatic =	-485.81	kcal/mol						
ΔE_{Tot} =	-112.41	kcal/mol						
ΔE_{Vdw} =	-17.69	kcal/mol						
ΔE_{Ele} =	-63.16	kcal/mol						
Initial Orientation	LB2	RS2 RB2 RS1	LS1 LB2 LS2		RS1	RS1 LB1	LS1	
Final Orientation	RS2	RS2 RB2 RS1	LS1 LS2 LB2			RS1 RB1	LS1	
Gd^{3+} chelates 2 SO_3^- @ 3 sites								
Total =	-233.83	kcal/mol						
Van der Waals =	74.41	kcal/mol						
Electrostatic =	-479.85	kcal/mol						
ΔE_{Tot} =	-111.31	kcal/mol						
ΔE_{Vdw} =	-28.48	kcal/mol						
ΔE_{Ele} =	-57.20	kcal/mol						

	Tyr10	His13	His14	Gln15	Lys16	Leu17	Val18	Phe20	Glu22
Initial Orientation	CS RB1		LB2				LB2		LB2
Final Orientation	CS		LB1 LB1				LB2		
Gd^{3+} chelates 2 SO_3^- @ 4 sites + 3 H_2O									
Total =	-215.96	kcal/mol							
Van der Waals =	83.65	kcal/mol							
Electrostatic =	-478.85	kcal/mol							
ΔE_{Tot} =	-93.45	kcal/mol							
ΔE_{Vdw} =	-19.24	kcal/mol							
ΔE_{Ele} =	-56.20	kcal/mol							
Initial Orientation		LB1			RB1 RS1			RS1	
Final Orientation		LB1 LNH			RB1 RS1			RS1	
Gd^{3+} chelates 2 SO_3^- @ 4 sites + 2 H_2O									
Total =	-215.20	kcal/mol							
Van der Waals =	87.94	kcal/mol							
Electrostatic =	-489.67	kcal/mol							
ΔE_{Tot} =	-92.69	kcal/mol							
ΔE_{Vdw} =	-14.95	kcal/mol							
ΔE_{Ele} =	-67.02	kcal/mol							
Initial Orientation	LS1	LS1	Gd^{3+} RS2 LS1			LB2			
Final Orientation	LS1	LS1	LS1 LS2			LS1 LB2	LB2		
Gd^{3+} chelates 1 SO_3^- @ 3 sites									
Total =	-250.55	kcal/mol							
Van der Waals =	78.59	kcal/mol							
Electrostatic =	-500.63	kcal/mol							
ΔE_{Tot} =	-128.03	kcal/mol							
ΔE_{Vdw} =	-24.30	kcal/mol							
ΔE_{Ele} =	-77.98	kcal/mol							

Table 6.16: The solution phase results of solapsone-Gd^{3+} interacting with the LVFF region of the 1AMB conformer of β-amyloid

	His13	Lys16	Leu17	Val18	Phe19	Phe20	Asp23	Val24	Lys28
Initial Orientation		LB1 LNH			CS		LB2 CS		
Final Orientation		LB1 LNH			LB1 CS	LB1 LB2	LB2 CS	LB2	
Gd^{3+} chelates 3 SO_3^- @ 6 sites + 2 H_2O									
Total =	-135.45 kcal/mol								
Van der Waals =	88.01 kcal/mol								
Electrostatic =	-476.73 kcal/mol								
ΔE_{Tot} =	-12.93 kcal/mol								
ΔE_{Vdw} =	-14.88 kcal/mol								
ΔE_{Ele} =	-54.08 kcal/mol								
Initial Orientation	RS1		RB1 RNH						LS1 LNH
Final Orientation	RS1		RB1						LS1 LNH
Gd^{3+} chelates 2 SO_3^- @ 6 sites + 1 H_2O									
Total =	-225.90 kcal/mol								
Van der Waals =	87.51 kcal/mol								
Electrostatic =	-482.70 kcal/mol								
ΔE_{Tot} =	-103.38 kcal/mol								
ΔE_{Vdw} =	-15.38 kcal/mol								
ΔE_{Ele} =	-60.05 kcal/mol								
Initial Orientation				RB2	LB2				
Final Orientation				RB2	LB2				
Gd^{3+} chelates 2 SO_3^- @ 4 sites + 1 H_2O									
Total =	-154.82 kcal/mol								
Van der Waals =	92.29 kcal/mol								
Electrostatic =	-467.83 kcal/mol								
ΔE_{Tot} =	-32.31 kcal/mol								
ΔE_{Vdw} =	-10.60 kcal/mol								
ΔE_{Ele} =	-45.18 kcal/mol								

	His13	Leu17	Val18	Phe19	Phe20	Ala21	Glu22	Gly25	Lys28
Initial Orientation	LS1	LB1			RB1				RS1
Final Orientation	LS1	LB1 LS1 CS			RB1 CS				RS1 RNH
Gd^{3+} chelates 2 SO_3^- @ 4 sites + 3 H_2O									
Total =	-231.41 kcal/mol								
Van der Waals =	82.93 kcal/mol								
Electrostatic =	-484.24 kcal/mol								
ΔE_{Tot} =	-108.90 kcal/mol								
ΔE_{Vdw} =	-19.97 kcal/mol								
ΔE_{Ele} =	-61.59 kcal/mol								
Initial Orientation			RB2		LB2	LB2			LS1
Final Orientation			RB2			LB2	RB2	LB2	LS1
Gd^{3+} chelates 2 SO_3^- @ 3 sites + 2 H_2O									
Total =	-220.27 kcal/mol								
Van der Waals =	88.94 kcal/mol								
Electrostatic =	-488.15 kcal/mol								
ΔE_{Tot} =	-97.75 kcal/mol								
ΔE_{Vdw} =	-13.95 kcal/mol								
ΔE_{Ele} =	-65.50 kcal/mol								
Initial Orientation	RB2	RB2 RS2							
Final Orientation	RB2	RB2 RS2	LB2						
Gd^{3+} chelates 2 SO_3^- @ 5 sites + 1 H_2O									
Total =	-216.83 kcal/mol								
Van der Waals =	97.34 kcal/mol								
Electrostatic =	-470.78 kcal/mol								
ΔE_{Tot} =	-94.31 kcal/mol								
ΔE_{Vdw} =	-5.56 kcal/mol								
ΔE_{Ele} =	-48.13 kcal/mol								

Table 6.17: The solution phase results of solapsone-Gd^{3+} interacting with the HHQK region of the 1AMC conformer of β-amyloid

	Tyr10	His13	His14	Gln15	Lys16	Leu17	Phe20	Tyr10	His13	His14	Gln15	Lys16	Leu17	Phe20
Initial Orientation	CS	LS1	RB1			LS1			RB2			LB2		LB1
	LB1		CS						RB2			LS2		
												RS2		
Final Orientation	LB1	LS1	RB1			LS1			RB2			LB2		LB1
	CS	LB1	LB1						RB2			LS2		
			RS1						RS2			RS2		
			CS											
Gd^{3+} chelates 2 SO_3^- @ 4 sites + 2 H_2O								Gd^{3+} chelates 3 SO_3^- @ 6 sites + 2 H_2O						
Total =	-189.11	kcal/mol						-218.76	kcal/mol					
Van der Waals =	93.59	kcal/mol						85.90	kcal/mol					
Electrostatic =	-458.63	kcal/mol						-472.52	kcal/mol					
ΔE_{Tot} =	-68.96	kcal/mol						-98.61	kcal/mol					
ΔE_{Vdw} =	-22.09	kcal/mol						-29.78	kcal/mol					
ΔE_{Ele} =	-43.86	kcal/mol						-57.75	kcal/mol					
Initial Orientation		RB2			LS1	RB2	LB2	LB2	RB2	LS2			RS2	
		RS1							RS2	LB2			LS2	
									LS2					
Final Orientation		RS1			LS1	RS2			RB2	LB2		RB2	RS2	
									RS2	LS2			LS2	
									LS2					
Gd^{3+} chelates 2 SO_3^- @ 2 sites + 3H_2O								Gd^{3+} chelates 2 SO_3^- @ 3 sites + 1 H_2O						
Total =	-188.56	kcal/mol						-230.5	kcal/mol					
Van der Waals =	97.45	kcal/mol						83.3	kcal/mol					
Electrostatic =	-464.24	kcal/mol						-512.8	kcal/mol					
ΔE_{Tot} =	-68.41	kcal/mol						-110.37	kcal/mol					
ΔE_{Vdw} =	-18.24	kcal/mol						-32.40	kcal/mol					
ΔE_{Ele} =	-49.46	kcal/mol						-98.08	kcal/mol					
Initial Orientation	RS1	RB1	RS1		LS1	LS1	LS1	RS2	LS2	RB2				
					LB1			RS1	LB2					
								LS2						
								RB2						
Final Orientation	RS1	RB1			LS1	LS1	LS1	RS2	LS1	RB2			LS2	
		RS1			LB1			RB2	LS2					
								RS1						
								LS1						
Gd^{3+} chelates 2 SO_3^- @ 4 sites + 1 H_2O								Gd^{3+} chelates 2 SO_3^- @ 3 sites						
Total =	-185.90	kcal/mol						-220.02	kcal/mol					
Van der Waals =	78.92	kcal/mol						82.54	kcal/mol					
Electrostatic =	-444.80	kcal/mol						-487.04	kcal/mol					
ΔE_{Tot} =	-65.75	kcal/mol						-99.87	kcal/mol					
ΔE_{Vdw} =	-36.76	kcal/mol						-33.14	kcal/mol					
ΔE_{Ele} =	-30.03	kcal/mol						-72.27	kcal/mol					

Table 6.18: The solution phase results of solapsone-Gd^{3+} interacting with the LVFF region of the 1AMC conformer of β-amyloid

	Gln15	Lys16	Leu17	Val18	Phe19	Phe20	Ala21	Glu22	His13	Lys16	Leu17	Val18	Phe19	Phe20	Lys28
Initial Orientation				RS2	LB2				LB2	RS2	LB2			RB2	
				RB2					RS2	RB2	RS2				
Final Orientation				RB2	LB2		RB2	LB2	LS2	RB2	LB2				
				RS2				LS2	LB2	RS2	RS2				
									RS2		LS2				
Gd^{3+} chelates 2 SO_3^- @ 5 sites + 1 site @ Glu22									Gd^{3+} chelates 3 SO_3^- @ 5 sites + 1 H_2O						
Total =	-218.82 kcal/mol								-214.91 kcal/mol						
Van der Waals =	107.43 kcal/mol								87.25 kcal/mol						
Electrostatic =	-514.19 kcal/mol								-486.99 kcal/mol						
ΔE_{Tot} =	-98.67 kcal/mol								-94.76 kcal/mol						
ΔE_{Vdw} =	-8.25 kcal/mol								-28.43 kcal/mol						
ΔE_{Ele} =	-99.42 kcal/mol								-72.22 kcal/mol						
Initial Orientation	LB1			LB1	RB1			RB1	LS1	LS1	LB2			RB1	
	CS				CS					LNH	LNH			CS	
														LB1	
Final Orientation	LB1				RB1			RB1	LS1	LS1	LB2			LB1	RB2
	CS				CS			LS2		LNH	LNH			CS	
								RS2							
Gd^{3+} chelates 2 SO_3^- @ 5 sites + 2 sites @ Glu22									Gd^{3+} chelates 2 SO_3^- @ 5 sites + 1 H_2O						
Total =	-234.87 kcal/mol								-229.24 kcal/mol						
Van der Waals =	93.30 kcal/mol								86.87 kcal/mol						
Electrostatic =	-529.51 kcal/mol								-501.00 kcal/mol						
ΔE_{Tot} =	-114.72 kcal/mol								-109.09 kcal/mol						
ΔE_{Vdw} =	-22.38 kcal/mol								-28.81 kcal/mol						
ΔE_{Ele} =	-114.74 kcal/mol								-86.23 kcal/mol						
Initial Orientation		RS1			LB1	RS1			RS1	RS1	RB1			LB2	
					RB1						RS1				
Final Orientation		RS1			LB2				RS1	RS1	RS1			LS2	LB1
					CS						RB1			LB2	
					RB1									LB1	
Gd^{3+} chelates 2 SO_3^- @ 4 sites + 1 H_2O									Gd^{3+} chelates 1 SO_3^- @ 2 sites + 4H_2O						
Total =	-213.15 kcal/mol								-202.00 kcal/mol						
Van der Waals =	80.56 kcal/mol								89.85 kcal/mol						
Electrostatic =	-484.06 kcal/mol								-476.35 kcal/mol						
ΔE_{Tot} =	-93.00 kcal/mol								-81.85 kcal/mol						
ΔE_{Vdw} =	-35.12 kcal/mol								-25.84 kcal/mol						
ΔE_{Ele} =	-69.29 kcal/mol								-61.58 kcal/mol						

Table 6.19: The solution phase results of solapsone-Gd^{3+} interacting with the HHQK region of the 1AML conformer of β-amyloid

	Tyr10	His13	His14	Gln15	Lys16	Leu17	Phe20	Val12	His13	His14	Gln15	Lys16
Initial Orientation	LB1	LB1	CS			LB1		LS2	LS1			RS1
		LS1						RS2				
		LNH										
Final Orientation	LB1	LS1	CS			CS		RS2	LS1			RS1
	LB1	LB1				LB1		LS2				
	CS	LNH										
Gd^{3+} chelates 3 SO_3^- @ 7 sites								Gd^{3+} chelates 2 SO_3^- @ 4 sites + 1H_2O				
Total =	-207.77	kcal/mol						-80.04	kcal/mol			
Van der Waals =	41.45	kcal/mol						109.77	kcal/mol			
Electrostatic =	-356.12	kcal/mol						-439.86	kcal/mol			
ΔE_{Tot} =	-231.43	kcal/mol						-103.70	kcal/mol			
ΔE_{Vdw} =	-90.24	kcal/mol						-21.92	kcal/mol			
ΔE_{Ele} =	-9.69	kcal/mol						-93.43	kcal/mol			
Initial Orientation		LS1			RS1			LS1	LS1			RB1
												LS1
												LB1
												RS1
Final Orientation		LS1			RS1				LS1			RB1
												RS1
												LS1
												LB1
Gd^{3+} chelates 2 SO_3^- @ 5 sites + 1 H_2O								Gd^{3+} chelates 2 SO_3^- @ 5 sites				
Total =	-48.94	kcal/mol						-75.3	kcal/mol			
Van der Waals =	137.61	kcal/mol						117.7	kcal/mol			
Electrostatic =	-445.33	kcal/mol						-438.8	kcal/mol			
ΔE_{Tot} =	-72.60	kcal/mol						-99.00	kcal/mol			
ΔE_{Vdw} =	5.92	kcal/mol						-14.02	kcal/mol			
ΔE_{Ele} =	-98.90	kcal/mol						-92.38	kcal/mol			
Initial Orientation					LB1		CS	RS1	RS1			LS2
					LNH		LB1					RS1
Final Orientation					LB1		CS	RS1	RS1			LS2
							LB1					RS1
Gd^{3+} chelates 2 SO_3^- @ 4 sites + 2 H_2O								Gd^{3+} chelates 2 SO_3^- @ 4 sites				
Total =	-62.85	kcal/mol						-53.04	kcal/mol			
Van der Waals =	113.75	kcal/mol						121.25	kcal/mol			
Electrostatic =	-426.12	kcal/mol						-423.96	kcal/mol			
ΔE_{Tot} =	-86.51	kcal/mol						-76.70	kcal/mol			
ΔE_{Vdw} =	-17.94	kcal/mol						-10.44	kcal/mol			
ΔE_{Ele} =	-79.69	kcal/mol						-77.53	kcal/mol			

Table 6.20: The solution phase results of solapsone-Gd^{3+} interacting with the LVFF region of the 1AML conformer of β-amyloid

	His13	Lys16	Leu17	Val18	Phe19	Phe20	Asp23	Ala30
Initial Orientation		LS1			LS1 LB2		LB2	
Final Orientation		LS1			LB2 LS1	LS1	LB2	
Gd^{3+} chelates 2 SO_3^- @ 5 sites + 1 H_2O								
Total =	-70.66 kcal/mol							
Van der Waals =	121.33 kcal/mol							
Electrostatic =	-437.88 kcal/mol							
ΔE_{Tot} =	-94.32 kcal/mol							
ΔE_{Vdw} =	-10.36 kcal/mol							
ΔE_{Ele} =	-91.44 kcal/mol							
Initial Orientation	RB2	RB2	RB2			RS2 LS2 LB2		RB2
Final Orientation	RB2	RB2	RB2			LB2 RB2 LS2 RS2	LB2	RB2
Gd^{3+} chelates 2 SO_3^- @ 4 sites								
Total =	-59.73 kcal/mol							
Van der Waals =	118.48 kcal/mol							
Electrostatic =	-435.25 kcal/mol							
ΔE_{Tot} =	-83.39 kcal/mol							
ΔE_{Vdw} =	-13.21 kcal/mol							
ΔE_{Ele} =	-88.82 kcal/mol							
Initial Orientation		RS1 RB1			RB1 CS	CS LB1	CS	
Final Orientation		RB1 RS1			CS RB1	LB1 CS	LB1 CS	
Gd^{3+} chelates 1 SO_3^- @ 2 sites + 2H_2O								
Total =	-23.53 kcal/mol							
Van der Waals =	127.86 kcal/mol							
Electrostatic =	-398.53 kcal/mol							
ΔE_{Tot} =	-47.19 kcal/mol							
ΔE_{Vdw} =	-3.83 kcal/mol							
ΔE_{Ele} =	-52.10 kcal/mol							

Table 6.21: The solution phase results of solapsone-Gd^{3+} interacting with the HHQK region of the 1BA4 conformer of β-amyloid

	Asp1	Glu3	His6	Asp7	Gly9	Tyr10	His13	His14	Gln15	Lys16	Gly9	Tyr10	His13	His14	Gln15	Lys16
Initial Orientation	LB2	LB2	LS1	LB2	LB2	RB2	RB2			LB2	RB2	LB2	LB2	LS1		
						RS2						RS2				
												RB2				
Final Orientation	LB2	LB2	LS1	LB2	LB2	RB2	RB2			LB2		LB2	LB2	LS1		
						RS2						RS2	LB2			
Gd^{3+} chelates 2 SO_3^- @ 5 sites + 1 H_2O											Gd^{3+} chelates 2 SO_3^- @ 3 sites + 1 H_2O					
Total =	-99.93 kcal/mol										-90.20 kcal/mol					
Van der Waals =	107.16 kcal/mol										119.14 kcal/mol					
Electrostatic =	-457.60 kcal/mol										-454.64 kcal/mol					
ΔE_{Tot} =	-97.78 kcal/mol										-88.06 kcal/mol					
ΔE_{Vdw} =	-25.90 kcal/mol										-13.91 kcal/mol					
ΔE_{Ele} =	-77.22 kcal/mol										-74.27 kcal/mol					
Initial Orientation						RB2	RB2	RS1		LB2			LS1	RS1		
						RS2										
Final Orientation						RB2	RS1	RS1		LB2			LS1	RS1		
						RS2	RB2							RB1		
Gd^{3+} chelates 2 SO_3^- @ 4 sites + 1H_2O											Gd^{3+} chelates 2 SO_3^- @ 5 sites + 1 H_2O					
Total =	-86.34 kcal/mol										-86.3 kcal/mol					
Van der Waals =	112.38 kcal/mol										122.3 kcal/mol					
Electrostatic =	-452.20 kcal/mol										-445.4 kcal/mol					
ΔE_{Tot} =	-84.19 kcal/mol										-84.19 kcal/mol					
ΔE_{Vdw} =	-20.68 kcal/mol										-10.75 kcal/mol					
ΔE_{Ele} =	-71.82 kcal/mol										-65.03 kcal/mol					
Initial Orientation							LS1	RS1					RS1	LS1		
								RB1					LS1			
Final Orientation							LS1	RS1					LS1	LS1		
							LS2	RB1					RS1			
Gd^{3+} chelates 2 SO_3^- @ 3 sites + 3 H_2O											Gd^{3+} chelates 2 SO_3^- @ 4 sites + 1H_2O					
Total =	-52.97 kcal/mol										-66.49 kcal/mol					
Van der Waals =	142.41 kcal/mol										134.18 kcal/mol					
Electrostatic =	-438.81 kcal/mol										-431.55 kcal/mol					
ΔE_{Tot} =	-50.82 kcal/mol										-64.34 kcal/mol					
ΔE_{Vdw} =	9.35 kcal/mol										1.12 kcal/mol					
ΔE_{Ele} =	-58.43 kcal/mol										-51.17 kcal/mol					

Table 6.22: The solution phase results of solapsone-Gd^{3+} interacting with the LVFF region of the 1BA4 conformer of β-amyloid

	His14	Gln15	Leu17	Val18	Phe19	Phe20	Glu22	His14	Gln15	Leu17	Val18	Phe19	Phe20	Glu22
Initial Orientation			RB2	LB2				LS1		LB1				
								LB1		CS				
								LNH						
Final Orientation			RB2	LB2				LS1		LB1				
								LB1		CS				
								LNH						
Gd^{3+} chelates 3 SO_3^- @ 6 sites + 1 H_2O								Gd^{3+} chelates 2 SO_3^- @ 4 sites + 1 H_2O						
Total =	-64.06 kcal/mol							-47.23 kcal/mol						
Van der Waals =	148.07 kcal/mol							123.38 kcal/mol						
Electrostatic =	-446.28 kcal/mol							-401.70 kcal/mol						
ΔE_{Tot} =	-61.92 kcal/mol							-45.09 kcal/mol						
ΔE_{Vdw} =	15.01 kcal/mol							-9.68 kcal/mol						
ΔE_{Ele} =	-65.90 kcal/mol							-21.32 kcal/mol						
Initial Orientation	LS1		LB2	LS2			RB2	LS1		RB1	LB1			
										RS1				
	LS1			LS2			RB2	LB1		RB1	LB1			
Final Orientation				RS2				LS1		RS1	CS			
										LB1				
Gd^{3+} chelates 2 SO_3^- @ 5 sites								Gd^{3+} chelates 2 SO_3^- @ 5 sites + 2 H_2O						
Total =	-95.13 kcal/mol							-109.35 kcal/mol						
Van der Waals =	124.38 kcal/mol							110.61 kcal/mol						
Electrostatic =	-455.35 kcal/mol							-458.02 kcal/mol						
ΔE_{Tot} =	-92.99 kcal/mol							-107.21 kcal/mol						
ΔE_{Vdw} =	-8.68 kcal/mol							-22.45 kcal/mol						
ΔE_{Ele} =	-74.97 kcal/mol							-77.64 kcal/mol						
Initial Orientation		CS			LB1		LS2		LB2	RB2	RS2			LB2
					CS		RS1				LS2			
Final Orientation		CS			CS		LS2		LB2	RB2	LS2			LB2
							CS				RS2			
							RS2							
							RB2							
Gd^{3+} chelates 2 SO_3^- @ 4 sites + Glu22 @ 1 site								Gd^{3+} chelates 2 SO_3^- @ 3 sites + 2 H_2O						
Total =	-87.29 kcal/mol							-19.10 kcal/mol						
Van der Waals =	235.74 kcal/mol							116.18 kcal/mol						
Electrostatic =	-420.33 kcal/mol							-373.70 kcal/mol						
ΔE_{Tot} =	-85.14 kcal/mol							-16.96 kcal/mol						
ΔE_{Vdw} =	102.68 kcal/mol							-16.88 kcal/mol						
ΔE_{Ele} =	-39.95 kcal/mol							6.68 kcal/mol						

Table 6.23: The solution phase results of solapsone-Gd^{3+} interacting with the HHQK region of the 1IYT conformer of β-amyloid

	Gly9	Tyr10	Val12	His13	His14	Gln15	Lys16	Leu17
Initial Orientation	LB2			LB2	RB1			
				LB2	CS			
				LB1				
Final Orientation	LB2	RB1	LB2	LB2	RB1			CS
		RNH		LB2	CS			
				LB1				
				CS				
Gd^{3+} chelates 3 SO_3^- @ 5 sites + 2 H_2O								
Total =	-127.87 kcal/mol							
Van der Waals =	114.23 kcal/mol							
Electrostatic =	-488.23 kcal/mol							
ΔE_{Tot} =	-52.59 kcal/mol							
ΔE_{Vdw} =	-8.41 kcal/mol							
ΔE_{Ele} =	-57.00 kcal/mol							
Initial Orientation				RS1	LS1			RB1
				RS2				LB1
Final Orientation				RS2	LS1			RB1
				RS1				LB1
Gd^{3+} chelates 2 SO_3^- @ 4 sites + 2 H_2O								
Total =	-86.38 kcal/mol							
Van der Waals =	112.68 kcal/mol							
Electrostatic =	-495.57 kcal/mol							
ΔE_{Tot} =	-11.10 kcal/mol							
ΔE_{Vdw} =	-9.96 kcal/mol							
ΔE_{Ele} =	-64.34 kcal/mol							
Initial Orientation				LS1	RS1			RB2
				LS2				
Final Orientation				Gd^{3+}	RB2			RS2
				LS2	RS1			RB2
				LS1				
				LB2				
				RS2				
Gd^{3+} chelates 2 SO_3^- @ 3 sites + 2 H_2O								
Total =	-52.97 kcal/mol							
Van der Waals =	142.41 kcal/mol							
Electrostatic =	-438.81 kcal/mol							
ΔE_{Tot} =	22.32 kcal/mol							
ΔE_{Vdw} =	19.77 kcal/mol							
ΔE_{Ele} =	-7.57 kcal/mol							

	Gly9	Tyr10	His13	His14	Gln15	Lys16	Leu17
		RS1	RB1	RS1			RB2
			LS1				
			LS2				
			RS2				
Final Orientation	RB1	RS1	LS1	RS1			RB2
			LS2				
			RB1				
Gd^{3+} chelates 2 SO_3^- @ 4 sites + 2 H_2O							
Total =	-126.68 kcal/mol						
Van der Waals =	114.09 kcal/mol						
Electrostatic =	-482.56 kcal/mol						
ΔE_{Tot} =	-51.40 kcal/mol						
ΔE_{Vdw} =	-8.55 kcal/mol						
ΔE_{Ele} =	-51.33 kcal/mol						
Initial Orientation		LB2	RS1	LS1			RB1
							LB1
Final Orientation		LS2	RS1	LS1			RB1
		LB2		LS2			
Gd^{3+} chelates 2 SO_3^- @ 5 sites + 1 H_2O							
Total =	-98.6 kcal/mol						
Van der Waals =	132.2 kcal/mol						
Electrostatic =	-477.1 kcal/mol						
ΔE_{Tot} =	-23.28 kcal/mol						
ΔE_{Vdw} =	9.53 kcal/mol						
ΔE_{Ele} =	-45.92 kcal/mol						
Initial Orientation			RS1			LS1	
Final Orientation			RS1			LS1	
Gd^{3+} chelates 2 SO_3^- @ 5 sites + 1 H_2O							
Total =	-100.56 kcal/mol						
Van der Waals =	113.09 kcal/mol						
Electrostatic =	-461.92 kcal/mol						
ΔE_{Tot} =	-25.28 kcal/mol						
ΔE_{Vdw} =	-9.55 kcal/mol						
ΔE_{Ele} =	-30.68 kcal/mol						

Table 6.24: The solution phase results of solapsone-Gd^{3+} interacting with the LVFF region of the 1IYT conformer of β-amyloid

	His14	Gln15	Lys16	Leu17	Val18	Phe19	Phe20	Asp23
Initial Orientation	RS1	RS1	LS1		RS1	LB1		
		LS1			RB1	LS1		
Final Orientation		LS2	LS1		RS1	LB1		
		LS1				LS1		
		RS2				LNH		
		RS1						
Gd^{3+} chelates 2 SO_3^- @ 4 sites + Gln15 @ 1 sites + $2H_2O$								
Total =	-127.96 kcal/mol							
Van der Waals =	109.91 kcal/mol							
Electrostatic =	-488.27 kcal/mol							
ΔE_{Tot} =	-52.68 kcal/mol							
ΔE_{Vdw} =	-12.73 kcal/mol							
ΔE_{Ele} =	-57.04 kcal/mol							
Initial Orientation			RB1				RB1	CS
Final Orientation			RB1				CS	CS
							RB1	
Gd^{3+} chelates 2 SO_3^- @ 3 sites + 2 H_2O								
Total =	-47.01 kcal/mol							
Van der Waals =	129.69 kcal/mol							
Electrostatic =	-425.91 kcal/mol							
ΔE_{Tot} =	28.28 kcal/mol							
ΔE_{Vdw} =	7.05 kcal/mol							
ΔE_{Ele} =	5.33 kcal/mol							
Initial Orientation			RB1			CS	LB1	CS
			LB1			RB1	CS	
			CS					
			RS1					
Final Orientation			RS1			RB1	CS	CS
			RB1			CS		
			CS					
Gd^{3+} chelates 1 SO_3^- @ 2 sites + $3H_2O$								
Total =	-21.05 kcal/mol							
Van der Waals =	117.69 kcal/mol							
Electrostatic =	-381.88 kcal/mol							
ΔE_{Tot} =	54.23 kcal/mol							
ΔE_{Vdw} =	-4.94 kcal/mol							
ΔE_{Ele} =	49.36 kcal/mol							

	His13	Lys16	Leu17	Val18	Phe19	Phe20	Ala21	Asp23
Initial Orientation	RB2	RS2	RB2			RB2		LB2
		LS2				RS2		
Final Orientation		RB2	RB2			RB2		LB2
		RS2				RS2		
						LS2		
Gd^{3+} chelates 2 SO_3^- @ 5 sites								
Total =	-82.28 kcal/mol							
Van der Waals =	106.56 kcal/mol							
Electrostatic =	-499.21 kcal/mol							
ΔE_{Tot} =	-7.00 kcal/mol							
ΔE_{Vdw} =	-16.08 kcal/mol							
ΔE_{Ele} =	-67.98 kcal/mol							
Initial Orientation	RB1		RB1			LB1		
	RB2					CS		
Final Orientation	RB2		RB1			LB1		
	RB1					CS		
	RNH							
Gd^{3+} chelates 2 SO_3^- @ 4 sites + 2 H_2O								
Total =	-34.86 kcal/mol							
Van der Waals =	130.54 kcal/mol							
Electrostatic =	-471.42 kcal/mol							
ΔE_{Tot} =	40.42 kcal/mol							
ΔE_{Vdw} =	7.90 kcal/mol							
ΔE_{Ele} =	-40.19 kcal/mol							
Initial Orientation			CS			RB1	CS	
			LB1			RS1		
Final Orientation			LS1			RB1	CS	
			LB1			RS1		
			CS					
			RB1					
Gd^{3+} chelates 2 SO_3^- @ 6 sites + 2 H_2O								
Total =	-13.72 kcal/mol							
Van der Waals =	132.45 kcal/mol							
Electrostatic =	-454.47 kcal/mol							
ΔE_{Tot} =	61.57 kcal/mol							
ΔE_{Vdw} =	9.81 kcal/mol							
ΔE_{Ele} =	-23.24 kcal/mol							

Table 6.25: The solution phase results of solapsone-Gd^{3+} interacting with the HHQK region of the 1Z0Q conformer of β-amyloid

	Gly9	Tyr10	His13	His14	Gln15	Lys16	Leu17	Gly9	Tyr10	His13	His14	Gln15	Lys16	Leu17
Initial Orientation	CS	CS	LB1	RS1		LS1		LS1	LB1	LS1	RS1			
Final Orientation		CS	LB1	RS1		LS1		LS1	CS	LS1	RS1			
			CS						LB1					
Gd^{3+} chelates 2 SO_3^- @ 4 sites + 2 H_2O								Gd^{3+} chelates 2 SO_3^- @ 3 sites + 2 H_2O						
Total =	-39.54 kcal/mol							-86.70 kcal/mol						
Van der Waals =	105.47 kcal/mol							113.23 kcal/mol						
Electrostatic =	-472.05 kcal/mol							-464.94 kcal/mol						
ΔE_{Tot} =	-46.11 kcal/mol							-93.28 kcal/mol						
ΔE_{Vdw} =	-22.79 kcal/mol							-15.04 kcal/mol						
ΔE_{Ele} =	-88.13 kcal/mol							-81.02 kcal/mol						
Initial Orientation			RS1	LS1			CS		LS1	RB2	LS1		RS1	
				LB1										
Final Orientation	RS1		RS1	LS1			CS	LS1	LS1	RB2	LS1		RS1	CS
Gd^{3+} chelates 2 SO_3^- @ 4 sites + 2 H_2O								Gd^{3+} chelates 2 SO_3^- @ 4 sites + 1H_2O						
Total =	-138.20 kcal/mol							-88.9 kcal/mol						
Van der Waals =	101.63 kcal/mol							130.2 kcal/mol						
Electrostatic =	-485.00 kcal/mol							-479.1 kcal/mol						
ΔE_{Tot} =	-144.77 kcal/mol							-95.42 kcal/mol						
ΔE_{Vdw} =	-26.64 kcal/mol							1.89 kcal/mol						
ΔE_{Ele} =	-101.08 kcal/mol							-95.21 kcal/mol						
Initial Orientation	RS2	LS1	RS1	LS1		RS1				LS1			RB1	
			RB2							CS			RS1	
			RS2											
Final Orientation		LS1	RS1	LS1		RS1				LS1			RS1	
			RS2							LB1			RB1	
										CS				
Gd^{3+} chelates 2 SO_3^- @ 6 sites + 1 H_2O								Gd^{3+} chelates 2 SO_3^- @ 3 sites + 2 H_2O						
Total =	-80.00 kcal/mol							-95.61 kcal/mol						
Van der Waals =	121.45 kcal/mol							118.61 kcal/mol						
Electrostatic =	-473.46 kcal/mol							-453.28 kcal/mol						
ΔE_{Tot} =	-86.57 kcal/mol							-102.18 kcal/mol						
ΔE_{Vdw} =	-6.82 kcal/mol							-9.66 kcal/mol						
ΔE_{Ele} =	-89.55 kcal/mol							-69.36 kcal/mol						

Table 6.26: The solution phase results of solapsone-Gd^{3+} interacting with the LVFF region of the 1Z0Q conformer of β-amyloid

	Lys16	Leu17	Val18	Phe19	Phe20	His14	Lys16	Leu17	Val18	Phe19	Phe20	Ala21	Glu22
Initial Orientation	LS1	LB1		CS	CS	LS1	RS1	CS	LB1			CS	
	LB1				RB1			RB1					
	LNH												
Final Orientation	LS1	CS		CS	RB1	LS1		CS	CS			LB1	
	CS	LB1			CS	RNH		RB1				CS	
	LB1												
	LNH												
Gd^{3+} chelates 3 SO_3^- @ 5 sites						Gd^{3+} chelates 2 SO_3^- @ 3 sites + 1 H_2O							
Total =	-105.95 kcal/mol					-89.80 kcal/mol							
Van der Waals =	106.34 kcal/mol					93.80 kcal/mol							
Electrostatic =	-468.66 kcal/mol					-443.33 kcal/mol							
ΔE_{Tot} =	-112.52 kcal/mol					-96.37 kcal/mol							
ΔE_{Vdw} =	-21.93 kcal/mol					-34.47 kcal/mol							
ΔE_{Ele} =	-84.74 kcal/mol					-59.42 kcal/mol							
Initial Orientation		RS2		RB1	RB1			LB2		RB2			
		RB2			RB2								
Final Orientation		RS2		RS2	RB2			RS2		RB2			
		RB2		RB1	RB1					RS2			
				CS	RNH								
Gd^{3+} chelates 3 SO_3^- @ 6 sites						Gd^{3+} chelates 3 SO_3^- @ 5 sites + 1H_2O							
Total =	-72.60 kcal/mol					-21.72 kcal/mol							
Van der Waals =	105.06 kcal/mol					103.68 kcal/mol							
Electrostatic =	-453.66 kcal/mol					-396.89 kcal/mol							
ΔE_{Tot} =	-79.17 kcal/mol					-28.29 kcal/mol							
ΔE_{Vdw} =	-23.20 kcal/mol					-24.59 kcal/mol							
ΔE_{Ele} =	-69.74 kcal/mol					-12.98 kcal/mol							
Initial Orientation		CS			LB1	RB1		LB1	CS			CS	CS
		RB1			CS							LB1	
Final Orientation	RB1	CS		CS	LB1	RB1		LS1	LB1				CS
		RB1		RB1	CS	LB1			CS				
						RNH							
Gd^{3+} chelates 2 SO_3^- @ 4 sites + 3H_2O						Gd^{3+} chelates 2 SO_3^- @ 6 sites + 1 H_2O							
Total =	-31.47 kcal/mol					-61.96 kcal/mol							
Van der Waals =	113.37 kcal/mol					117.61 kcal/mol							
Electrostatic =	-402.15 kcal/mol					-435.34 kcal/mol							
ΔE_{Tot} =	-38.04 kcal/mol					-68.53 kcal/mol							
ΔE_{Vdw} =	-14.90 kcal/mol					-10.65 kcal/mol							
ΔE_{Ele} =	-18.23 kcal/mol					-51.43 kcal/mol							

The solution phase optimized systems of β-amyloid and solapsone-Gd^{3+} showed binding could occur between the complex and the **HH**Q**K** and LVFF regions of interest. The orientation of the interactions tended to remain the same as in the gas phase system, and gadolinium was still capable of chelating to solapsone in the presence of water, and

even interacted with the protein in some instances. An example of the binding interactions can be seen in Figure 6.6, with the water molecules removed except for those interacting with gadolinium. The electrostatic energies are more favourable than the van der Waals energies of the systems. Binding occurs preferentially at His13-His14, followed by His13-Lys16 in the **HH**Q**K** region, while Leu17-Phe20, Phe19-Phe20, and Leu17-Val18 are favoured in the LVFF region.

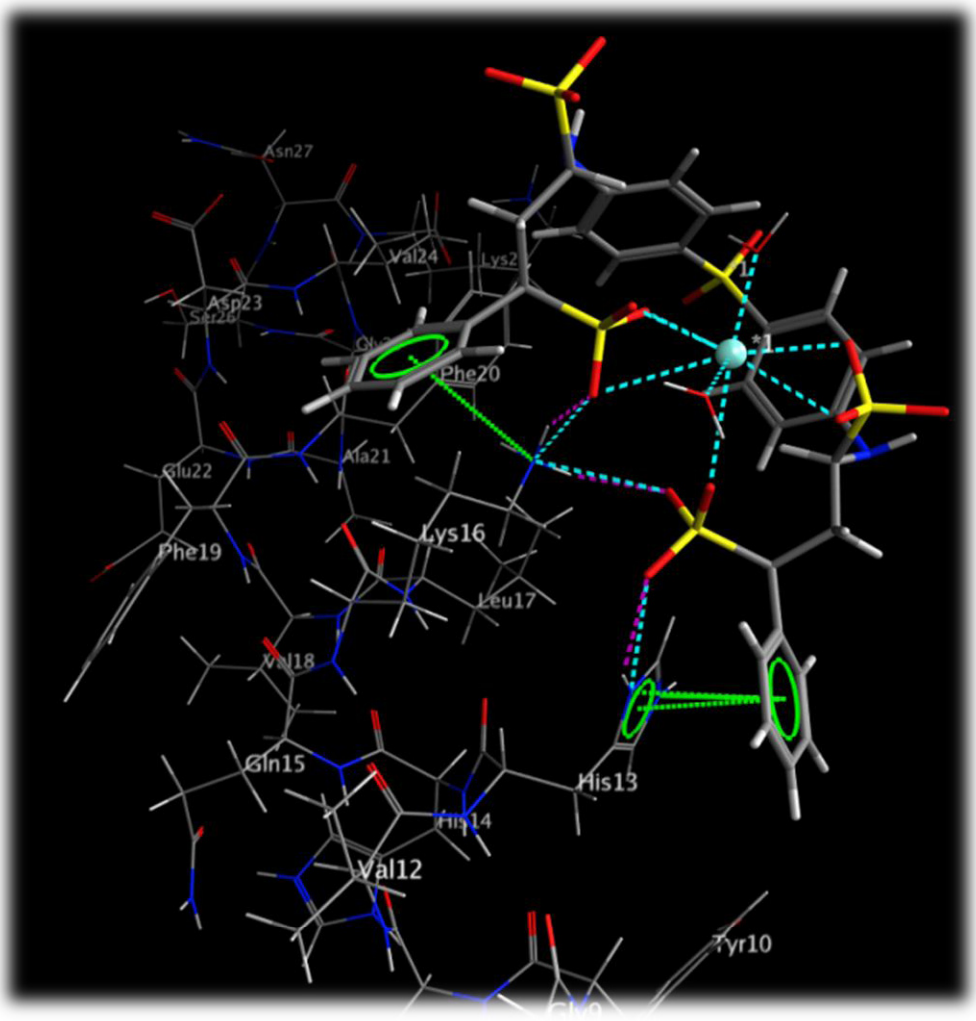

Figure 6.6: Solution phase interactions between the chelated solapsone-Gd^{3+} complex and β-amyloid. Dashed green lines indicate the formation of aromatic-aromatic and cation-aromatic interactions. Dashed purple lines represent the formation of hydrogen bonds, and dashed blue lines indicate metal-ligation interactions.

6.3 SOLAPSONE AS AN AMYLOID ANTI-AGGREGANT

Given the success of solapsone-Gd^{3+} binding to β-amyloid, solapsone was examined by itself as a potential inhibitor of Aβ aggregations. Both gas phase and solution phase optimizations were performed to determine solapsone's ability to bind to the β-amyloid protein.

6.3.1 GAS PHASE OPTIMIZATIONS OF SOLAPSONE WITH β-AMYLOID

Gas phase minimizations were performed for solapsone interacting with five different conformers of Aβ (the 1AMB and 1AMC conformers are nearly identical, so only one was used) using the CHARMM22 force field in the Molecular Operating Environment [48, 87]. Each system was set up such that a combination of two of the functional groups on solapsone were oriented towards two of the amino acid side chains on Aβ in one of three regions: **HH**Q**K**, LVFF and overlapping both **HH**Q**K** and LVFF. The functional groups were selected such that a combination of one group from each half of the molecule was selected, or one group from the side along with the central SO_2 group.

For these optimizations, the lowest energy structure identified from the systematic conformational search performed in section 6.1.1 was selected for use. The energies of the Aβ conformers, measured with a constrained protein backbone, are given in Appendix 6, and the energies of the optimized solapsone molecule are given in the following table.

Table 6.27: The gas phase energies of solapsone

	Energies (kcal/mol)		
	E_{tot}	E_{vdw}	E_{ele}
Solapsone	81.13	40.56	20.81

Using these energies, equations 6.4-6.6 were used to calculate the binding energies for the optimized systems.

$$\Delta E_{tot} = E_{tot} - E_{A\beta} - E_{Solapsone} \quad (6.4)$$

$$\Delta E_{vdw} = E_{vdw} - E_{vdwA\beta} - E_{vdwSolapsone} \quad (6.5)$$

$$\Delta E_{ele} = E_{ele} - E_{eleA\beta} - E_{eleSolapsone} \quad (6.6)$$

The total, ΔE_{tot}, van der Waals, ΔE_{vdw}, and electrostatic energies, ΔE_{ele}, were calculated by subtracting the energies of the individually optimized Aβ proteins and the solapsone molecule from the energies of the minimized protein-solapsone systems.

6.3.2 Results of the Gas Phase Optimization of Solapsone and β-Amyloid

The minimization of solapsone with five different conformations of β-amyloid resulted in a massive number of systems. From these systems, one fifth of the results for each of the three regions of Aβ were selected for solution phase optimizations, these are summarized in the following tables. Each table shows the initial and final orientation of solapsone, with the functional groups identified according to Figure 6.4. The amino acids are represented by their three letter abbreviations, and the different binding interactions are noted by colour: orange, green and blue are used for hydrogen bonds, cation-π, and π-π interactions; yellow, purple and lime green are used for interactions with the –NH-, C=O, and –CH- of the protein backbone; indigo is used for interactions occurring with the $–CH_2$- chain of the amino acids.

Table 6.28: The gas phase results of solapsone interacting with the HHQK region of the 1AMB conformer of β-amyloid

	His6	Gly9	Tyr10	His13	His14	Gln15	Lys16	Leu17	Phe20	Lys28
Initial Orientation				LB1			RS1			
Final Orientation	LS2	LS1	LS1	RB1			RS1	RS1	RS1	
	LS1			LB1			RS2			
	LB2			LS1						
Total =	-86.46 kcal/mol			ΔE_{Tot} =	-155.80 kcal/mol					
Van der Waals =	75.57 kcal/mol			ΔE_{Vdw} =	-20.27 kcal/mol					
Electrostatic =	-327.17 kcal/mol			ΔE_{Ele} =	-136.28 kcal/mol					
Initial Orientation				LS1			RB1			
Final Orientation			LB2	LB1	LS1		RS1	RS1	RS1	
				LS1			RS2	LB1		
				LS2				LS1		
Total =	-85.25 kcal/mol			ΔE_{Tot} =	-154.59 kcal/mol					
Van der Waals =	74.78 kcal/mol			ΔE_{Vdw} =	-21.06 kcal/mol					
Electrostatic =	-328.79 kcal/mol			ΔE_{Ele} =	-137.90 kcal/mol					
Initial Orientation				RB1			LS2			
Final Orientation			RS1	LS1	RS2		LS2		LB2	
			RS2	RB1			LS1			
				RNH						
				RS2						
Total =	-81.42 kcal/mol			ΔE_{Tot} =	-150.77 kcal/mol					
Van der Waals =	77.39 kcal/mol			ΔE_{Vdw} =	-18.45 kcal/mol					
Electrostatic =	-330.03 kcal/mol			ΔE_{Ele} =	-139.14 kcal/mol					
Initial Orientation				LB1			CS			
Final Orientation				LS1			LB1	RS1	RB1	RS2
							LS1		RS2	
							LS2		RS1	
Total =	-67.71 kcal/mol			ΔE_{Tot} =	-137.05 kcal/mol					
Van der Waals =	74.67 kcal/mol			ΔE_{Vdw} =	-21.17 kcal/mol					
Electrostatic =	-311.42 kcal/mol			ΔE_{Ele} =	-120.53 kcal/mol					
Initial Orientation				RS2			LS2			
Final Orientation				RS2			LS2	RS2	LB2	
				RS1			LS1		LS2	
Total =	-64.12 kcal/mol			ΔE_{Tot} =	-133.46 kcal/mol					
Van der Waals =	81.84 kcal/mol			ΔE_{Vdw} =	-14.00 kcal/mol					
Electrostatic =	-312.53 kcal/mol			ΔE_{Ele} =	-121.63 kcal/mol					

	His6	Gly9	Tyr10	His13	His14	Gln15	Lys16	Leu17	Phe20
Initial Orientation				CS			LS1		
Final Orientation	RS1	RS1	RS1	RB1			LS1	LS2	LS2
				LB1				LS1	LS1
				RNH				LB1	
				RS1					
Total =	-70.53 kcal/mol			ΔE_{Tot} =	-139.87 kcal/mol				
Van der Waals =	74.46 kcal/mol			ΔE_{Vdw} =	-21.38 kcal/mol				
Electrostatic =	-323.94 kcal/mol			ΔE_{Ele} =	-133.04 kcal/mol				
Initial Orientation				RB1			LB1		
Final Orientation		RS1	RS1	RB1			LS1		
				CS			LS2		
				RS2			RB1		
				RS1			CS		
Total =	-66.62 kcal/mol			ΔE_{Tot} =	-135.96 kcal/mol				
Van der Waals =	77.33 kcal/mol			ΔE_{Vdw} =	-18.51 kcal/mol				
Electrostatic =	-315.20 kcal/mol			ΔE_{Ele} =	-124.31 kcal/mol				
Initial Orientation				RS1			LB1		
Final Orientation			RB2	RS2			LS2	CS	LB1
				RS1			LB2	LB1	LNH
				RB1					LS1
									LB2
Total =	-62.14 kcal/mol			ΔE_{Tot} =	-131.48 kcal/mol				
Van der Waals =	77.90 kcal/mol			ΔE_{Vdw} =	-17.94 kcal/mol				
Electrostatic =	-316.21 kcal/mol			ΔE_{Ele} =	-125.32 kcal/mol				
Initial Orientation					RB2		LB2		
Final Orientation			RS2	LB1	RB2		LB2	LS2	LB2
				LS2			LS2	LB1	
				LS1					
Total =	-60.38 kcal/mol			ΔE_{Tot} =	-129.72 kcal/mol				
Van der Waals =	73.27 kcal/mol			ΔE_{Vdw} =	-22.57 kcal/mol				
Electrostatic =	-306.12 kcal/mol			ΔE_{Ele} =	-115.23 kcal/mol				
Initial Orientation				CS			RB1		
Final Orientation			LB2	LB1	LS1		RS1	RB1	RS1
			LS2	LS1					
				CS					
Total =	-62.55 kcal/mol			ΔE_{Tot} =	-131.89 kcal/mol				
Van der Waals =	79.22 kcal/mol			ΔE_{Vdw} =	-16.62 kcal/mol				
Electrostatic =	-313.27 kcal/mol			ΔE_{Ele} =	-122.38 kcal/mol				

Table 6.29: The gas phase results of solapsone interacting with the LVFF region of the 1AMB conformer of β-amyloid

	Val12	His13	His14	Gln15	Lys16	Leu17	Val18	Phe19	Phe20
Initial Orientation								RB1	LB1
Final Orientation	RS1	LS1		RS1	RS2			RS1	LB1
					RB1			RB1	LNH
					RS1			CS	
					LB1				
					LS1				
					LS2				
Total =	-59.60 kcal/mol			ΔE_{Tot} =	-128.94 kcal/mol				
Van der Waals =	68.57 kcal/mol			ΔE_{Vdw} =	-27.27 kcal/mol				
Electrostatic =	-303.53 kcal/mol			ΔE_{Ele} =	-112.63 kcal/mol				
Initial Orientation						RB2	LB2		
Final Orientation			LB2						
			LB2						
Total =	22.73 kcal/mol			ΔE_{Tot} =	-46.61 kcal/mol				
Van der Waals =	86.93 kcal/mol			ΔE_{Vdw} =	-8.91 kcal/mol				
Electrostatic =	-235.18 kcal/mol			ΔE_{Ele} =	-44.29 kcal/mol				
Initial Orientation								LB2	RB2
Final Orientation		RS2			LS2	RS2		LB2	RS2
					LNH	RB2			
					LB1				
					RS2				
Total =	-52.56 kcal/mol			ΔE_{Tot} =	-121.90 kcal/mol				
Van der Waals =	79.19 kcal/mol			ΔE_{Vdw} =	-16.65 kcal/mol				
Electrostatic =	-297.39 kcal/mol			ΔE_{Ele} =	-106.50 kcal/mol				

	His13	Lys16	Leu17	Val18	Phe19	Phe20	Val24	Lys28
Initial Orientation			LB2			RB2		
Final Orientation	LS2	LS1	LB2			RS2	RB2	RS2
	LS1					RB2		
Total =	-56.08 kcal/mol			ΔE_{Tot} =	-125.42 kcal/mol			
Van der Waals =	77.35 kcal/mol			ΔE_{Vdw} =	-18.49 kcal/mol			
Electrostatic =	-308.00 kcal/mol			ΔE_{Ele} =	-117.10 kcal/mol			
Initial Orientation			LB1			RB1		
Final Orientation	LS2	LS2	LS1			CS		RS1
	LS1	LS1				RB1		
		LB1						
Total =	-52.87 kcal/mol			ΔE_{Tot} =	-122.21 kcal/mol			
Van der Waals =	83.57 kcal/mol			ΔE_{Vdw} =	-12.27 kcal/mol			
Electrostatic =	-308.18 kcal/mol			ΔE_{Ele} =	-117.28 kcal/mol			
Initial Orientation			LB2			RB1		
Final Orientation		RS2	LB2			LS2		LS1
						LB1		LS2
						RB1		
Total =	-51.46 kcal/mol			ΔE_{Tot} =	-120.80 kcal/mol			
Van der Waals =	84.51 kcal/mol			ΔE_{Vdw} =	-11.33 kcal/mol			
Electrostatic =	-305.46 kcal/mol			ΔE_{Ele} =	-114.57 kcal/mol			

Table 6.30: The gas phase results of solapsone interacting with the HHQKLVFF region of the 1AMB conformer of β-amyloid

	Gly9	Tyr10	His13	His14	Gln15	Lys16	Leu17	Val18	Phe19	Phe20	Ala21	Val24	Gly25	Lys28
Initial Orientation			RB1				LB1							
Final Orientation	RS2	RS2	RB1				LB1			LS1				LS2
			RS1											
			RS2											
Total =	-83.43 kcal/mol			ΔE_{Tot} =	-152.77 kcal/mol									
Van der Waals =	75.19 kcal/mol			ΔE_{Vdw} =	-20.65 kcal/mol									
Electrostatic =	-329.61 kcal/mol			ΔE_{Ele} =	-138.71 kcal/mol									
Initial Orientation			RS2				LB2							
Final Orientation	RB2		RB1			RS2	LS2			LS2	LS2		LB2	LS1
			RB2								LB2			LB2
			RNH											
Total =	-74.11 kcal/mol			ΔE_{Tot} =	-143.45 kcal/mol									
Van der Waals =	72.86 kcal/mol			ΔE_{Vdw} =	-22.98 kcal/mol									
Electrostatic =	-318.46 kcal/mol			ΔE_{Ele} =	-127.57 kcal/mol									
Initial Orientation			LS1				RB1							
Final Orientation		LS1	LS1							RS1				RS2
			LS2											RS1
Total =	-72.21 kcal/mol			ΔE_{Tot} =	-141.55 kcal/mol									
Van der Waals =	79.44 kcal/mol			ΔE_{Vdw} =	-16.40 kcal/mol									
Electrostatic =	-323.23 kcal/mol			ΔE_{Ele} =	-132.34 kcal/mol									
Initial Orientation			LB1				RB1							
Final Orientation		LS1	LB1				RB1			RS1	RS1			RS1
			LS1											RS2
			LS2											
Total =	-70.35 kcal/mol			ΔE_{Tot} =	-139.69 kcal/mol									
Van der Waals =	76.49 kcal/mol			ΔE_{Vdw} =	-19.34 kcal/mol									
Electrostatic =	-315.76 kcal/mol			ΔE_{Ele} =	-124.87 kcal/mol									
Initial Orientation			RB2							LB2				
Final Orientation		RB2	RS2	RS2		LS2	RS2			LB1				
			RS1			LB1	RB1			LS1				
						LNH	LB1							
Total =	-68.31 kcal/mol			ΔE_{Tot} =	-137.65 kcal/mol									
Van der Waals =	73.38 kcal/mol			ΔE_{Vdw} =	-22.46 kcal/mol									
Electrostatic =	-309.77 kcal/mol			ΔE_{Ele} =	-118.88 kcal/mol									
Initial Orientation			LS2							RB1				
Final Orientation			LS1			LS2	LS2			CS				RS1
			LS2				LS1			RS2				
							LB1							
Total =	-64.80 kcal/mol			ΔE_{Tot} =	-134.14 kcal/mol									
Van der Waals =	78.01 kcal/mol			ΔE_{Vdw} =	-17.83 kcal/mol									
Electrostatic =	-314.12 kcal/mol			ΔE_{Ele} =	-123.23 kcal/mol									

Table 6.30: The gas phase results of solapsone interacting with the HHQKLVFF region of the 1AMB conformer of β-amyloid

	Gly9	Tyr10	His13	His14	Gln15	Lys16	Leu17	Val18	Phe19	Phe20	Ala21	Val24	Lys28
Initial Orientation				LS2			RB1						
Final Orientation		LB2	LS2	LS2			RS2			RS2		CS	RS1
							CS						RS2
							LB1						
Total =	-62.36 kcal/mol			ΔE_{Tot} =	-131.70 kcal/mol								
Van der Waals =	77.45 kcal/mol			ΔE_{Vdw} =	-18.39 kcal/mol								
Electrostatic =	-308.69 kcal/mol			ΔE_{Ele} =	-117.80 kcal/mol								
Initial Orientation			LB1							RB2			
Final Orientation	LS1	LS1	LB1			LB2	RNH			RB2			
			RB1			RS1	RB1			RS1			
			LB1			RNH							
			LNH			RB1							
			LS1										
Total	-62.08 kcal/mol			ΔE_{Tot} =	-131.42 kcal/mol								
Van der Waals	71.44 kcal/mol			ΔE_{Vdw} =	-24.40 kcal/mol								
Electrostatic	-305.99 kcal/mol			ΔE_{Ele} =	-115.10 kcal/mol								
Initial Orientation			RS1				LB1						
Final Orientation		RS1	RB2	RS1			LS1			LS1			LS2
		RS2	RB2				LB1						
			RNH										
			RS1										
Total	-59.01 kcal/mol			ΔE_{Tot} =	-128.35 kcal/mol								
Van der Waals	70.65 kcal/mol			ΔE_{Vdw} =	-25.19 kcal/mol								
Electrostatic	-300.95 kcal/mol			ΔE_{Ele} =	-110.06 kcal/mol								
Initial Orientation			RB1							LB2			
Final Orientation			RB2			RB2	LS1			LS1			LS2
			RS1							LB2			
			RNH										LB2
			RB1										
Total	-55.20 kcal/mol			ΔE_{Tot} =	-124.54 kcal/mol								
Van der Waals	76.56 kcal/mol			ΔE_{Vdw} =	-19.28 kcal/mol								
Electrostatic	-310.76 kcal/mol			ΔE_{Ele} =	-119.86 kcal/mol								
Initial Orientation			LS2				RB2						
Final Orientation			LS2	RS2		LS2	RB1	RS2			RB2		
			LB1			LNH	RS2	RB2					
						LB1	RB2						
Total	-54.86 kcal/mol			ΔE_{Tot} =	-124.20 kcal/mol								
Van der Waals	80.19 kcal/mol			ΔE_{Vdw} =	-15.65 kcal/mol								
Electrostatic	-303.44 kcal/mol			ΔE_{Ele} =	-112.55 kcal/mol								
Initial Orientation			LS2					RB1					
Final Orientation			LS2	RS2		LS2	RB1	RS2					
			LB1			LNH	RS2						
						LB2							
Total	-54.79 kcal/mol			ΔE_{Tot} =	-124.13 kcal/mol								
Van der Waals	84.03 kcal/mol			ΔE_{Vdw} =	-11.81 kcal/mol								
Electrostatic	-309.00 kcal/mol			ΔE_{Ele} =	-118.11 kcal/mol								

Table 6.30: The gas phase results of solapsone interacting with the HHQKLVFF region of the 1AMB conformer of β-amyloid

	Gly9	Tyr10	Val12	His13	His14	Gln15	Lys16	Leu17	Val18	Phe19	Phe20	Ala21	Val24	Lys28
Initial Orientation				CS				RB1						
Final Orientation				LB1			LS2	RS2			RS2			RB2
				LS1				RB1						
Total =	-78.98 kcal/mol			ΔE_{Tot} =	-148.32 kcal/mol									
Van der Waals =	77.21 kcal/mol			ΔE_{Vdw} =	-18.63 kcal/mol									
Electrostatic =	-323.94 kcal/mol			ΔE_{Ele} =	-133.05 kcal/mol									
Initial Orientation							RS2	LB2						
Final Orientation				RB2			RS2	RB1			LS2			LS1
				RS1			RB1							LS2
				RNH										
Total =	-73.59 kcal/mol			ΔE_{Tot} =	-142.93 kcal/mol									
Van der Waals =	71.76 kcal/mol			ΔE_{Vdw} =	-24.08 kcal/mol									
Electrostatic =	-314.61 kcal/mol			ΔE_{Ele} =	-123.72 kcal/mol									
Initial Orientation				LB2				RB2						
Final Orientation	LB2	LB2		LB2			LB1	RB2			RS1	RB2		RS1
				LB1			LNH				RNH			
				LNH			LS1							
Total =	-71.30 kcal/mol			ΔE_{Tot} =	-140.64 kcal/mol									
Van der Waals =	69.88 kcal/mol			ΔE_{Vdw} =	-25.95 kcal/mol									
Electrostatic =	-309.26 kcal/mol			ΔE_{Ele} =	-118.37 kcal/mol									
Initial Orientation							LS1	RB1						
Final Orientation				LS1			LS2	LS1			LB1			RS2
							LS1				CS			RS1
Total =	-69.14 kcal/mol			ΔE_{Tot} =	-138.48 kcal/mol									
Van der Waals =	78.19 kcal/mol			ΔE_{Vdw} =	-17.65 kcal/mol									
Electrostatic =	-317.42 kcal/mol			ΔE_{Ele} =	-126.53 kcal/mol									
Initial Orientation							RB1	LB2						
Final Orientation				RB2			RS2	LS2			LS2			LS1
														LS2
Total =	-68.14 kcal/mol			ΔE_{Tot} =	-137.48 kcal/mol									
Van der Waals =	77.03 kcal/mol			ΔE_{Vdw} =	-18.81 kcal/mol									
Electrostatic =	-315.12 kcal/mol			ΔE_{Ele} =	-124.22 kcal/mol									
Initial Orientation				LS2							RB2			
Final Orientation				LS2			LB1	LB1			RB2		RB2	RS2
				LS1			LS2				RS2		RS2	RB2
											RB1			
											CS			
Total =	-63.76 kcal/mol			ΔE_{Tot} =	-133.10 kcal/mol									
Van der Waals =	72.92 kcal/mol			ΔE_{Vdw} =	-22.92 kcal/mol									
Electrostatic =	-306.56 kcal/mol			ΔE_{Ele} =	-115.67 kcal/mol									

Table 6.30: The gas phase results of solapsone interacting with the HHQKLVFF region of the 1AMB conformer of β-amyloid

	Gly9	His13	His14	Gln15	Lys16	Leu17	Val18	Phe19	Phe20	Lys28
Initial Orientation					CS				LB1	
Final Orientation		RS1			RB1				CS	LS2
		RS2			RS2				LB1	
					CS				LS2	
					RS1					
Total =	-62.21 kcal/mol			ΔE_{Tot} =	-131.55 kcal/mol					
Van der Waals =	78.29 kcal/mol			ΔE_{Vdw} =	-17.55 kcal/mol					
Electrostatic =	-312.41 kcal/mol			ΔE_{Ele} =	-121.52 kcal/mol					
Initial Orientation		LS1							RB1	
Final Orientation		LB2			LS1	LS1			CS	RS2
		LS2			LS2					RS1
		LS1								
Total =	-59.24 kcal/mol			ΔE_{Tot} =	-128.58 kcal/mol					
Van der Waals =	82.18 kcal/mol			ΔE_{Vdw} =	-13.66 kcal/mol					
Electrostatic =	-312.37 kcal/mol			ΔE_{Ele} =	-121.48 kcal/mol					
Initial Orientation					RB2				LB1	
Final Orientation	RB2	RB2			RB1	RS1			CS	
		RS1			LS2					
					LB1					
Total =	-56.67 kcal/mol			ΔE_{Tot} =	-126.02 kcal/mol					
Van der Waals =	77.54 kcal/mol			ΔE_{Vdw} =	-18.30 kcal/mol					
Electrostatic =	-305.97 kcal/mol			ΔE_{Ele} =	-115.08 kcal/mol					
Initial Orientation		CS							LB2	
Final Orientation		RS2	RS2		LS2	RB2	RB2		LB2	
		LB1							LS2	
		CS								
		RB1								
Total =	-55.19 kcal/mol			ΔE_{Tot} =	-124.53 kcal/mol					
Van der Waals =	79.66 kcal/mol			ΔE_{Vdw} =	-16.18 kcal/mol					
Electrostatic =	-305.54 kcal/mol			ΔE_{Ele} =	-114.65 kcal/mol					
Initial Orientation		RS1							LB1	
Final Orientation		RS1			RS1	RS1			LS1	LS1
		RS2							LB1	
Total =	-54.44 kcal/mol			ΔE_{Tot} =	-123.78 kcal/mol					
Van der Waals =	85.48 kcal/mol			ΔE_{Vdw} =	-10.36 kcal/mol					
Electrostatic =	-306.72 kcal/mol			ΔE_{Ele} =	-115.82 kcal/mol					
Initial Orientation		RS2							LB2	
Final Orientation		RS2			RS2	RS2			LS2	
		RS1			LS1				LB2	
Total =	-62.47 kcal/mol			ΔE_{Tot} =	-131.81 kcal/mol					
Van der Waals =	82.02 kcal/mol			ΔE_{Vdw} =	-13.82 kcal/mol					
Electrostatic =	-121.07 kcal/mol			ΔE_{Ele} =	69.82 kcal/mol					

Table 6.31: The gas phase results of solapsone interacting with the HHQK region of the 1AML conformer of β-amyloid

	Ser8	Tyr10	Val12	His13	His14	Gln15	Ly16	Leu17	Val18	Phe20	Ala21	Ile31
Initial Orientation				LS2	RS2							
Final Orientation	RS2	LS1		LS2	RS2			LS2				LB2
		LB1		LS1	RB2							LS2
		CS										
		RB1										
Total =	102.54 kcal/mol			ΔE_{Tot} =	-164.25 kcal/mol							
Van der Waals =	112.36 kcal/mol			ΔE_{Vdw} =	-19.51 kcal/mol							
Electrostatic =	-257.90 kcal/mol			ΔE_{Ele} =	-148.17 kcal/mol							
Initial Orientation				LB1	RB2							
Final Orientation		RS2		LB1	RB2		LB2	RB1		LB2		RB1
		RB2		RB1			LS2	RS1				RS1
				LS2								
Total =	82.45 kcal/mol			ΔE_{Tot} =	-184.33 kcal/mol							
Van der Waals =	107.24 kcal/mol			ΔE_{Vdw} =	-24.62 kcal/mol							
Electrostatic =	-272.63 kcal/mol			ΔE_{Ele} =	-162.90 kcal/mol							
Initial Orientation				LB1			RB2					
Final Orientation		LS2	RB2	LB1	LS2		RB2	LS2				
		LB2		LB1			RS2					
				RS2								
				RB1								
				LS2								
Total =	86.32 kcal/mol			ΔE_{Tot} =	-180.46 kcal/mol							
Van der Waals =	111.15 kcal/mol			ΔE_{Vdw} =	-20.71 kcal/mol							
Electrostatic =	-272.26 kcal/mol			ΔE_{Ele} =	-162.54 kcal/mol							
Initial Orientation				RB2	LB1							
Final Orientation		RB1		RB2	LB1			LB2	LB2		LB2	
		RNH		RS2	LB1			RS2				
		RS1			LB2							
		RB2			LNH							
					RB1							
					RS2							
Total =	87.92 kcal/mol			ΔE_{Tot} =	-178.87 kcal/mol							
Van der Waals =	105.74 kcal/mol			ΔE_{Vdw} =	-26.12 kcal/mol							
Electrostatic =	-267.35 kcal/mol			ΔE_{Ele} =	-157.63 kcal/mol							

	Tyr10	Val12	His13	His14	Gln15	Lys16	Leu17	Ile31
Initial Orientation			LB2	RB2				
Final Orientation	RS1	LS2	LB1	RB2		LB2	LS2	RB2
			LS2			LS2		
			LNH					
			LS2					
Total =	82.08 kcal/mol		ΔE_{Tot} =	-184.70 kcal/mol				
Van der Waals =	107.93 kcal/mol		ΔE_{Vdw} =	-23.93 kcal/mol				
Electrostatic =	-275.64 kcal/mol		ΔE_{Ele} =	-165.92 kcal/mol				
Initial Orientation			CS	LS2				
Final Orientation	LB2	RS2	RB1	LS2		RS2	LS2	LS1
	LS2	RB2	RS2					LB1
			LS2					
			LB1					
Total =	85.31 kcal/mol		ΔE_{Tot} =	-181.47 kcal/mol				
Van der Waals =	108.60 kcal/mol		ΔE_{Vdw} =	-23.27 kcal/mol				
Electrostatic =	-268.43 kcal/mol		ΔE_{Ele} =	-158.70 kcal/mol				
Initial Orientation			RB1	LS2				
Final Orientation	LB2	RS2	RS2	LB2		RS2	LS2	LS1
	LS2	RB2	LS2	LS2				
			RB1					
Total =	87.59 kcal/mol		ΔE_{Tot} =	-179.20 kcal/mol				
Van der Waals =	109.61 kcal/mol		ΔE_{Vdw} =	-22.25 kcal/mol				
Electrostatic =	-271.81 kcal/mol		ΔE_{Ele} =	-162.08 kcal/mol				
Initial Orientation			CS	RS1				
Final Orientation	RS1		LS1	RS1			RS1	RS2
			LNH	RB2				
			LB1					
			RS1					
Total =	88.35 kcal/mol		ΔE_{Tot} =	-178.43 kcal/mol				
Van der Waals =	115.52 kcal/mol		ΔE_{Vdw} =	-16.35 kcal/mol				
Electrostatic =	-273.13 kcal/mol		ΔE_{Ele} =	-163.40 kcal/mol				

Table 6.31: The gas phase results of solapsone interacting with the HHQK region of the 1AML conformer of β-amyloid

	Tyr10	Val12	His13	His14	Gln15	Ly16	Leu17	Ala30	Ile31	Met35
Initial Orientation				LB2		RB2				
Final Orientation	LB1	RB2	RS2	LB2		RB2	LS2			
	LNH	RS2	RB1	LS2		RS2				
		RNH	LB1							
		RB1	LS2							
Total =	89.20 kcal/mol		ΔE_{Tot} =	-177.59 kcal/mol						
Van der Waals =	109.49 kcal/mol		ΔE_{Vdw} =	-22.37 kcal/mol						
Electrostatic =	-265.45 kcal/mol		ΔE_{Ele} =	-155.72 kcal/mol						
Initial Orientation			RS2	CS						
Final Orientation	LS2		RS2	LB1					CS	
	RS2			LS2					RB1	
	RB2			LS1					RS1	
Total =	91.68 kcal/mol		ΔE_{Tot} =	-175.11 kcal/mol						
Van der Waals =	102.88 kcal/mol		ΔE_{Vdw} =	-28.99 kcal/mol						
Electrostatic =	-260.36 kcal/mol		ΔE_{Ele} =	-150.63 kcal/mol						
Initial Orientation			CS	RB1						
Final Orientation	LS1		LB1	RS1		LS2	RB1		CS	RS2
			LS2				RS1		RB1	
			LS1						RS2	
			RB1							
Total =	94.32 kcal/mol		ΔE_{Tot} =	-172.47 kcal/mol						
Van der Waals =	109.47 kcal/mol		ΔE_{Vdw} =	-22.39 kcal/mol						
Electrostatic =	-265.25 kcal/mol		ΔE_{Ele} =	-155.52 kcal/mol						

	Tyr10	His13	His14	Gln15	Lys16	Leu17	Val18	Ala21	Ile31
Initial Orientation		RB1	LB2						
Final Orientation	LB1	LB1	LS2		RB2	LS2			LS1
	LS2	LB1			RS2				
	LB2	RB1							
		LS1							
		LS2							
Total =	90.05 kcal/mol		ΔE_{Tot} =	-176.73 kcal/mol					
Van der Waals =	111.04 kcal/mol		ΔE_{Vdw} =	-20.82 kcal/mol					
Electrostatic =	-267.29 kcal/mol		ΔE_{Ele} =	-157.56 kcal/mol					
Initial Orientation		RB1	LS1						
Final Orientation	RB1	RB1	LS2			LS1			
	CS	RB1	LS1						
	LB1	RS1							
	LS1	RNH							
		LS1							
Total =	92.27 kcal/mol		ΔE_{Tot} =	-174.51 kcal/mol					
Van der Waals =	108.97 kcal/mol		ΔE_{Vdw} =	-22.89 kcal/mol					
Electrostatic =	-266.00 kcal/mol		ΔE_{Ele} =	-156.28 kcal/mol					
Initial Orientation		LS2	RB1						
Final Orientation	LS1	LB2	RB1			LS2	RS2	RB2	
		LS2	LS2				RB2		
			RNH						
			RS2						
Total =	97.58 kcal/mol		ΔE_{Tot} =	-169.21 kcal/mol					
Van der Waals =	112.97 kcal/mol		ΔE_{Vdw} =	-18.89 kcal/mol					
Electrostatic =	-261.45 kcal/mol		ΔE_{Ele} =	-151.72 kcal/mol					

Table 6.32: The gas phase results of solapsone interacting with the LVFF region of the 1AML conformer of β-amyloid

	Arg5	Ser8	Tyr10	Val12	His13	His14	Lys16	Leu17	Val18	Phe19	Phe20	Ala21	Glu22	Ala30	Ile31
Initial Orientation								LB2	RB2						
Final Orientation	RS2		LB2		LB2	LB1		LS2	RS2						
			LS2		LS2	LS2			RB2						
						RB1									
Total =	94.30 kcal/mol			ΔE_{Tot} =	-172.49 kcal/mol										
Van der Waals =	110.92 kcal/mol			ΔE_{Vdw} =	-20.94 kcal/mol										
Electrostatic =	-264.34 kcal/mol			ΔE_{Ele} =	-154.62 kcal/mol										
Initial Orientation								LB2		RB2					
Final Orientation				LB1	LB2		LS2	LB2		RB2	LS2				
					LS1		RB1								
					LNH		RNH								
					LB1		RS2								
Total =	109.48 kcal/mol			ΔE_{Tot} =	-157.31 kcal/mol										
Van der Waals =	113.85 kcal/mol			ΔE_{Vdw} =	-18.02 kcal/mol										
Electrostatic =	-252.91 kcal/mol			ΔE_{Ele} =	-143.18 kcal/mol										
Initial Orientation								RB2			LB2				
Final Orientation			RS2		LB1	RB2	LS2	RS2			LB2				RB1
					RB1	RS2					LS2				RNH
					RS2										
Total =	96.27 kcal/mol			ΔE_{Tot} =	-170.52 kcal/mol										
Van der Waals =	110.67 kcal/mol			ΔE_{Vdw} =	-21.19 kcal/mol										
Electrostatic =	-261.60 kcal/mol			ΔE_{Ele} =	-151.88 kcal/mol										
Initial Orientation								RB2	LB2						
Final Orientation	LB2	LB1	RB1		RB2	RB1		RS2	LB2						RS2
	LS1		RS1			LB1		RB2							RB2
Total =	115.98 kcal/mol			ΔE_{Tot} =	-150.81 kcal/mol										
Van der Waals =	110.77 kcal/mol			ΔE_{Vdw} =	-21.09 kcal/mol										
Electrostatic =	-242.87 kcal/mol			ΔE_{Ele} =	-133.14 kcal/mol										

Table 6.33: The gas phase results of solapsone interacting with the HHQKLVFF region of the 1AML conformer of β-amyloid

	Arg5	Tyr10	Val12	His13	His14	Gln15	Lys16	Leu17	Val18	Phe19	Phe20	Glu22	Gly29	Ala30	Ile31
Initial Orientation					RB2				LB2						
Final Orientation	LB2	RS2		RS2	RB1			RS2	LB2						RS1
	LS1	RB2			LB1				LS2						
					RS2										
Total =	77.70 kcal/mol			ΔE_{Tot} =	-189.09 kcal/mol										
Van der Waals =	103.79 kcal/mol			ΔE_{Vdw} =	-28.07 kcal/mol										
Electrostatic =	-272.46 kcal/mol			ΔE_{Ele} =	-162.73 kcal/mol										
Initial Orientation					LB1				RB2						
Final Orientation	RB2	LB2		LB2	LB1			LS2	RS2			RB2			
	RS1	LS2		LS2	LS2				RB2						
					RB1										
					RS2										
Total =	94.00 kcal/mol			ΔE_{Tot} =	-172.79 kcal/mol										
Van der Waals =	106.26 kcal/mol			ΔE_{Vdw} =	-25.60 kcal/mol										
Electrostatic =	-263.29 kcal/mol			ΔE_{Ele} =	-153.56 kcal/mol										
Initial Orientation					RB2						LB2				
Final Orientation		RS2		LS2	RB2		LB2	RS2			LB2				RB1
				LB1	RS2		LS2								RNH
				RB1											
				RS2											
Total =	98.66 kcal/mol			ΔE_{Tot} =	-168.12 kcal/mol										
Van der Waals =	105.25 kcal/mol			ΔE_{Vdw} =	-26.62 kcal/mol										
Electrostatic =	-252.76 kcal/mol			ΔE_{Ele} =	-143.03 kcal/mol										
Initial Orientation				RB2							LB1				
Final Orientation			RB2	RS1			LB1	RS1		LB2	LB1			RS1	
				RB2			LS2			LNH	RB1				
							LNH								
							RB1								
							RNH								
							RS1								
							RB2								
Total =	102.45 kcal/mol			ΔE_{Tot} =	-164.34 kcal/mol										
Van der Waals =	106.46 kcal/mol			ΔE_{Vdw} =	-25.40 kcal/mol										
Electrostatic =	-252.08 kcal/mol			ΔE_{Ele} =	-142.36 kcal/mol										
Initial Orientation				CS							RB2				
Final Orientation				RB1			LS2	RS2			RB2		RB2	RB2	
				RS2			RS2	RS1						RS1	
				RS1											
				LB1			LB2								
Total =	106.81 kcal/mol			ΔE_{Tot} =	-159.98 kcal/mol										
Van der Waals =	116.91 kcal/mol			ΔE_{Vdw} =	-14.95 kcal/mol										
Electrostatic =	-266.85 kcal/mol			ΔE_{Ele} =	-157.12 kcal/mol										

Table 6.33: The gas phase results of solapsone interacting with the HHQKLVFF region of the 1AML conformer of β-amyloid

	Arg5	His6	Glu11	Val12	His13	His14	Gln15	Lys16	Leu17	Val18	Phe19	Phe20	Glu22	Lys28	Ile31
Initial Orientation					RS2							LB1			
Final Orientation					RB2			RS1				CS		LB2	
					RS2			RS2						LS2	
Total =	110.32 kcal/mol			ΔE_{Tot} =	-156.46 kcal/mol										
Van der Waals =	117.20 kcal/mol			ΔE_{Vdw} =	-14.67 kcal/mol										
Electrostatic =	-264.49 kcal/mol			ΔE_{Ele} =	-154.76 kcal/mol										
Initial Orientation						RB1				LB1					
Final Orientation	LS2					RB1			RS1	LS1			LS1		RS1
	LS1					RS1									
						RS2									
Total =	113.29 kcal/mol			ΔE_{Tot} =	-153.50 kcal/mol										
Van der Waals =	115.02 kcal/mol			ΔE_{Vdw} =	-16.84 kcal/mol										
Electrostatic =	-251.51 kcal/mol			ΔE_{Ele} =	-141.78 kcal/mol										
Initial Orientation					LS2							RB2			
Final Orientation				LS2	LS2			LS2			RNH	CS			
					LS1			LB1			RS1				
								RB1							
								RNH							
								RS1							
Total =	115.77 kcal/mol			ΔE_{Tot} =	-151.01 kcal/mol										
Van der Waals =	110.52 kcal/mol			ΔE_{Vdw} =	-21.34 kcal/mol										
Electrostatic =	-242.45 kcal/mol			ΔE_{Ele} =	-132.73 kcal/mol										
Initial Orientation					RB2						LB2				
Final Orientation		LB2			RB2			LS2			LS1				
					RS2			LNH			LNH				
								LB1							
Total =	112.03 kcal/mol			ΔE_{Tot} =	-154.75 kcal/mol										
Van der Waals =	114.10 kcal/mol			ΔE_{Vdw} =	-17.76 kcal/mol										
Electrostatic =	-247.53 kcal/mol			ΔE_{Ele} =	-137.80 kcal/mol										
Initial Orientation					LS1						RB2				
Final Orientation			RB1	LB1	LS1			LB1			RB2				
				CS				RB1							
								RS2							
Total =	115.60 kcal/mol			ΔE_{Tot} =	-151.19 kcal/mol										
Van der Waals =	118.51 kcal/mol			ΔE_{Vdw} =	-13.36 kcal/mol										
Electrostatic =	-254.84 kcal/mol			ΔE_{Ele} =	-145.11 kcal/mol										

Table 6.33: The gas phase results of solapsone interacting with the HHQKLVFF region of the 1AML conformer of β-amyloid

	Arg5	Tyr10	His13	His14	Gln15	Lys16	Leu17	Val18	Phe19	Phe20	Ala21	Gly29	Ala30	Ile31	Ile32	Met35
Initial Orientation			RB2					LB2								
Final Orientation		RS1	RS2	LB1			RS2				LB2			RS2	LS2	
				RB1										RB2		
				LNH												
Total =	92.36 kcal/mol			ΔE_{Tot} =	-174.42 kcal/mol											
Van der Waals =	111.48 kcal/mol			ΔE_{Vdw} =	-20.38 kcal/mol											
Electrostatic =	-269.37 kcal/mol			ΔE_{Ele} =	-159.64 kcal/mol											
Initial Orientation				LB2				RB2								
Final Orientation	RB2	LS2	LB2	RB1			LS2	RB2						LB1		
	RS2			LB1										LNH		
				LS2										LB2		
Total =	98.28 kcal/mol			ΔE_{Tot} =	-168.50 kcal/mol											
Van der Waals =	110.56 kcal/mol			ΔE_{Vdw} =	-21.31 kcal/mol											
Electrostatic =	-255.87 kcal/mol			ΔE_{Ele} =	-146.14 kcal/mol											
Initial Orientation			LB2					RB2								
Final Orientation	RB2	LB2	LB2	LB1			LS2	RB2						LB1		CS
		LS2	LS2	LS2												
				RB1												
				RS2												
Total =	100.46 kcal/mol			ΔE_{Tot} =	-166.33 kcal/mol											
Van der Waals =	106.94 kcal/mol			ΔE_{Vdw} =	-24.92 kcal/mol											
Electrostatic =	-262.13 kcal/mol			ΔE_{Ele} =	-152.40 kcal/mol											
Initial Orientation				LB2						RB2						
Final Orientation		LB1	RB1	LB2			LS2					RB2	RB2	LS2		
		LNH		LB2									RS2			
		LS1														
Total =	94.41 kcal/mol			ΔE_{Tot} =	-172.37 kcal/mol											
Van der Waals =	109.97 kcal/mol			ΔE_{Vdw} =	-21.89 kcal/mol											
Electrostatic =	-256.25 kcal/mol			ΔE_{Ele} =	-146.52 kcal/mol											
Initial Orientation						RS1				LB2						
Final Orientation			LB1			RB2	LS1		RB2	LS1						
			LS1			RNH										
			LS2			LB1										
						LNH										
						LS1										
Total =	109.03 kcal/mol			ΔE_{Tot} =	-157.76 kcal/mol											
Van der Waals =	107.90 kcal/mol			ΔE_{Vdw} =	-23.96 kcal/mol											
Electrostatic =	-256.69 kcal/mol			ΔE_{Ele} =	-146.97 kcal/mol											

Table 6.34: The gas phase results of solapsone interacting with the HHQK region of the 1BA4 conformer of β-amyloid

	His13	His14	Gln15	Lys16	Leu17	His13	His14	Gln15	Lys16
Initial Orientation	RS2	LB2				RS2	LS2		
Final Orientation	RB1	LS1	RS2			RS1	LS2		
	RB1	LS2				RS2	LS1		
	RS2								
	RS1								
Total =	31.01 kcal/mol					34.01 kcal/mol			
Van der Waals =	88.68 kcal/mol					94.79 kcal/mol			
Electrostatic =	-278.35 kcal/mol					-268.75 kcal/mol			
ΔE_{Tot} =	-141.83 kcal/mol					-138.83 kcal/mol			
ΔE_{Vdw} =	-13.01 kcal/mol					-6.90 kcal/mol			
ΔE_{Ele} =	-129.62 kcal/mol					-120.01 kcal/mol			
Initial Orientation	RB2	LB2				CS	RS1		
Final Orientation	LS2	LS2	LB2			LB1	RS1		
	RB1					LS2	RS2		
	RNH					LS1			
	RB2								
Total =	45.51 kcal/mol					46.29 kcal/mol			
Van der Waals =	85.74 kcal/mol					92.47 kcal/mol			
Electrostatic =	-262.02 kcal/mol					-267.83 kcal/mol			
ΔE_{Tot} =	-127.33 kcal/mol					-126.55 kcal/mol			
ΔE_{Vdw} =	-15.95 kcal/mol					-9.22 kcal/mol			
ΔE_{Ele} =	-113.28 kcal/mol					-119.09 kcal/mol			
Initial Orientation	LS2	RS2				CS	LS2		
Final Orientation	LB1	CS	CS		RS1	LB1	LS2		
	LS2	RB1				LS2	LS1		
		RS1				LS1			
		RS2				CS			
						RS2			
Total =	46.42 kcal/mol					49.63 kcal/mol			
Van der Waals =	87.71 kcal/mol					89.96 kcal/mol			
Electrostatic =	-261.28 kcal/mol					-263.92 kcal/mol			
ΔE_{Tot} =	-126.42 kcal/mol					-123.21 kcal/mol			
ΔE_{Vdw} =	-13.99 kcal/mol					-11.74 kcal/mol			
ΔE_{Ele} =	-112.55 kcal/mol					-115.19 kcal/mol			
Initial Orientation	LS2	CS							
Final Orientation	LS2	LB1			RS1				
		LS2			RS2				
		RB1							
		RS2							
Total =	49.67 kcal/mol								
Van der Waals =	90.52 kcal/mol								
Electrostatic =	-261.68 kcal/mol								
ΔE_{Tot} =	-123.17 kcal/mol								
ΔE_{Vdw} =	-11.17 kcal/mol								
ΔE_{Ele} =	-112.94 kcal/mol								

Table 6.35: The gas phase results of solapsone interacting with the LVFF region of the 1BA4 conformer of β-amyloid

	His14	Leu17	Val18	Phe19	Phe20	Ala21	Val24	Lys28
Initial Orientation			LB2		RB2			
Final Orientation	LS1	LB1	LB1			RB1	RB2	RB2
		LNH	LB2			CS		RS2
						LB1		
Total =	55.79 kcal/mol		ΔE_{Tot} =	-117.05 kcal/mol				
Van der Waals =	79.39 kcal/mol		ΔE_{Vdw} =	-22.30 kcal/mol				
Electrostatic =	-239.52 kcal/mol		ΔE_{Ele} =	-90.79 kcal/mol				
Initial Orientation		RB2			LB1			
Final Orientation	RS2	RS2			LB1			
		RNH						
		RB1						
Total =	83.54 kcal/mol		ΔE_{Tot} =	-89.30 kcal/mol				
Van der Waals =	91.23 kcal/mol		ΔE_{Vdw} =	-10.46 kcal/mol				
Electrostatic =	-238.55 kcal/mol		ΔE_{Ele} =	-89.82 kcal/mol				
Initial Orientation		RB1			LB2			
Final Orientation	RS2	RB1	RS2		LB2			
					LS2			
Total =	85.42 kcal/mol		ΔE_{Tot} =	-87.42 kcal/mol				
Van der Waals =	90.61 kcal/mol		ΔE_{Vdw} =	-11.08 kcal/mol				
Electrostatic =	-224.83 kcal/mol		ΔE_{Ele} =	-76.09 kcal/mol				

	His13	His14	Gln15	Lys16	Leu17	Val18	Phe19	Phe20	Val24	Lys28
Initial Orientation						RB1		LB1		
Final Orientation		RB1	RS1		LB1	RB1				
		RNH				RS1				
		RS1								
Total =	83.39 kcal/mol			ΔE_{Tot} =	-89.45 kcal/mol					
Van der Waals =	83.41 kcal/mol			ΔE_{Vdw} =	-18.28 kcal/mol					
Electrostatic =	-209.63 kcal/mol			ΔE_{Ele} =	-60.89 kcal/mol					
Initial Orientation						RB2		LB1		
Final Orientation	LB2			LB2	LB2			LB1	RS1	RS1
								RB1		
Total =	83.58 kcal/mol			ΔE_{Tot} =	-89.26 kcal/mol					
Van der Waals =	84.59 kcal/mol			ΔE_{Vdw} =	-17.10 kcal/mol					
Electrostatic =	-228.30 kcal/mol			ΔE_{Ele} =	-79.57 kcal/mol					
Initial Orientation					LB1	RB2				
Final Orientation	LS2	LS2			LB1	RB2				
						RS2				
Total =	86.05 kcal/mol			ΔE_{Tot} =	-86.79 kcal/mol					
Van der Waals =	88.26 kcal/mol			ΔE_{Vdw} =	-13.43 kcal/mol					
Electrostatic =	-210.98 kcal/mol			ΔE_{Ele} =	-62.24 kcal/mol					

Table 6.36: The gas phase results of solapsone interacting with the HHQKLVFF region of the 1BA4 conformer of β-amyloid

	His13	His14	Gln15	Lys16	Leu17	Val18	Phe19	Phe20	His13	His14	Gln15	Lys16	Leu17	Val18	Phe19	Phe20
Initial Orientation	RB2					LB1			RS1				LB2			
Final Orientation	RS1	LS2	RB1		LS2	LB1			RNH	LB1			LS1	LS1		
	RB2	LB1			LNH	CS			RS1	RB1						
		RB1			LB1				RB2	LS1						
		RB2								RNH						
										RS2						
Total =	44.20 kcal/mol			ΔE_{Tot} =	-128.64 kcal/mol				45.41 kcal/mol			ΔE_{Tot} =	-127.43 kcal/mol			
Van der Waals =	79.61 kcal/mol			ΔE_{Vdw} =	-22.09 kcal/mol				83.15 kcal/mol			ΔE_{Vdw} =	-18.54 kcal/mol			
Electrostatic =	-260.72 kcal/mol			ΔE_{Ele} =	-111.98 kcal/mol				-250.32 kcal/mol			ΔE_{Ele} =	-101.59 kcal/mol			
Initial Orientation		RB1			LB2				LB1							RB2
Final Orientation	RS2	RS2			LS2				RB1	LB1		RS1	RB2			RB2
	RS1	RB1			LB2				LB1	LB1			RS1			
		LS2							LS1	RB1						
										LNH						
										LB2						
Total =	51.89 kcal/mol			ΔE_{Tot} =	-120.95 kcal/mol				52.73 kcal/mol			ΔE_{Tot} =	-120.11 kcal/mol			
Van der Waals =	90.68 kcal/mol			ΔE_{Vdw} =	-11.01 kcal/mol				79.17 kcal/mol			ΔE_{Vdw} =	-22.52 kcal/mol			
Electrostatic =	-263.69 kcal/mol			ΔE_{Ele} =	-114.95 kcal/mol				-250.91 kcal/mol			ΔE_{Ele} =	-102.17 kcal/mol			
Initial Orientation		CS			RB1					LB2			RB2			
Final Orientation	LS2	LS1	LS1		RS1				LB2	RB1			RB2			
	LS1	LB1							LS2	LS2						
		RB1							LNH	LB1						
										RNH						
Total =	54.84 kcal/mol			ΔE_{Tot} =	-118.00 kcal/mol				55.58 kcal/mol			ΔE_{Tot} =	-117.26 kcal/mol			
Van der Waals =	89.51 kcal/mol			ΔE_{Vdw} =	-12.18 kcal/mol				83.97 kcal/mol			ΔE_{Vdw} =	-17.72 kcal/mol			
Electrostatic =	-259.82 kcal/mol			ΔE_{Ele} =	-111.08 kcal/mol				-254.38 kcal/mol			ΔE_{Ele} =	-105.64 kcal/mol			
Initial Orientation	RB1				LB2					RB1			LB1			
Final Orientation	RB1	RB2	LS1		LB2				RS1	RB1			LS1			
	RNH	LS1							RS2	RS1						
	RS1															
Total =	56.32 kcal/mol			ΔE_{Tot} =	-116.52 kcal/mol				56.78 kcal/mol			ΔE_{Tot} =	-116.06 kcal/mol			
Van der Waals =	83.38 kcal/mol			ΔE_{Vdw} =	-18.31 kcal/mol				90.71 kcal/mol			ΔE_{Vdw} =	-10.98 kcal/mol			
Electrostatic =	-257.31 kcal/mol			ΔE_{Ele} =	-108.58 kcal/mol				-255.38 kcal/mol			ΔE_{Ele} =	-106.65 kcal/mol			
Initial Orientation		RB2			LB1				RS2					LB2		
Final Orientation	RB2	RB1			LS2				RB2	LS2				LS2		
	RNH	RNH			LNH				RB2					LB2		
	RS1	RS2			LB1				RS2							
Total =	57.99 kcal/mol			ΔE_{Tot} =	-114.85 kcal/mol				58.36 kcal/mol			ΔE_{Tot} =	-114.48 kcal/mol			
Van der Waals =	81.15 kcal/mol			ΔE_{Vdw} =	-20.54 kcal/mol				91.72 kcal/mol			ΔE_{Vdw} =	-9.97 kcal/mol			
Electrostatic =	-242.98 kcal/mol			ΔE_{Ele} =	-94.24 kcal/mol				-244.10 kcal/mol			ΔE_{Ele} =	-95.36 kcal/mol			

Table 6.36: The gas phase results of solapsone interacting with the HHQKLVFF region of the 1BA4 conformer of β-amyloid

	His13	His14	Gln15	Lys16	Leu17	Val18	Phe19	Phe20	Val12	His13	His14	Gln15	Lys16	Leu17	Val18	Phe19	Phe20
Initial Orientation	LB1				RB2						RS1				LB2		
Final Orientation	RB1	RB1			RB2			RB2		LS1	LB1	LB2		RB1			
	LB1	RNH									RB1						
	LNH	LB1									RS1						
	LS1	LNH									RNH						
		LB2															
Total =	58.81 kcal/mol			ΔE_{Tot} =	-114.03 kcal/mol				59.38 kcal/mol			ΔE_{Tot} =	-113.46 kcal/mol				
Van der Waals =	83.76 kcal/mol			ΔE_{Vdw} =	-17.93 kcal/mol				86.95 kcal/mol			ΔE_{Vdw} =	-14.74 kcal/mol				
Electrostatic =	-252.23 kcal/mol			ΔE_{Ele} =	-103.49 kcal/mol				-253.90 kcal/mol			ΔE_{Ele} =	-105.16 kcal/mol				
Initial Orientation	RB2				LB1						LS2				RB2		
Final Orientation	LB2	LB1			LS1	CS				LB2	LS2				RB2		
	RNH	RB1			LB1					LS2							
	RS1									LS1							
Total =	61.17 kcal/mol			ΔE_{Tot} =	-111.67 kcal/mol				64.94 kcal/mol			ΔE_{Tot} =	-107.90 kcal/mol				
Van der Waals =	86.68 kcal/mol			ΔE_{Vdw} =	-15.01 kcal/mol				88.58 kcal/mol			ΔE_{Vdw} =	-13.11 kcal/mol				
Electrostatic =	-246.66 kcal/mol			ΔE_{Ele} =	-97.92 kcal/mol				-247.34 kcal/mol			ΔE_{Ele} =	-98.61 kcal/mol				
Initial Orientation		RB1				LB1					LS2			RB1			
Final Orientation	RS1	CS	CS			LB1				LS1	LB1			RS2			
	RS2	RB1				CS					LS2						
		RS1									LS1						
Total =	66.15 kcal/mol			ΔE_{Tot} =	-106.69 kcal/mol				67.15 kcal/mol			ΔE_{Tot} =	-105.69 kcal/mol				
Van der Waals =	85.73 kcal/mol			ΔE_{Vdw} =	-15.97 kcal/mol				90.63 kcal/mol			ΔE_{Vdw} =	-11.06 kcal/mol				
Electrostatic =	-242.59 kcal/mol			ΔE_{Ele} =	-93.85 kcal/mol				-245.26 kcal/mol			ΔE_{Ele} =	-96.53 kcal/mol				
Initial Orientation		RS1				LB1				LB2				RB1			
Final Orientation	RS1	RS1	CS			LB1			LS1	LB2	RB1			RS1			
										LB2	RB1						
										LS1	LB1						
										LNH	RNH						
											LNH						
Total =	67.18 kcal/mol			ΔE_{Tot} =	-105.66 kcal/mol				70.63 kcal/mol			ΔE_{Tot} =	-102.21 kcal/mol				
Van der Waals =	93.08 kcal/mol			ΔE_{Vdw} =	-8.61 kcal/mol				81.86 kcal/mol			ΔE_{Vdw} =	-19.83 kcal/mol				
Electrostatic =	-236.65 kcal/mol			ΔE_{Ele} =	-87.91 kcal/mol				-240.31 kcal/mol			ΔE_{Ele} =	-91.58 kcal/mol				

Table 6.37: The gas phase results of solapsone interacting with the HHQK region of the 1IYT conformer of β-amyloid

	Gly9	Tyr10	Val12	His13	His14	Gln15	Lys16	Leu17	Phe20
Initial Orientation				CS	LS2				
Final Orientation	LS2	LS2	RS2	RB1	LS1		RS1	LS1	
				LB1			RS2		
				LB1					
				LS1					
Total =	-12.90 kcal/mol			ΔE_{Tot} =	-146.95 kcal/mol				
Van der Waals =	75.90 kcal/mol			ΔE_{Vdw} =	-20.37 kcal/mol				
Electrostatic =	-305.24 kcal/mol			ΔE_{Ele} =	-125.79 kcal/mol				
Initial Orientation				LB1	RB2				
Final Orientation	RS2	RS2		LB1	RB2		LS2	LS2	LB2
				RB1	RS2		LS1		LS2
				RB1					
				LS2					
Total =	-4.98 kcal/mol			ΔE_{Tot} =	-139.03 kcal/mol				
Van der Waals =	68.42 kcal/mol			ΔE_{Vdw} =	-27.85 kcal/mol				
Electrostatic =	-293.09 kcal/mol			ΔE_{Ele} =	-113.65 kcal/mol				
Initial Orientation				RB1			LS2		
Final Orientation	RS1			RB1	RS2		LS2	RS2	
				RS1			LS1		
				RS2					
				RB2					
Total =	-1.70 kcal/mol			ΔE_{Tot} =	-135.75 kcal/mol				
Van der Waals =	78.30 kcal/mol			ΔE_{Vdw} =	-17.97 kcal/mol				
Electrostatic =	-301.33 kcal/mol			ΔE_{Ele} =	-121.88 kcal/mol				
Initial Orientation				RS2	LB2				
Final Orientation			RS2	RB1	LS2		RS2	CS	
				RS2	RB2		RS1	LB1	
				LB1				LS2	
				LS2					
Total =	1.45 kcal/mol			ΔE_{Tot} =	-132.60 kcal/mol				
Van der Waals =	75.24 kcal/mol			ΔE_{Vdw} =	-21.03 kcal/mol				
Electrostatic =	-290.00 kcal/mol			ΔE_{Ele} =	-110.55 kcal/mol				

	His6	Tyr10	Val12	His13	His14	Gln15	Lys16	Leu17	Phe20
Initial Orientation				LS2	RS2				
Final Orientation		RS2		LB1	RB2		LS2	LS2	LB2
				LS2	RS2			RB2	LS2
				LS1					
				RB1					
Total =	-10.19 kcal/mol			ΔE_{Tot} =	-144.24 kcal/mol				
Van der Waals =	70.93 kcal/mol			ΔE_{Vdw} =	-25.35 kcal/mol				
Electrostatic =	-295.20 kcal/mol			ΔE_{Ele} =	-115.75 kcal/mol				
Initial Orientation				LB1	RB1				
Final Orientation				LB1	RS1		LS2		LB2
				LS2					LS2
				LS1					
				RB1					
				RS1					
Total =	-4.18 kcal/mol			ΔE_{Tot} =	-138.23 kcal/mol				
Van der Waals =	75.97 kcal/mol			ΔE_{Vdw} =	-20.30 kcal/mol				
Electrostatic =	-292.82 kcal/mol			ΔE_{Ele} =	-113.37 kcal/mol				
Initial Orientation				RB1	LS2				
Final Orientation			RS2	RB1	LB2		RS1	LS2	
				LS2	LS2		RS2	LB1	
				LB1				CS	
				RNH					
				RS2					
Total =	1.03 kcal/mol			ΔE_{Tot} =	-133.02 kcal/mol				
Van der Waals =	76.12 kcal/mol			ΔE_{Vdw} =	-20.15 kcal/mol				
Electrostatic =	-294.24 kcal/mol			ΔE_{Ele} =	-114.80 kcal/mol				
Initial Orientation				CS			RB2		
Final Orientation	LS2		RS2	RB1			RS1		
	LB2			CS			RS2		
				RS1					
				RS2					
Total =	2.81 kcal/mol			ΔE_{Tot} =	-131.24 kcal/mol				
Van der Waals =	78.98 kcal/mol			ΔE_{Vdw} =	-17.29 kcal/mol				
Electrostatic =	-292.32 kcal/mol			ΔE_{Ele} =	-112.87 kcal/mol				

Table 6.37: The gas phase results of solapsone interacting with the HHQK region of the 1IYT conformer of β-amyloid

	Arg5	His6	Gly9	Tyr10	Val12	His13	His14	Gln15	Lys16	Leu17	Gly9	Tyr10	His13	His14	Gln15	Lys16	Leu17	Phe20
Initial Orientation						CS			RS2				RB1	LB2				
Final Orientation	LS2	LS2	LB1		CS	RB1			RS2				RB1	LB2		RS1	LB2	RB2
		LS1	CS		RS2	RS1							LB1					RS1
						CS							LB1					
													RS1					
													LNH					
Total =	6.90 kcal/mol		ΔE_{Tot} =		-127.15 kcal/mol						10.05 kcal/mol			ΔE_{Tot} =	-124.01 kcal/mol			
Van der Waals =	78.72 kcal/mol		ΔE_{Vdw} =		-17.55 kcal/mol						76.23 kcal/mol			ΔE_{Vdw} =	-20.05 kcal/mol			
Electrostatic =	-294.45 kcal/mol		ΔE_{Ele} =		-115.00 kcal/mol						-284.80 kcal/mol			ΔE_{Ele} =	-105.35 kcal/mol			
Initial Orientation						RB2	LB2						LS2	RB2				
Final Orientation				LB2	RB2	RB1	LB2		RB2	LS2	RS2	RS2	LS2	RB2		LS2		
						LS2	LS2		RS2				LB1	RS2				
						LB1												
						RNH												
						RS2												
Total =	13.13 kcal/mol		ΔE_{Tot} =		-120.92 kcal/mol						15.76 kcal/mol			ΔE_{Tot} =	-118.29 kcal/mol			
Van der Waals =	82.50 kcal/mol		ΔE_{Vdw} =		-13.77 kcal/mol						78.62 kcal/mol			ΔE_{Vdw} =	-17.66 kcal/mol			
Electrostatic =	-289.40 kcal/mol		ΔE_{Ele} =		-109.95 kcal/mol						-281.18 kcal/mol			ΔE_{Ele} =	-101.73 kcal/mol			
Initial Orientation						CS			LB1				LB1	RS2				
Final Orientation		RS1	RB1		LS1	LB1			LS2				LB1	RS2		LS2		
						CS			LS1				LS2					
						LS1							RB1					
Total =	16.14 kcal/mol		ΔE_{Tot} =		-117.91 kcal/mol						16.14 kcal/mol			ΔE_{Tot} =	-117.91 kcal/mol			
Van der Waals =	82.95 kcal/mol		ΔE_{Vdw} =		-13.32 kcal/mol						81.20 kcal/mol			ΔE_{Vdw} =	-15.07 kcal/mol			
Electrostatic =	-290.21 kcal/mol		ΔE_{Ele} =		-110.77 kcal/mol						-291.02 kcal/mol			ΔE_{Ele} =	-111.57 kcal/mol			
Initial Orientation							LB2		RB2									
Final Orientation			LB1	LS1		RB1	LB2		RB2									
			LNH						RS2									
			LS1															
Total =	21.10 kcal/mol		ΔE_{Tot} =		-112.95 kcal/mol													
Van der Waals =	82.65 kcal/mol		ΔE_{Vdw} =		-13.62 kcal/mol													
Electrostatic =	-280.51 kcal/mol		ΔE_{Ele} =		-101.07 kcal/mol													

Table 6.38: The gas phase results of solapsone interacting with the LVFF region of the 1IYT conformer of β-amyloid

	Val12	His13	His14	Lys16	Leu17	Val18	Phe19	Phe20	His13	His14	Lys16	Leu17	Val18	Phe19	Phe20	Asp23
Initial Orientation					RB1			LB1				RB1			LB2	
Final Orientation	LS1	LB1	RS1	LS2	CS			LS2	LB1	RS2	LS2	RS2			LS2	
		LS1		LS1	RB1				LS1		LS1	RB1			LB2	
		LNH							CS							
		RB1							LS2							
		RS1														
Total =	1.58 kcal/mol			ΔE_{Tot} =	-132.48 kcal/mol				12.50 kcal/mol			ΔE_{Tot} =	-121.55 kcal/mol			
Van der Waals =	74.94 kcal/mol			ΔE_{Vdw} =	-21.34 kcal/mol				73.70 kcal/mol			ΔE_{Vdw} =	-22.57 kcal/mol			
Electrostatic =	-287.03 kcal/mol			ΔE_{Ele} =	-107.59 kcal/mol				-282.13 kcal/mol			ΔE_{Ele} =	-102.68 kcal/mol			
Initial Orientation					RB2			LB1						LB1	RB1	
Final Orientation	LS2	LS2		LS1	RS2			CS	RS1		LB1			LS2	CS	CS
	LB2			LB1	RNH			LB1			LS1			LS1	RB1	
				LNH	RB1						LNH			LB1	RS2	
											RB1					
											RS1					
Total =	29.68 kcal/mol			ΔE_{Tot} =	-104.38 kcal/mol				37.83 kcal/mol			ΔE_{Tot} =	-96.22 kcal/mol			
Van der Waals =	77.51 kcal/mol			ΔE_{Vdw} =	-18.76 kcal/mol				75.40 kcal/mol			ΔE_{Vdw} =	-20.87 kcal/mol			
Electrostatic =	-267.83 kcal/mol			ΔE_{Ele} =	-88.38 kcal/mol				-261.18 kcal/mol			ΔE_{Ele} =	-81.73 kcal/mol			
Initial Orientation					LB1			RB1								
Final Orientation		LB1		CS	LB1			RB1								
		CS														
		LS1														
Total =	75.19 kcal/mol			ΔE_{Tot} =	-58.86 kcal/mol											
Van der Waals =	83.10 kcal/mol			ΔE_{Vdw} =	-13.17 kcal/mol											
Electrostatic =	-222.94 kcal/mol			ΔE_{Ele} =	-43.50 kcal/mol											

Table 6.39: The gas phase results of solapsone interacting with the HHQKLVFF region of the 1IYT conformer of β-amyloid

	Gly9	Tyr10	Val12	His13	His14	Gln15	Lys16	Leu17	Val18	Phe19	Phe20
Initial Orientation					LS2			RB1			
Final Orientation	LS2	LS2		RB1	LS1		RS2	CS			
				LB1				LS1			
				LS2							
Total =	-3.79 kcal/mol			ΔE_{Tot} =	-137.84 kcal/mol						
Van der Waals =	77.30 kcal/mol			ΔE_{Vdw} =	-18.97 kcal/mol						
Electrostatic =	-298.03 kcal/mol			ΔE_{Ele} =	-118.58 kcal/mol						
Initial Orientation							LB2			RB2	
Final Orientation			LS2	LS1			RB1			RB2	
				LS2			LS1				
				LB2							
Total =	4.93 kcal/mol			ΔE_{Tot} =	-129.12 kcal/mol						
Van der Waals =	77.43 kcal/mol			ΔE_{Vdw} =	-18.84 kcal/mol						
Electrostatic =	-290.83 kcal/mol			ΔE_{Ele} =	-111.38 kcal/mol						
Initial Orientation							RS2	LB1			
Final Orientation				RB1	LS2		RS2	CS			
				LS2				LS1			
Total =	7.46 kcal/mol			ΔE_{Tot} =	-126.59 kcal/mol						
Van der Waals =	81.90 kcal/mol			ΔE_{Vdw} =	-14.37 kcal/mol						
Electrostatic =	-289.93 kcal/mol			ΔE_{Ele} =	-110.48 kcal/mol						
Initial Orientation							RB1	LB2			
Final Orientation			RB1	LB2			RS2	LB2		RS2	LS1
				LS2			LS2	LS2			
				LB1							
Total =	8.52 kcal/mol			ΔE_{Tot} =	-125.53 kcal/mol						
Van der Waals =	76.03 kcal/mol			ΔE_{Vdw} =	-20.24 kcal/mol						
Electrostatic =	-280.89 kcal/mol			ΔE_{Ele} =	-101.44 kcal/mol						
Initial Orientation					RS2						LB2
Final Orientation		RS1		LS2	RS1		LS2	LS2			LB2
				LS1	RS2			RS2			LS2
				LB1							
Total =	9.75 kcal/mol			ΔE_{Tot} =	-124.30 kcal/mol						
Van der Waals =	79.30 kcal/mol			ΔE_{Vdw} =	-16.98 kcal/mol						
Electrostatic =	-285.87 kcal/mol			ΔE_{Ele} =	-106.42 kcal/mol						

	Tyr10	Val12	His13	His14	Gln15	Lys16	Leu17	Val18	Phe19	Phe20
Initial Orientation						LB1				RB2
Final Orientation			RS1		LS2	LB1			LS2	RS2
			RS2		LB2	RS2			LB2	
						LS2				
Total =	1.71 kcal/mol			ΔE_{Tot} =	-132.35 kcal/mol					
Van der Waals =	75.51 kcal/mol			ΔE_{Vdw} =	-20.76 kcal/mol					
Electrostatic =	-289.47 kcal/mol			ΔE_{Ele} =	-110.03 kcal/mol					
Initial Orientation			LB1				RB2			
Final Orientation	RS2	LS2	LB1	RB2		LB1	RB1			
			LS1	RS2		LS2				
			RS2			LB2				
			RB1							
			LS2							
Total =	7.28 kcal/mol			ΔE_{Tot} =	-126.77 kcal/mol					
Van der Waals =	75.28 kcal/mol			ΔE_{Vdw} =	-20.99 kcal/mol					
Electrostatic =	-286.57 kcal/mol			ΔE_{Ele} =	-107.12 kcal/mol					
Initial Orientation			LS2				RB2			
Final Orientation			LB1	RS2		LB2	RS2			LB2
			LS1			LS2	RB1			LS2
			CS							
			LS2							
Total =	8.08 kcal/mol			ΔE_{Tot} =	-125.98 kcal/mol					
Van der Waals =	77.12 kcal/mol			ΔE_{Vdw} =	-19.15 kcal/mol					
Electrostatic =	-284.23 kcal/mol			ΔE_{Ele} =	-104.78 kcal/mol					
Initial Orientation			CS				LB1			
Final Orientation			RB1			RS1	LS1			
			RS2							
			LB1							
			LS1							
Total =	9.38 kcal/mol			ΔE_{Tot} =	-124.67 kcal/mol					
Van der Waals =	83.75 kcal/mol			ΔE_{Vdw} =	-12.52 kcal/mol					
Electrostatic =	-293.75 kcal/mol			ΔE_{Ele} =	-114.30 kcal/mol					
Initial Orientation						RB1				LB2
Final Orientation		RB1	LB1			RB2	LS1		RS1	LB2
			LS1			LS1				
						LNH				
						LB1				
						RNH				
						RS1				
Total =	9.79 kcal/mol			ΔE_{Tot} =	-124.26 kcal/mol					
Van der Waals =	66.25 kcal/mol			ΔE_{Vdw} =	-30.02 kcal/mol					
Electrostatic =	-285.95 kcal/mol			ΔE_{Ele} =	-106.51 kcal/mol					

Table 6.39: The gas phase results of solapsone interacting with the HHQKLVFF region of the 1IYT conformer of β-amyloid

	Val12	His13	His14	Gln15	Lys16	Leu17	Val18	Phe19	Phe20
Initial Orientation		RB1				LB1			
Final Orientation		RB1			LS1	LS1			
		RS2							
		LB1							
		LS1							
Total =	10.20 kcal/mol			ΔE_{Tot} =	-123.85 kcal/mol				
Van der Waals =	84.05 kcal/mol			ΔE_{Vdw} =	-12.23 kcal/mol				
Electrostatic =	-293.05 kcal/mol			ΔE_{Ele} =	-113.60 kcal/mol				
Initial Orientation			LS1						RB2
Final Orientation		RB1	LS1		RS1	LB1			RB2
		LB1				LNH			RS1
		LS1							
Total =	14.57 kcal/mol			ΔE_{Tot} =	-119.48 kcal/mol				
Van der Waals =	75.26 kcal/mol			ΔE_{Vdw} =	-21.01 kcal/mol				
Electrostatic =	-276.30 kcal/mol			ΔE_{Ele} =	-96.85 kcal/mol				
Initial Orientation		LS2					RB2		
Final Orientation		LB1	RS2		LS2	LS2			LB2
		LS1				RB1			
		LS2				RB2			
Total =	16.52 kcal/mol			ΔE_{Tot} =	-117.54 kcal/mol				
Van der Waals =	73.67 kcal/mol			ΔE_{Vdw} =	-22.60 kcal/mol				
Electrostatic =	-274.94 kcal/mol			ΔE_{Ele} =	-95.50 kcal/mol				
Initial Orientation		LB1							RB2
Final Orientation		RB1			RB2	LS1			RB2
		LS1			RNH	LNH			
		LB1				LB1			
		RNH							
		RS1							
Total =	17.70 kcal/mol			ΔE_{Tot} =	-116.35 kcal/mol				
Van der Waals =	76.58 kcal/mol			ΔE_{Vdw} =	-19.69 kcal/mol				
Electrostatic =	-277.28 kcal/mol			ΔE_{Ele} =	-97.83 kcal/mol				
Initial Orientation					RB2	LB2			
Final Orientation	RB2	LB1			RS1	LS2			
	RS2	RS2			RS2	LB2			
		LNH							
		LB2							
Total =	22.00 kcal/mol			ΔE_{Tot} =	-112.05 kcal/mol				
Van der Waals =	82.30 kcal/mol			ΔE_{Vdw} =	-13.97 kcal/mol				
Electrostatic =	-277.77 kcal/mol			ΔE_{Ele} =	-98.32 kcal/mol				

	Val12	His13	His14	Gln15	Lys16	Leu17	Val18	Phe19	Phe20
Initial Orientation					RB1			LB1	
Final Orientation	RS1	RS1			LB1			LS1	
		RS2			RS2				
		RB2							
Total =	13.81 kcal/mol			ΔE_{Tot} =	-120.24 kcal/mol				
Van der Waals =	81.13 kcal/mol			ΔE_{Vdw} =	-15.14 kcal/mol				
Electrostatic =	-285.25 kcal/mol			ΔE_{Ele} =	-105.80 kcal/mol				
Initial Orientation					RS2	LB2			
Final Orientation	RS2	LB2			RB1	LS2			LB1
		LS2			RS1	LB2			LS1
					RS2				
					LS2				
Total =	16.13 kcal/mol			ΔE_{Tot} =	-117.93 kcal/mol				
Van der Waals =	76.82 kcal/mol			ΔE_{Vdw} =	-19.45 kcal/mol				
Electrostatic =	-280.83 kcal/mol			ΔE_{Ele} =	-101.39 kcal/mol				
Initial Orientation					LB1			RB2	
Final Orientation		LS1		RS1	RB1			RB2	LB2
					LB1			RS1	
					RS1			RNH	
					RNH			RB1	
					LNH				
					LS1				
Total =	16.92 kcal/mol			ΔE_{Tot} =	-117.13 kcal/mol				
Van der Waals =	73.62 kcal/mol			ΔE_{Vdw} =	-22.65 kcal/mol				
Electrostatic =	-279.53 kcal/mol			ΔE_{Ele} =	-100.08 kcal/mol				
Initial Orientation					RS2			LB2	
Final Orientation		RS2			RB1			LB2	RB2
					LS2			LS2	
					LB1				
					RS2				
Total =	18.12 kcal/mol			ΔE_{Tot} =	-115.93 kcal/mol				
Van der Waals =	76.04 kcal/mol			ΔE_{Vdw} =	-20.23 kcal/mol				
Electrostatic =	-276.20 kcal/mol			ΔE_{Ele} =	-96.76 kcal/mol				
Initial Orientation					RB2				LB1
Final Orientation	RS2	LB2			RB1	LS2			LS2
		LS2			LS2				LB1
					CS				CS
					RS1				
					RS2				
Total =	22.22 kcal/mol			ΔE_{Tot} =	-111.83 kcal/mol				
Van der Waals =	75.34 kcal/mol			ΔE_{Vdw} =	-20.93 kcal/mol				
Electrostatic =	-272.58 kcal/mol			ΔE_{Ele} =	-93.14 kcal/mol				

Table 6.39: The gas phase results of solapsone interacting with the HHQKLVFF region of the 1IYT conformer of β-amyloid

	Val12	His13	His14	Gln15	Lys16	Leu17	Val18	Phe19	Phe20
Initial Orientation					RB2			LB1	
Final Orientation	RS2	RB2		LS2	RB1			LB1	
		RS2		LB2	LB1			LNH	
					RS2			LS1	
								LB2	
Total =	23.03 kcal/mol			ΔE_{Tot} =	-111.02 kcal/mol				
Van der Waals =	75.84 kcal/mol			ΔE_{Vdw} =	-20.43 kcal/mol				
Electrostatic =	-269.36 kcal/mol			ΔE_{Ele} =	-89.92 kcal/mol				
Initial Orientation					LB1	RB2			
Final Orientation		RS2			LB1	RS2			RB1
		RB2			LS2	RB2			
					LNH				
					RS2				
Total =	23.71 kcal/mol			ΔE_{Tot} =	-110.34 kcal/mol				
Van der Waals =	78.43 kcal/mol			ΔE_{Vdw} =	-17.84 kcal/mol				
Electrostatic =	-274.36 kcal/mol			ΔE_{Ele} =	-94.91 kcal/mol				
Initial Orientation					RB1			LB2	
Final Orientation		RS2			RB1			LB2	RB2
					LS2			LS2	
					RS2				
Total =	24.06 kcal/mol			ΔE_{Tot} =	-110.00 kcal/mol				
Van der Waals =	81.32 kcal/mol			ΔE_{Vdw} =	-14.95 kcal/mol				
Electrostatic =	-275.91 kcal/mol			ΔE_{Ele} =	-96.46 kcal/mol				

	His13	His14	Gln15	Lys16	Leu17	Val18	Phe19	Phe20
Initial Orientation	RS1				LB1			
Final Orientation	RB1	LS1		RB2	RS1			RS1
	RS2			RS2	LB1			
	RS1			RS1				
	CS							
Total =	23.69 kcal/mol			ΔE_{Tot} =	-110.37 kcal/mol			
Van der Waals =	75.60 kcal/mol			ΔE_{Vdw} =	-20.67 kcal/mol			
Electrostatic =	-272.74 kcal/mol			ΔE_{Ele} =	-93.29 kcal/mol			
Initial Orientation				RB2			LB2	
Final Orientation	RS2			RB1			LS2	RB2
				LS2			LB2	
				RS2				
Total =	23.82 kcal/mol			ΔE_{Tot} =	-110.23 kcal/mol			
Van der Waals =	79.67 kcal/mol			ΔE_{Vdw} =	-16.60 kcal/mol			
Electrostatic =	-271.64 kcal/mol			ΔE_{Ele} =	-92.20 kcal/mol			

Table 6.40: The gas phase results of solapsone interacting with the HHQK region of the 1Z0Q conformer of β-amyloid

	Gly9	Tyr10	His13	His14	Gln15	Lys16	Leu17	Val18
Initial Orientation				RS2		LS2		
Final Orientation	CS	CS	LB1	RS1		LS2	RS2	RS2
			LS1	RS2				
			CS					
Total =	94.27 kcal/mol			ΔE_{Tot} =	-150.30 kcal/mol			
Van der Waals =	106.03 kcal/mol			ΔE_{Vdw} =	-15.67 kcal/mol			
Electrostatic =	-295.62 kcal/mol			ΔE_{Ele} =	-135.38 kcal/mol			
Initial Orientation				LS2		CS		
Final Orientation		LS2	RS2	LS2		RB1	LS1	
			LS2	LB2		RS1		
						LS1		
Total =	98.55 kcal/mol			ΔE_{Tot} =	-146.03 kcal/mol			
Van der Waals =	106.87 kcal/mol			ΔE_{Vdw} =	-14.84 kcal/mol			
Electrostatic =	-292.23 kcal/mol			ΔE_{Ele} =	-131.99 kcal/mol			
Initial Orientation			CS	RS2				
Final Orientation	CS	CS	LB1	RS2		LS2		
			LS1	RS1		RS2		
			LS2					
Total =	99.51 kcal/mol			ΔE_{Tot} =	-145.07 kcal/mol			
Van der Waals =	109.29 kcal/mol			ΔE_{Vdw} =	-12.41 kcal/mol			
Electrostatic =	-293.14 kcal/mol			ΔE_{Ele} =	-132.90 kcal/mol			
Initial Orientation			RB1	LB1				
Final Orientation	RB1		RB1	LS2		LS1		
			RNH	LS1				
			RS1					
			RB2					
Total =	106.00 kcal/mol			ΔE_{Tot} =	-138.58 kcal/mol			
Van der Waals =	105.86 kcal/mol			ΔE_{Vdw} =	-15.84 kcal/mol			
Electrostatic =	-288.01 kcal/mol			ΔE_{Ele} =	-127.76 kcal/mol			
Initial Orientation			RB1	LB2				
Final Orientation	LB1	LS1	LB1	LB2		RS2		
		LNH	RB1	LS1		RB1		
		LB1	RB1					
			LNH					
			RNH					
Total =	107.41 kcal/mol			ΔE_{Tot} =	-137.16 kcal/mol			
Van der Waals =	97.73 kcal/mol			ΔE_{Vdw} =	-23.97 kcal/mol			
Electrostatic =	-275.24 kcal/mol			ΔE_{Ele} =	-115.00 kcal/mol			

	Gly9	Tyr10	Val12	His13	His14	Gln15	Lys16	Leu17	Val18
Initial Orientation				LB1	RS2				
Final Orientation	CS	CS		LB1	RS2		LS2		
				LS1	RS1		RS2		
				LS2					
Total =	98.47 kcal/mol			ΔE_{Tot} =	-146.11 kcal/mol				
Van der Waals =	104.36 kcal/mol			ΔE_{Vdw} =	-17.34 kcal/mol				
Electrostatic =	-292.45 kcal/mol			ΔE_{Ele} =	-132.21 kcal/mol				
Initial Orientation				LS2	RB1				
Final Orientation	LS1	CS		LB1	RB1		LB2	RS2	RS2
				LS2	CS		LS2		
				LS1	RS1				
					RS2				
Total =	99.12 kcal/mol			ΔE_{Tot} =	-145.46 kcal/mol				
Van der Waals =	100.02 kcal/mol			ΔE_{Vdw} =	-21.69 kcal/mol				
Electrostatic =	-291.07 kcal/mol			ΔE_{Ele} =	-130.83 kcal/mol				
Initial Orientation				CS	LS1				
Final Orientation				RB1	LS2		RS1		
				RS1	LS1		RB1		
				RS2			RNH		
Total =	105.31 kcal/mol			ΔE_{Tot} =	-139.27 kcal/mol				
Van der Waals =	110.47 kcal/mol			ΔE_{Vdw} =	-11.23 kcal/mol				
Electrostatic =	-291.80 kcal/mol			ΔE_{Ele} =	-131.56 kcal/mol				
Initial Orientation				LS2	RS2				
Final Orientation		CS		LS2	RB1		LB2		
				LS1	RS1		LS2		
					RS2				
Total =	106.18 kcal/mol			ΔE_{Tot} =	-138.39 kcal/mol				
Van der Waals =	107.61 kcal/mol			ΔE_{Vdw} =	-14.09 kcal/mol				
Electrostatic =	-285.38 kcal/mol			ΔE_{Ele} =	-125.14 kcal/mol				
Initial Orientation				LS2	RB2				
Final Orientation				LS2	RB2		LS2		RB2
				LS1					
Total =	107.91 kcal/mol			ΔE_{Tot} =	-136.66 kcal/mol				
Van der Waals =	105.29 kcal/mol			ΔE_{Vdw} =	-16.42 kcal/mol				
Electrostatic =	-282.70 kcal/mol			ΔE_{Ele} =	-122.46 kcal/mol				

Table 6.40: The gas phase results of solapsone interacting with the HHQK region of the 1Z0Q conformer of β-amyloid

	Tyr10	His13	His14	Gln15	Lys16	Leu17	Val18
Initial Orientation		LS1	CS				
Final Orientation	CS	LS1	RB1		LB1		
		CS	RS2		LS2		
			CS		LS1		
			RS1				
Total =	108.86 kcal/mol			ΔE_{Tot} =	-135.72 kcal/mol		
Van der Waals =	104.22 kcal/mol			ΔE_{Vdw} =	-17.48 kcal/mol		
Electrostatic =	-287.62 kcal/mol			ΔE_{Ele} =	-127.38 kcal/mol		
Initial Orientation			CS		RS2		
Final Orientation	LS2	RS2	LS1		RS2		
		CS	CS		RS1		
					CS		
Total =	110.37 kcal/mol			ΔE_{Tot} =	-134.21 kcal/mol		
Van der Waals =	106.66 kcal/mol			ΔE_{Vdw} =	-15.04 kcal/mol		
Electrostatic =	-285.89 kcal/mol			ΔE_{Ele} =	-125.65 kcal/mol		
Initial Orientation		RS2	CS				
Final Orientation		RS2	LB1		RS1	CS	
			LS1		CS		
			CS				
Total =	113.76 kcal/mol			ΔE_{Tot} =	-130.82 kcal/mol		
Van der Waals =	105.47 kcal/mol			ΔE_{Vdw} =	-16.23 kcal/mol		
Electrostatic =	-278.63 kcal/mol			ΔE_{Ele} =	-118.39 kcal/mol		
Initial Orientation			LB2		RS2		
Final Orientation		RB2	LB2		RS2	CS	LB2
		RS1	LNH		CS		
					RB1		
Total =	116.63 kcal/mol			ΔE_{Tot} =	-127.94 kcal/mol		
Van der Waals =	104.70 kcal/mol			ΔE_{Vdw} =	-17.00 kcal/mol		
Electrostatic =	-275.83 kcal/mol			ΔE_{Ele} =	-115.59 kcal/mol		

	Gly9	Tyr10	His13	His14	Gln15	Lys16	Leu17	Val18	Ala21
Initial Orientation			RS1	CS					
Final Orientation	RS2		RS2	LS1		RS1			
			RS1	LS2					
Total =	110.05 kcal/mol			ΔE_{Tot} =	-134.53 kcal/mol				
Van der Waals =	109.65 kcal/mol			ΔE_{Vdw} =	-12.05 kcal/mol				
Electrostatic =	-284.10 kcal/mol			ΔE_{Ele} =	-123.85 kcal/mol				
Initial Orientation				LB2		RB2			
Final Orientation			RB2	LNH		RS2		LB2	LB2
			RS1	LS1		RB1			
			RNH						
			RB1						
Total =	112.24 kcal/mol			ΔE_{Tot} =	-132.34 kcal/mol				
Van der Waals =	103.13 kcal/mol			ΔE_{Vdw} =	-18.57 kcal/mol				
Electrostatic =	-280.21 kcal/mol			ΔE_{Ele} =	-119.96 kcal/mol				
Initial Orientation			RS2	LS2					
Final Orientation			RB2	LS2		RS1	CS		
			RS2			RS2			
						RB1			
						CS			
Total =	114.82 kcal/mol			ΔE_{Tot} =	-129.75 kcal/mol				
Van der Waals =	106.72 kcal/mol			ΔE_{Vdw} =	-14.99 kcal/mol				
Electrostatic =	-279.91 kcal/mol			ΔE_{Ele} =	-119.67 kcal/mol				

Table 6.41: The gas phase results of solapsone interacting with the LVFF region of the 1Z0Q conformer of β-amyloid

	His14	Lys16	Leu17	Val18	Phe19	Phe20	Ala21	Glu22	Asp23	Val24	Lys28
Initial Orientation			RB1	LB2							
Final Orientation	LB2	RS1	RB1	LB2							
	LS1	RNH	LB1								
Total =	156.16 kcal/mol		ΔE_{Tot} =		-88.42 kcal/mol						
Van der Waals =	107.95 kcal/mol		ΔE_{Vdw} =		-13.75 kcal/mol						
Electrostatic =	-249.60 kcal/mol		ΔE_{Ele} =		-89.36 kcal/mol						
Initial Orientation				LB2		RB2					
Final Orientation	LB2	LS1	LS1	LB2		RS2	LB2	LB2			
	LS2		LNH			RB2	LB1				
	LS1		LB1								
Total =	161.66 kcal/mol		ΔE_{Tot} =		-82.92 kcal/mol						
Van der Waals =	104.25 kcal/mol		ΔE_{Vdw} =		-17.45 kcal/mol						
Electrostatic =	-233.26 kcal/mol		ΔE_{Ele} =		-73.02 kcal/mol						
Initial Orientation			LB2			RB1					
Final Orientation		LB2	LB2			RB1					RS1
						LB1					RNH
Total =	167.30 kcal/mol		ΔE_{Tot} =		-77.27 kcal/mol						
Van der Waals =	108.22 kcal/mol		ΔE_{Vdw} =		-13.49 kcal/mol						
Electrostatic =	-233.09 kcal/mol		ΔE_{Ele} =		-72.84 kcal/mol						
Initial Orientation					RB2	LB1					
Final Orientation			LS2			RB2			RB2	RS2	RS2
						RS2					RB2
						RB1					
						CS					
						LS2					
Total =	179.19 kcal/mol		ΔE_{Tot} =		-65.39 kcal/mol						
Van der Waals =	108.95 kcal/mol		ΔE_{Vdw} =		-12.75 kcal/mol						
Electrostatic =	-204.46 kcal/mol		ΔE_{Ele} =		-44.22 kcal/mol						

	Val12	His14	Gln15	Lys16	Leu17	Val18	Phe19	Phe20	Val24	Lys28
Initial Orientation					LB1	RB2				
Final Orientation		RB2		LS2	LB1	RB2				
		RS2		LB1	RB1					
Total =	161.25 kcal/mol			ΔE_{Tot} =	-83.33 kcal/mol					
Van der Waals =	110.05 kcal/mol			ΔE_{Vdw} =	-11.65 kcal/mol					
Electrostatic =	-233.71 kcal/mol			ΔE_{Ele} =	-73.47 kcal/mol					
Initial Orientation					LB2		RB1			
Final Orientation	RB2		RB2	RB1	LB2		RB1	LS2		
				RB2	LS2		RS2			
Total =	164.34 kcal/mol			ΔE_{Tot} =	-80.24 kcal/mol					
Van der Waals =	102.52 kcal/mol			ΔE_{Vdw} =	-19.18 kcal/mol					
Electrostatic =	-226.59 kcal/mol			ΔE_{Ele} =	-66.35 kcal/mol					
Initial Orientation							RB1	LB1		
Final Orientation							RS1	LB1	LS1	LS1
								RB1		LNH
Total =	172.55 kcal/mol			ΔE_{Tot} =	-72.02 kcal/mol					
Van der Waals =	110.96 kcal/mol			ΔE_{Vdw} =	-10.74 kcal/mol					
Electrostatic =	-223.02 kcal/mol			ΔE_{Ele} =	-62.78 kcal/mol					

Table 6.42: The gas phase results of solapsone interacting with the HHQKLVFF region of the 1Z0Q conformer of β-amyloid

	His13	His14	Gln15	Lys16	Leu17	Val18	Phe19	Phe20	Ala21
Initial Orientation	RB2					LB2			
Final Orientation	RS2 RB1	LS1		RS1 RS2	LS2				LB2
Total =	108.84 kcal/mol			ΔE_{Tot} =	-135.74 kcal/mol				
Van der Waals =	105.35 kcal/mol			ΔE_{Vdw} =	-16.35 kcal/mol				
Electrostatic =	-285.60 kcal/mol			ΔE_{Ele} =	-125.36 kcal/mol				
Initial Orientation				RS2			LB2		
Final Orientation	RS1 RS2			LB1 RB1 RS2			LB2		
Total =	119.08 kcal/mol			ΔE_{Tot} =	-125.50 kcal/mol				
Van der Waals =	113.42 kcal/mol			ΔE_{Vdw} =	-8.28 kcal/mol				
Electrostatic =	-279.96 kcal/mol			ΔE_{Ele} =	-119.72 kcal/mol				
Initial Orientation				LS2		RB2			
Final Orientation	LS2	RB2 RS2		LS2 LNH LB1 RS2		RB2			
Total =	122.12 kcal/mol			ΔE_{Tot} =	-122.46 kcal/mol				
Van der Waals =	112.06 kcal/mol			ΔE_{Vdw} =	-9.65 kcal/mol				
Electrostatic =	-274.47 kcal/mol			ΔE_{Ele} =	-114.23 kcal/mol				
Initial Orientation				RB2		LB2			
Final Orientation	RS1	LB2		RS2 RB1 RNH		LB2			LB2
Total =	125.77 kcal/mol			ΔE_{Tot} =	-118.80 kcal/mol				
Van der Waals =	108.75 kcal/mol			ΔE_{Vdw} =	-12.95 kcal/mol				
Electrostatic =	-267.81 kcal/mol			ΔE_{Ele} =	-107.57 kcal/mol				
Initial Orientation	LS2				RB2				
Final Orientation	LS2			LB1 RS2	RS2				
Total =	127.73 kcal/mol			ΔE_{Tot} =	-116.85 kcal/mol				
Van der Waals =	109.47 kcal/mol			ΔE_{Vdw} =	-12.23 kcal/mol				
Electrostatic =	-265.92 kcal/mol			ΔE_{Ele} =	-105.68 kcal/mol				
Initial Orientation	RS2						LB2		
Final Orientation	RS1 RS2			RS2			LB2		
Total =	135.23 kcal/mol			ΔE_{Tot} =	-109.35 kcal/mol				
Van der Waals =	115.56 kcal/mol			ΔE_{Vdw} =	-6.14 kcal/mol				
Electrostatic =	-267.74 kcal/mol			ΔE_{Ele} =	-107.50 kcal/mol				

	Gly9	Tyr10	His13	His14	Gln15	Lys16	Leu17	Val18	Phe19	Phe20	Ala21
Initial Orientation						RS2		LB2			
Final Orientation			RS1 RNH RB1	LS1 LB2		RS2	LS1	LS1 LB2			LB2
Total =	118.88 kcal/mol			ΔE_{Tot} =	-125.70 kcal/mol						
Van der Waals =	106.61 kcal/mol			ΔE_{Vdw} =	-15.09 kcal/mol						
Electrostatic =	-276.19 kcal/mol			ΔE_{Ele} =	-115.95 kcal/mol						
Initial Orientation						LS2	RB2				
Final Orientation			LS2	RS2		LS2 LS1 LB1 RS2	RS2				
Total =	121.89 kcal/mol			ΔE_{Tot} =	-122.69 kcal/mol						
Van der Waals =	113.12 kcal/mol			ΔE_{Vdw} =	-8.58 kcal/mol						
Electrostatic =	-277.75 kcal/mol			ΔE_{Ele} =	-117.51 kcal/mol						
Initial Orientation			LS1					RB1			
Final Orientation	LS1	LS1	LS1	RB1 LB1 CS RNH		LB1 LS2 CS	CS	RB1			RS1
Total =	125.60 kcal/mol			ΔE_{Tot} =	-118.98 kcal/mol						
Van der Waals =	102.17 kcal/mol			ΔE_{Vdw} =	-19.53 kcal/mol						
Electrostatic =	-262.57 kcal/mol			ΔE_{Ele} =	-102.33 kcal/mol						
Initial Orientation			RS2				LB2				
Final Orientation	RS1	RS2 RB2	RS2 RS1			LS2 LB1	LB2				
Total =	127.71 kcal/mol			ΔE_{Tot} =	-116.87 kcal/mol						
Van der Waals =	112.24 kcal/mol			ΔE_{Vdw} =	-9.47 kcal/mol						
Electrostatic =	-267.96 kcal/mol			ΔE_{Ele} =	-107.71 kcal/mol						
Initial Orientation						RB1			LB2		
Final Orientation			RS1			RS2 LB1			LS2 LB2		
Total =	132.82 kcal/mol			ΔE_{Tot} =	-111.76 kcal/mol						
Van der Waals =	114.73 kcal/mol			ΔE_{Vdw} =	-6.97 kcal/mol						
Electrostatic =	-265.21 kcal/mol			ΔE_{Ele} =	-104.97 kcal/mol						
Initial Orientation			RB2				LB1				
Final Orientation	RB2	RB2	RB2	RNH RS1		LS1 LNH LB1 RB1	LB1				
Total =	136.87 kcal/mol			ΔE_{Tot} =	-107.70 kcal/mol						
Van der Waals =	104.65 kcal/mol			ΔE_{Vdw} =	-17.05 kcal/mol						
Electrostatic =	-255.22 kcal/mol			ΔE_{Ele} =	-94.98 kcal/mol						

Table 6.42: The gas phase results of solapsone interacting with the HHQKLVFF region of the 1Z0Q conformer of β-amyloid

	Gly9	Tyr10	His13	His14	Gln15	Lys16	Leu17	Val18	Phe19	Phe20
Initial Orientation			LS1				RB2			
Final Orientation			LB2	LB2		LB1	RB2			
			LS1			RB1				
						LNH				
						RNH				
Total =	137.40 kcal/mol			ΔE_{Tot} =	-107.18 kcal/mol					
Van der Waals =	107.18 kcal/mol			ΔE_{Vdw} =	-14.52 kcal/mol					
Electrostatic =	-264.72 kcal/mol			ΔE_{Ele} =	-104.48 kcal/mol					
Initial Orientation						RB1		LB2		
Final Orientation		LS1	LS1	LB2		RB1	LS2	LB2		
			LB1	LS1		LB1	LB2			
			LNH			RNH				
						LNH				
Total =	142.47 kcal/mol			ΔE_{Tot} =	-102.11 kcal/mol					
Van der Waals =	105.05 kcal/mol			ΔE_{Vdw} =	-16.66 kcal/mol					
Electrostatic =	-248.71 kcal/mol			ΔE_{Ele} =	-88.47 kcal/mol					
Initial Orientation				CS			LB2			
Final Orientation		CS		LB1		LS1	LB2	LS2		
				LS2						
				CS						
				LS1						
Total =	144.59 kcal/mol			ΔE_{Tot} =	-99.99 kcal/mol					
Van der Waals =	109.13 kcal/mol			ΔE_{Vdw} =	-12.57 kcal/mol					
Electrostatic =	-247.97 kcal/mol			ΔE_{Ele} =	-87.73 kcal/mol					
Initial Orientation			RB2							LB2
Final Orientation			RS2			LB1	LB2			LB2
			RB2			RB1	LS1			
						RS2				
Total =	146.92 kcal/mol			ΔE_{Tot} =	-97.65 kcal/mol					
Van der Waals =	110.40 kcal/mol			ΔE_{Vdw} =	-11.31 kcal/mol					
Electrostatic =	-251.28 kcal/mol			ΔE_{Ele} =	-91.04 kcal/mol					
Initial Orientation			RB2				LB2			
Final Orientation	RB2		RS1			RS2	LS2			
			RS2			RB1				
Total =	148.46 kcal/mol			ΔE_{Tot} =	-96.12 kcal/mol					
Van der Waals =	113.46 kcal/mol			ΔE_{Vdw} =	-8.24 kcal/mol					
Electrostatic =	-257.56 kcal/mol			ΔE_{Ele} =	-97.31 kcal/mol					
Initial Orientation			LB1						RB2	
Final Orientation			LB1			LS2			RB2	
			LNH							
			LS1							
Total =	152.12 kcal/mol			ΔE_{Tot} =	-92.46 kcal/mol					
Van der Waals =	106.49 kcal/mol			ΔE_{Vdw} =	-15.22 kcal/mol					
Electrostatic =	-243.86 kcal/mol			ΔE_{Ele} =	-83.62 kcal/mol					

	Val12	His13	His14	Gln15	Lys16	Leu17	Val18	Phe19	Phe20
Initial Orientation					CS				RB2
Final Orientation	LS2	LS2			LB1	RS2		RS2	RB2
		LS1			LS2				
Total =	142.08 kcal/mol			ΔE_{Tot} =	-102.50 kcal/mol				
Van der Waals =	106.75 kcal/mol			ΔE_{Vdw} =	-14.95 kcal/mol				
Electrostatic =	-255.05 kcal/mol			ΔE_{Ele} =	-94.81 kcal/mol				
Initial Orientation		LB2						RB2	
Final Orientation		LNH	LB2		RB1			RB2	
		LS1			LB1				
		LB2			LB2				
Total =	143.74 kcal/mol			ΔE_{Tot} =	-100.84 kcal/mol				
Van der Waals =	111.76 kcal/mol			ΔE_{Vdw} =	-9.94 kcal/mol				
Electrostatic =	-252.84 kcal/mol			ΔE_{Ele} =	-92.60 kcal/mol				
Initial Orientation		RS1				LB2			
Final Orientation		RB2			RS2	LB2			
		RB1			RB1				
		RNH							
		RS1							
Total =	145.72 kcal/mol			ΔE_{Tot} =	-98.86 kcal/mol				
Van der Waals =	107.64 kcal/mol			ΔE_{Vdw} =	-14.06 kcal/mol				
Electrostatic =	-251.98 kcal/mol			ΔE_{Ele} =	-91.74 kcal/mol				
Initial Orientation		LS1				RB1			
Final Orientation		LS1			RB1	RS1			
					LB1				
Total =	148.25 kcal/mol			ΔE_{Tot} =	-96.33 kcal/mol				
Van der Waals =	117.81 kcal/mol			ΔE_{Vdw} =	-3.89 kcal/mol				
Electrostatic =	-258.28 kcal/mol			ΔE_{Ele} =	-98.04 kcal/mol				
Initial Orientation					CS	RB1			
Final Orientation		LS2			LB1	RS1			
					LS1				
					RB1				
					RS1				
Total =	148.76 kcal/mol			ΔE_{Tot} =	-95.82 kcal/mol				
Van der Waals =	113.86 kcal/mol			ΔE_{Vdw} =	-7.84 kcal/mol				
Electrostatic =	-252.04 kcal/mol			ΔE_{Ele} =	-91.80 kcal/mol				

The gas phase minimization of solapsone with β-amyloid indicated that it was indeed capable of binding to the **HH**Q**K**, LVFF and overlapping regions on the protein in an energetically favourable fashion. The electrostatic energies were much lower than the van der Waals energies.

These systems were selected for optimization in an aqueous environment based on two criteria: they must have the lowest energy possible, and binding interactions must occur with at least two amino acids in the Aβ region of interest.

6.3.3 Results of the Solution Phase Optimization of Solapsone with β-Amyloid

Minimization of the solvated systems followed the same process as in section 6.2.3. The energies of the optimized β-amyloid conformers are listed in Appendix 6, and the energies of solapsone upon minimization in a solvated environment (and ignoring the solvent contribution) are summarized in Table 6.43.

Table 6.43: The solution phase energies of solapsone

	Energies (kcal/mol)		
	E_{tot}	E_{vdw}	E_{ele}
Solapsone	93.96	46.55	21.82

The energies were calculated using equations 6.4-6.6 (these were measured ignoring solvent contributions and with constrained protein backbones), both the measured and calculated energies are summarized in the following tables. The amino acids are indicated by their three letter abbreviations, and the initial and final orientations of solapsone are given. Hydrogen bonds are represented in orange, cation-π interactions in green, and π-π in blue. Purple, lime green, and yellow are used for interactions with the protein backbone, at the C=O. –CH-, and –NH- groups. Potential binding occurring with the $–CH_2$- chain of the amino acid side chains is denoted by indigo-coloured cells.

Table 6.44: The solution phase results of solapsone interacting with the HHQK region of the 1AMB conformer of β-amyloid

	His6	Gly9	Tyr10	His13	His14	Gln15	Lys16	Leu17	Phe20	Ala21	Lys28
Initial Orientation	LS2 LS1 LB2	LS1	LS1	RB1 LB1 LS1			RS1 RS2	RS1	RS1		
Final Orientation	LS2		LS1	RB1 LB1 LS1			RS1 RS2	RS1	RS1		
Total =	-76.95 kcal/mol										
Van der Waals =	72.86 kcal/mol										
Electrostatic =	-314.60 kcal/mol										
ΔE_{Tot} =	-178.85 kcal/mol										
ΔE_{Vdw} =	-25.57 kcal/mol										
ΔE_{Ele} =	-124.50 kcal/mol										
Initial Orientation			LB2	LB1 LS1 LS2	LS1		RS1 RS2	RS1 LB1 LS1	RS1		
Final Orientation			LS2 LB2	LB1 LS1 LS2	LS1		RS2 RS1	RS1 LS1	RS1		
Total =	-55.15 kcal/mol										
Van der Waals =	70.42 kcal/mol										
Electrostatic =	-309.14 kcal/mol										
ΔE_{Tot} =	-157.06 kcal/mol										
ΔE_{Vdw} =	-28.01 kcal/mol										
ΔE_{Ele} =	-119.04 kcal/mol										
Initial Orientation			RS1 RS2	LS1 RB1 RNH RS2	RS2		LS2 LS1		LB2		
Final Orientation			RS2	LB1 RB1 RS2 RB2	RS2		LS2 LS1	RB2	LB2 LS2		
Total =	-60.47 kcal/mol										
Van der Waals =	71.39 kcal/mol										
Electrostatic =	-304.93 kcal/mol										
ΔE_{Tot} =	-162.37 kcal/mol										
ΔE_{Vdw} =	-27.04 kcal/mol										
ΔE_{Ele} =	-114.83 kcal/mol										
Initial Orientation				LS1			LB1 LS1 LS2	RS1	RB1 RS2 RS1		RS2
Final Orientation				LS1			LB1 LS2 LS1	RS1	CS RB1 RS1 RS2	RS1	RS2
Total =	-50.87 kcal/mol										
Van der Waals =	74.94 kcal/mol										
Electrostatic =	-305.18 kcal/mol										
ΔE_{Tot} =	-152.77 kcal/mol										
ΔE_{Vdw} =	-23.49 kcal/mol										
ΔE_{Ele} =	-115.08 kcal/mol										
Initial Orientation				RS2 RS1			LS2 LS1	RS2	LB2 LS2		
Final Orientation				RS2 RS1			LS2 LS1	RS2	LS2		
Total =	-38.65 kcal/mol										
Van der Waals =	85.14 kcal/mol										
Electrostatic =	-300.56 kcal/mol										
ΔE_{Tot} =	-140.56 kcal/mol										
ΔE_{Vdw} =	-13.29 kcal/mol										
ΔE_{Ele} =	-110.46 kcal/mol										

	His6	Gly9	Tyr10	His13	His14	Gln15	Lys16	Leu17	Phe20
Initial Orientation	RS1	RS1	RS1	RB1 LB1 RNH RS1			LS1	LS2 LS1 LB1	LS2 LS1
Final Orientation	RS1	RS1	RS1	RB1 RS1 RNH LB1			LS1	LS1 LS2	LS1 LS2
Total =	-24.60 kcal/mol								
Van der Waals =	82.19 kcal/mol								
Electrostatic =	-293.79 kcal/mol								
ΔE_{Tot} =	-126.50 kcal/mol								
ΔE_{Vdw} =	-16.24 kcal/mol								
ΔE_{Ele} =	-103.69 kcal/mol								
Initial Orientation		RS1	RS1	RB1 CS RS2 RS1			LS1 LS2 RB1 CS		
Final Orientation	RS1	RS1	RS1	RB1 CS RS1 RS2			LS1 LS2		LS2
Total =	-65.18 kcal/mol								
Van der Waals =	72.97 kcal/mol								
Electrostatic =	-307.20 kcal/mol								
ΔE_{Tot} =	-167.08 kcal/mol								
ΔE_{Vdw} =	-25.46 kcal/mol								
ΔE_{Ele} =	-117.10 kcal/mol								
Initial Orientation			RB2	RS2 RS1 RB1			LS2 LB2	CS LB1	LB1 LNH LS1 LB2
Final Orientation				RS2 RS1 RB1			LB1 LS2 LB2	CS LB1	LB1 LNH LS1
Total =	-60.71 kcal/mol								
Van der Waals =	71.48 kcal/mol								
Electrostatic =	-302.84 kcal/mol								
ΔE_{Tot} =	-162.62 kcal/mol								
ΔE_{Vdw} =	-26.95 kcal/mol								
ΔE_{Ele} =	-112.74 kcal/mol								
Initial Orientation			RS2	LB1 LS2 LS1	RB2		LB2 LS2	LS2 LB1	LB2
Final Orientation			RS2	LB1 LS2 LS1	RB2		LB2 LS2	LS2 RB1	LB2
Total =	-32.93 kcal/mol								
Van der Waals =	79.28 kcal/mol								
Electrostatic =	-308.30 kcal/mol								
ΔE_{Tot} =	-134.83 kcal/mol								
ΔE_{Vdw} =	-19.15 kcal/mol								
ΔE_{Ele} =	-118.20 kcal/mol								
Initial Orientation			LB2 LS2	LB1 LS1 CS	LS1		RS1	RB1	RS1
Final Orientation			LS2 LB2	RB1 LB1 LS1	LS1		RS1	RB1 LS1	RS1
Total =	24.10 kcal/mol								
Van der Waals =	82.82 kcal/mol								
Electrostatic =	-289.31 kcal/mol								
ΔE_{Tot} =	-77.81 kcal/mol								
ΔE_{Vdw} =	-15.61 kcal/mol								
ΔE_{Ele} =	-99.21 kcal/mol								

Table 6.45: The solution phase results of solapsone interacting with the LVFF region of the 1AMB conformer of β-amyloid

	Tyr10	Val12	His13	His14	Gln15	Lys16	Leu17	Val18	Phe19	Phe20	Ala21	Lys28	His13	Lys16	Leu17	Val18	Phe19	Phe20	Val24	Lys28
Initial Orientation		RS1	LS1		RS1	RS2			RS1	LB1			LS2	LS1	LB2			RS2	RB2	RS2
						RB1			RB1	LNH			LS1					RB2		
						RS1			CS											
						LB1														
						LS1														
						LS2														
Final Orientation		RS1	LS1		RS1	RS2			CS	LNH			LB2	LS1	LB2			RS2	RB2	RS2
						LB1			RB1	LB1			LS1		LS1					RB2
						RB1			RS1											
						RS1														
Total =	-52.03 kcal/mol												-35.97 kcal/mol							
Van der Waals =	71.88 kcal/mol												72.38 kcal/mol							
Electrostatic =	-292.54 kcal/mol												-288.04 kcal/mol							
ΔE_{Tot} =	-153.93 kcal/mol												-137.88 kcal/mol							
ΔE_{Vdw} =	-26.55 kcal/mol												-26.05 kcal/mol							
ΔE_{Ele} =	-102.44 kcal/mol												-97.94 kcal/mol							
Initial Orientation				LB2									LS2	LS2	LS1			CS		RS1
				LB2									LS1	LS1				RB1		
														LB1						
Final Orientation	RB2		LS1	LB2			RB1				RB2	RB2	LS1	LS2	LS1			CS		RS1
	LS1			LB2			LB1					RS2	LS2	LS1				RB1		2
				LS1										LB1						
Total =	-43.69 kcal/mol												-35.57 kcal/mol							
Van der Waals =	67.41 kcal/mol												84.63 kcal/mol							
Electrostatic =	-277.36 kcal/mol												-301.07 kcal/mol							
ΔE_{Tot} =	-145.60 kcal/mol												-137.47 kcal/mol							
ΔE_{Vdw} =	-31.02 kcal/mol												-13.80 kcal/mol							
ΔE_{Ele} =	-87.26 kcal/mol												-110.97 kcal/mol							
Initial Orientation			RS2			LS2	RS2		LB2	RS2				RS2	LB2			LS2		LS1
						LNH	RB2											LB1		LS2
						LB1												RB1		
						RS2														
Final Orientation			RB2			RS2	RB2		LB2	RS2				RS2				LS2		LB1
			RS2			LB1	RS2		LS2									RB1		LS1
						LNH														LS2
						LS2														
Total =	-43.29 kcal/mol												-34.63 kcal/mol							
Van der Waals =	81.90 kcal/mol												81.57 kcal/mol							
Electrostatic =	-290.21 kcal/mol												-290.07 kcal/mol							
ΔE_{Tot} =	-145.19 kcal/mol												-136.54 kcal/mol							
ΔE_{Vdw} =	-16.53 kcal/mol												-16.85 kcal/mol							
ΔE_{Ele} =	-100.12 kcal/mol												-99.97 kcal/mol							

Table 6.46: The solution phase results of solapsone interacting with the HHQKLVFF region of the 1AMB conformer of β-amyloid

	Gly9	Tyr10	His13	His14	Gln15	Lys16	Leu17	Val18	Phe19	Phe20	Ala21	Val24	Gly25	Lys28
Initial Orientation	RS2	RS2	RB1				LB1			LS1				LS2
			RS1											
			RS2											
Final Orientation	RS2	RS2	RB1			RS1	LB1			LS1				LS2
			RS1				LS1							
			RS2											
Total =	-65.97 kcal/mol													
Van der Waals =	69.00 kcal/mol													
Electrostatic =	-310.62 kcal/mol													
ΔE_{Tot} =	-167.88 kcal/mol													
ΔE_{Vdw} =	-29.43 kcal/mol													
ΔE_{Ele} =	-120.52 kcal/mol													
Initial Orientation	RB2		RB1			RS2	LS2			LS2	LS2		LB2	LS1
			RB2								LB2			LB2
			RNH											
Final Orientation	RB2		RB1			RS2	LS2			LS2	LB2	LS2	LB2	
			RS2				LB1							
			RNH											
			RB2											
Total =	-31.54 kcal/mol													
Van der Waals =	88.42 kcal/mol													
Electrostatic =	-302.23 kcal/mol													
ΔE_{Tot} =	-133.45 kcal/mol													
ΔE_{Vdw} =	-10.01 kcal/mol													
ΔE_{Ele} =	-112.13 kcal/mol													
Initial Orientation		LS1	LS1							RS1				RS2
			LS2											RS1
Final Orientation			LS2							RS1				RS1
			LS1											
			LB1											
Total =	-34.21 kcal/mol													
Van der Waals =	74.63 kcal/mol													
Electrostatic =	-301.13 kcal/mol													
ΔE_{Tot} =	-136.11 kcal/mol													
ΔE_{Vdw} =	-23.80 kcal/mol													
ΔE_{Ele} =	-111.03 kcal/mol													
Initial Orientation		LS1	LB1				RB1			RS1	RS1			RS1
			LS1											RS2
			LS2											
Final Orientation		LS1	LB1				RS1			RS1				RS1
			LS1				RB1							RS2
			LS2				CS							
Total =	-67.22 kcal/mol													
Van der Waals =	78.72 kcal/mol													
Electrostatic =	-305.76 kcal/mol													
ΔE_{Tot} =	-169.13 kcal/mol													
ΔE_{Vdw} =	-19.71 kcal/mol													
ΔE_{Ele} =	-115.67 kcal/mol													
Initial Orientation		RB2	RS2	RS2		LS2	RS2			LB1				
			RS1			LB1	RB1			LS1				
						LNH	LB1							
Final Orientation		RB2	RB1	RS2		LNH	LB1			LB2				LS2
			RS1			LB1	RS2			LS1				
			RS2							LNH				
										LB1				
Total =	-83.73 kcal/mol													
Van der Waals =	67.58 kcal/mol													
Electrostatic =	-319.50 kcal/mol													
ΔE_{Tot} =	-185.63 kcal/mol													
ΔE_{Vdw} =	-30.85 kcal/mol													
ΔE_{Ele} =	-129.40 kcal/mol													
Initial Orientation			LS1			LS2	LS2			CS				RS1
			LS2				LS1			RS2				
							LB1							
Final Orientation			LS1			LS2	LB1			RS2				RS1
			LS2							CS				
										LB1				
Total =	-45.36 kcal/mol													
Van der Waals =	74.06 kcal/mol													
Electrostatic =	-302.59 kcal/mol													
ΔE_{Tot} =	-147.26 kcal/mol													
ΔE_{Vdw} =	-24.37 kcal/mol													
ΔE_{Ele} =	-112.49 kcal/mol													

Table 6.46: The solution phase results of solapsone interacting with the HHQKLVFF region of the 1AMB conformer of β-amyloid

	His6	Gly9	Tyr10	His13	His14	Gln15	Lys16	Leu17	Val18	Phe19	Phe20	Ala21	Val24	Gly25	Lys28
Initial Orientation			LB2	LS2	LS2			RS2 CS LB1			RS2		CS		RS1 RS2
Final Orientation			LB2	LS2	LS2			CS RS2 RB2			RS2		CS		RS1 RS2
Total =	-46.50 kcal/mol														
Van der Waals =	74.26 kcal/mol														
Electrostatic =	-297.53 kcal/mol														
ΔE_{Tot} =	-148.41 kcal/mol														
ΔE_{Vdw} =	-24.17 kcal/mol														
ΔE_{Ele} =	-107.43 kcal/mol														
Initial Orientation		LS1	LS1	LB1 RB1 LB1 LNH LS1			LB2 RS1 RNH RB1	RNH RB1			RB2 RS1				
Final Orientation	LB2 LS1	LS1	LS1	RB1 LB1 LB1 LNH LS1			RS1 RNH RB1	RNH RB1			RB2 RS1				
Total =	16.07 kcal/mol														
Van der Waals =	63.83 kcal/mol														
Electrostatic =	-287.80 kcal/mol														
ΔE_{Tot} =	-85.84 kcal/mol														
ΔE_{Vdw} =	-34.60 kcal/mol														
ΔE_{Ele} =	-97.70 kcal/mol														
Initial Orientation			RS1 RS2	RB2 RB2 RNH RS1	RS1			LS1 LB1			LS1				LS2
Final Orientation			RS1 RS2 RB2	RB2 RNH RS1	RS1			LS1 LB1			LS1				LS2 LB2
Total =	-57.20 kcal/mol														
Van der Waals =	69.17 kcal/mol														
Electrostatic =	-291.85 kcal/mol														
ΔE_{Tot} =	-159.10 kcal/mol														
ΔE_{Vdw} =	-29.26 kcal/mol														
ΔE_{Ele} =	-101.75 kcal/mol														
Initial Orientation				RB2 RS1 RNH RB1			RB2	LS1			LS1 LB2				LS2 LB2
Final Orientation				RB2 RB1 RNH RS1				LS1 RB2			LS1		LB2		LB2 LS2
Total =	-33.48 kcal/mol														
Van der Waals =	86.33 kcal/mol														
Electrostatic =	-289.60 kcal/mol														
ΔE_{Tot} =	-135.39 kcal/mol														
ΔE_{Vdw} =	-12.10 kcal/mol														
ΔE_{Ele} =	-99.50 kcal/mol														
Initial Orientation				LS2 LB1	RS2		LS2 LNH LB1	RB1 RS2 RB2	RS2 RB2			RB2			
Final Orientation				LS2 LB1	RS2		LS2	RS2	RS2			RB2			
Total =	8.63 kcal/mol														
Van der Waals =	80.37 kcal/mol														
Electrostatic =	-295.43 kcal/mol														
ΔE_{Tot} =	-93.28 kcal/mol														
ΔE_{Vdw} =	-18.06 kcal/mol														
ΔE_{Ele} =	-105.34 kcal/mol														
Initial Orientation				LS2 LB1	RS2		LS2 LNH LB2	RB1 RS2	RS2						
Final Orientation				LB1 LS2	RS2		LB2	LB1 RB1 RS2	RS2 RB2						
Total =	-33.25 kcal/mol														
Van der Waals =	79.01 kcal/mol														
Electrostatic =	-296.44 kcal/mol														
ΔE_{Tot} =	-135.15 kcal/mol														
ΔE_{Vdw} =	-19.42 kcal/mol														
ΔE_{Ele} =	-106.34 kcal/mol														

Table 6.46: The solution phase results of solapsone interacting with the HHQKLVFF region of the 1AMB conformer of β-amyloid

	Gly9	Tyr10	Val12	His13	His14	Gln15	Lys16	Leu17	Val18	Phe19	Phe20	Ala21	Val24	Lys28
Initial Orientation				LB1 LS1 LS2			LS2	RS2 RB1			RS2			RB2
Final Orientation				LB1 LS1 LS2			LS2	RS2 LB1			RB2 RS2			RB2
Total =	-16.42 kcal/mol													
Van der Waals =	73.97 kcal/mol													
Electrostatic =	-311.30 kcal/mol													
ΔE_{Tot} =	-118.33 kcal/mol													
ΔE_{Vdw} =	-24.46 kcal/mol													
ΔE_{Ele} =	-121.20 kcal/mol													
Initial Orientation				RB2 RS1 RNH			RS2 RB1	RB1			LS2			LS1 LS2
Final Orientation				RS1 RNH RB2			RS2 RB1 RNH RB2	LS2 RB1			LS2 LB1 CS RB1	LS2		LS1 LS2
Total =	8.25 kcal/mol													
Van der Waals =	77.07 kcal/mol													
Electrostatic =	-292.22 kcal/mol													
ΔE_{Tot} =	-93.65 kcal/mol													
ΔE_{Vdw} =	-21.36 kcal/mol													
ΔE_{Ele} =	-102.12 kcal/mol													
Initial Orientation	LB2	LB2		LB2 LB1 LNH			LB1 LNH LS1	RB2			RS1 RNH	RB2		RS1 2
Final Orientation	LB2	LB2		LB2 LB2 LB1 LNH			LB1 LNH LS1	RB2			RS1 RNH RB1			RS1 2
Total =	-57.28 kcal/mol													
Van der Waals =	71.09 kcal/mol													
Electrostatic =	-301.47 kcal/mol													
ΔE_{Tot} =	-159.18 kcal/mol													
ΔE_{Vdw} =	-27.34 kcal/mol													
ΔE_{Ele} =	-111.37 kcal/mol													
Initial Orientation				LS1			LS2 LS1	LS1			LB1 CS			RS2 RS1
Final Orientation				LS1			LS1 LS2	LB1 LS1			LB1 CS LS1 LS2			RS2 RS1
Total =	25.83 kcal/mol													
Van der Waals =	91.66 kcal/mol													
Electrostatic =	-296.88 kcal/mol													
ΔE_{Tot} =	-76.07 kcal/mol													
ΔE_{Vdw} =	-6.77 kcal/mol													
ΔE_{Ele} =	-106.78 kcal/mol													
Initial Orientation				RB2			RS2	LS2			LS2			LS1 LS2
Final Orientation				RB2			RS2 RB1 RNH RB2	LS2			LS2			LS1
Total =	-49.60 kcal/mol													
Van der Waals =	75.85 kcal/mol													
Electrostatic =	-293.75 kcal/mol													
ΔE_{Tot} =	-151.51 kcal/mol													
ΔE_{Vdw} =	-22.58 kcal/mol													
ΔE_{Ele} =	-103.65 kcal/mol													
Initial Orientation				LS2 LS1			LB1 LS2	LB1			RB2 RS2 RB1 CS		RB2 RS2	RS2 RB2
Final Orientation				LS2 LS1			LS2	LB1 LS1			RS2 RB1 CS		RB2	RS2
Total =	-65.55 kcal/mol													
Van der Waals =	65.29 kcal/mol													
Electrostatic =	-308.05 kcal/mol													
ΔE_{Tot} =	-167.45 kcal/mol													
ΔE_{Vdw} =	-33.14 kcal/mol													
ΔE_{Ele} =	-117.95 kcal/mol													

Table 6.46: The solution phase results of solapsone interacting with the HHQKLVFF region of the 1AMB conformer of β-amyloid

	Gly9	Tyr10	Val12	His13	His14	Gln15	Lys16	Leu17	Val18	Phe19	Phe20	Ala21	Val24	Lys28
Initial Orientation				RS1			RB1				CS			LS2
				RS2			RS2				LB1			
							CS				LS2			
							RS1							
Final Orientation				RS1			RB1				LS2			LS2
				RS2			CS				LB1			
							RS1				CS			
Total =	-36.95 kcal/mol													
Van der Waals =	80.72 kcal/mol													
Electrostatic =	-296.56 kcal/mol													
ΔE_{Tot} =	-138.85 kcal/mol													
ΔE_{Vdw} =	-17.71 kcal/mol													
ΔE_{Ele} =	-106.46 kcal/mol													
Initial Orientation				LB2			LS1	LS1			CS			RS2
				LS2			LS2							RS1
				LS1										
Final Orientation				LB2			LS1	LS1			CS			RS2
							LS2							RS1
Total =	-37.01 kcal/mol													
Van der Waals =	93.54 kcal/mol													
Electrostatic =	-309.25 kcal/mol													
ΔE_{Tot} =	-138.92 kcal/mol													
ΔE_{Vdw} =	-4.89 kcal/mol													
ΔE_{Ele} =	-119.15 kcal/mol													
Initial Orientation	RB2			RB2			RB1	RS1			CS			
				RS1			LS2							
							LB1							
Final Orientation	RB2		RB2	RB2			RB1	RS1			LB1			
				RS1			LS2				CS			
							LB1				RB1			
							RNH							
Total =	4.96 kcal/mol													
Van der Waals =	68.20 kcal/mol													
Electrostatic =	-287.12 kcal/mol													
ΔE_{Tot} =	-96.95 kcal/mol													
ΔE_{Vdw} =	-30.22 kcal/mol													
ΔE_{Ele} =	-97.02 kcal/mol													
Initial Orientation				RS2	RS2		LS2	RB2	RB2		LB2			
				LB1							LS2			
				CS										
				RB1										
Final Orientation				RS2	RS2		LS2	LS2	RB2		LB2			
				LB1	RB2						LS2			
				CS										
				RB1										
Total =	-54.96 kcal/mol													
Van der Waals =	75.90 kcal/mol													
Electrostatic =	-299.57 kcal/mol													
ΔE_{Tot} =	-156.86 kcal/mol													
ΔE_{Vdw} =	-22.53 kcal/mol													
ΔE_{Ele} =	-109.47 kcal/mol													
Initial Orientation				RS1			RS1	RS1			LS1			LS1
				RS2							LB1			
Final Orientation				RS2			RS1	RS1			LS1			LS1
				RS1							LB1			
Total =	-34.06 kcal/mol													
Van der Waals =	80.91 kcal/mol													
Electrostatic =	-295.46 kcal/mol													
ΔE_{Tot} =	-135.96 kcal/mol													
ΔE_{Vdw} =	-17.52 kcal/mol													
ΔE_{Ele} =	-105.36 kcal/mol													
Initial Orientation				RS2			RS2	RS2			LS2			
				RS1			LS1				LB2			
Final Orientation				RS2			LS2	RS2			LB2			
				RS1			LS1				LS2			
Total =	-48.63 kcal/mol													
Van der Waals =	84.99 kcal/mol													
Electrostatic =	-303.59 kcal/mol													
ΔE_{Tot} =	-150.53 kcal/mol													
ΔE_{Vdw} =	-13.44 kcal/mol													
ΔE_{Ele} =	-113.49 kcal/mol													

Table 6.47: The solution phase results of solapsone interacting with the HHQK region of the 1AML conformer of β-amyloid

	Ser8	Tyr10	Val12	His13	His14	Gln15	Ly16	Leu17	Val18	Phe20	Ala21	Ile31	Tyr10	Val12	His13	His14	Gln15	Lys16	Leu17	Ile31
Initial Orientation	RS2	LS1		LS2	RS2			LS2				LB2	RS1	LS2	LB1	RB2		LB2	LS2	RB2
		LB1		LS1	RB2							LS2			LS2			LS2		
		CS													LNH					
		RB1													LS2					
Final Orientation	RS2	LS1		LS2	RB1			LS2				LB2		LS2	LB1	RS2		LB2	RS2	RB2
		LB1		LS1	RS2							LS2			LS2	RB2				
		CS													RB1					
		RB1													RS2					
Total =	89.59 kcal/mol												66.76 kcal/mol							
Van der Waals =	100.34 kcal/mol												106.46 kcal/mol							
Electrostatic =	-250.39 kcal/mol												-275.08 kcal/mol							
ΔE_{Tot} =	-158.49 kcal/mol												-181.32 kcal/mol							
ΔE_{Vdw} =	-26.89 kcal/mol												-20.77 kcal/mol							
ΔE_{Ele} =	-136.51 kcal/mol												-161.20 kcal/mol							
Initial Orientation		RS2		LB1	RB2		LB2	RB1		LB2		RB1	LB2	RS2	RB1	LS2		RS2	LS2	LS1
		RB2		RB1			LS2	RS1				RS1	LS2	RB2	RS2					LB1
				LS2											LS2					
															LB1					
Final Orientation		RS2		RB1	RB2		LB2	RB1		LB2		CS	LB2		RB1	LS2		RS2	LS2	LS1
				RB1			LS2	RNH				RB1	LS2		RB1					CS
				LB1				RS1				RS1			LS2					
				LS2											CS					
				RS2											RNH					
															RS2					
Total =	76.59 kcal/mol												96.45 kcal/mol							
Van der Waals =	93.80 kcal/mol												105.98 kcal/mol							
Electrostatic =	-258.71 kcal/mol												-265.81 kcal/mol							
ΔE_{Tot} =	-171.49 kcal/mol												-151.63 kcal/mol							
ΔE_{Vdw} =	-33.43 kcal/mol												-21.25 kcal/mol							
ΔE_{Ele} =	-144.83 kcal/mol												-151.93 kcal/mol							
Initial Orientation		LS2	RB2	LB1	LS2		RB2	LS2					LB2	RS2	RS2	LB2		RS2	LS2	LS1
		LB2		LB1			RS2						LS2	RB2	LS2	LS2				
				RS2											RB1					
				RB1																
				LS2																
Final Orientation		LB2	RB2	LB1	LS2		RS2	LS2					LS2	RB2	LB1	LS2		RS2	LS2	LS1
		LS2		LB1			RB2						LB2	RS2	RS2	LB2				
		LNH		LS2											RB1					
		LB1		RS2											LS2					
Total =	120.64 kcal/mol												107.15 kcal/mol							
Van der Waals =	119.72 kcal/mol												118.38 kcal/mol							
Electrostatic =	-255.65 kcal/mol												-251.61 kcal/mol							
ΔE_{Tot} =	-127.44 kcal/mol												-140.93 kcal/mol							
ΔE_{Vdw} =	-7.50 kcal/mol												-8.85 kcal/mol							
ΔE_{Ele} =	-141.77 kcal/mol												-137.73 kcal/mol							
Initial Orientation		RB1		RB2	LB1			LB2	LB2		LB2		RS1		LS1	RS1			RS1	RS2
		RNH		RS2	LB1			RS2							LNH	RB2				
		RS1			LB2										LB1					
		RB2			LNH										RS1					
					RB1															
					RS2															
Final Orientation		RS1		RB2	LB1			LB2	LB2		LB2		RB1		LS1	RS1			RS1	RS2
		RB2		RB2	LB1			RS2					RS1		LNH	RB2				
				RS2	RB1										LB1					
					RB1										RS1					
					LB2															
					RNH															
					RS2															
Total =	114.32 kcal/mol												109.57 kcal/mol							
Van der Waals =	102.71 kcal/mol												122.36 kcal/mol							
Electrostatic =	-247.81 kcal/mol												-256.63 kcal/mol							
ΔE_{Tot} =	-133.75 kcal/mol												-138.51 kcal/mol							
ΔE_{Vdw} =	-24.52 kcal/mol												-4.87 kcal/mol							
ΔE_{Ele} =	-133.93 kcal/mol												-142.75 kcal/mol							

Table 6.47: The solution phase results of solapsone interacting with the HHQK region of the 1AML conformer of β-amyloid

	Tyr10	Val12	His13	His14	Gln15	Ly16	Leu17	Ala30	Ile31	Met35
Initial Orientation	LB1	RB2	RS2	LB2		RB2	LS2			
	LNH	RS2	RB1	LS2		RS2				
		RNH	LB1							
		RB1	LS2							
Final Orientation	LNH	RB1	LS2	LB2		RS2	LS2			
	LB1	RS2	LB1	LS2		RB2				
	RB1	RB2	RS2							
Total =	116.21 kcal/mol									
Van der Waals =	103.76 kcal/mol									
Electrostatic =	-234.17 kcal/mol									
ΔE_{Tot} =	-131.87 kcal/mol									
ΔE_{Vdw} =	-23.47 kcal/mol									
ΔE_{Ele} =	-120.29 kcal/mol									
Initial Orientation	LS2		RS2	LB1					CS	
	RS2			LS2					RB1	
	RB2			LS1					RS1	
Final Orientation	LS2		RS2	LB1			RS2		CS	
	RS2			LS2					RB1	
	RB2			LS1					RS1	
Total =	81.45 kcal/mol									
Van der Waals =	97.09 kcal/mol									
Electrostatic =	-259.08 kcal/mol									
ΔE_{Tot} =	-166.63 kcal/mol									
ΔE_{Vdw} =	-30.14 kcal/mol									
ΔE_{Ele} =	-145.19 kcal/mol									
Initial Orientation	LS1		LB1	RS1		LS2	RB1		CS	RS2
			LS2				RS1		RB1	
			LS1						RS2	
			RB1							
Final Orientation	LS1	LS1	LB1	RS1		LS2	RB1	CS	CS	RS2
			LS2						RB1	
			LS1						RS1	
			RB1						RS2	
Total =	88.28 kcal/mol									
Van der Waals =	98.35 kcal/mol									
Electrostatic =	-253.03 kcal/mol									
ΔE_{Tot} =	-159.80 kcal/mol									
ΔE_{Vdw} =	-28.88 kcal/mol									
ΔE_{Ele} =	-139.15 kcal/mol									

	Tyr10	His13	His14	Gln15	Lys16	Leu17	Val18	Ala21	Ile31
Initial Orientation	LB1	LB1	LS2		RB2	LS2			LS1
	LS2	LB1			RS2				
	LB2	RB1							
		LS1							
		LS2							
Final Orientation	LB2	LS2	LS2		RB2	LS2			LS1
	LB1	LB1			RS2				
		RB1							
		RS2							
Total =	109.90 kcal/mol								
Van der Waals =	126.32 kcal/mol								
Electrostatic =	-258.13 kcal/mol								
ΔE_{Tot} =	-138.18 kcal/mol								
ΔE_{Vdw} =	-0.91 kcal/mol								
ΔE_{Ele} =	-144.25 kcal/mol								
Initial Orientation	RB1	RB1	LS2			LS1			
	CS	RB1	LS1						
	LB1	RS1							
	LS1	RNH							
		LS1							
Final Orientation	LS2	RB1	LS2			LS1			LS1
	LS1	RB1	LS1						
	LB1	LS1							
	CS	LB1							
	RB1	RNH							
		RS1							
Total =	91.40 kcal/mol								
Van der Waals =	96.51 kcal/mol								
Electrostatic =	-253.51 kcal/mol								
ΔE_{Tot} =	-156.68 kcal/mol								
ΔE_{Vdw} =	-30.72 kcal/mol								
ΔE_{Ele} =	-139.63 kcal/mol								
Initial Orientation	LS1	LB2	RB1			LS2	RS2	RB2	
		LS2	LS2				RB2		
			RNH						
			RS2						
Final Orientation	LS2	LB2	RB1				RS2	RB2	LS2
	LS1	LS2	LS2				RB2		
			RNH						
Total =	88.48 kcal/mol								
Van der Waals =	90.49 kcal/mol								
Electrostatic =	-241.06 kcal/mol								
ΔE_{Tot} =	-159.60 kcal/mol								
ΔE_{Vdw} =	-36.73 kcal/mol								
ΔE_{Ele} =	-127.18 kcal/mol								

Table 6.48: The solution phase results of solapsone interacting with the LVFF region of the 1AML conformer of β-amyloid

	Arg5	Ser8	Tyr10	Val12	His13	His14	Lys16	Leu17	Val18	Phe19	Phe20	Ala21	Glu22	Ala30	Ile31
Initial Orientation	RS2		LB2		LB2	LB1		LS2	RS2						
			LS2		LS2	LS2			RB2						
						RB1									
Final Orientation	RS2		LB2		LB2	LB1		LS2	RS2			RB2	RB2		LB1
			LS2		LS2	LS2									
Total =	117.95 kcal/mol														
Van der Waals =	101.62 kcal/mol														
Electrostatic =	-244.30 kcal/mol														
ΔE_{Tot} =	-130.13 kcal/mol														
ΔE_{Vdw} =	-25.60 kcal/mol														
ΔE_{Ele} =	-130.42 kcal/mol														
Initial Orientation				LB1	LB2		LS2	LB2		RB2	LS2				
					LS1		RB1								
					LNH		RNH								
					LB1		RS2								
Final Orientation				LB1	LB2		RB1	LB2			LS2				LB2
					LNH		LS2				RB2				
							LB1								
							RNH								
Total =	90.23 kcal/mol														
Van der Waals =	105.51 kcal/mol														
Electrostatic =	-265.43 kcal/mol														
ΔE_{Tot} =	-157.85 kcal/mol														
ΔE_{Vdw} =	-21.72 kcal/mol														
ΔE_{Ele} =	-151.55 kcal/mol														
Initial Orientation			RS2		LB1	RB2	LS2	RS2				LB2			RB1
					RB1	RS2						LS2			RNH
					RS2										
Final Orientation					RB1	RB2	LS2	RS2				LS2		RB1	RB1
					RS2	RS2									RNH
															RB2
Total =	112.44 kcal/mol														
Van der Waals =	116.00 kcal/mol														
Electrostatic =	-250.68 kcal/mol														
ΔE_{Tot} =	-135.64 kcal/mol														
ΔE_{Vdw} =	-11.23 kcal/mol														
ΔE_{Ele} =	-136.80 kcal/mol														
Initial Orientation	LB2	LB1	RB1		RB2	RB1		RS2	LB2						RS2
	LS1		RS1			LB1		RB2							RB2
Final Orientation	LB2	CS	RS1		RB2	RB1		RB2	LB2						RB2
	LS1	LB1	RB1			RB1									RS2
						LB1									
Total =	98.51 kcal/mol														
Van der Waals =	93.82 kcal/mol														
Electrostatic =	-239.88 kcal/mol														
ΔE_{Tot} =	-149.56 kcal/mol														
ΔE_{Vdw} =	-33.41 kcal/mol														
ΔE_{Ele} =	-126.00 kcal/mol														

Table 6.49: The solution phase results of solapsone interacting with the HHQKLVFF region of the 1AML conformer of β-amyloid

	Arg5	Tyr10	Val12	His13	His14	Gln15	Lys16	Leu17	Val18	Phe19	Phe20	Glu22	Gly29	Ala30	Ile31
Initial Orientation	LB2	RS2		RS2	RB1			RS2	LB2						RS1
	LS1	RB2			LB1				LS2						
					RS2										
Final Orientation	LB2	RS2		RS2	RB1			RS2	LB2			LB2			RS1
	LS1				LB1										
					RNH										
					RS2										
Total =	78.37 kcal/mol														
Van der Waals =	92.69 kcal/mol														
Electrostatic =	-262.76 kcal/mol														
ΔE_{Tot} =	-169.71 kcal/mol														
ΔE_{Vdw} =	-34.54 kcal/mol														
ΔE_{Ele} =	-148.88 kcal/mol														
Initial Orientation	RB2	LB2		LB2	LB1			LS2	RS2			RB2			
	RS1	LS2		LS2	LS2				RB2						
					RB1										
					RS2										
Final Orientation	RB2	LB2		LB2	LS2	RS2		LS2	RS2			RB2			
	RS1	LS2		LS2	RB1				RB2						
		LS1			RS2										
Total =	72.10 kcal/mol														
Van der Waals =	95.92 kcal/mol														
Electrostatic =	-267.61 kcal/mol														
ΔE_{Tot} =	-175.97 kcal/mol														
ΔE_{Vdw} =	-31.31 kcal/mol														
ΔE_{Ele} =	-153.73 kcal/mol														
Initial Orientation		RS2		LS2	RB2		LB2	RS2			LB2				RB1
				LB1	RS2		LS2								RNH
				RB1											
				RS2											
Final Orientation		RS2		LS2	RB2		LB2	RS2			LB2				RB1
				LB1	RS2		LS2	RB2							RB2
				RB1											
				RS2											
Total =	116.12 kcal/mol														
Van der Waals =	112.15 kcal/mol														
Electrostatic =	-233.90 kcal/mol														
ΔE_{Tot} =	-131.96 kcal/mol														
ΔE_{Vdw} =	-15.07 kcal/mol														
ΔE_{Ele} =	-120.02 kcal/mol														
Initial Orientation			RB2	RS1			LB1	RS1		LB2	LB1			RS1	
				RB2			LS2			LNH	RB1				
							LNH								
							RB1								
							RNH								
							RS1								
							RB2								
Final Orientation			RB2	RS1			LB1	RS1		LB1	RB1			RS1	
				RB2			LS2			LNH	LB1				
							RS1			LB2					
							RNH								
							RB1								
							LNH								
Total =	88.65 kcal/mol														
Van der Waals =	100.71 kcal/mol														
Electrostatic =	-250.53 kcal/mol														
ΔE_{Tot} =	-159.43 kcal/mol														
ΔE_{Vdw} =	-26.52 kcal/mol														
ΔE_{Ele} =	-136.65 kcal/mol														
Initial Orientation				RB1			LS2	RS2			RB2		RB2	RB2	
				RS2			RS2	RS1						RS1	
				RS1											
				LB1			LB2								
Final Orientation				RB1			LB2	RS2			RB2		RB2	RS1	
				RNH			LS2							RB2	
				RS2			RS2								
Total =	95.53 kcal/mol														
Van der Waals =	109.82 kcal/mol														
Electrostatic =	-271.08 kcal/mol														
ΔE_{Tot} =	-152.55 kcal/mol														
ΔE_{Vdw} =	-17.41 kcal/mol														
ΔE_{Ele} =	-157.20 kcal/mol														

Table 6.49: The solution phase results of solapsone interacting with the HHQKLVFF region of the 1AML conformer of β-amyloid

	Arg5	His6	Glu11	Val12	His13	His14	Gln15	Lys16	Leu17	Val18	Phe19	Phe20	Glu22	Asp23	Lys28	Gly29	Ile31
Initial Orientation					RB2			RS1				CS			LB2		
					RS2			RS2							LS2		
Final Orientation					RB2			RS1				LB1			LS2	LS2	
					RS2			RS2				CS			LB2		
Total =	71.99 kcal/mol																
Van der Waals =	118.68 kcal/mol																
Electrostatic =	-279.85 kcal/mol																
ΔE_{Tot} =	-176.09 kcal/mol																
ΔE_{Vdw} =	-8.55 kcal/mol																
ΔE_{Ele} =	-165.97 kcal/mol																
Initial Orientation	LS2					RB1			RS1	LS1			LS1				RS1
	LS1					RS1											
						RS2											
Final Orientation	LS2					RB1			RS1	LS1			LS1				RS1
	LS1					CS											
						RS1											
						RS2											
Total =	117.35 kcal/mol																
Van der Waals =	107.93 kcal/mol																
Electrostatic =	-231.10 kcal/mol																
ΔE_{Tot} =	-130.72 kcal/mol																
ΔE_{Vdw} =	-19.30 kcal/mol																
ΔE_{Ele} =	-117.22 kcal/mol																
Initial Orientation				LS2	LS2			LS2			RNH	CS					
					LS1			LB1			RS1						
								RB1									
								RNH									
								RS1									
Final Orientation				LS2	LS2			LB1			RS1	CS		RB2			
				LB2	LS1			RS1			RNH						
								CS			RB1						
								LS2									
Total =	135.62 kcal/mol																
Van der Waals =	105.56 kcal/mol																
Electrostatic =	-225.33 kcal/mol																
ΔE_{Tot} =	-112.46 kcal/mol																
ΔE_{Vdw} =	-21.67 kcal/mol																
ΔE_{Ele} =	-111.45 kcal/mol																
Initial Orientation		LB2			RB2			LS2			LS1						
					RS2			LNH			LNH						
								LB1									
Final Orientation					RB2			LS2			LB2						
					RS2			LB1			LS1						
								RS2			LB1						
Total =	133.01 kcal/mol																
Van der Waals =	119.36 kcal/mol																
Electrostatic =	-233.36 kcal/mol																
ΔE_{Tot} =	-115.07 kcal/mol																
ΔE_{Vdw} =	-7.86 kcal/mol																
ΔE_{Ele} =	-119.48 kcal/mol																
Initial Orientation			RB1	LB1	LS1			LB1			RB2						
				CS				RB1									
								RS2									
Final Orientation				RB1	LS1			RB1			RB2						
				CS				RS2									
								LB1									
Total =	106.29 kcal/mol																
Van der Waals =	106.36 kcal/mol																
Electrostatic =	-245.49 kcal/mol																
ΔE_{Tot} =	-141.79 kcal/mol																
ΔE_{Vdw} =	-20.86 kcal/mol																
ΔE_{Ele} =	-131.61 kcal/mol																

Table 6.49: The solution phase results of solapsone interacting with the HHQKLVFF region of the 1AML conformer of β-amyloid

	Arg5	Tyr10	His13	His14	Gln15	Lys16	Leu17	Val18	Phe19	Phe20	Ala21	Gly29	Ala30	Ile31	Ile32	Met35
Initial Orientation		RS1	RS2	LB1			RS2				LB2			RS2	LS2	
				RB1										RB2		
				LNH												
Final Orientation		RS1	RS1	LB1			RS2				LB2			RS2	LS2	
			RS2	RB1												
				LNH												
Total =	109.14 kcal/mol															
Van der Waals =	111.26 kcal/mol															
Electrostatic =	-252.63 kcal/mol															
ΔE_{Tot} =	-138.94 kcal/mol															
ΔE_{Vdw} =	-15.97 kcal/mol															
ΔE_{Ele} =	-138.75 kcal/mol															
Initial Orientation	RB2	LS2	LB2	RB1			LS2	RB2						LB1		
	RS2			LB1										LNH		
				LS2										LB2		
Final Orientation	RS2	LS2	LB2	RB1			LS2							LB1		
	RB2		LS2	LB1										LNH		
				LS2										LB2		
Total =	111.37 kcal/mol															
Van der Waals =	107.33 kcal/mol															
Electrostatic =	-245.00 kcal/mol															
ΔE_{Tot} =	-136.71 kcal/mol															
ΔE_{Vdw} =	-19.89 kcal/mol															
ΔE_{Ele} =	-131.12 kcal/mol															
Initial Orientation	RB2	LB2	LB2	LB1			LS2	RB2						LB1		CS
		LS2	LS2	LS2												
				RB1												
				RS2												
Final Orientation	RB2	LS2	LB2	LS2			LS2	RB2						LB1		CS
		LS1	LS2	LS1												
				LB1												
				RB1												
				RS2												
Total =	97.41 kcal/mol															
Van der Waals =	104.32 kcal/mol															
Electrostatic =	-264.29 kcal/mol															
ΔE_{Tot} =	-150.67 kcal/mol															
ΔE_{Vdw} =	-22.91 kcal/mol															
ΔE_{Ele} =	-150.41 kcal/mol															
Initial Orientation		LB1	RB1	LB2			LS2					RB2	RB2	LS2		
		LNH		LB2									RS2			
		LS1														
Final Orientation		LS1	RB1	LB2			LS2			RB2		RB2	RS2	LS2		
			LB1	LS1									RB2			
			RNH													
Total =	94.41 kcal/mol															
Van der Waals =	109.97 kcal/mol															
Electrostatic =	-256.25 kcal/mol															
ΔE_{Tot} =	-153.67 kcal/mol															
ΔE_{Vdw} =	-17.26 kcal/mol															
ΔE_{Ele} =	-142.36 kcal/mol															
Initial Orientation			LB1			RB2	LS1		RB2	LS1						
			LS1			RNH										
			LS2			LB1										
						LNH										
						LS1										
Final Orientation			LS1			RB2	LS1		RB2	LS1			LS1			
			LS2			LB1										
						LNH										
						LS1										
Total =	89.69 kcal/mol															
Van der Waals =	87.11 kcal/mol															
Electrostatic =	-259.20 kcal/mol															
ΔE_{Tot} =	-158.39 kcal/mol															
ΔE_{Vdw} =	-40.12 kcal/mol															
ΔE_{Ele} =	-145.32 kcal/mol															

Table 6.50: The solution phase results of solapsone interacting with the HHQK region of the 1BA4 conformer of β-amyloid

	Tyr10	His13	His14	Gln15	Lys16	Leu17	His13	His14	Gln15	Lys16
Initial Orientation		RB1	LS1	RS2			RS1	LS2		
		RB1	LS2				RS2	LS1		
		RS2								
		RS1								
Final Orientation		RS2	LS1	RB2			RS1	LS2		
		RS1	RS2	RS2			RS2	LS1		
		RB1	LS2							
Total =	64.47	kcal/mol					82.04	kcal/mol		
Van der Waals =	129.64	kcal/mol					130.42	kcal/mol		
Electrostatic =	-303.24	kcal/mol					-276.42	kcal/mol		
ΔE_{Tot} =	-157.81	kcal/mol					-140.23	kcal/mol		
ΔE_{Vdw} =	1.04	kcal/mol					1.82	kcal/mol		
ΔE_{Ele} =	-155.41	kcal/mol					-128.59	kcal/mol		
Initial Orientation		LS2	LS2	LB2			LB1	RS1		
		RB1					LS2	RS2		
		RNH					LS1			
		RB2								
Final Orientation	RB2	RB2	LS2				LS2	RS1		
		RNH	LS2*				LS1	RS2		
		RB1	*-NH-							
		LS2	LS1							
Total =	113.33	kcal/mol					73.19	kcal/mol		
Van der Waals =	119.25	kcal/mol					116.74	kcal/mol		
Electrostatic =	-256.84	kcal/mol					-273.24	kcal/mol		
ΔE_{Tot} =	-108.95	kcal/mol					-149.08	kcal/mol		
ΔE_{Vdw} =	-9.35	kcal/mol					-11.86	kcal/mol		
ΔE_{Ele} =	-109.01	kcal/mol					-125.41	kcal/mol		
Initial Orientation		LB1	CS	CS		RS1	LB1	LS2		
		LS2	RB1				LS2	LS1		
			RS1				LS1			
			RS2				CS			
							RS2			
Final Orientation		LS2	CS	CS			RB1	LS2		
			RB1				RS2	LS1		
			RS1				LB1			
			RS2				LS2			
Total =	90.81	kcal/mol					93.67	kcal/mol		
Van der Waals =	117.58	kcal/mol					128.36	kcal/mol		
Electrostatic =	-263.22	kcal/mol					-275.53	kcal/mol		
ΔE_{Tot} =	-131.47	kcal/mol					-128.61	kcal/mol		
ΔE_{Vdw} =	-11.01	kcal/mol					-0.24	kcal/mol		
ΔE_{Ele} =	-115.39	kcal/mol					-127.70	kcal/mol		
Initial Orientation		LS2	LB1			RS1				
			LS2			RS2				
			RB1							
			RS2							
Final Orientation		LS2	LS2			RB1				
		LS1	RS2			RS1				
						RS2				
Total =	102.63	kcal/mol								
Van der Waals =	117.75	kcal/mol								
Electrostatic =	-258.68	kcal/mol								
ΔE_{Tot} =	-119.64	kcal/mol								
ΔE_{Vdw} =	-10.85	kcal/mol								
ΔE_{Ele} =	-110.85	kcal/mol								

Table 6.51: The solution phase results of solapsone interacting with the LVFF region of the 1BA4 conformer of β-amyloid

	His14	Gln15	Leu17	Val18	Phe19	Phe20	Ala21	Val24	Lys28
Initial Orientation	LS1		LB1	LB1			RB1	RB2	RB2
			LNH	LB2			CS		RS2
							LB1		
Final Orientation	LS1	LB2	LS1	LB2			RB1	RNH	RB2
			LNH	LB1				RB2	RS2
			LB1						
Total =	136.79 kcal/mol								
Van der Waals =	127.19 kcal/mol								
Electrostatic =	-229.63 kcal/mol								
ΔE_{Tot} =	-85.49 kcal/mol								
ΔE_{Vdw} =	-1.41 kcal/mol								
ΔE_{Ele} =	-81.81 kcal/mol								
Initial Orientation	RS2		RS2			LB1			
			RNH						
			RB1						
Final Orientation	RS2		RB1			LB1			
			RS2			CS			
Total =	136.03 kcal/mol								
Van der Waals =	113.61 kcal/mol								
Electrostatic =	-222.88 kcal/mol								
ΔE_{Tot} =	-86.24 kcal/mol								
ΔE_{Vdw} =	-14.99 kcal/mol								
ΔE_{Ele} =	-75.05 kcal/mol								
Initial Orientation	RS2		RB1	RS2		LB2			
						LS2			
Final Orientation	RS2		RS2			LS2			
			LS2			LB2			
Total =	161.13 kcal/mol								
Van der Waals =	131.97 kcal/mol								
Electrostatic =	-208.03 kcal/mol								
ΔE_{Tot} =	-61.14 kcal/mol								
ΔE_{Vdw} =	3.38 kcal/mol								
ΔE_{Ele} =	-60.20 kcal/mol								

	His13	His14	Gln15	Lys16	Leu17	Val18	Phe19	Phe20	Ala21	Val24	Lys28
Initial Orientation		RB1	RS1		LB1	RB1					
		RNH				RS1					
		RS1									
Final Orientation		RNH	RS1		LB1	CS			LB1		
		RS1				RB1					
		RB2				RS1					
Total =	136.23 kcal/mol										
Van der Waals =	112.16 kcal/mol										
Electrostatic =	-216.21 kcal/mol										
ΔE_{Tot} =	-86.05 kcal/mol										
ΔE_{Vdw} =	-16.44 kcal/mol										
ΔE_{Ele} =	-68.38 kcal/mol										
Initial Orientation	LB2			LB2	LB2			LB1		RS1	RS1
								RB1			
Final Orientation	LB2	LB2			LB2			RB1		RS1	RS1
								LB1			
Total =	209.50 kcal/mol										
Van der Waals =	109.60 kcal/mol										
Electrostatic =	-210.14 kcal/mol										
ΔE_{Tot} =	-12.77 kcal/mol										
ΔE_{Vdw} =	-19.00 kcal/mol										
ΔE_{Ele} =	-62.31 kcal/mol										
Initial Orientation	LS2	LS2			LB1	RB2					
						RS2					
Final Orientation		LS2		LB2	LB2	RS2					
					LS2	RB2					
					LB1						
Total =	147.41 kcal/mol										
Van der Waals =	123.34 kcal/mol										
Electrostatic =	-210.45 kcal/mol										
ΔE_{Tot} =	-74.87 kcal/mol										
ΔE_{Vdw} =	-5.26 kcal/mol										
ΔE_{Ele} =	-62.63 kcal/mol										

Table 6.52: The solution phase results of solapsone interacting with the HHQKLVFF region of the 1BA4 conformer of β-amyloid

	His13	His14	Gln15	Lys16	Leu17	Val18	Phe19	Phe20	His13	His14	Gln15	Lys16	Leu17	Val18	Phe19	Phe20
Initial Orientation	RS1	LS2	RB1		LS2	LB1			RNH	LB1			LS1	LS1		
	RB2	LB1			LNH	CS			RS1	RB1						
		RB1			LB1				RB2	LS1						
		RB2								RNH						
										RS2						
Final Orientation	RS1	RS1	RS2						RB2	LB1			LS1	LS1		
	RS2	RS2							RS1	RB1			LB2			
									RNH	RS2						
										LNH						
Total =	97.61 kcal/mol								85.00 kcal/mol							
Van der Waals =	119.43 kcal/mol								113.01 kcal/mol							
Electrostatic =	-260.65 kcal/mol								-273.13 kcal/mol							
ΔE_{Tot} =	-124.66 kcal/mol								-137.28 kcal/mol							
ΔE_{Vdw} =	-9.17 kcal/mol								-15.59 kcal/mol							
ΔE_{Ele} =	-112.82 kcal/mol								-125.30 kcal/mol							
Initial Orientation	RS2	RS2			LS2				RB1	LB1		RS1	RB2			RB2
	RS1	RB1			LB2				LB1	LB1			RS1			
		LS2							LS1	RB1						
										LNH						
										LB2						
Final Orientation	RS1	LS2			LB2				RB1	LB1		RS1	RB2			RB2
	RS2	RB1			LS2				LB1	RB1			RNH			
		RS2							LNH	LB2						
									LS1							
Total =	89.36 kcal/mol								120.33 kcal/mol							
Van der Waals =	122.71 kcal/mol								118.50 kcal/mol							
Electrostatic =	-273.24 kcal/mol								-249.36 kcal/mol							
ΔE_{Tot} =	-132.91 kcal/mol								-101.94 kcal/mol							
ΔE_{Vdw} =	-5.89 kcal/mol								-10.09 kcal/mol							
ΔE_{Ele} =	-125.41 kcal/mol								-101.54 kcal/mol							
Initial Orientation	LS2	LS1	LS1		RS1				LB2	RB1			RB2			
	LS1	LB1							LS2	LS2						
		RB1							LNH	LB1						
										RNH						
Final Orientation	LS1	LS1	LS1		RS1				RB1	LS2	LS2		RS1			
	LS2	LB1							RB1				RNH			
									LB1							
									LB1							
									LNH							
									LS2							
									LB2							
Total =	105.80 kcal/mol								109.39 kcal/mol							
Van der Waals =	126.63 kcal/mol								114.73 kcal/mol							
Electrostatic =	-272.90 kcal/mol								-264.01 kcal/mol							
ΔE_{Tot} =	-116.48 kcal/mol								-112.88 kcal/mol							
ΔE_{Vdw} =	-1.96 kcal/mol								-13.87 kcal/mol							
ΔE_{Ele} =	-125.07 kcal/mol								-116.18 kcal/mol							
Initial Orientation	RB1	RB2	LS1		LB2				RS1	RB1			LS1			
	RNH	LS1							RS2	RS1						
	RS1															
Final Orientation	RS1	RB2	LS1		LB2				RS1	RB1			LS1			
	RNH	RB1	LS1*						RS2	RNH						
	RB1	LS1	*-NH-							RS1						
		LB2														
Total =	113.31 kcal/mol								104.07 kcal/mol							
Van der Waals =	118.89 kcal/mol								123.77 kcal/mol							
Electrostatic =	-249.08 kcal/mol								-256.77 kcal/mol							
ΔE_{Tot} =	-108.96 kcal/mol								-118.21 kcal/mol							
ΔE_{Vdw} =	-9.71 kcal/mol								-4.83 kcal/mol							
ΔE_{Ele} =	-101.25 kcal/mol								-108.95 kcal/mol							
Initial Orientation	RB2	RB1			LS2				RB2	LS2				LS2		
	RNH	RNH			LNH				RB2					LB2		
	RS1	RS2			LB1				RS2							
Final Orientation	RS1	RB1			LB1				RB2	LS2			LS2	LB2		
		RS2			LNH				RS2							
		RNH			LS2											
		LB1														
Total =	81.09 kcal/mol								110.33 kcal/mol							
Van der Waals =	104.40 kcal/mol								111.06 kcal/mol							
Electrostatic =	-263.54 kcal/mol								-239.62 kcal/mol							
ΔE_{Tot} =	-141.18 kcal/mol								-111.95 kcal/mol							
ΔE_{Vdw} =	-24.20 kcal/mol								-17.54 kcal/mol							
ΔE_{Ele} =	-115.71 kcal/mol								-91.79 kcal/mol							

Table 6.52: The solution phase results of solapsone interacting with the HHQKLVFF region of the 1BA4 conformer of β-amyloid

	His13	His14	Gln15	Lys16	Leu17	Val18	Phe19	Phe20
Initial Orientation	RB1	RB1			RB2			RB2
	LB1	RNH						
	LNH	LB1						
	LS1	LNH						
		LB2						
Final Orientation	RB1	RB1			RB2			RB2
	LB1	LB1						
	LNH	LB2						
	LS1							
Total =	103.24 kcal/mol							
Van der Waals =	92.63 kcal/mol							
Electrostatic =	-246.60 kcal/mol							
ΔE_{Tot} =	-119.03 kcal/mol							
ΔE_{Vdw} =	-35.97 kcal/mol							
ΔE_{Ele} =	-98.78 kcal/mol							
Initial Orientation	LB2	LB1			LS1	CS		
	RNH	RB1			LB1			
	RS1							
Final Orientation	RNH	LB1			LS1			
	RS1	RB1			LB1			
	RB2							
Total =	86.21 kcal/mol							
Van der Waals =	124.42 kcal/mol							
Electrostatic =	-271.66 kcal/mol							
ΔE_{Tot} =	-136.06 kcal/mol							
ΔE_{Vdw} =	-4.17 kcal/mol							
ΔE_{Ele} =	-123.83 kcal/mol							
Initial Orientation	RS1	CS	CS			LB1		
	RS2	RB1				CS		
		RS1						
Final Orientation	RS1	CS	CS			LB1		
	RS2	RB1				CS		
		RS1						
Total =	100.07 kcal/mol							
Van der Waals =	112.26 kcal/mol							
Electrostatic =	-260.74 kcal/mol							
ΔE_{Tot} =	-122.21 kcal/mol							
ΔE_{Vdw} =	-16.33 kcal/mol							
ΔE_{Ele} =	-112.91 kcal/mol							
Initial Orientation	RS1	RS1	CS			LB1		
Final Orientation	RS1	RS1	CS			LB1		
		-NH-	RB1					
Total =	86.61 kcal/mol							
Van der Waals =	125.71 kcal/mol							
Electrostatic =	-273.54 kcal/mol							
ΔE_{Tot} =	-135.67 kcal/mol							
ΔE_{Vdw} =	-2.88 kcal/mol							
ΔE_{Ele} =	-125.71 kcal/mol							

	Val12	His13	His14	Gln15	Lys16	Leu17	Val18	Phe19	Phe20
Initial Orientation		LS1	LB1	LB2		RB1			
			RB1						
			RS1						
			RNH						
Final Orientation	LS1	LS1	LB1	LB2		RB1			
		LNH	RB1						
			RS1						
			RNH						
Total =	77.59 kcal/mol								
Van der Waals =	121.98 kcal/mol								
Electrostatic =	-283.25 kcal/mol								
ΔE_{Tot} =	-144.68 kcal/mol								
ΔE_{Vdw} =	-6.61 kcal/mol								
ΔE_{Ele} =	-135.43 kcal/mol								
Initial Orientation		LB2	LS2				RB2		
		LS2							
		LS1							
Final Orientation		LS1	LB1			RB2	RB2		
		LS2	LS2						
		LB2							
Total =	84.82 kcal/mol								
Van der Waals =	113.31 kcal/mol								
Electrostatic =	-277.48 kcal/mol								
ΔE_{Tot} =	-137.45 kcal/mol								
ΔE_{Vdw} =	-15.29 kcal/mol								
ΔE_{Ele} =	-129.66 kcal/mol								
Initial Orientation		LS1	LB1			RS2			
			LS2						
			LS1						
Final Orientation		LS1	LB1			RS2			
			LS1						
			LS2						
Total =	140.28 kcal/mol								
Van der Waals =	136.05 kcal/mol								
Electrostatic =	-250.64 kcal/mol								
ΔE_{Tot} =	-82.00 kcal/mol								
ΔE_{Vdw} =	7.46 kcal/mol								
ΔE_{Ele} =	-102.81 kcal/mol								
Initial Orientation	LS1	LB2	RB1			RS1			
		LB2	RB1						
		LS1	LB1						
		LNH	RNH						
			LNH						
Final Orientation		LB2	LB1			RS1			
		LS1	RB1						
			RB1						
			RNH						
			LNH						
Total =	115.20 kcal/mol								
Van der Waals =	121.92 kcal/mol								
Electrostatic =	-252.02 kcal/mol								
ΔE_{Tot} =	-107.07 kcal/mol								
ΔE_{Vdw} =	-6.68 kcal/mol								
ΔE_{Ele} =	-104.20 kcal/mol								

Table 6.53: The solution phase results of solapsone interacting with the HHQK region of the 1IYT conformer of β-amyloid

	Gly9	Tyr10	Val12	His13	His14	Gln15	Lys16	Leu17	Phe19	Phe20	Asp23
Initial Orientation	LS2	LS2	RS2	RB1	LS1		RS1	LS1			
				LB1			RS2				
				LB1							
				LS1							
Final Orientation	LS2	LS2	RS2	RB1	LS1		RS2				
			LS2	LB1			RS1				
				LB1							
				RS2							
				LS1							
				LS2							
Total =	66.28 kcal/mol										
Van der Waals =	109.30 kcal/mol										
Electrostatic =	-296.85 kcal/mol										
ΔE_{Tot} =	-82.85 kcal/mol										
ΔE_{Vdw} =	-8.88 kcal/mol										
ΔE_{Ele} =	-98.17 kcal/mol										
Initial Orientation	RS2	RS2		LB1	RB2		LS2	LS2		LB2	
				RB1	RS2		LS1			LS2	
				RB1							
				LS2							
Final Orientation		RS2		LB1	RB2		LS1	LS2		LB2	
				RB1	RS2		LS2				
				RB1							
				RS2							
				RNH							
				LS2							
Total =	78.13 kcal/mol										
Van der Waals =	106.48 kcal/mol										
Electrostatic =	-278.19 kcal/mol										
ΔE_{Tot} =	-71.01 kcal/mol										
ΔE_{Vdw} =	-11.70 kcal/mol										
ΔE_{Ele} =	-79.51 kcal/mol										
Initial Orientation	RS1			RB1	RS2		LS2	RS2			
				RS1			LS1				
				RS2							
				RB2							
Final Orientation	RS2		RS2	RS2			LS2		LB2		LB2
				RB2							
Total =	151.70 kcal/mol										
Van der Waals =	124.41 kcal/mol										
Electrostatic =	-225.50 kcal/mol										
ΔE_{Tot} =	2.56 kcal/mol										
ΔE_{Vdw} =	6.24 kcal/mol										
ΔE_{Ele} =	-26.82 kcal/mol										
Initial Orientation			RS2	RB1	LS2		RS2	CS			
				RS2	RB2		RS1	LB1			
				LB1				LS2			
				LS2							
Final Orientation			RS2	RB1	LB2		RS1	LB1			
				LS2	LS2		RS2	CS			
				LB1							
				RS2							
Total =	80.87 kcal/mol										
Van der Waals =	111.60 kcal/mol										
Electrostatic =	-282.14 kcal/mol										
ΔE_{Tot} =	-68.27 kcal/mol										
ΔE_{Vdw} =	-6.58 kcal/mol										
ΔE_{Ele} =	-83.46 kcal/mol										

	His6	Gly9	Tyr10	Val12	His13	His14	Gln15	Lys16	Leu17	Phe20
Initial Orientation			RS2		LB1	RB2		LS2	LS2	LB2
					LS2	RS2			RB2	LS2
					LS1					
					RB1					
Final Orientation			RS2		LB1	RB2		LS2	LS2	LB2
					LS2	RS2		LS1		
					LS1					
					RB1					
					RB2					
Total =	62.95 kcal/mol									
Van der Waals =	107.01 kcal/mol									
Electrostatic =	-275.90 kcal/mol									
ΔE_{Tot} =	-86.18 kcal/mol									
ΔE_{Vdw} =	-11.17 kcal/mol									
ΔE_{Ele} =	-77.22 kcal/mol									
Initial Orientation					LB1	RS1		LS2		LB2
					LS2					LS2
					LS1					
					RB1					
					RS1					
Final Orientation					LB1	RS1		LS1	LS2	LS2
					RB1			LS2		LB2
					LS1					
					RS1					
Total =	78.00 kcal/mol									
Van der Waals =	113.29 kcal/mol									
Electrostatic =	-286.24 kcal/mol									
ΔE_{Tot} =	-71.14 kcal/mol									
ΔE_{Vdw} =	-4.88 kcal/mol									
ΔE_{Ele} =	-87.56 kcal/mol									
Initial Orientation				RS2	RB1	LB2		RS1	LS2	
					LS2	LS2		RS2	LB1	
					LB1				CS	
					RNH					
					RS2					
Final Orientation			LS2	RS2	RB1	LS2		RS1	RB1	
					RS2			RS2	CS	
					RNH				LB1	
					LB1					
					LS2					
Total =	87.59 kcal/mol									
Van der Waals =	101.04 kcal/mol									
Electrostatic =	-289.46 kcal/mol									
ΔE_{Tot} =	-61.54 kcal/mol									
ΔE_{Vdw} =	-17.14 kcal/mol									
ΔE_{Ele} =	-90.78 kcal/mol									
Initial Orientation	LS2			RS2	RB1			RS1		
	LB2				CS			RS2		
					RS1					
					RS2					
Final Orientation	LS2	LS2		RS2	RB1			RB2		
					RS2			RS2		
	LB2				RS1			RS1		
					CS					
Total =	93.93 kcal/mol									
Van der Waals =	111.61 kcal/mol									
Electrostatic =	-275.35 kcal/mol									
ΔE_{Tot} =	-55.21 kcal/mol									
ΔE_{Vdw} =	-6.56 kcal/mol									
ΔE_{Ele} =	-76.67 kcal/mol									

Table 6.53: The solution phase results of solapsone interacting with the HHQK region of the 1IYT conformer of β-amyloid

	Arg5	His6	Gly9	Tyr10	Val12	His13	His14	Gln15	Lys16	Leu17	Gly9	Tyr10	His13	His14	Gln15	Lys16	Leu17	Phe20
Initial Orientation	LS2	LS2	LB1		CS	RB1			RS2				RB1	LB2		RS1	LB2	RB2
		LS1	CS		RS2	RS1							LB1					RS1
						CS							LB1					
													RS1					
													LNH					
Final Orientation	LS2	LS2	CS		CS	RB1			RS2				LB1	LB2		RS1	RS1	RB2
		LS1			RS2	RS1			RB2				LB1				RNH	RS1
						RS2							RB1					
													RS1					
													LNH					
													LB2					
Total =	55.70 kcal/mol										95.16 kcal/mol							
Van der Waals =	110.93 kcal/mol										107.05 kcal/mol							
Electrostatic =	-298.49 kcal/mol										-255.24 kcal/mol							
ΔE_{Tot} =	-93.44 kcal/mol										-53.98 kcal/mol							
ΔE_{Vdw} =	-7.25 kcal/mol										-11.13 kcal/mol							
ΔE_{Ele} =	-99.81 kcal/mol										-56.56 kcal/mol							
Initial Orientation				LB2	RB2	RB1	LB2		RB2	LS2	RS2	RS2	LS2	RB2		LS2		
						LS2	LS2		RS2				LB1	RS2				
						LB1												
						RNH												
						RS2												
Final Orientation				LB2		RB1	LB2		RB2		RS2	RS2	LS2	RB2		LS2		
						RS2	LS2		RS2			RB2	LB1	RS2				
						LS2							RB1					
						LB1							RS2					
						RNH												
Total =	86.78 kcal/mol										80.04 kcal/mol							
Van der Waals =	123.63 kcal/mol										110.15 kcal/mol							
Electrostatic =	-281.33 kcal/mol										-275.89 kcal/mol							
ΔE_{Tot} =	-62.36 kcal/mol										-69.10 kcal/mol							
ΔE_{Vdw} =	5.46 kcal/mol										-8.03 kcal/mol							
ΔE_{Ele} =	-82.65 kcal/mol										-77.21 kcal/mol							
Initial Orientation		RS1	RB1		LS1	LB1			LS2				LB1	RS2		LS2		
						CS			LS1				LS2					
						LS1							RB1					
Final Orientation		RS1	RB1		LB1	LB1			LS2			RS2	LB1	RS2		LS2	LS2	
					LS1	CS			LS1				LS2					
						LS1												
						LS2												
Total =	96.17 kcal/mol										90.98 kcal/mol							
Van der Waals =	118.77 kcal/mol										107.51 kcal/mol							
Electrostatic =	-281.41 kcal/mol										-278.19 kcal/mol							
ΔE_{Tot} =	-52.97 kcal/mol										-58.16 kcal/mol							
ΔE_{Vdw} =	0.59 kcal/mol										-10.67 kcal/mol							
ΔE_{Ele} =	-82.73 kcal/mol										-79.51 kcal/mol							
Initial Orientation			LB1	LS1		RB1	LB2		RB2									
			LNH						RS2									
			LS1															
Final Orientation			LB1	LB1	LNH	LB1	LB2		RB2									
			LNH			LS2			RS2									
			LS1			LB2												
Total =	115.21 kcal/mol																	
Van der Waals =	129.58 kcal/mol																	
Electrostatic =	-265.31 kcal/mol																	
ΔE_{Tot} =	-33.93 kcal/mol																	
ΔE_{Vdw} =	11.40 kcal/mol																	
ΔE_{Ele} =	-66.63 kcal/mol																	

Table 6.54: The solution phase results of solapsone interacting with the LVFF region of the 1IYT conformer of β-amyloid

	Val12	His13	His14	Lys16	Leu17	Val18	Phe19	Phe20	His13	His14	Lys16	Leu17	Val18	Phe19	Phe20	Asp23
Initial Orientation	LS1	LB1	RS1	LS2	CS			LS2	LB1	RS2	LS2	RS2			LS2	
		LS1		LS1	RB1				LS1		LS1	RB1			LB2	
		LNH							CS							
		RB1							LS2							
		RS1														
Final Orientation	LS1	LB1	RS1	LS2	LB1			LS2	LB1	RS2	LS2	RB1			LS2	
		LNH		LS1	CS				LB1			LS2			LB2	
		RB1			RB1				LS1							
		RS1							RS2							
									CS							
									LS2							
Total =	94.40 kcal/mol								98.63 kcal/mol							
Van der Waals =	108.60 kcal/mol								102.71 kcal/mol							
Electrostatic =	-297.85 kcal/mol								-259.19 kcal/mol							
ΔE_{Tot} =	-54.73 kcal/mol								-50.51 kcal/mol							
ΔE_{Vdw} =	-9.58 kcal/mol								-15.47 kcal/mol							
ΔE_{Ele} =	-99.17 kcal/mol								-60.51 kcal/mol							
Initial Orientation	LS2	LS2		LS1	RS2			CS	RS1		LB1			LS2	CS	CS
	LB2			LB1	RNH			LB1			LS1			LS1	RB1	
				LNH	RB1						LNH			LB1	RS2	
											RB1					
											RS1					
Final Orientation	LS2	LS2		LS1	RB2			LB1			LB1			LB1	RS2	CS
	LB2			LNH	RB1						RS1			LS1	RB1	
				LB2							RB1				CS	
											LNH					
											LS1					
Total =	124.38 kcal/mol								100.40 kcal/mol							
Van der Waals =	118.62 kcal/mol								101.49 kcal/mol							
Electrostatic =	-254.62 kcal/mol								-243.91 kcal/mol							
ΔE_{Tot} =	-24.76 kcal/mol								-48.74 kcal/mol							
ΔE_{Vdw} =	0.45 kcal/mol								-16.69 kcal/mol							
ΔE_{Ele} =	-55.94 kcal/mol								-45.23 kcal/mol							
Initial Orientation		LB1		CS	LB1			RB1								
		CS														
		LS1														
Final Orientation		CS		CS	LS1			RB1								
					LB1			RNH								
Total =	164.58 kcal/mol															
Van der Waals =	125.82 kcal/mol															
Electrostatic =	-203.80 kcal/mol															
ΔE_{Tot} =	15.44 kcal/mol															
ΔE_{Vdw} =	7.65 kcal/mol															
ΔE_{Ele} =	-5.12 kcal/mol															

Table 6.55: The solution phase results of solapsone interacting with the HHQKLVFF region of the 1IYT conformer of β-amyloid

	Gly9	Tyr10	Val12	His13	His14	Gln15	Lys16	Leu17	Val18	Phe19	Phe20
Initial Orientation	LS2	LS2		RB1 LB1 LS2	LS1		RS2	CS LS1			
Final Orientation	LS2 LB2	LB2		RB1 LB1 LS2	LS1		RS2	LS1			
Total =	113.62 kcal/mol										
Van der Waals =	121.38 kcal/mol										
Electrostatic =	-277.13 kcal/mol										
ΔE_{Tot} =	-35.52 kcal/mol										
ΔE_{Vdw} =	3.21 kcal/mol										
ΔE_{Ele} =	-78.45 kcal/mol										
Initial Orientation			LS2	LS1 LS2 LB2			RB1 LS1			RB2	
Final Orientation			LS2	LS1 LS2 LB2			LB1 RB1 LS1			RB1	
Total =	65.91 kcal/mol										
Van der Waals =	98.74 kcal/mol										
Electrostatic =	-272.65 kcal/mol										
ΔE_{Tot} =	-83.22 kcal/mol										
ΔE_{Vdw} =	-19.44 kcal/mol										
ΔE_{Ele} =	-73.97 kcal/mol										
Initial Orientation				RB1 LS2	LS2		RS2	CS LS1			
Final Orientation				RB1 LS2	LS2		RS2	CS LB1 LS1			
Total =	81.20 kcal/mol										
Van der Waals =	115.81 kcal/mol										
Electrostatic =	-274.88 kcal/mol										
ΔE_{Tot} =	-67.94 kcal/mol										
ΔE_{Vdw} =	-2.37 kcal/mol										
ΔE_{Ele} =	-76.20 kcal/mol										
Initial Orientation			RB1	LB2 LS2 LB1			RS2 LS2	LB2 LS2		RS2	LS1
Final Orientation			RB1	LB1 LS2 LB2			RS2 LS2	LS2 LB2		RS2	LS1
Total =	92.61 kcal/mol										
Van der Waals =	116.08 kcal/mol										
Electrostatic =	-265.70 kcal/mol										
ΔE_{Tot} =	-56.52 kcal/mol										
ΔE_{Vdw} =	-2.10 kcal/mol										
ΔE_{Ele} =	-67.02 kcal/mol										
Initial Orientation		RS1		LS2 LS1 LB1	RS1 RS2		LS2	LS2 RS2			LB2 LS2
Final Orientation		RS1		LB1 LS1 LS2	RS1		LS2	LS2			LB2 LS2
Total =	111.17 kcal/mol										
Van der Waals =	116.32 kcal/mol										
Electrostatic =	-251.32 kcal/mol										
ΔE_{Tot} =	-37.96 kcal/mol										
ΔE_{Vdw} =	-1.86 kcal/mol										
ΔE_{Ele} =	-52.64 kcal/mol										

	Tyr10	Val12	His13	His14	Gln15	Lys16	Leu17	Val18	Phe19	Phe20
Initial Orientation			RS1 RS2		LS2 LB2	LB1 RS2 LS2			LS2 LB2	RS2
Final Orientation			RS1 RS2		LS2 LB2	LB1 RS2 RB1 LS2	RB2 RS2		LS2 LB2	RB2 RS2
Total =	96.04 kcal/mol									
Van der Waals =	105.89 kcal/mol									
Electrostatic =	-252.91 kcal/mol									
ΔE_{Tot} =	-53.10 kcal/mol									
ΔE_{Vdw} =	-12.29 kcal/mol									
ΔE_{Ele} =	-54.23 kcal/mol									
Initial Orientation	RS2	LS2	LB1 LS1 RS2 RB1 LS2	RB2 RS2		LB1 LS2 LB2	RB1			
Final Orientation		LS2	LS1 LS2 LB1 RB1 RS2	RB2 RS2		LB2 LS2 LNH LB1	LB1 RB1 RNH			
Total =	68.21 kcal/mol									
Van der Waals =	112.63 kcal/mol									
Electrostatic =	-183.64 kcal/mol									
ΔE_{Tot} =	-80.93 kcal/mol									
ΔE_{Vdw} =	-5.54 kcal/mol									
ΔE_{Ele} =	15.04 kcal/mol									
Initial Orientation			LB1 LS1 CS LS2	RS2		LB2 LS2	RS2 RB1			LB2 LS2
Final Orientation			LB1 LS2 LS1 CS RS2	RS2		LB2 LS2	RB1			LB2 LS2
Total =	73.74 kcal/mol									
Van der Waals =	112.22 kcal/mol									
Electrostatic =	-283.82 kcal/mol									
ΔE_{Tot} =	-75.39 kcal/mol									
ΔE_{Vdw} =	-5.96 kcal/mol									
ΔE_{Ele} =	-85.14 kcal/mol									
Initial Orientation			RB1 RS2 LB1 LS1			RS1	LS1			
Final Orientation			LS1 LB1 RB1 RS2			RS1	LS1			
Total =	108.00 kcal/mol									
Van der Waals =	107.26 kcal/mol									
Electrostatic =	-300.86 kcal/mol									
ΔE_{Tot} =	-41.13 kcal/mol									
ΔE_{Vdw} =	-10.92 kcal/mol									
ΔE_{Ele} =	-102.18 kcal/mol									
Initial Orientation		RB1	LB1 LS1			RB2 LS1 LNH LB1 RNH RS1	LS1		RS1	LB2
Final Orientation		RB1 LB1	LB1 LS1			RB2 RS1 RNH LS1	LS1		RS1	LB2
Total =	85.58 kcal/mol									
Van der Waals =	107.26 kcal/mol									
Electrostatic =	-273.62 kcal/mol									
ΔE_{Tot} =	-63.55 kcal/mol									
ΔE_{Vdw} =	-10.92 kcal/mol									
ΔE_{Ele} =	-74.94 kcal/mol									

Table 6.55: The solution phase results of solapsone interacting with the HHQKLVFF region of the 1IYT conformer of β-amyloid

	Val12	His13	His14	Gln15	Lys16	Leu17	Val18	Phe19	Phe20	Val12	His13	His14	Gln15	Lys16	Leu17	Val18	Phe19	Phe20
Initial Orientation		RB1			LS1	LS1				RS1	RS1			LB1			LS1	
		RS2									RS2			RS2				
		LB1									RB2							
		LS1																
Final Orientation		RB1			RS1	LS1				RS2	RS1			RS1			LS1	
		RS2									RS2							
		LS1																
		LB1																
Total =	85.08 kcal/mol									74.01 kcal/mol								
Van der Waals =	121.99 kcal/mol									109.00 kcal/mol								
Electrostatic =	-278.95 kcal/mol									-281.01 kcal/mol								
ΔE_{Tot} =	-64.06 kcal/mol									-75.13 kcal/mol								
ΔE_{Vdw} =	3.82 kcal/mol									-9.18 kcal/mol								
ΔE_{Ele} =	-80.27 kcal/mol									-82.33 kcal/mol								
Initial Orientation		RB1	LS1		RS1	LB1			RB2	RS2	LB2			RB1	LS2			LB1
		LB1				LNH			RS1		LS2			RS1	LB2			LS1
		LS1												RS2				
														LS2				
Final Orientation		LNH	LS1		RS1	LB1			RS1	RS2	LB2			RB1	LS2			LB1
		LB1				RB1					LS2			RS1				LS1
		RB1				RNH								LS2				
Total =	98.79 kcal/mol									104.66 kcal/mol								
Van der Waals =	104.81 kcal/mol									115.21 kcal/mol								
Electrostatic =	-258.33 kcal/mol									-266.22 kcal/mol								
ΔE_{Tot} =	-50.35 kcal/mol									-44.48 kcal/mol								
ΔE_{Vdw} =	-13.37 kcal/mol									-2.97 kcal/mol								
ΔE_{Ele} =	-59.65 kcal/mol									-67.54 kcal/mol								
Initial Orientation		LB1	RS2		LS2	LS2			LB2		LS1		RS1	RB1			RB2	LB2
		LS1				RB1								LB1			RS1	
		LS2				RB2								RS1			RNH	
														RNH			RB1	
														LNH				
														LS1				
Final Orientation	LS2	LS2			RS2			RB2			LS1		RS1	LB1			RB2	LB2
	LB2	LB2			LS2			RS2						RB1			RS1	
														RS1			RNH	
														RNH			RB1	
														LNH				
														LS1				
Total =	125.61 kcal/mol									96.27 kcal/mol								
Van der Waals =	119.33 kcal/mol									100.62 kcal/mol								
Electrostatic =	-238.21 kcal/mol									-260.55 kcal/mol								
ΔE_{Tot} =	-23.53 kcal/mol									-52.87 kcal/mol								
ΔE_{Vdw} =	1.16 kcal/mol									-17.55 kcal/mol								
ΔE_{Ele} =	-39.53 kcal/mol									-61.87 kcal/mol								
Initial Orientation		RB1			RB2	LS1			RB2		RS2			RB1			LB2	RB2
		LS1			RNH	LNH								LS2			LS2	
		LB1				LB1								LB1				
		RNH												RS2				
		RS1																
Final Orientation		RB1			RB2	LS1			RB2		RS2			RB1	RB2		LS2	RB2
		LS1			RNH	LB1								LS2			LB2	
		LB1												LB1				
		RS1																
Total =	59.09 kcal/mol									105.51 kcal/mol								
Van der Waals =	98.00 kcal/mol									115.49 kcal/mol								
Electrostatic =	-287.23 kcal/mol									-266.74 kcal/mol								
ΔE_{Tot} =	-90.04 kcal/mol									-43.62 kcal/mol								
ΔE_{Vdw} =	-20.18 kcal/mol									-2.69 kcal/mol								
ΔE_{Ele} =	-88.55 kcal/mol									-68.06 kcal/mol								
Initial Orientation	RB2	LB1			RS1	LS2				RS2	LB2			RB1	LS2			LS2
	RS2	RS2			RS2	LB2					LS2			LS2				LB1
		LNH												CS				CS
		LB2												RS1				
														RS2				
Final Orientation	RS2	LB1			RS1	LS2				RS2	LB2			RB1	LS2			CS
		RS2			RS2						LB2			RS1	LB2			LB1
		RB1												RS2				LS2
		LNH												CS				
		LB2												LS2				
Total =	108.58 kcal/mol									150.22 kcal/mol								
Van der Waals =	118.01 kcal/mol									136.96 kcal/mol								
Electrostatic =	-251.14 kcal/mol									-252.43 kcal/mol								
ΔE_{Tot} =	-40.56 kcal/mol									1.09 kcal/mol								
ΔE_{Vdw} =	-0.17 kcal/mol									18.78 kcal/mol								
ΔE_{Ele} =	-52.46 kcal/mol									-53.75 kcal/mol								

Table 6.55: The solution phase results of solapsone interacting with the HHQKLVFF region of the 1IYT conformer of β-amyloid

	Val12	His13	His14	Gln15	Lys16	Leu17	Val18	Phe19	Phe20	His13	His14	Gln15	Lys16	Leu17	Val18	Phe19	Phe20
Initial Orientation	RS2	RB2		LS2	RB1			LB1		RB1	LS1		RB2	RS1			RS1
		RS2		LB2	LB1			LNH		RS2			RS2	LB1			
					RS2			LS1		RS1			RS1				
								LB2		CS							
Final Orientation	RS2	RB2		LS2	RB1			LB2		RB1	LS1		RS1	RS1			RS1
		RS2		LB2	LB1			LNH		RB1			RS2				RB2
					RS2			LB1		CS			RB2				
										RS1							
										RS2							
Total =	95.08 kcal/mol									152.71 kcal/mol							
Van der Waals =	99.70 kcal/mol									126.30 kcal/mol							
Electrostatic =	-262.39 kcal/mol									-235.86 kcal/mol							
ΔE_{Tot} =	-54.06 kcal/mol									3.57 kcal/mol							
ΔE_{Vdw} =	-18.48 kcal/mol									8.12 kcal/mol							
ΔE_{Ele} =	-63.71 kcal/mol									-37.18 kcal/mol							
Initial Orientation		RS2			LB1	RS2			RB1	RS2			RB1			LS2	RB2
		RB2			LS2	RB2							LS2			LB2	
					LNH								RS2				
					RS2												
Final Orientation		RS2			LB1	RB2			RB1	RS2			RB1	RB2		LB2	RB2
					RS2	RS2							LS2			LS2	RNH
					LNH								RS2				
Total =	104.55 kcal/mol									87.19 kcal/mol							
Van der Waals =	114.34 kcal/mol									117.35 kcal/mol							
Electrostatic =	-240.99 kcal/mol									-272.28 kcal/mol							
ΔE_{Tot} =	-44.59 kcal/mol									-61.94 kcal/mol							
ΔE_{Vdw} =	-3.83 kcal/mol									-0.83 kcal/mol							
ΔE_{Ele} =	-42.31 kcal/mol									-73.60 kcal/mol							
Initial Orientation		RS2			RB1			LB2	RB2								
					LS2			LS2									
					RS2												
Final Orientation		RS2			RB1	RB2		LB2	RB2								
					LS2	RS2			RS1								
					RS2				RNH								
Total =	70.69 kcal/mol																
Van der Waals =	103.22 kcal/mol																
Electrostatic =	-265.84 kcal/mol																
ΔE_{Tot} =	-78.44 kcal/mol																
ΔE_{Vdw} =	-14.95 kcal/mol																
ΔE_{Ele} =	-67.16 kcal/mol																

Table 6.56: The solution phase results of solapsone interacting with the HHQK region of the 1Z0Q conformer of β-amyloid

	Gly9	Tyr10	His13	His14	Gln15	Lys16	Leu17	Val18
Initial Orientation	CS	CS	LB1 LS1 CS	RS1 RS2		LS2	RS2	RS2
Final Orientation		CS	LB1 CS LS1	RS1 RS2		LS2 RS2	RS2	RS2
Total =	61.47 kcal/mol							
Van der Waals =	90.80 kcal/mol							
Electrostatic =	-295.15 kcal/mol							
ΔE_{Tot} =	-169.52 kcal/mol							
ΔE_{Vdw} =	-33.01 kcal/mol							
ΔE_{Ele} =	-143.78 kcal/mol							
Initial Orientation		LS2	RS2 LS2	LS2 LB2		RB1 RS1 LS1	LS1	
Final Orientation	LS2	LS2	RS2 LS2	LS1 LS2 LB2		RB1 RS1 LB1 LS1	LS1 -NH-	
Total =	105.04 kcal/mol							
Van der Waals =	115.26 kcal/mol							
Electrostatic =	-278.29 kcal/mol							
ΔE_{Tot} =	-125.95 kcal/mol							
ΔE_{Vdw} =	-8.55 kcal/mol							
ΔE_{Ele} =	-126.92 kcal/mol							
Initial Orientation	CS	CS	LB1 LS1 LS2	RS2 RS1		LS2 RS2		
Final Orientation	CS	CS	LS1 LB1 RS2	RS1 RS2		LS2	RS2 RB2	
Total =	78.98 kcal/mol							
Van der Waals =	98.36 kcal/mol							
Electrostatic =	-270.63 kcal/mol							
ΔE_{Tot} =	-152.01 kcal/mol							
ΔE_{Vdw} =	-25.44 kcal/mol							
ΔE_{Ele} =	-119.27 kcal/mol							
Initial Orientation	RB1		RB1 RNH RS1 RB2	LS2 LS1		LS1		
Final Orientation	RB1	CS	RB2 RS1 RNH RB1	LS2 LS1		LS1		
Total =	92.66 kcal/mol							
Van der Waals =	103.89 kcal/mol							
Electrostatic =	-274.39 kcal/mol							
ΔE_{Tot} =	-138.33 kcal/mol							
ΔE_{Vdw} =	-19.91 kcal/mol							
ΔE_{Ele} =	-123.03 kcal/mol							
Initial Orientation	LB1	LS1 LNH LB1	LB1 RB1 RB1 LNH RNH	LB2 LS1		RS2 RB1		
Final Orientation	LB1	LB1 LS1	LB1 RB1	LB2 LS1		RS2 RB1	LB2	LB2
Total =	77.71 kcal/mol							
Van der Waals =	106.97 kcal/mol							
Electrostatic =	-284.21 kcal/mol							
ΔE_{Tot} =	-153.29 kcal/mol							
ΔE_{Vdw} =	-16.83 kcal/mol							
ΔE_{Ele} =	-132.85 kcal/mol							

	Gly9	Tyr10	Val12	His13	His14	Gln15	Lys16	Leu17	Val18	Ala21
Initial Orientation	CS	CS		LB1 LS1 LS2	RS2 RS1		LS2 RS2			
Final Orientation		CS		LS1 LS2 LB1	RS1 RS2		LS2 LB2		RS2	
Total =	86.68 kcal/mol									
Van der Waals =	107.33 kcal/mol									
Electrostatic =	-286.32 kcal/mol									
ΔE_{Tot} =	-144.31 kcal/mol									
ΔE_{Vdw} =	-16.48 kcal/mol									
ΔE_{Ele} =	-134.96 kcal/mol									
Initial Orientation	LS1	CS		LB1 LS2 LS1	RB1 CS RS1 RS2		LB2 LS2	RS2	RS2	
Final Orientation		CS		LB1 LS1 LS2	RB1 RS2 RS1 CS LB1		LB2 LS2	RB2 RS2	RS2	RB2
Total =	89.70 kcal/mol									
Van der Waals =	104.70 kcal/mol									
Electrostatic =	-265.21 kcal/mol									
ΔE_{Tot} =	-141.29 kcal/mol									
ΔE_{Vdw} =	-19.11 kcal/mol									
ΔE_{Ele} =	-113.85 kcal/mol									
Initial Orientation				RB1 RS1 RS2	LS2 LS1		RS1 RB1 RNH			
Final Orientation				RB1 RS1 RS2	LS2 LS1		RB1 RNH RS1		LS1	
Total =	80.91 kcal/mol									
Van der Waals =	107.01 kcal/mol									
Electrostatic =	-286.02 kcal/mol									
ΔE_{Tot} =	-150.08 kcal/mol									
ΔE_{Vdw} =	-16.80 kcal/mol									
ΔE_{Ele} =	-134.65 kcal/mol									
Initial Orientation		CS		LS2 LS1	RB1 RS1 RS2		LB2 LS2			
Final Orientation		CS		LB1 RS1 LS1 LS2	RS2		LB2 LS2		RS2	
Total =	96.34 kcal/mol									
Van der Waals =	123.05 kcal/mol									
Electrostatic =	-285.13 kcal/mol									
ΔE_{Tot} =	-134.66 kcal/mol									
ΔE_{Vdw} =	-0.76 kcal/mol									
ΔE_{Ele} =	-133.76 kcal/mol									
Initial Orientation				LS2 LS1	RB2		LS2		RB2	
Final Orientation			LS2	LS2 LS1	RS2		LS2 LB2		RB2	
Total =	99.54 kcal/mol									
Van der Waals =	112.06 kcal/mol									
Electrostatic =	-269.73 kcal/mol									
ΔE_{Tot} =	-131.45 kcal/mol									
ΔE_{Vdw} =	-11.74 kcal/mol									
ΔE_{Ele} =	-118.37 kcal/mol									

Table 6.56: The solution phase results of solapsone interacting with the HHQK region of the 1Z0Q conformer of β-amyloid

	Gly9	Tyr10	His13	His14	Gln15	Lys16	Leu17	Val18
Initial Orientation		CS	LS1	RB1		LB1		
			CS	RS2		LS2		
				CS		LS1		
				RS1				
Final Orientation		CS	LS1	RB1		LS2		
				RB1				
				RS2		LS1		
				CS				
Total =	81.46 kcal/mol							
Van der Waals =	98.03 kcal/mol							
Electrostatic =	-294.67 kcal/mol							
ΔE_{Tot} =	-149.53 kcal/mol							
ΔE_{Vdw} =	-25.78 kcal/mol							
ΔE_{Ele} =	-143.30 kcal/mol							
Initial Orientation		LS2	RS2	LS1		RS2		
			CS	CS		RS1		
						CS		
Final Orientation		LS2	RS2	LS1		RS1		
			CS	CS		RS2		
						CS		
Total =	95.97 kcal/mol							
Van der Waals =	106.83 kcal/mol							
Electrostatic =	-279.21 kcal/mol							
ΔE_{Tot} =	-135.02 kcal/mol							
ΔE_{Vdw} =	-16.98 kcal/mol							
ΔE_{Ele} =	-127.84 kcal/mol							
Initial Orientation			RS2	LB1		RS1	CS	
				LS1		CS		
				CS				
Final Orientation	RS2		RS2	LB1		RS1	CS	CS
			RB1	LS1				
				CS				
Total =	135.81 kcal/mol							
Van der Waals =	98.88 kcal/mol							
Electrostatic =	-286.81 kcal/mol							
ΔE_{Tot} =	-95.18 kcal/mol							
ΔE_{Vdw} =	-24.92 kcal/mol							
ΔE_{Ele} =	-135.45 kcal/mol							
Initial Orientation			RB2	LB2		RS2	CS	LB2
			RS1	LNH		CS		
						RB1		
Final Orientation			RB2	LB2		RS2	LB1	LB2
			RS1	LS1		CS	CS	
				LNH		RB1		
				LB1				
Total =	99.92 kcal/mol							
Van der Waals =	101.42 kcal/mol							
Electrostatic =	-260.23 kcal/mol							
ΔE_{Tot} =	-131.07 kcal/mol							
ΔE_{Vdw} =	-22.39 kcal/mol							
ΔE_{Ele} =	-108.86 kcal/mol							

	Gly9	Tyr10	His13	His14	Gln15	Lys16	Leu17	Val18	Ala21	Glu22
Initial Orientation	RS2		RS2	LS1		RS1				
			RS1	LS2						
Final Orientation	RS2	CS	RS2	LS1		RS1		LS1		
			RS1	RS1						
				LB1						
				LS2						
Total =	87.11 kcal/mol									
Van der Waals =	95.49 kcal/mol									
Electrostatic =	-291.66 kcal/mol									
ΔE_{Tot} =	-143.88 kcal/mol									
ΔE_{Vdw} =	-28.32 kcal/mol									
ΔE_{Ele} =	-140.30 kcal/mol									
Initial Orientation			RB2	LNH		RS2		LB2	LB2	
			RS1	LS1		RB1				
			RNH							
			RB1							
Final Orientation			RB1	LS1		RS2	LS2	LB2	LB2	LB2
			RNH	LNH			LB1			
			RS1							
			RB2							
Total =	65.78 kcal/mol									
Van der Waals =	105.04 kcal/mol									
Electrostatic =	-285.56 kcal/mol									
ΔE_{Tot} =	-165.21 kcal/mol									
ΔE_{Vdw} =	-18.76 kcal/mol									
ΔE_{Ele} =	-134.19 kcal/mol									
Initial Orientation			RB2	LS2		RS1	CS			
			RS2			RS2				
						RB1				
						CS				
Final Orientation			RB2	CS		RS1	CS			
			RS2	LS2		CS				
Total =	88.89 kcal/mol									
Van der Waals =	100.60 kcal/mol									
Electrostatic =	-279.59 kcal/mol									
ΔE_{Tot} =	-142.10 kcal/mol									
ΔE_{Vdw} =	-23.21 kcal/mol									
ΔE_{Ele} =	-128.23 kcal/mol									

Table 6.57: The solution phase results of solapsone interacting with the LVFF region of the 1Z0Q conformer of β-amyloid

	His14	Lys16	Leu17	Val18	Phe19	Phe20	Ala21	Glu22	Asp23	Val24	Lys28
Initial Orientation	LB2	RS1	RB1	LB2							
	LS1	RNH	LB1								
Final Orientation	LB2	RS1	LB1	LB2			LB2				
	LS1	RNH	RB1								
Total =	123.99 kcal/mol										
Van der Waals =	91.09 kcal/mol										
Electrostatic =	-239.26 kcal/mol										
ΔE_{Tot} =	-107.00 kcal/mol										
ΔE_{Vdw} =	-32.71 kcal/mol										
ΔE_{Ele} =	-87.90 kcal/mol										
Initial Orientation	LB2	LS1	LS1	LB2		RS2	LB2	LB2			
	LS2		LNH			RB2	LB1				
	LS1		LB1								
Final Orientation	LS1		LB1	LB2		RS2	LB2	LB2			
	LB2		LNH								
			LS1								
Total =	140.06 kcal/mol										
Van der Waals =	89.57 kcal/mol										
Electrostatic =	-216.73 kcal/mol										
ΔE_{Tot} =	-90.93 kcal/mol										
ΔE_{Vdw} =	-34.24 kcal/mol										
ΔE_{Ele} =	-65.36 kcal/mol										
Initial Orientation		LB2	LB2			RB1					RS1
						LB1					RNH
Final Orientation		LB2	LNH			RB1				RNH	RS1
			LB2			LB1					RNH
Total =	123.37 kcal/mol										
Van der Waals =	103.45 kcal/mol										
Electrostatic =	-246.04 kcal/mol										
ΔE_{Tot} =	-107.62 kcal/mol										
ΔE_{Vdw} =	-20.35 kcal/mol										
ΔE_{Ele} =	-94.67 kcal/mol										
Initial Orientation			LS2			RB2			RB2	RS2	RS2
						RS2					RB2
						RB1					
						CS					
						LS2					
Final Orientation			LB2		RB2	LS2			RB2	RS2	RS2
			LS2			RB1					RB2
						RS2					
						RB2					
Total =	165.22 kcal/mol										
Van der Waals =	107.33 kcal/mol										
Electrostatic =	-204.46 kcal/mol										
ΔE_{Tot} =	-65.77 kcal/mol										
ΔE_{Vdw} =	-16.48 kcal/mol										
ΔE_{Ele} =	-53.10 kcal/mol										

	Val12	His14	Gln15	Lys16	Leu17	Val18	Phe19	Phe20	Val24	Lys28
Initial Orientation		RB2		LS2	LB1	RB2				
		RS2		LB1	RB1					
Final Orientation		RB2		LS2	LB1	RB2				
		RS2		LB1	RB1					
Total =	157.95 kcal/mol									
Van der Waals =	74.05 kcal/mol									
Electrostatic =	-246.76 kcal/mol									
ΔE_{Tot} =	-73.04 kcal/mol									
ΔE_{Vdw} =	-49.76 kcal/mol									
ΔE_{Ele} =	-95.40 kcal/mol									
Initial Orientation	RB2		RB2	RB1	LB2		RB1	LS2		
				RB2	LS2		RS2			
Final Orientation	RB2		RB2	RB1	LS2		RS2	CS		
				RB2	LB2		RB1			
				LB1						
Total =	180.86 kcal/mol									
Van der Waals =	100.81 kcal/mol									
Electrostatic =	-245.74 kcal/mol									
ΔE_{Tot} =	-50.13 kcal/mol									
ΔE_{Vdw} =	-22.99 kcal/mol									
ΔE_{Ele} =	-94.38 kcal/mol									
Initial Orientation							RS1	LB1	LS1	LS1
								RB1		LNH
Final Orientation							RNH	LB1	LS1	LS1
								CS		LNH
								RB1		
Total =	159.14 kcal/mol									
Van der Waals =	126.30 kcal/mol									
Electrostatic =	-222.41 kcal/mol									
ΔE_{Tot} =	-71.85 kcal/mol									
ΔE_{Vdw} =	2.49 kcal/mol									
ΔE_{Ele} =	-71.05 kcal/mol									

Table 6.58: The solution phase results of solapsone interacting with the HHQKLVFF region of the 1Z0Q conformer of β-amyloid

	His13	His14	Gln15	Lys16	Leu17	Val18	Phe19	Phe20	Ala21
Initial Orientation	RS2 RB1	LS1		RS1 RS2	LS2				LB2
Final Orientation	RB2 RS2 RB1	LB1 LNH LS1		RS1 RS2	LS2 LB2	LB2			LB2
Total =	93.57 kcal/mol								
Van der Waals =	108.79 kcal/mol								
Electrostatic =	-279.42 kcal/mol								
ΔE_{Tot} =	-137.43 kcal/mol								
ΔE_{Vdw} =	-15.01 kcal/mol								
ΔE_{Ele} =	-128.06 kcal/mol								
Initial Orientation	RS1 RS2			LB1 RB1 RS2			LB2		
Final Orientation	RS1 RS2			RB1 RS2			LB2		
Total =	119.94 kcal/mol								
Van der Waals =	120.35 kcal/mol								
Electrostatic =	-258.00 kcal/mol								
ΔE_{Tot} =	-111.05 kcal/mol								
ΔE_{Vdw} =	-3.45 kcal/mol								
ΔE_{Ele} =	-106.63 kcal/mol								
Initial Orientation	LS2	RB2 RS2		LS2 LNH LB1 RS2		RB2			
Final Orientation	LS2	RB2 RS2		LS2 LB1	RB2	RB2			
Total =	127.83 kcal/mol								
Van der Waals =	113.03 kcal/mol								
Electrostatic =	-241.42 kcal/mol								
ΔE_{Tot} =	-103.16 kcal/mol								
ΔE_{Vdw} =	-10.77 kcal/mol								
ΔE_{Ele} =	-90.05 kcal/mol								
Initial Orientation	RS1	LB2		RS2 RB1 RNH		LB2			LB2
Final Orientation	RS1	LB2		RS2 RB2 RB1		LB2			
Total =	98.04 kcal/mol								
Van der Waals =	112.02 kcal/mol								
Electrostatic =	-263.50 kcal/mol								
ΔE_{Tot} =	-132.96 kcal/mol								
ΔE_{Vdw} =	-11.78 kcal/mol								
ΔE_{Ele} =	-112.14 kcal/mol								
Initial Orientation	LS2			LB1 RS2	RS2				
Final Orientation	LS2			LB1 LS2 LNH RS2					
Total =	113.72 kcal/mol								
Van der Waals =	121.57 kcal/mol								
Electrostatic =	-269.69 kcal/mol								
ΔE_{Tot} =	-117.28 kcal/mol								
ΔE_{Vdw} =	-2.23 kcal/mol								
ΔE_{Ele} =	-118.33 kcal/mol								
Initial Orientation	RS1 RS2			RS2			LB2		
Final Orientation	RB2 RS2 RS1			RS2			LB2		
Total =	148.90 kcal/mol								
Van der Waals =	123.58 kcal/mol								
Electrostatic =	-252.48 kcal/mol								
ΔE_{Tot} =	-82.09 kcal/mol								
ΔE_{Vdw} =	-0.23 kcal/mol								
ΔE_{Ele} =	-101.11 kcal/mol								

	Gly9	Tyr10	Val12	His13	His14	Gln15	Lys16	Leu17	Val18	Phe19	Phe20	Ala21
Initial Orientation				RS1 RNH RB1	LS1 LB2		RS2	LS1	LS1 LB2			LB2
Final Orientation				RB2 RS1 RNH	LS2		RS2 RB2	LS2	LS2 LB2			
Total =	95.27 kcal/mol											
Van der Waals =	101.71 kcal/mol											
Electrostatic =	-260.11 kcal/mol											
ΔE_{Tot} =	-135.72 kcal/mol											
ΔE_{Vdw} =	-22.10 kcal/mol											
ΔE_{Ele} =	-108.75 kcal/mol											
Initial Orientation				LS2	RS2		LS2 LS1 LB1 RS2	RS2				
Final Orientation				LS2 RS2	RB2 RS2		RS2 LB1 LNH LS2	RB2 RS2	RS2			
Total =	133.89 kcal/mol											
Van der Waals =	101.96 kcal/mol											
Electrostatic =	-249.93 kcal/mol											
ΔE_{Tot} =	-97.10 kcal/mol											
ΔE_{Vdw} =	-21.84 kcal/mol											
ΔE_{Ele} =	-98.56 kcal/mol											
Initial Orientation	LS1	LS1		LS1	RB1 LB1 CS RNH		LB1 LS2 CS	CS	RB1			RS1
Final Orientation			LB1 CS	LB1 LS2 LS1		CS	LS1 LB1			RB1		
Total =	123.93 kcal/mol											
Van der Waals =	112.96 kcal/mol											
Electrostatic =	-242.54 kcal/mol											
ΔE_{Tot} =	-107.06 kcal/mol											
ΔE_{Vdw} =	-10.85 kcal/mol											
ΔE_{Ele} =	-91.17 kcal/mol											
Initial Orientation	RS1	RS2 RB2		RS2 RS1			LS2 LB1	LB2				
Final Orientation	RS2 RS1	RB2 RS2		RS1 RS2	RS2		LB1 LNH LS2					
Total =	92.59 kcal/mol											
Van der Waals =	93.88 kcal/mol											
Electrostatic =	-266.74 kcal/mol											
ΔE_{Tot} =	-138.40 kcal/mol											
ΔE_{Vdw} =	-29.93 kcal/mol											
ΔE_{Ele} =	-115.38 kcal/mol											
Initial Orientation				RS1			RS2 LB1			LS2 LB2		
Final Orientation				RS2 RS1			LS2 RS2 LB1			LB2		
Total =	85.13 kcal/mol											
Van der Waals =	98.00 kcal/mol											
Electrostatic =	-271.55 kcal/mol											
ΔE_{Tot} =	-145.86 kcal/mol											
ΔE_{Vdw} =	-25.80 kcal/mol											
ΔE_{Ele} =	-120.18 kcal/mol											
Initial Orientation	RB2	RB2		RB2	RNH RS1		LS1 LNH LB1 RB1	LB1				
Final Orientation	RB2	RS1		RNH RB2	RB1 RNH RS1		LS2 LNH LB1	LB1				
Total =	177.03 kcal/mol											
Van der Waals =	90.37 kcal/mol											
Electrostatic =	-249.01 kcal/mol											
ΔE_{Tot} =	-53.97 kcal/mol											
ΔE_{Vdw} =	-33.43 kcal/mol											
ΔE_{Ele} =	-97.65 kcal/mol											

Table 6.58: The solution phase results of solapsone interacting with the HHQKLVFF region of the 1Z0Q conformer of β-amyloid

	Gly9	Tyr10	His13	His14	Gln15	Lys16	Leu17	Val18	Phe19	Phe20
Initial Orientation			LB2 LS1	LB2		LB1 RB1 LNH RNH	RB2			
Final Orientation			LB2 LS1	LB2		LB1 RB1 LNH RNH	RB2			
Total =	179.90 kcal/mol									
Van der Waals =	110.11 kcal/mol									
Electrostatic =	-264.31 kcal/mol									
ΔE_{Tot} =	-51.10 kcal/mol									
ΔE_{Vdw} =	-13.69 kcal/mol									
ΔE_{Ele} =	-112.95 kcal/mol									
Initial Orientation		LS1	LS1 LB1 LNH	LB2 LS1		RB1 LB1 RNH LNH	LS2 LB2	LB2		
Final Orientation	LS1	LS1	LS1 LNH* *C=O LB1	LB2 LS1		RB1 LB1 RNH	LB2	LB2		
Total =	104.45 kcal/mol									
Van der Waals =	104.49 kcal/mol									
Electrostatic =	-251.10 kcal/mol									
ΔE_{Tot} =	-126.54 kcal/mol									
ΔE_{Vdw} =	-19.32 kcal/mol									
ΔE_{Ele} =	-99.74 kcal/mol									
Initial Orientation		CS		LB1 LS2 CS LS1		LS1	LB2	LS2		
Final Orientation		CS		LB1 CS LS1		LS1	LS2	LS2		
Total =	145.19 kcal/mol									
Van der Waals =	104.62 kcal/mol									
Electrostatic =	-239.18 kcal/mol									
ΔE_{Tot} =	-85.80 kcal/mol									
ΔE_{Vdw} =	-19.19 kcal/mol									
ΔE_{Ele} =	-87.82 kcal/mol									
Initial Orientation			RS2 RB2			LB1 RB1 RS2	LB2 LS1			LB2
Final Orientation			RB2 RS2			RB1 RS2 LB1	LS1 LB2			LB2
Total =	120.12 kcal/mol									
Van der Waals =	101.57 kcal/mol									
Electrostatic =	-246.72 kcal/mol									
ΔE_{Tot} =	-110.87 kcal/mol									
ΔE_{Vdw} =	-22.23 kcal/mol									
ΔE_{Ele} =	-95.36 kcal/mol									
Initial Orientation	RB2		RS1 RS2			RS2 RB1	LS2			
Final Orientation	RB2		RS1 RS2	RS2		RB1 RS1	LS2 LB2			
Total =	121.98 kcal/mol									
Van der Waals =	111.63 kcal/mol									
Electrostatic =	-272.47 kcal/mol									
ΔE_{Tot} =	-109.01 kcal/mol									
ΔE_{Vdw} =	-12.17 kcal/mol									
ΔE_{Ele} =	-121.11 kcal/mol									
Initial Orientation			LB1 LNH LS1			LS2			RB2	
Final Orientation			LB1 LNH LS1			LS2			RB2	
Total =	171.88 kcal/mol									
Van der Waals =	125.38 kcal/mol									
Electrostatic =	-217.11 kcal/mol									
ΔE_{Tot} =	-59.11 kcal/mol									
ΔE_{Vdw} =	1.58 kcal/mol									
ΔE_{Ele} =	-65.75 kcal/mol									

	Val12	His13	His14	Gln15	Lys16	Leu17	Val18	Phe19	Phe20
Initial Orientation	LS2	LS2 LS1			LB1 LS2	RS2		RS2	RB2
Final Orientation	LB2 LS2	LS2 LS1			LB1 LS2 RB1 RS2	RS2		RS2 RB2	RS2 RB2
Total =	134.98 kcal/mol								
Van der Waals =	86.53 kcal/mol								
Electrostatic =	-231.01 kcal/mol								
ΔE_{Tot} =	-96.01 kcal/mol								
ΔE_{Vdw} =	-37.28 kcal/mol								
ΔE_{Ele} =	-79.64 kcal/mol								
Initial Orientation		LNH LS1 LB2	LB2		RB1 LB1 LB2			RB2	
Final Orientation		LNH LS1 LB2	LB2		RB1 RB2 LB1			RB2	
Total =	166.92 kcal/mol								
Van der Waals =	110.29 kcal/mol								
Electrostatic =	-255.24 kcal/mol								
ΔE_{Tot} =	-64.07 kcal/mol								
ΔE_{Vdw} =	-13.52 kcal/mol								
ΔE_{Ele} =	-103.88 kcal/mol								
Initial Orientation		RB2 RB1 RNH RS1			RS2 RB1	LB2			
Final Orientation	RB2	RB2 RNH RB1			RB1 RS2 LB2	LB2			
Total =	117.58 kcal/mol								
Van der Waals =	103.64 kcal/mol								
Electrostatic =	-241.77 kcal/mol								
ΔE_{Tot} =	-113.41 kcal/mol								
ΔE_{Vdw} =	-20.17 kcal/mol								
ΔE_{Ele} =	-90.41 kcal/mol								
Initial Orientation		LS1			RB1 LB1	RS1			
Final Orientation		LS1			RB1 LB1	RS1			
Total =	142.52 kcal/mol								
Van der Waals =	110.36 kcal/mol								
Electrostatic =	-255.42 kcal/mol								
ΔE_{Tot} =	-88.47 kcal/mol								
ΔE_{Vdw} =	-13.45 kcal/mol								
ΔE_{Ele} =	-104.06 kcal/mol								
Initial Orientation		LS2			LB1 LS1 RB1 RS1	RS1			
Final Orientation		LB2 LS2			RB1 LS1 LB1 RNH RS1	RS1		RS1	
Total =	126.28 kcal/mol								
Van der Waals =	111.98 kcal/mol								
Electrostatic =	-251.85 kcal/mol								
ΔE_{Tot} =	-104.71 kcal/mol								
ΔE_{Vdw} =	-11.82 kcal/mol								
ΔE_{Ele} =	-100.48 kcal/mol								

The addition of water molecules into the solapsone-Aβ systems has minimal effect on the binding interactions that occur. Overall the electrostatic energies tend to be significantly more favourable than the van der Waals energies in the binding interactions. Solapsone is capable of forming multiple binding interactions within the **HH**Q**K** and LVFF regions, as well as overlapping both regions. An example of binding occurring with the **HH**Q**K** region can be seen in Figure 6.7.

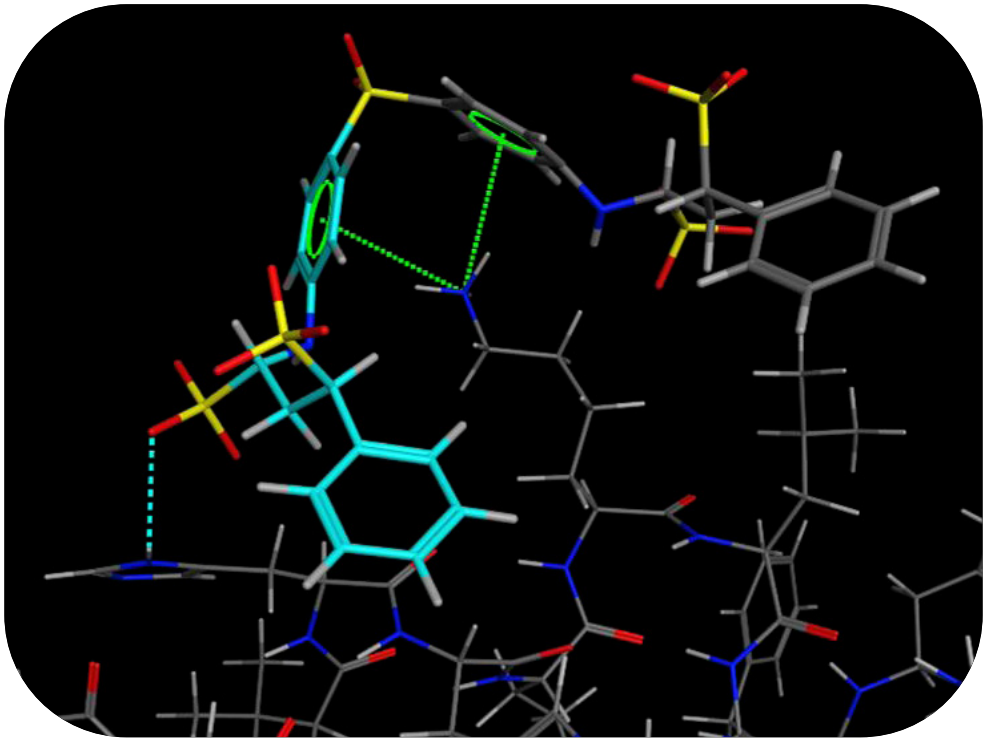

Figure 6.7: Solapsone interacting with β-amyloid after solution phase optimization. Water molecules have been removed for clarity. Dashed green lines indicate cation-π interactions between the aromatic rings and Lys16. The dashed blue line indicates an electrostatic type interaction between one of the sulfonate groups and His13.

6.4 Biological Validation of Solapsone-Gd^{3+} as an Imaging Agent

Given the positive *in silico* results of solapsone-Gd^{3+} interacting with β-amyloid, as well as solapsone binding to Aβ, it was determined that solapsone should be tested for its *in vitro* capacity to bind to the protein.

As solapsone is no longer commercially available, the compound had to be synthesized and then complexed with gadolinium in a 1:1 and 2:1 ratio of solapsone to metal ion (*in silico* studies showed that gadolinium could chelate with two solapsone molecules simultaneously). Solapsone was synthesized (by Dr. Arun Yadav) via the following scheme in Figure 6.5.

A thioflavin-T assay was performed by Rose Chen to compare the anti-aggregation ability of solapsone and solapsone-Gd^{3+}. The results are given in Figure 6.9.

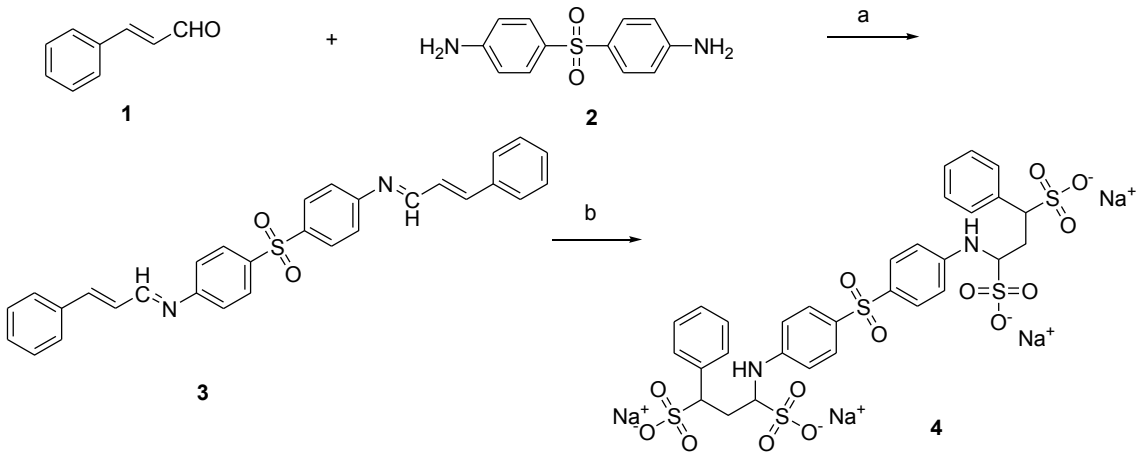

Figure 6.8: Synthesis of solapsone

A thioflavin-T assay was performed by Rose Chen to compare the anti-aggregation ability of solapsone and solapsone-Gd^{3+}. The results are given in Figure 6.9.

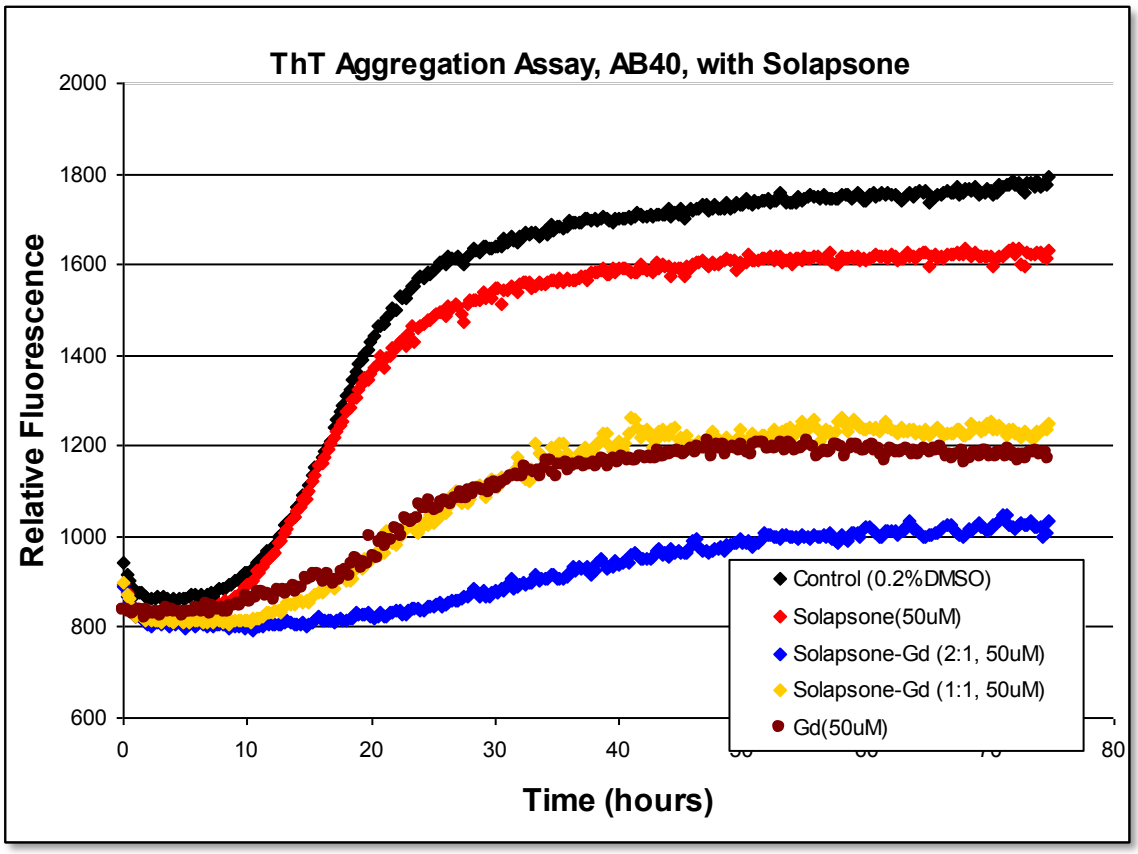

Figure 6.9: Thioflavin T assay of solapsone and solapsone-Gd^{3+}

The results of the ThT assay show that solapsone is capable of binding to Aβ to prevent aggregation from occurring. A 1:1 complex of solapsone-Gd^{3+} decreases aggregation significantly, meaning that it can bind to the smaller soluble forms of β-amyloid. The 2:1 complex binds even more strongly to Aβ than the 1:1 complex. Interestingly, gadolinium on its own demonstrates a capacity to inhibit amyloid aggregation; however, the goal is to cure AD, not kill the patient in the process, as would occur with giving patients a heavy metal such as gadolinium. Only miniscule amounts of

gadolinium would be required to complex with solapsone to make a viable imaging agent, and thus would be well tolerated (given gadolinium is used in current MRI agents).

Furthermore, an animal study is underway to test the efficacy of solapsone-Gd^{3+} as an imaging agent for MRI. This study involves the use of an APP/PS1 doubly transgenic mouse model of AD. At six months of age, the mice will be injected with the solapsone-Gd^{3+} complex at a single dose of 25 mg/kg. MRI images will be captured at 15, 30 and 60 minutes after injection to determine how well the imaging agent performs.

6.5 Conclusions on Solapsone as a Diagnostic Imaging Agent for Alzheimer's Disease

The *in silico* and *in vitro* studies of solapsone-Gd^{3+} as a diagnostic agent are quite favourable. The molecular modelling suggests that solapsone is more than capable of binding to β-amyloid while also chelating a paramagnetic ion such as gadolinium. This is further supported by *in vitro* testing showing a decrease in amyloid aggregation. This truly is a novel diagnostic agent, as all of the currently available imaging agents for AD being developed are being analogued from molecules used to bind to the aggregated forms of β-amyloid, and they only bind to the plaques. Solapsone has already been used in humans, and thus would be more market ready, and given that it binds to the soluble forms of Aβ that are responsible for the disease, it would allow for earlier diagnosis of the disease. The fact that solapsone-Gd^{3+} could be used in MRI imaging is also a boon, as most all hospitals have a MRI machine (this is not the case for PET imaging).

Overall solapsone presents itself as an excellent potential imaging agent for Alzheimer's disease, and a provisional patent for the solapsone-Gd^{3+} complex (which also includes a novel synthetic route for solapsone) has been filed.

6.6 INTERPRETATION

The *in silico* optimization of solapsone-Gd^{3+} with different conformations of β-amyloid suggests that the complex can bind to monomeric forms in order to allow for their identification. Solapsone can chelate gadolinium with a binding energy similar to those of known chelators, indicating that the metal-ligand interactions are fairly strong. Binding interactions within the LVFF region sometimes overlapped into the **HH**Q**K** region, and vice versa. For some conformations, the solapsone-Gd^{3+} complex did bind outside the **HH**Q**K** region, but it can be seen that this is a result of the complex surrounding the amyloid peptide.

The *in vitro* results support the *in silico* evidence that solapsone-Gd^{3+} can bind to Aβ in a monomeric or at least in the soluble forms, as aggregation was inhibited. As the blood vessels in the region of Aβ aggregation become damaged in the disease process, and given the evidence that solapsone can cross the blood-brain barrier, it is entirely possible that this complex will be able to enter the brain and bind to the soluble forms of Aβ, and potentially the plaques as well.

The *in vitro* results also show that a complex ratio of two solapsone molecules to one gadolinium ion can bind to β-amyloid more effectively. *In silico* studies suggest that a variety of orientations are possible for this complex, and it may be that with the 2:1 complex, two or more separate monomers of Aβ could be bound. The decreased

aggregation observed relative to the 1:1 ratio suggests a similar action may be occurring *in vitro*.

The mouse model will allow for *in vivo* verification of this hypothesis, and if it should prove successful will present a readily accessible MRI contrast agent to allow for earlier diagnosis of AD than compounds that are currently available. This is also a favourable complex of interest, as solapsone has a very low toxicity, and chelated gadolinium also has reduced toxicity. The potential side-effects of the administration of this complex may therefore be minimal.

The *in silico* studies also suggest that solapsone can bind to different conformations of β-amyloid on its own. The molecule can interact with both the **HH**Q**K** and LVFF regions, as well as overlapping the two. This is possible as the larger size of solapsone allows it to wrap itself around the amyloid protein to prevent conformational conversion. The binding energies of these systems are also favourable, and multiple binding interactions can form between the protein and small molecule. Although its activity *in vitro* is less than that of complexed solapsone-Gd^{3+}, it does show some capacity to inhibit Aβ aggregation which is a beneficial outcome. Thus a known drug can be repurposed to target other diseases in need of new therapeutic approaches.

CHAPTER 7: CONCLUSIONS

Through the course of this research computational methods have been used to identify endogenous molecules within the human brain that have the potential to bind to β-amyloid to prevent neurotoxic aggregation from occurring, and the results have potential significance.

7.1 PHOSPHOSERINE

Phosphoserine has demonstrated by *in silico* and *in vitro* means that it is capable of binding to the monomeric form of β-amyloid to prevent aggregation. Phosphoserine can also bind to other proteins involved in AD bearing a common **BB**X**B** motif. In fact, it binds well to these proteins and demonstrated itself as more energetically favourable in binding to them relative to other species that were investigated. Thus phosphoserine may act in a multi-faceted approach, to not only prevent Aβ aggregation, but inhibit the damaging inflammatory responses that occur.

Further research of phosphoserine as an anti-AD drug is warranted. As the pathways involved in the synthesis and degradation of the molecule are known, drugs could be designed to increase the concentration of phosphoserine in the brain. Phosphoserine could also be used as a lead molecule to develop analogues with even more efficacy.

7.2 HHQK AS A TARGET FOR ANTI-ALZHEIMER'S DRUGS

The research presented demonstrates that the **HH**Q**K** region of Aβ, which plays an important role in the misfolding, is a viable target for anti-AD drugs. The indentified

endogenous molecules, such as phenylalanine, dopamine, and 3-hydroxyanthranilic acid, were all capable of binding to **HH**Q**K**, and are of interest for further development. The positive computational results, supported by *in vitro* assays, led to the development of a novel series of analogues of 3HAA, and the activity of these new analogues has been increased. Further QSARs will be performed to continue to improve the efficacy of these drugs.

7.3 BBXB AND THE "PROMISCUOUS DRUG" CONCEPT

The molecular mechanics studies of a series of synthetic molecules interacting with the **BB**X**B** motif on multiple proteins support the concept of a "promiscuous drug". All five compounds were capable of binding to the concentrated region of basic amino acids on multiple proteins involved in Alzheimer's disease. Certain compounds were more efficacious at forming these binding interactions; however, they were all able to target **BB**X**B**. This supports the concept that a single drug could target multiple proteins involved in the disease process.

One particular compound of interest, NCE-0217, was "analogued" further and a QSAR was performed to provide direction on which compounds should be synthesized next. This process will be repeated as necessary to improve the activity of the molecules.

7.4 EVHHQK AS A TARGET FOR ANTI-ALZHEIMER'S DRUGS

Studies on the interactions between both endogenous and synthetic molecules with the EV**HH**Q**K** region of β-amyloid support its potential for another binding target to

prevent aggregation. Therefore, small molecules containing both anionic and cationic moieties could interact with EV**HH**Q**K** in a preventative manner.

The results indicate that the anionic groups on these molecules play a role in the strength of binding interactions, where $SO_3^- > PO_3^- > CO_2^-$. This indicates that a search for molecules with sulfonate groups would yield compounds with a greater chance of positive binding interactions than those with carboxylate groups. The size of the molecule is also a factor in its ability to bind to β-amyloid, as β-alanine was not as capable as GABA for forming interactions with the protein.

7.5 LVFF AS A TARGET FOR ANTI-ALZHEIMER'S DRUGS

The *in silico* studies of small molecules comparing the binding strength of the **HH**Q**K** region to the LVFF region of β-amyloid demonstrate the viability of LVFF as another drug target. Compounds with aromatic rings are capable of targeting both **HH**Q**K** and LVFF, and may bind even more strongly to the LVFF region of Aβ. Thus, we can design and develop drug molecules capable of targeting both regions of the protein to better promote stability in the monomeric form.

7.6 SOLAPSONE AS AN IMAGING AGENT FOR ALZHEIMER'S DISEASE

The results of the minimization of solapsone chelating gadolinium with β-amyloid are favourable for its use as a diagnostic agent. Optimizations in both the gas phase and solution phase demonstrated multiple interactions formed between solapsone-Gd^{3+} and the **HH**Q**K** and LVFF regions of Aβ, which was further supported by *in vitro* results. The

next phase of this project will be to obtain the results of animal study in order to proceed with its development.

Solapsone may also be capable of acting as an amyloid anti-aggregant. The *in silico* studies showed that it would form many binding interactions, not only with **HH**Q**K** or LVFF, but overlapping both regions. It should be quite capable of keeping β-amyloid in its non-toxic form by binding around these regions.

7.7 General Conclusions

The use of computational techniques has facilitated the identification, design and development of novel therapeutics for Alzheimer's disease. The identification of endogenous molecules of the brain as anti-Alzheimer's drugs is an approach that has not previously been postulated. These identified compounds have shown great promise as leads in the development of putative anti-AD drugs. Computational methods were also of use in the design and development of novel molecules for inhibiting amyloid aggregation, as they allowed for more focused research and positive results to be obtained with less synthetic cost.

Furthermore, through the use of these computational techniques, the idea of "physinformatics" was developed, this would allow for the discovery of potentially useful molecules based on specific functional groups and electronic arrangements in order to better target an identified region. Drugs may also be repurposed through these means of discovery, as with the identification of solapsone (formerly used to treat leprosy), and its subsequent development as a diagnostic imaging agent for Alzheimer's disease.

References

[1] Parihar, M. S., Hemnani, T. *J. Clin. Neurosci*. **2004**, ***11***, 456-467.

[2] Grossberg, G. T. *J Clin Pyschiatry.* **2003**, ***64*** (suppl 9), 3-6.

[3] Brookmeyer, R., Johnson, E., Zeigler-Graham, K., Arrighi, H. M. *Alzheimer's & Dementia.* **2007**, ***3***, 186-191.

[4] Easwaramoorthy, B., Pichika, R., Collins, D., Potkin, S.G., Leslie, F.M., Mukherjee, J. *Synapse.* **2007**, ***61***, 29-36.

[5] Wenk, G. L. *J Clin Psychiatry*, **2003**, **64** (suppl 9), 7-10.

[6] Purves, D. & Williams, S.M. *Neuroscience,* 3rd ed; Sinauer Associates: Sunderland, MA, **2004**.

[7] Nestler, E.J., Hyman, S.E. & Malenka, R.C. *Molecular Neuropharmacology: A Foundation for Clinical Neuroscience.* The McGraw-Hill Companies, Inc.: Toronto, ON **2001**.

[8] Lahiri, D. K., Greig, N. H. *Neurobiol. Aging*. **2004**, ***25***, 581-587.

[9] Walsh, D. M., Selkoe, D. J. *J. Neurochem*. **2007**, ***101***, 1172-1184.

[10] Maltseva, E., Kerth, A., Blume, A., Mohwald, H., Brezesinski, G. *ChemBioChem*. **2005**, ***6***, 1817-1824.

[11] Verdile, G., Fuller, S., Atwood, C. S., Laws, S. M., Gandy, S. E., Martins, R. N. *Pharmacol. Res*. **2004**, ***50***, 397-409.

[12] Gandy, S. *J. Clin. Invest*. **2005**, ***115***, 1121-1129.

[13] Buchet, R., Pikula, S. *Acta Biochim. Pol*. **2000**, ***47***, 725-733.

[14] LaFeria, F. M., Green, K. N., Oddo, S. *Nat. Rev. Neurosci.* **2007**, ***8***, 499-508.

[15] Gouras, G. K., Almeida, C. G., Takahashi, R. H. *Neurobiol. Aging*. **2005**, ***26***, 1235-1244.

[16] Morita, M., Vestergaard, M., Hamada, T., Takagi, M. *Biophys. Chem*. **2010**, ***147***, 81-86.

[17] Yoda, M., Miura, T., Takeuchi, H. *Biochem. Bioph. Res. Co.* **2008**, ***376***, 56-59.

[18] Fändrich, M., Schmidt, M., Grigorieff, N. *Trends Biochem. Sci*. **2011**, ***36***, 338-345.

[19] Oddo, S., Caccamo, A., Tran, L., Lambert, M. P., Glabe, C. G., Klein, W. L., LaFeria, F. M. *J. Biol. Chem*. **2006**, ***281***, 1599-1604.

[20] Minati, L., Edginton, T., Bruzzone, M. G., Giaccone, G. *Am J Alzheimers Dis*. **2009**, ***24***, 95-121.

[21] Vijayan, S., El-Akkad, E., Grundke-Iqbal, I., Iqbal, K. *FEBS Lett*. **2001**, ***507***, 375-381.

[22] Karp, G. *Cell and Molecular Biology: Concepts and Experiment,*. 3rd ed.; John Wiley & Sons, Inc.: Hoboken, NJ **2003**.

[23] Butterfield, D. A., Bush, A. I. *Neurobiol. Aging*. **2004**, ***25***, 563-568.

[24] *World Alzheimer Report*. Alzheimer's Disease International: London **2009**.

[25] Diamond, J. "A Report of Alzheimer's Disease and Current Research." *Alzheimer Society*.Toronto, ON, **2006**.

[26] Alzheimer Treatment: Drug Treatments. *Alzheimer Society of Canada.* **2007**. <http://www.alzheimer.ca/english/treatment/treatments-into.htm> 21 Dec. 2007.

[27] Robinson, D. M., Keating, G. M. *Drugs*. **2006**, ***66***, 1515-1534.

[28] Sugimoto, H., Yamanishi, Y., Iimura, Y. & Kawakami, Y. *Curr. Med. Chem*. **2000**,*7*, 303-339.

[29] Bar-On, P., Millard, C.B., Harel, M., Dvir, H., Enz, A., Sussman, J.L., Silman, I. *Biochemistry*. **2002**, ***41***, 3555-3564.

[30] Pilger, C., Bartolucci, C., Lamba, D., Tropsha, A., Fels, G. *J. Mol. Graphics Modell.* **2001**, ***19***, 288-296.

[31] Mangialasche, F., Solomon, A., Winblad, B., Mecocci, P, Kivipelto, M. *Lancet Neurol.* **2010**, ***9***, 702-716.

[32] Adlard, P.A., Cherny, R. A., Finkelstein, D. I., Gautier, E., Robb, E., Coretes, M., Volitakis, I., Liu, X., Smith, J. P., Perez, K., Laughton, K., Li, Q-X., Charman, S. A., Nicolazzo, J. A., Wilkins, S., Deleva, K., Lynch, T., Barnham, K. J., Bush, A. I. *Neuron*. **2008**, ***59***, 43-55.

[33] Salloway, S., Sperling, R., Keren, R., Porsteinsson, A. P., van Dyck, C. H., Tariot, P. N., Gilman, S., Arnold, D., Abushakra, S., Hernandez, C., Crans, G., Liang, E., Quinn, G., Bairu, M., Pastrak, A., Cedarbaum, J. M. *Neurology*. **2011**, *77*, 1253-1262.

[34] Townsend, M. *J. Alzheimer's Dis*. **2011**, ***24***, 43-52.

[35] Humpel. C. *Trends Biotechnol*. **2011**, ***29***, 26-32.

[36] Hampel, H., Frank, R., Brioch, K., Teipel, S. J., Katz, R. G., Hardy, J., Herholz, K., Bokde, A. L. W., Jessen, F., Hoessler, Y. C., Sanhai, W. R., Zetterberg, H., Woodcock, J., Blennow, K. *Nat. Rev. Drug Discov*. **2010**, ***9***, 560-574.

[37] Lin, K.-J., Hsu, W.-C., Hsiao, I.-T., Wey, S.-P., Jin, L.-W., Skovronsky, D., Wai, Y.-Y., Chang, H.-P., Lo, C.-W., Yao, C. H., Yen, T.-C., Kung, M.-P. *Nucl. Med. Biol.* **2010**, ***37***, 497-508.

[38] Ono, M., Saji, H. *Int. J. Mol. Imaging*. **2011**, 1-12.

[39] Nogrady, T., Weaver D. F. *Medicinal Chemistry: A Molecular and Biochemical Approach.* 3rd ed.; Oxford University Press, Inc.: Toronto, ON **2005**.

[40] Lipinski, C. A., Lombardo, F., Dominy, B. W., Feeny, P. J. *Adv. Drug Deliv. Rev*. **2001**, ***46***, 3-26.

[41] Stephenson, V. C., Heyding, R. A., Weaver, D. F. *FEBS Lett*. **2005**, ***579***, 1338-1342.

[42] Leach, A. R. *Molecular Modelling: Principles and Applications.* 2nd Ed. Toronto : Pearson Educated Limited, **2001**.

[43] Mayo, S. L., Olafson, B. D., Goaddard III, W. A. *J. Phys. Chem.* **1990**, ***94***, 8897-8909.

[44] Brooks, B. R., Bruccoleri, R. E., Olafson, B. D., Sates, D. J., Swaminathan, S., Karplus, M. *J. Comput. Chem.* **1983**, ***4,*** 187-217.

[45] *Cerius*^{2}. Version 4.10. Accelrys Inc., **2005**.

[46] *QUANTA2005*. Version 05.0417. Accelrys Software Inc., **2006.**

[47] *Molecular Operating Environment*. Version 2008.10. Chemical Computing Group Inc., **2009**.

[48] MacKerell Jr., A. D., Basford, D,. Bellott, M., Dunbrack Jr., R. L., Evanseck, J. D., Field, M. J., Fischer, S., Gao, J., Guo, H., Ha, S., Joseph-McCarthy, D., Kuchnir, L., Kuezera, K., Lau, F. T. K., Mattos, C., Michnick, S., Ngo, T., Nguyen, D. T., Prodhom, B., Reiher III, W. E., Roux, B., Schlenkrich, M., Smith, J. C., Stote, R., Straub, J., Watanabe, M., Wiórkiewicz-Kuczera, J., Yin, D., Karpus, M. *J Phys Chem B*. **1998**, ***102***, 3586-3616.

[49] QUANTA 2005 Basic Operations. *2005.* San Diego : Accelrys Inc.

[50] "CHARMM: The Energy Function and Its Parameterization." *Encyclopedia of Computational Chemistry.* John Wiley and Sons Ltd.: Chichester, New York **1998**, 271-277.

[51] *Molecular Operating Environment*. Chemical Computing Group Inc.: Montreal, Quebec **2009**.

[52] *Cerius^{2}4.10L Forcefield-Based Simulations*. Accelrys Software Inc.: San Diego **2005**.

[53] Labute, P. *JCCG*. **1995**.

[54] Carbó-Dorca, R., Robert, D., Amat, Ll., Gironés, X., Besalú, E. *Molecular Quantum Similarity in QSAR and Drug Design.* Springer-Verlag: Berlin **2000**.

[55] Mannhold, R. *Molecular Drug Properties: Measurement and Prediction*. Wiley-VCH Verlag GmbH & Co. KGaA: Weinheim **2008**.

[56] *Cerius^2 Version 4.10 QSAR*. Accelrys Software Inc.: San Diego **2005**.

[57] Labute, P. *Pacific Symposium on Biocomputing*. **1999**, ***4***, 444-455.

[58] Cohen, J. *Educ. Psychol. Meas*. **1960**, ***20***, 37-46.

[59] Szegedi, V., Juhász, G., Rózsa, E., Juhász-Vedres, G., Datki, Z., Fülöp, L., Bozsó, Z., Lakatos, A., Laczkó, I. , Farkas, T., Kis, Z., Tóth, G., Soós, K., Zarándi, M., Budai, D.,Toldi, J., Penke, B. *FASEB J*. **2006**, ***20***, E324-333.

[60] Klunk, W. E., McClure, R. J., Richard, J., Pettegrew, J. W. *Mol. Chem. Neuropathol*. **1991**, ***15***, 51-73.

[61] Mason, R. P., Trumbore, M. W., Pettegrew, J. W. *Neurobiol. Aging*. **1995**, ***16***, 531-539.

[62] Molina, J. A., Jiménez-Jiménez, F. J., Vargas, C., Gómez, P., de Bustos, F., Ortí-Pareja, M., Tallón-Barranco, A., Benito-León, J., Arenas, J., Enríquez-de-Salamanca, R. *J. Neural Transm*. **1998**, ***105***, 279-286.

[63] Klunk, W. E., McClure, R. J., Pettegrew, J. W. *J. Neurochem*. **1991**, ***56***, 1997-2003.

[64] Mason, R. P., Trumbore, M. W., Pettegrew, J. W. *Ann. NY Acad, Sci*. **1996**, ***17***, 368-373.

[65] Wu, S-Z., Bodles, A. M., Porter, M. M., Griffin, W. S. T., Basile, A. S., Barger, S. W. *J. Neuroninflamm*. **2004**, 1.

[66] Wood, P. L., Hawkinson, J. E., Goodnough, D. B. *J. Neurochem*. **1996**, ***67***, 1485-1490.

[67] Berman, H. M., Westbrook, J., Feng, Z., Gililand, G., Bhat, T. N., Weissig, H., Shindyalov, I. N., Bourne, P. E. *Nucleic Acids Res*. **200**, ***28***, 235-242.

[68] McGrath, M. E., Vasquez, J. R., Craik, C. S., Yang, A. S., Honig, B., Fletterick, R. J. *Biochemistry*, **1992**, ***31***, 3059-3064.

[69] Talafous, J., Marcinowski, K. J., Klopman, G., Zagorski, M. G. *Biochemistry*, **1994**, ***33***, 7788-7796.

[70] Sticht, H., Bayer, P., Willbold, D., Dames, S., Hilbich, C., Beyreuther K., Frank, R. W., Rosch, P. *Eur. J. Biochem*. **1995**, ***233***, 293-298.

[71] Coles, M., Bicknell, W., Watson, A. A., Fairlie, D. P., Craik, D. J. *Biochemistry*. **1998**, ***37***, 11064-11077.

[72] Crescenzi, O., Tomaselli, S., Guerrini, R., Salvadori, S., D'Ursi, A. M., Temussi, P. A., Picone, D. *Eur. J. Biochem*. **2002**, ***269***, 5642-5648.

[73] Zirah, S., Kozin, S. A., Mazur, A. K., Blond, A., Cheminant, M., Segalas-Milazzo, I., Debey, P., Rebuffat, S. *J. Biol. Chem*. **2006**, ***281***, 2151-2161.

[74] Gasteiger, J., Marsili, M. *Tetrahedron.* **1980***,* ***36***, 3219-3288.

[75] Kraich, M., Klein, M., Patiño, E., Harrer, H., Nickel, J., Sebald, W., Mueller, T. D. *BMC Biol*. **2006**, ***4***:13.

[76] Yoon, C., Johnston, S. C., Tang, J., Stahl, M., Tobin, J. F., Somers, W. S. *EMBO J.* **2000**, ***19***, 3530-3541.

[77] LaPorte, S. L., Juo, Z. S., Vaclavikova, J., Colf, L. A., Qi, X., Heller, N. M., Keegan, A. D., Garcia, K. C. *Cell*. **2008**, ***132***, 259-272.

[78] Smith, S. P., Shaw, G. S. *Structure*. **1998**, ***8***, 211-222.

[79] Chung, C., Cooke, R. M., Proudfoot, A. E. I., Wells, T. N. C. *Biochemistry*. **1995**, ***34***, 9307-9314.

[80] Bella, J., Kolatkar, P. R., Marlor, C. W., Greve, J. M., Rossman, M. G. *Proc. Natl. Acad. Sci*. **1998**, ***95***, 4140-4145.

[81] Atwood, C. S., Martins, R. N., Smith, M. A., Perry, G., *Peptides*. **2002**, ***23***, 1343-1350.

[82] Liu, R., McAllister, C., Lyubchenko, Y., Sierks, M. R. *J. Neurosci. Res*. **2004**, ***75***, 162-171.

[83] Tomaselli, S., Esposito, V., Vangone, P., van Nuland, N.A., Bonvin, A.M., Guerrini, R., Tancredi, T., Temussi, P.A., Picone, D. *ChemBioChem*. **2006**, *7*, 257-267.

[84] Fonteh, A. N., Harrington, R. J., Tsai, A., Liao, P., Harrington, M. G. *Amino Acids*. **2007**, ***32***, 213-224.

[85] Yates, C. M., Allison, Y., Simpson, J., Maloney, A. F. J., Gordon, A. *Lancet*. **1979**, ***2***, 851-852.

[86] Richard, D. M., Dawes, M. A., Mathias, C. W., Acherson, A., Hill-Kapturczak, N., Dougherty, D. M. *IJTR*. **2009**, ***2***, 45-60.

[87] *Molecular Operating Environment*. Version 2009.10. Chemical Computing Group Inc., **2009**.

[88] *Molecular Operating Environment*. Version 2010.10. Chemical Computing Group Inc., **2010**.

[89] Krause, D., Suh, H.-S., Tarassishin, L., Cui, Q. L., Durafourt, B. A., Choi, N., Bauman, A., Cosenza-Nashat, M., Antel, J. P., Zhao, M.-L., Lee, S. C. *Am. J. Pathol*. **2011**, ***179***, 1330-1372.

[90] Patani, G. A., LaVoie, E. J. *Chem. Rev*. **1996**, ***96***, 3147-3176.

[91] Lima, L. M., Barreiro, E. J. *Curr. Med. Chem*. **2005**, ***12***, 23-49.

[92] Gooptu, B., Hazes, B., Chang, W.-S., W., Dafforn, T. R., Carrell, R. W., Read, R. J., Lomas, D., A. *PNAS*. **2000**, ***97***, 62-72.

[93] Harrel, M., Sussman, J. L. 2J3D. **2009**.

[94] Mahley, R. W., Weisgraber, K. H., Huang, Y. *PNAS*. **2006**, ***103***, 5644-5654.

[95] Verderame, J. R., Kantardjieff, K., Segelke, B., Weisgraber, K., Rupp, N. 1GS9. **2009**.

[96] Ikemizu, S., Gilbert, R. J. C., Fennelly, J. A., Collins, A. V., Harlos, K., Davis, S. J. *Immunity*. **2000**, ***12***, 51-60.

[97] Evans, J. C., Huddler, D. P., Jiracek, J., Castro, C., Millian, N. S., Garrow, T. A., Ludwig, M. L. *Structure*. **2002**, ***10***, 1159-1171.

[98] Païdassi, H., Tacnet-Delorme, P., Garlatti, V., Darnault, C., Ghebrehiwet, B., Gaboriauld, C., Arlaud, G. J., Frachet, P. *J. Immunol*. **2008**, ***180***, 2329-2338.

[99] Landar, A., Curry, B., Parker, M. H., DiGiacomo, R., Indelicato, S. R., Nagabhushan, T. L., Rizzi, G., Walter, M. R. *J. Mol. Biol*. **2000**, ***299***, 169-179.

[100] Wilson, K. P., Black, J.-A. F., Thomson, J. A., Kim, E. E., Griffith, J. P., Navla, M. A., Murcko, M. A., Chambers, S. P., Aldape, R. A., Raybuck, S. A., Livingston, D. J. *Nature*. **1994**, ***370***, 270-274.

[101] Ren, M., Guo, Q., Guo, L., Lenz, M., Qian, F., Koenen, R. R., Xu, H., Schilling, A. B., Weber, C., Ye, R. D., Dinner, A. R., Tang, W.-J. *EMBO J*. **2010**, ***29***, 3952-3966.

[102] Glossop, M. S., Bazin, R. J., Dack, K. N., Fox, D. N. A., MacDonald, G. A., Mills, M., Owen, D. R., Phillips, C., Reeves, K. A., Ringer, T. J., Strang, R. S., Watson, C. A. L. *Bioorg. Med. Chem. Lett*. **2011**, ***21***, 3404-3406.

[103] Crump, M. P., Gong, J.-H., Loetscher, P., Rajarathnam, K., Amara, A., Arenzana-Seisdedos, F., Virelizier, J.-L., Baggiolini, M., Sykes, B. D., Clark-Lewis, I. *EMBO J*. **1997**, ***16***, 6996-7007.

[104] Eckenroth, B. E., Steere, A. N., Chasteen, D., Everse, S. J., Mason, A. B. *PNAS*. **2011**, ***108***, 13089-13094.

[105] Gervais, F., Paquette, J., Morissette, C., Kryzwkowski, P., Yu, M., Azzi, M., Lacombe, D., Kong, X., Aman, A., Laurin, J., Szarek, W. A., Tremblay, P. *Neurobiol. Aging*. **2007**, ***28***, 537-547.

[106] Dewar, M. J. S., Zoebisch, E. G., Healy, E. F., Stewart, J. J. P. *J. Am. Chem. Soc.* **1985**, ***107***, 3902-3909.

[107] *Gaussian 09W*. Version 7.0. Gaussian, Inc. **2009**.

[108] Carr, D. H., Brown, J., Bydder, G. M., Weinmann, H.J., Speck, U., Thomas, D. J., Young, I. R. *Lancet*. **1984**, ***323***, 484-486.

[109] Jopling, W. H. *Postgrad Med. J*. **1960**, ***36***, 634-637.

[110] Brownlee, G., Green, A. F., Woodbine, M. *Brit. J. Pharmacol*. **1948**, ***3***, 15-28.

[111] Brownlee, G. *Lancet*. **1948**, ***252***, 131-134.

[112] Runge, V. M. *J. Magn. Reson. Imaging*. **2000**, ***12***, 205-213.

[113] Tirkkonen, B., Aukrust, A., Couture, E., Grace, D., Haile, Y., Holm, K. M, Hope, H., Larsen, å., Sivertsen Lunde, H, Sjøgren, C. E. *Acta Radiol*. **1997**, ***38***, 780-789.

Appendix 1: The Library of Endogenous Molecules of the Brain

(S)13-hydroxyoctadecadienoic acid

(S)1-benzyl-1,2,3,4-TIQ

(S)1-phenyl-1,2,3,4-TIQ

(S)1-phenyl-N-methyl-1,2,3,4-TIQ

(S)-norcoclaurine

(S)-reticuline

(S)-salsoline

(S)-salsolinol

(S)-tetrahydropapaveroline

1,2,3,4-TIQ

1,2-dimethyl-6,7-dihydroxyisoquinolinium

1,2-N-dimethyl-1,2,3,6-tetrahydroisoquinoline

1,3-butadiene

1,3-P-D-glycerate

10-formylTHF

11beta-17alpha-21-trihydroxy-5beta-pregnane-3,20-dione

11beta-21-dihydroxy-3,20-oxo-5beta-pregnan- 18-al

11beta-hydroxy-4-androstene-3,17-dione

11-cis-retinal

11-deoxycortisol

11-hydroxyeicosatetraenoic acid

12-hydroxyeicosatetraenoic acid

14-desmethyllanosterol

15-hydroxyeicosatetraenoic acid

16alpha-hydroxydehydroepiandrosterone

16alpha-hydroxyestrone

17alpha-21-didyhroxy-5beta-pregnane-3,11,20-trione

17alpha-hydroxypregnenolone

17alpha-hydroxyprogesterone

18-hydroxycorticosterone

19-hydroxyandrost-4-ene-3,17-dione

19-hydroxy-PGA1

19-hydroxy-PGA2

19-hydroxy-PGB1

19-hydroxy-PGB2

19-hydroxytestosterone

1-carboxy(S)salsolinol

1D-myo-inositol,1,4,5-P3

1L-myo-inositol-1-P

1-lysolecithin

1-lysophosphatidylethanolamine

1-methyl-1,2,3,4-THBC

1-methyl-1,2,3,4-THBC-3-carboxylic acid

1-methylimidazole-4-acetic acid

1-monoacylglycerol

1-phosphatidyl-1D-myo-inositol

1-phosphatidyl-1D-myo-inositol-3,4-P2

1-phosphatidyl-1D-myo-inositol-3P

1-phosphatidyl-1D-myo-inositol-4,5-P2

1-phosphatidyl-1D-myo-inositol-4P

1-pyrroline2-carboxylate

1-pyrroline-4-hydroxy-2-carboxylate

2(N)-methyl-1,2,3,4-TIQ

2(N)-methyl-norsalsolinol

2,3-dioxo-L-gulonate

2,3-P-D-glycerate

2,5-dihydroxypyridine

2,9-dimethyl-beta-carbolinium

2,9-dimethyl-harmanium

20-alpha-22-beta-dihydroxycholesterol

20-carboxy-LTB4

20-hydroxy-LTB4

22beta-hydroxycholesterol

23P-D-glycerateb

24(S)-hydroxycholesterol

2-alpha-hydroxyethyl-ThPP

2-alpha-lactoyl-ThPP-r

2-alpha-lactoyl-ThPP-s

2-amino-3-carboxymuconatesemialdehyde

2-amino-3-oxadipate

2-aminomuconate

2-aminomuconatesemialdehyde

2-arachidonylglycerol

2-dehydro-3-deoxy-6-P-gluconate

2-dehydro-L-gulonolactone

2-deoxyadenosine

2-deoxyadenosine-5-diphosphate

2-deoxyadenosine-5-phosphate

2-deoxyadenosine-5-triphosphate

2-deoxycytidine

2-deoxycytidine-5-diphosphate

2-deoxycytidine-5-phosphate

2-deoxycytidine-5-triphosphate

2-deoxy-D-glucose

2-deoxyguanosine

2-deoxyguanosine-5-diphosphate

2-deoxyguanosine-5-phosphate

2-deoxyguanosine-5-triphosphate

2-deoxyinosine

2-deoxyribose

2-deoxythymidine

2-deoxythymidine-5-diphosphate

2-deoxythymidine-5-phosphate

2-deoxythymidine-5-triphosphate

2-deoxyuridine

2-deoxyuridine-5-diphosphate

2-deoxyuridine-5-phosphate

2-deoxyuridine-5-triphosphate

2-hydroxy-3-ketoadipate

2-hydroxy-3-oxoadipate

2-hydroxyestradiol-17b

2-hydroxyestrone

2-hydroxyglutarate

2-hydroxyputrescine

2-hydroxystearic acid

2-lysolecithin

2-lysophosphatidylethanolamine

2-methoxyestradiol-17b

2-methoxyestrone

2-methyl-3-hydroxybutyryl CoA

2-methylacetoacetyl CoA

2-methyl-beta-carbolinium

2-methylbutyryl CoA

2-methyl-harmanium

2-methylheptanone

2-methyl-THBC

2-monoacylglycerol

2-octyl-gamma-bromoacetoacetate

2-oxo-3-methylvalerate

2-oxo-5-aminovalerate

2-oxoadipate

2-oxobutyrate

2-oxoglutaramate

2-oxoglutarate

2-oxoisocaproate

2-oxoisovalerate

2-P-D-glycerate

3,3,5-triiodothyronine

3,3-diiodothyronine

3,4,5-trihydroxy-2-oxo-L-valeraldehyde

3,4-dihydroxy-5-decaprenylbenzoate

3,4-dihydroxy-5-heptaprenylbenzoate

3,4-dihydroxy-5-hexaprenylbenzoate

3,4-dihydroxy-5-nonaprenylbenzoate

3,4-dihydroxy-5-octaprenylbenzoate

3,4-Dihydroxyphenylglycol

3,5,3-triiodothyronine

3,5-diiodothyronine

3alpha-11beta-21-trihydroxy-20-oxo-5beta-pregnan-18-al

3alpha-17beta-dihydroxyandrostane

3alpha-hydroxy-5beta-pregnan-20-one

3beta-17beta-dihydroxy-5-androstene

3beta-dimethylallylalcohol

3-dehydro-L-gulonate

3-dehydrosphinganine

3-dehydrothreonate

3-hydroxyanthranilate

3-hydroxyisobutyrate

3-hydroxy-L-kynurenine

3-hydroxypyruvate

3-hydroxytrimethyllysine

3-iodothyronine

3-isopropylmalate

3-mercaptopyruvate

3-methoxy-4-hydroxy-5-decaprenylbenzoate

3-methoxy-4-hydroxy-5-heptaprenylbenzoate

3-methoxy-4-hydroxy-5-hexaprenylbenzoate

3-methoxy-4-hydroxy-5-nonaprenylbenzoate

3-methoxy-4-hydroxy-5-octaprenylbenzoate

3-methoxy-4-hydroxymandelaldehyde

3-methoxy-4-hydroxymandelate

3-methoxy-4-hydroxyphenylethyleneglycolsulfate

3-methoxy-4-hydroxyphenylglycol

3-methoxy-DOPA

3-methoxytyramine

3-methylcrotonate

3-methylcrotonyl CoA

3-O-acetyl-sphingosine

3-O-methyl-sphingosine

3-O-sulfoglucuronic acid

3-P-D-glycerate

3-phosphatidylethanolamine

3-phosphatidyl-L-glycerol-1P

3-P-hydroxypyruvate

3-P-serine

3-sulfinoalanine

3-sulfinylpyruvate

3-ureidoisobutyrate

3-ureidopropionate

4,7,10,13,16,19-docosahexenoic acid

4-aminobutyraldehyde

4-aminobutyrate

4-androstene-3,17-dione

4-aspartyl-P

4-fumarylacetoacetate

4-hydroxy-3-decaprenylbenzoate

4-hydroxy-3-heptaprenylbenzoate

4-hydroxy-3-hexaprenylbenzoate

4-hydroxy-3-methoxyphenylalanine

4-hydroxy-3-nonaprenylbenzoate

4-hydroxy-3-octaprenylbenzoate

4-hydroxynonenal

4-hydroxyphenylpyruvate

4-hydroxytrimethyllysine

4-imidazolone-5-propionate

4-maleylacetoacetate

4-pyridoxate

5,10-methenyl-THF

5,10-methylene-THF

5,6-dihetre

5,6-dihydrouracil

5,6-epetre

5,7-cholestadien-3-ol

5alpha-androstane-3,17-dione

5alpha-androstane-3alpha-7beta-diol

5alpha-dihydrotestosterone

5alpha-pregnan-3alpha-ol-20-one

5alpha-pregnane-3,20-dione

5-aminoimidazole ribotide

5-aminoimidazole-4-carboxamide ribotide

5-aminoimidazole-4-Nsuccinylocarboxamide ribotide

5-amino-levulinate

5beta-androstane-3,17-dione

5beta-pregnane-3,20-dione

5-formaminoimidazole-4-carboxamide ribotide

5-formyl THF

5-hete

5-hpete

5-hydroxyindoleacetaldehyde

5-hydroxyindoleacetate

5-hydroxytryptophan

5-hydroxytryptophol

5-methoxy-N,N-dimethyltryptamine

5-methyl THF

5-methylcytosine

5-methyltetrahydrofolate

5-oxoproline

5-P-B-D-ribosylamine

5-S-cysteinyl-3,4-dihydroxyphenylacetic acid

5-S-cysteinyl-3,4-dihydroxyphenylalanine

5-S-cysteinyldopamine

6-acetylmorphine

6-amino-2-oxohexanoate

6-hydroxymelatonin

6-hydroxymelatonin sulfate

6-hydroxynicotinate

6-ketoprostaglandin,F2alpha

6-methoxy-2-decaprenylphenol

6-methoxy-2-heptaprenylphenol

6-methoxy-2-hexaprenylphenol

6-methoxy-2-nonaprenylphenol

6-methoxy-2-octaprenylphenol

6-methoxytryptoline

6-R-5,6,7,8-tetrahydrobiopterin

6-R-pyruvoylterahydropterin

6-S-acetyl-dihydrolipoamide

7,8-diaminononanoate

7,8-dihydrofolate

7-dehydrocholesterol

8-amino-7-oxononanoate

9-hydroxyoctadecadienoic acid

acetaldehyde

acetate

acetoacetate

acetoacetylCoA

acetyl-CoA

acetylcholine

acetylcholine-solv

acetyl-L-carnitine

acetylputrescine

aconitate

adenine

adenosine

adenosine-5-phosphate

adenosine-5-phosphosulfate

adenylosuccinate

ADP

ADP-glucose

Adrenic acid

adrenosterone

alcylglycerone-P

aldimine

aldosterone

aldosterone-hemiacetal-R

aldosterone-hemiacetal-S

alkylacylglycerol

alkylglycerol-3P

alkylglycerone-P

all-trans retinal

allo-4-hydroxy-D-proline

alpha-aminobutyric acid

alpha-carotene

alpha-D-fucose

alpha-D-galactose

alpha-D-galactose-1-P

alpha-D-GalNAc

alpha-D-GlcNAc

alpha-D-glucosamine

alpha-D-glucose-1-6P

alpha-D-glucose-1P

alpha-D-glucose-6P

alpha-D-glucuronate

alpha-D-glucuronate-f

alpha-D-mannose

alpha-D-mannose-6P

alpha-D-mannose-6-P

alpha-D-ribose-1-phosphate

alpha-D-ribose5-P

alpha-glycero-P

alpha-ketoadipate

alpha-L-fucose

alpha-tocopherol

alpha-tocopherol-quinone

alph-hydroxy-nervonic acid

aminoacrylate

aminobutanesulfonic acid

aminomethanesulfonic acid

aminopentanesulfonic acid

ammonia

anandamide

androst-4-enedione

androstenediol

androstenedione

androsterone

anthranilate

APS

Arachidic acid

Arachidonic acid

ARA-S

ATP

auxin

behenic acid

beta-alanine

beta-aminoisobutyrate

beta-carotene

beta-D-fructose-1-6P

beta-D-fructose-1P

beta-D-fructose-6P

beta-D-fucose

beta-D-GalNAc

beta-D-GlcNAc

beta-D-glucosamine

beta-D-glucuronate

beta-D-glucuronate-f

beta-estradiol

beta-hydroxybutyric acid

betaine

betaine aldehyde

beta-L-fucose

beta-N-acetylgalactosamine

beta-phenylethylamine

beta-sulfopyruvate

bicarbonate

bilirubin

biliverdin IXa

bilrubin-B-diglucuronide

biotin

c18-sphingosine

calcitriol

cAMP

campesterol

carbamate

Carbamoly-P

carbamoyl-P

carbon dioxide

carboxyaminoimidazole ribotide

carnitine

carnosine

CDP-1,2-diacyl-glycerol

CDP-choline

CDP-ethanolamine

ceramide-C18

cerebrodiene

cerebronic acid-R

cerebronic acid-S

cerebroside

cGMP

cholesterol

choline

cisaconitate

cis-vaccenic acid

citrate

CMP-N-acetylneuraminate

CoA-SH

coproporphyrinogen III

cortexone

corticosterone

cortisol

cortisone

cortol

cortolone

creatine

creatinine

crotonyl-CoA

cyclohexa-2,5-diene-1,4-dione

cyclo-L-His-L-Pro

cyclo-L-Gly-L-Pro

cytidine

cytidinediphosphate choline

cytidine-5-diphosphate

cytidine-5-phosphate

cytidine-5-triphosphate

cytochromes-a

cytosine

D-3-hydroxybutyrate

d3-isopentenyl-PP

D-4-hydroxy-2-oxoglutarate

d5,7,24-cholestadien-3beta-ol

D-6-P-gluconate

D-6-P-glucono-1,5-lactone

d7,24-cholestadien-3beta-ol

deamino-NAD+

dehydroascorbate

dehydroepiandrosterone

dehydroepiandrosterone sulfate

dephosphoCoA-SH

D-erythrose-4P

desmosterol

dethiobiotin

dexamthasone

D-fructose

D-fructose2-6P

D-GalNAcol

D-glucarate

D-gluconate

D-glucono-1,5-lactone

D-glucosamine-6-P

D-glucose

D-glucuronate

D-glucuronate-1-P

D-glucuronolactone

D-glyceraldehyde

D-glyceraldehyde-3-P

D-glyceraldehyde-3P

D-glycerate

DHA

DHF

diacylglycerol

dihomo-gamma-linolenic acid

dihydroceramide

dihydrolipoamide

dihydroneopterin

dihydroneopterin-P3

dihydrosphingosine-1-P

dihydrothymine

dihydrouracil

dihydroxyacetone-P

dihydroxyphenylacetate

diiodo-L-tyrosine

dimethylglycine

dimethylallyl-PP

dimethylcitraconate

diphosphate

diphosphatidylglycerol

D-lactate

DL-dipalmitoyllecithin

D-mannose

Docosahexaenoic acid

Dopa

dopamine

Dopaquin

D-pantothenic acid

D-proline

D-ribitol

D-ribose

D-ribose-5-P

D-ribulose

D-ribulose-5-P

D-ribulose-a

D-ribulose-b

D-sedoheptulose-7-P

D-serine

D-sorbitol

D-xylose

D-xylulose

D-xylulose-5-P

D-xylulose-a

D-xylulose-b

Eicosapentaenoic acid

Eicosatrienoic acid

enoloxaloacetate

epinephrine

estradiol

estriol

estrone

ethanol

ethanolamine

ethanolamine-P

etiocholan-3alpha-ol-17-one

FAD

FADH2

f-aminoevulinic acid

fatty acid C16

fatty acid C18

fatty acid C20

fatty acid C22

fatty acid C23

fatty acid C24

fatty acid C25

fatty acid D11-C20-1

fatty acid D13-C22-1

fatty acid D6,9-C18-2

fatty acid D8,11-C20-2

fluorocitrate

FMN

folic acid

formic acid

formimglutglutamate

formylglycinamide ribotide

formylglycinamidine ribotide

fumarate

GABA

galabiosylceramide

galactitol

galactosylceramide

galactosylceramide

galactosylceramide sulfate

galactosylsphingosine

gamma-butyrobetaine

gamma-hydroxybutyric acid

gangliotriaosylceramide

GDP

GDP-4-dehydro-6-deoxy-D-mannose

GDP-4-dehydro-L-fucose

GDP-alpha-L-fucose

GDP-D-mannose

geranyl-PP

globotriaosylceramide

glucosylceramide

glutaconyl-CoA

glutamate

glutaryl-CoA

glyceraldehyde-P

glycero-3-phosphoethanolamine

glycero-3-phospoethanolamine

glycerol

glycerol-3P

glycerol-3-phosphoethanolamine

glycerone-P

GlyceroneP

glycerophosphoethanolamine

glycinamide ribotide

glycine

glycogen

glycolate

glyoxylate

GSH

GSSG

GTP

guanine

guanosine

guanosine-5-phosphate

harman

histamine

homogentisate

homotaurine

homovanillate

hydantoin propionate

hydrogen phosphate

hydrogen sulfide

hydroperoxide

hydroxymethylbilane

hydroxypyruvate

hypochlorite

hypotaurine

hypoxanthine

imidazole acetaldehyde

imidazole acetate

indole-3-acetic acid

Indole-5,6-Quinone

indoleacetaldehyde

indolelactate

indolepyruvate

inosine

inosine-5-phosphate

inositol-1,3,4,5,6-P5

inositol-1,3,4,5-P4

inositol-1,3,4,6-P4

inositol-1,3,4-P3

inositol-1,3-P2

inositol-1,4,5,6-P4

inositol-1,4,5-P3

inositol-1,4-P2

inositol-1-P

inositol-3,4,5,6-P4

inositol-3,4-P2

inositol-3-P

inositol-4-P

isobutyryl CoA

isocaproic aldehyde

isocitrate

isoethionic acid

isoleucine

isovaleric acid

isovaleryl CoA

itaconate

ketamine

kynurenate

L-1-glycero-3-phosphocholine

L-1-pyrroline-2-carboxylate

L-1-pyrroline-3-hydroxy-5-carboxylate

L-1-pyrroline-5-carboxylate

L-2-aminoacetoacetate

L-2-aminoadipate

L-4-hydroxyproline

L-5-hydroxylysine

laciotriaosulceramide

lactosylceramide

L-alanine

lanosterol

L-arabinose

L-arginine

L-argininosuccinate

L-ascorbate

L-asparagine

L-aspartate

lathosterol

lauric acid

L-citrulline

L-cystathionine

L-cysteate

L-cysteine

L-cysteinylglycine

L-DOPA

lecithin

L-erythro-4-hydroxyglutamate

L-erythro-ascorbate

leu enkephalin

leucine

leukotriene B4

leukotriene C4

leukotriene D4

leukotriene E4

L-gamma-carboxyglutamate

L-gamma-glutamylalanine

L-gamma-glutamylarginine

L-gamma-glutamylasparagine

L-gamma-glutamylaspartate

L-gamma-glutamylcysteine

L-gamma-glutamylglutamate

L-gamma-glutamylglutamine

L-gamma-glutamylglycine

L-gamma-glutamylhistidine

L-gamma-glutamylisoleucine

L-gamma-glutamylleucine

L-gamma-glutamyllycine

L-gamma-glutamylmethionine

L-gamma-glutamylphenylalanine

L-gamma-glutamylproline

L-gamma-glutamylserine

L-gamma-glutamylthreonine

L-gamma-glutamyltryptophan

L-gamma-glutamyltyrosine

L-gamma-glutamylvaline

L-glutamate

L-glutamate-5-semialdehyde

L-glutamine

L-glutamyl-5P

L-glutamyl-5-P

L-gulonate

L-gulonolactone

L-histidine

L-homocysteine

L-iduronic acid

lignoceric acid

linoleamide

linoleic acid

linolenic acid

L-kynurenine

L-lactate

L-lysine

L-ornithine

L-oxosuccinamate

L-phosphatidate

L-proline

L-ribulose-5-P

L-selenocysteine

L-serine

L-threonate

L-thyroxine

L-tryptophan

lysophosphatidate

malate

maleamate

maleate

malonate

malondialdehyde

malonylCoA

mannose-1-P

mannosylglucosylceramide

melatonin

met enkephalin

metanephrine

methacrylyl CoA

methanol

methionine

methionine sulfone

methtryptoline

mevalonate

mevalonate-5P

mevalonate-5PP

MoCo-dimer

MoCo-dimer-ADP

MoCo-dimer-ADPx2

MoCo-dimer-CDP

MoCo-dimer-CDPx2

MoCo-dimer-GDP

MoCo-dimer-GDPx2

MoCo-dimer-hypoxanthineDP

MoCo-dimer-hypoxanthineDPx2

MoCo-O

MoCo-O-ADP

MoCo-O-CDP

MoCo-O-GDP

MoCo-O-hypoxanthineDP

monoiodo-L-tyrosine

MPT

myo-inositol

myo-inositol-hexakisphosphate

myo-inositol-1,2-cyclic-P

myo-inositol-5-phosphate

myristic acid

N,N-dimethyltryptamine

N-acetyl-5-hydroxytryptamine

N-acetyl-aspartate

N-acetylaspartatic acid

N-acetyl-D-glucosamine

N-acetyl-D-glucosamine-1-P

N-acetyl-D-glucosamine-6-P

N-acetyl-D-mannosamine

N-acetyl-D-mannosamine-6-P

N-acetyl-L-lysine

N-acetylneuraminate

N-acetylneuraminate-9-P

N-acetyl-spermidine

N-acetyl-spermine

NAD+

NADH

NADP+

NADPH

N-carbamoyl-L-aspartate

nervonic acid

N-formylkynurenine

nicotinamide

nicotinamide nucleotide

nicotinate

nicotinate nucleotide

nitric oxide

N-methylhistamine

N-methyl-norsalsolinol

N-oleoylethanolamine

norepinephrine

norharman

normetanephrine

N-palmitoylethanolamine

N-stearoylethanolamine

Nw-hydroxyarginine

o-acetylcholine

oleamide

oleic aicd

oleylCoA

o-phosphocholine

o-phospho-ethanolamine

orotate

orotidine-5-phosphate

O-succinyl-acetyl-L-homoserine

oxalate

oxaloacetate

oxalocrotonate

oxalosuccinate

oxidized alpha-lipoic acid

oxytocin

PAF

palmitic acid

palmitoleic acid

palmitoylCoA

pantetheine

PAP

PAPS

P-creatine

PEP

phenylalanine

phenyllactate

Phenyl-Pyruvate

phosphatidylethanolamine

phosphatidylinositol

phosphatidylserine

phosphatidylserine-dioleic

phosphatidylserine-distearic

phosphatidylserine-oleic-stearic

phosphatidylserine-stearic-oleic

phosphocholine

phosphorylethanolamine

phtanic acid-R

phtanic acid-S

phytanic acid

phytate

picolinate

pipecolic acid

plasmalogen

plasmanylcholine

plasmanylethanolamine

porphobilinogen

porphobilinogen derivative

precursor-z

pregnanediol

pregnenolone

pregnenolone sulfate

previtamin D3

procollagen-5-hydroxy-L-lysine

progesterone

propionyl-CoA

prostaglandin A1

prostaglandin A2

prostaglandin B1

prostaglandin B2

prostaglandin D2

prostaglandin E1

prostaglandin E2

prostaglandin E3

prostaglandin F1a

prostaglandin F2alpha

prostaglandin G2

prostaglandin I2

protoheme

protoporphyrin IXmsf

protoporphyrinogen IX

PRPP

pseudouridine

psychosine

pterin-4alpha-carbinolamine

pterine-6-carboxylate

putrescine

pyridoxal

pyridoxal-P

pyridoxamine

pyridoxamine-5-P

pyridoxamine-P

pyridoxine

pyridoxine-P

pyruvate

quinoid

quinolate

quinolinate

quinolinate nucleotide

r-3-aminoisobutyrate

r-4P-N-pantothenoylcysteine

r-4P-pantetheine

r-4P-pantothenate

retinoate

r-methylmalonyl-CoA

r-pantothenate

r-pantothenol

s-3-aminoisobutyrate

s-3-hydroxy-3-methylglutaryl CoA

s-3-hydroxyisobutyrate

s-3-hydroxyisobutyryl CoA

s-4,5-dihydro-orotate

s-adenosyl-L-homocysteine

s-adenosyl-L-methionine

sarcosine

serotonin

sialolactosylceramide

s-malate

s-methylmalonate semialdehyde

s-methylmalonyl-CoA

sn-glycerol3P

sn-glycerol-3P

spermidine

spermine

sphinganine

sphinganine

sphingomyelin

sphingomyelin-C14

sphingomyelin-C16

sphingomyelin-C17

sphingomyelin-C19

sphingomyelin-C20

sphingomyelin-C21

sphingomyelin-C22

sphingomyelin-C22-1

sphingomyelin-C23

sphingomyelin-C23-1

sphingomyelin-C24

sphingomyelin-C25

sphingomyelin-C25-1

sphingomyelin-C26

sphingomyelin-C26-1

sphingomyelin-nervonic acid

sphingomyelin-stearic acid

sphingosine

sphingosine-1-P

sphingosylphosphorylcholine

spiro-intermediate

squalene

s-squalene-2,3-epoxide

stearic acid

stearoylCoA

stigmasterol

succinate

succinate semialdehyde

succinylCoA

sulfate

sulfatide

sulfite

taurine

testosterone

thebaine

THF

thiamine

thiamine pyrophosphate

thiamine-P

thiocyanic acid

thiocysteine

threonine

thromboxane A2

thromboxane B2

thymidine

thymidylic acid

thymine

tiglyl CoA

trans-trans-cis-geranylgeranyl-PP

trans-trans-farnesol

trans-trans-farnesyl-PP

trans-3-methylglutaconyl CoA

TRH

triacylglyceride

trimethyllysine

triphosophate

triphosphoinositide-arachidonic-eicosatrienoic

triphosphoinositide-diarachidonic

triphosphoinositide-diC16

triphosphoinositide-dieicosapentaenoic

triphosphoinositide-dieicosatrienoic

triphosphoinositide-dioleic

triphosphoinositide-distearic

triphosphoinositide-eicosapentaenoic-C16

triphosphoinositide-oleic-stearic

tryptamine

tryptoline

tryptophol

tyramine

tyrosine

ubiquinol-10

ubiquinol-6

ubiquinol-7

ubiquinol-8

ubiquinol-9

ubiquinone-10

ubiquinone-6

ubiquinone-7

ubiquinone-8

ubiquinone-9

UDP-D-glucuronate

UDP-glucose

UDP-G-glucuronate

UDP-L-iduronate

UDP-N-acetyl-D-glucosamine

UDP-N-acetyl-galactosamine

uracil

urate

urate enolate

uridine

uridine-5-diphosphate

uridine-5-phosphate

uridine-5-triphosphate

urocanoate

urocortisol

urocortisone

uroporphyrinogen I

uroporphyrinogen III

valine

vasopressin

vitamin A

vitamin D2

vitamin D3

vitamin E

vitamin K hydroquinone

vitamin K quinone

vitamin K quinone epoxide

xanthine

xanthosine

xanthosine-5-phosphate

xanthurenate

zymosterol

(peptide/AminoAcid)=AA

(peptide/AminoAcid)=AAKKAAI

(peptide/AminoAcid)=Ac-alpha-DE, "NAAG"

(peptide/AminoAcid)=Ac-DQYG-NH2

(peptide/AminoAcid)=AGPE

(peptide/AminoAcid)=AL

(peptide/AminoAcid)=alpha-DA

(peptide/AminoAcid)=ANKFNKEQ

(peptide/AminoAcid)=AVL

(peptide/AminoAcid)=AYYF

(peptide/AminoAcid)=beta-A-alpha-hyp

(peptide/AminoAcid)=beta-A-alpha-K

(peptide/AminoAcid)=beta-A-L-methyl-H, "anserine"

(peptide/AminoAcid)=beta-AH, "carnosine"

(peptide/AminoAcid)=beta-D-Taurine

(peptide/AminoAcid)=beta-DG

(peptide/AminoAcid)=CG

(peptide/AminoAcid)=cyclo-PG

(peptide/AminoAcid)=DA

(peptide/AminoAcid)=DKGNV, "alpha-globin6-10"

(peptide/AminoAcid)=EEP

(peptide/AminoAcid)=EFP-NH2, "Phe2TRH"

(peptide/AminoAcid)=EGEPNL

(peptide/AminoAcid)=EHP, "TRH-deamidated-non-pyro"

(peptide/AminoAcid)=EHP-NH2, "TRH"

(peptide/AminoAcid)=EHPG, "TRH-Gly"

(peptide/AminoAcid)=ELFNPY, "chroogranin-B-precursor520-526"

(peptide/AminoAcid)=ELP-NH2, "Leu2-TRH"

(peptide/AminoAcid)=ETP-NH2, "Thr2-TRH"

(peptide/AminoAcid)=EV

(peptide/AminoAcid)=EVGGEAL, "beta-globin21-27"

(peptide/AminoAcid)=EVGGEALG, "beta-globin21-28"

(peptide/AminoAcid)=EVP-NH2, "Val2-TRH"

(peptide/AminoAcid)=EYP-NH2, "Tyr2-TRH"

(peptide/AminoAcid)=FGFQKVP

(peptide/AminoAcid)=FISNHAY

(peptide/AminoAcid)=FIVH, "GTP-ase-activator304-307"

(peptide/AminoAcid)=FL

(peptide/AminoAcid)=FLPGH

(peptide/AminoAcid)=FPNEPM

(peptide/AminoAcid)=FRNPLAK

(peptide/AminoAcid)=Gaba-hypusine

(peptide/AminoAcid)=Gaba-K

(peptide/AminoAcid)=Gaba-L-methyl-H, "homoanserine"

(peptide/AminoAcid)=Gaba-H, "Homocarnosine"

(peptide/AminoAcid)=gamma-E-beta-Aib

(peptide/AminoAcid)=gamma-E-cysteate-G

(peptide/AminoAcid)=gamma-E-Gaba

(peptide/AminoAcid)=gamma-E-Taurine

(peptide/AminoAcid)=gamma-QE

(peptide/AminoAcid)=gamma-ECG, "glutathione, GSH"

(peptide/AminoAcid)=GG

(peptide/AminoAcid)=GGE, "beta-globin23-25"

(peptide/AminoAcid)=GKNVP, "cytochrome-c-oxidase-precursor-chain-VIIA32-40"

(peptide/AminoAcid)=GQ

(peptide/AminoAcid)=GQFFE

(peptide/AminoAcid)=GVFTPP

(peptide/AminoAcid)=GWMDF-NH2, "CCK-5"

(peptide/AminoAcid)=HP-DKP, "HP-Diketopiperazine=TRH-metab"

(peptide/AminoAcid)=IEG

(peptide/AminoAcid)=IEWNPS, "cytochrome-c-oxidase-VIIB70-75"

(peptide/AminoAcid)=INLFFIVL

(peptide/AminoAcid)=INNPFIL

(peptide/AminoAcid)=KIPYIL, "Neuromedin-N"

(peptide/AminoAcid)=KV

(peptide/AminoAcid)=KVNPD, "beta-globin16-20"

(peptide/AminoAcid)=LEPPP

(peptide/AminoAcid)=LG

(peptide/AminoAcid)=LL

(peptide/AminoAcid)=LMYP

(peptide/AminoAcid)=LS

(peptide/AminoAcid)=LSAL, "5-HT-moduline"

(peptide/AminoAcid)=LSHSL, "alpha-globin101-105"

(peptide/AminoAcid)=LVLFPGK

(peptide/AminoAcid)=LVVYP, "beta-globin31-35"

(peptide/AminoAcid)=LVVYPW, "beta-globin32-37"

(peptide/AminoAcid)=LVVYPWT, "beta-globin32-38"

(peptide/AminoAcid)=LVVYPWTQ, "beta-globin32-39"

(peptide/AminoAcid)=MLT, "beta-globin1-3"

(peptide/AminoAcid)=MLTAEEKA, "beta-globin1-8"

(peptide/AminoAcid)=NKVP, "cytochrome-c-oxidase-VIIA12-15"

(peptide/AminoAcid)=pEHP, "TRH-deamidated"

(peptide/AminoAcid)=pEHP-NH2, "TRH"

(peptide/AminoAcid)=pEHPG, "TRH-Gly"

(peptide/AminoAcid)=PLFP

(peptide/AminoAcid)=PLG-NH2, "MIF-1"

(peptide/AminoAcid)=PVDNSSP

(peptide/AminoAcid)=S-methyl-gamma-ECG, "S-methylglutathione"

(peptide/AminoAcid)=SRDKR-NH2

(peptide/AminoAcid)=SV

(peptide/AminoAcid)=SVQCPFGG, "aldehyde-dehydrogenase461-468"

(peptide/AminoAcid)=TQLPAEEI

(peptide/AminoAcid)=TSKY, "alpha-globins137-140, neokyotorphin1-4"

(peptide/AminoAcid)=TSKY, "alpha-globins137-141, neokyotorphin"

(peptide/AminoAcid)=TVLTSKY

(peptide/AminoAcid)=TVLTSKYR

(peptide/AminoAcid)=VAYKN

(peptide/AminoAcid)=VE

(peptide/AminoAcid)=VHLTDAEK

(peptide/AminoAcid)=VLGQV

(peptide/AminoAcid)=VLNP

(peptide/AminoAcid)=VLS

(peptide/AminoAcid)=VS

(peptide/AminoAcid)=VVGQV

(peptide/AminoAcid)=VVVL

(peptide/AminoAcid)=VVYP

(peptide/AminoAcid)=VVYPW

(peptide/AminoAcid)=VVYPWT

(peptide/AminoAcid)=VVYPWTQ

(peptide/AminoAcid)=VYPWT

(peptide/AminoAcid)=VYPWTQ

(peptide/AminoAcid)=VYYFPG

(peptide/AminoAcid)=WMDF-NH2

(peptide/AminoAcid)=WVAMQT

(peptide/AminoAcid)=YAYYY

(peptide/AminoAcid)=YEAVAL

(peptide/AminoAcid)=YEQLSGK

(peptide/AminoAcid)=YG

(peptide/AminoAcid)=YGG

(peptide/AminoAcid)=YGGFL, "leu-enkephalin"

(peptide/AminoAcid)=YGGFM, "Met-enkephalin"

(peptide/AminoAcid)=YGGFMRF, "met-enkephalin-arg6-phe7"

(peptide/AminoAcid)=YGGFMRGL, "Met-Enk-arg-gly-leu"

(peptide/AminoAcid)=YGGFMRRV-NH2, "metorphamide"

(peptide/AminoAcid)=YKVIPKS

(peptide/AminoAcid)=YLE

(peptide/AminoAcid)=YPFF-NH2, "endomorphin-2"

(peptide/AminoAcid)=YPKG-NH2

(peptide/AminoAcid)=YPLG-NH2, "Tyr-MIF-1"

(peptide/AminoAcid)=YPWF-NH2, endomorphon-1"

(peptide/AminoAcid)=YPWG-NH2

(peptide/AminoAcid)=YR, "kyotorphin"

Appendix 2: Method for Uniting Two 30 Å Water Boxes in QUANTA

Step 1: Turn capture commands on (save as .inp file).

Step 2: Under solvate structure, select the 30 Å length (water) box and place it on an atom in the system.

Step 3: Turn capture commands off.

Step 4: Open the saved input file captured in steps 1-3 using an available editing program (in this thesis vi was used). See Appendix 3 for a sample file.

Step 5: Note the atom number in SET 2 for future reference.

Step 6: Select the text from READ COOR CARD FREE to the end of the atoms involved in the system (not including water molecules) and copy into a new .txt file.

Step 7: Using the file outlined in Appendix 4, delete lines between READ COOR CARD FREE and COOR ORIE NOROT SELE BYNUM @2 end.

Step 8: Read the .txt from step 6 into the space created by the deletion in step 7.

Step 9: Set the number in SET 2 to the number recorded from SET 2 in the initially captured file.

Step 10: Set 3 to an appropriate atomic number from the system being studied.

Step 11: Save the resulting file in .STR format.

Step 12: Stream the .STR file into QUANTA using the stream CHARMm file option (the system must be free from solvent before this can occur).

Step 13: Adjust the number in SET 3 as necessary to minimize overlap of the two united water boxes.

Step 14: If the overlap is minimal and is deemed acceptable, delete overlapping water bonds or water molecule fragments as necessary to produce proper water molecules.

Appendix 3: Sample Initial File for Solvation in QUANTA Using United Water Boxes

Text immediately preceding and following the section used in the .txt file for input into the CHARMm streaming file has been included as reference.

```
* Script file produced by QUANTA
*
* Script to read parameter, psf, and ic files
*
reset
open read unit 21 card name $CHM_DATA/MASSES.RTF
read rtf unit 21 card
close unit 20
open read unit 20 card name ".charmmprm"
read param unit 20 card
close unit 20
open read unit 20 card name ".charmmpsf"
read psf unit 20 card
close unit 20
open read unit 20 card name ".charmmic"
ic read unit 20 card
close unit 20
! Script for reading RTF
!
OPEN READ UNIT 77 CARD NAME -
 "TIP3.RTF"
READ RTF CARD UNIT 77 APPEND
CLOSE UNIT 77
!set some variables
!
SET 1 1
SET 2 24

! QUANTA coordinates included in script file

READ COOR CARD FREE
* current QUANTA coordinates written for free read
*
464
   1    1   MINI  CA     -7.308962   10.064661   -2.405315 MINI    1   0.0
   2    1   MINI  HA     -7.914192   10.877570   -2.004334 MINI    1   0.0
   3    1   MINI  CB     -7.960489    9.491540   -3.668795 MINI    1   0.0
   4    1   MINI  HB1    -8.944982    9.085988   -3.430853 MINI    1   0.0
   5    1   MINI  HB2    -8.122888   10.289052   -4.394613 MINI    1   0.0
   6    1   MINI  CG     -7.112230    8.420467   -4.302016 MINI    1   0.0
   7    1   MINI  CD1    -6.058426    8.760720   -5.145370 MINI    1   0.0
   8    1   MINI  HD1    -5.840714    9.799349   -5.347174 MINI    1   0.0
   9    1   MINI  CD2    -7.368808    7.075675   -4.053276 MINI    1   0.0
  10    1   MINI  HD2    -8.179193    6.793570   -3.399433 MINI    1   0.0
  11    1   MINI  CE1    -5.278129    7.772991   -5.731510 MINI    1   0.0
  12    1   MINI  O1     -4.224179    8.117190   -6.552227 MINI    1   0.0
```

13	1	MINI	CE2	-6.593439	6.086135	-4.641974	MINI	1	0.0
14	1	MINI	HE2	-6.803187	5.046315	-4.441598	MINI	1	0.0
15	1	MINI	CZ	-5.551493	6.434802	-5.488376	MINI	1	0.0
16	1	MINI	O2	-4.791917	5.456796	-6.096515	MINI	1	0.0
17	1	MINI	H1	-6.322476	10.471231	-2.628883	MINI	1	0.0
18	1	MINI	N1	-7.149965	9.078195	-1.343117	MINI	1	0.0
19	1	MINI	H2	-3.587694	7.411913	-6.542690	MINI	1	0.0
20	1	MINI	H3	-4.312234	5.841283	-6.818595	MINI	1	0.0
21	1	MINI	H4	-6.695127	9.530078	-0.524174	MINI	1	0.0
22	1	MINI	H5	-6.559151	8.293039	-1.684175	MINI	1	0.0
23	1	MINI	H6	-8.087923	8.723651	-1.071054	MINI	1	0.0
24	2	ASP	N	19.777775	-0.609759	1.064205	AAMB	1	0.0
25	2	ASP	CA	19.041170	0.412852	1.823377	AAMB	1	0.0
26	2	ASP	C	17.933453	0.933095	1.021516	AAMB	1	0.0
27	2	ASP	O	16.766161	0.674886	1.402760	AAMB	1	0.0
28	2	ASP	CB	19.930069	1.538161	2.379704	AAMB	1	0.0
29	2	ASP	CG	19.108906	2.493291	3.266880	AAMB	1	0.0
30	2	ASP	OD1	18.637297	2.057324	4.315971	AAMB	1	0.0
31	2	ASP	OD2	18.937716	3.650251	2.886323	AAMB	1	0.0
32	2	ASP	H1	19.122427	-1.356153	0.755510	AAMB	1	0.0
33	2	ASP	H2	20.217154	-0.167099	0.231754	AAMB	1	0.0
34	2	ASP	H3	20.517815	-1.020694	1.667922	AAMB	1	0.0
35	2	ASP	HA	18.610788	-0.162236	2.653509	AAMB	1	0.0
36	2	ASP	HB1	20.734478	1.116608	2.983014	AAMB	1	0.0
37	2	ASP	HB2	20.404535	2.098895	1.572696	AAMB	1	0.0
38	3	ALA	N	18.160498	1.642654	-0.100774	AAMB	1	0.0
39	3	ALA	CA	17.094845	2.143059	-0.915015	AAMB	1	0.0
40	3	ALA	C	16.254911	1.052349	-1.423196	AAMB	1	0.0
41	3	ALA	O	15.054347	1.068294	-1.075329	AAMB	1	0.0
42	3	ALA	CB	17.693850	2.943579	-2.079667	AAMB	1	0.0
43	3	ALA	HN	19.074314	1.839025	-0.364898	AAMB	1	0.0
44	3	ALA	HA	16.493011	2.824638	-0.300168	AAMB	1	0.0
45	3	ALA	HB1	18.346439	2.330746	-2.702714	AAMB	1	0.0
46	3	ALA	HB2	16.912722	3.358833	-2.718083	AAMB	1	0.0
47	3	ALA	HB3	18.287046	3.778799	-1.706802	AAMB	1	0.0
48	4	GLU	N	16.766771	0.108776	-2.238868	AAMB	1	0.0
49	4	GLU	CA	15.982441	-0.984445	-2.721450	AAMB	1	0.0
50	4	GLU	C	15.336887	-1.714932	-1.622579	AAMB	1	0.0
51	4	GLU	O	14.235341	-2.266397	-1.856518	AAMB	1	0.0
52	4	GLU	CB	16.917519	-1.940748	-3.488229	AAMB	1	0.0
53	4	GLU	CG	18.039606	-2.571616	-2.637842	AAMB	1	0.0
54	4	GLU	CD	19.012463	-3.366955	-3.521243	AAMB	1	0.0
55	4	GLU	OE1	18.620823	-4.416527	-4.029042	AAMB	1	0.0
56	4	GLU	OE2	20.149826	-2.927709	-3.691912	AAMB	1	0.0
57	4	GLU	HN	17.696264	0.177130	-2.510961	AAMB	1	0.0
58	4	GLU	HA	15.271745	-0.619510	-3.458186	AAMB	1	0.0
59	4	GLU	HB1	16.324903	-2.733285	-3.949845	AAMB	1	0.0
60	4	GLU	HB2	17.364010	-1.387508	-4.315942	AAMB	1	0.0
61	4	GLU	HG1	18.596556	-1.806110	-2.096667	AAMB	1	0.0
62	4	GLU	HG2	17.629417	-3.252203	-1.891811	AAMB	1	0.0
63	5	PHE	N	15.919147	-1.782670	-0.408540	AAMB	1	0.0
64	5	PHE	CA	15.307195	-2.459879	0.694823	AAMB	1	0.0
65	5	PHE	C	14.023937	-1.843083	1.055299	AAMB	1	0.0
66	5	PHE	O	12.972171	-2.524466	0.949426	AAMB	1	0.0
67	5	PHE	CB	16.279289	-2.527469	1.885281	AAMB	1	0.0
68	5	PHE	CG	15.739032	-3.373315	3.008089	AAMB	1	0.0

69	5	PHE	CD1	15.829038	-4.760987	2.951096	AAMB	1	0.0
70	5	PHE	CD2	15.136943	-2.778950	4.113894	AAMB	1	0.0
71	5	PHE	CE1	15.324374	-5.542925	3.981631	AAMB	1	0.0
72	5	PHE	CE2	14.630987	-3.558754	5.144966	AAMB	1	0.0
73	5	PHE	CZ	14.724332	-4.941813	5.079098	AAMB	1	0.0
74	5	PHE	HN	16.751390	-1.312392	-0.272539	AAMB	1	0.0
75	5	PHE	HA	15.091137	-3.477376	0.342844	AAMB	1	0.0
76	5	PHE	HB1	17.229969	-2.950082	1.559053	AAMB	1	0.0
77	5	PHE	HB2	16.505520	-1.533824	2.267890	AAMB	1	0.0
78	5	PHE	HD1	16.292446	-5.239335	2.100450	AAMB	1	0.0
79	5	PHE	HD2	15.058798	-1.702938	4.175553	AAMB	1	0.0
80	5	PHE	HE1	15.400675	-6.619709	3.932070	AAMB	1	0.0
81	5	PHE	HE2	14.167374	-3.089276	6.000203	AAMB	1	0.0
82	5	PHE	HZ	14.334185	-5.549905	5.882122	AAMB	1	0.0
83	6	ARG	N	13.973029	-0.583468	1.540645	AAMB	1	0.0
84	6	ARG	CA	12.735288	0.057283	1.876006	AAMB	1	0.0
85	6	ARG	C	11.947042	0.320672	0.666657	AAMB	1	0.0
86	6	ARG	O	10.776729	0.746743	0.824206	AAMB	1	0.0
87	6	ARG	CB	13.092020	1.395360	2.551799	AAMB	1	0.0
88	6	ARG	CG	14.014983	1.223515	3.769409	AAMB	1	0.0
89	6	ARG	CD	14.358479	2.554219	4.443905	AAMB	1	0.0
90	6	ARG	NE	15.328096	2.312673	5.503546	AAMB	1	0.0
91	6	ARG	CZ	15.798455	3.294541	6.300189	AAMB	1	0.0
92	6	ARG	NH1	15.372872	4.548343	6.182192	AAMB	1	0.0
93	6	ARG	NH2	16.707289	3.000172	7.220729	AAMB	1	0.0
94	6	ARG	HN	14.801904	-0.091048	1.579415	AAMB	1	0.0
95	6	ARG	HA	12.176013	-0.551757	2.589055	AAMB	1	0.0
96	6	ARG	HB1	13.585172	2.054682	1.834535	AAMB	1	0.0
97	6	ARG	HB2	12.179491	1.906087	2.863252	AAMB	1	0.0
98	6	ARG	HG1	13.546998	0.556514	4.493953	AAMB	1	0.0
99	6	ARG	HG2	14.948694	0.747324	3.468746	AAMB	1	0.0
100	6	ARG	HD1	14.815233	3.249584	3.737501	AAMB	1	0.0
101	6	ARG	HD2	13.476509	3.018210	4.888027	AAMB	1	0.0
102	6	ARG	HE	15.684490	1.386206	5.624157	AAMB	1	0.0
103	6	ARG	HH11	14.686085	4.782607	5.494776	AAMB	1	0.0
104	6	ARG	HH12	15.737885	5.260526	6.782176	AAMB	1	0.0
105	6	ARG	HH21	17.045107	2.063514	7.311261	AAMB	1	0.0
106	6	ARG	HH22	17.058128	3.715544	7.825210	AAMB	1	0.0
107	7	HIS	N	12.477256	0.090535	-0.550493	AAMB	1	0.0
108	7	HIS	CA	11.744717	0.312759	-1.758953	AAMB	1	0.0
109	7	HIS	C	10.796138	-0.782060	-1.978250	AAMB	1	0.0
110	7	HIS	O	9.589708	-0.479645	-1.876704	AAMB	1	0.0
111	7	HIS	CB	12.670664	0.470988	-2.976635	AAMB	1	0.0
112	7	HIS	CG	11.853472	0.800605	-4.207127	AAMB	1	0.0
113	7	HIS	ND1	11.174619	1.956473	-4.369656	AAMB	1	0.0
114	7	HIS	CD2	11.632096	-0.006237	-5.336245	AAMB	1	0.0
115	7	HIS	CE1	10.558787	1.856300	-5.559719	AAMB	1	0.0
116	7	HIS	NE2	10.815231	0.683228	-6.165370	AAMB	1	0.0
117	7	HIS	HN	13.376023	-0.258575	-0.621651	AAMB	1	0.0
118	7	HIS	HA	11.189747	1.253068	-1.633207	AAMB	1	0.0
119	7	HIS	HB1	13.391198	1.271157	-2.816208	AAMB	1	0.0
120	7	HIS	HB2	13.221879	-0.444952	-3.165380	AAMB	1	0.0
121	7	HIS	HD1	11.136872	2.709538	-3.744411	AAMB	1	0.0
122	7	HIS	HD2	12.032319	-0.994756	-5.506828	AAMB	1	0.0
123	7	HIS	HE1	9.930161	2.626813	-5.980333	AAMB	1	0.0
124	7	HIS	H1	10.482866	0.387524	-7.037562	AAMB	1	0.0

125	8	ASP	N	11.233445	-2.023194	-2.281511	AAMB	1	0.0
126	8	ASP	CA	10.336828	-3.122818	-2.458477	AAMB	1	0.0
127	8	ASP	C	9.481910	-3.294824	-1.276572	AAMB	1	0.0
128	8	ASP	O	8.295098	-3.664217	-1.457893	AAMB	1	0.0
129	8	ASP	CB	11.157777	-4.409196	-2.672501	AAMB	1	0.0
130	8	ASP	CG	11.973235	-4.345119	-3.976825	AAMB	1	0.0
131	8	ASP	OD1	11.374281	-4.144149	-5.033825	AAMB	1	0.0
132	8	ASP	OD2	13.194413	-4.495240	-3.924402	AAMB	1	0.0
133	8	ASP	HN	12.188498	-2.180787	-2.348245	AAMB	1	0.0
134	8	ASP	HA	9.733404	-2.936532	-3.343399	AAMB	1	0.0
135	8	ASP	HB1	11.833135	-4.579036	-1.831377	AAMB	1	0.0
136	8	ASP	HB2	10.502279	-5.279665	-2.734753	AAMB	1	0.0
137	9	SER	N	9.988587	-3.138769	-0.034572	AAMB	1	0.0
138	9	SER	CA	9.176601	-3.262035	1.137976	AAMB	1	0.0
139	9	SER	C	8.022375	-2.358343	1.073562	AAMB	1	0.0
140	9	SER	O	6.868747	-2.855776	1.073585	AAMB	1	0.0
141	9	SER	CB	10.068615	-2.965061	2.355839	AAMB	1	0.0
142	9	SER	OG	9.355240	-3.135004	3.573644	AAMB	1	0.0
143	9	SER	HN	10.925159	-2.918284	0.068418	AAMB	1	0.0
144	9	SER	HA	8.817378	-4.297300	1.180070	AAMB	1	0.0
145	9	SER	HB1	10.930118	-3.641708	2.333718	AAMB	1	0.0
146	9	SER	HB2	10.455923	-1.943617	2.286220	AAMB	1	0.0
147	9	SER	HG	9.915859	-2.967490	4.327736	AAMB	1	0.0
148	10	GLY	N	8.198386	-1.021602	1.008988	AAMB	1	0.0
149	10	GLY	CA	7.094239	-0.121842	0.900155	AAMB	1	0.0
150	10	GLY	C	6.454493	-0.233650	-0.411757	AAMB	1	0.0
151	10	GLY	O	5.464347	0.490092	-0.620506	AAMB	1	0.0
152	10	GLY	HN	9.096245	-0.652911	0.994446	AAMB	1	0.0
153	10	GLY	HA1	6.379829	-0.274391	1.706055	AAMB	1	0.0
154	10	GLY	HA2	7.484860	0.892686	0.999122	AAMB	1	0.0
155	11	TYR	N	6.983341	-1.033271	-1.360520	AAMB	1	0.0
156	11	TYR	CA	6.388818	-1.190931	-2.650550	AAMB	1	0.0
157	11	TYR	C	5.169522	-2.002688	-2.575299	AAMB	1	0.0
158	11	TYR	O	4.083598	-1.530204	-2.994898	AAMB	1	0.0
159	11	TYR	CB	7.350282	-1.753478	-3.713031	AAMB	1	0.0
160	11	TYR	CG	6.796342	-1.622310	-5.108879	AAMB	1	0.0
161	11	TYR	CD1	6.946820	-0.433889	-5.817184	AAMB	1	0.0
162	11	TYR	CD2	6.123273	-2.683400	-5.708284	AAMB	1	0.0
163	11	TYR	CE1	6.430960	-0.306970	-7.100461	AAMB	1	0.0
164	11	TYR	CE2	5.607652	-2.560893	-6.992030	AAMB	1	0.0
165	11	TYR	CZ	5.761763	-1.369484	-7.691957	AAMB	1	0.0
166	11	TYR	OH	5.255615	-1.225814	-8.969693	AAMB	1	0.0
167	11	TYR	HN	7.757517	-1.570586	-1.156951	AAMB	1	0.0
168	11	TYR	HA	6.096994	-0.185557	-2.971601	AAMB	1	0.0
169	11	TYR	HB1	8.295371	-1.216645	-3.688034	AAMB	1	0.0
170	11	TYR	HB2	7.569117	-2.803098	-3.529725	AAMB	1	0.0
171	11	TYR	HD1	7.467752	0.399982	-5.369175	AAMB	1	0.0
172	11	TYR	HD2	5.990994	-3.612691	-5.173663	AAMB	1	0.0
173	11	TYR	HE1	6.549152	0.620338	-7.642038	AAMB	1	0.0
174	11	TYR	HE2	5.083165	-3.399038	-7.427675	AAMB	1	0.0
175	11	TYR	HH	5.439033	-1.998519	-9.487761	AAMB	1	0.0
176	12	GLU	N	5.214782	-3.259125	-2.090118	AAMB	1	0.0
177	12	GLU	CA	4.044102	-4.064106	-1.970570	AAMB	1	0.0
178	12	GLU	C	3.232757	-3.556814	-0.869093	AAMB	1	0.0
179	12	GLU	O	1.983533	-3.602206	-0.998179	AAMB	1	0.0
180	12	GLU	CB	4.517496	-5.503375	-1.724126	AAMB	1	0.0

181	12	GLU	CG	5.322128	-6.050351	-2.920312	AAMB	1	0.0
182	12	GLU	CD	6.149025	-7.281702	-2.523667	AAMB	1	0.0
183	12	GLU	OE1	7.378289	-7.199483	-2.546176	AAMB	1	0.0
184	12	GLU	OE2	5.553935	-8.305547	-2.195225	AAMB	1	0.0
185	12	GLU	HN	6.073738	-3.598763	-1.784515	AAMB	1	0.0
186	12	GLU	HA	3.471385	-4.003354	-2.898062	AAMB	1	0.0
187	12	GLU	HB1	5.134706	-5.521853	-0.823157	AAMB	1	0.0
188	12	GLU	HB2	3.667104	-6.158360	-1.528040	AAMB	1	0.0
189	12	GLU	HG1	4.651354	-6.317287	-3.737273	AAMB	1	0.0
190	12	GLU	HG2	6.007466	-5.301211	-3.317899	AAMB	1	0.0
191	13	VAL	N	3.814550	-3.109827	0.251651	AAMB	1	0.0
192	13	VAL	CA	3.053213	-2.556596	1.319859	AAMB	1	0.0
193	13	VAL	C	2.326123	-1.396080	0.844176	AAMB	1	0.0
194	13	VAL	O	1.248710	-1.084186	1.408288	AAMB	1	0.0
195	13	VAL	CB	3.977241	-2.253151	2.518477	AAMB	1	0.0
196	13	VAL	CG1	3.262727	-1.508710	3.659647	AAMB	1	0.0
197	13	VAL	CG2	4.608006	-3.544752	3.065091	AAMB	1	0.0
198	13	VAL	HN	4.783776	-3.122324	0.330963	AAMB	1	0.0
199	13	VAL	HA	2.343054	-3.321087	1.616117	AAMB	1	0.0
200	13	VAL	HB	4.783395	-1.613705	2.166303	AAMB	1	0.0
201	13	VAL	HG11	2.396917	-2.068810	4.013923	AAMB	1	0.0
202	13	VAL	HG12	3.933859	-1.357831	4.505430	AAMB	1	0.0
203	13	VAL	HG13	2.919914	-0.523229	3.344039	AAMB	1	0.0
204	13	VAL	HG21	5.136044	-4.104921	2.294390	AAMB	1	0.0
205	13	VAL	HG22	5.326916	-3.323920	3.854645	AAMB	1	0.0
206	13	VAL	HG23	3.846898	-4.204151	3.482245	AAMB	1	0.0
207	14	HIS	N	2.870301	-0.601688	-0.085326	AAMB	1	0.0
208	14	HIS	CA	2.147757	0.486269	-0.649232	AAMB	1	0.0
209	14	HIS	C	0.906444	-0.041158	-1.187686	AAMB	1	0.0
210	14	HIS	O	-0.162553	0.551120	-0.892737	AAMB	1	0.0
211	14	HIS	CB	2.936666	1.288229	-1.707480	AAMB	1	0.0
212	14	HIS	CG	2.015913	2.187256	-2.510916	AAMB	1	0.0
213	14	HIS	ND1	1.357392	3.253081	-2.004886	AAMB	1	0.0
214	14	HIS	CD2	1.667202	2.053854	-3.865278	AAMB	1	0.0
215	14	HIS	CE1	0.631821	3.749829	-3.021202	AAMB	1	0.0
216	14	HIS	NE2	0.797974	3.046414	-4.154242	AAMB	1	0.0
217	14	HIS	HN	3.751224	-0.804321	-0.429730	AAMB	1	0.0
218	14	HIS	HA	1.901805	1.165849	0.177339	AAMB	1	0.0
219	14	HIS	HB1	3.682687	1.917218	-1.224643	AAMB	1	0.0
220	14	HIS	HB2	3.462702	0.633453	-2.396213	AAMB	1	0.0
221	14	HIS	HD1	1.394027	3.589149	-1.085397	AAMB	1	0.0
222	14	HIS	HD2	2.023841	1.294254	-4.545117	AAMB	1	0.0
223	14	HIS	HE1	-0.010105	4.613591	-2.942399	AAMB	1	0.0
224	14	HIS	H1	0.370479	3.221088	-5.018197	AAMB	1	0.0
225	15	HIS	N	0.946838	-1.035730	-2.092577	AAMB	1	0.0
226	15	HIS	CA	-0.236731	-1.644258	-2.613684	AAMB	1	0.0
227	15	HIS	C	-1.127244	-2.033749	-1.516683	AAMB	1	0.0
228	15	HIS	O	-2.353407	-2.056832	-1.743800	AAMB	1	0.0
229	15	HIS	CB	0.025579	-2.709569	-3.709244	AAMB	1	0.0
230	15	HIS	CG	0.080974	-4.150737	-3.231872	AAMB	1	0.0
231	15	HIS	ND1	1.178463	-4.932372	-3.311204	AAMB	1	0.0
232	15	HIS	CD2	-0.954665	-4.924392	-2.676597	AAMB	1	0.0
233	15	HIS	CE1	0.824723	-6.131931	-2.821561	AAMB	1	0.0
234	15	HIS	NE2	-0.461154	-6.157293	-2.429128	AAMB	1	0.0
235	15	HIS	HN	1.815019	-1.381073	-2.354747	AAMB	1	0.0
236	15	HIS	HA	-0.745348	-0.819196	-3.128792	AAMB	1	0.0

237	15	HIS	HB1	-0.783553	-2.658721	-4.438816	AAMB	1	0.0
238	15	HIS	HB2	0.938850	-2.468493	-4.254772	AAMB	1	0.0
239	15	HIS	HD1	2.053021	-4.682819	-3.671699	AAMB	1	0.0
240	15	HIS	HD2	-1.965244	-4.600068	-2.481699	AAMB	1	0.0
241	15	HIS	HE1	1.495636	-6.975162	-2.752990	AAMB	1	0.0
242	15	HIS	H1	-0.940965	-6.918912	-2.043189	AAMB	1	0.0
243	16	GLN	N	-0.618183	-2.353164	-0.307480	AAMB	1	0.0
244	16	GLN	CA	-1.446121	-2.722356	0.796756	AAMB	1	0.0
245	16	GLN	C	-2.285527	-1.597471	1.225606	AAMB	1	0.0
246	16	GLN	O	-3.507591	-1.806687	1.390926	AAMB	1	0.0
247	16	GLN	CB	-0.645303	-3.321538	1.967379	AAMB	1	0.0
248	16	GLN	CG	-1.523450	-4.059809	2.993394	AAMB	1	0.0
249	16	GLN	CD	-2.214256	-5.289377	2.386834	AAMB	1	0.0
250	16	GLN	OE1	-3.431685	-5.356618	2.278814	AAMB	1	0.0
251	16	GLN	NE2	-1.358961	-6.255718	2.009510	AAMB	1	0.0
252	16	GLN	HN	0.340554	-2.337373	-0.191350	AAMB	1	0.0
253	16	GLN	HA	-2.113590	-3.506227	0.416273	AAMB	1	0.0
254	16	GLN	HB1	0.112989	-3.999655	1.575492	AAMB	1	0.0
255	16	GLN	HB2	-0.108893	-2.544837	2.506401	AAMB	1	0.0
256	16	GLN	HG1	-0.918609	-4.387672	3.838799	AAMB	1	0.0
257	16	GLN	HG2	-2.289382	-3.394150	3.392277	AAMB	1	0.0
258	16	GLN	HE21	-1.720738	-7.108796	1.631888	AAMB	1	0.0
259	16	GLN	HE22	-0.368933	-6.149203	2.098950	AAMB	1	0.0
260	17	LYS	N	-1.746697	-0.373374	1.393378	AAMB	1	0.0
261	17	LYS	CA	-2.527025	0.763398	1.782422	AAMB	1	0.0
262	17	LYS	C	-3.514591	1.121618	0.760728	AAMB	1	0.0
263	17	LYS	O	-4.674531	1.411898	1.132969	AAMB	1	0.0
264	17	LYS	CB	-1.530368	1.907630	2.045236	AAMB	1	0.0
265	17	LYS	CG	-2.140560	3.293662	2.336305	AAMB	1	0.0
266	17	LYS	CD	-2.438395	4.155569	1.093334	AAMB	1	0.0
267	17	LYS	CE	-1.220231	4.337471	0.175319	AAMB	1	0.0
268	17	LYS	NZ	-1.398108	5.389336	-0.817685	AAMB	1	0.0
269	17	LYS	HN	-0.792302	-0.283311	1.248828	AAMB	1	0.0
270	17	LYS	HA	-3.048416	0.512863	2.714864	AAMB	1	0.0
271	17	LYS	HB1	-0.936101	1.616875	2.911986	AAMB	1	0.0
272	17	LYS	HB2	-0.810949	1.972501	1.230316	AAMB	1	0.0
273	17	LYS	HG1	-3.041641	3.182692	2.940636	AAMB	1	0.0
274	17	LYS	HG2	-1.433862	3.847651	2.955751	AAMB	1	0.0
275	17	LYS	HD1	-3.271389	3.749475	0.521260	AAMB	1	0.0
276	17	LYS	HD2	-2.771108	5.136537	1.434701	AAMB	1	0.0
277	17	LYS	HE1	-0.335867	4.594476	0.758380	AAMB	1	0.0
278	17	LYS	HE2	-1.003431	3.418928	-0.369616	AAMB	1	0.0
279	17	LYS	HZ1	-1.586084	6.290607	-0.333286	AAMB	1	0.0
280	17	LYS	HZ2	-0.537215	5.471690	-1.396080	AAMB	1	0.0
281	17	LYS	HZ3	-2.210231	5.150732	-1.423035	AAMB	1	0.0
282	18	LEU	N	-3.174159	1.156810	-0.543538	AAMB	1	0.0
283	18	LEU	CA	-4.113560	1.484990	-1.567282	AAMB	1	0.0
284	18	LEU	C	-5.176423	0.471401	-1.659226	AAMB	1	0.0
285	18	LEU	O	-6.329594	0.840865	-1.994066	AAMB	1	0.0
286	18	LEU	CB	-3.312541	1.591564	-2.885684	AAMB	1	0.0
287	18	LEU	CG	-3.764131	2.712226	-3.836073	AAMB	1	0.0
288	18	LEU	CD1	-5.230063	2.568621	-4.262001	AAMB	1	0.0
289	18	LEU	CD2	-3.466871	4.099277	-3.248059	AAMB	1	0.0
290	18	LEU	HN	-2.262553	0.934893	-0.775909	AAMB	1	0.0
291	18	LEU	HA	-4.577597	2.434096	-1.285496	AAMB	1	0.0
292	18	LEU	HB1	-2.261363	1.775138	-2.654881	AAMB	1	0.0

293	18	LEU	HB2	-3.309213	0.635576	-3.413471	AAMB	1	0.0
294	18	LEU	HG	-3.158692	2.615662	-4.738280	AAMB	1	0.0
295	18	LEU	HD11	-5.449493	1.549911	-4.582293	AAMB	1	0.0
296	18	LEU	HD12	-5.907969	2.822372	-3.447451	AAMB	1	0.0
297	18	LEU	HD13	-5.459674	3.227573	-5.097718	AAMB	1	0.0
298	18	LEU	HD21	-2.419458	4.179615	-2.959273	AAMB	1	0.0
299	18	LEU	HD22	-3.660022	4.886509	-3.973520	AAMB	1	0.0
300	18	LEU	HD23	-4.074741	4.306821	-2.367718	AAMB	1	0.0
301	19	VAL	N	-4.932119	-0.810388	-1.315467	AAMB	1	0.0
302	19	VAL	CA	-5.943285	-1.823956	-1.356185	AAMB	1	0.0
303	19	VAL	C	-6.797062	-1.714142	-0.169165	AAMB	1	0.0
304	19	VAL	O	-8.010448	-1.991933	-0.292257	AAMB	1	0.0
305	19	VAL	CB	-5.283894	-3.214997	-1.505604	AAMB	1	0.0
306	19	VAL	CG1	-6.216343	-4.386761	-1.146817	AAMB	1	0.0
307	19	VAL	CG2	-4.768979	-3.403587	-2.941956	AAMB	1	0.0
308	19	VAL	HN	-4.041923	-1.068045	-1.045009	AAMB	1	0.0
309	19	VAL	HA	-6.592118	-1.648055	-2.224685	AAMB	1	0.0
310	19	VAL	HB	-4.431998	-3.263937	-0.825355	AAMB	1	0.0
311	19	VAL	HG11	-7.127732	-4.364471	-1.745230	AAMB	1	0.0
312	19	VAL	HG12	-5.724566	-5.343723	-1.322303	AAMB	1	0.0
313	19	VAL	HG13	-6.505972	-4.365598	-0.095801	AAMB	1	0.0
314	19	VAL	HG21	-4.124856	-2.585130	-3.260045	AAMB	1	0.0
315	19	VAL	HG22	-4.201437	-4.328980	-3.037664	AAMB	1	0.0
316	19	VAL	HG23	-5.598280	-3.450290	-3.648001	AAMB	1	0.0
317	20	PHE	N	-6.305319	-1.202374	0.975365	AAMB	1	0.0
318	20	PHE	CA	-7.101325	-1.045330	2.153176	AAMB	1	0.0
319	20	PHE	C	-8.025386	0.078303	1.983149	AAMB	1	0.0
320	20	PHE	O	-9.174790	0.006741	2.481483	AAMB	1	0.0
321	20	PHE	CB	-6.164958	-0.817445	3.353059	AAMB	1	0.0
322	20	PHE	CG	-6.918325	-0.599432	4.640983	AAMB	1	0.0
323	20	PHE	CD1	-7.091969	0.686183	5.147894	AAMB	1	0.0
324	20	PHE	CD2	-7.463361	-1.676588	5.333272	AAMB	1	0.0
325	20	PHE	CE1	-7.800352	0.892975	6.324309	AAMB	1	0.0
326	20	PHE	CE2	-8.171719	-1.472138	6.510238	AAMB	1	0.0
327	20	PHE	CZ	-8.340724	-0.187380	7.006686	AAMB	1	0.0
328	20	PHE	HN	-5.371571	-0.965666	1.007602	AAMB	1	0.0
329	20	PHE	HA	-7.680093	-1.966908	2.294902	AAMB	1	0.0
330	20	PHE	HB1	-5.506618	-1.678745	3.471618	AAMB	1	0.0
331	20	PHE	HB2	-5.513167	0.037280	3.168236	AAMB	1	0.0
332	20	PHE	HD1	-6.681209	1.534905	4.620530	AAMB	1	0.0
333	20	PHE	HD2	-7.345307	-2.681495	4.954969	AAMB	1	0.0
334	20	PHE	HE1	-7.933961	1.894438	6.706670	AAMB	1	0.0
335	20	PHE	HE2	-8.596709	-2.313291	7.038013	AAMB	1	0.0
336	20	PHE	HZ	-8.893896	-0.030313	7.921391	AAMB	1	0.0
337	21	PHE	N	-7.673174	1.132797	1.221871	AAMB	1	0.0
338	21	PHE	CA	-8.544904	2.242817	0.996134	AAMB	1	0.0
339	21	PHE	C	-9.594489	1.882055	0.039219	AAMB	1	0.0
340	21	PHE	O	-10.734620	2.340141	0.209890	AAMB	1	0.0
341	21	PHE	CB	-7.630144	3.339085	0.406048	AAMB	1	0.0
342	21	PHE	CG	-8.279858	4.689785	0.243046	AAMB	1	0.0
343	21	PHE	CD1	-9.033857	4.982680	-0.889980	AAMB	1	0.0
344	21	PHE	CD2	-8.114664	5.673143	1.214872	AAMB	1	0.0
345	21	PHE	CE1	-9.610301	6.235482	-1.050958	AAMB	1	0.0
346	21	PHE	CE2	-8.682891	6.930295	1.052681	AAMB	1	0.0
347	21	PHE	CZ	-9.431198	7.211647	-0.081760	AAMB	1	0.0
348	21	PHE	HN	-6.783930	1.133674	0.845026	AAMB	1	0.0

349	21	PHE	HA	-8.990414	2.589137	1.936806	AAMB	1	0.0
350	21	PHE	HB1	-6.758051	3.460793	1.050660	AAMB	1	0.0
351	21	PHE	HB2	-7.229529	3.023388	-0.559345	AAMB	1	0.0
352	21	PHE	HD1	-9.172157	4.231207	-1.654119	AAMB	1	0.0
353	21	PHE	HD2	-7.534697	5.461709	2.101659	AAMB	1	0.0
354	21	PHE	HE1	-10.201106	6.449576	-1.929776	AAMB	1	0.0
355	21	PHE	HE2	-8.543750	7.689849	1.808443	AAMB	1	0.0
356	21	PHE	HZ	-9.876211	8.187594	-0.210358	AAMB	1	0.0
357	22	ALA	N	-9.328560	1.117209	-1.035786	AAMB	1	0.0
358	22	ALA	CA	-10.350311	0.737008	-1.961846	AAMB	1	0.0
359	22	ALA	C	-11.245373	-0.265703	-1.365418	AAMB	1	0.0
360	22	ALA	O	-12.307265	-0.557771	-1.942278	AAMB	1	0.0
361	22	ALA	CB	-9.670074	0.152686	-3.205822	AAMB	1	0.0
362	22	ALA	HN	-8.420064	0.809104	-1.179925	AAMB	1	0.0
363	22	ALA	HA	-10.940668	1.615099	-2.245142	AAMB	1	0.0
364	22	ALA	HB1	-9.004342	0.886258	-3.661141	AAMB	1	0.0
365	22	ALA	HB2	-9.070167	-0.724423	-2.957659	AAMB	1	0.0
366	22	ALA	HB3	-10.401347	-0.141039	-3.960057	AAMB	1	0.0
367	23	GLU	N	-10.821669	-1.054320	-0.355770	AAMB	1	0.0
368	23	GLU	CA	-11.671812	-2.020930	0.266841	AAMB	1	0.0
369	23	GLU	C	-12.599527	-1.352089	1.179854	AAMB	1	0.0
370	23	GLU	O	-13.772074	-1.752651	1.183833	AAMB	1	0.0
371	23	GLU	CB	-10.786191	-3.005298	1.055466	AAMB	1	0.0
372	23	GLU	CG	-10.072260	-4.031264	0.157045	AAMB	1	0.0
373	23	GLU	CD	-11.003459	-5.190736	-0.227515	AAMB	1	0.0
374	23	GLU	OE1	-11.254838	-6.049382	0.618023	AAMB	1	0.0
375	23	GLU	OE2	-11.469094	-5.230234	-1.365911	AAMB	1	0.0
376	23	GLU	HN	-9.929513	-0.930140	-0.003553	AAMB	1	0.0
377	23	GLU	HA	-12.248537	-2.569595	-0.489512	AAMB	1	0.0
378	23	GLU	HB1	-10.038554	-2.439721	1.613465	AAMB	1	0.0
379	23	GLU	HB2	-11.367321	-3.537548	1.811626	AAMB	1	0.0
380	23	GLU	HG1	-9.698793	-3.567060	-0.754756	AAMB	1	0.0
381	23	GLU	HG2	-9.208701	-4.445973	0.677601	AAMB	1	0.0
382	24	ASP	N	-12.177330	-0.354410	1.977433	AAMB	1	0.0
383	24	ASP	CA	-13.065334	0.361538	2.837221	AAMB	1	0.0
384	24	ASP	C	-13.743554	1.391010	2.052543	AAMB	1	0.0
385	24	ASP	O	-14.992313	1.328216	1.946455	AAMB	1	0.0
386	24	ASP	CB	-12.257605	0.997838	3.984617	AAMB	1	0.0
387	24	ASP	CG	-11.773894	-0.060520	4.995178	AAMB	1	0.0
388	24	ASP	OD1	-12.179153	0.006625	6.155449	AAMB	1	0.0
389	24	ASP	OD2	-10.999251	-0.938578	4.617404	AAMB	1	0.0
390	24	ASP	HN	-11.239460	-0.117474	1.970835	AAMB	1	0.0
391	24	ASP	HA	-13.825746	-0.321635	3.237243	AAMB	1	0.0
392	24	ASP	HB1	-11.387917	1.532624	3.599510	AAMB	1	0.0
393	24	ASP	HB2	-12.866926	1.730987	4.517014	AAMB	1	0.0
394	25	VAL	N	-13.033711	2.400514	1.517171	AAMB	1	0.0
395	25	VAL	CA	-13.627054	3.411602	0.703844	AAMB	1	0.0
396	25	VAL	C	-14.398943	2.830595	-0.395773	AAMB	1	0.0
397	25	VAL	O	-15.560534	3.262855	-0.588836	AAMB	1	0.0
398	25	VAL	CB	-12.657796	4.541532	0.304691	AAMB	1	0.0
399	25	VAL	CG1	-13.392541	5.713545	-0.365649	AAMB	1	0.0
400	25	VAL	CG2	-11.899372	5.035639	1.547065	AAMB	1	0.0
401	25	VAL	HN	-12.081930	2.420543	1.672284	AAMB	1	0.0
402	25	VAL	HA	-14.366833	3.867602	1.376663	AAMB	1	0.0
403	25	VAL	HB	-11.940532	4.177545	-0.427518	AAMB	1	0.0
404	25	VAL	HG11	-13.847574	5.406779	-1.306554	AAMB	1	0.0

405	25	VAL	HG12	-14.181201	6.107159	0.276092	AAMB	1	0.0
406	25	VAL	HG13	-12.705975	6.529413	-0.591897	AAMB	1	0.0
407	25	VAL	HG21	-12.588413	5.275250	2.357176	AAMB	1	0.0
408	25	VAL	HG22	-11.195408	4.289235	1.915162	AAMB	1	0.0
409	25	VAL	HG23	-11.335196	5.938540	1.333591	AAMB	1	0.0
410	26	GLY	N	-13.897909	1.806942	-1.109662	AAMB	1	0.0
411	26	GLY	CA	-14.634172	1.199144	-2.163104	AAMB	1	0.0
412	26	GLY	C	-15.754764	0.428300	-1.636873	AAMB	1	0.0
413	26	GLY	O	-16.810810	0.459768	-2.314776	AAMB	1	0.0
414	26	GLY	HN	-13.017754	1.473277	-0.889328	AAMB	1	0.0
415	26	GLY	HA1	-14.927588	1.958454	-2.865408	AAMB	1	0.0
416	26	GLY	HA2	-14.053854	0.540123	-2.786183	AAMB	1	0.0
417	27	SER	N	-15.607442	-0.352578	-0.547584	AAMB	1	0.0
418	27	SER	CA	-16.715082	-1.065141	0.019772	AAMB	1	0.0
419	27	SER	C	-17.905237	-0.211181	0.102507	AAMB	1	0.0
420	27	SER	O	-18.980049	-0.652926	-0.379306	AAMB	1	0.0
421	27	SER	CB	-16.459150	-1.687217	1.412520	AAMB	1	0.0
422	27	SER	OG	-17.627197	-2.027590	2.144411	AAMB	1	0.0
423	27	SER	HN	-14.748532	-0.419415	-0.115161	AAMB	1	0.0
424	27	SER	HA	-16.934277	-1.868156	-0.693759	AAMB	1	0.0
425	27	SER	HB1	-15.859401	-2.595108	1.317549	AAMB	1	0.0
426	27	SER	HB2	-15.903035	-0.987941	2.035828	AAMB	1	0.0
427	27	SER	HG	-18.252108	-2.452096	1.564978	AAMB	1	0.0
428	28	ASN	N	-17.828413	1.017654	0.655349	AAMB	1	0.0
429	28	ASN	CA	-18.949713	1.902397	0.746077	AAMB	1	0.0
430	28	ASN	C	-18.805429	3.008193	-0.214104	AAMB	1	0.0
431	28	ASN	O	-18.979372	4.178142	0.210553	AAMB	1	0.0
432	28	ASN	CB	-19.186373	2.356376	2.203287	AAMB	1	0.0
433	28	ASN	CG	-17.994606	3.060821	2.876493	AAMB	1	0.0
434	28	ASN	OD1	-17.876747	4.279554	2.875591	AAMB	1	0.0
435	28	ASN	ND2	-17.159494	2.222300	3.510754	AAMB	1	0.0
436	28	ASN	HN	-16.969990	1.309415	1.001629	AAMB	1	0.0
437	28	ASN	HA	-19.878851	1.413835	0.435057	AAMB	1	0.0
438	28	ASN	HB1	-20.043367	3.028956	2.253181	AAMB	1	0.0
439	28	ASN	HB2	-19.452908	1.489117	2.807838	AAMB	1	0.0
440	28	ASN	HD21	-16.399454	2.589891	4.044052	AAMB	1	0.0
441	28	ASN	HD22	-17.275978	1.231059	3.450246	AAMB	1	0.0
442	29	LYS	N	-18.527422	2.773166	-1.515061	AAMB	1	0.0
443	29	LYS	CA	-18.354721	3.826449	-2.471390	AAMB	1	0.0
444	29	LYS	C	-19.492424	3.881565	-3.367871	AAMB	1	0.0
445	29	LYS	O	-19.854271	2.898005	-4.056283	AAMB	1	0.0
446	29	LYS	CB	-17.088192	3.650053	-3.327225	AAMB	1	0.0
447	29	LYS	CG	-16.037207	4.749557	-3.110100	AAMB	1	0.0
448	29	LYS	CD	-16.355852	6.036693	-3.877877	AAMB	1	0.0
449	29	LYS	CE	-15.298275	7.119374	-3.638209	AAMB	1	0.0
450	29	LYS	NZ	-15.605159	8.364956	-4.330549	AAMB	1	0.0
451	29	LYS	OXT	-20.106014	4.955043	-3.577588	AAMB	1	0.0
452	29	LYS	HN	-18.407160	1.860785	-1.813810	AAMB	1	0.0
453	29	LYS	HA	-18.309614	4.804605	-1.985870	AAMB	1	0.0
454	29	LYS	HB1	-16.700270	2.679095	-3.084668	AAMB	1	0.0
455	29	LYS	HB2	-17.287268	3.583776	-4.399544	AAMB	1	0.0
456	29	LYS	HG1	-15.960933	4.994623	-2.053224	AAMB	1	0.0
457	29	LYS	HG2	-15.058952	4.379163	-3.417967	AAMB	1	0.0
458	29	LYS	HD1	-16.424520	5.823281	-4.945067	AAMB	1	0.0
459	29	LYS	HD2	-17.333387	6.411322	-3.572547	AAMB	1	0.0
460	29	LYS	HE1	-15.215751	7.347436	-2.575213	AAMB	1	0.0

```
  461    29   LYS   HE2   -14.319218    6.783948   -3.980606 AAMB    1   0.0
  462    29   LYS   HZ1   -16.516441    8.733411   -3.990545 AAMB    1   0.0
  463    29   LYS   HZ2   -14.854439    9.058959   -4.139287 AAMB    1   0.0
  464    29   LYS   HZ3   -15.661006    8.185925   -5.353293 AAMB    1   0.0

! ...
! Copyright (c) 1986, 1987, 1988, 1989, 1990, 1991  Polygen Corporation
! Confidential and Proprietary: All Rights Reserved
! ...
! ...
!

if 1 eq 0 COOR ORIE NOROT
if 1 eq 1 COOR ORIE NOROT SELE BYNUM @2 end
```

Appendix 4: CHARMM .STR File for Uniting Two 30 Å Water Boxes for Solvating Larger Systems

Water molecules have been removed, with .... used to indicate that there are more molecules included in the system than shown.

```
* Script file produced by QUANTA
*
! Startup script for CHARMm
!
UPPER ! case for files to write
open write card unit 7 name CHARMM.LOG
outu 7
banner
bomblevel -2
wrnlev 0
prnlev 5
* Script to read parameter, psf, and ic files
*
reset
open read unit 21 card name $CHM_DATA/MASSES.RTF
read rtf unit 21 card
close unit 20
open read unit 20 card name ".charmmprm"
read param unit 20 card
close unit 20
open read unit 20 card name ".charmmpsf"
read psf unit 20 card
close unit 20
open read unit 20 card name ".charmmic"
ic read unit 20 card
close unit 20
! Script for reading RTF
!
OPEN READ UNIT 77 CARD NAME -
 "TIP3.RTF"
READ RTF CARD UNIT 77 APPEND
CLOSE UNIT 77
!set some variables
!
SET 1 1
SET 2 1
SET 3 367

! QUANTA coordinates included in script file

! Copyright (c) 1986, 1987, 1988, 1989, 1990, 1991  Polygen Corporation
! Confidential and Proprietary: All Rights Reserved
! ...
! ...
READ COOR CARD FREE
* current QUANTA coordinates written for free read
```

```
*
464
  1   1  ASP  N     19.777775  -0.609759   1.064205 AAMB   1   0.0
  2   1  ASP  CA    19.041170   0.412852   1.823377 AAMB   1   0.0
  3   1  ASP  C     17.933453   0.933095   1.021516 AAMB   1   0.0
  4   1  ASP  O     16.766161   0.674886   1.402760 AAMB   1   0.0
  5   1  ASP  CB    19.933836   1.535490   2.379036 AAMB   1   0.0
  6   1  ASP  CG    19.121866   2.487353   3.277849 AAMB   1   0.0
  7   1  ASP  OD1   18.632879   2.039340   4.313909 AAMB   1   0.0
  8   1  ASP  OD2   18.976418   3.655082   2.920227 AAMB   1   0.0
  9   1  ASP  H1    19.121496  -1.354191   0.752547 AAMB   1   0.0
 10   1  ASP  H2    20.220243  -0.166533   0.233697 AAMB   1   0.0
 11   1  ASP  H3    20.515404  -1.023449   1.668909 AAMB   1   0.0
 12   1  ASP  HA    18.610788  -0.162236   2.653509 AAMB   1   0.0
 13   1  ASP  HB1   20.742023   1.110273   2.974636 AAMB   1   0.0
 14   1  ASP  HB2   20.403439   2.099329   1.571359 AAMB   1   0.0
 15   2  ALA  N     18.160498   1.642654  -0.100774 AAMB   1   0.0
 16   2  ALA  CA    17.094845   2.143059  -0.915015 AAMB   1   0.0
 17   2  ALA  C     16.254911   1.052349  -1.423196 AAMB   1   0.0
 18   2  ALA  O     15.054347   1.068294  -1.075329 AAMB   1   0.0
 19   2  ALA  CB    17.694002   2.943519  -2.079650 AAMB   1   0.0
 20   2  ALA  HN    19.074314   1.839025  -0.364898 AAMB   1   0.0
 21   2  ALA  HA    16.493011   2.824638  -0.300168 AAMB   1   0.0
 22   2  ALA  HB1   18.346489   2.330650  -2.702799 AAMB   1   0.0
 23   2  ALA  HB2   16.912779   3.358901  -2.717892 AAMB   1   0.0
 24   2  ALA  HB3   18.287169   3.778764  -1.706802 AAMB   1   0.0
 25   3  GLU  N     16.766771   0.108776  -2.238868 AAMB   1   0.0
 26   3  GLU  CA    15.982441  -0.984445  -2.721450 AAMB   1   0.0
 27   3  GLU  C     15.336887  -1.714932  -1.622579 AAMB   1   0.0
 28   3  GLU  O     14.235341  -2.266397  -1.856518 AAMB   1   0.0
 29   3  GLU  CB    16.912476  -1.943119  -3.491119 AAMB   1   0.0
 30   3  GLU  CG    18.027748  -2.588000  -2.643043 AAMB   1   0.0
 31   3  GLU  CD    18.976223  -3.410681  -3.527524 AAMB   1   0.0
 32   3  GLU  OE1   18.561335  -4.460563  -4.015923 AAMB   1   0.0
 33   3  GLU  OE2   20.118059  -2.992227  -3.718383 AAMB   1   0.0
 34   3  GLU  HN    17.696264   0.177130  -2.510961 AAMB   1   0.0
 35   3  GLU  HA    15.271745  -0.619510  -3.458186 AAMB   1   0.0
 36   3  GLU  HB1   16.313803  -2.728753  -3.956718 AAMB   1   0.0
 37   3  GLU  HB2   17.364645  -1.390374  -4.316061 AAMB   1   0.0
 38   3  GLU  HG1   18.602930  -1.828216  -2.112981 AAMB   1   0.0
 39   3  GLU  HG2   17.610920  -3.255042  -1.888543 AAMB   1   0.0
 40   4  PHE  N     15.919147  -1.782670  -0.408540 AAMB   1   0.0
 41   4  PHE  CA    15.307195  -2.459879   0.694823 AAMB   1   0.0
 42   4  PHE  C     14.023937  -1.843083   1.055299 AAMB   1   0.0
 43   4  PHE  O     12.972171  -2.524466   0.949426 AAMB   1   0.0
 44   4  PHE  CB    16.279325  -2.527560   1.885257 AAMB   1   0.0
 45   4  PHE  CG    15.739339  -3.373469   3.008183 AAMB   1   0.0
 46   4  PHE  CD1   15.827451  -4.761220   2.950030 AAMB   1   0.0
 47   4  PHE  CD2   15.139515  -2.779069   4.115228 AAMB   1   0.0
 48   4  PHE  CE1   15.323042  -5.543265   3.980633 AAMB   1   0.0
 49   4  PHE  CE2   14.634054  -3.558976   5.146505 AAMB   1   0.0
 50   4  PHE  CZ    14.725373  -4.942125   5.079395 AAMB   1   0.0
 51   4  PHE  HN    16.751390  -1.312392  -0.272539 AAMB   1   0.0
 52   4  PHE  HA    15.091137  -3.477376   0.342844 AAMB   1   0.0
 53   4  PHE  HB1   17.229939  -2.950183   1.558902 AAMB   1   0.0
 54   4  PHE  HB2   16.505716  -1.533943   2.267781 AAMB   1   0.0
```

55	4	PHE	HD1	16.289227	-5.239542	2.098484	AAMB	1	0.0
56	4	PHE	HD2	15.062601	-1.703010	4.177594	AAMB	1	0.0
57	4	PHE	HE1	15.397733	-6.620112	3.930117	AAMB	1	0.0
58	4	PHE	HE2	14.172368	-3.089531	6.002832	AAMB	1	0.0
59	4	PHE	HZ	14.335523	-5.550326	5.882483	AAMB	1	0.0
60	5	ARG	N	13.973029	-0.583468	1.540645	AAMB	1	0.0
61	5	ARG	CA	12.735288	0.057283	1.876006	AAMB	1	0.0
62	5	ARG	C	11.947042	0.320672	0.666657	AAMB	1	0.0
63	5	ARG	O	10.776729	0.746743	0.824206	AAMB	1	0.0
64	5	ARG	CB	13.090855	1.396300	2.549845	AAMB	1	0.0
65	5	ARG	CG	14.012118	1.225855	3.768469	AAMB	1	0.0
66	5	ARG	CD	14.358644	2.557881	4.438255	AAMB	1	0.0
67	5	ARG	NE	15.332176	2.317842	5.494621	AAMB	1	0.0
68	5	ARG	CZ	15.810915	3.302024	6.283080	AAMB	1	0.0
69	5	ARG	NH1	15.389730	4.556768	6.160191	AAMB	1	0.0
70	5	ARG	NH2	16.723600	3.009213	7.200159	AAMB	1	0.0
71	5	ARG	HN	14.801904	-0.091048	1.579415	AAMB	1	0.0
72	5	ARG	HA	12.176013	-0.551757	2.589055	AAMB	1	0.0
73	5	ARG	HB1	13.585042	2.054208	1.831977	AAMB	1	0.0
74	5	ARG	HB2	12.177840	1.907795	2.858794	AAMB	1	0.0
75	5	ARG	HG1	13.541816	0.562265	4.494619	AAMB	1	0.0
76	5	ARG	HG2	14.944643	0.746375	3.469539	AAMB	1	0.0
77	5	ARG	HD1	14.812840	3.250935	3.727876	AAMB	1	0.0
78	5	ARG	HD2	13.478590	3.023529	4.884431	AAMB	1	0.0
79	5	ARG	HE	15.685361	1.390481	5.618040	AAMB	1	0.0
80	5	ARG	HH11	14.699955	4.790350	5.475661	AAMB	1	0.0
81	5	ARG	HH12	15.761321	5.270680	6.754082	AAMB	1	0.0
82	5	ARG	HH21	17.058340	2.071859	7.294514	AAMB	1	0.0
83	5	ARG	HH22	17.080513	3.726822	7.798309	AAMB	1	0.0
84	6	HIS	N	12.477256	0.090535	-0.550493	AAMB	1	0.0
85	6	HIS	CA	11.744717	0.312759	-1.758953	AAMB	1	0.0
86	6	HIS	C	10.796138	-0.782060	-1.978250	AAMB	1	0.0
87	6	HIS	O	9.589708	-0.479645	-1.876704	AAMB	1	0.0
88	6	HIS	CB	12.669912	0.466814	-2.978475	AAMB	1	0.0
89	6	HIS	CG	11.850272	0.746600	-4.220493	AAMB	1	0.0
90	6	HIS	ND1	11.024459	1.806971	-4.352235	AAMB	1	0.0
91	6	HIS	CD2	11.767838	-0.026044	-5.391406	AAMB	1	0.0
92	6	HIS	CE1	10.456316	1.683361	-5.563576	AAMB	1	0.0
93	6	HIS	NE2	10.884850	0.586773	-6.213204	AAMB	1	0.0
94	6	HIS	HN	13.376023	-0.258575	-0.621651	AAMB	1	0.0
95	6	HIS	HA	11.189747	1.253068	-1.633207	AAMB	1	0.0
96	6	HIS	HB1	13.376599	1.282532	-2.833537	AAMB	1	0.0
97	6	HIS	HB2	13.235850	-0.443755	-3.144358	AAMB	1	0.0
98	6	HIS	HD1	10.866956	2.516039	-3.694793	AAMB	1	0.0
99	6	HIS	HD2	12.302275	-0.942279	-5.594612	AAMB	1	0.0
100	6	HIS	HE1	9.738291	2.381361	-5.967376	AAMB	1	0.0
101	6	HIS	H1	10.618958	0.291678	-7.108222	AAMB	1	0.0
102	7	ASP	N	11.233445	-2.023194	-2.281511	AAMB	1	0.0
103	7	ASP	CA	10.336828	-3.122818	-2.458477	AAMB	1	0.0
104	7	ASP	C	9.481910	-3.294824	-1.276572	AAMB	1	0.0
105	7	ASP	O	8.295098	-3.664217	-1.457893	AAMB	1	0.0
106	7	ASP	CB	11.158020	-4.409654	-2.672259	AAMB	1	0.0
107	7	ASP	CG	12.009846	-4.344454	-3.954447	AAMB	1	0.0
108	7	ASP	OD1	11.486812	-3.933098	-4.991384	AAMB	1	0.0
109	7	ASP	OD2	13.186305	-4.707085	-3.903346	AAMB	1	0.0
110	7	ASP	HN	12.188498	-2.180787	-2.348245	AAMB	1	0.0

111	7	ASP	HA	9.733404	-2.936532	-3.343399	AAMB	1	0.0
112	7	ASP	HB1	11.812886	-4.589718	-1.817311	AAMB	1	0.0
113	7	ASP	HB2	10.499928	-5.275890	-2.757493	AAMB	1	0.0
114	8	SER	N	9.988587	-3.138769	-0.034572	AAMB	1	0.0
115	8	SER	CA	9.176601	-3.262035	1.137976	AAMB	1	0.0
116	8	SER	C	8.022375	-2.358343	1.073562	AAMB	1	0.0
117	8	SER	O	6.868747	-2.855776	1.073585	AAMB	1	0.0
118	8	SER	CB	10.068766	-2.962929	2.355190	AAMB	1	0.0
119	8	SER	OG	9.357747	-3.133594	3.574400	AAMB	1	0.0
120	8	SER	HN	10.925159	-2.918284	0.068418	AAMB	1	0.0
121	8	SER	HA	8.817378	-4.297300	1.180070	AAMB	1	0.0
122	8	SER	HB1	10.931597	-3.637786	2.332720	AAMB	1	0.0
123	8	SER	HB2	10.454106	-1.940798	2.283954	AAMB	1	0.0
124	8	SER	HG	9.918180	-2.960077	4.327270	AAMB	1	0.0
125	9	GLY	N	8.198386	-1.021602	1.008988	AAMB	1	0.0
126	9	GLY	CA	7.094239	-0.121842	0.900155	AAMB	1	0.0
127	9	GLY	C	6.454493	-0.233650	-0.411757	AAMB	1	0.0
128	9	GLY	O	5.464347	0.490092	-0.620506	AAMB	1	0.0
129	9	GLY	HN	9.096245	-0.652911	0.994446	AAMB	1	0.0
130	9	GLY	HA1	6.379829	-0.274391	1.706055	AAMB	1	0.0
131	9	GLY	HA2	7.484860	0.892686	0.999122	AAMB	1	0.0
132	10	TYR	N	6.983341	-1.033271	-1.360520	AAMB	1	0.0
133	10	TYR	CA	6.388818	-1.190931	-2.650550	AAMB	1	0.0
134	10	TYR	C	5.169522	-2.002688	-2.575299	AAMB	1	0.0
135	10	TYR	O	4.083598	-1.530204	-2.994898	AAMB	1	0.0
136	10	TYR	CB	7.345534	-1.742988	-3.722003	AAMB	1	0.0
137	10	TYR	CG	6.780235	-1.568047	-5.108628	AAMB	1	0.0
138	10	TYR	CD1	6.875566	-0.338809	-5.754462	AAMB	1	0.0
139	10	TYR	CD2	6.144049	-2.622742	-5.757461	AAMB	1	0.0
140	10	TYR	CE1	6.336807	-0.163243	-7.022114	AAMB	1	0.0
141	10	TYR	CE2	5.606416	-2.451428	-7.026970	AAMB	1	0.0
142	10	TYR	CZ	5.700393	-1.217822	-7.661445	AAMB	1	0.0
143	10	TYR	OH	5.164546	-1.024396	-8.920258	AAMB	1	0.0
144	10	TYR	HN	7.757517	-1.570586	-1.156951	AAMB	1	0.0
145	10	TYR	HA	6.096994	-0.185557	-2.971601	AAMB	1	0.0
146	10	TYR	HB1	8.294446	-1.213179	-3.691091	AAMB	1	0.0
147	10	TYR	HB2	7.558067	-2.797953	-3.559109	AAMB	1	0.0
148	10	TYR	HD1	7.367125	0.491326	-5.267713	AAMB	1	0.0
149	10	TYR	HD2	6.056268	-3.584122	-5.272258	AAMB	1	0.0
150	10	TYR	HE1	6.410582	0.796421	-7.512625	AAMB	1	0.0
151	10	TYR	HE2	5.111298	-3.284590	-7.504464	AAMB	1	0.0
152	10	TYR	HH	5.410977	-1.736432	-9.496549	AAMB	1	0.0
153	11	GLU	N	5.214782	-3.259125	-2.090118	AAMB	1	0.0
154	11	GLU	CA	4.044102	-4.064106	-1.970570	AAMB	1	0.0
155	11	GLU	C	3.232757	-3.556814	-0.869093	AAMB	1	0.0
156	11	GLU	O	1.983533	-3.602206	-0.998179	AAMB	1	0.0
157	11	GLU	CB	4.508585	-5.504136	-1.700698	AAMB	1	0.0
158	11	GLU	CG	5.352304	-6.073346	-2.858341	AAMB	1	0.0
159	11	GLU	CD	6.046267	-7.385198	-2.456297	AAMB	1	0.0
160	11	GLU	OE1	7.271055	-7.465412	-2.563812	AAMB	1	0.0
161	11	GLU	OE2	5.353405	-8.310934	-2.037041	AAMB	1	0.0
162	11	GLU	HN	6.073738	-3.598763	-1.784515	AAMB	1	0.0
163	11	GLU	HA	3.471385	-4.003354	-2.898062	AAMB	1	0.0
164	11	GLU	HB1	5.097457	-5.521979	-0.780948	AAMB	1	0.0
165	11	GLU	HB2	3.647953	-6.151681	-1.525591	AAMB	1	0.0
166	11	GLU	HG1	4.723450	-6.259685	-3.729042	AAMB	1	0.0

167	11	GLU	HG2	6.119726	-5.364998	-3.172588	AAMB	1	0.0
168	12	VAL	N	3.814550	-3.109827	0.251651	AAMB	1	0.0
169	12	VAL	CA	3.053213	-2.556596	1.319859	AAMB	1	0.0
170	12	VAL	C	2.326123	-1.396080	0.844176	AAMB	1	0.0
171	12	VAL	O	1.248710	-1.084186	1.408288	AAMB	1	0.0
172	12	VAL	CB	3.977703	-2.252757	2.517904	AAMB	1	0.0
173	12	VAL	CG1	3.264524	-1.506013	3.658383	AAMB	1	0.0
174	12	VAL	CG2	4.606677	-3.544638	3.065645	AAMB	1	0.0
175	12	VAL	HN	4.783776	-3.122324	0.330963	AAMB	1	0.0
176	12	VAL	HA	2.343054	-3.321087	1.616117	AAMB	1	0.0
177	12	VAL	HB	4.785039	-1.615181	2.165269	AAMB	1	0.0
178	12	VAL	HG11	2.397423	-2.064084	4.012671	AAMB	1	0.0
179	12	VAL	HG12	3.935966	-1.356168	4.504056	AAMB	1	0.0
180	12	VAL	HG13	2.923978	-0.519927	3.342626	AAMB	1	0.0
181	12	VAL	HG21	5.134048	-4.105847	2.295260	AAMB	1	0.0
182	12	VAL	HG22	5.325817	-3.323709	3.854879	AAMB	1	0.0
183	12	VAL	HG23	3.844441	-4.202545	3.482995	AAMB	1	0.0
184	13	HIS	N	2.870301	-0.601688	-0.085326	AAMB	1	0.0
185	13	HIS	CA	2.147757	0.486269	-0.649232	AAMB	1	0.0
186	13	HIS	C	0.906444	-0.041158	-1.187686	AAMB	1	0.0
187	13	HIS	O	-0.162553	0.551120	-0.892737	AAMB	1	0.0
188	13	HIS	CB	2.931556	1.290516	-1.710533	AAMB	1	0.0
189	13	HIS	CG	2.001103	2.197772	-2.492605	AAMB	1	0.0
190	13	HIS	ND1	1.418068	3.307247	-1.989043	AAMB	1	0.0
191	13	HIS	CD2	1.562221	2.028737	-3.816505	AAMB	1	0.0
192	13	HIS	CE1	0.647256	3.795218	-2.975793	AAMB	1	0.0
193	13	HIS	NE2	0.714894	3.044284	-4.088673	AAMB	1	0.0
194	13	HIS	HN	3.751224	-0.804321	-0.429730	AAMB	1	0.0
195	13	HIS	HA	1.901805	1.165849	0.177339	AAMB	1	0.0
196	13	HIS	HB1	3.685525	1.914498	-1.233498	AAMB	1	0.0
197	13	HIS	HB2	3.446121	0.639142	-2.411343	AAMB	1	0.0
198	13	HIS	HD1	1.526666	3.676201	-1.087930	AAMB	1	0.0
199	13	HIS	HD2	1.846090	1.232338	-4.488090	AAMB	1	0.0
200	13	HIS	HE1	0.047480	4.688235	-2.890903	AAMB	1	0.0
201	13	HIS	H1	0.240240	3.206418	-4.930442	AAMB	1	0.0
202	14	HIS	N	0.946838	-1.035730	-2.092577	AAMB	1	0.0
203	14	HIS	CA	-0.236731	-1.644258	-2.613684	AAMB	1	0.0
204	14	HIS	C	-1.127244	-2.033749	-1.516683	AAMB	1	0.0
205	14	HIS	O	-2.353407	-2.056832	-1.743800	AAMB	1	0.0
206	14	HIS	CB	0.008137	-2.701402	-3.719336	AAMB	1	0.0
207	14	HIS	CG	0.135380	-4.139705	-3.249672	AAMB	1	0.0
208	14	HIS	ND1	1.244685	-4.886912	-3.421677	AAMB	1	0.0
209	14	HIS	CD2	-0.829846	-4.945433	-2.617420	AAMB	1	0.0
210	14	HIS	CE1	0.966844	-6.097539	-2.913075	AAMB	1	0.0
211	14	HIS	NE2	-0.281356	-6.164334	-2.418308	AAMB	1	0.0
212	14	HIS	HN	1.815019	-1.381073	-2.354747	AAMB	1	0.0
213	14	HIS	HA	-0.745348	-0.819196	-3.128792	AAMB	1	0.0
214	14	HIS	HB1	-0.834490	-2.677860	-4.411414	AAMB	1	0.0
215	14	HIS	HB2	0.887401	-2.429862	-4.304904	AAMB	1	0.0
216	14	HIS	HD1	2.081094	-4.607575	-3.845982	AAMB	1	0.0
217	14	HIS	HD2	-1.832204	-4.653473	-2.341948	AAMB	1	0.0
218	14	HIS	HE1	1.665944	-6.920380	-2.903794	AAMB	1	0.0
219	14	HIS	H1	-0.705399	-6.941513	-1.999400	AAMB	1	0.0
220	15	GLN	N	-0.618183	-2.353164	-0.307480	AAMB	1	0.0
221	15	GLN	CA	-1.446121	-2.722356	0.796756	AAMB	1	0.0
222	15	GLN	C	-2.285527	-1.597471	1.225606	AAMB	1	0.0

223	15	GLN	O	-3.507591	-1.806687	1.390926	AAMB	1	0.0
224	15	GLN	CB	-0.646446	-3.324816	1.966519	AAMB	1	0.0
225	15	GLN	CG	-1.525218	-4.062795	2.993101	AAMB	1	0.0
226	15	GLN	CD	-2.235078	-5.284182	2.389935	AAMB	1	0.0
227	15	GLN	OE1	-3.455738	-5.372842	2.365419	AAMB	1	0.0
228	15	GLN	NE2	-1.392638	-6.222067	1.922573	AAMB	1	0.0
229	15	GLN	HN	0.340554	-2.337373	-0.191350	AAMB	1	0.0
230	15	GLN	HA	-2.113590	-3.506227	0.416273	AAMB	1	0.0
231	15	GLN	HB1	0.110819	-4.003546	1.573723	AAMB	1	0.0
232	15	GLN	HB2	-0.107666	-2.549977	2.505945	AAMB	1	0.0
233	15	GLN	HG1	-0.917151	-4.400835	3.832102	AAMB	1	0.0
234	15	GLN	HG2	-2.281023	-3.391980	3.402313	AAMB	1	0.0
235	15	GLN	HE21	-1.763429	-7.075501	1.554611	AAMB	1	0.0
236	15	GLN	HE22	-0.401695	-6.089486	1.933481	AAMB	1	0.0
237	16	LYS	N	-1.746697	-0.373374	1.393378	AAMB	1	0.0
238	16	LYS	CA	-2.527025	0.763398	1.782422	AAMB	1	0.0
239	16	LYS	C	-3.514591	1.121618	0.760728	AAMB	1	0.0
240	16	LYS	O	-4.674531	1.411898	1.132969	AAMB	1	0.0
241	16	LYS	CB	-1.529032	1.904917	2.049959	AAMB	1	0.0
242	16	LYS	CG	-2.139030	3.286984	2.356941	AAMB	1	0.0
243	16	LYS	CD	-2.452783	4.154167	1.122408	AAMB	1	0.0
244	16	LYS	CE	-1.242841	4.352679	0.197316	AAMB	1	0.0
245	16	LYS	NZ	-1.453694	5.393516	-0.798794	AAMB	1	0.0
246	16	LYS	HN	-0.792302	-0.283311	1.248828	AAMB	1	0.0
247	16	LYS	HA	-3.048416	0.512863	2.714864	AAMB	1	0.0
248	16	LYS	HB1	-0.930709	1.606689	2.911505	AAMB	1	0.0
249	16	LYS	HB2	-0.813467	1.977020	1.232241	AAMB	1	0.0
250	16	LYS	HG1	-3.033640	3.169272	2.969662	AAMB	1	0.0
251	16	LYS	HG2	-1.427783	3.839292	2.972631	AAMB	1	0.0
252	16	LYS	HD1	-3.286161	3.744693	0.553417	AAMB	1	0.0
253	16	LYS	HD2	-2.791710	5.129979	1.472394	AAMB	1	0.0
254	16	LYS	HE1	-0.360971	4.633786	0.772934	AAMB	1	0.0
255	16	LYS	HE2	-1.009074	3.436814	-0.344935	AAMB	1	0.0
256	16	LYS	HZ1	-1.675055	6.288345	-0.316544	AAMB	1	0.0
257	16	LYS	HZ2	-0.595514	5.509400	-1.376210	AAMB	1	0.0
258	16	LYS	HZ3	-2.255284	5.126222	-1.406323	AAMB	1	0.0
259	17	LEU	N	-3.174159	1.156810	-0.543538	AAMB	1	0.0
260	17	LEU	CA	-4.113560	1.484990	-1.567282	AAMB	1	0.0
261	17	LEU	C	-5.176423	0.471401	-1.659226	AAMB	1	0.0
262	17	LEU	O	-6.329594	0.840865	-1.994066	AAMB	1	0.0
263	17	LEU	CB	-3.325880	1.610585	-2.892667	AAMB	1	0.0
264	17	LEU	CG	-3.785712	2.747661	-3.824523	AAMB	1	0.0
265	17	LEU	CD1	-5.271036	2.654594	-4.195492	AAMB	1	0.0
266	17	LEU	CD2	-3.435913	4.129725	-3.254340	AAMB	1	0.0
267	17	LEU	HN	-2.262553	0.934893	-0.775909	AAMB	1	0.0
268	17	LEU	HA	-4.577597	2.434096	-1.285496	AAMB	1	0.0
269	17	LEU	HB1	-2.271438	1.785138	-2.670066	AAMB	1	0.0
270	17	LEU	HB2	-3.333622	0.662522	-3.434430	AAMB	1	0.0
271	17	LEU	HG	-3.218442	2.637896	-4.749746	AAMB	1	0.0
272	17	LEU	HD11	-5.526294	1.658127	-4.556837	AAMB	1	0.0
273	17	LEU	HD12	-5.908995	2.880983	-3.341547	AAMB	1	0.0
274	17	LEU	HD13	-5.520473	3.365987	-4.982799	AAMB	1	0.0
275	17	LEU	HD21	-2.367505	4.209018	-3.054261	AAMB	1	0.0
276	17	LEU	HD22	-3.696604	4.920219	-3.958532	AAMB	1	0.0
277	17	LEU	HD23	-3.965827	4.328816	-2.322925	AAMB	1	0.0
278	18	VAL	N	-4.932119	-0.810388	-1.315467	AAMB	1	0.0

279	18	VAL	CA	-5.943285	-1.823956	-1.356185	AAMB	1	0.0
280	18	VAL	C	-6.797062	-1.714142	-0.169165	AAMB	1	0.0
281	18	VAL	O	-8.010448	-1.991933	-0.292257	AAMB	1	0.0
282	18	VAL	CB	-5.279749	-3.213930	-1.499511	AAMB	1	0.0
283	18	VAL	CG1	-6.213015	-4.387560	-1.148586	AAMB	1	0.0
284	18	VAL	CG2	-4.746875	-3.403572	-2.929430	AAMB	1	0.0
285	18	VAL	HN	-4.041923	-1.068045	-1.045009	AAMB	1	0.0
286	18	VAL	HA	-6.592118	-1.648055	-2.224685	AAMB	1	0.0
287	18	VAL	HB	-4.434917	-3.259472	-0.810178	AAMB	1	0.0
288	18	VAL	HG11	-7.118831	-4.366127	-1.755462	AAMB	1	0.0
289	18	VAL	HG12	-5.718055	-5.343682	-1.319533	AAMB	1	0.0
290	18	VAL	HG13	-6.512504	-4.366134	-0.100362	AAMB	1	0.0
291	18	VAL	HG21	-4.128042	-2.568224	-3.253778	AAMB	1	0.0
292	18	VAL	HG22	-4.146474	-4.310209	-3.007163	AAMB	1	0.0
293	18	VAL	HG23	-5.568073	-3.486960	-3.641508	AAMB	1	0.0
294	19	PHE	N	-6.305319	-1.202374	0.975365	AAMB	1	0.0
295	19	PHE	CA	-7.101325	-1.045330	2.153176	AAMB	1	0.0
296	19	PHE	C	-8.025386	0.078303	1.983149	AAMB	1	0.0
297	19	PHE	O	-9.174790	0.006741	2.481483	AAMB	1	0.0
298	19	PHE	CB	-6.161346	-0.814749	3.349294	AAMB	1	0.0
299	19	PHE	CG	-6.910186	-0.615058	4.642385	AAMB	1	0.0
300	19	PHE	CD1	-7.101917	0.664793	5.157448	AAMB	1	0.0
301	19	PHE	CD2	-7.431925	-1.705304	5.332189	AAMB	1	0.0
302	19	PHE	CE1	-7.804758	0.852190	6.340706	AAMB	1	0.0
303	19	PHE	CE2	-8.134746	-1.520186	6.515602	AAMB	1	0.0
304	19	PHE	CZ	-8.321570	-0.241290	7.020770	AAMB	1	0.0
305	19	PHE	HN	-5.371571	-0.965666	1.007602	AAMB	1	0.0
306	19	PHE	HA	-7.680093	-1.966908	2.294902	AAMB	1	0.0
307	19	PHE	HB1	-5.492814	-1.669469	3.458332	AAMB	1	0.0
308	19	PHE	HB2	-5.519492	0.048129	3.166873	AAMB	1	0.0
309	19	PHE	HD1	-6.709713	1.523271	4.631473	AAMB	1	0.0
310	19	PHE	HD2	-7.299407	-2.705380	4.946207	AAMB	1	0.0
311	19	PHE	HE1	-7.953233	1.847965	6.732335	AAMB	1	0.0
312	19	PHE	HE2	-8.541384	-2.371681	7.041228	AAMB	1	0.0
313	19	PHE	HZ	-8.870526	-0.098073	7.940141	AAMB	1	0.0
314	20	PHE	N	-7.673174	1.132797	1.221871	AAMB	1	0.0
315	20	PHE	CA	-8.544904	2.242817	0.996134	AAMB	1	0.0
316	20	PHE	C	-9.594489	1.882055	0.039219	AAMB	1	0.0
317	20	PHE	O	-10.734620	2.340141	0.209890	AAMB	1	0.0
318	20	PHE	CB	-7.618481	3.328862	0.405096	AAMB	1	0.0
319	20	PHE	CG	-8.251472	4.681148	0.196232	AAMB	1	0.0
320	20	PHE	CD1	-8.960198	4.960293	-0.969232	AAMB	1	0.0
321	20	PHE	CD2	-8.106814	5.682682	1.152657	AAMB	1	0.0
322	20	PHE	CE1	-9.504410	6.220169	-1.181649	AAMB	1	0.0
323	20	PHE	CE2	-8.644730	6.945993	0.940669	AAMB	1	0.0
324	20	PHE	CZ	-9.341792	7.216188	-0.228950	AAMB	1	0.0
325	20	PHE	HN	-6.783930	1.133674	0.845026	AAMB	1	0.0
326	20	PHE	HA	-8.990414	2.589137	1.936806	AAMB	1	0.0
327	20	PHE	HB1	-6.758616	3.459482	1.064263	AAMB	1	0.0
328	20	PHE	HB2	-7.198933	2.992059	-0.544946	AAMB	1	0.0
329	20	PHE	HD1	-9.085909	4.193028	-1.719779	AAMB	1	0.0
330	20	PHE	HD2	-7.564674	5.481259	2.065264	AAMB	1	0.0
331	20	PHE	HE1	-10.057606	6.423938	-2.087032	AAMB	1	0.0
332	20	PHE	HE2	-8.521981	7.719291	1.685306	AAMB	1	0.0
333	20	PHE	HZ	-9.762511	8.197178	-0.395628	AAMB	1	0.0
334	21	ALA	N	-9.328560	1.117209	-1.035786	AAMB	1	0.0

335	21	ALA	CA	-10.350311	0.737008	-1.961846	AAMB	1	0.0
336	21	ALA	C	-11.245373	-0.265703	-1.365418	AAMB	1	0.0
337	21	ALA	O	-12.307265	-0.557771	-1.942278	AAMB	1	0.0
338	21	ALA	CB	-9.669854	0.152794	-3.205755	AAMB	1	0.0
339	21	ALA	HN	-8.420064	0.809104	-1.179925	AAMB	1	0.0
340	21	ALA	HA	-10.940668	1.615099	-2.245142	AAMB	1	0.0
341	21	ALA	HB1	-9.003704	0.886374	-3.660519	AAMB	1	0.0
342	21	ALA	HB2	-9.070508	-0.724749	-2.957741	AAMB	1	0.0
343	21	ALA	HB3	-10.401311	-0.140363	-3.960104	AAMB	1	0.0
344	22	GLU	N	-10.821669	-1.054320	-0.355770	AAMB	1	0.0
345	22	GLU	CA	-11.671812	-2.020930	0.266841	AAMB	1	0.0
346	22	GLU	C	-12.599527	-1.352089	1.179854	AAMB	1	0.0
347	22	GLU	O	-13.772074	-1.752651	1.183833	AAMB	1	0.0
348	22	GLU	CB	-10.790043	-3.008301	1.056825	AAMB	1	0.0
349	22	GLU	CG	-10.069926	-4.032821	0.161508	AAMB	1	0.0
350	22	GLU	CD	-11.000795	-5.181879	-0.253294	AAMB	1	0.0
351	22	GLU	OE1	-11.283941	-6.042099	0.580723	AAMB	1	0.0
352	22	GLU	OE2	-11.432377	-5.211642	-1.405437	AAMB	1	0.0
353	22	GLU	HN	-9.929513	-0.930140	-0.003553	AAMB	1	0.0
354	22	GLU	HA	-12.248537	-2.569595	-0.489512	AAMB	1	0.0
355	22	GLU	HB1	-10.046156	-2.444288	1.621465	AAMB	1	0.0
356	22	GLU	HB2	-11.376102	-3.543640	1.807014	AAMB	1	0.0
357	22	GLU	HG1	-9.678091	-3.563277	-0.739589	AAMB	1	0.0
358	22	GLU	HG2	-9.218993	-4.459637	0.693020	AAMB	1	0.0
359	23	ASP	N	-12.177330	-0.354410	1.977433	AAMB	1	0.0
360	23	ASP	CA	-13.065334	0.361538	2.837221	AAMB	1	0.0
361	23	ASP	C	-13.743554	1.391010	2.052543	AAMB	1	0.0
362	23	ASP	O	-14.992313	1.328216	1.946455	AAMB	1	0.0
363	23	ASP	CB	-12.266554	0.983707	3.997362	AAMB	1	0.0
364	23	ASP	CG	-11.808397	-0.095633	4.997859	AAMB	1	0.0
365	23	ASP	OD1	-12.314987	-0.112497	6.120143	AAMB	1	0.0
366	23	ASP	OD2	-10.953807	-0.908598	4.648471	AAMB	1	0.0
367	23	ASP	HN	-11.239460	-0.117474	1.970835	AAMB	1	0.0
368	23	ASP	HA	-13.825746	-0.321635	3.237243	AAMB	1	0.0
369	23	ASP	HB1	-11.389018	1.516296	3.627135	AAMB	1	0.0
370	23	ASP	HB2	-12.876906	1.714050	4.532335	AAMB	1	0.0
371	24	VAL	N	-13.033711	2.400514	1.517171	AAMB	1	0.0
372	24	VAL	CA	-13.627054	3.411602	0.703844	AAMB	1	0.0
373	24	VAL	C	-14.398943	2.830595	-0.395773	AAMB	1	0.0
374	24	VAL	O	-15.560534	3.262855	-0.588836	AAMB	1	0.0
375	24	VAL	CB	-12.652191	4.532939	0.287577	AAMB	1	0.0
376	24	VAL	CG1	-13.384815	5.709221	-0.377373	AAMB	1	0.0
377	24	VAL	CG2	-11.863484	5.030176	1.509347	AAMB	1	0.0
378	24	VAL	HN	-12.081930	2.420543	1.672284	AAMB	1	0.0
379	24	VAL	HA	-14.366833	3.867602	1.376663	AAMB	1	0.0
380	24	VAL	HB	-11.950670	4.158913	-0.455073	AAMB	1	0.0
381	24	VAL	HG11	-13.856360	5.403377	-1.310308	AAMB	1	0.0
382	24	VAL	HG12	-14.159917	6.113651	0.274056	AAMB	1	0.0
383	24	VAL	HG13	-12.693000	6.516822	-0.617229	AAMB	1	0.0
384	24	VAL	HG21	-12.535227	5.315455	2.319210	AAMB	1	0.0
385	24	VAL	HG22	-11.182512	4.269599	1.890988	AAMB	1	0.0
386	24	VAL	HG23	-11.267399	5.904689	1.262430	AAMB	1	0.0
387	25	GLY	N	-13.897909	1.806942	-1.109662	AAMB	1	0.0
388	25	GLY	CA	-14.634172	1.199144	-2.163104	AAMB	1	0.0
389	25	GLY	C	-15.754764	0.428300	-1.636873	AAMB	1	0.0
390	25	GLY	O	-16.810810	0.459768	-2.314776	AAMB	1	0.0

391	25	GLY	HN	-13.017754	1.473277	-0.889328	AAMB	1	0.0
392	25	GLY	HA1	-14.927588	1.958454	-2.865408	AAMB	1	0.0
393	25	GLY	HA2	-14.053854	0.540123	-2.786183	AAMB	1	0.0
394	26	SER	N	-15.607442	-0.352578	-0.547584	AAMB	1	0.0
395	26	SER	CA	-16.715082	-1.065141	0.019772	AAMB	1	0.0
396	26	SER	C	-17.905237	-0.211181	0.102507	AAMB	1	0.0
397	26	SER	O	-18.980049	-0.652926	-0.379306	AAMB	1	0.0
398	26	SER	CB	-16.458445	-1.687199	1.412190	AAMB	1	0.0
399	26	SER	OG	-17.626175	-2.028486	2.144185	AAMB	1	0.0
400	26	SER	HN	-14.748532	-0.419415	-0.115161	AAMB	1	0.0
401	26	SER	HA	-16.934277	-1.868156	-0.693759	AAMB	1	0.0
402	26	SER	HB1	-15.858155	-2.594639	1.316521	AAMB	1	0.0
403	26	SER	HB2	-15.902379	-0.987645	2.035284	AAMB	1	0.0
404	26	SER	HG	-18.251007	-2.453056	1.564705	AAMB	1	0.0
405	27	ASN	N	-17.828413	1.017654	0.655349	AAMB	1	0.0
406	27	ASN	CA	-18.949713	1.902397	0.746077	AAMB	1	0.0
407	27	ASN	C	-18.805429	3.008193	-0.214104	AAMB	1	0.0
408	27	ASN	O	-18.979372	4.178142	0.210553	AAMB	1	0.0
409	27	ASN	CB	-19.194557	2.352446	2.203225	AAMB	1	0.0
410	27	ASN	CG	-18.020664	3.081731	2.880505	AAMB	1	0.0
411	27	ASN	OD1	-17.948967	4.303613	2.911146	AAMB	1	0.0
412	27	ASN	ND2	-17.149233	2.259248	3.485601	AAMB	1	0.0
413	27	ASN	HN	-16.969990	1.309415	1.001629	AAMB	1	0.0
414	27	ASN	HA	-19.878851	1.413835	0.435057	AAMB	1	0.0
415	27	ASN	HB1	-20.064405	3.008574	2.250322	AAMB	1	0.0
416	27	ASN	HB2	-19.445787	1.480943	2.808213	AAMB	1	0.0
417	27	ASN	HD21	-16.398821	2.643177	4.021193	AAMB	1	0.0
418	27	ASN	HD22	-17.225565	1.266129	3.398957	AAMB	1	0.0
419	28	LYS	N	-18.527422	2.773166	-1.515061	AAMB	1	0.0
420	28	LYS	CA	-18.354721	3.826449	-2.471390	AAMB	1	0.0
421	28	LYS	C	-19.492424	3.881565	-3.367871	AAMB	1	0.0
422	28	LYS	O	-19.854271	2.898005	-4.056283	AAMB	1	0.0
423	28	LYS	CB	-17.088057	3.649163	-3.326386	AAMB	1	0.0
424	28	LYS	CG	-16.039965	4.752141	-3.114206	AAMB	1	0.0
425	28	LYS	CD	-16.363916	6.034773	-3.887490	AAMB	1	0.0
426	28	LYS	CE	-15.312076	7.123820	-3.652524	AAMB	1	0.0
427	28	LYS	NZ	-15.622320	8.362862	-4.355102	AAMB	1	0.0
428	28	LYS	OXT	-20.106014	4.955043	-3.577588	AAMB	1	0.0
429	28	LYS	HN	-18.407160	1.860785	-1.813810	AAMB	1	0.0
430	28	LYS	HA	-18.309614	4.804605	-1.985870	AAMB	1	0.0
431	28	LYS	HB1	-16.697926	2.681018	-3.077460	AAMB	1	0.0
432	28	LYS	HB2	-17.286669	3.576143	-4.398309	AAMB	1	0.0
433	28	LYS	HG1	-15.963959	5.000231	-2.057859	AAMB	1	0.0
434	28	LYS	HG2	-15.060901	4.383323	-3.421366	AAMB	1	0.0
435	28	LYS	HD1	-16.431326	5.816101	-4.953671	AAMB	1	0.0
436	28	LYS	HD2	-17.343597	6.406069	-3.584526	AAMB	1	0.0
437	28	LYS	HE1	-15.234143	7.359888	-2.590948	AAMB	1	0.0
438	28	LYS	HE2	-14.330296	6.790445	-3.989171	AAMB	1	0.0
439	28	LYS	HZ1	-16.537807	8.727137	-4.022856	AAMB	1	0.0
440	28	LYS	HZ2	-14.878768	9.064148	-4.163210	AAMB	1	0.0
441	28	LYS	HZ3	-15.671393	8.177383	-5.377058	AAMB	1	0.0
442	29	MINI	CA	0.801935	7.774904	-1.808129	MINI	1	0.0
443	29	MINI	HA	0.566938	8.545598	-1.074308	MINI	1	0.0
444	29	MINI	CB	1.945340	8.232927	-2.719579	MINI	1	0.0
445	29	MINI	HB1	1.666320	9.148425	-3.242029	MINI	1	0.0
446	29	MINI	HB2	2.825317	8.470255	-2.121215	MINI	1	0.0

```
 447    29   MINI  CG      2.299530    7.168966   -3.721584 MINI    1   0.0
 448    29   MINI  CD1     3.194309    6.160393   -3.383742 MINI    1   0.0
 449    29   MINI  HD1     3.653621    6.151380   -2.406369 MINI    1   0.0
 450    29   MINI  CD2     1.725775    7.168845   -4.989739 MINI    1   0.0
 451    29   MINI  HD2     1.031304    7.948564   -5.267232 MINI    1   0.0
 452    29   MINI  CE1     3.495388    5.156970   -4.292325 MINI    1   0.0
 453    29   MINI  O1      4.362177    4.143554   -3.942663 MINI    1   0.0
 454    29   MINI  CE2     2.031391    6.170089   -5.905367 MINI    1   0.0
 455    29   MINI  HE2     1.561771    6.200259   -6.877861 MINI    1   0.0
 456    29   MINI  CZ      2.916948    5.156667   -5.552899 MINI    1   0.0
 457    29   MINI  O2      3.233977    4.132008   -6.425073 MINI    1   0.0
 458    29   MINI  H1      1.076688    6.872482   -1.261128 MINI    1   0.0
 459    29   MINI  N1     -0.420729    7.485872   -2.547294 MINI    1   0.0
 460    29   MINI  H2      4.387321    3.503186   -4.644748 MINI    1   0.0
 461    29   MINI  H3      3.209215    4.441852   -7.321945 MINI    1   0.0
 462    29   MINI  H4     -1.167603    7.194327   -1.884370 MINI    1   0.0
 463    29   MINI  H5     -0.241900    6.719477   -3.227988 MINI    1   0.0
 464    29   MINI  H6     -0.725669    8.339811   -3.056801 MINI    1   0.0
!

COOR ORIE NOROT SELE BYNUM @2 end

READ SEQU TIP3 1000
GENE SOLV SETU NOANGLE NODIHE
READ COOR CARD APPE
*1000 water molecules in 30 angstrom cube
*
 3000
   1    1 TIP3 OH2   10.72971  13.82612  -4.91916 SEG1 1      0.00000
   2    1 TIP3 H1     9.79544  13.62522  -4.97383 SEG1 1      0.00000
   3    1 TIP3 H2    10.91210  13.86591  -3.98035 SEG1 1      0.00000
   .
   .
   .
   .
   .
 2998 1000 TIP3 OH2   -2.08570  -3.85276  11.60936 SEG8 1000   0.00000
 2999 1000 TIP3 H1    -1.37778  -3.80913  10.96658 SEG8 1000   0.00000
 3000 1000 TIP3 H2    -2.68185  -3.14730  11.35804 SEG8 1000   0.00000


COOR ORIE NOROT SELE BYNUM @3 end

READ SEQU TIP3 1000
GENE SOLW SETU NOANGLE NODIHE
READ COOR CARD APPE
*1000 water molecules in 30 angstrom cube
*
 3000
   1    1 TIP3 OH2   10.72971  13.82612  -4.91916 SEG1 1      0.00000
   2    1 TIP3 H1     9.79544  13.62522  -4.97383 SEG1 1      0.00000
   3    1 TIP3 H2    10.91210  13.86591  -3.98035 SEG1 1      0.00000
   .
   .
   .
   .
```

```
    .
    .
 2998 1000 TIP3 OH2   -2.08570  -3.85276  11.60936 SEG8 1000   0.00000
 2999 1000 TIP3 H1    -1.37778  -3.80913  10.96658 SEG8 1000   0.00000
 3000 1000 TIP3 H2    -2.68185  -3.14730  11.35804 SEG8 1000   0.00000
DELE ATOM SELE ( .BYRES. ( (SEGID SOLV .OR. SEGID SOLW) .AND. TYPE OH2 .AND. -
     ( ( .NOT. SEGID SOLW .AND. .NOT. SEGID SOLV .AND. .NOT. HYDROGEN ) -
     .AROUND. 2.80 ) ) ) END


RETURN
STOP
```

Appendix 5: Methodology of Biological Assays

Materials for *In Vitro* Assays. $A\beta_{40}$ and $A\beta_{42}$ (AnaSpec, San Jose, CA, >95%) were stored at -80 ^{o}C until used. Tau441 was provided by Oligomerix Inc. (New York, NY) as frozen aliquots (8.3 mg/mL, 60 µL) in Tris-HCl (50 mM, pH 7.4). 1,1,1,3,3,3-Hexafluoroisopropanol (HFIP), and other reagents were obtained from Aldrich (St. Louis, MO) and were of the highest grade. All water used in the *in vitro* studies was micropore filtered and deionized.

$A\beta_{40}$ Stock Solutions. $A\beta_{40}$ (1.0 mg) was pre-treated in a 1.5 mL microfuge tube with HFIP (1 mL) and sonicated for 20 min. to disassemble any pre-formed Aβ aggregates. The HFIP was removed with a stream of argon and the Aβ dissolved in Tris base (5.8 mL, 20 mM, pH ~10). The pH was adjusted to 7.4 with concentrated HCl (~ 10 µL) and the solution filtered using a syringe filter (0.2 µm) before being used. Similar procedures were used for $A\beta_{42}$.

ThT Aβ Aggregation Assay. The kinetic ThT assay for Aβ aggregation was done as follows. Briefly, pre-treated Aβ1-40 (40 µM in 20 mM Tris, pH 7.4), was diluted with an equal volume of 8 µM ThT in Tris (20 mM, pH 7.4, 300 mM NaCl). Aliquots of Aβ/ThT (200 µL) were added to wells of a black polystyrene 96-well plate, followed by 2µL of a test compound in DMSO (of variable concentration), or DMSO alone (controls). Incubations were performed in triplicate and contained 20 µM Aβ and various concentration of compound in 20mM Tris, pH 7.4, 150 mM NaCl, 1% DMSO. Plates were covered with clear polystyrene lids and incubated at 37°C in a Tecan Genios microplate reader. Fluorescence readings (λ_{ex} = 450 nm, λ_{em} = 480 nm) were taken every 15 min., after first shaking at high intensity for 15 sec. and allowing to settle for 10 sec. before each reading. Active compounds attenuated the increase in fluorescence over time that occurred in controls.

ThS Tau Aggregation Assay. Frozen aliquots of tau441 were allowed to thaw at room temperature (RT) before being diluted with Tris-HCl (2.64 mL, 50 mM, pH 7.4) containing dithiothreitol (DTT, 1 mM) to prevent disulfide bonds. After allowing to stand at RT for 1 h, Thioflavin S (ThS) was added (2.5 µL, 10.8 mM), followed by the aggregation inducer heparin (20 µL, 1.08 g/mL). Aggregation was then monitored in a plate reader in the same manner as in the Aβ/ThT assay.

Circular Dichroism (CD). Aliquots (220 µL) of HFIP-pretreated Aβ (40 µM in 20 mM Tris, pH 7.4) were added directly to 1 mm quartz CD cells, followed by 2.2 µL compound (variable concentration) in methanol or methanol alone (controls). Solutions were incubated at 37°C for up to 6 days. CD scans were performed on a Jasco J-810 spectropolarimeter between 190 and 250 nm, with a resolution of 0.1 nm and bandwidth of 1 nm. Ten scans were obtained for each reading. Active compounds were those that inhibited the random-coil to β-sheet transition.

Transmission Electron Microscopy (TEM). $A\beta_{42}$ stock solution (40 µM in 20 mM Tris, pH 7.4) was incubated (37°C) in the absence and presence of the test compound

(100 μM). After 3 days, solutions were analyzed following the procedure of Cohen et al. (*Biochemistry* 2006, **45**: 4727-35) for TEM analysis. Briefly, a 10 μL sample was placed on a 400 mesh copper grid covered by carbon-stabilized Formvar film and allowed to stand for 1.5 min. Excess fluid was then removed and the grids negatively stained for 2 min with uranyl acetate (10 μL, 2% solution). Excess fluid was again removed and the samples viewed using an electron microscope operating at 80 kV.

Appendix 6: Protein Energies of Aβ

The gas phase energies of the 1AMB, 1AMC, 1AML, 1BA4, 1IYT, and 1Z0Q conformers of Aβ as optimized in QUANTA using the CHARMM22 force field are summarized as follows and calculated with a constrained protein backbone:

	Energies (kcal/mol)		
Conformer	E_{tot}	E_{ele}	E_{vdw}
1AMB	-125.85	-62.91	-118.83
1AMC	-124.84	-66.16	-117.54
1AML	-152.79	-54.14	-169.05
1BA4	-186.59	-65.48	-181.57
1IYT	-188.37	-83.14	-176.62
1Z0Q	-134.31	-64.92	-171.67

The solution phase energies of the 1AMB, 1AMC, 1AML, 1BA4, 1IYT, and 1Z0Q conformers of Aβ as optimized in QUANTA using the CHARMM22 force field are summarized as follows, and were calculated with the solvent removed:

	Energies (kcal/mol)		
Conformer	E_{tot}	E_{ele}	E_{vdw}
1AMB	-314.52	-270.43	-132.28
1AMC	-314.53	-280.48	-160.67
1AML	-404.92	-346.18	-212.50
1BA4	-420.10	-369.83	-206.17
1IYT	-530.26	-404.59	-240.00
1Z0Q	-448.37	-366.93	-237.08

The gas phase energies of the 1AMB, 1AMC, 1AML, 1BA4, 1IYT, and 1Z0Q conformers of Aβ as optimized in MOE using the CHARMM22 force field are summarized as follows and were measured with a constrained protein backbone:

	Energies (kcal/mol)		
Conformer	E_{tot}	E_{ele}	E_{vdw}
1AMB	-0.79	53.93	-209.47
1AMC	-11.92	55.13	-233.99
1AML	142.72	92.67	-172.78
1BA4	91.73	61.10	-169.48
1IYT	52.92	55.64	-200.21
1Z0Q	167.87	86.20	-187.97

The solution phase energies of the 1AMB, 1AMC, 1AML, 1BA4, 1IYT, and 1Z0Q conformers of Aβ as optimized in MOE using the CHARMM22 force field are summarized as follows (Used for Tryptophan and 3HAA):

	Energies (kcal/mol)		
Conformer	E_{tot}	E_{ele}	E_{vdw}
1AMB	-1.65	46.77	-198.00
1AMC	-27.22	45.27	-220.50
1AML	126.29	67.92	-159.13
1BA4	141.41	91.81	-169.50
1IYT	76.65	88.19	-216.55
1Z0Q	121.78	72.47	-185.37

The solution phase energies of the 1AMB, 1AMC, 1AML, 1BA4, 1IYT, and 1Z0Q conformers of Aβ as optimized in MOE using the CHARMM22 force field are summarized as follows (Used for Tryptamine):

	Energies (kcal/mol)		
Conformer	E_{tot}	E_{ele}	E_{vdw}
1AMB	-0.43	46.82	-206.95
1AMC	-19.95	52.82	-226.14
1AML	132.19	63.10	-155.00
1BA4	112.06	66.31	-181.81
1IYT	94.26	65.26	-199.04
1Z0Q	141.51	86.36	-190.99

The gas phase energies of the 1AMB, 1AMC, 1AML, 1BA4, 1IYT, and 1Z0Q conformers of Aβ as optimized in MOE using the CHARMM22 force field are summarized as follows and were measured with a constrained protein backbone (For Chapter 4 and Chapter 5 calculations):

	Energies (kcal/mol)		
Conformer	E_{tot}	E_{ele}	E_{vdw}
1AMB	-11.92	51.40	-217.02
1AMC	-11.92	55.13	-233.99
1AML	142.72	92.67	-172.78
1BA4	91.73	61.10	-169.48
1IYT	52.92	55.64	-200.21
1Z0Q	167.87	86.19	-187.97

The solution phase energies of the 1AMB, 1AMC, 1AML, 1BA4, 1IYT, and 1Z0Q conformers of Aβ as optimized in MOE using the CHARMM22 force field are summarized as follows and were measured with a constrained protein backbone (For Chapter 4 calculations):

	Energies (kcal/mol)		
Conformer	E_{tot}	E_{ele}	E_{vdw}
1AMB	14.39	48.15	-194.23
1AMC	-30.43	35.97	-229.64
1AML	119.31	69.45	-171.10
1BA4	126.85	71.13	-163.32
1IYT	149.83	76.11	-207.04
1Z0Q	136.73	81.21	-181.63

The gas phase energies of the 1AMB, 1AMC, 1AML, 1BA4, 1IYT, and 1Z0Q conformers of Aβ as calculated in Gaussian 09W using the AM1 level of theory (For Chapter 4 and Chapter 5 calculations):

Conformer		
1AMB	-1.074072433	Hartree
	-673.990	kcal/mol
1AMC	-1.082807729	Hartrees
	-679.472	kcal/mol
1AML	-1.436624016	Hartrees
	-901.494	kcal/mol
1BA4	-1.64754945	Hartrees
	-1033.852	kcal/mol
1IYT	-2.174795784	Hartrees
	-1364.704	kcal/mol
1Z0Q	-1.286585655	Hartrees
	-807.344	kcal/mol

The gas phase energies of the isolated LVFF and HHQK regions of Aβ used for calculations in Chapter 5:

	HHQK Energies (kcal/mol)		
Conformer	E_{tot}	E_{ele}	E_{vdw}
1AMB	91.02	37.71	-43.34
1AMC	61.45	40.54	-49.48
1AML	109.55	40.95	-7.18
1BA4	86.87	34.28	-29.80
1IYT	58.56	28.34	-28.12
1Z0Q	78.88	34.77	-28.44

	LVFF Energies (kcal/mol)		
Conformer	E_{tot}	E_{ele}	E_{vdw}
1AMB	101.13	19.04	8.05
1AMC	109.87	26.88	2.98
1AML	106.79	30.38	3.68
1BA4	86.30	19.00	-8.86
1IYT	89.33	20.41	2.77
1Z0Q	142.12	30.61	26.10

The solution phase energies of the isolated LVFF and HHQK regions of Aβ used for calculations in Chapter 5:

	HHQK Energies (kcal/mol)		
Conformer	E_{tot}	E_{ele}	E_{vdw}
1AMB	91.02	37.71	-43.34
1AMC	61.45	40.54	-49.48
1AML	109.55	40.95	-7.18
1BA4	86.87	34.28	-29.80
1IYT	58.56	28.34	-28.12
1Z0Q	78.88	34.77	-28.44

	LVFF Energies (kcal/mol)		
Conformer	E_{tot}	E_{ele}	E_{vdw}
1AMB	101.13	19.04	8.05
1AMC	109.87	26.88	2.98
1AML	106.79	30.38	3.68
1BA4	86.30	19.00	-8.86
1IYT	89.33	20.41	2.77
1Z0Q	142.12	30.61	26.10

The gas phase energies of the 1AMB, 1AMC, 1AML, 1BA4, 1IYT, and 1Z0Q conformers of Aβ as optimized in MOE using the CHARMM22 force field are summarized as follows and were measured with a constrained protein backbone (For Chapter 6 solapsone-Gd^{3+} calculations):

	Energies (kcal/mol)		
Conformer	E_{tot}	E_{ele}	E_{vdw}
1AMB	-8.68	51.70	-211.55
1AMC	2.50	62.41	-225.21
1AML	185.65	91.31	-130.54
1BA4	91.71	61.14	-169.55
1IYT	52.92	55.72	-200.26
1Z0Q	163.45	81.15	-171.67

The solution phase energies of the 1AMB, 1AMC, 1AML, 1BA4, 1IYT, and 1Z0Q conformers of Aβ as optimized in MOE using the CHARMM22 force field are summarized as follows and were measured with a constrained protein backbone (For Chapter 6 solapsone-Gd^{3+} calculations):

	Energies (kcal/mol)		
Conformer	E_{tot}	E_{ele}	E_{vdw}
1AMB	7.95	51.88	-211.92
1AMC	10.31	64.67	-204.04
1AML	154.12	80.68	-135.70
1BA4	128.32	82.05	-169.65
1IYT	55.18	71.63	-220.50
1Z0Q	137.04	77.26	-173.19

The gas phase energies of the 1AMB, 1AML, 1BA4, 1IYT, and 1Z0Q conformers of Aβ as optimized in MOE using the CHARMM22 force field are summarized as follows and were measured with a constrained protein backbone (For Chapter 6 solapsone-Aβ calculations):

	Energies (kcal/mol)		
Conformer	E_{tot}	E_{ele}	E_{vdw}
1AMB	-11.78	55.28	-211.70
1AML	185.65	91.31	-130.54
1BA4	91.71	61.14	-169.55
1IYT	52.92	55.72	-200.26
1Z0Q	163.45	81.15	-181.05

The solution phase energies of the 1AMB, 1AML, 1BA4, 1IYT, and 1Z0Q conformers of Aβ as optimized in MOE using the CHARMM22 force field are summarized as follows and were measured with a constrained protein backbone (For Chapter 6 solapsone calculations):

	Energies (kcal/mol)		
Conformer	E_{tot}	E_{ele}	E_{vdw}
1AMB	7.95	51.88	-211.92
1AML	154.12	80.68	-135.70
1BA4	128.32	82.05	-169.65
1IYT	55.18	71.63	-220.50
1Z0Q	137.04	77.26	-173.19

Appendix 7: Analogues of 3-Hydroxyanthranilic Acid

Test-03

2-amino-3-mercaptobenzoic acid

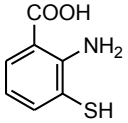

Test-08

3-hydroxy-2-(methylamino)benzoic acid

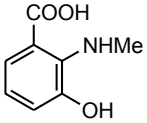

Test-09

3-hydroxy-2-(phenylamino)benzoic acid

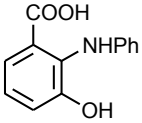

Test-10

2-(benzylamino)-3-hydroxybenzoic acid

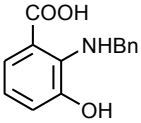

Test-11

2-amino-3-(1*H*-tetrazol-5-yl)phenol

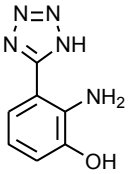

Test-12

2-amino-3-(1-methyl-1*H*-tetrazol-5-yl)phenol

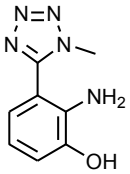

Test-14

2-amino-3-hydroxybenzamide

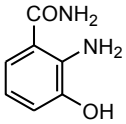

Test-15

2-amino-3-hydroxybenzenesulfonamide

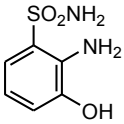

Test-16

2-amino-3-hydroxybenzenesulfonic acid

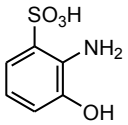

Test-17

2-amino-3-hydroxyphenylphosphonic acid

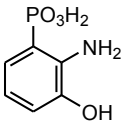

Test-18

2-amino-3',5'-difluorobiphenyl-3,4'-diol

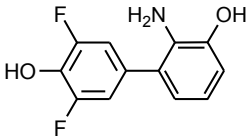

Test-19

2'-amino-2,4-difluorobiphenyl-3,3'-diol

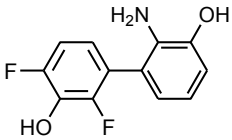

Test-20

2-amino-3-(2,2,2-trifluoro-1-hydroxyethyl)phenol

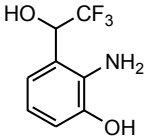

Test-21

2-amino-3-fluorophenol

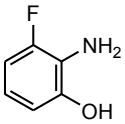

Test-22

2-amino-3-chlorophenol

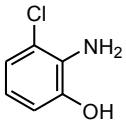

Test-23

2-amino-3-hydroxybenzonitrile

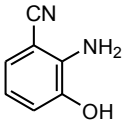

Test-24

3-methylbenzene-1,2-diol

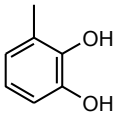

Test-26

3-methyl-2-(methylamino)phenol

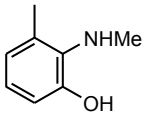

Test-27

3-methyl-2-(phenylamino)phenol

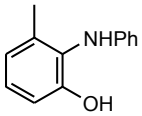

Test-28

2-(benzylamino)-3-methylphenol

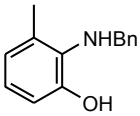

Test-29

3-methylbenzene-1,2-diamine

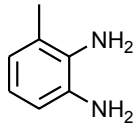

Test-30

N-(2-amino-3-methylphenyl)methanesulfonamide

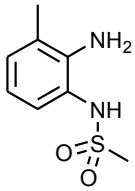

Test-31

2-amino-3-methylbenzenethiol

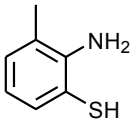

Test-32

2-chloro-6-methylaniline

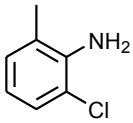

Test-33

1-(2-amino-3-methylphenyl)urea

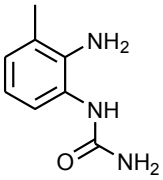

Test-34

N^1,6-dimethylbenzene-1,2-diamine

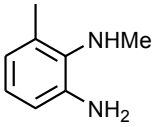

Test-35

3-fluorobenzene-1,2-diamine

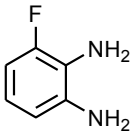

Test-36

N^1,N^2,3-trimethylbenzene-1,2-diamine

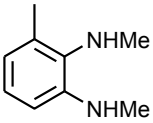

Test-37

2-(thiophen-2-yl)phenol

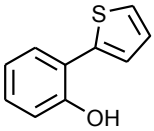

Test-38

3-fluoro-2-(phenylamino)phenol

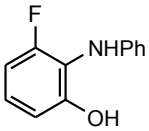

Test-39

4-methyl-2-(phenylamino)phenol

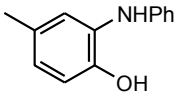

Test-40

5-methyl-2-(phenylamino)phenol

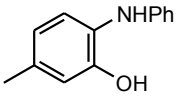

Test-41

2-methyl-6-(phenylamino)phenol

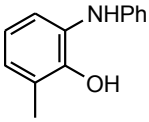

Test-42

2-(diphenylamino)phenol

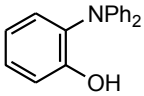

Test-43

N^1-phenylbenzene-1,2-diamine

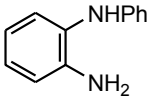

Test-44

2-methyl-*N*-phenylaniline

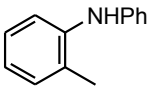

Test-45

N-(2-(phenylamino)phenyl)methanesulfonamide

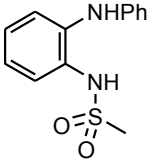

Test-46

2-(phenylamino)benzenethiol

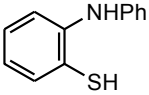

Test-47

2-chloro-*N*-phenylaniline

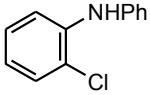

Test-48

2-azido-*N*-phenylaniline

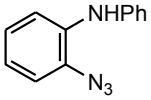

Test-49

1-(2-(phenylamino)phenyl)urea

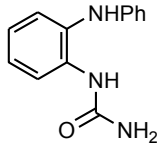

Test-50

4-(dimethylamino)phenol

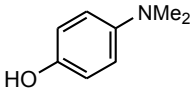

Test-51

N^1-methylbenzene-1,4-diamine

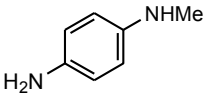

Test-52

N^1,N^4-dimethylbenzene-1,4-diamine

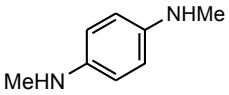

Test-53

N,4-dimethylaniline

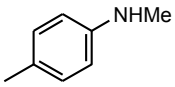

Test-54

N-(4-(methylamino)phenyl)methanesulfonamide

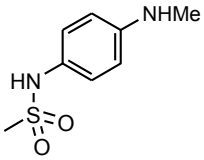

Test-55

4-(methylamino)benzenethiol

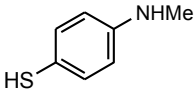

Test-56

4-chloro-*N*-methylaniline

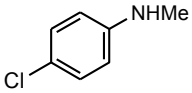

Test-57

4-azido-*N*-methylaniline

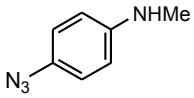

Test-58

1-(4-(methylamino)phenyl)urea

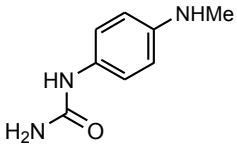

Test-61

p-cresol

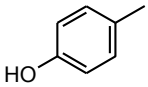

Test-62

3-methyl-4-(methylamino)phenol

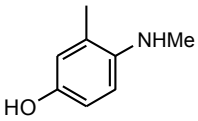

Test-63

2-methyl-4-(methylamino)phenol

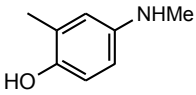

Test-64

2,5-dimethyl-4-(methylamino)phenol

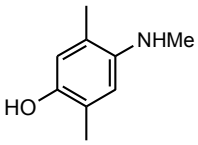

Test-65

3,5-dimethyl-4-(methylamino)phenol

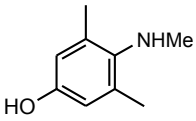

Test-66

3-fluoro-4-(methylamino)phenol

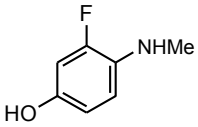

Test-67

2-fluoro-4-(methylamino)phenol

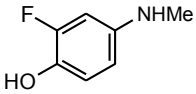

Test-68

2,5-difluoro-4-(methylamino)phenol

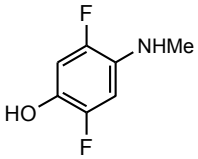

Appendix 8: BBXB Protein Energies

	Energy (kcal/mol)		
Protein	Total	Van der Waals	electrostatic
Aβ	-188.37	-176.62	-83.14
AChE	-11824.15	-3505.07	-11006.67
α_1-ACT	-2535.93	-2571.00	-815.11
Apoε4	-4771.46	-870.30	-4652.69
B7-1	-1235.34	-1364.49	-387.79
BHMT	-13535.79	-4781.19	-11386.05
C1qA	-13234.02	-5566.68	-10374.84
ICAM-1	-1119.97	-1258.12	-462.30
IFN-γ	-12827.01	-3611.30	-11148.04
IL-1βCE	-7775.87	-1526.68	-7483.63
IL-4	-962.15	-954.61	-294.30
IL-12	-2430.07	-2807.22	-768.53
IL-13	-388.29	-554.99	-79.10
MIP-1α	-1832.98	-2179.97	-625.66
MIP-1β	-1996.41	-2273.27	-654.33
NEP	-20607.56	-4580.47	-19329.89
RANTES	-1634.97	-690.39	-1634.48
S100β	-977.29	-1054.54	-481.74
SDF-1	-2190.99	-302.72	-2254.47
Transferrin	-3289.34	-3436.47	-1067.03

Appendix 9: Analogues of NCE-0217

Analogues of NCE-0217 used in the QSAR

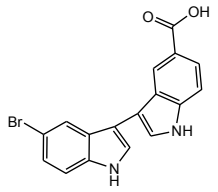

103

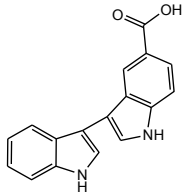

104

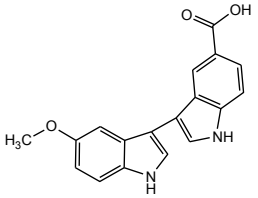

105

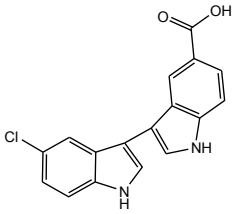

106

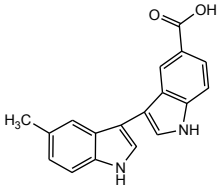

107

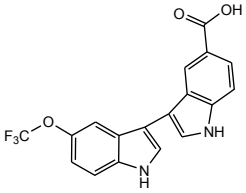

108

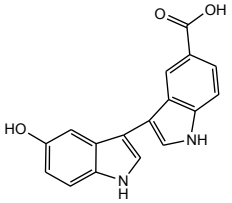

109

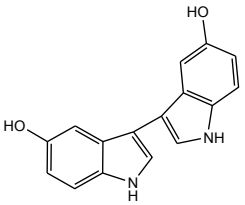

110

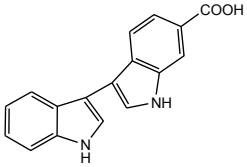

111

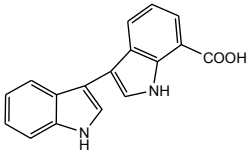

112

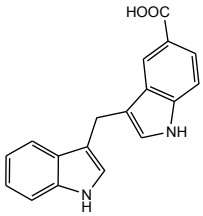

115

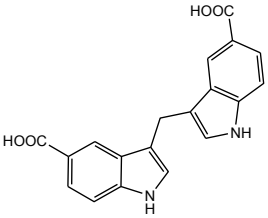

116

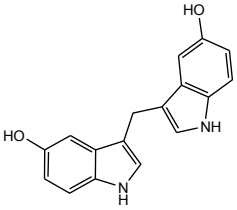

117

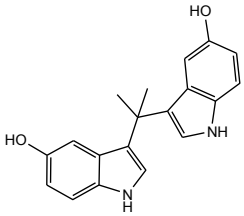

120

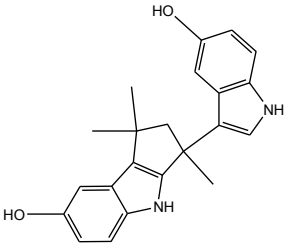

121

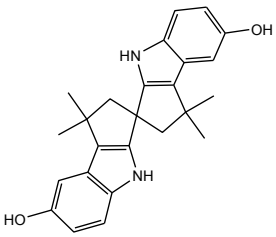

122

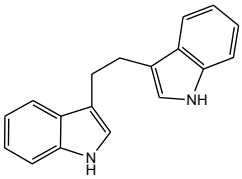

123

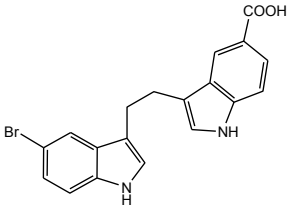

124

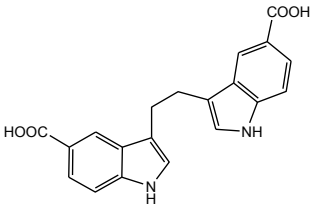

125

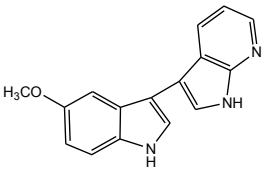

132

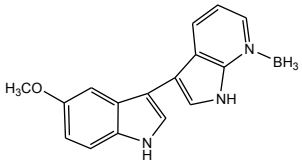

133

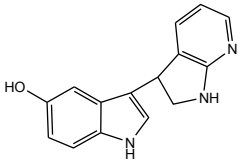

134

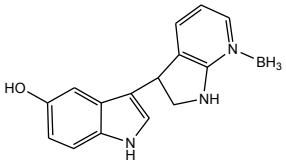

135

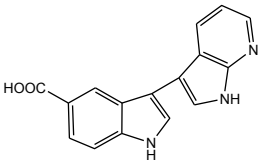

136

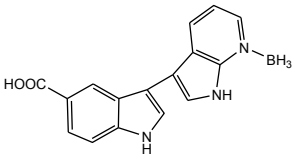

137

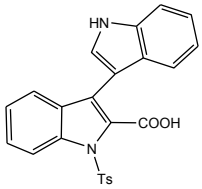

155

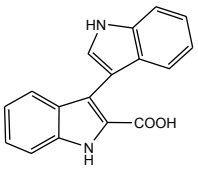

156

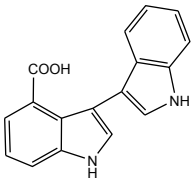

157

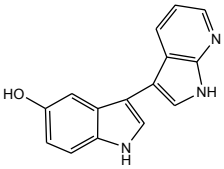

161

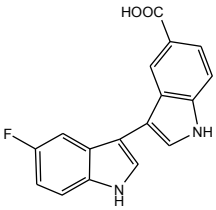

163

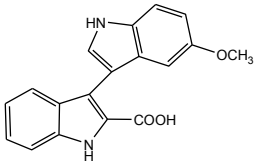

168

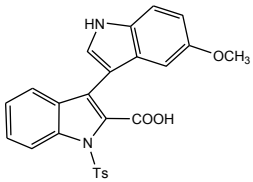

169

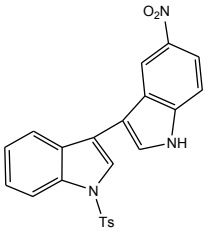

170

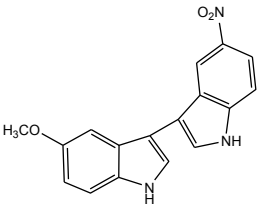

171

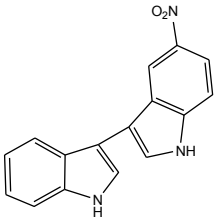

172

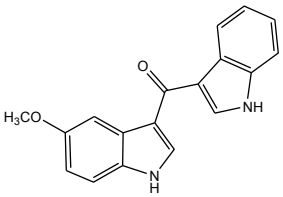

173

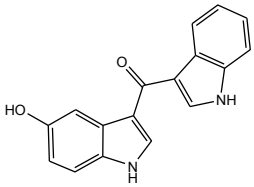

174

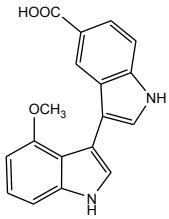

175

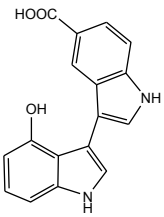

176

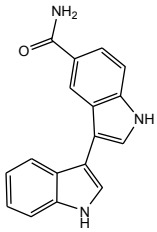

177

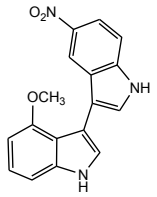

179

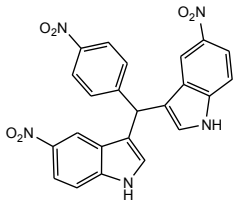

181

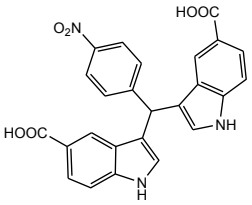

182

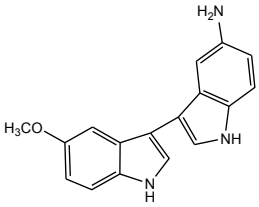

185

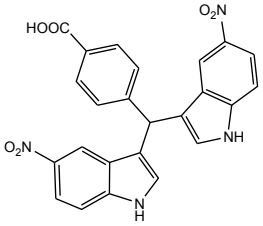

190

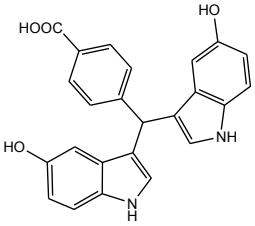

191

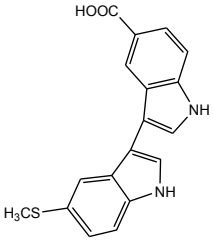

200

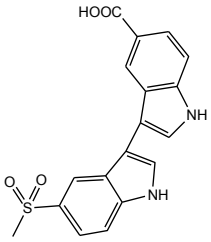

201

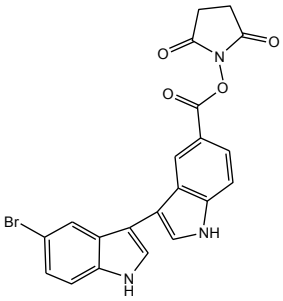

213

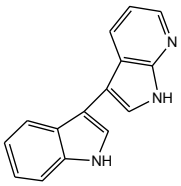

218

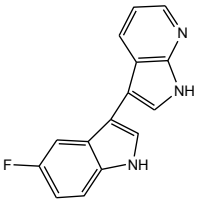

230

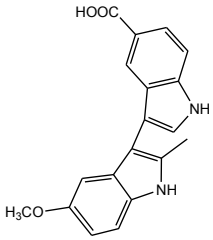

235

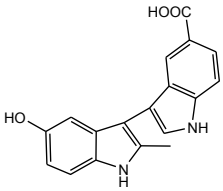

236

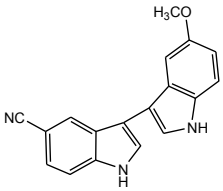

238

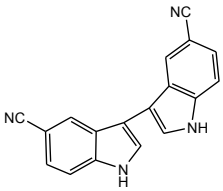

239

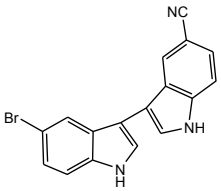

240

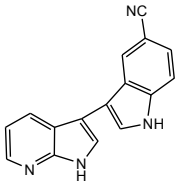

241

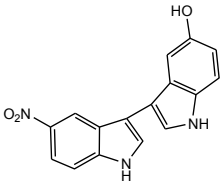

251

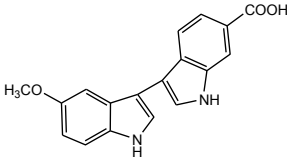

252

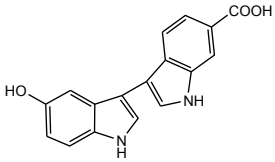

253

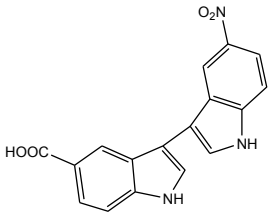

254

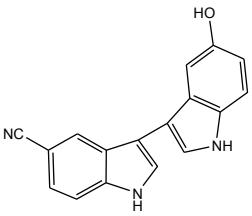

276

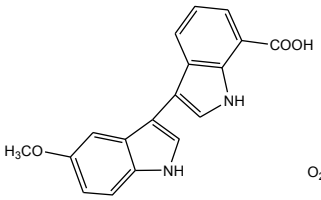

289

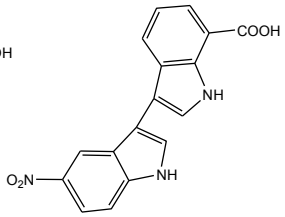

295

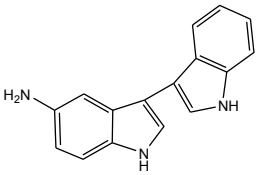

300

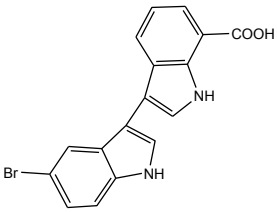

303

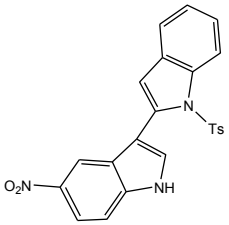

309

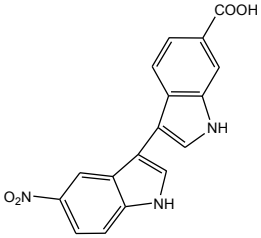

327

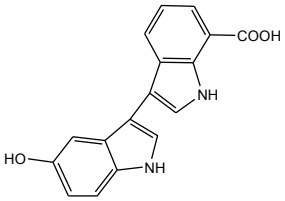

329

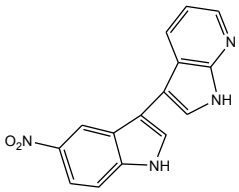

332

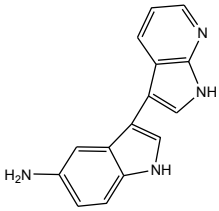

334

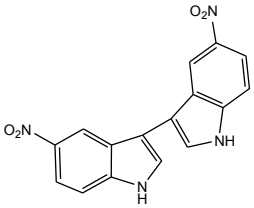

335

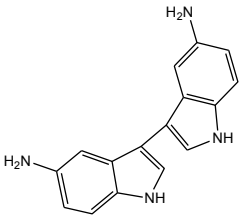

336

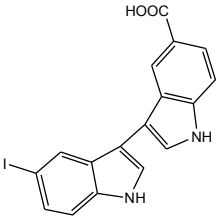

342

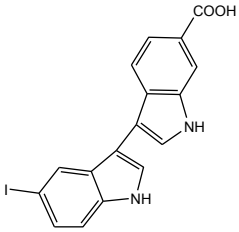

343

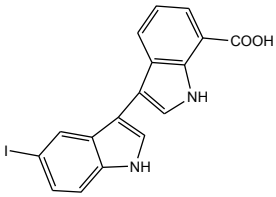

353

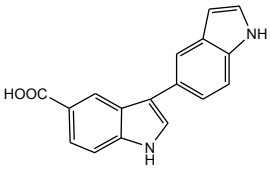

354

QSAR predictions of activity for test compounds of biindoles

Compound	Structure	Active/ Inactive
1	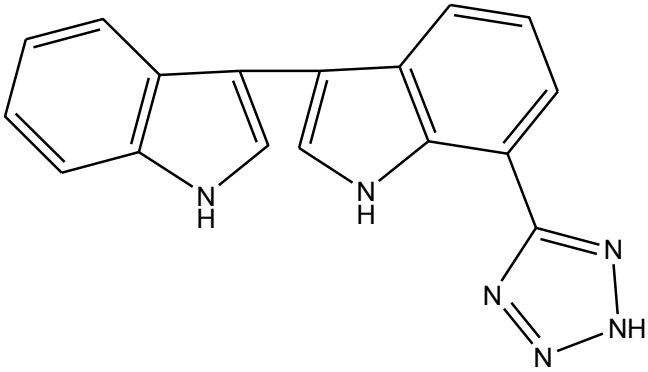	Inactive
2	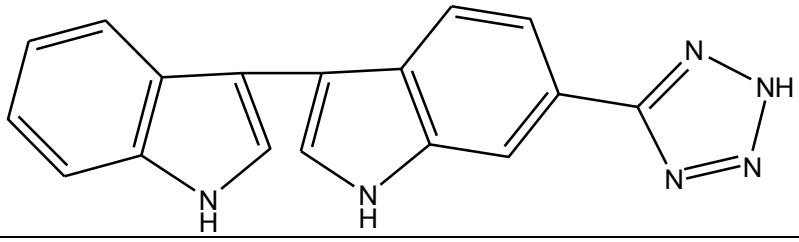	Inactive
3	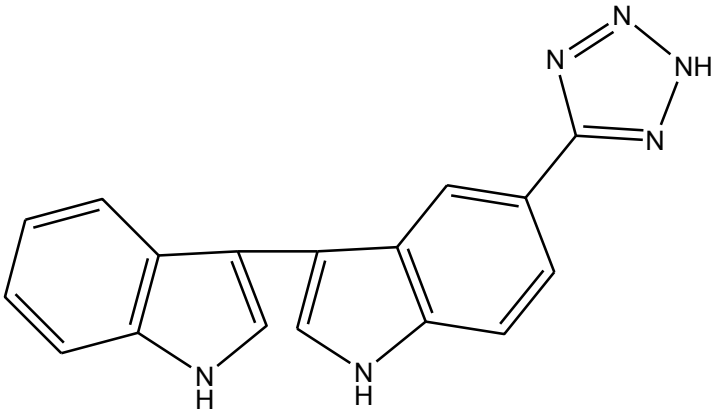	Inactive
4	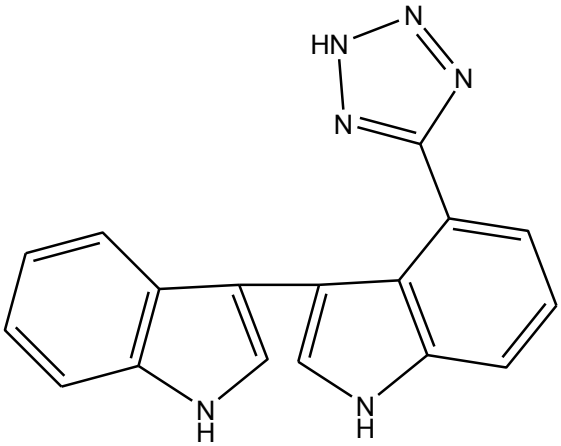	Inactive

5	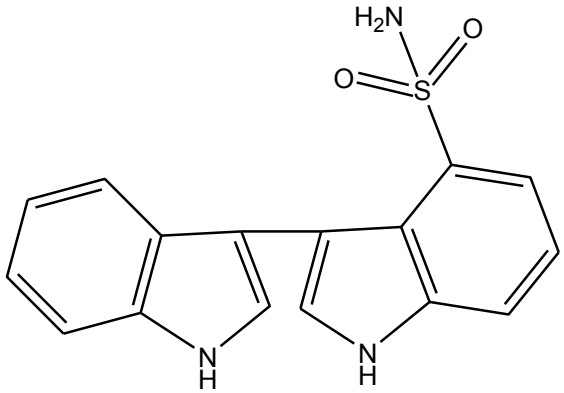	Active
6	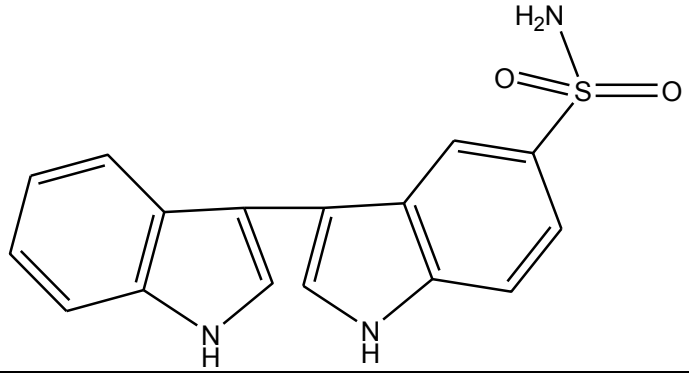	Active
7	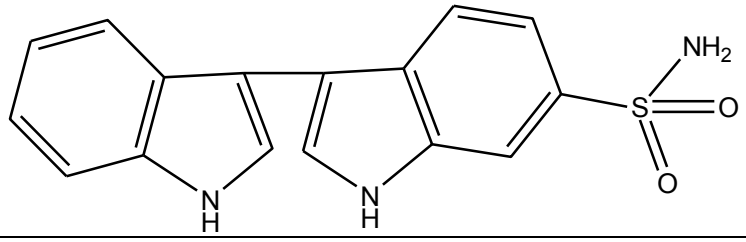	Active
8	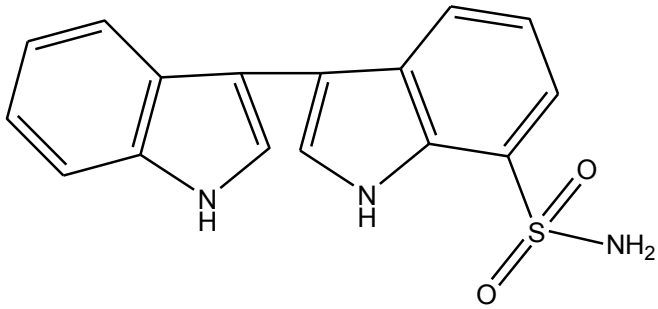	Active
9	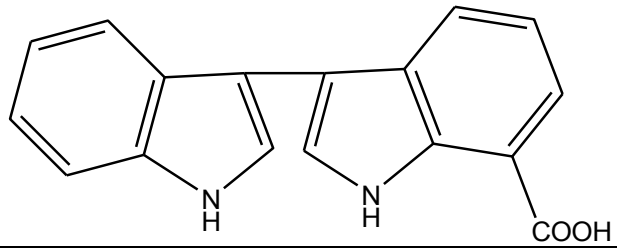	Active

10	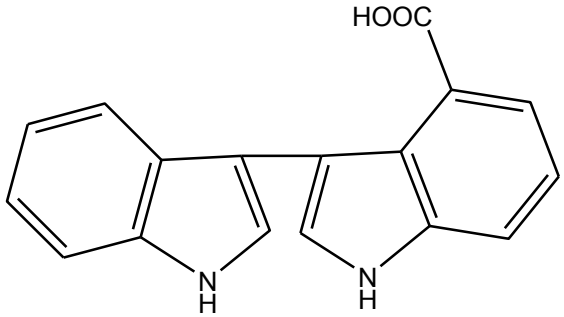	Inactive
11	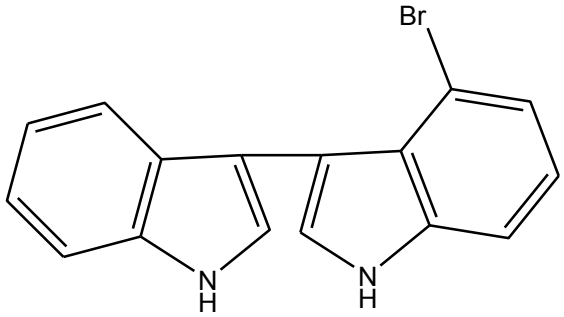	Active
12	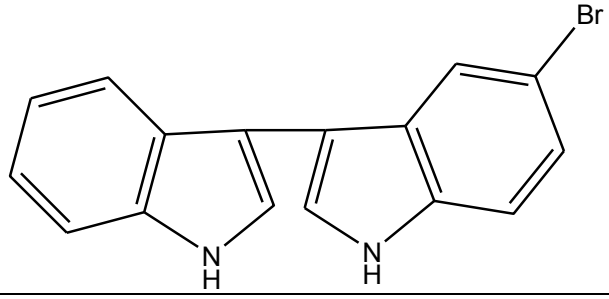	Inactive
13	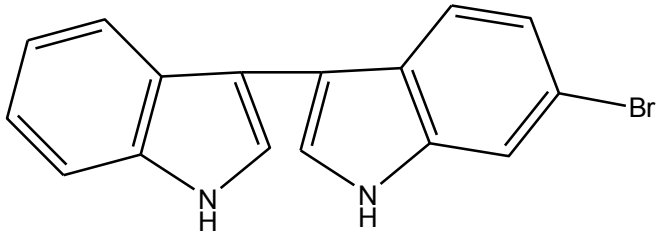	Active
14	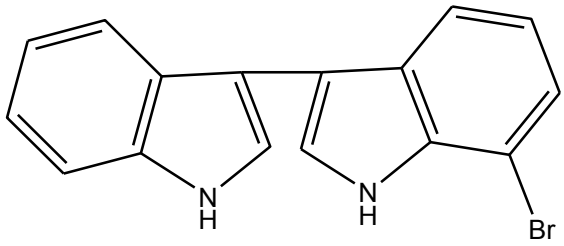	Inactive

15	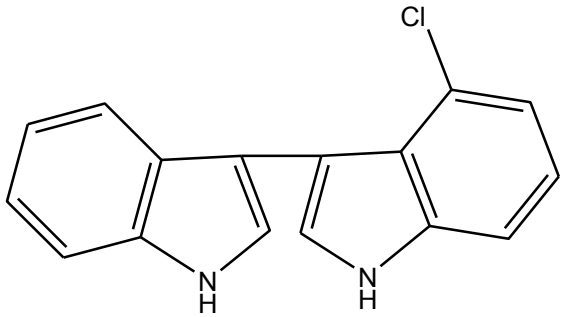	Active
16	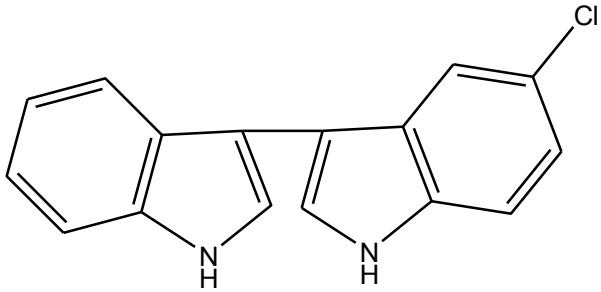	Active
17	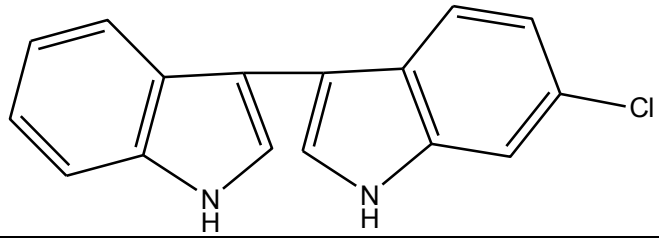	Active
18	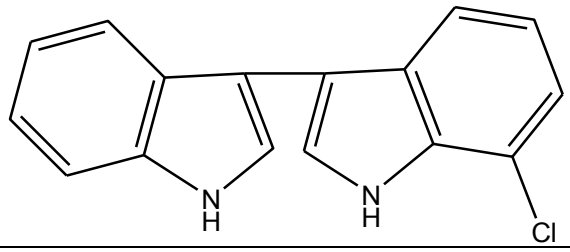	Active
19	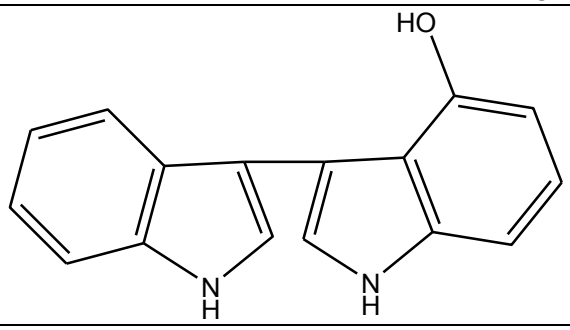	Active
20	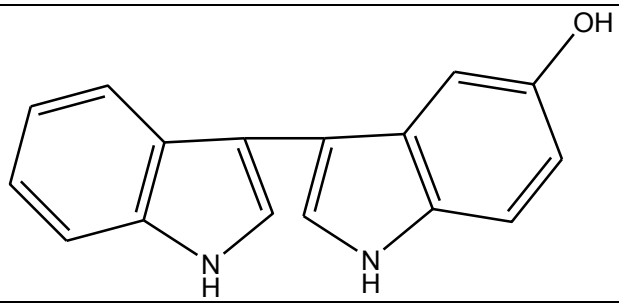	Active

21	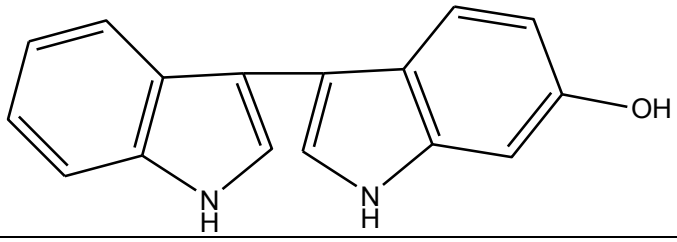	Active
22	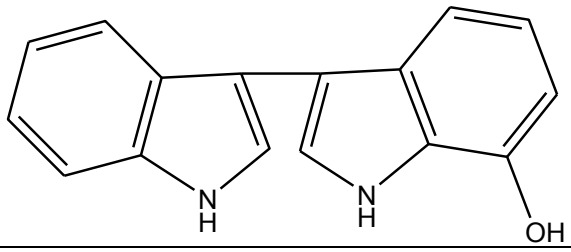	Active
23	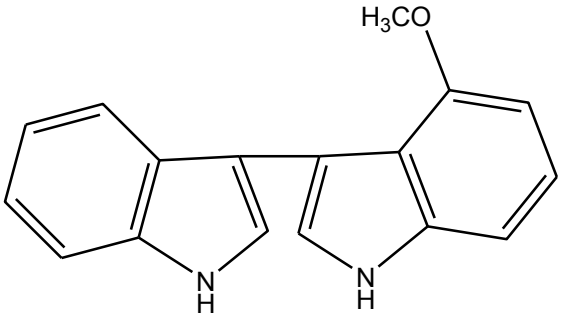	Inactive
24	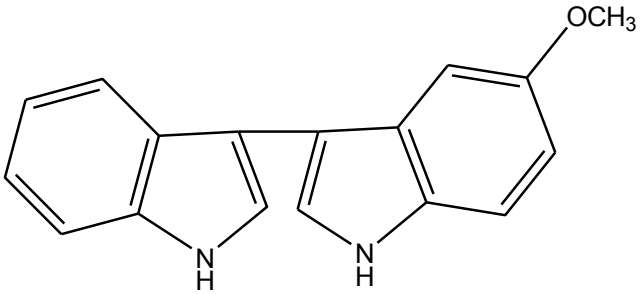	Inactive
25	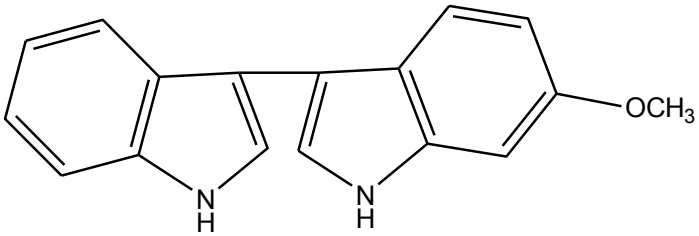	Active
26	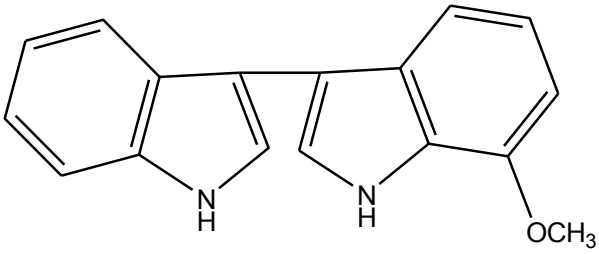	Active

27	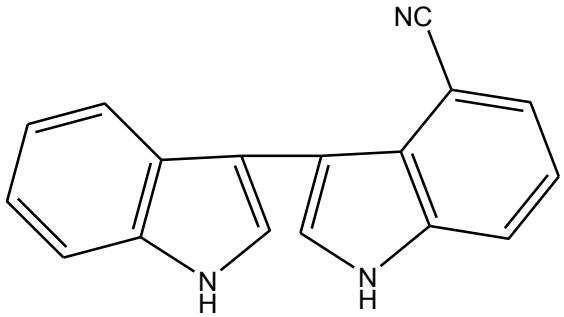	Inactive
28	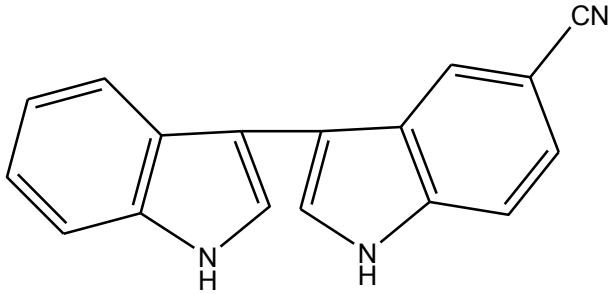	Inactive
29	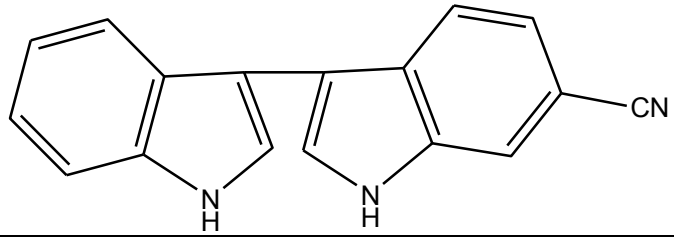	Inactive
30	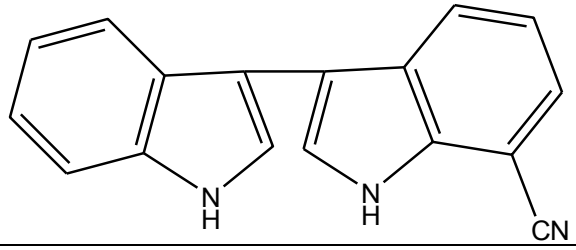	Inactive
31	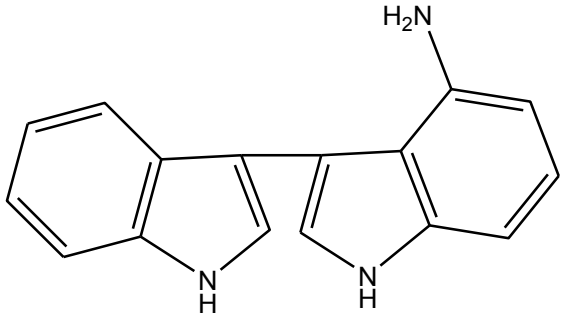	Active
32	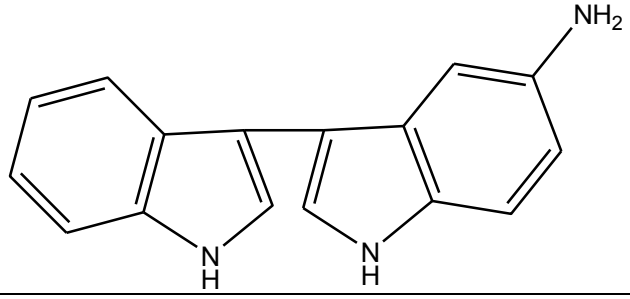	Active

33	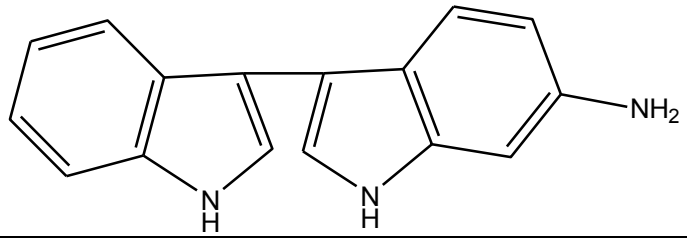	Active
34	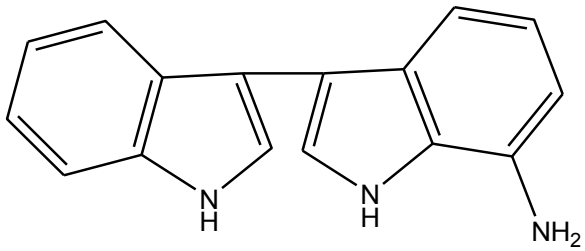	Active
35	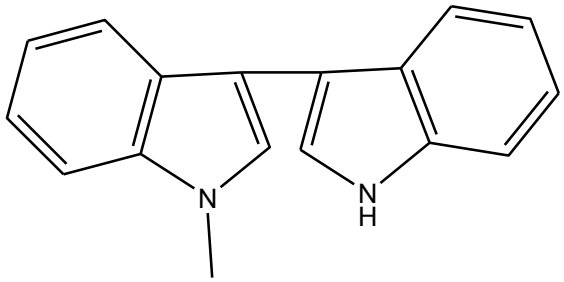	Inactive
36	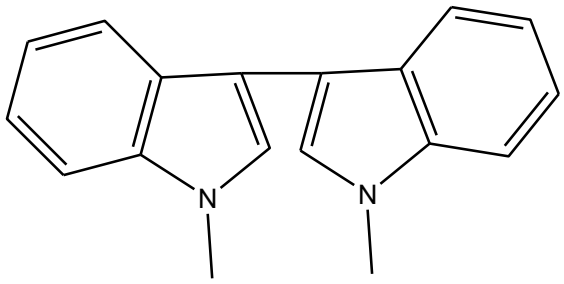	Active
37	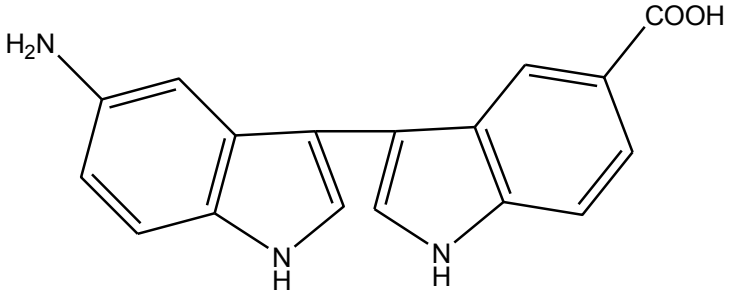	Inactive

38	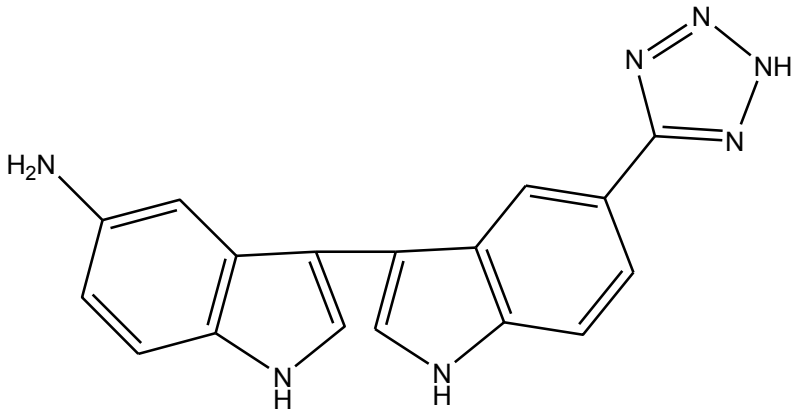	Inactive
39	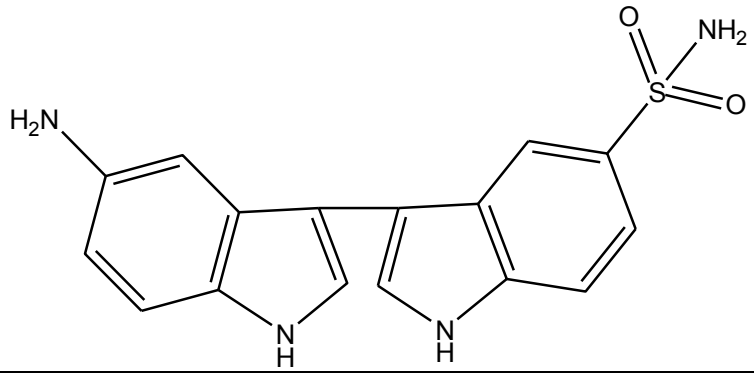	Active
40	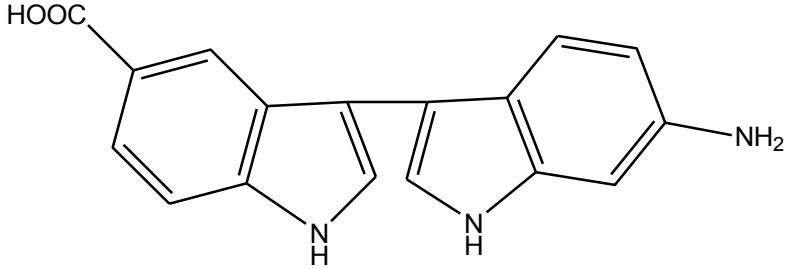	Inactive
41	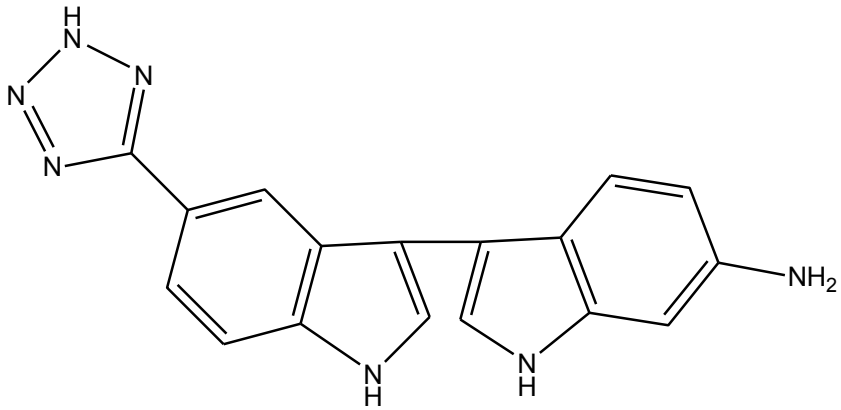	Active

42	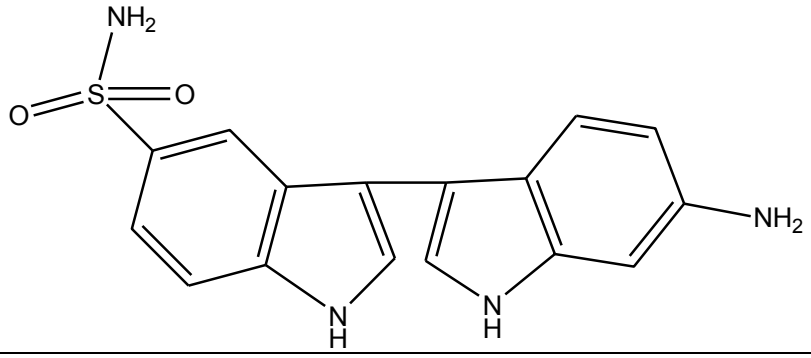	Active
43	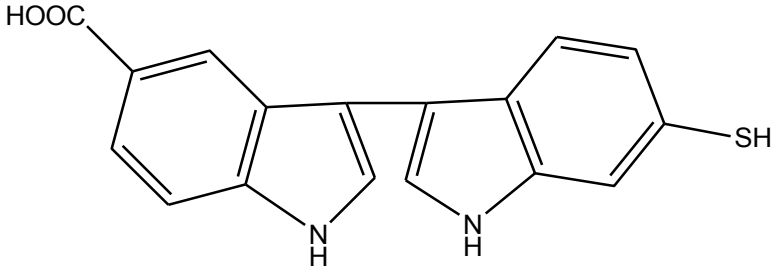	Active
44	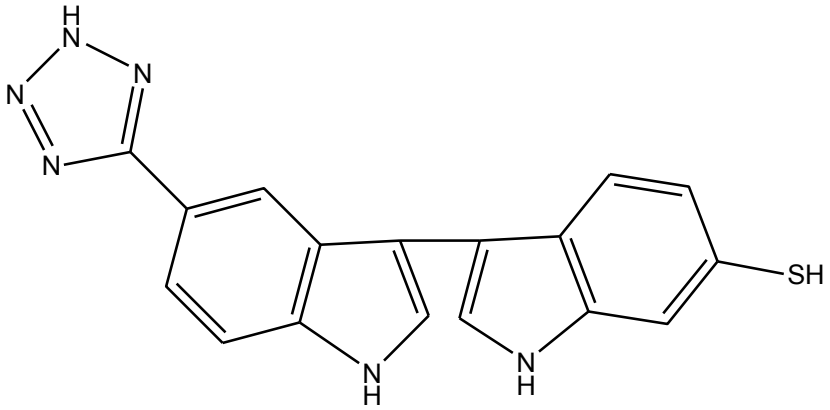	Active
45	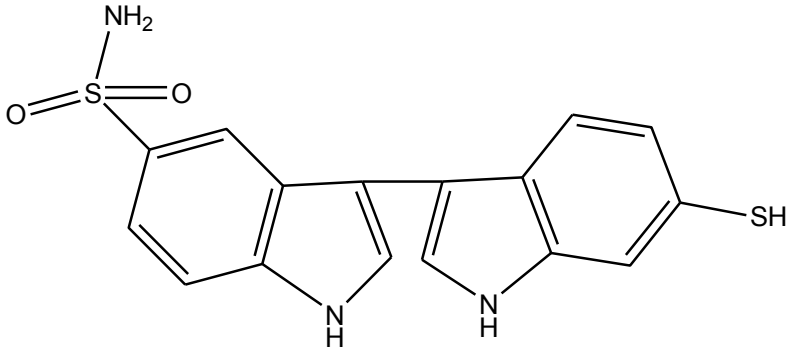	Active
46	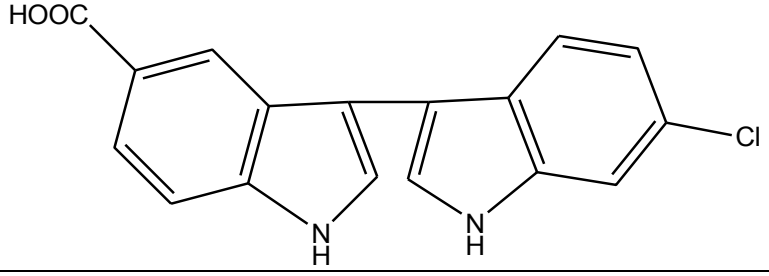	Active

47	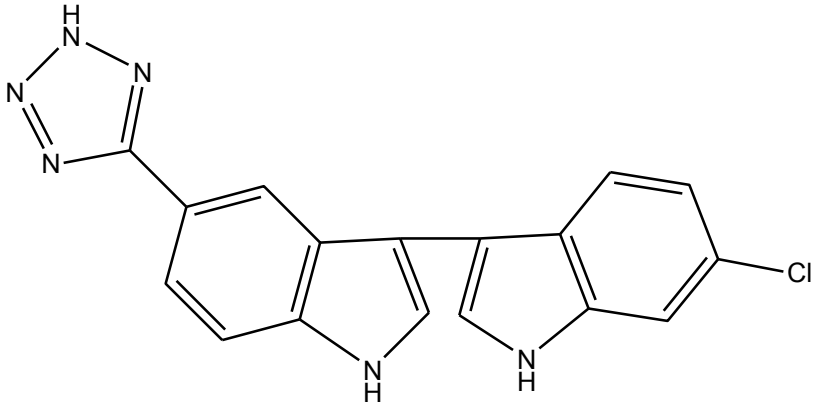	Inactive
48	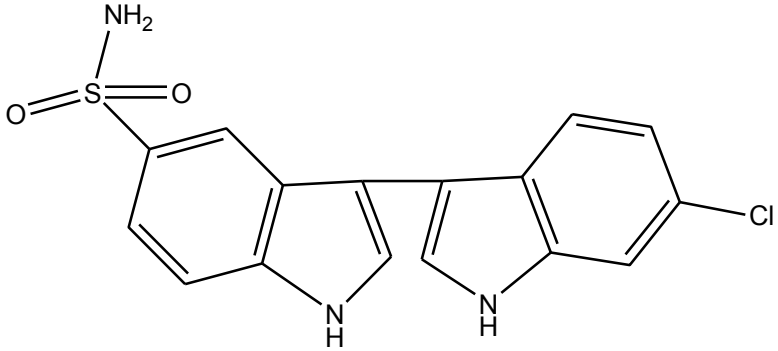	Active
49	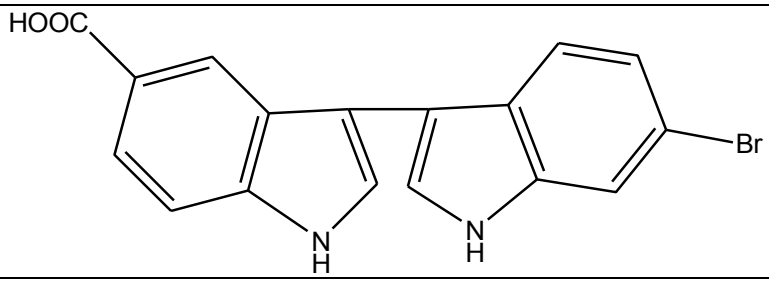	Active
50	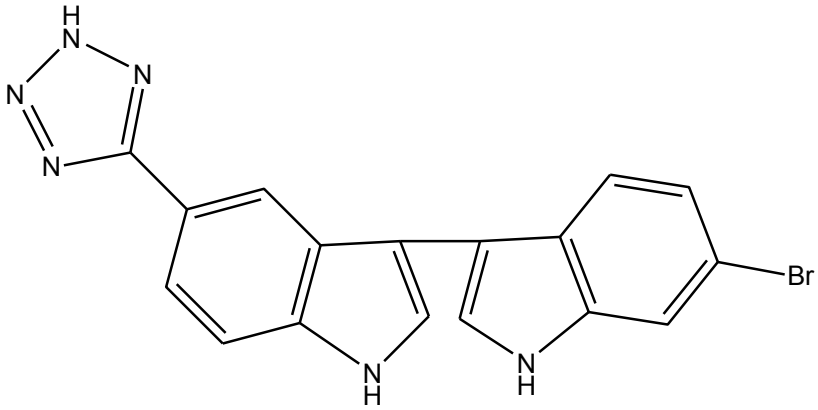	Inactive

51	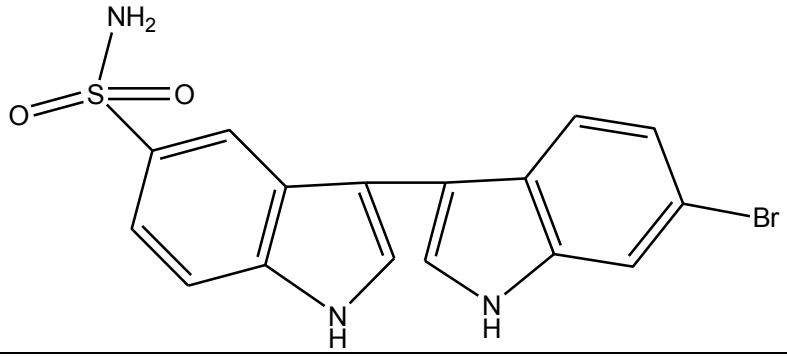	Active
52	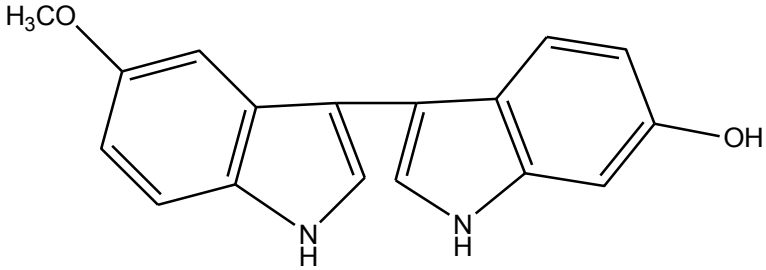	Active
53	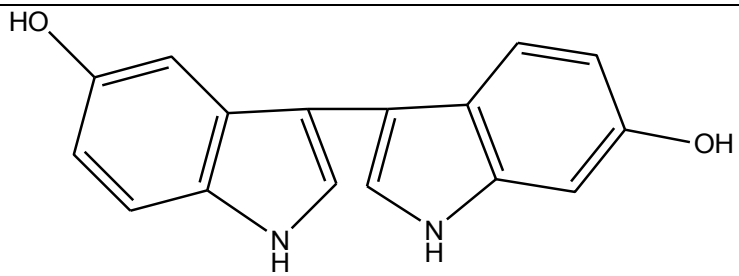	Active
54	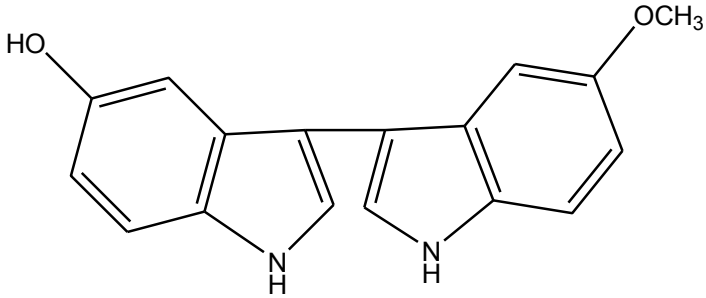	Active
55	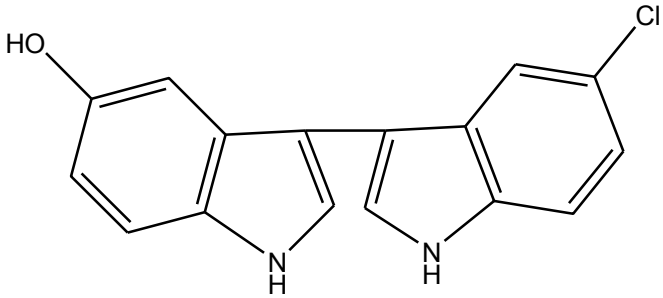	Active

56	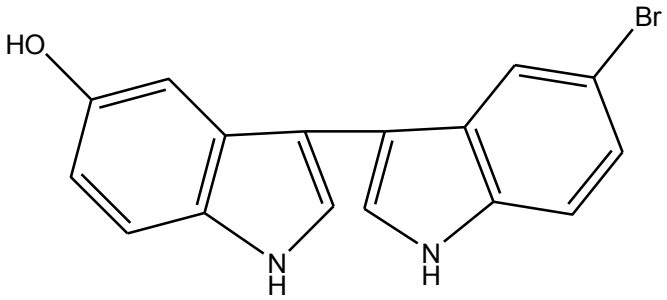	Active
57	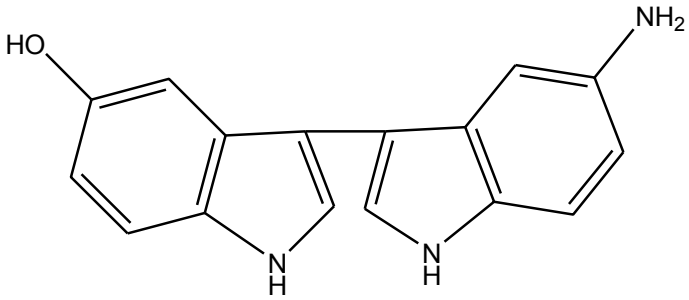	Active
58	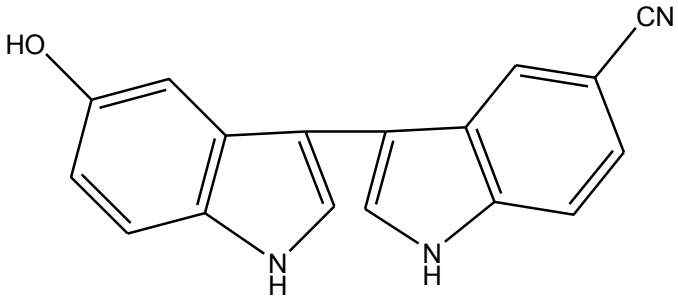	Inactive
59	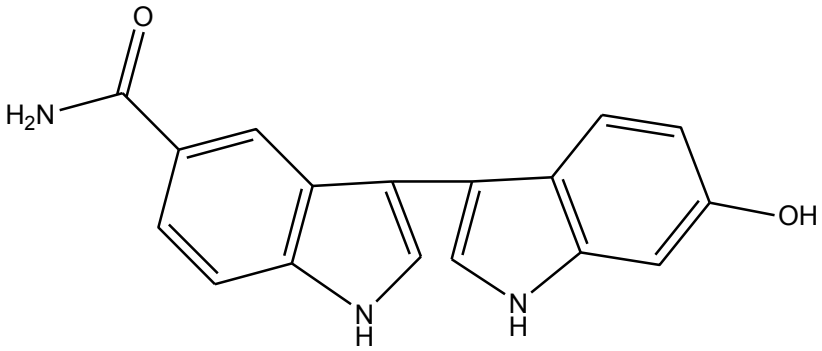	Active
60	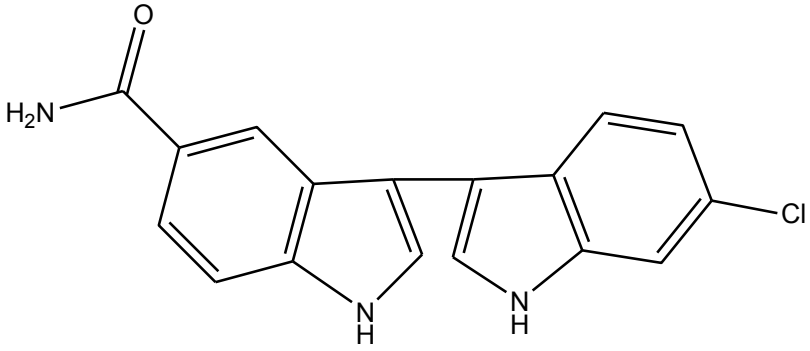	Active

61	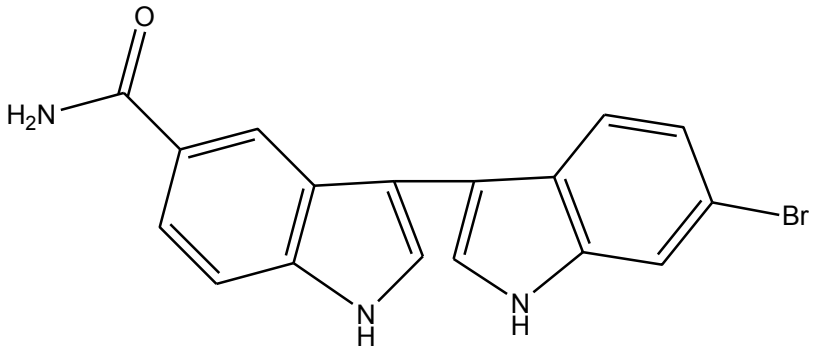	Inactive
62	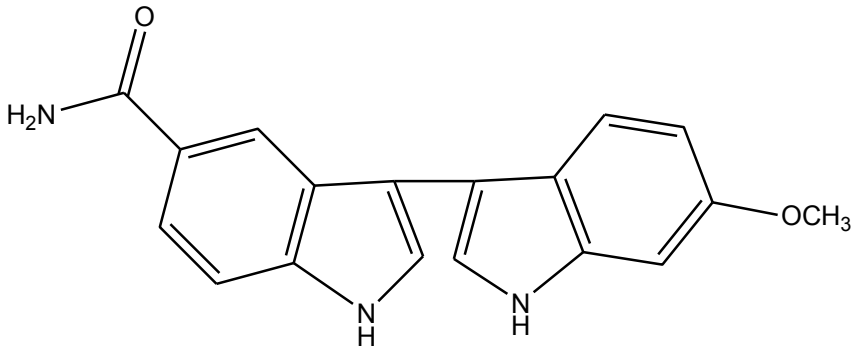	Inactive
63	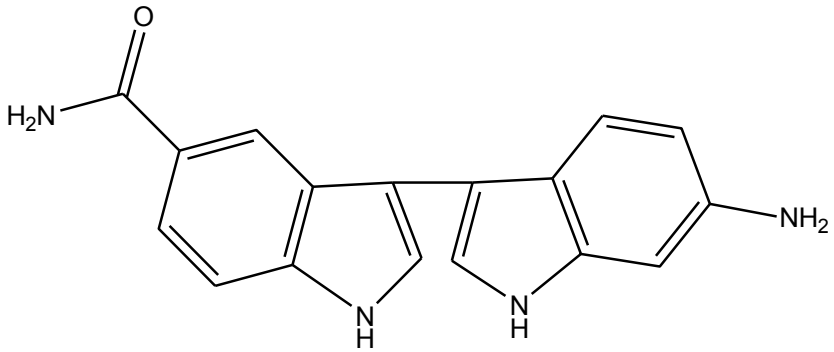	Active

Appendix 10: Library of Known Drugs

abacavir suflate

abciximab

acarbose

acebutolol hydrochloride

acetaminophen

acetylcysteine

acetylsalicylic acid (ASA)

acitretin

acyclovir

adapalene

adenosine

alendronate

alfacalcidol

alfentanil hydrochloride

alfuzosin

alginic acid

alitetinoin

allopurinol

alpha tocopherol

alprazolam

alprostadil

altretamine

aluminum hydroxide

amantadine hydrochloride

amcinonide

amikacin sulfate

amiloride hydrochloride

aminocaproic acid

aminophylline

amiodarone hydrochloride

amitriptyline hydrochloride

amlodipine besylate

amobarbital sodium

amoxicillin trihydrate

amphotericin B

ampicillin

amprenavir

amsacrine

anagrelide hydrochloride

anakinra

anastrozole

ancestim

anthralin

aprotinin

articaine hydrochloride

ascorbic acid

atenolol

atorvastatin calcium

atovaquone

atracurium besylate

atropine sulfate

attapulgite, activated

aurothioglucose

azatadine maleate

azathioprine

azithromycin

bacampicillin hydrochloride

bacitracin

baclofen

basiliximab

beclomethasone dipropionate

benazepril

benzocaine

benzoyl peroxide

benztropine mesylate

beractant

betamethasone acetate

betamethasone sodium phosphate

bethanechol chloride

bezafibrate

bicalutamide

biperiden hydrochloride

bisacodyl

bismuth subsalicylate

bisoprolol fumarate

bleomycin sulfate

bosentan

botulinum toxin type A

bovine lipid extract surfactant

bretylium tosylate

bromazepam

bromocriptine mesylate

brompheniramine maleate

budesonide

bumetanide

bupivacaine hydrochloride

bupropion hydrochloride

buserelin

buspirone hydrochloride

busulfan

butalbital

butorphanol tartrate

butyl methoxydibenzoylmethane (Parsol 1789)

calcipotriol

calcitonin salmon

calcitriol

calcium carbonate

candesartan cilexetil

cantharidin

capecitabine

capsaicin

captopril

carbamazepine

carboplatin

carisoprodol

carmustine

carvedilol

cascara

caspofungin acetate

cefaclor

cefadroxil

cefazolin sodium

cefepime hydrochloride

cefixime

cefotaxime sodium

cefotetan disodium

cefoxitin sodium

cefprozil

ceftazidime

ceftazidime pentahydrate

ceftizoxime sodium

ceftriaxone sodium

cefuroxime sodium

celecoxib

cephalexin

cetirizine hydrochloride

cevonorgesterl/ethinyl estradiol

chloral hydrate

chlorambucil

chloramphenicol

chlordiazepoxide hydrochloride

chlorhexidine acetate

chloroprocaine hydrochloride

chloroquine phosphate

chlorphenesin

chlorpheniramine maleate

chlorpromazine hydrochloride

chlorpropamide

chlortetracycline hydrochloride

chlorthalidone

cholecalciferol

cholestyramine resin

choline salicylate

ciazepam

ciclopirox olamine

cilazapril

cimetidine

ciprofloxacin

ciprofloxacin hydrochloride

cisatracurium besylate

cisplatin

citalopram hydrobromide

cladribine

clarithromycin

clemastine hydrogen fumarate

clindamycin hydochloride

clioquinol

clobazam

clobetasol 17-propionate

clodronate disodium

clofibrate

clomiphene citrate

clomipramine hydrochloride

clonazepam

clonidine hydrochloride

clopidogrel bisulfate

clorazepate dipotassium

clotrimazole

cloxacillin sodium

clozapine

cocaine hydrochloride

codeine phosphate

colchicine

colestipol hydrochloride

colistimethate sodium

cortisone acetate

crythromycin

cyanocobalamin

cyclizine lactate

cyclobenzaprine hydrochloride

cyclophosphamide

cycloserine

cyclosporine

cyproheptadine hydrochloride

cyproterone acetate

cytarabine

dacarbazine

daclizumab

dactinomycin

dalteparin sodium

danaparoid sodium

danazol

dantrolene sodium

dapsone

daunorubicin

deferoxamine mesylate

delavirdine mesylate

desflurane

desipramine hydrochloride

desloratadine

desmopressin acetate

desonide

desoximetasone

dexamphetamine

diazepam

diazoxide

diclofenac potassium

dicyclomine

didanosine (ddl)

didanosine (ddl)

diethylpropion hydrochloride

diethylstilbestrol sodium diphosphate

diflucortolone valerate

diflunisal

digoxin

dihydroergotamine mesylate

dihydrotachysterol

diltiazem hydrochloride

dimenhydrinate

diphenhydramine

dipyridamole

disopyramide

dobutamine hydrochloride

docetaxel

docusate calcium

dolasetron mesylate

donepezil hydrochloride

dopamine hydrochloride

doperidone maleate

dornase alfa, recombinant

doxacurium chloride

doxazosin

doxepin hydrochloride

doxercalciferol

doxorubicin hydrochloride

doxycycline hyclate

doxylamine succinate

dronabinol

econazole nitrate

efavirenz

enalapril maleate

enalaprilat

enflurane

enoxaparin sodium

entacapone

epinephrine

epirubicin hydrochloride

epoprostenol sodium

eprosartan mesylate

eptifibatide

ergocalciferol (calciferol)

erythromycin

esmolol hydrochloride

estradiol

estramustine sodium phosphate

estrone

estropipate

etanercept

ethacrynate sodium

ethacrynic acid

ethambutol hydrochloride

ethinyl estradiol

ethopropazine hydrochloride

ethosuximide

etidronate

etodolac

etoposide

exemestane

famciclovir

famotidne

felodipine

fenofibrate (micronized)

fenoprofen calcium

fenoterol hydrobromide

fentanyl citrate

ferrous sulfate

fexofenadine hydrochloride

filgrastim

finasteride

flavoxate hydrochloride

flecainide acetate

floctafenine

fluconazole

flucytosine

fludarabine phosphate

fludrocortisone acetate

flumazenil

flumethasone pivalate

flunarizine hydrochloride

fluocinonide

fluorouracil

fluoxetine hydrochloride

flupenthixol decanoate

fluphenazine decanoate

flurazepam hydrochloride

flurbiprofen

flutamide

fluticasone propionate

fluvastatin sodium

fluvoxamine maleate

folic acid

fomepizol

fondaparins sodium

formoterol fumarate

fosfomycin tromethamine

fosinopril sodium

fosphenytoin sodium

framycetin sulfate

furosemide

fusidic acid

gabapentin

galantamine hydrobromide

ganciclovir sodium

ganirelix acetate

gatifloxacin

gemcitabine hydrochloride

gemfibrozil

gentamicin sulfate

gliclazide

glyburide

glycolic acid

gonadorelin acetate

goserelin acetate

granisetron hydrochloride

griseofulvin

halcinonide

halobetasol propionate

haloperidol

homosalate

hydralazine hydrochloride

hydrochlorothiazide

hydrocortisone

hydroquinone

hydroxocobalamin

hydroxychloroquine sulfate

hydroxyurea

hydroxyzine hydrochloride

hyoscine hydrobromide

ibuprofen

ibutilide fumarate

idarubicin hydrochloride

idoxuridine

ifosfamide

imatinib mesylate

imipramine hydrochloride

imiquimod

indapamide

indapamine

indinavir sulfate

indomethacin

iodoquinol

ipecac

irbsartan

irinotecan hydrochloride

isoflurane

isoniazid

isoniazid

isoproterenol

isoproterenol hydrochloride

isosorbide dinitrate

isotretinoin

itraconazole

ketamine hydrochloride

ketoconazole

ketoproen

ketorolac tromethamine

labetalol hydrochloride

lactulose

lamivudine (3TC)

lamivudine (3TC)

lamotrigine

lansoprazole

leflunomide

lepirudin

letrozole

leuprolide acetate

levodopa

levofloxacin

levonorgestrel

levothyroxine sodium

lidocaine

limepiride

lincomycin hydrochloride monohydrate

linezolid

liothyronine sodium

lisinopril

lithium carbonate

lomustine

loperamide hydrochloride

loratadine

lorazepam

losartan potassium

lovastatin

loxapine

l-tryptohan

magaldrate

magnesium citrate

mannitol

maprotiline hydrochloride

mazindol

mebendazole

mechlorethamine hydrochloride

meclizine hydrochloride

medrogestone

medroxypogesterone acetate

mefenamic acid

mefloquine hydrochloride

megestrol acetate

meloxicam

melphalan

menthol

mentronidazole

meperidine hydrochloride (pethidine)

mepivacaine hydrochloride

mercaptopurine

meropenem

mesoridazine besylate

mestranol/norethindrone

metformin hydrochloride

methadone

methenamine mandelate

methimazole

methocarbamol

methohexital sodium

methotrimeprazine maleate

methoxamine hydrochloride

methoxsalen

methsuximide

methyldopa

methylphenidate

methylprednisolone

methysergide maleate

metoclopramide hydrochloride

metolazone

metoprolol tartrate

metronidazole

mexiletine hydrochloride

miconazole nitrate

midazolam hydrochloride

milrinone lactate

minocycline hydrochloride

minoxidil

misoprostol

mitomycin

mitotane

mitoxantrone hydrochloride

mivacurium chloride

moclobemide

modafinil

mometasone furoate

montelukast sodium

morphine hydrochloride

moxifloxacin hydrochloride

mupirocin

mycophenolate mofetil

nabilone

nabumetone

nadolol

nadroparin calcium

nafarelin acetate

naftifine hydrochloride

nalbuphine hydrochloride

nalidixic acid

naloxone hydrochloride

naltexone hydrochloride

nandrolone decanoate

naparoxen

naproxen sodium

naratriptan hydrochloride

nateglinide

nedocromil sodium

nefazodone hydrochloride

nelfinavir

neomycin sulfate

netilmicin sulfate

nevirapine

niacin

niacinamide

nicotine

nicoumalone

nifedipine

nilutamide

nitrazepam

nitrofurantion

nitroglycerin

nizatidne

nonoxynol-9

norelgestromin/ethinyl estradiol

norepinephrine bitartrate

norethindrone

norfloxacin

nortriptyline hydrochloride

nylidrin hydrochloride

nystatin

octocrylene

octreotide acetate

octyl dimethyl PABA (Padimate O)

octyl methoxycinnamate (Parsol MCX)

octyl salicylate

ofloxacin

olanzapine

omeprazole magnesium

ondansetron

orciprenaline sulfate

orlistat

orphenandrine citrate

oseltamivir

oxaprozin

oxazepam

oxbenzoneterephthalylidene dicamphor sulfonic acid

oxcarbazepine

oxiconazole nitrate

oxprenolol hydrochloride

oxtriphylline

oxybutynin chloride

oxycodone hydrochloride

oxymorphone hydrochloride

oxytocin

paclitaxel

pamabrom

pamidronate disodium

pancuronium bromide

pantoprazole sodium

pantothenic acid (calcium pantothenate)

papaverine hydrochloride

para-aminosalicylate sodium (PAS sodium)

paraldehyde

paromomycin sulfate

paroxetine

penicillamine

penicillin G sodium

pentamidine isethionate

pentazocine hydrochloride

pentobarbital sodium

pentostatin

pentoxifylline

pergolide mesylate

pericyazine

perindopril erbumine

perphenazine

phenazopyridine hydrochloride

phenelzine sulfate

phenobarbital

phenoxymethyl penicillin

phentermine

phentolamine mesylate

phenylbenzymidazole sulfonic acid (Parsol HS)

phenylbutazone

phenylephrine hydrochloride
phenytoin
phytonadione
pimozide
pinaverium bromide
pindolol
pioglitzaone
piperacillin sodium
pipotiazine palmitate
piroxicam
pivampicillin
pizotifen
podofilox
polymyxin B sulfate
polysiloxane/silicone dioxide
porfimer sodium
povidone-iodine
pralidoxime chloride
pramipexole dihydrochloride
pravastatin sodium
praziquantel
prazosin hydrochloride
prednisolone
prednisolone sodium phosphate
prednisone
prilocaine hydrochloride
primaquine phosphate
primidone
probenecid
procainamide hydrochloride
procaine hydrochloride
procarbazine hydrochloride
prochlorperazine
procyclidine hydrochloride
proguanil
promazine hydrochloride
promethazine hydrochloride
propafenone hydrochloride
propantheline bromide
propofol
propoxyphene napsylate
propranolol hydrochloride
propylthiouracil
protamine sulfate
pyrantel pamoate
pyrazinamide
pyridostigmine bromide
pyridoxine hydrochloride
pyrimethamine
pyrvinium pamoate

quetiapine fumarate

quinapril hydrochloride

quinidine bisulfate

quinupristin/dalfopristin

rabavirin

rabeprazole

rabeprazole sodium

raloxifene hydrochloride

raltitrexed disodium

ramipril

ranitidie hydrochloride

ranitidine hydrochloride

remifentanil hydrochloride

repaglinide

retinol

riboflavin

rifabutin

rifabutin

rifampin

risedronate

risperidone

ritonavir

rivastigmine tartrate

rizatriptan benzoate

rocuronium bromide

rofecoxib

ropinirole hydrochloride

ropivacaine hydrochloride

rosiglitazone

salbutamol

salicylic acid

salmeterol xinafoate

saquinavir

scopolamine

secobarbital sodium

selegiline hydrochloride

selenium sulfide

sertaline hydrochloride

sertraline

sevelamer hydrochloride

sevoflurane

sibutramine

sildenafil citrate

silver sulfadizaine

simethicone

simvastatin

sirolimus

slfadiazine

sodium alginate

sodium arothiomalate

sodium fusidate

sodium nitroprusside

sodium phosphates

sodium thiosulfate

solapsone

somatostatin

somatropin

sorbitol

sotalol hydrochloride

spiramycin

spironolactone

spironolactone

stavudine (d4T)

stavudine (d4T)

sterculia gum

streptomycin sulfate

streptomycin sulfate

streptozocin

strontium chloride

succinylcholine chloride

sucralfate

sufentanil citrate

sulfamethoxazole

sulfapyridine

sulfasalazine

sulfinpyrazone

sulindac

sumatriptan succinate

tacrolimus

tamoxifen citrate

tamsulosin hydrochloride

taxaroten

tazarotene

tazarotene

telmisartan

temazepam

temozolomide

teniposide

tenoxicam

terazosin hydrochloride

terbinafine hydrochloride

terbutaline sulfate

terbutaline sulfate

terconazole

testosterone

tetracaine

tetracycline hydrochloride

theophylline

thiamine hydrochloride

thioguanine

thioproperazine mesylate

thioridazine hydrochloride

thiotepa

thiothixene

tiaprofenic acid

ticarcillin disodium

ticlipidine hydrochloride

timolol maleate

tinzaparin sodium

tioconazole

tirofiban hydrochloride

tizanidine

tobramycin sulfate

tolbutamide

tolmetin sodium

tolnaftate

tolterodine L-tartrate

topiramate

topotecan hydrochloride

trandolapril

tranexamic acid

tranylcypromine sulfate

trazodone hydrochloride

tretinion

triamcinolone

triamterene

triamterene /hydrochlorothiazide

triclosan

triethanolamine salicylate

trifluoperazine hydrochloride

trifluridine

trifuoperazine hydrochloride

trihexyphenidyl hydrochloride

trimcinolone

trimebutine

trimeprazine tartrate

trimethoprim

trimipramine maleate

trizolam

undecylenic acid

ursodiol

valacyclovir hydrochloride

valganciclovir

valproic acid

valrubicin

valsartan

vancomycin hydrochloride

vasopressin

vecuronium bromide

venlafaxine

verapamil hydrochloride

vigabatrin

vinblastine sulfate

vincristine sulfate

vinorelbine tartrate

warfarin sodium

zafirlukast

zalcitabine (ddC)

zaleplon

zanamivir

zidovudine (AZT)

zoledronic acid

zolmitriptan

zopiclone

zuclope

Appendix 11: Gas Phase Results of Solapsone-Gd^{3+} and Solapsone

For all tables, purple cells indicate cation-π interations, blue indicates π-π and orange indicates hydrogen bonds

Gas phase results of Solapsone-Gd^{3+} and the 1AMB conformer of Aβ

	H	H	Q	K	Tyr10		
Initial orientation	LB2	RB2					
Final Orientation		RB2			LS1		
Gd^{3+} chelates 3 SO_3^- @	2 sites each						
Total Energy	-206.263						
van der Waals	91.113						
electrostatic	-485.772						
ΔEs	-47.427						
	-8.008						
	-50.493						

	H	H	Q	K	Tyr10	Val18	Glu22
Initial orientation	RB1	LB1					
Final Orientation		LB2			CS	LB2	LB2
					RB1		
Gd^{3+} chelates 2 SO_3^- @	2 sites each						
Total Energy	-238.032						
van der Waals	86.985						
electrostatic	-502.925						
ΔEs	-79.196						
	-12.136						
	-67.646						

	H	H	Q	K	Tyr10	Leu17	Val18
Initial orientation	LS1	RS1					
Final Orientation	RB1	RS1			CS	LS1	RS2
	LB1						RB2
	LS1						
Gd^{3+} chelates 2 SO_3^- @	5 sites (2 + 3)						
Total Energy	-233.529						
van der Waals	82.133						
electrostatic	-497.803						
ΔEs	-74.693						
	-16.988						
	-62.524						

	H	H	Q	K	Leu17	Phe20
Initial orientation	RB1			LB1		
Final Orientation	RB1			LB1	LB1	LB1
	CS					LS1
Gd^{3+} chelates 2 SO_3^- @	6 sites (3 each)					
Total Energy	-224.646					
van der Waals	85.647					
electrostatic	-491.822					
ΔEs	-65.81					
	-13.474					
	-56.543					

	H	H	Q	K	His6	Tyr10
Initial orientation	RB2			LB2		
Final Orientation	RB2			LS1	RS1	RB2
				2Hbond		
Gd^{3+} chelates 2 SO_3^- @	4 sites (2 each)					
Total Energy	-226.003					
van der Waals	89.617					
electrostatic	-499.098					
ΔEs	-67.167					
	-9.504					
	-63.819					

	H	H	Q	K	Tyr10	Leu17
Initial orientation	LS1	RS2				
Final Orientation	LS1	Gd^{3+}			LS1	LB2
		RS2			C=O	
		LS1				
		-CH2-				
Gd^{3+} chelates 2 SO_3^- @	5 sites (3L + 2R)					
Total Energy	-235.169					
van der Waals	84.987					
electrostatic	-505.238					
ΔEs	-76.333					
	-14.134					
	-69.959					

	H	H	Q	K
Initial orientation	LB1			RB1
Final Orientation	LB1			RB1
	LB1			RS1
	CS			2 Hbonds
Gd^{3+} chelates 2 SO_3^- @	4 sites (2L + 2R)			
Total Energy	-223.191			
van der Waals	89.175			
electrostatic	-497.51			
ΔEs	-64.355			
	-9.946			
	-62.231			

	H	H	Q	K
Initial orientation	LB2			RB2
Final Orientation	LB2			
Gd^{3+} chelates 2 SO_3^- @	3 sites (2R + 1L)			
Total Energy	-183.091			
van der Waals	82.931			
electrostatic	-458.915			
ΔEs	-24.255			
	-16.19			
	-23.636			

	H	H	Q	K	Leu17	Phe20
Initial orientation	RS1			LS1		
Final Orientation	RB1			LS1	RS1	LS1
				2 Hbonds		
Gd^{3+} chelates 2 SO_3^- @	5 sites (3L + 2R)					
Total Energy	-241.321					
van der Waals	78.068					
electrostatic	-506.181					
ΔEs	-82.485					
	-21.053					
	-70.902					

	H	H	Q	K	Leu17	Phe20
Initial orientation	LS1			RS1		
Final Orientation	LS1			RS1	CS	RS1
				RB1		
Gd^{3+} chelates 2 SO_3^- @	6 sites (3 each)					
Total Energy	-211.061					
van der Waals	89.649					
electrostatic	-480.806					
ΔEs	-52.225					
	-9.472					
	-45.527					

	H	H	Q	K	Tyr10
Initial orientation	RB2	LB2			
Final Orientation	RB2	LB2			LB2
	RS2				LS2
Gd^{3+} chelates 2 SO_3^- @	4 sites (2 each)				
Total Energy	-211.64				
van der Waals	87.759				
electrostatic	-480.945				
ΔEs	-52.804				
	-11.362				
	-45.666				

	H	H	Q	K	Tyr10	Leu17	Val18
Initial orientation	RS2	LS1					
Final Orientation	RS2	LS1			RS1	LB2	RS1	LS1
	RB2	LB2					LB1
	RS1	LS2					
		-CH2-					
Gd^{3+} chelates 2 SO_3^- @	4 sites (2 each)						
Total Energy	-248.404						
van der Waals	77.417						
electrostatic	-506.112						
ΔEs	-89.568						
	-21.704						
	-70.833						

	H	H	Q	K	Leu17	Phe20
Initial orientation	RS1			LS2		
Final Orientation	RS1			RS1	RS1	Gd^{3+}
				LS2	RS2	LS2
				LS1		LB2
				-CH2-		
Gd^{3+} chelates 2 SO_3^- @	5 sites (3R + 2L)					
Total Energy	-228.838					
van der Waals	81.443					
electrostatic	-488.473					
ΔEs	-70.002					
	-17.678					
	-53.194					

	H	H	Q	K	Leu17
Initial orientation	LS2			RS1	
Final Orientation	LS1			RS1	LS1	RS1
Gd^{3+} chelates 2 SO_3^- @	5 sites (3L + 2R)				
Total Energy	-214.508				
van der Waals	91.245				
electrostatic	-485.579				
ΔEs	-55.672				
	-7.876				
	-50.3				

	H	H	Q	K	Leu17
Initial orientation	LS2			RS2	
Final Orientation	LS1			RS1	LS1
				2	
Gd^{3+} chelates 2 SO_3^- @	5 sites (3L + 2R)				
Total Energy	-218.219				
van der Waals	93.365				
electrostatic	-490.309				
ΔEs	-59.383				
	-5.756				
	-55.03				

	H	H	Q	K	Leu17	Phe20
Initial orientation	LS2			RS2		
Final Orientation	LS1			RB2	LS1	LB1
Gd^{3+} chelates 3 SO_3^- @	6 sites (2R + 2L + 2L)					
Total Energy	-216.515					
van der Waals	84.462					
electrostatic	-485.249					
ΔEs	-57.679					
	-14.659					
	-49.97					

	H	H	Q	K	Phe20
Initial orientation	LS1			RS2	
Final Orientation	LS1			RS2	RB2
Gd^{3+} chelates 2 SO_3^- @	5 sites (3L + 2R)				
Total Energy	-206.592				
van der Waals	92.684				
electrostatic	-480.249				
ΔEs	-47.756				
	-6.437				
	-44.97				

	H	H	Q	K	Leu17
Initial orientation		LB2		RB2	
Final Orientation	LS2	LB2		RB2	RS2
		-CH2-			RB2
		LS2			
		-CH-			
Gd^{3+} chelates 2 SO_3^- @	4 sites (2 each)				
Total Energy	-228.906				
van der Waals	83.88				
electrostatic	-492.195				
ΔEs	-70.07				
	-15.241				
	-56.916				

	H	H	Q	K	Leu17
Initial orientation		RB2			
Final Orientation	LB2	RB2			RS2
					LS2
					LB2
Gd^{3+} chelates 2 SO_3^- @	3 sites (2L + 1R)				
Total Energy	-218.66				
van der Waals	81.656				
electrostatic	-478.411				
ΔEs	-59.824				
	-17.465				
	-43.132				

	L	V	F	F
Initial orientation			RB2	LB2
Final Orientation			RB2	
Gd^{3+} chelates 2 SO_3^- @	5 sites (2 + 3)			
Total Energy	-191.485			
van der Waals	92.94			
electrostatic	-462.602			
ΔEs	-32.649			
	-6.181			
	-27.323			

	L	V	F	F	His13
Initial orientation		LB2	RB2		
Final Orientation	RB2				RB2
	RS2				
Gd^{3+} chelates 2 SO_3^- @	5 sites (3L + 2R)				
Total Energy	-212.106				
van der Waals	92.231				
electrostatic	-479.733				
ΔEs	-53.27				
	-6.89				
	-44.454				

	L	V	F	F	Lys16
Initial orientation			LB1	RB1	
Final Orientation					RB1
Gd^{3+} chelates 2 SO_3^- @	6 sites - 3 each				
Total Energy	-196.265				
van der Waals	85.138				
electrostatic	-460.946				
ΔEs	-37.429				
	-13.983				
	-25.667				

	L	V	F	F	Asp23
Initial orientation			LB2	RB2	
Final Orientation				RB2	RB2
Gd^{3+} chelates 2 SO_3^- @	5 sites (3L + 2R)				
Total Energy	-215.555				
van der Waals	93.234				
electrostatic	-490.155				
ΔEs	-56.719				
	-5.887				
	-54.876				

	L	V	F	F
Initial orientation		RB2	LB2	
Final Orientation		RB2	LB2	
Gd^{3+} chelates 2 SO_3^- @	5 sites (3L + 2R)			
Total Energy	-214.701			
van der Waals	89.395			
electrostatic	-480.931			
ΔEs	-55.865			
	-9.726			
	-45.652			

	L	V	F	F	Lys16	Asp23
Initial orientation			RB1	LB1		
Final Orientation			CS*		LB1	LB2
					LNH	CS
Gd^{3+} chelates 3 SO_3^- @	6 sites, 2 each (R has 2 SO3 L has 1)					
Total Energy	-237.856	* w/CH2 of side chain				
van der Waals	86.535					
electrostatic	-513.324					
ΔEs	-79.02					
	-12.586					
	-78.045					

	L	V	F	F	His13	Gln15
Initial orientation		LB1	RB1			
Final Orientation		RB1	CS		RS1	RB1
			LB1			CS
Gd^{3+} chelates 2 SO_3^- @	5 sites (3L + 2R)					
Total Energy	-192.333					
van der Waals	89.118					
electrostatic	-454.094					
ΔEs	-33.497					
	-10.003					
	-18.815					

	L	V	F	F	His13	Lys28
Initial orientation	RB1			LB1		
Final Orientation	RB1				RS1	LS1
	RNH					LNH
Gd^{3+} chelates 2 SO_3^- @	6 sites (3 each)					
Total Energy	-225.033					
van der Waals	87.41					
electrostatic	-497.616					
ΔEs	-66.197					
	-11.711					
	-62.337					

	L	V	F	F	Gln15
Initial orientation		RB1	LB1		
Final Orientation		RB1	LB1		CS
			CS		
Gd^{3+} chelates 2 SO_3^- @	5 sites (3L + 2R)				
Total Energy	-194.654				
van der Waals	88.431				
electrostatic	-452.907				
ΔEs	-35.818				
	-10.69				
	-17.628				

	L	V	F	F	His13	Lys28
Initial orientation	LB1			RB1		
Final Orientation	LB1			RB1	LS1	RS1
Gd^{3+} chelates 2 SO_3^- @	5 sites (3R + 2L)					
Total Energy	-232.85					
van der Waals	88.43					
electrostatic	-503.133					
ΔEs	-74.014					
	-10.691					
	-67.854					

	L	V	F	F	Ala21	Lys28
Initial orientation		RB2		LB2		
Final Orientation		RB2		LB2	LB2	LS1
Gd^{3+} chelates 2 SO_3^- @	4 sites (2 each)					
Total Energy	-216.817					
van der Waals	82.737					
electrostatic	-482.741					
ΔEs	-57.981					
	-16.384					
	-47.462					

	L	V	F	F
Initial orientation	RB2			LB2
Final Orientation	RB2			
Gd^{3+} chelates 2 SO_3^- @	5 sites (3L + 2R)			
Total Energy	-174.26			
van der Waals	94.836			
electrostatic	-449.527			
ΔEs	-15.424			
	-4.285			
	-14.248			

	L	V	F	F	Gly25
Initial orientation		LB2		RB2	
Final Orientation					RB2
Gd^{3+} chelates 2 SO_3^- @	5 sites (3L + 2R)				
Total Energy	-209.847				
van der Waals	89.957				
electrostatic	-483.479				
ΔEs	-51.011				
	-9.164				
	-48.2				

	L	V	F	F	Lys28
Initial orientation	LB2			RB2	
Final Orientation				RB2	RS1
Gd^{3+} chelates 2 SO_3^- @	5 sites (3L + 2R)				
Total Energy	-196.093				
van der Waals	92.946				
electrostatic	-469.645				
ΔEs	-37.257				
	-6.175				
	-34.366				

Gas phase results of Solapsone-Gd^{3+} and the 1AMC conformer of Aβ

	H	H	Q	K	Tyr10
Initial orientation	LB2	RB2			
Final Orientation	LB2	RB2			LS2
Gd^{3+} chelates 2 SO_3^- @	5 sites (2R & 3L)				
Total Energy	-195.765				
van der Waals	104.78				
electrostatic	-499.452				
ΔEs	-48.103				
	-5.05				
	-50.517				

	H	H	Q	K	Leu17	Phe20
Initial orientation	RS2			LS2		
Final Orientation	RB2			LS1	RB2	LB2
	RS1			2		
Gd^{3+} chelates 2 SO_3^- @	6 sites (3L & 3R)					
Total Energy	-207.886					
van der Waals	104.263					
electrostatic	-504.147					
ΔEs	-60.224					
	-5.567					
	-55.212					

	H	H	Q	K	Leu17
Initial orientation	RB2	LB2			
Final Orientation	RB2	LB2			RB2
	RS2	LB2			LS1
Gd^{3+} chelates 2 SO_3^- @	4 sites (2L & 2R)				
Total Energy	-201.584				
van der Waals	94.463				
electrostatic	-488.395				
ΔEs	-53.922				
	-15.367				
	-39.46				

	H	H	Q	K	Leu17
Initial orientation	LB1			RB1	
Final Orientation	LB1			RS1	CS
	LB1				
Gd^{3+} chelates 2 SO_3^- @	6 sites (3L & 3R)				
Total Energy	-204.639				
van der Waals	97.662				
electrostatic	-500.604				
ΔEs	-56.977				
	-12.168				
	-51.669				

	H	H	Q	K	Tyr10	
Initial orientation	RB1	LB1				
Final Orientation	RB1	LB1			LB1	
	CS	-CH2-				
Gd^{3+} chelates 2 SO_3^- @	6 sites (3L & 3R)					
Total Energy	-197.934					
van der Waals	100.293					
electrostatic	-489.578					
ΔEs	-50.272					
	-9.537					
	-40.643					

	H	H	Q	K	Leu17	Phe20
Initial orientation	RB1			LB1		
Final Orientation	CS			LB1	CS	LS1
				-CH2-		
Gd^{3+} chelates 2 SO_3^- @	5 sites (2R & 3L)					
Total Energy	-198.939					
van der Waals	103.295					
electrostatic	-492.027					
ΔEs	-51.277					
	-6.535					
	-43.092					

	H	H	Q	K	Tyr10	Leu17
Initial orientation	LB1	RB1				
Final Orientation	LS1	RB1			CS	LS1
		CS			LB1	
Gd^{3+} chelates 2 SO_3^- @	6 sites (3L & 3R)					
Total Energy	-218.345					
van der Waals	97.452					
electrostatic	-506.372					
ΔEs	-70.683					
	-12.378					
	-57.437					

	H	H	Q	K	Leu17	Phe20
Initial orientation	LS1			RS1		
Final Orientation	LB1			RS1	LB1	RS1
	LS1			RB1	CS	
Gd^{3+} chelates 2 SO_3^- @	6 sites (3L & 3R)					
Total Energy	-202.506					
van der Waals	99.885					
electrostatic	-495.451					
ΔEs	-54.844					
	-9.945					
	-46.516					

	H	H	Q	K
Initial orientation	LB2			RB2
Final Orientation	LB2			RB2
Gd^{3+} chelates 2 SO_3^- @	5 sites (2R & 3L)			
Total Energy	-183.466			
van der Waals	102.853			
electrostatic	-484.495			
ΔEs	-35.804			
	-6.977			
	-35.56			

	H	H	Q	K	Leu17
Initial orientation	RS1			LS1	
Final Orientation	RS1			LS1	RS1
	RB1				
Gd^{3+} chelates 2 SO_3^- @	6 sites (3L & 3R)				
Total Energy	-205.393				
van der Waals	99.724				
electrostatic	-497.001				
ΔEs	-57.731				
	-10.106				
	-48.066				

	H	H	Q	K	Phe20
Initial orientation	RB2			LB2	
Final Orientation	RB2			LB2	LB1
	RB2			LS2	
				RS2	
Gd^{3+} chelates 3 SO_3^- @	6 sites (3L & 2R & 1R)				
Total Energy	-208.953				
van der Waals	95.955				
electrostatic	-496.192				
ΔEs	-61.291				
	-13.875				
	-47.257				

	H	H	Q	K	Tyr10
Initial orientation		RB2		LB2	
Final Orientation	LS2	RB2			RS2
	LB2	-CH2-			RS1
					LS2
					RB2
Gd^{3+} chelates 2 SO_3^- @	3 sites (2R & 2L)				
Total Energy	-218.045				
van der Waals	86.523				
electrostatic	-498.937				
ΔEs	-70.383				
	-23.307				
	-50.002				

	H	H	Q	K	Tyr10	Leu17
Initial orientation		LB2		RB2		
Final Orientation	RB2	LS2			LB2	RS2
	RS2	-CH-				LS2
	LS2	LB2				
		-CH2-				
Gd^{3+} chelates 3 SO_3^- @	5 sites (2L & 1L & 2R)					
Total Energy	-229.735					
van der Waals	94.325					
electrostatic	-518.809					
ΔEs	-82.073					
	-15.505					
	-69.874					

	H	H	Q	K	Leu17
Initial orientation	RS1			LS2	
Final Orientation	RS1			LS1	RS1
				LS2	
Gd^{3+} chelates 2 SO_3^- @	5 sites (2R & 3L)				
Total Energy	-207.725				
van der Waals	102.109				
electrostatic	-508.407				
ΔEs	-60.063				
	-7.721				
	-59.472				

	H	H	Q	K	Tyr10	Leu17
Initial orientation	LS2			RS1		
Final Orientation	LB1			RB1	LS1	CS
	LS1			RS1		
	LS2			2		
Gd^{3+} chelates 2 SO_3^- @	5 sites (2R & 3L)					
Total Energy	-205.009					
van der Waals	98.398					
electrostatic	-497.754					
ΔEs	-57.347					
	-11.432					
	-48.819					

	H	H	Q	K	Phe20
Initial orientation	LS1			RS2	
Final Orientation	LS1			RS2	RB2
				2	
Gd^{3+} chelates 2 SO_3^- @	5 sites (2R & 3L)				
Total Energy	-191.081				
van der Waals	105.299				
electrostatic	-490.172				
ΔEs	-43.419				
	-4.531				
	-41.237				

	H	H	Q	K	Tyr10	Leu17	Phe20
Initial orientation	RS2			LS1			
Final Orientation	RB1	RS1		LS1	RS1	LS1	LS1
				LB1			
Gd^{3+} chelates 2 SO_3^- @	6 sites (3L & 3R)						
Total Energy	-223.142						
van der Waals	97.643						
electrostatic	-514.301						
ΔEs	-75.48						
	-12.187						
	-65.366						

	L	V	F	F	His13	Ala21
Initial orientation	LB2	RB2				
Final Orientation	LB2	RB2			LB2	RB2
Gd^{3+} chelates 2 SO_3^- @	4 sites (2L & 2R)					
Total Energy	-186.508					
van der Waals	95.002					
electrostatic	-475.067					
ΔEs	-38.846					
	-14.828					
	-26.132					

	L	V	F	F	Val12	Lys16
Initial orientation		RB1	LB1			
Final Orientation		RB1	LB1		RS1	LB1
						LS1
Gd^{3+} chelates 2 SO_3^- @	6 sites (3L & 3R)					
Total Energy	-204.005					
van der Waals	93.3					
electrostatic	-491.278					
ΔEs	-56.343					
	-16.53					
	-42.343					

	L	V	F	F		
Initial orientation	RB2	LB2				
Final Orientation	RB2	LB2				
Gd^{3+} chelates 2 SO_3^- @	5 sites (2R & 3L)					
Total Energy	-170.378					
van der Waals	102.679					
electrostatic	-467.903					
ΔEs	-22.716					
	-7.151					
	-18.968					

	L	V	F	F	Lys16	
Initial orientation		LB1	RB1			
Final Orientation		LB1	RS1		RS1	
		RB1				
Gd^{3+} chelates 2 SO_3^- @	5 sites (2R & 3L)	-CH2-				
Total Energy	-213.926					
van der Waals	92.888					
electrostatic	-500.231					
ΔEs	-66.264					
	-16.942					
	-51.296					

	L	V	F	F		
Initial orientation	LB1	RB1				
Final Orientation	LB1	CS				
	CS					
Gd^{3+} chelates 2 SO_3^- @	5 sites (2R & 3L)					
Total Energy	-182.583					
van der Waals	106.438					
electrostatic	-484.526					
ΔEs	-34.921					
	-3.392					
	-35.591					

	L	V	F	F	His13	Lys16
Initial orientation		RB2				
Final Orientation		RB2			LB2	RS2
					RS2	RB2
Gd^{3+} chelates 3 SO_3^- @	6 sites (2L & 2L & 2R)					
Total Energy	-230.053					
van der Waals	97.692					
electrostatic	-522.929					
ΔEs	-82.391					
	-12.138					
	-73.994					

	L	V	F	F	Tyr10	His13
Initial orientation	RB1	LB1				
Final Orientation	RB1	CS			RB2	RS1
					RS2	
Gd^{3+} chelates 2 SO_3^- @	5 sites (2R & 3L)					
Total Energy	-207.366					
van der Waals	96.413					
electrostatic	-494.721					
ΔEs	-59.704					
	-13.417					
	-45.786					

	L	V	F	F		
Initial orientation	RB2			LB2		
Final Orientation	RB2			LB2		
Gd^{3+} chelates 2 SO_3^- @	4 sites (2L & 2R)					
Total Energy	-182.787					
van der Waals	105.725					
electrostatic	-480.351					
ΔEs	-35.125					
	-4.105					
	-31.416					

	L	V	F	F	Gln15	
Initial orientation		LB2	RB2		RB2	
Final Orientation			RB2		-CH2-	
					RS2	
Gd^{3+} chelates 2 SO_3^- @	5 sites (2R & 3L)					
Total Energy	-180.092					
van der Waals	103.516					
electrostatic	-479.083					
ΔEs	-32.43					
	-6.314					
	-30.148					

	L	V	F	F	Lys16	His13
Initial orientation	RB1			LB1		
Final Orientation	RB1			LB2	RS1	RS1
	RS1					
Gd^{3+} chelates 2 SO_3^- @	5 sites (2R & 3L)					
Total Energy	-211.674					
van der Waals	94.831					
electrostatic	-502.584					
ΔEs	-64.012					
	-14.999					
	-53.649					

	L	V	F	F	Glu22	
Initial orientation		RB2	LB2			
Final Orientation		RB2	LB2		LB2	
Gd^{3+} chelates 2 SO_3^- @	6 sites (3L & 3R)					
Total Energy	-185.121					
van der Waals	105.033					
electrostatic	-483.797					
ΔEs	-37.459					
	-4.797					
	-34.862					

	L	V	F	F	His13	Lys16
Initial orientation	LB1			RB1		
Final Orientation	LB2			RB1	LS1	LS1
	LNH			CS		LNH
				LB1		
Gd^{3+} chelates 2 SO_3^- @	5 sites (2R & 3L)					
Total Energy	-221.577					
van der Waals	97.62					
electrostatic	-516.356					
ΔEs	-73.915					
	-12.21					
	-67.421					

	L	V	F	F	Gln15	Glu22
Initial orientation		LB1	RB1			
Final Orientation		LB1	RB1		LB1	RB1
			CS		CS	
Gd^{3+} chelates 2 SO_3^- @	4 sites (2L & 2R) and Glu22 @ 2 sites					
Total Energy	-221.776					
van der Waals	96.535					
electrostatic	-527.107					
ΔEs	-74.114					
	-13.295					
	-78.172					

	L	V	F	F		
Initial orientation		RB2	LB2			
Final Orientation		RB2	LB2			
Gd^{3+} chelates 2 SO_3^- @	5 sites (2R & 3L)					
Total Energy	-168.877					
van der Waals	104.062					
electrostatic	-466.488					
ΔEs	-21.215					
	-5.768					
	-17.553					

	L	V	F	F	Gln15	
Initial orientation		RB1	LB1			
Final Orientation		RB1	LB1		CS	
		CS	CS			
Gd^{3+} chelates 2 SO_3^- @	4 sites (3L & 1R) and Glu22 @ 2 sites					
Total Energy	-210.708					
van der Waals	99.258					
electrostatic	-506.405					
ΔEs	-63.046					
	-10.572					
	-57.47					

	L	V	F	F		
Initial orientation		LB2				
Final Orientation		LB2				
Gd^{3+} chelates 3 SO_3^- @	5 sites (2R & 3L)					
Total Energy	-211.151					
van der Waals	102.366					
electrostatic	-509.153					
ΔEs	-63.489					
	-7.464					
	-60.218					

	L	V	F	F		
Initial orientation			RB2	LB2		
Final Orientation			RB2			
Gd^{3+} chelates 2 SO_3^- @	6 sites (3L & 2R & 1R)					
Total Energy	-187.245					
van der Waals	106.971					
electrostatic	-487.614					
ΔEs	-39.583					
	-2.859					
	-38.679					

	L	V	F	F		
Initial orientation			LB2	RB2		
Final Orientation						
Gd^{3+} chelates 2 SO_3^- @	5 sites (2R & 3L)					
Total Energy	-169.798					
van der Waals	109.671					
electrostatic	-474.804					
ΔEs	-22.136					
	-0.159					
	-25.869					

	L	V	F	F		
Initial orientation	RB2		LB2			
Final Orientation		RS2	LB2			
		RB2				
Gd^{3+} chelates 2 SO_3^- @	5 sites (3R & 2L) and Glu22 @ 1 site					
Total Energy	-234.218					
van der Waals	102.274					
electrostatic	-531.47					
ΔEs	-86.556					
	-7.556					
	-82.535					

Gas phase results of Solapsone-Gd^{3+} and the 1AML conformer of Aβ

	H	H	Q	K		
Initial orientation	LB2	RB2				
Final Orientation	LB2	RB2				
Gd^{3+} chelates 2 SO_4^- @	5 sites (2R & 3L)					
Total Energy	7.462					
van der Waals	136.518					
electrostatic	-386.106					
ΔEs	-28.031					
	-2.212					
	-31.841					

	H	H	Q	K	Tyr10	Leu17
Initial orientation	LB1	RB1				
Final Orientation	LB1	CS			LB1	LB1
	LS1					
	LNH					
Gd^{3+} chelates 3 SO_4^- @	7 sites (3L & 2R & 2R)					
Total Energy	-79.292					
van der Waals	131.807					
electrostatic	-467.126					
ΔEs	-114.785					
	-6.923					
	-112.861					

	H	H	Q	K
Initial orientation	LB2			RB2
Final Orientation	LB2			RB2
Gd^{3+} chelates 2 SO_4^- @	5 sites (2R & 3L)			
Total Energy	-8.883			
van der Waals	131.525			
electrostatic	-394.301			
ΔEs	-44.376			
	-7.205			
	-40.036			

	H	H	Q	K	Val12
Initial orientation	LB1			RB1	
Final Orientation	LB1			RB1	CS
	LNH			CS (-CH2-)	LB1
					(C=O)
Gd^{3+} chelates 2 SO_4^- @	6 sites (3L & 3R)				
Total Energy	-34.66				
van der Waals	129.853				
electrostatic	-421.609				
ΔEs	-70.153				
	-8.877				
	-67.344				

	H	H	Q	K
Initial orientation	LS1			RS1
Final Orientation	LS1			RS1
Gd^{3+} chelates 2 SO_4^- @	6 sites (3L & 3R)			
Total Energy	-74.527			
van der Waals	135.243			
electrostatic	-465.655			
ΔEs	-110.02			
	-3.487			
	-111.39			

	H	H	Q	K
Initial orientation	RS2			LS1
Final Orientation	RS2			LS1
Gd^{3+} chelates 2 SO_4^- @	4 sites (3L & 1R)			
Total Energy	-44.994			
van der Waals	136.427			
electrostatic	-440.038			
ΔEs	-80.487			
	-2.303			
	-85.773			

	H	H	Q	K	Val12
Initial orientation	LS2			RS1	
Final Orientation	LS1			RS1	LS2
					RS2
Gd^{3+} chelates 2 SO_4^- @	5 sites (2R & 3L)				
Total Energy	-89.716				
van der Waals	129.602				
electrostatic	-471.853				
ΔEs	-125.209				
	-9.128				
	-117.588				

	L	V	F	F
Initial orientation			RB2	LB2
Final Orientation				
Gd^{3+} chelates 2 SO_4^- @	5 sites (2R & 3L)			
Total Energy	13.099			
van der Waals	138.446			
electrostatic	-377.041			
ΔEs	-22.394			
	-0.284			
	-22.776			

	L	V	F	F	Lys16	Asp23
Initial orientation			RB1	LB1		
Final Orientation			RB1	CS	RS1	CS
			CS	LB1	RB1	-CH2-
Gd^{3+} chelates 2 SO_4^- @	6 sites (3L & 3R)					
Total Energy	-55.202					
van der Waals	126.536					
electrostatic	-454.143					
ΔEs	-90.695					
	-12.194					
	-99.878					

	L	V	F	F
Initial orientation	LB2		RB2	
Final Orientation				LS2
Gd^{3+} chelates 2 SO_4^- @	5 sites (2R & 3L)			
Total Energy	-26.14			
van der Waals	127.539			
electrostatic	-407.102			
ΔEs	-61.633			
	-11.191			
	-52.837			

	H	H	Q	K	Tyr10		
Initial orientation	RB2	LB2					
Final Orientation		LB2			RS2		
Gd^{3+} chelates 2 SO_4^- @	4 sites (2R & 2L)						
Total Energy	-27.892						
van der Waals	132.759						
electrostatic	-414.173						
ΔEs	-63.385						
	-5.971						
	-59.908						

	H	H	Q	K	Tyr10	Leu17	Ile31
Initial orientation	RB1	LB1					
Final Orientation	RS1	CS			RS1	RB1	RB1
		LB1				CS	CS
							LB1
Gd^{3+} chelates 2 SO_4^- @	6 sites (3L & 3R)						
Total Energy	-54.43						
van der Waals	129.965						
electrostatic	-435.194						
ΔEs	-89.923						
	-8.765						
	-80.929						

	H	H	Q	K	Tyr10
Initial orientation	RB2			LB2	
Final Orientation	RB2				RB2
	RB2				
Gd^{3+} chelates 2 SO_4^- @	5 sites (2R & 3L)				
Total Energy	-53.334				
van der Waals	129.286				
electrostatic	-429.627				
ΔEs	-88.827				
	-9.444				
	-75.362				

	H	H	Q	K	Phe20
Initial orientation	RB1			LB1	
Final Orientation				LB1	CS
				-CH2-	LB1
				LNH	
Gd^{3+} chelates 2 SO_4^- @	6 sites (3L & 3R)				
Total Energy	-60.487				
van der Waals	126.233				
electrostatic	-441.386				
ΔEs	-95.98				
	-12.497				
	-87.121				

	H	H	Q	K	Val12
Initial orientation	RS1			LS1	
Final Orientation	RS1			LS1	CS
				2	
Gd^{3+} chelates 2 SO_4^- @	6 sites (3L & 3R)				
Total Energy	-23.292				
van der Waals	134.324				
electrostatic	-411.531				
ΔEs	-58.785				
	-4.406				
	-57.266				

	H	H	Q	K	Val12
Initial orientation	LS1			RS2	
Final Orientation	LS1			RB1	LS1
				LS1*	C=O
				LB1*	
				-CH2-	
				RS1	
Gd^{3+} chelates 2 SO_4^- @	6 sites (3L & 3R)				
Total Energy	-68.856				
van der Waals	130.098				
electrostatic	-465.387				
ΔEs	-104.349				
	-8.632				
	-111.122				

	H	H	Q	K	Val12
Initial orientation	RS1			LS2	
Final Orientation	RS1			LS2	RS1
				RS1	
				-CH2-	
Gd^{3+} chelates 2 SO_4^- @	4 sites (2L & 2R)				
Total Energy	-60.352				
van der Waals	129.737				
electrostatic	-440.576				
ΔEs	-95.845				
	-8.993				
	-86.311				

	L	V	F	F	Lys16	Asp23
Initial orientation			LB2	RB2		
Final Orientation			LS1		LS1	LB2
			LB2		2	
Gd^{3+} chelates 2 SO_4^- @	6 sites (3L & 3R)					
Total Energy	-70.149					
van der Waals	132.058					
electrostatic	-456.32					
ΔEs	-105.642					
	-6.672					
	-102.055					

	L	V	F	F
Initial orientation			LB1	RB1
Final Orientation				
Gd^{3+} chelates 2 SO_4^- @	5 sites (2R & 3L)			
Total Energy	20.025			
van der Waals	135.429			
electrostatic	-367.064			
ΔEs	-15.468			
	-3.301			
	-12.799			

	L	V	F	F	His13	Lys16	Ala30
Initial orientation	RB2		LB2				
Final Orientation	RB2			RS2	RB2	RB2	RB2
				LS2		-CH2-	
				LB2			
Gd^{3+} chelates 2 SO_4^- @	4 sites (2L & 2R)						
Total Energy	-60.285						
van der Waals	123.812						
electrostatic	-440.733						
ΔEs	-95.778						
	-14.918						
	-86.468						

Gas phase results of Solapsone-Gd^{3+} and the 1BA4 conformer of Aβ

	H	H	Q	K						
Initial orientation	RB2	LB2								
Final Orientation	RB2									
Gd^{3+} chelates 2 SO_3^- @	5 sites (2R & 3L)									
Total Energy	-82.819									
van der Waals	105.686									
electrostatic	-418.894									
ΔEs	-24.366									
	-2.871									
	-25.618									

	H	H	Q	K						
Initial orientation	LB2	RB2								
Final Orientation	LB2									
	LS2									
Gd^{3+} chelates 2 SO_3^- @	4 sites (2L & 2R)									
Total Energy	-121.23									
van der Waals	101.278									
electrostatic	-445.844									
ΔEs	-62.777									
	-7.279									
	-52.568									

	H	H	Q	K						
Initial orientation	LB1	RB1								
Final Orientation	LS1	RS1								
Gd^{3+} chelates 2 SO_3^- @	6 sites (3L & 3R)									
Total Energy	-127.595									
van der Waals	101.57									
electrostatic	-454.871									
ΔEs	-69.142									
	-6.987									
	-61.595									

	H	H	Q	K						
Initial orientation	RB1	LB1								
Final Orientation	RS1	RS1								
		RB1								
Gd^{3+} chelates 2 SO_3^- @	5 sites (2R & 3L)									
Total Energy	-108.338									
van der Waals	102.36									
electrostatic	-437.455									
ΔEs	-49.885									
	-6.197									
	-44.179									

	H	H	Q	K						
Initial orientation	RS1	LS1								
Final Orientation	RS1	LS1								
Gd^{3+} chelates 2 SO_3^- @	6 sites (3L & 3R)									
Total Energy	-112.131									
van der Waals	104.871									
electrostatic	-446.028									
ΔEs	-53.678									
	-3.686									
	-52.752									

	H	H	Q	K						
Initial orientation	LS1	RS1								
Final Orientation	LS1	RS1								
Gd^{3+} chelates 2 SO_3^- @	5 sites (2R & 3L)									
Total Energy	-103.617									
van der Waals	108.071									
electrostatic	-437.607									
ΔEs	-45.164									
	-0.486									
	-44.331									

	H	H	Q	K	Tyr10					
Initial orientation	RB2			LB2						
Final Orientation	RB2	RS1		LB2	RB2					
					RS2					
					-CH2-					
Gd^{3+} chelates 2 SO_3^- @	5 sites (2R & 3L)									
Total Energy	-139.151									
van der Waals	93.593									
electrostatic	-469.703									
ΔEs	-80.698									
	-14.964									
	-76.427									

	H	H	Q	K	Gly9	Tyr10
Initial orientation	LB2			RB2		
Final Orientation	LB2	LS1			RB2	LB2
					-NH	RS2
						-CH2-
Gd^{3+} chelates 2 SO_3^- @	4 sites (2L & 2R)					RB2
						-CH-
Total Energy	-143.452					
van der Waals	91.58					
electrostatic	-469.77					
ΔEs	-84.999					
	-16.977					
	-76.494					

	H	H	Q	K	Asp1	Glu3	His6	Asp7	Gly9	Tyr10
Initial orientation		RB2		LB2						
Final Orientation	RB2			LB2	LB2	LB2	LS1	LB2	LB2	RB2
					-NH3+			C=O		RS2
										-CH2-
Gd^{3+} chelates 2 SO_3^- @	5 sites (2R & 3L)									
Total Energy	-144.663									
van der Waals	92.843									
electrostatic	-469.321									
ΔEs	-86.21									
	-15.714									
	-76.045									

	H	H	Q	K	His6	Gly9
Initial orientation		LB2		RB2		
Final Orientation					RS1	RB2
						-NH-
Gd^{3+} chelates 2 SO_3^- @	5 sites (2R & 3L)					
Total Energy	-103.562					
van der Waals	101.296					
electrostatic	-438.781					
ΔEs	-45.109					
	-7.261					
	-45.505					

	H	H	Q	K		
Initial orientation	LS2	RS2				
Final Orientation	LS1	RB1				
		RS2				
		RS1				
Gd^{3+} chelates 2 SO_3^- @	6 sites (3L & 3R)					
Total Energy	-123.388					
van der Waals	102.375					
electrostatic	-452.891					
ΔEs	-64.935					
	-6.182					
	-59.615					

	H	H	Q	K		
Initial orientation	RS2	LS2				
Final Orientation	RS1	LS1				
		LS2				
		LB2				
Gd^{3+} chelates 2 SO_3^- @	5 sites (2R & 3L)					
Total Energy	-107.676					
van der Waals	102.832					
electrostatic	-440.322					
ΔEs	-49.223					
	-5.725					
	-47.046					

	H	H	Q	K		
Initial orientation	RS1	LS2				
Final Orientation	LS1	RS1				
		LS2				
Gd^{3+} chelates 2 SO_3^- @	5 sites (2R & 3L)					
Total Energy	-96.799					
van der Waals	104					
electrostatic	-427.323					
ΔEs	-38.346					
	-4.557					
	-34.047					

	H	H	Q	K		
Initial orientation	LS2	RS1				
Final Orientation	LS1	RS1				
	2	RB1				
Gd^{3+} chelates 2 SO_3^- @	5 sites (2L & 3R)					
Total Energy	-130.154					
van der Waals	102.547					
electrostatic	-460.94					
ΔEs	-71.701					
	-6.01					
	-67.664					

	H	H	Q	K		
Initial orientation	LS1	RS2				
Final Orientation	LS1	RS2				
	LB2	LS2				
	LB2	LS1				
Gd^{3+} chelates 2 SO_3^- @	5 sites (2R & 3L)					
Total Energy	-123.114					
van der Waals	94.718					
electrostatic	-451.398					
ΔEs	-64.661					
	-13.839					
	-58.122					

	H	H	Q	K		
Initial orientation	RS2	LS1				
Final Orientation	RS1	LS1				
	LS1					
Gd^{3+} chelates 2 SO_3^- @	5 sites (2R & 3L)					
Total Energy	-124.556					
van der Waals	102.651					
electrostatic	-452.962					
ΔEs	-66.103					
	-5.906					
	-59.686					

	L	V	F	F	His14	Glu22
Initial orientation	LB2		RB2			
Final Orientation	LB2	LS2			LS1	RB2
Gd^{3+} chelates 2 SO_3^- @	6 sites (3L & 3R)					
Total Energy	-141.471					
van der Waals	99.109					
electrostatic	-469.084					
ΔEs	-83.018					
	-9.448					
	-75.808					

	L	V	F	F	His14	Glu22
Initial orientation	RB2		LB2			
Final Orientation	RB2	RS2			LB2	LB2
		LS2				
Gd^{3+} chelates 2 SO_3^- @	5 sites (2R & 3L)					
Total Energy	-112.926					
van der Waals	98.713					
electrostatic	-434.898					
ΔEs	-54.473					
	-9.844					
	-41.622					

	L	V	F	F	Gln15	Glu22
Initial orientation		LB1	RB1			
Final Orientation		CS			LS2	CS
					RB1	
					RS1	
Gd^{3+} chelates 2 SO_3^- @	5 sites (2R & 3L)					
Total Energy	-112.086					
van der Waals	95.241					
electrostatic	-432.619					
ΔEs	-53.633					
	-13.316					
	-39.343					

	L	V	F	F	Gln15	Glu22
Initial orientation		RB1	LB1			
Final Orientation			LB1		CS	LS2
			CS			RS1
Gd^{3+} chelates 2 SO_3^- @	6 sites (3L & 3R) and Glu22 @ 1 site					
Total Energy	-133.478					
van der Waals	101.993					
electrostatic	-470.459					
ΔEs	-75.025					
	-6.564					
	-77.183					

	L	V	F	F	His14	Gln15
Initial orientation	LB2	RB2				
Final Orientation	RS2				RS2	RB2
Gd^{3+} chelates 2 SO_3^- @	5 sites (2R & 3L)					
Total Energy	-111.113					
van der Waals	97.968					
electrostatic	-438.131					
ΔEs	-52.66					
	-10.589					
	-44.855					

	L	V	F	F
Initial orientation	RB2	LB2		
Final Orientation	RB2	LB2		
Gd^{3+} chelates 3 SO_3^- @	7 sites (3R & 2L & 2L)			
Total Energy	-128.899			
van der Waals	100.406			
electrostatic	-445.858			
ΔEs	-70.446			
	-8.151			
	-52.582			

	L	V	F	F
Initial orientation	LB2		RB2	
Final Orientation			RB2	
Gd^{3+} chelates 2 SO_3^- @	5 sites (2L & 3R)			
Total Energy	-89.166			
van der Waals	102.459			
electrostatic	-419.116			
ΔEs	-30.713			
	-6.098			
	-25.84			

	L	V	F	F
Initial orientation	RB2			LB2
Final Orientation				LB2
Gd^{3+} chelates 2 SO_3^- @	5 sites (2R & 3L)			
Total Energy	-64.469			
van der Waals	106.748			
electrostatic	-397.596			
ΔEs	-6.016			
	-1.809			
	-4.32			

	L	V	F	F
Initial orientation	RB1			LB1
Final Orientation	RB1			LB2
	CS			
Gd^{3+} chelates 2 SO_3^- @	5 sites (2R & 3L)			
Total Energy	-89.511			
van der Waals	102.625			
electrostatic	-420.863			
ΔEs	-31.058			
	-5.932			
	-27.587			

	L	V	F	F	His14
Initial orientation	LB1			RB1	
Final Orientation	LB1				LS1
	CS				LB1
					LNH
Gd^{3+} chelates 2 SO_3^- @	6 sites (3L & 3R)				
Total Energy	-102.772				
van der Waals	99.134				
electrostatic	-425.454				
ΔEs	-44.319				
	-9.423				
	-32.178				

	L	V	F	F	Glu22
Initial orientation		LB2	RB2		
Final Orientation		LS2			LS2
		LB2			RS2
Gd^{3+} chelates 2 SO_3^- @	6 sites (3L & 3R) and Glu22 @ 1 site				
Total Energy	-113.386				
van der Waals	100.368				
electrostatic	-439.467				
ΔEs	-54.933				
	-8.189				
	-46.191				

	L	V	F	F	Gln15
Initial orientation		RB2	LB2		
Final Orientation		RB2			RS2
					RB2
Gd^{3+} chelates 2 SO_3^- @	5 sites (2R & 3L)				
Total Energy	-100.875				
van der Waals	104.577				
electrostatic	-428.22				
ΔEs	-42.422				
	-3.98				
	-34.944				

	L	V	F	F
Initial orientation		LB2		RB2
Final Orientation		LB2		
Gd^{3+} chelates 2 SO_3^- @	6 sites (3L & 3R)			
Total Energy	-92.015			
van der Waals	103.244			
electrostatic	-408.383			
ΔEs	-33.562			
	-5.313			
	-15.107			

	L	V	F	F	Ala21
Initial orientation		RB2		LB2	
Final Orientation	RB2				RB2
Gd^{3+} chelates 2 SO_3^- @	6 sites (3L & 3R)				
Total Energy	-71.138				
van der Waals	104.975				
electrostatic	-402.969				
ΔEs	-12.685				
	-3.582				
	-9.693				

	L	V	F	F	Ala21
Initial orientation	LB1	RB1			
Final Orientation	CS	RB1			CS
Gd^{3+} chelates 3 SO_3^- @	7 sites (3L & 2R & 2R)				
Total Energy	-99.926				
van der Waals	102.601				
electrostatic	-430.295				
ΔEs	-41.473				
	-5.956				
	-37.019				

	L	V	F	F	His14
Initial orientation	RB1	LB1			
Final Orientation	RB1	LB1			LS1
	RS1				
Gd^{3+} chelates 2 SO_3^- @	6 sites (3L & 3R)				
Total Energy	-141.52				
van der Waals	97.757				
electrostatic	-458.762				
ΔEs	-83.067				
	-10.8				
	-65.486				

Gas phase results of Solapsone-Gd^{3+} and the 1IYT conformer of Aβ

	H	H	Q	K	Leu17
Initial orientation	RB2	LB2			
Final Orientation	RB2	LB2			RB2
		LB2			RS2
Gd^{3+} chelates 3 SO_3^- @	5 sites (2R & 2L & 1L)				
Total Energy	-141.591				
van der Waals	89.125				
electrostatic	-456.242				
ΔEs	-44.35				
	-14.012				
	-32.257				

	H	H	Q	K
Initial orientation	LB2	RB2		
Final Orientation	LB2			
Gd^{3+} chelates 3 SO_3^- @	6 sites (3L &2R & 1R)			
Total Energy	-141.608			
van der Waals	95.575			
electrostatic	-460.869			
ΔEs	-44.367			
	-7.562			
	-36.884			

	H	H	Q	K
Initial orientation	RB1	LB1		
Final Orientation	RB1			
	RB1			
	CS			
	-CH2-			
Gd^{3+} chelates 2 SO_3^- @	6 sites (3R & 3L)			
Total Energy	-143.545			
van der Waals	97.022			
electrostatic	-465.065			
ΔEs	-46.304			
	-6.115			
	-41.08			

	H	H	Q	K	Gly9
Initial orientation	LB1	RB1			
Final Orientation	LB2	RB1			LB2
	LB2	CS			C=O
	LB1				
Gd^{3+} chelates 3 SO_3^- @	7 sites (3L & 2R & 2R)				
Total Energy	-174.374				
van der Waals	88.304				
electrostatic	-487.173				
ΔEs	-77.133				
	-14.833				
	-63.188				

	H	H	Q	K	Leu17
Initial orientation	LS1	RS1			
Final Orientation	LS1	RS1			RB2
	LS2				
Gd^{3+} chelates 2 SO_3^- @	5 sites (2R & 3L)				
Total Energy	-162.665				
van der Waals	90.547				
electrostatic	-478.553				
ΔEs	-65.424				
	-12.59				
	-54.568				

	H	H	Q	K	Leu17
Initial orientation	RS1	LS1			
Final Orientation	RS1	LS1			CS
	2				
	RB1				
Gd^{3+} chelates 2 SO_3^- @	5 sites (2R & 3L)				
Total Energy	-138.639				
van der Waals	99.072				
electrostatic	-460.098				
ΔEs	-41.398				
	-4.065				
	-36.113				

	H	H	Q	K
Initial orientation	LB2			RB2
Final Orientation	LB2			RB2
Gd^{3+} chelates 2 SO_3^- @	5 sites (2R & 3L)			
Total Energy	-119.625			
van der Waals	101.002			
electrostatic	-449.446			
ΔEs	-22.384			
	-2.135			
	-25.461			

	H	H	Q	K
Initial orientation	RB2			LB2
Final Orientation				
Gd^{3+} chelates 2 SO_3^- @	5 sites (2R & 3L)			
Total Energy	-123.108			
van der Waals	102.049			
electrostatic	-448.481			
ΔEs	-25.867			
	-1.088			
	-24.496			

	H	H	Q	K	Val12
Initial orientation	LB1			RB1	
Final Orientation	LB1			RS1	
	CS				
Gd^{3+} chelates 2 SO_3^- @	6 sites (3R & 3L)				
Total Energy	-152.622				
van der Waals	94.052				
electrostatic	-472.187				
ΔEs	-55.381				
	-9.085				
	-48.202				

	H	H	Q	K	Val12
Initial orientation	RB1			LB1	
Final Orientation	CS			LB1	CS
				LNH	
Gd^{3+} chelates 2 SO_3^- @	5 sites (2R & 3L)				
Total Energy	-134.33				
van der Waals	95.398				
electrostatic	-450.786				
ΔEs	-37.089				
	-7.739				
	-26.801				

	H	H	Q	K
Initial orientation	LS1			RS1
Final Orientation	LS1			RS1
Gd^{3+} chelates 2 SO_3^- @	5 sites (2R & 3L)			
Total Energy	-154.501			
van der Waals	97.145			
electrostatic	-472.797			
ΔEs	-57.26			
	-5.992			
	-48.812			

	H	H	Q	K
Initial orientation	RS1			LS1
Final Orientation	RS1			LS1
Gd^{3+} chelates 2 SO_3^- @	6 sites (3R & 3L)			
Total Energy	-161.525			
van der Waals	99.369			
electrostatic	-484.591			
ΔEs	-64.284			
	-3.768			
	-60.606			

	H	H	Q	K
Initial orientation	LS1			RS2
Final Orientation	LS1			LS1
				-CH2-
Gd^{3+} chelates 2 SO_3^- @	5 sites (2R & 3L)			
Total Energy	-143.833			
van der Waals	101.725			
electrostatic	-472.613			
ΔEs	-46.592			
	-1.412			
	-48.628			

	H	H	Q	K
Initial orientation	RS2			LS1
Final Orientation				LS1
Gd^{3+} chelates 2 SO_3^- @	4 sites (2L & 2R)			
Total Energy	-153.091			
van der Waals	96.523			
electrostatic	-470.832			
ΔEs	-55.85			
	-6.614			
	-46.847			

Initial orientation	RS1			LS2		
Final Orientation	RS1			LS2	LB2	
	LS1					
	LB2					
Gd^{3+} chelates 2 SO_3^- @	4 sites (2L & 2R)					
Total Energy	-156.797					
van der Waals	89.143					
electrostatic	-474.829					
ΔEs	-59.556					
	-13.994					
	-50.844					

	H	H	Q	K	Tyr10	Leu17
Initial orientation	LS2	RS1				
Final Orientation	RB1	RS1			RS1	RB2
	LS1					
	LS2					
	RS2					
Gd^{3+} chelates 2 SO_3^- @	5 sites (2R & 3L)					
Total Energy	-168.281					
van der Waals	88.104					
electrostatic	-482.299					
ΔEs	-71.04					
	-15.033					
	-58.314					

	H	H	Q	K	Leu17	
Initial orientation	RS2	LS1				
Final Orientation	RS1	LS1			RB1	
	RS2				LB1	
Gd^{3+} chelates 2 SO_3^- @	5 sites (2R & 3L)					
Total Energy	-164.573					
van der Waals	90.553					
electrostatic	-479.415					
ΔEs	-67.332					
	-12.584					
	-55.43					

	L	V	F	F		
Initial orientation	LB2	RB2				
Final Orientation		RB2				
Gd^{3+} chelates 2 SO_3^- @	5 sites (2R & 3L)					
Total Energy	-107.872					
van der Waals	102.762					
electrostatic	-435.377					
ΔEs	-10.631					
	-0.375					
	-11.392					

	L	V	F	F	Ala21	
Initial orientation	LB1	RB1				
Final Orientation	CS	CS			CS	
	LB1					
Gd^{3+} chelates 2 SO_3^- @	5 sites (2R & 3L)					
Total Energy	-119.66					
van der Waals	97.725					
electrostatic	-441.631					
ΔEs	-22.419					
	-5.412					
	-17.646					

	L	V	F	F		
Initial orientation		LB2	RB2			
Final Orientation						
Gd^{3+} chelates 2 SO_3^- @	5 sites (2R & 3L)					
Total Energy	-105.688					
van der Waals	99.973					
electrostatic	-430.959					
ΔEs	-8.447					
	-3.164					
	-6.974					

	L	V	F	F	Gln15	
Initial orientation		LB1	RB1			
Final Orientation		LB1			RB1	
		CS				
Gd^{3+} chelates 2 SO_3^- @	5 sites (2R & 3L)					
Total Energy	-131.417					
van der Waals	96.099					
electrostatic	-456.565					
ΔEs	-34.176					
	-7.038					
	-32.58					

Initial orientation	LS2			RS1		
Final Orientation				RS1		
Gd^{3+} chelates 2 SO_3^- @	5 sites (2R & 3L)					
Total Energy	-146.669					
van der Waals	102.184					
electrostatic	-475.052					
ΔEs	-49.428					
	-0.953					
	-51.067					

	H	H	Q	K	Tyr10	Leu17
Initial orientation	RS1	LS2				
Final Orientation	RS1	LS1			LB2	RB1
						LB1
Gd^{3+} chelates 2 SO_3^- @	6 sites (3R & 3L)					
Total Energy	-163.068					
van der Waals	96.339					
electrostatic	-487.4					
ΔEs	-65.827					
	-6.798					
	-63.415					

	L	V	F	F	His13	Lys16	Asp23
Initial orientation	RB2		LB2				
Final Orientation	RB2			RB2	RB2	RS2	LB2
				RS2		-CH2-	
						LS2	
Gd^{3+} chelates 2 SO_3^- @	5 sites (2R & 3L)						
Total Energy	-147.545						
van der Waals	92.242						
electrostatic	-471.439						
ΔEs	-50.304						
	-10.895						
	-47.454						

	L	V	F	F		
Initial orientation	RB2	LB2				
Final Orientation	RB2	LB2				
Gd^{3+} chelates 2 SO_3^- @	5 sites (2R & 3L)					
Total Energy	-119.017					
van der Waals	97.302					
electrostatic	-441.955					
ΔEs	-21.776					
	-5.835					
	-17.97					

	L	V	F	F	His14	
Initial orientation	RB1	LB1				
Final Orientation	CS	LB1			CS	
					-CH2-	
Gd^{3+} chelates 2 SO_3^- @	5 sites (2R & 3L)					
Total Energy	-123.924					
van der Waals	98.639					
electrostatic	-447.056					
ΔEs	-26.683					
	-4.498					
	-23.071					

	L	V	F	F		
Initial orientation		RB2	LB2			
Final Orientation			LB2			
Gd^{3+} chelates 2 SO_3^- @	6 sites (3R & 3L)					
Total Energy	-129.067					
van der Waals	100.634					
electrostatic	-456.136					
ΔEs	-31.826					
	-2.503					
	-32.151					

	L	V	F	F	His14	Gln15	Lys16
Initial orientation		RB1	LB1				
Final Orientation		RS1	LB1		RS1	RS1	LS1
		RB1	LS1		C=O	LS1	
			LNH				
Gd^{3+} chelates 2 SO_3^- @	5 sites (2R & 3L) and Gln15 @ 1 site						
Total Energy	-200.371						
van der Waals	84.014						
electrostatic	-504.165						
ΔEs	-103.13						
	-19.123						
	-80.18						

	L	V	F	F	His13	
Initial orientation	RB2			LB2		
Final Orientation					RB2	
Gd^{3+} chelates 2 SO_3^- @	4 sites (2L & 2R)					
Total Energy	-118.512					
van der Waals	97.496					
electrostatic	-441.275					
ΔEs	-21.271					
	-5.641					
	-17.29					

	L	V	F	F	Ala21	
Initial orientation	LB1			RB1		
Final Orientation	CS			RB1	CS	
	LB1			RS1		
Gd^{3+} chelates 2 SO_3^- @	6 sites (3R & 3L)					
Total Energy	-134.722					
van der Waals	92.936					
electrostatic	-452.022					
ΔEs	-37.481					
	-10.201					
	-28.037					

	L	V	F	F	Asp23	
Initial orientation			RB2	LB2		
Final Orientation					RB2	
Gd^{3+} chelates 2 SO_3^- @	5 sites (2R & 3L)					
Total Energy	-133.558					
van der Waals	99.75					
electrostatic	-460.299					
ΔEs	-36.317					
	-3.387					
	-36.314					

	L	V	F	F	Lys16	Asp23
Initial orientation			LB1	RB1		
Final Orientation				RB1	RB1	CS
Gd^{3+} chelates 3 SO_3^- @	7 sites (3R & 2L & 2L)					
Total Energy	-139.108					
van der Waals	94.479					
electrostatic	-461.082					
ΔEs	-41.867					
	-8.658					
	-37.097					

	L	V	F	F	Ala21	Lys28
Initial orientation		LB2		RB2		
Final Orientation					RB2	RS1
Gd^{3+} chelates 2 SO_3^- @	5 sites (2R & 3L)					
Total Energy	-148.741					
van der Waals	95.511					
electrostatic	-475.794					
ΔEs	-51.5					
	-7.626					
	-51.809					

	L	V	F	F		
Initial orientation	LB2			RB2		
Final Orientation						
Gd^{3+} chelates 3 SO_3^- @	6 sites (3L & 2R & 1R)					
Total Energy	-137.932					
van der Waals	99.749					
electrostatic	-458.98					
ΔEs	-40.691					
	-3.388					
	-34.995					

	L	V	F	F	His13	
Initial orientation	RB1			LB1		
Final Orientation	RB1			LB1	RB1	
				CS	RB2	
					RNH	
Gd^{3+} chelates 2 SO_3^- @	5 sites (2R & 3L)					
Total Energy	-136.958					
van der Waals	88.444					
electrostatic	-455.313					
ΔEs	-39.717					
	-14.693					
	-31.328					

	L	V	F	F		
Initial orientation			LB2	RB2		
Final Orientation			LB2			
Gd^{3+} chelates 2 SO_3^- @	5 sites (2R & 3L)					
Total Energy	-126.371					
van der Waals	98.232					
electrostatic	-450.218					
ΔEs	-29.13					
	-4.905					
	-26.233					

	L	V	F	F	Lys16	Asp23
Initial orientation			RB1	LB1		
Final Orientation			CS	LB1	RB1	CS
			RB1	CS	LB1	
					CS	
Gd^{3+} chelates 2 SO_3^- @	6 sites (3R & 3L)				RS1	
Total Energy	-136.626					
van der Waals	90.847					
electrostatic	-451.454					
ΔEs	-39.385					
	-12.29					
	-27.469					

	L	V	F	F		
Initial orientation		RB2		LB2		
Final Orientation						
Gd^{3+} chelates 2 SO_3^- @	5 sites (2R & 3L)					
Total Energy	-120.919					
van der Waals	101.347					
electrostatic	-449.503					
ΔEs	-23.678					
	-1.79					
	-25.518					

Gas phase results of Solapsone-Gd^{3+} and the 1Z0Q conformer of Aβ

	H	H	Q	K	Gly9	
Initial orientation	LB2	RB2				
Final Orientation		RB2			LB2	
					C=O	
Gd^{3+} chelates 2 SO_3^- @	5 sites (3L & 2R)					
Total Energy	-13.469					
van der Waals	126.557					
electrostatic	-436.104					
ΔEs	-26.753					
	-2.012					
	-31.325					

	H	H	Q	K	Gly9
Initial orientation	RB2	LB2			
Final Orientation	LB2				RB2
					C=O
Gd^{3+} chelates 2 SO_3^- @	5 sites (3L & 2R)				
Total Energy	-13.601				
van der Waals	125.012				
electrostatic	-429.435				
ΔEs	-26.885				
	-3.557				
	-24.656				

	H	H	Q	K	Tyr10
Initial orientation	RB1	LB1			
Final Orientation	RS1	CS			CS
	RB1				-CH2-
	-CH2-				
Gd^{3+} chelates 2 SO_3^- @	6 sites (3L & 3R)				
Total Energy	-35.425				
van der Waals	115.699				
electrostatic	-441.13				
ΔEs	-48.709				
	-12.87				
	-36.351				

	H	H	Q	K
Initial orientation	LB1	RB1		
Final Orientation	LB1	RB1		CS
		CS		-CH2-
		-CH-		LB1
Gd^{3+} chelates 2 SO_3^- @	5 sites (3L & 2R)			
Total Energy	-43.557			
van der Waals	116.453			
electrostatic	-451.368			
ΔEs	-56.841			
	-12.116			
	-46.589			

	H	H	Q	K	Gly9	Tyr10
Initial orientation	LS1	RS1				
Final Orientation	LS1	RS1			LS1	LB1
					C=O	-CH2-
Gd^{3+} chelates 2 SO_3^- @	4 sites (2R & 2L)					
Total Energy	-64.808					
van der Waals	121.901					
electrostatic	-480.659					
ΔEs	-78.092					
	-6.668					
	-75.88					

	H	H	Q	K	Leu17
Initial orientation	RS1	LS1			
Final Orientation	RS1	LS1			CS
		LB1			
Gd^{3+} chelates 2 SO_3^- @	6 sites (3L & 3R)				
Total Energy	-62.752				
van der Waals	118.78				
electrostatic	-475.264				
ΔEs	-76.036				
	-9.789				
	-70.485				

	H	H	Q	K	Gly9	Tyr10
Initial orientation	LS1	RS2				
Final Orientation	LS1	RS2			LS1	LS1
		RS1			C=O	-CH2-
Gd^{3+} chelates 2 SO_3^- @	5 sites (3L & 2R)					
Total Energy	-46.413					
van der Waals	119.419					
electrostatic	-457.88					
ΔEs	-59.697					
	-9.15					
	-53.101					

	H	H	Q	K	Gly9	Tyr10
Initial orientation	RS2	LS1				
Final Orientation	RS1	LS1		RS1	RS2	LS1
	RB2				C=O	
	RS2					
Gd^{3+} chelates 2 SO_3^- @	6 sites (3L & 3R)					
Total Energy	-59.7					
van der Waals	116.266					
electrostatic	-473.408					
ΔEs	-72.984					
	-12.303					
	-68.629					

	H	H	Q	K
Initial orientation	RB2			LB2
Final Orientation	RB2			
Gd^{3+} chelates 2 SO_3^- @	5 sites (3L & 2R)			
Total Energy	-5.112			
van der Waals	128.211			
electrostatic	-427.083			
ΔEs	-18.396			
	-0.358			
	-22.304			

	H	H	Q	K
Initial orientation	LB2			RB2
Final Orientation				RB2
Gd^{3+} chelates 2 SO_3^- @	4 sites (2R & 2L)			
Total Energy	2.001			
van der Waals	123.436			
electrostatic	-414.633			
ΔEs	-11.283			
	-5.133			
	-9.854			

	H	H	Q	K
Initial orientation	LB1			RB1
Final Orientation	LS1			RB1
	CS			RS1
	-CH2-			2
Gd^{3+} chelates 2 SO_3^- @	6 sites (3L & 3R)			
Total Energy	-47.759			
van der Waals	121.271			
electrostatic	-462.808			
ΔEs	-61.043			
	-7.298			
	-58.029			

	H	H	Q	K
Initial orientation	RB1			LB1
Final Orientation	RS1			LB1
	RB1			
Gd^{3+} chelates 2 SO_3^- @	6 sites (3L & 3R)			
Total Energy	-39.749			
van der Waals	123.227			
electrostatic	-461.035			
ΔEs	-53.033			
	-5.342			
	-56.256			

	H	H	Q	K
Initial orientation	LS1			SR1
Final Orientation	LS1			SR1
Gd^{3+} chelates 2 SO_3^- @	6 sites (3L & 3R)			
Total Energy	-39.902			
van der Waals	124.088			
electrostatic	-455.965			
ΔEs	-53.186			
	-4.481			
	-51.186			

	H	H	Q	K
Initial orientation	RS1			LS1
Final Orientation	RS1			LS1
				2
Gd^{3+} chelates 2 SO_3^- @	5 sites (3L & 2R)			
Total Energy	-42.868			
van der Waals	127.927			
electrostatic	-458.958			
ΔEs	-56.152			
	-0.642			
	-54.179			

	H	H	Q	K	Gly9	Tyr10	
Initial orientation	LS2			RS1			
Final Orientation	LS2	LS1		RS1	LB2	LS1	
	LS1	-NH-			C=O	-CH2-	
	-CH2-						
Gd^{3+} chelates 2 SO_3^- @	5 sites (3L & 2R)						
Total Energy	-43.614						
van der Waals	120.136						
electrostatic	-459.888						
ΔEs	-56.898						
	-8.433						
	-55.109						

	H	H	Q	K			
Initial orientation	RS1			LS2			
Final Orientation	RS1			LS1			
Gd^{3+} chelates 2 SO_3^- @	6 sites (3L & 3R)						
Total Energy	-32.737						
van der Waals	125.674						
electrostatic	-449.807						
ΔEs	-46.021						
	-2.895						
	-45.028						

	H	H	Q	K			
Initial orientation	LS1			RS2			
Final Orientation	LS1			RS1			
				-CH2-			
Gd^{3+} chelates 2 SO_3^- @	5 sites (3L & 2R)						
Total Energy	-32.379						
van der Waals	123.86						
electrostatic	-447.177						
ΔEs	-45.663						
	-4.709						
	-42.398						

	H	H	Q	K			
Initial orientation	RS2			LS1			
Final Orientation	LS1			LS1			
Gd^{3+} chelates 2 SO_3^- @	5 sites (3L & 2R)						
Total Energy	-37.648						
van der Waals	124.363						
electrostatic	-456.059						
ΔEs	-50.932						
	-4.206						
	-51.28						

	H	H	Q	K			
Initial orientation		RB2		LB2			
Final Orientation		RB2					
Gd^{3+} chelates 2 SO_3^- @	5 sites (3L & 2R)						
Total Energy	-10.22						
van der Waals	125.242						
electrostatic	-429.447						
ΔEs	-23.504						
	-3.327						
	-24.668						

	H	H	Q	K	Leu17		
Initial orientation		LB2		RB2			
Final Orientation		LB2		RB2	RS2		
				RS2			
				-CH2-			
Gd^{3+} chelates 2 SO_3^- @	5 sites (3L & 2R)						
Total Energy	-20.754						
van der Waals	120.767						
electrostatic	-438.291						
ΔEs	-34.038						
	-7.802						
	-33.512						

	H	H	Q	K	Tyr10		
Initial orientation		LS1		RS1			
Final Orientation	RB2	LS1		RS1	LS1		
				2	-CH2-		
Gd^{3+} chelates 2 SO_3^- @	5 sites (3L & 2R)						
Total Energy	-62.557						
van der Waals	119.035						
electrostatic	-474.412						
ΔEs	-75.841						
	-9.534						
	-69.633						

	H	H	Q	K	Gly9	Tyr10	
Initial orientation		RS1		LS1			
Final Orientation	LB1	RS1		LS1	CS	CS	
					C=O	-CH2-	
Gd^{3+} chelates 2 SO_3^- @	6 sites (3L & 3R)						
Total Energy	-72.103						
van der Waals	121.535						
electrostatic	-484.648						
ΔEs	-85.387						
	-7.034						
	-79.869						

	L	V	F	F	Ala21		
Initial orientation	LB2	RB2					
Final Orientation	LB2				RB2		
Gd^{3+} chelates 2 SO_3^- @	5 sites (3L & 2R)						
Total Energy	-8.364						
van der Waals	122.979						
electrostatic	-425.819						
ΔEs	-21.648						
	-5.59						
	-21.04						

	L	V	F	F	Ala21		
Initial orientation	RB2	LB2					
Final Orientation	RB2			RB2	LB2		
					C=O		
Gd^{3+} chelates 2 SO_3^- @	5 sites (3L & 2R)						
Total Energy	-19.887						
van der Waals	119.496						
electrostatic	-434.914						
ΔEs	-33.171						
	-9.073						
	-30.135						

	L	V	F	F	His14	Ala21	Glu22
Initial orientation	LB1	RB1					
Final Orientation	LB1	CS			RB1	CS	CS
					RNH	LB1	-CH2-
Gd^{3+} chelates 2 SO_3^- @	6 sites (3L & 3R)						
Total Energy	-23.729						
van der Waals	111.479						
electrostatic	-427.482						
ΔEs	-37.013						
	-17.09						
	-22.703						

	L	V	F	F	His14	Lys16	Ala21
Initial orientation	RB1	LB1					
Final Orientation	CS	LB1			LS1	RS1	CS
	RB1					-CH2-	
Gd^{3+} chelates 2 SO_3^- @	6 sites (3L & 3R)						
Total Energy	-47.102						
van der Waals	114.657						
electrostatic	-452.594						
ΔEs	-60.386						
	-13.912						
	-47.815						

	L	V	F	F			
Initial orientation	RB2			LB2			
Final Orientation	RB2						
Gd^{3+} chelates 2 SO_3^- @	5 sites (3L & 2R)						
Total Energy	10.709						
van der Waals	125.845						
electrostatic	-405.989						
ΔEs	-2.575						
	-2.724						
	-1.21						

	L	V	F	F			
Initial orientation	LB2			RB2			
Final Orientation							
Gd^{3+} chelates 2 SO_3^- @	5 sites (3L & 2R)						
Total Energy	12.822						
van der Waals	126.816						
electrostatic	-405.075						
ΔEs	-0.462						
	-1.753						
	-0.296						

	L	V	F	F				L	V	F	F		
Initial orientation	RB1			LB1			Initial orientation	LB1			RB1		
Final Orientation	RB1			LB1			Final Orientation	LB1			RB1		
				CS							CS		
Gd^{3+} chelates 2 SO_3^- @	5 sites (3L & 2R)						Gd^{3+} chelates 2 SO_3^- @	5 sites (3L & 2R)					
Total Energy	1.62						Total Energy	-11.024					
van der Waals	122.113						van der Waals	121.182					
electrostatic	-405.695						electrostatic	-430.89					
ΔEs	-11.664						ΔEs	-24.308					
	-6.456							-7.387					
	-0.916							-26.111					
	L	V	F	F				L	V	F	F	Gln15	
Initial orientation		LB2	RB2				Initial orientation		RB2	LB2			
Final Orientation							Final Orientation		RB2			RB2	
Gd^{3+} chelates 2 SO_3^- @	5 sites (3L & 2R)						Gd^{3+} chelates 2 SO_3^- @	6 sites (3L & 3R)					
Total Energy	-51.289						Total Energy	-51.939					
van der Waals	124.161						van der Waals	128.101					
electrostatic	-468.293						electrostatic	-474.913					
ΔEs	-64.573						ΔEs	-65.223					
	-4.408							-0.468					
	-63.514							-70.134					
	L	V	F	F				L	V	F	F	Ala21	Val24
Initial orientation		LB2		RB2			Initial orientation		RB2		LB2		
Final Orientation							Final Orientation	RB2	RB2			RS2	LB2
Gd^{3+} chelates 2 SO_3^- @	5 sites (3L & 2R)						Gd^{3+} chelates 2 SO_3^- @	5 sites (3L & 2R)					
Total Energy	-16.594						Total Energy	-23.358					
van der Waals	124.503						van der Waals	117.829					
electrostatic	-435.428						electrostatic	-439.61					
ΔEs	-29.878						ΔEs	-36.642					
	-4.066							-10.74					
	-30.649							-34.831					
	L	V	F	F				L	V	F	F		
Initial orientation	RB2		LB2				Initial orientation	LB2		RB2			
Final Orientation	RB2						Final Orientation	LB2		RB2			
Gd^{3+} chelates 2 SO_3^- @	5 sites (3L & 2R)						Gd^{3+} chelates 3 SO_3^- @	7 sites (3L & 2R & 2R)					
Total Energy	-7.003						Total Energy	-33.049					
van der Waals	124.71						van der Waals	122.21					
electrostatic	-424.977						electrostatic	-450.006					
ΔEs	-20.287						ΔEs	-46.333					
	-3.859							-6.359					
	-20.198							-45.227					
	L	V	F	F	Lys16			L	V	F	F		
Initial orientation	LB1		RB1				Initial orientation	RB1		LB1			
Final Orientation	LB1		CS	CS	LS1		Final Orientation	RB1			CS		
				-CH2-	LB1								
				RB1	LNH								
Gd^{3+} chelates 3 SO_3^- @	7 sites (3L & 2R & 2R)						Gd^{3+} chelates 2 SO_3^- @	5 sites (3L & 2R)					
Total Energy	-62.934						Total Energy	-3.936					
van der Waals	115.145						van der Waals	121.682					
electrostatic	-476.384						electrostatic	-415.945					
ΔEs	-76.218						ΔEs	-17.22					
	-13.424							-6.887					
	-71.605							-11.166					
	L	V	F	F				L	V	F	F		
Initial orientation			RB2	LB2			Initial orientation			LB2	RB2		
Final Orientation							Final Orientation				RB2		
Gd^{3+} chelates 2 SO_3^- @	5 sites (3L & 2R)						Gd^{3+} chelates 2 SO_3^- @	5 sites (3L & 2R)					
Total Energy	9.348						Total Energy	5.17					
van der Waals	126.144						van der Waals	125.277					
electrostatic	-407.448						electrostatic	-410.119					
ΔEs	-3.936						ΔEs	-8.114					
	-2.425							-3.292					
	-2.669							-5.34					
	L	V	F	F				L	V	F	F		
Initial orientation			LB1	RB1			Initial orientation			RB1	LB1		
Final Orientation	RS2		RB1	RB1			Final Orientation	CS			LB1		
	RB2			RB2				RB1			CS		
Gd^{3+} chelates 3 SO_3^- @	7 sites (3L & 2R & 2R)						Gd^{3+} chelates 2 SO_3^- @	5 sites (3L & 2R)					
Total Energy	-36.079						Total Energy	-29.971					
van der Waals	118.414						van der Waals	119.226					
electrostatic	-443.942						electrostatic	-442.937					
ΔEs	-49.363						ΔEs	-43.255					
	-10.155							-9.343					
	-39.163							-38.158					

Gas phase results of solapsone and the 1AMB conformer of Aβ

	H	H	Q	K	Tyr10				H	H	Q	K	Leu17		
Initial Orientation	RB2	LB2						Initial Orientation	LB2	RB2					
Final Orientation		LB2			RB2			Final Orientation	LB1	RB2		LS1	RB1		
		LB2			RNH				LS2	RB2		LB2	LB1		
										RS2			LNH		
Total Energy	14.658							Total Energy	-35.275						
van der Waals	90.634							van der Waals	79.81						
electrostatic	-245.836							electrostatic	-288.134						
ΔEs	-54.683							ΔEs	-104.616						
	-5.204								-16.028						
	-54.943								-97.241						
	H	H	Q	K	Leu17				H	H	Q	K	Leu17		
Initial Orientation	LB1	RB1						Initial Orientation	RB1	LB1					
Final Orientation	LS1	RS1			LS1			Final Orientation	RS1	LB1			RS1		
										LS1			RNH		
Total Energy	-7.541							Total Energy	-0.643						
van der Waals	87.459							van der Waals	85.713						
electrostatic	-262.09							electrostatic	-254.618						
ΔEs	-76.882							ΔEs	-69.984						
	-8.379								-10.125						
	-71.197								-63.725						
	H	H	Q	K	Tyr10	Leu17			H	H	Q	K	Leu17		
Initial Orientation	LS2	RS2						Initial Orientation	RS2	LS2					
Final Orientation	LS2	RS2			LB1	LS2		Final Orientation	RS2	LS2			RS2		
					CS				RB2						
Total Energy	-2.225							Total Energy	-3.11						
van der Waals	88.489							van der Waals	88.411						
electrostatic	-256.779							electrostatic	-258.513						
ΔEs	-71.566							ΔEs	-72.451						
	-7.349								-7.427						
	-65.886								-67.62						
	H	H	Q	K					H	H	Q	K	Tyr10	Phe20	
Initial Orientation	LB2			RB2				Initial Orientation	RB2			LB2			
Final Orientation	LS2			RS2				Final Orientation	RB1			LNH	RS2	LS2	
				RB2					RS2				RB2		
Total Energy	-26.291							Total Energy	-44.369						
van der Waals	89.911							van der Waals	82.756						
electrostatic	-283.522							electrostatic	-301.915						
ΔEs	-95.632							ΔEs	-113.71						
	-5.927								-13.082						
	-92.629								-111.022						
	H	H	Q	K	Gly9	Tyr10			H	H	Q	K	Tyr10	Leu17	Phe20
Initial Orientation	RB1			LB1				Initial Orientation	LB1			RB1			
Final Orientation	RB1			LS1	RS1	RS1		Final Orientation	LB1			RS1	LS1	RS1	RS1
	CS			LS2	C=O				LS1			RS2			
	RS2			RB1*								2			
	RS1*			CS*											
	*-CH2-			*-CH2-											
Total Energy	-66.619							Total Energy	-59.55						
van der Waals	77.328							van der Waals	82.213						
electrostatic	-315.198							electrostatic	-311.885						
ΔEs	-135.96							ΔEs	-128.891						
	-18.51								-13.625						
	-124.305								-120.992						
	H	H	Q	K	Leu17	Phe20			H	H	Q	K	Leu17	Phe20	
Initial Orientation	LS2			RS2				Initial Orientation	RS2			LS2			
Final Orientation	LS2			RS2	LB1	RB1		Final Orientation	RS2			LS2	RS2	LB2	
				2	LS2	RS2			2			2		LS2	
						RS1			RS1			LS1			
						CS						-CH2-			
Total Energy	-36.571							Total Energy	-64.123						
van der Waals	80.846							van der Waals	81.842						
electrostatic	-282.505							electrostatic	-312.527						
ΔEs	-105.912							ΔEs	-133.464						
	-14.992								-13.996						
	-91.612								-121.634						
	H	H	Q	K	Phe20				H	H	Q	K	Leu17	PHe20	
Initial Orientation	CS			LS2				Initial Orientation	LS2			CS			
Final Orientation	RS2			LS2	LB2			Final Orientation	LS2			RB1	CS	RB1	
	2			2					RS2			RS2	LB1	CS	
				LS1									LS1		
Total Energy	-57.396			-CH2-				Total Energy	-50.849						
van der Waals	85.969							van der Waals	80.284						
electrostatic	-309.595							electrostatic	-302.776						
ΔEs	-126.737							ΔEs	-120.19						
	-9.869								-15.554						
	-118.702								-111.883						
	H	H	Q	K	Phe20				H	H	Q	K	Tyr10	Leu17	Phe20
Initial Orientation	RS2			CS				Initial Orientation	CS			RS2			
Final Orientation	RS2			CS	LS2			Final Orientation	RB1			RS2	LS2	RS1	RS1
	RS1			RB1					CS					RB1	
									LS2					CS	
Total Energy	-36.365							Total Energy	-57.995						
van der Waals	85.483							van der Waals	79.286						
electrostatic	-291.551							electrostatic	-306.139						
ΔEs	-105.706							ΔEs	-127.336						
	-10.355								-16.552						
	-100.658								-115.246						

	H	H	Q	K	His6	Gly9	Tyr10	Leu17	Phe20
Initial Orientation	CS			LS1					
Final Orientation	RB1			LS1	RS1	RS1	RS1	LS2	LS2
	LB1			2		C=O		LS1	LS1
	RNH							LB1	-CH2-
	RS1								
	-CH2-								
Total Energy	-70.529								
van der Waals	74.462								
electrostatic	-323.936								
ΔEs	-139.87								
	-21.376								
	-133.043								

	H	H	Q	K	Leu17	Phe20	Lys28
Initial Orientation	RS1			CS			
Final Orientation	RS2			RB1	RB1	LB1	LS2
	RS1			RS1	RS2	CS	
				CS			
Total Energy	-54.786						
van der Waals	80.166						
electrostatic	-303.796						
ΔEs	-124.127						
	-15.672						
	-112.903						

	H	H	Q	K	Leu17	Phe20
Initial Orientation	CS			LB1		
Final Orientation	RB1			LS1	CS	LS1
	CS					LS2
Total Energy	-16.694					
van der Waals	90.638					
electrostatic	-273.387					
ΔEs	-86.035					
	-5.2					
	-82.494					

	H	H	Q	K	Tyr10	Leu17
Initial Orientation	RB1			CS		
Final Orientation	RB1			LS1	RS1	CS
	RS1					
Total Energy	-49.527					
van der Waals	85.642					
electrostatic	-301.77					
ΔEs	-118.868					
	-10.196					
	-110.877					

	H	H	Q	K	His6	Gly9	Tyr10	Leu17	Phe20
Initial Orientation	LB1			RS1					
Final Orientation	RB1			RS1	LS2	LS1	LS1	RS1	RS1
	LB1			RS2	LS1	C=O			
	LS1				LB2				
	-CH2-								
Total Energy	-86.458								
van der Waals	75.566								
electrostatic	-327.173								
ΔEs	-155.799								
	-20.272								
	-136.28								

	H	H	Q	K	Leu17
Initial Orientation	RB1			LS1	
Final Orientation	LB1			LS2	CS
	CS			LS1	
	RB1			-CH2-	
Total Energy	-39.046				
van der Waals	87.14				
electrostatic	-292.786				
ΔEs	-108.387				
	-8.698				
	-101.893				

	H	H	Q	K
Initial Orientation	RS2			LB2
Final Orientation	RB1			LS2
	RS2			LB2
Total Energy	-35.007			
van der Waals	85.816			
electrostatic	-290.411			
ΔEs	-104.348			
	-10.022			
	-99.518			

	H	H	Q	K	His6	Gly9	Tyr10	Leu17	Phe20
Initial Orientation	LB1			RS2					
Final Orientation	LB1			RS1	LB2	LB2	LS2	CS	RS1
	LS2			RS2		C=O	LB2		
	LB2			-CH2-					
Total Energy	-58.545								
van der Waals	73.264								
electrostatic	-302.24								
ΔEs	-127.886								
	-22.574								
	-111.347								

	H	H	Q	K	Leu17	Phe20	Lys28
Initial Orientation	LS1			CS			
Final Orientation	LS1			LB1	CS	RB1	RS1
	LB1			LS2	LB1	RS1	
				LS1		CS	
				-CH2-			
Total Energy	-44.148						
van der Waals	79.772						
electrostatic	-298.529						
ΔEs	-113.489						
	-16.066						
	-107.636						

	H	H	Q	K	Leu17
Initial Orientation	CS			RS1	
Final Orientation	RB1			RS1	RS1
	CS				
	RS1				
	RS2				
Total Energy	-35.809				
van der Waals	87.059				
electrostatic	-290.215				
ΔEs	-105.15				
	-8.779				
	-99.322				

	H	H	Q	K	Leu17	Phe20	Lys28
Initial Orientation	LB1			CS			
Final Orientation	LS1			LB1	RS1	RB1	RS2
				LS1		RS2	
				LS2		RS1	
				-CH2-			
Total Energy	-67.71						
van der Waals	74.669						
electrostatic	-311.419						
ΔEs	-137.051						
	-21.169						
	-120.526						

	H	H	Q	K	Tyr10	Leu17	Phe20
Initial Orientation	CS			RB1			
Final Orientation	LB1	LS1		RS1	LB2	RB1	RS1
	LS1	-CH2-		2	LS2		
	CS						
Total Energy	-62.546						
van der Waals	79.218						
electrostatic	-313.269						
ΔEs	-131.887						
	-16.62						
	-122.376						

	H	H	Q	K	Tyr10	Leu17	Phe20
Initial Orientation	RS1			LB1			
Final Orientation	RS2			LS2	RB2	CS	LB1
	RS1			2		LB1	LNH
	RB1			LB2			LS1
				-CH2-			LB2
Total Energy	-62.135						
van der Waals	77.901						
electrostatic	-316.209						
ΔEs	-131.476						
	-17.937						
	-125.316						

	H	H	Q	K	Tyr10	Leu17	Phe20
Initial Orientation	LS1			RB1			
Final Orientation	LB1	LS1		RS1	LB2	RS1	RS1
	LS1	-CH2-		RS2		LB1	
	LS2			2		LS1	
Total Energy	-85.251						
van der Waals	74.781						
electrostatic	-328.792						
ΔEs	-154.592						
	-21.057						
	-137.899						

	H	H	Q	K
Initial Orientation	LB2			RS2
Final Orientation	LS2			RS2
				2
Total Energy	-23.542			
van der Waals	93.314			
electrostatic	-283.717			
ΔEs	-92.883			
	-2.524			
	-92.824			

	H	H	Q	K	Tyr10	Phe20
Initial Orientation	RB1			LS2		
Final Orientation	LS1	RS2		LS2	RS1	LB2
	RB1	-CH-		2	RS2	
	RNH			LS1	C=O	
	RS2			-CH2-		
Total Energy	-81.424					
van der Waals	77.391					
electrostatic	-330.032					
ΔEs	-150.765					
	-18.447					
	-139.139					

	H	H	Q	K													
Initial Orientation	LS2			RB1													
Final Orientation	LS2			RS2													
Total Energy	-18.394																
van der Waals	93.624																
electrostatic	-281.066																
ΔEs	-87.735																
	-2.214																
	-90.173																
	H	H	Q	K	Tyr10	Val18						H	H	Q	K	Tyr10	Val18
Initial Orientation	RS1	CS									Initial Orientation	CS	RS1				
Final Orientation	RS1	RS1			RS2	CS					Final Orientation	LB1	CS			LB1	RS1
		-CH-										LS2	-CH-			CS	
		CS										LS1	RS1			RB1	
												CS					
Total Energy	-0.188										Total Energy	-36.629					
van der Waals	84.607										van der Waals	76.849					
electrostatic	-253.202										electrostatic	-289.707					
ΔEs	-69.529										ΔEs	-105.97					
	-11.231											-18.989					
	-62.309											-98.814					
	H	H	Q	K	Tyr10	Leu17	Phe20					H	H	Q	K	Try10	Leu17	Val18
Initial Orientation	CS	RS2									Initial Orientation	RS2	CS					
Final Orientation	LB1	RS2		LS2	RS1	LS2	LS2				Final Orientation	RS2	RB1			RS2	RS1	RS1
		-CH2-		2			LB2						CS			C=O		
													RS1					
													-CH-					
													RS2					
													-CH2-					
Total Energy	-54.42										Total Energy	-6.136					
van der Waals	82.737										van der Waals	81.385					
electrostatic	-310.403										electrostatic	-259.023					
ΔEs	-123.761										ΔEs	-75.477					
	-13.101											-14.453					
	-119.51											-68.13					
	H	H	Q	K	Tyr10	Glu11	Leu17	Val18	Glu22			H	H	Q	K	His6	Gly9	Tyr10
Initial Orientation	LS2	CS									Initial Orientation	CS	LS2					
Final Orientation	LS2	RS2	RS2		LS1	CS	LB1	RB2	RB2		Final Orientation	RB1	CS			RB2	RS2	RS2
		2				-CH2-						RS2	-CH2-				C=O	RB1
		RB1										CS	LS2					
		CS																
		LB1																
		LS2																
		-CH2-																
Total Energy	-26.567										Total Energy	-39.49					
van der Waals	75.552										van der Waals	71.273					
electrostatic	-272.675										electrostatic	-288.886					
ΔEs	-95.908										ΔEs	-108.831					
	-20.286											-24.565					
	-81.782											-97.993					
	H	H	Q	K	Tyr10	Leu17						H	H	Q	K	Tyr10	
Initial Orientation	LB1	RS1									Initial Orientation	RS1	LB1				
Final Orientation	LB1	CS			LS1	CS					Final Orientation	RS1	LB1	LS1		RS2	
	LS2	-CH-			LB1								LS1				
	LS1	RB1											RS1				
	CS	-CH2-											-CH2-				
		RS1											LNH				
Total Energy	-37.222										Total Energy	-14.897					
van der Waals	78.84										van der Waals	82.849					
electrostatic	-286.891										electrostatic	-265.747					
ΔEs	-106.563										ΔEs	-84.238					
	-16.998											-12.989					
	-95.998											-74.854					
	H	H	Q	K	Leu17							H	H	Q	K	Tyr10	Leu17
Initial Orientation	LS1	RB1									Initial Orientation	RB1	LS2				
Final Orientation	LS1	RS1			LS1						Final Orientation	RB1	LS2			RS2	CS
												RS1					
												RS2					
Total Energy	-7.563										Total Energy	-37.813					
van der Waals	87.6										van der Waals	81.639					
electrostatic	-262.152										electrostatic	-290.705					
ΔEs	-76.904										ΔEs	-107.154					
	-8.238											-14.199					
	-71.259											-99.812					
	H	H	Q	K	Tyr10	Leu17	Val18					H	H	Q	K	Leu17	Val18
Initial Orientation	LB1	RS2									Initial Orientation	RS2	LB2				
Final Orientation	LB1	RS2		LS2	CS	LS2	RS2				Final Orientation	RB1	LB2		RS2	LS2	LS2
	LS2					LB1						RS2	LS2				
	LS1											RNH	-CH2-				
Total Energy	-42.851										Total Energy	-54.195					
van der Waals	81.753										van der Waals	75.935					
electrostatic	-297.33										electrostatic	-302.613					
ΔEs	-112.192										ΔEs	-123.536					
	-14.085											-19.903					
	-106.437											-111.72					
	H	H	Q	K	Tyr10	Leu17						H	H	Q	K	Glu11	Leu17
Initial Orientation	LB2	RS2									Initial Orientation	RB2	LS2				
Final Orientation	LB2	LS2	RS2		LS1	LB2					Final Orientation	RB1	LB2		RS2	LB2	RB1
	LS2	-CH2-	RB2			LS2						RS2	LS1		2		
		RS2															
		RB2															
Total Energy	-25.724										Total Energy	-43.477					
van der Waals	79.387										van der Waals	81.892					
electrostatic	-273.467										electrostatic	-295.929					
ΔEs	-95.065										ΔEs	-112.818					
	-16.451											-13.946					
	-82.574											-105.036					
	H	H	Q	K	Tyr10	Leu17	Phe20					H	H	Q	K	Glu11	Leu17	Val18
Initial Orientation		RB2		LB2							Initial Orientation		LB2		RB2			
Final Orientation	LB1	RB2		LB2	RS2	LS2	LB2				Final Orientation	RB1	LB2		RB2	LB2	RS2	LS2
	LS2			LS2		LB1						RNH	LB2		RS2			
	LS1												LS2					
Total Energy	-60.376										Total Energy	-31.426					
van der Waals	73.27										van der Waals	82.152					
electrostatic	-306.118										electrostatic	-284.056					
ΔEs	-129.717										ΔEs	-100.767					
	-22.568											-13.686					
	-115.225											-93.163					

	L	V	F	F	Ala21	Lys28
Initial Orientation	LB1	RB1				
Final Orientation	LS1			LS1	CS	LS2
Total Energy	-17.898					
van der Waals	84.625					
electrostatic	-269.275					
ΔFs	-87.239					
	-11.213					
	-78.382					

	L	V	F	F	Ala21	Lys28
Initial Orientation	RB1	LB1				
Final Orientation	CS			RS1	RS1	RB2
	RB1					RS1
Total Energy	-16.438					
van der Waals	80.217					
electrostatic	-265.083					
ΔFs	-85.779					
	-15.621					
	-74.19					

	L	V	F	F	His13	His14	Lys16
Initial Orientation	LB1	RB2					
Final Orientation	LS2	RS2	RB2	LB2	LS2	RS2	LB2
							LS2
Total Energy	-29.528						
van der Waals	82.827						
electrostatic	-279.741						
ΔFs	-98.869						
	-13.011						
	-88.848						

	L	V	F	F	His14
Initial Orientation	RB2	LB2			
Final Orientation					LB2
					LB2
Total Energy	22.727				
van der Waals	86.961				
electrostatic	-235.178				
ΔFs	-46.614				
	-8.877				
	-44.285				

	L	V	F	F	Glu22
Initial Orientation	RB2		LB2		
Final Orientation					LB2
Total Energy	62.194				
van der Waals	92.234				
electrostatic	-200.117				
ΔFs	-7.147				
	-3.604				
	-9.224				

	L	V	F	F
Initial Orientation	LB2		RB2	
Final Orientation				
Total Energy	55.716			
van der Waals	95.509			
electrostatic	-205.188			
ΔFs	-13.625			
	-0.329			
	-14.295			

	L	V	F	F	His13	Lys16	Lys28
Initial Orientation	LB1			RB1			
Final Orientation	LS1			CS	LS2	LS2	RS1
				RB1	LS1	LS1	
						LB1	
Total Energy	-52.866						
van der Waals	83.566						
electrostatic	-308.175						
ΔFs	-122.207						
	-12.272						
	-117.282						

	L	V	F	F	His13	Lys16	Lys28
Initial Orientation	RB1			LB1			
Final Orientation	RS1			CS	RS1	LS2	
	RB1			LB1		2	
				LS1			
Total Energy	-26.326						
van der Waals	85.752						
electrostatic	-280.005						
ΔFs	-95.667						
	-10.086						
	-89.112						

	L	V	F	F	Lys16	Lys28
Initial Orientation	LB2			RB1		
Final Orientation	LB2			LS2	RS2	LS1
				LB1		LS2
				RB1		
Total Energy	-51.46					
van der Waals	84.505					
electrostatic	-305.46					
ΔFs	-120.801					
	-11.333					
	-114.567					

	L	V	F	F	Lys16	Lys28
Initial Orientation	RB2			LB1		
Final Orientation	RS2			LS2	LS2	RS1
				LB1		2
				RB1		RB1
				RS2		
Total Energy	-44.287					
van der Waals	81.673					
electrostatic	-294.105					
ΔFs	-113.628					
	-14.165					
	-103.212					

	L	V	F	F	His13	His14	Lys16
Initial Orientation	LB1			RB2			
Final Orientation	LS1	LB2		RB2	LS1	LS1	RS1
	LNH					-CH2-	
Total Energy	-34.515						
van der Waals	75.784						
electrostatic	-286.116						
ΔFs	-103.856						
	-20.054						
	-95.223						

	L	V	F	F	Tyr10	His13	His14	Ala21	Lys28
Initial Orientation	RB2	LB2							
Final Orientation	RB1			RB2	LS1	LS1	LB2	RB2	RB2
	LB1						LB2		RS2
							LS1		2
							-CH2-		
Total Energy	-54.145								
van der Waals	68.047								
electrostatic	-293.864								
ΔFs	-123.486								
	-27.791								
	-102.971								

	L	V	F	F	His14
Initial Orientation	LB2	RB2			
Final Orientation		RS2			RB2
					RB2
					RS2
Total Energy	19.905				
van der Waals	89.169				
electrostatic	-237.685				
ΔFs	-49.436				
	-6.669				
	-46.792				

	L	V	F	F	His13	His14	Lys16
Initial Orientation	RB2			LB2			
Final Orientation	RS2			LB1	RB2	RS2	LS1
				LNH	RS2		
				LS2			
Total Energy	-48.346						
van der Waals	81.514						
electrostatic	-304.457						
ΔFs	-117.687						
	-14.324						
	-113.564						

	L	V	F	F	His13	Lys16	Val24	Lys28
Initial Orientation	LB2			RB2				
Final Orientation	LB2			RS2	LS2	LS1	RB2	RS2
				RB2	LS1			
Total Energy	-56.079							
van der Waals	77.346							
electrostatic	-307.997							
ΔFs	-125.42							
	-18.492							
	-117.104							

	L	V	F	F	Gln15
Initial Orientation		RB1	LB1		
Final Orientation		CS	CS		CS
		RB1			
Total Energy	61.491				
van der Waals	89.798				
electrostatic	-193.531				
ΔFs	-7.85				
	-6.04				
	-2.638				

	L	V	F	F	Glu22					L	V	F	F	His14	Gln15	Lys16	
Initial Orientation		LB1	RB1						Initial Orientation		RB2	LB1					
Final Orientation		LB1	RS1		CS				Final Orientation		RS2	LB1		RB2	RNH	LS2	
		LS1			-CH2-							LNH			RB1	LB2	
												LS2				-CH2-	
Total Energy	42.68								Total Energy	0.03							
van der Waals	89.222								van der Waals	84.524							
electrostatic	-216.652								electrostatic	-253.93							
ΔEs	-26.661								ΔEs	-69.311							
	-6.616									-11.314							
	-25.759									-63.037							
	L	V	F	F						L	V	F	F				
Initial Orientation		LB2	RB1						Initial Orientation		RB2	LB2					
Final Orientation		LB2	RB1						Final Orientation			LB2					
Total Energy	46.169								Total Energy	56.345							
van der Waals	87.319								van der Waals	92.647							
electrostatic	-208.605								electrostatic	-201.862							
ΔEs	-23.172								ΔEs	-12.996							
	-8.519									-3.191							
	-17.712									-10.969							
	L	V	F	F	Gln15					L	V	F	F	His14	Lys28		
Initial Orientation		LB2	RB2						Initial Orientation		RB2		LB2				
Final Orientation					RB2				Final Orientation	RS2	RS2			RB2	LS1		
											RB2			RS2			
														-CH2-			
Total Energy	39.194								Total Energy	-15.154							
van der Waals	91.989								van der Waals	83.048							
electrostatic	-217.886								electrostatic	-266.074							
ΔEs	-30.147								ΔEs	-84.495							
	-3.849									-12.79							
	-26.993									-75.181							
	L	V	F	F	Ala21	Glu22	Lys28			L	V	F	F	Val12	His13	Gln15	Lys16
Initial Orientation		LB2		RB2					Initial Orientation			RB1	LB1				
Final Orientation				RB2	LB2	LB2	RS2		Final Orientation			RS1	LB1*	RS1	LS1	RS1	RS2
				RS2			2					RB1	LNH*			-CH2-	RB1
												CS	*-CH2-				RS1*
												-CH2-					LB1*
Total Energy	-9.463								Total Energy	-59.595							LS1*
van der Waals	82.769								van der Waals	68.572							*-CH2-
electrostatic	-258.718								electrostatic	-303.526							LS2
ΔEs	-78.804								ΔEs	-128.936							
	-13.069									-27.266							
	-67.825									-112.633							
	L	V	F	F	Lys16	Val24				L	V	F	F	Gln15	Lys16		
Initial Orientation			LB1	RB1					Initial Orientation			LB1	RB2				
Final Orientation			LS1	RS1	LB1	CS			Final Orientation			RB1		LS2	RB2		
				RB1	RS1							CS			RS2		
					RB1							LB1			2		
					LNH							LS2					
Total Energy	-33.13				LS1				Total Energy	-0.123							
van der Waals	80.492				-CH2-				van der Waals	83.544							
electrostatic	-286.645								electrostatic	-255.682							
ΔEs	-102.471								ΔEs	-69.464							
	-15.346									-12.294							
	-95.752									-64.789							
	L	V	F	F	His13	Lys16				L	V	F	F	His13	Lys16		
Initial Orientation			RB2	LB1					Initial Orientation			RB1	LB2				
Final Orientation	LS2		RB2		LB2	RB1			Final Orientation			RB2	LB2	LS1	LB1		
					LS2	RS2						RS1			RB1		
						LS2									RNH*		
						-CH2-									LNH*		
Total Energy	-48.492					RNH			Total Energy	-47.676					LS1*		
van der Waals	77.575					RS2			van der Waals	78.354					*-CH2-		
electrostatic	-294.481								electrostatic	-300.436							
ΔEs	-117.833								ΔEs	-117.017							
	-18.263									-17.484							
	-103.588									-109.543							
	L	V	F	F	Lys16	Lys28				L	V	F	F	Lys16			
Initial Orientation			LB2	RB1					Initial Orientation			RB2	LB2				
Final Orientation				LB1	LS2	RS1			Final Orientation			RB2	LB2	LB1			
				RB1	LB2	RNH						RS2		LNH			
				RB2										LS1			
														-CH2-			
Total Energy	-28.859								Total Energy	-14.425							
van der Waals	80.05								van der Waals	87.505							
electrostatic	-285.561								electrostatic	-270.715							
ΔEs	-98.2								ΔEs	-83.766							
	-15.788									-8.333							
	-94.668									-79.822							
	L	V	F	F	His13	Lys16											
Initial Orientation			LB2	RB2													
Final Orientation	RS2		LB2	RS2	RS2	LS2											
	RB2			-CH2-		LNH											
						LB1											
						RS2											
Total Energy	-52.56					-CH2-											
van der Waals	79.19																
electrostatic	-297.391																
ΔEs	-121.901																
	-16.648																
	-106.498																

	H	H	Q	K	L	V	F	F	Lys28			
Initial Orientatio	CS				LB1							
Final Orientatio	RB1				CS			LS1	LB2			
	CS				LB1							
					LS1							
Total Energy	-27.757											
van der Waals	82.473											
electrostatic	-275.278											
ΔEs	-97.098											
	-13.365											
	-84.385											

	H	H	Q	K	L	V	F	F	Lys28
Initial Orientatio	CS				RB1				
Final Orientatio	LB1			LS2	RS2			RS2	RB2
	LS1				RB1				
	LS2								
Total Energy	-78.978								
van der Waals	76.494								
electrostatic	-323.94								
ΔEs	-148.319								
	-18.631								
	-133.047								

	H	H	Q	K	L	V	F	F	Gly9	Tyr10	Lys28
Initial Orientatio	RB1				LB1						
Final Orientatio	RB1				LB1			LS1	RS2	RS2	LS2
	RS1								C=O		2
	RS2										
Total Energy	-83.432										
van der Waals	75.187										
electrostatic	-329.605										
ΔEs	-152.773										
	-20.651										
	-138.712										

	H	H	Q	K	L	V	F	F	Tyr10	Ala21	Lys28
Initial Orientatio	LB1				RB1						
Final Orientatio	RS1				RB1			RS1	LS1	RS1	RS1
	LS1										RS2
	LS2										
Total Energy	-70.35										
van der Waals	76.494										
electrostatic	-315.763										
ΔEs	-139.691										
	-19.344										
	-124.87										

	H	H	Q	K	L	V	F	F	Tyr10	Lys28		
Initial Orientatio	RS1				LB1							
Final Orientatio	RB2	RS1			LS1			LS1	RS1	LS2		
	RB2	-CH2-			LB1				RS2			
	RNH											
	RS1											
Total Energy	-59.013											
van der Waals	70.646											
electrostatic	-300.95											
ΔEs	-128.354											
	-25.192											
	-110.057											

	H	H	Q	K	L	V	F	F	Tyr10	Ala21	Lys28
Initial Orientatio	RS2				LB1						
Final Orientatio	RS1			RS1	LS2				RS2	LS2	LS1
	RS2				CS						2
					RB1						
Total Energy	-53.758										
van der Waals	82.104										
electrostatic	-305.243										
ΔEs	-123.099										
	-13.734										
	-114.35										

	H	H	Q	K	L	V	F	F	
Initial Orientatio	LB1				RB2				
Final Orientatio	LS2			LS2*	RB2				
	2			LB2*	RS2				
	RS2			*-CH2-					
Total Energy	-35.508								
van der Waals	83.701								
electrostatic	-285.068								
ΔEs	-104.849								
	-12.137								
	-94.175								

	H	H	Q	K	L	V	F	F	Ala21
Initial Orientatio	LB2				RB1				
Final Orientatio	LS2			LB2	RB1				RS1
				LS2	RNH				
					RS1				
Total Energy	-13.592								
van der Waals	85.429								
electrostatic	-264.497								
ΔEs	-82.933								
	-10.409								
	-73.604								

	H	H	Q	K	L	V	F	F	Ala21	Lys28
Initial Orientatio	RB2				LB2					
Final Orientatio	RB2			RS2						
	RB2									
	RS2									
Total Energy	-44.934									
van der Waals	81.659									
electrostatic	-298.15									
ΔEs	-114.275									
	-14.179									
	-107.257									

	H	H	Q	K	L	V	F	F	Ala21	Gly9	Tyr10	Ala21	Lys28
Initial Orientatio	LB2				RB2								
Final Orientatio	LB2			LB1	RB2			RS1	LB2	LB2	RB2	RS1	
	LB1			LNH				RNH				2	
	LNH			LS1									
				-CH2-									
Total Energy	-71.297												
van der Waals	69.884												
electrostatic	-309.261												
ΔEs	-140.638												
	-25.954												
	-118.368												

	H	H	Q	K	L	V	F	F	Gly9	Ala21	Gly25	Lys28
Initial Orientatio	RS2				LB2							
Final Orientatio	RB1			RS2	LS2			LS2	RB2	LS2	LB2	LS1
	RB2			2						LB2		LB2
	-CH2-											
	RNH											
Total Energy	-74.106											
van der Waals	72.855											
electrostatic	-318.463											
ΔEs	-143.447											
	-22.983											
	-127.57											

	H	H	Q	K	L	V	F	F	Ala21
Initial Orientatio	LS2				RB2				
Final Orientatio	LS2	RS2		LS2	RB1	RS2			RB2
	LB1	-CH2-		LNH	RS2	RB2			
				LB1	RB2				
Total Energy	-54.858								
van der Waals	80.191								
electrostatic	-303.442								
ΔEs	-124.199								
	-15.647								
	-112.549								

	H	H	Q	K	L	V	F	F	Gly25
Initial Orientatio	RB1					LB1			
Final Orientatio	RB1			RS1	LB1				LB2
	RS1				RB1				
					RNH				
Total Energy	-13.726								
van der Waals	81.547								
electrostatic	-267.666								
ΔEs	-83.067								
	-14.291								
	-76.773								

	H	H	Q	K	L	V	F	F
Initial Orientatio	RB1					RB1		
Final Orientatio	LS1	RB1			LB1	RB1		
	LNH	-CH2-						
	LB1	RNH						
		RS1						
Total Energy	-13.499							
van der Waals	78.792							
electrostatic	-259.862							
ΔEs	-82.84							
	-17.046							
	-68.969							

	H	H	Q	K	L	V	F	F	
Initial Orientatio	LS1					RB1			
Final Orientatio	LS1				LB1	CS			
	LB1				CS	RB1			
Total Energy	8.404								
van der Waals	83.888								
electrostatic	-242.365								
ΔEs	-60.937								
	-11.95								
	-51.472								

	H	H	Q	K	L	V	F	F
Initial Orientatio	RS1					LB1			
Final Orientatio	RS1				RS1				
	2				RB1				
Total Energy	16.33								
van der Waals	88.664								
electrostatic	-240.513								
ΔEs	-53.011								
	-7.174								
	-49.62								

	H	H	Q	K	L	V	F	F	Tyr10
Initial Orientatio	RS2					LB1			
Final Orientatio	RS2	LS2			RS2	LS2			RB2
Total Energy	18.04								
van der Waals	83.238								
electrostatic	-234.993								
ΔEs	-51.301								
	-12.6								
	-44.1								

	H	H	Q	K	L	V	F	F	Gly9
Initial Orientatio	RS2					LB2			
Final Orientatio	RB1				LS2	LB2			RB2
	RNH					LS2			
	RS2								
	RB2								
	-CH2-								
Total Energy	-20.07								
van der Waals	80.448								
electrostatic	-269.632								
ΔEs	-89.411								
	-15.39								
	-78.739								

	H	H	Q	K	L	V	F	F	
Initial Orientatio	LS2					RB1			
Final Orientatio	LS2	RS2		LNH	RS2	RS2			
	2			LS2	RB1				
	LB1			-CH2-					
				LB2					
Total Energy	-54.79								
van der Waals	84.029								
electrostatic	-309.001								
ΔEs	-124.131								
	-11.809								
	-118.108								

	H	H	Q	K	L	V	F	F	Tyr10	Ala21	Glu22
Initial Orientatio	RB2					LB2					
Final Orientatio	RB2	RS2			RS2	LB2			RB2	LB2	LB2
	RS2	-CH-			RS1						
Total Energy	-10.353										
van der Waals	79.454										
electrostatic	-263.467										
ΔEs	-79.694										
	-16.384										
	-72.574										

	H	H	Q	K	L	V	F	F	Tyr10	
Initial Orientatio	LB2					RB2				
Final Orientatio	LS2								LS2	
	LB2									
Total Energy	-4.358									
van der Waals	88.106									
electrostatic	-260.234									
ΔEs	-73.699									
	-7.732									
	-69.341									

	H	H	Q	K	L	V	F	F	Gly9	
Initial Orientatio	LS2						RB2			
Final Orientatio	LS2			LB1			RB2	RS2	LB2	
				RS2				RB2	C=O	
				RB1						
Total Energy	-40.908									
van der Waals	77.432									
electrostatic	-288.22									
ΔEs	-110.249									
	-18.406									
	-97.327									

	H	H	Q	K	L	V	F	F	
Initial Orientatio	RB2						LB2		
Final Orientatio	RB2			RS1			LB2		
				RNH					
				RB2					
Total Energy	11.949								
van der Waals	92.656								
electrostatic	-250.098								
ΔEs	-57.392								
	-3.182								
	-59.205								

	H	H	Q	K	L	V	F	F	
Initial Orientatio	CS							LB2	
Final Orientatio	RS2	RS2		LS2	RB2	RB2		LB2	
	LB1	-CH-		2				LS2	
	CS								
	RB1								
Total Energy	-55.192								
van der Waals	79.656								
electrostatic	-305.543								
ΔEs	-124.533								
	-16.182								
	-114.65								

	H	H	Q	K	L	V	F	F	Lys28	
Initial Orientatio	LS1							RB1		
Final Orientatio	LB2			LS1	LS1			CS	RS2	
	LS2			LS2					RS1	
	LS1									
Total Energy	-59.236									
van der Waals	82.176									
electrostatic	-312.374									
ΔEs	-128.577									
	-13.662									
	-121.481									

	H	H	Q	K	L	V	F	F	Gly9	Tyr10
Initial Orientatio	LB1							RB2		
Final Orientatio	LB1			LB2	RNH			RB2	LS1	LS1
	RB1			RS1	RB1			RS1	C=O	
	LB1			RNH						
	LNH			RB1						
	LS1									
	-CH2-									
Total Energy	-62.082									
van der Waals	71.44									
electrostatic	-305.988									
ΔEs	-131.423									
	-24.398									
	-115.095									

	H	H	Q	K	L	V	F	F	Lys28	
Initial Orientatio	RB1							LB2		
Final Orientatio	RB2			RB2	LS1			LS1	LS2	
	RS1							LB2	2	
	RNH								LB2	
	RB1									
Total Energy	-55.2									
van der Waals	76.561									
electrostatic	-310.755									
ΔEs	-124.541									
	-19.277									
	-119.862									

	H	H	Q	K	L	V	F	F	
Initial Orientatio	LS1							RB2	
Final Orientatio	LB1			LB1					
	LS1			RB1					
	LNH								
Total Energy	-17.741								
van der Waals	86.851								
electrostatic	-273.744								
ΔEs	-87.082								
	-8.987								
	-82.851								

	H	H	Q	K	L	V	F	F	Val24	Lys28
Initial Orientatio	LS2							RB2		
Final Orientatio	LS2			LB1	LB1			RB2	RB2	RS2
	2			LS2				RS2	RS2	RB2
	LS1			-CH2-				RB1		
								CS		
Total Energy	-63.762									
van der Waals	72.921									
electrostatic	-306.561									
ΔEs	-133.103									
	-22.917									
	-115.668									

	H	H	Q	K	L	V	F	F	Tyr10	
Initial Orientatio	RB2							LB2		
Final Orientatio	RS2	RS2		LS2	RS2			LB1	RB2	
	RS1	-CH-		LB1	RB1			LS1		
				LNH	LB1					
Total Energy	-68.307									
van der Waals	73.381									
electrostatic	-309.769									
ΔEs	-137.648									
	-22.457									
	-118.876									

	H	H	Q	K	L	V	F	F	Tyr10	Lys28
Initial Orientatio	LS1				RB1					
Final Orientatio	LS1							RS1	LS1	RS2
	LS2									RS1
Total Energy	-72.212									
van der Waals	79.442									
electrostatic	-323.231									
ΔEs	-141.553									
	-16.396									
	-132.338									

	H	H	Q	K	L	V	F	F	Val12
Initial Orientatio	RS2						RB2		
Final Orientatio	RS2			RB2			LB2		LS2
	2			RS2					
				-CH2-					
Total Energy	-4.967								
van der Waals	87.255								
electrostatic	-262.454								
ΔEs	-74.308								
	-8.583								
	-71.561								

	H	H	Q	K	L	V	F	F	Val12
Initial Orientatio	LS1						RB1		
Final Orientatio	LS1			LS1			RS1		CS
	2			LNH					
				LB1					
Total Energy	-12.353								
van der Waals	86.291								
electrostatic	-271.565								
ΔEs	-81.694								
	-9.547								
	-80.672								

	H	H	Q	K	L	V	F	F
Initial Orientatio	LB2						RB2	
Final Orientatio								
Total Energy	33.277							
van der Waals	95.985							
electrostatic	-231.427							
ΔEs	-36.064							
	0.147							
	-40.534							

	H	H	Q	K	L	V	F	F	Lys28
Initial Orientatio	RS1							LB1	
Final Orientatio	RS1			RS1	RS1			LS1	LS1
	RS2							LB1	
Total Energy	-54.442								
van der Waals	85.477								
electrostatic	-306.715								
ΔEs	-123.783								
	-10.361								
	-115.822								

	H	H	Q	K	L	V	F	F	Lys28
Initial Orientatio	LS2							RB1	
Final Orientatio	LS1			LS2	LS2			CS	RS1
	LS2				LS1			RS2	
					LB1				
Total Energy	-64.797								
van der Waals	78.013								
electrostatic	-314.118								
ΔEs	-134.138								
	-17.825								
	-123.225								

	H	H	Q	K	L	V	F	F	Val24	Lys28
Initial Orientatio	RB2							LB1		
Final Orientatio	RB2			RB2	RS1			LB1	LS1	LS2
	RS1									
Total Energy	-31.06									
van der Waals	86.198									
electrostatic	-287.006									
ΔEs	-100.401									
	-9.64									
	-96.113									

	H	H	Q	K	L	V	F	F	Lys28
Initial Orientatio	LB2							RB1	
Final Orientatio	LB2			LS1				LB1	RS1
				LNH				RB1	
				RS2					
Total Energy	-38.24								
van der Waals	83.121								
electrostatic	-294.816								
ΔEs	-107.581								
	-12.717								
	-103.923								

	H	H	Q	K	L	V	F	F	Val24	Lys28
Initial Orientatio	RS1							LB2		
Final Orientatio	RS1			RNH				LB2	LB2	LB2
				RS1				LS2		-CH2-
				-CH2-						
Total Energy	-34.549									
van der Waals	85.808									
electrostatic	-288.857									
ΔEs	-103.89									
	-10.03									
	-97.964									

	H	H	Q	K	L	V	F	F
Initial Orientatio	RS2							LB2
Final Orientatio	RS2			RS2	RS2			LS2
	2			2				LB2
	RS1			LS1				
				-CH2-				
Total Energy	-62.47							
van der Waals	82.021							
electrostatic	-311.965							
ΔEs	-131.811							
	-13.817							
	-121.072							

	H	H	Q	K	L	V	F	F
Initial Orientatio	LB2							RB2
Final Orientatio	LB2			RS2	LB2			RS1
	LS1			2				RS2
	LNH			RB2				
				-CH2-				
Total Energy	-33.276							
van der Waals	82.303							
electrostatic	-284.036							
ΔEs	-102.617							
	-13.535							
	-93.143							

	H	H	Q	K	L	V	F	F
Initial Orientation								
Final Orientation								
Total Energy								
van der Waals								
electrostatic								
ΔEs	-69.341							
	-95.838							
	190.893							

	H	H	Q	K	L	V	F	F			
Initial Orientation		LB1			RB1						
Final Orientation	RS1	LB1			RS1						
	2	RB1*			RNH						
	RB1	CS*									
		*-CH2-									
		LS1									
Total Energy	-2.771										
van der Waals	83.765										
electrostatic	-259.134										
ΔEs	-72.112										
	-12.073										
	-68.241										

	H	H	Q	K	L	V	F	F	Lys28		
Initial Orientation		LS1			RB1						
Final Orientation		LS1			CS	LS1			RS1		
Total Energy	-19.925										
van der Waals	88.25										
electrostatic	-277.919										
ΔEs	-89.266										
	-7.588										
	-87.026										

	H	H	Q	K	L	V	F	F	Ala21	Gly25	Lys28
Initial Orientation		RS2			LB1						
Final Orientation		RS2			LB1	RS2		LS2	LB2	LB2	LB2
					CS				LS2		-CH2-
Total Energy	-19.689										
van der Waals	73.923										
electrostatic	-265.45										
ΔEs	-89.03										
	-21.915										
	-74.557										

	H	H	Q	K	L	V	F	F	Tyr10	Ala21	Lys28
Initial Orientation		LS2			RB1						
Final Orientation	LS2	LS2			RS2			RS2	LB2	CS	RS1
		-CH2-			CS						RS2
					LB1						
Total Energy	-62.359										
van der Waals	77.452										
electrostatic	-308.691										
ΔEs	-131.7										
	-18.386										
	-117.798										

	H	H	Q	K	L	V	F	F	Glu11		
Initial Orientation		RB2			LB1						
Final Orientation		RB2			LB1				RB2		
Total Energy	12.423										
van der Waals	90.594										
electrostatic	-246.221										
ΔEs	-56.918										
	-5.244										
	-55.328										

	H	H	Q	K	L	V	F	F	Tyr10
Initial Orientation		LB1			RB2				
Final Orientation	RS1	LB1	LS1		RB2				RS1
		LNH							
		RB1							
Total Energy	1.488								
van der Waals	80.227								
electrostatic	-246.967								
ΔEs	-67.853								
	-15.611								
	-56.074								

	H	H	Q	K	L	V	F	F	Tyr10	Glu11	
Initial Orientation		LS1			RB2						
Final Orientation	RS1	LB1			RB2	LB2			CS	LS1	
	2	LNH			RS1					-CH2-	
	RB1	LS1			RNH						
					RB1						
Total Energy	-16.451										
van der Waals	79.561										
electrostatic	-266.042										
ΔEs	-85.792										
	-16.277										
	-75.149										

	H	H	Q	K	L	V	F	F
Initial Orientation		RS2			LB2			
Final Orientation	LS2	RB2	RB2		LNH			
	2	RS2			LS2			
Total Energy	-1.717							
van der Waals	86.488							
electrostatic	-260.365							
ΔEs	-71.058							
	-9.35							
	-69.472							

	H	H	Q	K	L	V	F	F	Glu11		
Initial Orientation		LB2			RB2						
Final Orientation		LB2							LB2		
		LS2									
Total Energy	48.225										
van der Waals	90.679										
electrostatic	-208.211										
ΔEs	-21.116										
	-5.159										
	-17.318										

	H	H	Q	K	L	V	F	F
Initial Orientation		RB2			LB2			
Final Orientation		RB2						RB2
		RB2						
		RS2						
		-CH2-						
Total Energy	30.482							
van der Waals	88.155							
electrostatic	-226.179							
ΔEs	-38.859							
	-7.683							
	-35.286							

	H	H	Q	K	L	V	F	F	Tyr10		
Initial Orientation		CS				LB1					
Final Orientation		CS				CS			RS1		
Total Energy	43.169										
van der Waals	89.197										
electrostatic	-212.143										
ΔEs	-26.172										
	-6.641										
	-21.25										

	H	H	Q	K	L	V	F	F
Initial Orientation		CS				RB1		
Final Orientation		CS			RS1	RB1		
						RS1		
Total Energy	35.535							
van der Waals	89.543							
electrostatic	-221.813							
ΔEs	-33.806							
	-6.295							
	-30.92							

	H	H	Q	K	L	V	F	F			
Initial Orientation		LB1				RB1					
Final Orientation		LS1	LS1			CS					
Total Energy	60.809										
van der Waals	90.591										
electrostatic	-197.759										
ΔEs	-8.532										
	-5.247										
	-6.866										

	H	H	Q	K	L	V	F	F
Initial Orientation		RB1				LB1		
Final Orientation		RS1	RS1			CS		
		RB1						
Total Energy	48.306							
van der Waals	90.239							
electrostatic	-208.562							
ΔEs	-21.035							
	-5.599							
	-17.669							

	H	H	Q	K	L	V	F	F			
Initial Orientation		RS1				LB1					
Final Orientation		RS1	RS1			RB1					
		RNH									
Total Energy	28.338										
van der Waals	87.651										
electrostatic	-231.463										
ΔEs	-41.003										
	-8.187										
	-40.57										

	H	H	Q	K	L	V	F	F
Initial Orientation		LS1				RB1		
Final Orientation		LS1						
		LB1						
Total Energy	57.508							
van der Waals	90.715							
electrostatic	-199.601							
ΔEs	-11.833							
	-5.123							
	-8.708							

	H	H	Q	K	L	V	F	F	Tyr10		
Initial Orientation		RS2				LB1					
Final Orientation		RS2							RB2		
Total Energy	17.3										
van der Waals	89.417										
electrostatic	-241.995										
ΔEs	-52.041										
	-6.421										
	-51.102										

	H	H	Q	K	L	V	F	F	Glu22		
Initial Orientation		LS2				RB1					
Final Orientation		LS1							CS		
Total Energy	50.07										
van der Waals	92.576										
electrostatic	-208.731										
ΔEs	-19.271										
	-3.262										
	-17.838										

	H	H	Q	K	L	V	F	F	Glu11	
Initial Orientation		RB1				LB2				
Final Orientation		RB1	RNH		LB2	LS2	RB2		CS	
		LS2	RS2		LS2					
		-CH2-								
		LB1								
		CS								
Total Energy	-14.541									
van der Waals	78.278									
electrostatic	-264.396									
ΔEs	-83.882									
	-17.56									
	-73.503									

	H	H	Q	K	L	V	F	F	Glu11	Ala21
Initial Orientation		RB2				LB1				
Final Orientation	LB2	RB1	RNH		LB2	LB1			RB2	LS1
			RB1			LNH				
Total Energy	18.183									
van der Waals	78.01									
electrostatic	-230.849									
ΔEs	-51.158									
	-17.828									
	-39.956									

	H	H	Q	K	L	V	F	F
Initial Orientation		RB1					LB1	
Final Orientation		RB1	CS			RB1		
		RS1	RB1			RS1		
Total Energy	44.5							
van der Waals	85.287							
electrostatic	-211.214							
ΔEs	-24.841							
	-10.551							
	-20.321							

	H	H	Q	K	L	V	F	F
Initial Orientation		LS1					RB1	
Final Orientation		LS1	LS1				CS	
			LB1					
			CS					
Total Energy	43.204							
van der Waals	90.891							
electrostatic	-212.264							
ΔEs	-26.137							
	-4.947							
	-21.371							

	H	H	Q	K	L	V	F	F
Initial Orientation		LS2					RB1	
Final Orientation		LS2						
Total Energy	51.216							
van der Waals	88.868							
electrostatic	-203.72							
ΔEs	-18.125							
	-6.97							
	-12.827							

	H	H	Q	K	L	V	F	F	Val12
Initial Orientation		LB1					RB1		
Final Orientation			LB2	RS1			RB1		RB2
			LS2	RNH			LB1		
				RB2					
				-CH2-					
Total Energy	-13.63								
van der Waals	80.981								
electrostatic	-268.043								
ΔEs	-82.971								
	-14.857								
	-77.15								

	H	H	Q	K	L	V	F	F
Initial Orientation		LS2					RB2	
Final Orientation		CS	RS2			LS2	RB2	
		LB1	RB1				RS2	
		LS2	CS					
Total Energy	12.337							
van der Waals	81.182							
electrostatic	-237.761							
ΔEs	-57.004							
	-14.656							
	-46.868							

	H	H	Q	K	L	V	F	F
Initial Orientation		LB2					RB2	
Final Orientation		LB2	LS2				RB2	
		LB2						
		LS2						
Total Energy	40.715							
van der Waals	88.621							
electrostatic	-214.551							
ΔEs	-28.626							
	-7.217							
	-23.658							

	H	H	Q	K	L	V	F	F	Val24	Lys28
Initial Orientation		RS2						LB2		
Final Orientation		RB2			LS2	RS2		LS2	LB2	LB2
		RB2						LB2		
		RS2								
Total Energy	-37.743									
van der Waals	77.248									
electrostatic	-283.646									
ΔEs	-107.084									
	-18.59									
	-92.753									

	H	H	Q	K	L	V	F	F	Lys28
Initial Orientation		RB2						LB2	
Final Orientation		RB2				RB2			LS1
									LB2
									-CH2-
Total Energy	3.3								
van der Waals	80.77								
electrostatic	-247.88								
ΔEs	-66.041								
	-15.068								
	-56.987								

	H	H	Q	K	L	V	F	F	Tyr10		
Initial Orientation		LB1				RB2					
Final Orientation		LB1	LS1		RB2				RS1		
		RB1	LNH								
		RB1	LB`								
		RNH									
		-CH2-									
Total Energy	-3.189										
van der Waals	76.683										
electrostatic	-253.952										
ΔEs	-72.53										
	-19.155										
	-63.059										

	H	H	Q	K	L	V	F	F
Initial Orientation		LB1					RB1	
Final Orientation		LB1	LB1			CS	RB1	
			CS				RS1	
			RB1					
Total Energy	-16.969							
van der Waals	88.106							
electrostatic	-207.598							
ΔEs	-86.31							
	-7.732							
	-16.705							

	H	H	Q	K	L	V	F	F
Initial Orientation		RS1					LB1	
Final Orientation		RS1	RS1					
			RB1					
Total Energy	44.738							
van der Waals	88.544							
electrostatic	-211.438							
ΔEs	-24.603							
	-7.294							
	-20.545							

	H	H	Q	K	L	V	F	F	Glu11
Initial Orientation		RS2					LB1		
Final Orientation		RB2	RB2				LB1		RB2
							LNH		
							LS2		
Total Energy	44.274								
van der Waals	86.677								
electrostatic	-208.726								
ΔEs	-25.067								
	-9.161								
	-17.833								

	H	H	Q	K	L	V	F	F
Initial Orientation		RB1					LB2	
Final Orientation		LB1	LS1				LB2	
		RB1	LNH				LS1	
		RNH	LB1					
Total Energy	22.051							
van der Waals	80.284							
electrostatic	-228.875							
ΔEs	-47.29							
	-15.554							
	-37.982							

	H	H	Q	K	L	V	F	F	Glu11	Glu22
Initial Orientation		RB2					LB1			
Final Orientation		RB2				CS	LS2		RB2	CS
		RS2					LB1			
Total Energy	46.124									
van der Waals	81.069									
electrostatic	-204.002									
ΔEs	-23.217									
	-14.769									
	-13.109									

	H	H	Q	K	L	V	F	F
Initial Orientation		RB2					LB2	
Final Orientation		RB2					LS2	
							LB2	
Total Energy	63.099							
van der Waals	91.872							
electrostatic	-194.249							
ΔEs	-6.242							
	-3.966							
	-3.356							

	H	H	Q	K	L	V	F	F	Ala21
Initial Orientation		RB2						LB1	
Final Orientation				LS2	RB1			LB1	RB1
				LB2	LB1			LNH	
					LS2			LS1	
								LB2	
Total Energy	-18.854								
van der Waals	78.251								
electrostatic	-266.998								
ΔEs	-88.195								
	-17.587								
	-76.105								

	H	H	Q	K	L	V	F	F	Glu11	Val24	Lys28
Initial Orientation		LB2						RB2			
Final Orientation		LB2			RS1			RB2	LB2	RB2	RB2
											RS2
Total Energy	-11.851										
van der Waals	80.481										
electrostatic	-259.121										
ΔEs	-81.192										
	-15.357										
	-68.228										

	H	H	Q	K	L	V	F	F
Initial Orientation								
Final Orientation								
Total Energy								
van der Waals								
electrostatic								
ΔEs	-69.341							
	-95.838							
	190.893							

	H	H	Q	K	L	V	F	F	Lys28
Initial Orientation				CS	RB1				
Final Orientation	LS1			LS1	RS1			RB1	RS2
				LB1				CS	
								RS1	
								RS2	
Total Energy	-48.47								
van der Waals	80.07								
electrostatic	-303.75								
ΔEs	-117.811								
	-15.768								
	-112.857								

	H	H	Q	K	L	V	F	F
Initial Orientation				CS	LB1			
Final Orientation	LB1			RS1	LS1			RS1
	LS1			CS	LB1			
	LS2			-CH2-				
	CS			RB1				
				RS2				
Total Energy	-50.239							
van der Waals	81.169							
electrostatic	-300.455							
ΔEs	-119.58							
	-14.669							
	-109.562							

	H	H	Q	K	L	V	F	F
Initial Orientation				RB1	LB1			
Final Orientation	RS2			RS1	CS			
	CS				RB1			
	RB1				RS1			
Total Energy	-34.195							
van der Waals	86.786							
electrostatic	-285.656							
ΔEs	-103.536							
	-9.052							
	-94.763							

	H	H	Q	K	L	V	F	F
Initial Orientation				LB1	RB1			
Final Orientation	RS1			LB1	RS1			CS
				LS1	RB1			
				-CH2-				
Total Energy	-7.175							
van der Waals	87.066							
electrostatic	-263.3							
ΔEs	-76.516							
	-8.772							
	-72.407							

	H	H	Q	K	L	V	F	F	
Initial Orientation				RS1	LB1				
Final Orientation				RS1	CS			RS1	
Total Energy	3.608								
van der Waals	92.176								
electrostatic	-254.844								
ΔEs	-65.733								
	-3.662								
	-63.951								

	H	H	Q	K	L	V	F	F	F	Lys28
Initial Orientation					RB1					
Final Orientation	LS1			LS2	LS1				LB1	RS2
				2					CS	2
				LS1						RS1
				-CH2-						
Total Energy	-69.143									
van der Waals	78.185									
electrostatic	-317.423									
ΔEs	-138.484									
	-17.653									
	-126.53									

	H	H	Q	K	L	V	F	F
Initial Orientation				RS2	LB1			
Final Orientation	LS2			RS2	LB1			RB1
				2	LS1			RS2
								RS1
								CS
Total Energy	-52.386							
van der Waals	79.773							
electrostatic	-297.078							
ΔEs	-121.727							
	-16.065							
	-106.185							

	H	H	Q	K	L	V	F	F	Lys28
Initial Orientation				LS2	RB1				
Final Orientation	LB1			RS2	LB1			RS2	RB2
	LS2				RS1				RS2
	LS1								2
Total Energy	-39.953								
van der Waals	82.806								
electrostatic	-322.053								
ΔEs	-109.294								
	-13.032								
	-131.16								

	H	H	Q	K	L	V	F	F
Initial Orientation				RB2	LB1			
Final Orientation	RB1	LB2		RS2	LS2			
	RS2	-CH2-						
		LS2						
		-CH-						
Total Energy	-40.782							
van der Waals	81.424							
electrostatic	-288.41							
ΔEs	-110.123							
	-14.414							
	-97.517							

	H	H	Q	K	L	V	F	F	Lys28
Initial Orientation				RB1	LB2				
Final Orientation	RB2			RS2	LS2			LS2	LS1
									LS2
Total Energy	-68.14								
van der Waals	77.03								
electrostatic	-315.116								
ΔEs	-137.481								
	-18.808								
	-124.223								

	H	H	Q	K	L	V	F	F
Initial Orientation				LS2	RB2			
Final Orientation				LS2	RS2			
					RB2			
Total Energy	-18.752							
van der Waals	87.046							
electrostatic	-271.267							
ΔEs	-88.093							
	-8.792							
	-80.374							

	H	H	Q	K	L	V	F	F	Lys28
Initial Orientation				RS2	LB2				
Final Orientation	RB2			RS2	RB1			LS2	LS1
	RS1			RB1					LS2
	RNH								
Total Energy	-73.585								
van der Waals	71.756								
electrostatic	-314.61								
ΔEs	-142.926								
	-24.082								
	-123.717								

	H	H	Q	K	L	V	F	F	Lys28
Initial Orientation				LB2	RB2				
Final Orientation				LB1				RB1	RS1
				LNH					3
				LS2					
				-CH2-					
Total Energy	-42.684								
van der Waals	84.36								
electrostatic	-293.107								
ΔEs	-112.025								
	-11.478								
	-102.214								

	H	H	Q	K	L	V	F	F	Lys28
Initial Orientation				RB2	LB2				
Final Orientation	RB1			RS2	LB1				LB2
				RB1	RB1				LS2
				RNH					
Total Energy	-39.588								
van der Waals	82.574								
electrostatic	-288.247								
ΔEs	-108.929								
	-13.264								
	-97.354								

	H	H	Q	K	L	V	F	F
Initial Orientation				LS2		RB2		
Final Orientation	RS2	RS2		LS2	LB1	RB2		
		-CH-		LNH	RB2			
		RB2		LB1				
		-CH2-						
Total Energy	-52.335							
van der Waals	74.538							
electrostatic	-295.775							
ΔEs	-121.676							
	-21.3							
	-104.882							

	H	H	Q	K	L	V	F	F	Lys28
Initial Orientation				LB2		RB2			
Final Orientation				LS2	LS2			LS1	RS1
				LB2	LB1			LNH	RB1
								LB1	
Total Energy	-37.662								
van der Waals	85.084								
electrostatic	-287								
ΔEs	-107.003								
	-10.754								
	-96.107								

	H	H	Q	K	L	V	F	F		
Initial Orientation				RB2		LB2				
Final Orientatior	RB2	LB2		RS2	RS2	LB2				
	RS2	-CH2-			RB1					
					LS2					
					LB2					
Total Energy	-21.884									
van der Waals	81.331									
electrostatic	-270.576									
ΔEs	-91.225									
	-14.507									
	-79.683									

	H	H	Q	K	L	V	F	F		
Initial Orientation				RB1			LB1			
Final Orientation				LB1			LS1			
				RS1						
Total Energy	-14.149									
van der Waals	89.324									
electrostatic	-269.992									
ΔEs	-83.49									
	-6.514									
	-79.099									

	H	H	Q	K	L	V	F	F		
Initial Orientation				LB1			RB1			
Final Orientatior	LS1			LB1	LS1		RS1			
				RB1						
				RNH						
				LNH*						
Total Energy	-46.24			LS1*						
van der Waals	80.693			*-CH2-						
electrostatic	-300.724									
ΔEs	-115.581									
	-15.145									
	-109.831									

	H	H	Q	K	L	V	F	F		
Initial Orientation				LS2			RB1			
Final Orientation				LB1			CS			
				LS2						
				CS						
				-CH2-						
Total Energy	-5.647									
van der Waals	87.962									
electrostatic	-263.058									
ΔEs	-74.988									
	-7.876									
	-72.165									

	H	H	Q	K	L	V	F	F		
Initial Orientation				LB1			RB2			
Final Orientation				LB1				LS2		
				RB1				RB1		
				RNH						
				-CH2-						
Total Energy	-5.83									
van der Waals	85.38									
electrostatic	-262.567									
ΔEs	-75.171									
	-10.458									
	-71.674									

	H	H	Q	K	L	V	F	F		
Initial Orientation				RB1			LB2			
Final Orientation				LNH*			LB2			
				RB1*			LS1			
				RNH*						
Total Energy	-25.321			RS1						
van der Waals	78.233			*-CH2-						
electrostatic	-275.851									
ΔEs	-94.662									
	-17.605									
	-84.958									

	H	H	Q	K	L	V	F	F	Glu22	Asp23
Initial Orientation				LB2			RB1			
Final Orientation				LB2			RB2		RB2	RB2
				LNH*			-CH2-		-CH2-	-CH2-
				LS1*			RS1			
				*-CH2-			RNH			
Total Energy	14.898						RB1			
van der Waals	80.228									
electrostatic	-235.453									
ΔEs	-54.443									
	-15.61									
	-44.56									

	H	H	Q	K	L	V	F	F		
Initial Orientation				RS2			LB2			
Final Orientation			LS2	RS2			LB2			
			-CH2-	LS2			RS1			
				-CH2-						
Total Energy	-32.091									
van der Waals	83.972									
electrostatic	-286.08									
ΔEs	-101.432									
	-11.866									
	-95.187									

	H	H	Q	K	L	V	F	F		
Initial Orientation				LS2			RB2			
Final Orientation				LB1			RB2			
				LS2			RS2			
Total Energy	-9.579									
van der Waals	92.517									
electrostatic	-267.648									
ΔEs	-78.92									
	-3.321									
	-76.755									

	H	H	Q	K	L	V	F	F		
Initial Orientation				RB2			LB2			
Final Orientation				RB2			RB2			
				RS2			RS2			
				2						
Total Energy	21.325									
van der Waals	93.529									
electrostatic	-239.239									
ΔEs	-48.016									
	-2.309									
	-48.346									

	H	H	Q	K	L	V	F	F		
Initial Orientation				LB2			RB2			
Final Orientation				LS2			RB2			
				-CH2-						
Total Energy	-24.343									
van der Waals	86.177									
electrostatic	-278.1									
ΔEs	-93.684									
	-9.661									
	-87.207									

	H	H	Q	K	L	V	F	F	Val24	Lys28
Initial Orientation				CS				RB1		
Final Orientation				LS2	CS			CS	RS2	RS1
				2				RB1		RS2
				LS1				RS2		
				-CH2-						
Total Energy	-40.894									
van der Waals	83.068									
electrostatic	-295.759									
ΔEs	-110.235									
	-12.77									
	-104.866									

	H	H	Q	K	L	V	F	F	Lys28	
Initial Orientation				CS				LB1		
Final Orientatior	RS1			RB1				CS	LS2	
	RS2			RS2				LB1		
				CS				LS2		
				RS1						
Total Energy	-62.208			-CH2-						
van der Waals	78.286									
electrostatic	-312.409									
ΔEs	-131.549									
	-17.552									
	-121.516									

	H	H	Q	K	L	V	F	F		
Initial Orientation				LB1				LB1		
Final Orientation				LB1				CS	RS1	
				LS1				RB1		
				LS2				RS1		
Total Energy	-44.063									
van der Waals	85.885									
electrostatic	-303.131									
ΔEs	-113.404									
	-9.953									
	-112.238									

	H	H	Q	K	L	V	F	F		
Initial Orientation				RB1				LB1		
Final Orientatior	LS1			RB1				LB1		
	2			LS1				CS		
				CS						
Total Energy	-11.684									
van der Waals	89.208									
electrostatic	-269.846									
ΔEs	-81.025									
	-6.63									
	-78.953									

	H	H	Q	K	L	V	F	F		
Initial Orientation				RS1				LB1		
Final Orientatior	RS1			RNH	RS1			LB1		
				RS1				RB1		
				-CH2-						
Total Energy	-31.653									
van der Waals	81.432									
electrostatic	-281.939									
ΔEs	-100.994									
	-14.406									
	-91.046									

	H	H	Q	K	L	V	F	F		
Initial Orientation				LS1				RB1		
Final Orientatior	LS1			LB1	LS1			RB1		
				LS1				CS		
				LS2				LB1		
				-CH2-						
Total Energy	-46.4									
van der Waals	80.147									
electrostatic	-294.424									
ΔEs	-115.741									
	-15.691									
	-103.531									

	H	H	Q	K	L	V	F	F		
Initial Orientation				RS2				LB1		
Final Orientation	RB2			RB1	RS2			LS2	LS2	
	RS2			RS1				LB1		
				RS2				CS		
				-CH2-						
Total Energy	-53.062									
van der Waals	80.447									
electrostatic	-307.573									
ΔEs	-122.403									
	-15.391									
	-116.68									

	H	H	Q	K	L	V	F	F	Val24
Initial Orientation				LS2				RB1	
Final Orientation	LS2			LS2				LB1	RS2
				-CH2-				CS	
Total Energy	-11.258								
van der Waals	86.191								
electrostatic	-268.434								
ΔEs	-80.599								
	-9.647								
	-77.541								

	H	H	Q	K	L	V	F	F	Lys28
Initial Orientation				RB1				LB2	
Final Orientation	RS1			RB1				LS1	LB2
				RNH				LNH	
				RS1					
				-CH2-					
Total Energy	-40.857								
van der Waals	85.143								
electrostatic	-295.218								
ΔEs	-110.198								
	-10.695								
	-104.325								

	H	H	Q	K	L	V	F	F	Gly9
Initial Orientation				RB2				LB1	
Final Orientation	RB2			RB1	RS1			CS	RB2
	RS1			LS2					
				2					
				LB1					
Total Energy	-56.674								
van der Waals	77.541								
electrostatic	-305.972								
ΔEs	-126.015								
	-18.297								
	-115.079								

	H	H	Q	K	L	V	F	F	Asp23	Val24
Initial Orientation				RS2				LB2		
Final Orientation	RB2			LS2	RB2			LS2	LB2	LB2
	RS2			RS2						
	2			-CH2-						
Total Energy	-25.536									
van der Waals	86.441									
electrostatic	-281.399									
ΔEs	-94.877									
	-9.397									
	-90.506									

	H	H	Q	K	L	V	F	F	Lys28
Initial Orientation				LB2				RB2	
Final Orientation	LB2			LNH				RB1	RS1
	LS2			LB1					
Total Energy	-43.448								
van der Waals	82.689								
electrostatic	-296.426								
ΔEs	-112.789								
	-13.149								
	-105.533								

	H	H	Q	K	L	V	F	F
Initial Orientation				LB1				RB2
Final Orientation	LS1			LB1				
				RB1				
Total Energy	-26.417							
van der Waals	84.438							
electrostatic	-277.858							
ΔEs	-95.758							
	-11.4							
	-86.965							

	H	H	Q	K	L	V	F	F	Gly9
Initial Orientation				LB2				RB1	
Final Orientation	LB2			RS2	LS2			CS	LB2
	LS2			LS2				RS2	
				-CH2-					
				LB1					
Total Energy	-37.886								
van der Waals	76.771								
electrostatic	-291.851								
ΔEs	-107.227								
	-19.067								
	-100.958								

	H	H	Q	K	L	V	F	F	Val24	Lys28
Initial Orientation				LS2				RB2		
Final Orientation	LS2			LS2				RS2	RS2	RS2
				LB2					RB2	RB2
Total Energy	-32.457									
van der Waals	83.03									
electrostatic	-284.734									
ΔEs	-101.798									
	-12.808									
	-93.841									

	H	H	Q	K	L	V	F	F
Initial Orientation				RB2				LB2
Final Orientation	RB2			RS2				LS2
				RB2				LB2
				-CH2-				
Total Energy	-29.571							
van der Waals	84.295							
electrostatic	-287.401							
ΔEs	-98.912							
	-11.543							
	-96.508							

Gas phase results of solapsone and the 1AML conformer of Aβ

	H	H	Q	K	Tyr10	Leu17	Ile31
Initial Orientation	LB1	CS					
Final Orientation	LS1	CS			RB1	CS	LS1
	LB1	RB1					LB1
		RS1					CS
Total Energy	141.601						
van der Waals	113.753						
electrostatic	-222.828						
ΔEs	-125.184						
	-18.11						
	-113.101						

	H	H	Q	K	Tyr10	Ala30	Ile31
Initial Orientation	CS	LB1					
Final Orientation	RB1	LS1			CS	RS1	RS1
	CS	LB1			LS2		
	RS2				LB1		
Total Energy	128.155						
van der Waals	108.913						
electrostatic	-232.366						
ΔEs	-138.63						
	-22.95						
	-122.639						

	H	H	Q	K	Tyr10	Leu17	Ile31	Met35
Initial Orientation	CS	RB1						
Final Orientation	LB1	RS1		LS2	LS1	RB1	CS	RS2
	LS2			-CH2-		RS1	RB1	
	LS1						RS2	
	RB1							
Total Energy	94.318							
van der Waals	109.47							
electrostatic	-265.249							
ΔEs	-172.467							
	-22.393							
	-155.522							

	H	H	Q	K	Tyr10	Leu17	Ile31
Initial Orientation	RS1	CS					
Final Orientation	RS1	LB1			RS2	LS1	LB1
	RS2	LB1			CS		
		LS1					
		LNH					
		RB1					
Total Energy	113.581						
van der Waals	113.63						
electrostatic	-249.063						
ΔEs	-153.204						
	-18.233						
	-139.336						

	H	H	Q	K	Tyr10	Leu17	Ile31
Initial Orientation	CS	RS1					
Final Orientation	LS1	RS1			RS1	RS1	RS2
	LNH	RB2					
	LB1						
	RS1						
Total Energy	88.354						
van der Waals	115.515						
electrostatic	-273.129						
ΔEs	-178.431						
	-16.348						
	-163.402						

	H	H	Q	K	Tyr10	Leu17	Ile31
Initial Orientation	CS	LS1					
Final Orientation	LB1	LS1			RS2	LS1	LB1
	CS				LS1		
	LS1						
Total Energy	131.421						
van der Waals	114.396						
electrostatic	-225.763						
ΔEs	-135.364						
	-17.467						
	-116.036						

	H	H	Q	K	Ser8	Tyr10			
Initial Orientatior	LS1	CS							
Final Orientation	LS1	RB1			RS1	LS1			
		RNH							
		RS1							
Total Energy	153.364								
van der Waals	124.57								
electrostatic	-221.332								
ΔEs	-113.421								
	-7.293								
	-111.605								

	H	H	Q	K	Tyr10	Ala30	Ile31	Leu34
Initial Orientatior	CS	RS2						
Final Orientation	LB1	RS2			CS	LS2	LS2	LB2
	CS				RB1			LS2
	RB1				RS1			
Total Energy	128.272							
van der Waals	107.93							
electrostatic	-229.8							
ΔEs	-138.513							
	-23.933							
	-120.073							

	H	H	Q	K	Tyr10	Leu17	Met35
Initial Orientatior	LS2	CS					
Final Orientation	LS2	LS2			LS2	LS2	RS2
		LB1			LS1		
		CS					
Total Energy	157.065						
van der Waals	115.325						
electrostatic	-205.955						
ΔEs	-109.72						
	-16.538						
	-96.228						

	H	H	Q	K	Tyr10	Ile31
Initial Orientatior	LB1	RB1				
Final Orientation	LB1	RB1			RB1	CS
	LB1	RS1			RNH	
	LS1				RS1	
	LNH					
Total Energy	162.629					
van der Waals	116.196					
electrostatic	-204.363					
ΔEs	-104.156					
	-15.667					
	-94.636					

	H	H	Q	K	Tyr10	Val12
Initial Orientatior	LB1	RS1				
Final Orientation	LB1	RS1			RB1	LS1
	LS1				RS1	
	LS2				RNH	
					LB1	
Total Energy	125.642					
van der Waals	115.672					
electrostatic	-243.755					
ΔEs	-141.143					
	-16.191					
	-134.028					

	H	H	Q	K	Tyr10	Leu17
Initial Orientatior	RB1	LS1				
Final Orientation	RB1	LS2			RB1	LS1
	RB1	LS1			CS	
	RS1				LB1	
	RNH				LS1	
	LS1					
Total Energy	92.271					
van der Waals	108.973					
electrostatic	-266.004					
ΔEs	-174.514					
	-22.89					
	-156.277					

	H	H	Q	K	Tyr10	Ile31	Met35
Initial Orientatior	RS2	LB1					
Final Orientation	RS2	LS2			RB2	RB1	CS
					RS2	RS1	
Total Energy	123.772						
van der Waals	115.656						
electrostatic	-237.171						
ΔEs	-143.013						
	-16.207						
	-127.444						

	H	H	Q	K	Tyr10	Val12	Leu17	Ile31
Initial Orientatior	RB1	LS2						
Final Orientation	RS2	LB2		RS2	LB2	RS2	LS2	LS1
	2	LS2		-CH2-	LS2	C=O		
	LS2					RB2		
	RB1							
Total Energy	87.586							
van der Waals	109.614							
electrostatic	-271.806							
ΔEs	-179.199							
	-22.249							
	-162.079							

	H	H	Q	K	Tyr10	Leu17	Phe20	Ile31
Initial Orientatior	LB1	RB2						
Final Orientation	LB1	RB2		LB2	RS2	RB1	LB2	RB1
	RB1			LS2	RB2	RS1		RS1
	LS2			-CH2-				
Total Energy	82.454							
van der Waals	107.24							
electrostatic	-272.631							
ΔEs	-184.331							
	-24.623							
	-162.904							

	H	H	Q	K	Tyr10	Ile31		
Initial Orientatio	RS2	CS						
Final Orientatior	RS2	LB1			LS2	CS		
		LS2			RS2	RB1		
		LS1			RB2	RS1		
Total Energy	91.679							
van der Waals	102.876							
electrostatic	-260.357							
ΔEs	-175.106							
	-28.987							
	-150.63							

	H	H	Q	K	Tyr10	Val12	Leu17	Ile31
Initial Orientatio	CS	LS2						
Final Orientation	RB1	LS2		RS2	LB2	RS2	LS2	LS1
	RS2			-CH2-	LS2	C=O		LB1
	LS2					RB2		
	LB1							
Total Energy	85.313							
van der Waals	108.596							
electrostatic	-268.431							
ΔEs	-181.472							
	-23.267							
	-158.704							

	H	H	Q	K	Tyr10	Leu17	Leu34
Initial Orientatio	RB1	LB1					
Final Orientatior	LS1	LS2			LS2	LS1	RB2
	RB1	LB2			LS1		
	RNH	LS1			LB1		
	RS1				CS		
Total Energy	106.999						
van der Waals	110.726						
electrostatic	-255.044						
ΔEs	-159.786						
	-21.137						
	-145.317						

	H	H	Q	K	Tyr10	Leu17	Ile31
Initial Orientatio	RS1	LB1					
Final Orientatior	RS2	LB1			RB1	RS1	RS1
	RS1	LS1			CS		
		2					
		CS					
Total Energy	124.873						
van der Waals	119.455						
electrostatic	-240.452						
ΔEs	-141.912						
	-12.408						
	-130.725						

	H	H	Q	K	Ser8	Tyr10	Leu17	Ile31
Initial Orientatio	LS1	RB1						
Final Orientatior	LS1	RB1			RB2	LS2	LB1	LS1
	LNH	RB1						
		RNH						
		RS1						
Total Energy	133.63							
van der Waals	113.598							
electrostatic	-230.653							
ΔEs	-133.155							
	-18.265							
	-120.926							

	H	H	Q	K	Tyr10	Leu17	Ile31
Initial Orientatio	LB1	RS2					
Final Orientation	LB1	RS2		LS2	RB1	RS2	RB2
	LS2	RB2		-CH2-	RS1		
	RB1				RS2		
	RS2						
Total Energy	112.594						
van der Waals	106.729						
electrostatic	-243.017						
ΔEs	-154.191						
	-25.134						
	-133.29						

	H	H	Q	K	Tyr10	Leu17	Val18	Ala21
Initial Orientatio	LS2	RB1						
Final Orientatior	LB2	RB1			LS1	LS2	RS2	RB2
	LS2	LS2					RB2	
		RNH						
		RS2						
Total Energy	97.578							
van der Waals	112.972							
electrostatic	-261.451							
ΔEs	-169.207							
	-18.891							
	-151.724							

	H	H	Q	K	Tyr10	Leu17	Val18	Ala21
Initial Orientatio	RB2	LB1						
Final Orientation	RB2	LB1			RB1	LB2	LB2	LB2
	RS2	LB1			RNH	RS2		
		LB2			RS1			
		LNH			RB2			
		RB1						
		RS2						
Total Energy	87.918							
van der Waals	105.741							
electrostatic	-267.353							
ΔEs	-178.867							
	-26.122							
	-157.626							

	H	H	Q	K	Tyr10	Leu17	Ile31
Initial Orientatio	RB1	LB2					
Final Orientation	LB1	LS2		RB2	LB1	LS2	LS1
	LB1			RS2	LS2		
	RB1				LB2		
	LS1						
	LS2						
Total Energy	90.053						
van der Waals	111.041						
electrostatic	-267.29						
ΔEs	-176.732						
	-20.822						
	-157.563						

	H	H	Q	K	Tyr10	Leu17	Val18	Ile31
Initial Orientatio	LB2	RB1						
Final Orientation	LB2	LB1			LB2	LB1	RB2	LS1
		RS2			LS2			LB1
Total Energy	129.34							
van der Waals	118.303							
electrostatic	-243.475							
ΔEs	-137.445							
	-13.56							
	-133.748							

	H	H	Q	K	Tyr10	Leu17	Ile31
Initial Orientatio	RS2	LS2					
Final Orientation	RS2	LS1			LS2	LS2	CS
	RB2	LS2			LB2		LB1
	LS2						
Total Energy	118.153						
van der Waals	113.636						
electrostatic	-244.455						
ΔEs	-148.632						
	-18.227						
	-134.728						

	H	H	Q	K	Ser8	Tyr10	Leu17	Ile31
Initial Orientatio	LS2	RS2						
Final Orientation	LS2	RS2			RS2	LS1	LS2	LB2
	LS1	RB2				LB1		LS2
						CS		
						RB1		
Total Energy	102.539							
van der Waals	112.356							
electrostatic	-257.899							
ΔEs	-164.246							
	-19.507							
	-148.172							

	H	H	Q	K	Tyr10	Val12	Leu17	Ile31	Met35
Initial Orientatio	RB2	LS2							
Final Orientation	RS2	LB2			LS2	RB2	LS2	LS1	LS1
	RB1	LS2							LB1
	RB2								
Total Energy	100.525								
van der Waals	112.295								
electrostatic	-259.332								
ΔEs	-166.26								
	-19.568								
	-149.605								

	H	H	Q	K	Tyr10	Leu17	Phe20
Initial Orientatio	LS2	RB2					
Final Orientation	LS2	RS2		LB2*	RS1	LB2	LB2
	LB1	RB2		LS2*		RS2	
	RS2			*-CH2-			
Total Energy	79.309						
van der Waals	105.496						
electrostatic	-271.216						
ΔEs	-187.476						
	-26.367						
	-161.489						

	H	H	Q	K	Tyr10	Val12	Leu17	Ile31
Initial Orientatio	RS2	LB2						
Final Orientation	RB2	LS2			LS2	RB2	LS2	LB1
	RS2	LB2			LB2			LS1
	RNH							
	RB1							
Total Energy	100.405							
van der Waals	112.374							
electrostatic	-258.507							
ΔEs	-166.38							
	-19.489							
	-148.78							

	H	H	Q	K	Tyr10
Initial Orientatio	LB2	RS2			
Final Orientation	LB2	RB2			LS2
	LS2	RS2			
Total Energy	175.468				
van der Waals	126.321				
electrostatic	-200.736				
ΔEs	-91.317				
	-5.542				
	-91.009				

	H	H	Q	K	Tyr10
Initial Orientatio	RB2	LB2			
Final Orientation	RB2	LS2			LB1
	RS2	LB2			RB1
Total Energy	133.402				
van der Waals	119.431				
electrostatic	-234.103				
ΔEs	-133.383				
	-12.432				
	-124.376				

	H	H	Q	K	Tyr10	Val12	Leu17	Ile31
Initial Orientatio	LB2	RB2						
Final Orientation	LB1	RB2		LB2	RS1	LS2	LS2	RB2
	LS2			LS2		C=O		
	LNH			-CH2-				
	LS2							
Total Energy	82.081							
van der Waals	107.931							
electrostatic	-275.642							
ΔEs	-184.704							
	-23.932							
	-165.915							

	H	H	Q	K	Tyr10	Val12
Initial Orientatio	CS			RB1		
Final Orientation	CS			RB2	RS1	
				RNH	RB1	
				RS1*		
				RB1*		
				*-CH2-		
Total Energy	155.141					
van der Waals	119.296					
electrostatic	-212.451					
ΔEs	-111.644					
	-12.567					
	-102.724					

	H	H	Q	K	Val12
Initial Orientatio	CS			LB1	
Final Orientation	CS			LS1	CS
				LB1	C=O
Total Energy	203.203				
van der Waals	124.276				
electrostatic	-170.014				
ΔEs	-63.582				
	-7.587				
	-60.287				

	H	H	Q	K
Initial Orientatio	CS			RS1
Final Orientation	CS			RS1
Total Energy	172.739			
van der Waals	130.443			
electrostatic	-201.862			
ΔEs	-94.046			
	-1.42			
	-92.135			

	H	H	Q	K	Val12
Initial Orientatio	RS1			CS	
Final Orientation	RS1			RB1	RS1
	RS2			CS	
				RS2	
Total Energy	180.046				
van der Waals	123.299				
electrostatic	-190.264				
ΔEs	-86.739				
	-8.564				
	-80.537				

	H	H	Q	K	Val12
Initial Orientatio	CS			LS1	
Final Orientation	RB1			LS1	CS
	CS			LS2	LB1
	RS1			2	
				CS	
Total Energy	131.771			-CH2-	
van der Waals	120.688				
electrostatic	-234.21				
ΔEs	-135.014				
	-11.175				
	-124.483				

	H	H	Q	K	Val12
Initial Orientatio	LS1			CS	
Final Orientation	LS2			RB1	LS2
	LS1			LS1	
				-CH2-	
				LB1	
Total Energy	112.348				
van der Waals	118.4				
electrostatic	-250.78				
ΔEs	-154.437				
	-13.463				
	-141.053				

	H	H	Q	K
Initial Orientatio	LS2			CS
Final Orientation	LS2			RB1
				RS2
				LB1
				LS2
Total Energy	130.305			-CH2-
van der Waals	124.737			
electrostatic	-248.375			
ΔEs	-136.48			
	-7.126			
	-138.648			

	H	H	Q	K	Val12
Initial Orientatio	CS			LS2	
Final Orientation	LB1			LS2	LS1
	LS1			LS1	
	CS			-CH2-	
Total Energy	151.659				
van der Waals	123.952				
electrostatic	-223.431				
ΔEs	-115.126				
	-7.911				
	-113.704				

	H	H	Q	K	Tyr10
Initial Orientatio	CS			RS2	
Final Orientation	LB1			RS1	LS2
	LS2			RS2	
	CS*				
	RB1*				
	*-CH2-				
Total Energy	115.748				
van der Waals	119.89				
electrostatic	-250.767				
ΔEs	-151.037				
	-11.973				
	-141.04				

	H	H	Q	K	Val12	Phe19
Initial Orientatio	RS2			CS		
Final Orientation	RS1			LB1	RS1	LB2
	RS2			LS2		
	RB2			RS2		
				-CH2-		
Total Energy	140.666					
van der Waals	120.545					
electrostatic	-228.979					
ΔEs	-126.119					
	-11.318					
	-119.252					

	H	H	Q	K	Phe19
Initial Orientatio	LB1			RB1	
Final Orientation	LS1			RS1	RS1
	LNH			RB1	
	LB1			RNH	
Total Energy	144.492				
van der Waals	120.031				
electrostatic	-226.666				
ΔEs	-122.293				
	-11.832				
	-116.939				

	H	H	Q	K				
Initial Orientatio	RB1			LB1				
Final Orientation	RB1			LB1				
	RNH			LS1				
	RS1			CS				
				-CH2-				
Total Energy	144.383							
van der Waals	123.62							
electrostatic	-227.609							
ΔEs	-122.402							
	-8.243							
	-117.882							

	H	H	Q	K				
Initial Orientatio	LB1			RS1				
Final Orientation	LB1			RS1	LS1	LB2		
	LB1							
	LS1							
	LNH							
Total Energy	113.661							
van der Waals	120.14							
electrostatic	-258.648							
ΔEs	-153.124							
	-11.723							
	-148.921							

	H	H	Q	K				
Initial Orientatio	RS1			LB1				
Final Orientation				LB1				
				LS1				
				RS1				
				RB1				
Total Energy	139.916			-CH2-				
van der Waals	124.296							
electrostatic	-232.346							
ΔEs	-126.869							
	-7.567							
	-122.619							

	H	H	Q	K	Val12			
Initial Orientatio	LS1			RB1				
Final Orientation	LS1			RB1	CS			
				RS1	LB1			
					LS1			
Total Energy	140.142							
van der Waals	124.617							
electrostatic	-239.846							
ΔEs	-126.643							
	-7.246							
	-130.119							

	H	H	Q	K	Tyr10			
Initial Orientatio	RB1			LS1				
Final Orientation	RS2			LB1	RS1			
	RB1			LS2				
	RS1			2				
				LS1				
Total Energy	116.5			CS				
van der Waals	123.199			-CH2-				
electrostatic	-260.676							
ΔEs	-150.285							
	-8.664							
	-150.949							

	H	H	Q	K	Tyr10			
Initial Orientatio	LB1			RS2				
Final Orientation	LB1			RS2	LS2			
	LS2			2	2			
	LS1			CS				
				-CH2-				
Total Energy	125.551							
van der Waals	120.292							
electrostatic	-240.486							
ΔEs	-141.234							
	-11.571							
	-130.759							

	H	H	Q	K	Val12			
Initial Orientatio	RS2			LB1				
Final Orientation	RB2			LS2	RS2			
	RS2			RS2				
	2			-CH2-				
				RB1				
Total Energy	133.363							
van der Waals	119.563							
electrostatic	-230.059							
ΔEs	-133.422							
	-12.3							
	-120.332							

	H	H	Q	K	Val12	Phe19		
Initial Orientatio	LS2			RB1				
Final Orientation	LS2			LB1	LS2	RB1		
				RB1	C=O	RS1		
				RS2		RS2		
				LS2				
Total Energy	109.588			-CH2-				
van der Waals	113.086			RNH				
electrostatic	-253.445							
ΔEs	-157.197							
	-18.777							
	-143.718							

	H	H	Q	K	Val12			
Initial Orientatio	RB1			LS2				
Final Orientation	RS2			LS2	CS			
Total Energy	150.103							
van der Waals	125.883							
electrostatic	-219.597							
ΔEs	-116.682							
	-5.98							
	-109.87							

	H	H	Q	K	Tyr10	Val12	Leu17	
Initial Orientatio	LB1			RB2				
Final Orientation	LB1	LS2		RB2	LS2	RB2	LS2	
	LB1			RS2	LB2			
	RS2							
	RB1							
	LS2							
Total Energy	86.324							
van der Waals	111.154							
electrostatic	-272.262							
ΔEs	-180.461							
	-20.709							
	-162.535							

	H	H	Q	K				
Initial Orientatio	RB2			LB1				
Final Orientation				LB1				
				RB1				
Total Energy	159.296							
van der Waals	124.35							
electrostatic	-210.94							
ΔEs	-107.489							
	-7.513							
	-101.213							

	H	H	Q	K	His6	Glu11	Val12	
Initial Orientatio	LB2			RB1				
Final Orientation	LS2		RS2	RB1	RS2	RB2	LS2	
	LB2		-CH2-	LS2	RB2	-CH2-	C=O	
				-CH2-				
				LB1				
Total Energy	149.065							
van der Waals	117.135							
electrostatic	-214.03							
ΔEs	-117.72							
	-14.728							
	-104.303							

	H	H	Q	K	Tyr10			
Initial Orientatio	RB1			LB2				
Final Orientation	RB1			LB2	RNH			
	RB1			LS1	RS1			
	LB1				RB2			
	RNH							
	RS1							
Total Energy	114.264							
van der Waals	112.566							
electrostatic	-245.194							
ΔEs	-152.521							
	-19.297							
	-135.467							

	H	H	Q	K	Tyr10			
Initial Orientatio	LB2			RS1				
Final Orientation	LB1			RS1	LS1			
	LB2			RB1				
	LS1			RNH				
	LNH							
Total Energy	133.015							
van der Waals	115.889							
electrostatic	-231.039							
ΔEs	-133.77							
	-15.974							
	-121.312							

	H	H	Q	K	Val12	Leu17	Phe20	
Initial Orientatio	RS2			LS2				
Final Orientation	RS2			RB1	RB1	RS2	RB2	
				LS2	CS			
				RS2				
				-CH2-				
Total Energy	98.592							
van der Waals	114.767							
electrostatic	-262.539							
ΔEs	-168.193							
	-17.096							
	-152.812							

	H	H	Q	K				
Initial Orientatio	LS2			RS2				
Final Orientation	RB2			RS2				
	RB2			RS2				
	RS2			RB1				
				RS2				
Total Energy	114.082							
van der Waals	123.289							
electrostatic	-256.233							
ΔEs	-152.703							
	-8.574							
	-146.506							

	H	H	Q	K	Tyr10	Val12	Phe19	
Initial Orientatio	RB2			LS2				
Final Orientation	RB2			LS2	RB2	RS2	LB2	
	RB2			LNH				
	RS2			LB1				
Total Energy	143.321							
van der Waals	121.255							
electrostatic	-234.803							
ΔEs	-123.464							
	-10.608							
	-125.076							

	H	H	Q	K	His6	Glu11		
Initial Orientatio	LB2			RS2				
Final Orientation	LS2		RB2	LS2	RB2	RB2		
	LB2			-CH2-		C=O		
				RS2				
Total Energy	125.484							
van der Waals	120.78							
electrostatic	-251.266							
ΔEs	-141.301							
	-11.083							
	-141.539							

	H	H	Q	K	Glu11	Phe19	
Initial Orientatio	RS2			LB2			
Final Orientation	RS2		LB2	LB1	LS2	LB2	
			LS2	LS2	C=O		
			-CH2-	RB1			
				RS2			
Total Energy	105.8			-CH2-			
van der Waals	108.479						
electrostatic	-250.285						
ΔEs	-160.985						
	-23.384						
	-140.558						

	H	H	Q	K				
Initial Orientatior	LB2			RB2				
Final Orientation	LS2			RS2				
				RB1				
Total Energy	119.734							
van der Waals	121.746							
electrostatic	-248.885							
ΔEs	-147.051							
	-10.117							
	-139.158							

	H	H	Q	K	Phe19	Ala30		
Initial Orientatio	RB2			LB2				
Final Orientatior	RB2			LS2	LB2	RB2		
	RS2			RS2				
				-CH2-				
				LB1				
Total Energy	120.241			LNH				
van der Waals	123.502							
electrostatic	-250.331							
ΔEs	-146.544							
	-8.361							
	-140.604							

	H	H	Q	K	Tyr10	Val12	Leu17	
Initial Orientation		LB2		RB2				
Final Orientation	RS2	LB2		RB2	LB1	RB2	LS2	
	RB1	LS2		RS2	LNH	RS2		
	LB1			-CH2-		C=O		
	LS2					RNH		
						RB1		
Total Energy	89.198							
van der Waals	109.493							
electrostatic	-265.449							
ΔEs	-177.587							
	-22.37							
	-155.722							

	H	H	Q	K	Tyr10	Val12	Leu17	Ile31
Initial Orientation		RB2		LB2				
Final Orientatior	LB1	RB2		LB2	RS2	LS2	RS2	RB2
	RB1	RS2		LS2			RB2	
	LS2							
	RS2							
Total Energy	104.356							
van der Waals	112.157							
electrostatic	-252.406							
ΔEs	-162.429							
	-19.706							
	-142.679							

	L	V	F	F	Arg5	Ser8	Tyr10	His13	His14	Ile31
Initial Orientatior	RB2	LB2								
Final Orientation	RS2	LB2			LB2	LB1	RB1	RB2	RB1	RS2
	RB2				LS1		RS1		LB1	RB2
Total Energy	115.978									
van der Waals	110.769									
electrostatic	-242.869									
ΔEs	-150.807									
	-21.094									
	-133.142									

	L	V	F	F	Arg5	Tyr10	His13	His14
Initial Orientatior	LB2							
Final Orientatior	LS2				RS2	LB2	LB2	LB1
						LS2	LS2	LS2
								RB1
Total Energy	94.296							
van der Waals	110.923							
electrostatic	-264.344							
ΔEs	-172.489							
	-20.94							
	-154.617							

	L	V	F	F	Val12	His13	Lys16
Initial Orientatior	LB2		RB2				
Final Orientation	LB2		RB2	LS2	LB1	LB2	LS2
					C=O	LS1	-CH2-
						LNH	RB1
						LB1	RNH
Total Energy	109.477						RS2
van der Waals	113.847						
electrostatic	-252.906						
ΔEs	-157.308						
	-18.016						
	-143.179						

	L	V	F	F	His13	Lys16	Ala30
Initial Orientatio	RB2		LB2				
Final Orientatior	RB2		LB2	CS	RS2	LS2	RB2
			LS2	RB1	RB2	LS1	
						RB2	
						-CH2-	
Total Energy	120.796						
van der Waals	114.273						
electrostatic	-237.58						
ΔEs	-145.989						
	-17.59						
	-127.853						

	L	V	F	F	Tyr10	His13	His14	Lys16	Ile31
Initial Orientatior	RB2			LB2					
Final Orientation	RS2			LB2	RS2	LB1	RB2	LS2	RB1
				LS2		RB1	RS2		RNH
						RS2			
Total Energy	96.269								
van der Waals	110.673								
electrostatic	-261.604								
ΔEs	-170.516								
	-21.19								
	-151.877								

	L	V	F	F	His13	Ile31
Initial Orientatio	LB2			RB2		
Final Orientatior	LB2				LNH	LS2
					LB2	LB2
Total Energy	179.879					
van der Waals	121.365					
electrostatic	-186.753					
ΔEs	-86.906					
	-10.498					
	-77.026					

	L	V	F	F	Arg5	Ala21	Asp23
Initial Orientation		RB2	LB2				
Final Orientation					RS1	RB2	LB2
Total Energy	240.003						
van der Waals	122.529						
electrostatic	-132.045						
ΔEs	-26.782						
	-9.334						
	-22.318						

	L	V	F	F	Arg5
Initial Orientation		LB2	RB2		
Final Orientation					LS2
Total Energy	245.612				
van der Waals	128.819				
electrostatic	-132.831				
ΔEs	-21.173				
	-3.044				
	-23.104				

	L	V	F	F	Lys16
Initial Orientation			LB1	RB1	
Final Orientation			LS1	RB1	LS1
					2
					LB1
Total Energy	205.134				
van der Waals	125.216				
electrostatic	-169.977				
ΔEs	-61.651				
	-6.647				
	-60.25				

	L	V	F	F	Lys16
Initial Orientation			RB1	LB1	
Final Orientation			CS	LS1	RB1
			RB1	LB1	RS2
			RS1	CS	CS
Total Energy	161.237				
van der Waals	118.675				
electrostatic	-212.044				
ΔEs	-105.548				
	-13.188				
	-102.317				

	L	V	F	F	Lys16
Initial Orientation			RB2	LB1	
Final Orientation			RB2	RB1	RB2
					RS1
					2
Total Energy	201.536				
van der Waals	125.789				
electrostatic	-172.429				
ΔEs	-65.249				
	-6.074				
	-62.702				

	L	V	F	F	Lys16
Initial Orientation			LB1	RB2	
Final Orientation			LB1	RS2	RB1
			CS		RS2
					2
Total Energy	174.261				
van der Waals	120.488				
electrostatic	-193.565				
ΔEs	-92.524				
	-11.375				
	-83.838				

	L	V	F	F	Val12	His13	Lys16
Initial Orientation			LB2	RB1			
Final Orientation			LB2	RB1	RB2	RB2	RB1
						RS1	LS2
							LB1
							RNH*
Total Energy	139.756						RS1*
van der Waals	114.317						*-CH2-
electrostatic	-222.72						
ΔEs	-127.029						
	-17.546						
	-112.993						

	L	V	F	F	Lys16
Initial Orientation			RB1	LB2	
Final Orientation				LB2	LB1
					LNH
					LS1
Total Energy	214.669				
van der Waals	127.212				
electrostatic	-156.966				
ΔEs	-52.116				
	-4.651				
	-47.239				

	L	V	F	F	Lys16
Initial Orientation			LB2	RB2	
Final Orientation			LS2		LS2
			LB2		2
Total Energy	175.798				
van der Waals	129.1				
electrostatic	-198.029				
ΔEs	-90.987				
	-2.763				
	-88.302				

	L	V	F	F	Lys16
Initial Orientation			RB2	LB2	
Final Orientation			RB2		RS1
					2
Total Energy	191.417				
van der Waals	127.44				
electrostatic	-180.8				
ΔEs	-75.368				
	-4.423				
	-71.073				

	H	H	Q	K	L	V	F	F	Arg5	Tyr10	Ile31	Met35
Initial Orientation	LB2					RB2						
Final Orientation	LB2	LB1			LS2	RB2			RB2	LB2	LB1	CS
	LS2	LS2								LS2		
		RB1										
		RS2										
Total Energy	100.457											
van der Waals	106.939											
electrostatic	-262.125											
ΔEs	-166.328											
	-24.924											
	-152.398											

	H	H	Q	K	L	V	F	F	Glu11	Val12
Initial Orientation	LS1						RB2			
Final Orientation	LS1			LB1			RB2		RB1	LB1
				-CH2-					C=O	CS
				RB1						
				RS2						
Total Energy	115.6									
van der Waals	118.507									
electrostatic	-254.839									
ΔEs	-151.185									
	-13.356									
	-145.112									

	H	H	Q	K	L	V	F	F	Val12
Initial Orientation	LS2						RB2		
Final Orientation	LS2			RS2			RS2		LS2
	LS1			2			RB2		
				RB1					
Total Energy	124.179								
van der Waals	115.307								
electrostatic	-234.341								
ΔEs	-142.606								
	-16.556								
	-124.614								

	H	H	Q	K	L	V	F	F	Val12
Initial Orientation	LB2						RB2		
Final Orientation	LB2			RS2			RS1	RB2	LNH
	LS2			RB1			RB2		LB1
Total Energy	124.332								
van der Waals	113.258								
electrostatic	-236.964								
ΔEs	-142.453								
	-18.605								
	-127.237								

	H	H	Q	K	L	V	F	F	Ala30	Ile31
Initial Orientation	CS							RB1		
Final Orientation	LS2			RS1	CS			RB1	RS1	RS1
	LB1			RS2					LB1	
				CS*						
				RB1*						
				*-CH2-						
Total Energy	144.712									
van der Waals	108.961									
electrostatic	-210.574									
ΔEs	-122.073									
	-22.902									
	-100.847									

	H	H	Q	K	L	V	F	F
Initial Orientation	CS							LB2
Final Orientation	LB1			LS1				LB2
	CS			LS2				LS2
Total Energy	139.484							
van der Waals	121.098							
electrostatic	-230.755							
ΔEs	-127.301							
	-10.765							
	-121.028							

	H	H	Q	K	L	V	F	F	Gly29	Ala30
Initial Orientation	RB1							LB1		
Final Orientation	RS1							LB1	CS	CS
	RB1								C=O	
Total Energy	223.416									
van der Waals	124.67									
electrostatic	-146.555									
ΔEs	-43.369									
	-7.193									
	-36.828									

	H	H	Q	K	L	V	F	F
Initial Orientation	LS1							RB1
Final Orientation	LS1			LB1				CS
				LS2				
				LS1				
				-CH2-				
Total Energy	182.782							
van der Waals	120.544							
electrostatic	-186.453							
ΔEs	-84.003							
	-11.319							
	-76.726							

	H	H	Q	K	L	V	F	F	Tyr10	Ala21	Ile31	Ile32
Initial Orientatio	RB2					LB2						
Final Orientatior	RS2	LB1			RS2				RS1	LB2	RS2	LS2
		RB1									RB2	
		LNH										
Total Energy	92.363											
van der Waals	111.484											
electrostatic	-269.366											
ΔEs	-174.422											
	-20.379											
	-159.639											

	H	H	Q	K	L	V	F	F	His6	Val12
Initial Orientatio	RB2						LB1			
Final Orientation	RB2			LB1			LS1		LB2	RB2
	RS1			RB1			LB1			
				RNH*						
				RS1*						
Total Energy	151.262			*-CH2-						
van der Waals	110.167									
electrostatic	-214.008									
ΔEs	-115.523									
	-21.696									
	-104.281									

	H	H	Q	K	L	V	F	F	Val12
Initial Orientatio	RB1						LB2		
Final Orientation	RS1			LB1			LB2		RS1
	RB1			LNH					
Total Energy	173.478								
van der Waals	116.807								
electrostatic	-193.952								
ΔEs	-93.307								
	-15.056								
	-84.225								

	H	H	Q	K	L	V	F	F
Initial Orientatio	RS1						LB2	
Final Orientation	RS1			RB1			LB2	LB1
				LS2				CS
				LB1				
Total Energy	160.442							
van der Waals	119.645							
electrostatic	-203.803							
ΔEs	-106.343							
	-12.218							
	-94.076							

	H	H	Q	K	L	V	F	F
Initial Orientatio	RS2						LB2	
Final Orientatior	RS2			LS2			LB2	
	RB2			RS2				
				-CH2-				
Total Energy	177.297							
van der Waals	124.2							
electrostatic	-190.09							
ΔEs	-89.488							
	-7.663							
	-80.363							

	H	H	Q	K	L	V	F	F	His6
Initial Orientatio	RB2						LB2		
Final Orientation	RB2			LS2			LS1		LB2
	RS2			LNH			LNH		
				LB1					
				RS2					
Total Energy	112.034			-CH2-					
van der Waals	114.1								
electrostatic	247.527								
ΔEs	-154.751								
	-17.763								
	357.254								

	H	H	Q	K	L	V	F	F	Gly29	Ala30
Initial Orientatio	CS							RB2		
Final Orientation	RB1			LS2	RS2			RB2	RB2	RB2
	RS2			RS2	RS1				C=O	RS1
	RS1			-CH2-						
	LB1			LB2						
Total Energy	106.808									
van der Waals	116.914									
electrostatic	-266.849									
ΔEs	-159.977									
	-14.949									
	-157.122									

	H	H	Q	K	L	V	F	F
Initial Orientatio	LB1							RB1
Final Orientatior	LS1							
Total Energy	232.751							
van der Waals	128.9							
electrostatic	-142.427							
ΔEs	-34.034							
	-2.963							
	-32.7							

	H	H	Q	K	L	V	F	F	Val12
Initial Orientatio	RS1							LB1	
Final Orientation	RS1			RS1					RS1
	RS2			-CH2-					
Total Energy	158.871								
van der Waals	123.077								
electrostatic	-209.897								
ΔEs	-107.914								
	-8.786								
	-100.17								

	H	H	Q	K	L	V	F	F	Val12
Initial Orientatio	LS2							RB1	
Final Orientation	LS2			RS2				CS	LS2
	LS1			LS2*				RB1	
				LB1*					
				CS*					
Total Energy	117.873			*-CH2-					
van der Waals	112.473			RB1					
electrostatic	-240.863								
ΔEs	-148.912								
	-19.39								
	-131.136								

	H	H	Q	K	L	V	F	F	Lys28
Initial Orientation	RS2							LB1	
Final Orientation	RB2			RS1				CS	LB2
	RS2			2					LS2
				RS2					
				-CH2-					
Total Energy	110.321								
van der Waals	117.198								
electrostatic	-264.49								
ΔEs	-156.464								
	-14.665								
	-154.763								

	H	H	Q	K	L	V	F	F	Tyr10	Ile31
Initial Orientation	LB1							RB2		
Final Orientation	LB1			RS1					LS1	LB2
	LB1									
	LS1									
	RB1									
Total Energy	109.697									
van der Waals	114.288									
electrostatic	-252.191									
ΔEs	-157.088									
	-17.575									
	-142.464									

	H	H	Q	K	L	V	F	F	Val12	Ala30
Initial Orientation	RB2							LB1		
Final Orientation	RS1			LB1	RS1		LB2	LB1	RB2	RS1
	RB2			LS2			LNH	RB1		
				LNH						
				RB1						
				RNH*						
Total Energy	102.45			RS1*						
van der Waals	106.463			RB2*						
electrostatic	-252.083			*-CH2-						
ΔEs	-164.335									
	-25.4									
	-142.356									

	H	H	Q	K	L	V	F	F	Val12	Gly29
Initial Orientation	RB1							LB2		
Final Orientation	RS1			RS2				LB2	RS1	LS1
	RB1							LS1		C=O
	RNH									
Total Energy	143.087									
van der Waals	117.447									
electrostatic	-235.114									
ΔEs	-123.698									
	-14.416									
	-125.387									

	H	H	Q	K	L	V	F	F	Lys28	Gly29
Initial Orientation	RS1							LB2		
Final Orientation	RS1			RNH*				LB1	LS1	LS1*
	RS1*									LNH*
	*-CH2-									LB1*
	RB2									*C=O
Total Energy	151.948									
van der Waals	118.16									
electrostatic	-215.342									
ΔEs	-114.837									
	-13.703									
	-105.615									

	H	H	Q	K	L	V	F	F		
Initial Orientation	RS2							LB2		
Final Orientation	RS2			LS2				LB2		
	2									
Total Energy	148.022									
van der Waals	130.638									
electrostatic	-233.8									
ΔEs	-118.763									
	-1.225									
	-124.073									

	H	H	Q	K	L	V	F	F	Tyr10	Val12
Initial Orientation	RB2							LB2		
Final Orientation	RB2								RB2	RS2
	RB2									C=O
	RS2									RB2
Total Energy	163.689									
van der Waals	121.443									
electrostatic	-200.727									
ΔEs	-103.096									
	-10.42									
	-91									

	H	H	Q	K	L	V	F	F	Lys28
Initial Orientation	RS2							LB1	
Final Orientation	RB2			RS1				CS	LB2
	RS2			2					LS2
				RS2					
				-CH2-					
Total Energy	110.321								
van der Waals	117.198								
electrostatic	-264.49								
ΔEs	-156.464								
	-14.665								
	-154.763								

	H	H	Q	K	L	V	F	F	Tyr10	Ile31
Initial Orientation	LB1							RB2		
Final Orientation	LB1			RS1					LS1	LB2
	LB1									
	LS1									
	RB1									
Total Energy	109.697									
van der Waals	114.288									
electrostatic	-252.191									
ΔEs	-157.088									
	-17.575									
	-142.464									

	H	H	Q	K	L	V	F	F	Val12	Ala30
Initial Orientation	RB2							LB1		
Final Orientation	RS1			LB1	RS1		LB2	LB1	RB2	RS1
	RB2			LS2			LNH	RB1		
				LNH						
				RB1						
				RNH*						
Total Energy	102.45			RS1*						
van der Waals	106.463			RB2*						
electrostatic	-252.083			*-CH2-						
ΔEs	-164.335									
	-25.4									
	-142.356									

	H	H	Q	K	L	V	F	F	Val12	Gly29
Initial Orientation	RB1							LB2		
Final Orientation	RS1			RS2				LB2	RS1	LS1
	RB1							LS1		C=O
	RNH									
Total Energy	143.087									
van der Waals	117.447									
electrostatic	-235.114									
ΔEs	-123.698									
	-14.416									
	-125.387									

	H	H	Q	K	L	V	F	F	Lys28	Gly29
Initial Orientation	RS1							LB2		
Final Orientation	RS1			RNH*				LB1	LS1	LS1*
	RS1*									LNH*
	*-CH2-									LB1*
	RB2									*C=O
Total Energy	151.948									
van der Waals	118.16									
electrostatic	-215.342									
ΔEs	-114.837									
	-13.703									
	-105.615									

	H	H	Q	K	L	V	F	F		
Initial Orientation	RS2							LB2		
Final Orientation	RS2			LS2				LB2		
	2									
Total Energy	148.022									
van der Waals	130.638									
electrostatic	-233.8									
ΔEs	-118.763									
	-1.225									
	-124.073									

	H	H	Q	K	L	V	F	F	Tyr10	Val12
Initial Orientation	RB2							LB2		
Final Orientation	RB2								RB2	RS2
	RB2									C=O
	RS2									RB2
Total Energy	163.689									
van der Waals	121.443									
electrostatic	-200.727									
ΔEs	-103.096									
	-10.42									
	-91									

	H	H	Q	K	L	V	F	F	Glu22	Ile31	Ile32
Initial Orientatic		CS				RB1					
Final Orientation		RB1			LS2	CS			RS1	LS2	CS
		LS2							-CH2-		
		LS1									
Total Energy	143.487										
van der Waals	109.72										
electrostatic	-221.231										
ΔEs	-123.298										
	-22.143										
	-111.504										

	H	H	Q	K	L	V	F	F	Phe4	Arg5	Ile31	Ile32	Met35
Initial Orientation		CS				LB1							
Final Orientation		RB1			RS1	LB1			LS1	LS1	RS1	RS1	RB2
		CS								LS2	RB2		
		RS1											
		RS2											
Total Energy	124.995												
van der Waals	111.889												
electrostatic	-234.434												
ΔEs	-141.79												
	-19.974												
	-124.707												

	H	H	Q	K	L	V	F	F	Arg5	Ile31	Ile32	Met35
Initial Orientatic		LB1				RB1						
Final Orientation		LS1			LS1				RB2	LS2	LB1	LS2
		LB1							RS1			
Total Energy	116.543											
van der Waals	113.55											
electrostatic	-247.665											
ΔEs	-150.242											
	-18.313											
	-137.938											

	H	H	Q	K	L	V	F	F	Arg5	Glu22
Initial Orientation		RB1				LB1				
Final Orientation		RB1				CS			CS	LB1
Total Energy	113.29									
van der Waals	115.022									
electrostatic	-251.507									
ΔEs	-153.495									
	-16.841									
	-141.78									

	H	H	Q	K	L	V	F	F	Arg5	Glu22
Initial Orientatic		RS1				CS				
Final Orientation		RS1				CS			CS	LB1
Total Energy	197.194									
van der Waals	122.207									
electrostatic	-176.384									
ΔEs	-69.591									
	-9.656									
	-66.657									

	H	H	Q	K	L	V	F	F	Ala21	Glu22
Initial Orientation		LS1				RB1				
Final Orientation		LS1							RS1	RS1
		LB1								-CH2-
Total Energy	222.478									
van der Waals	122.271									
electrostatic	-146.347									
ΔEs	-44.307									
	-9.592									
	-36.62									

	H	H	Q	K	L	V	F	F	Arg5	Tyr10	Glu22
Initial Orientatic		LB1				RB2					
Final Orientatio	LB2	LB1			LS2	RS2			RB2	LB2	RB2
	LS2	LS2				RB2			RS1	LS2	
		RB1									
		RS2									
Total Energy	93.997										
van der Waals	106.261										
electrostatic	-263.289										
ΔEs	-172.788										
	-25.602										
	-153.562										

	H	H	Q	K	L	V	F	F	Arg5	Tyr10	Ile31
Initial Orientation		RB2				LB2					
Final Orientation	RS2	RB1			RS2	LB2			LB2	RS2	RS1
		LB1				LS2			LS1	RB2	
		RS2									
Total Energy	77.699										
van der Waals	103.791										
electrostatic	-272.457										
ΔEs	-189.086										
	-28.072										
	-162.73										

	H	H	Q	K	L	V	F	F	Arg5	Tyr10	Ile31
Initial Orientatic		LB2				RB2					
Final Orientatio	LB2	RB1			LS2	RB2			RB2	LS2	LB1
		LB1							RS2		LNH
		LS2									LB2
Total Energy	98.284										
van der Waals	110.558										
electrostatic	-255.866										
ΔEs	-168.501										
	-21.305										
	-146.139										

	H	H	Q	K	L	V	F	F	Val12
Initial Orientation				CS			RB1		
Final Orientation	LS1			RS1			RS1	LB2	LS1
				LS1*					C=O
				LNH*					
				*-CH2-					
Total Energy	124.222								
van der Waals	119.022								
electrostatic	-244.528								
ΔEs	-142.563								
	-12.841								
	-134.801								

	H	H	Q	K	L	V	F	F
Initial Orientation				CS			LB1	
Final Orientation				LS2			LS1	
				2				
Total Energy	161.984							
van der Waals	126.065							
electrostatic	-214.478							
ΔEs	-104.801							
	-5.798							
	-104.751							

	H	H	Q	K	L	V	F	F	Val12
Initial Orientation				RB1			LB1		
Final Orientation				RB1			LB1		RS1
				RS2			CS		
				RS1					
Total Energy	168.37								
van der Waals	122.108								
electrostatic	-197.595								
ΔEs	-98.415								
	-9.755								
	-87.868								

	H	H	Q	K	L	V	F	F
Initial Orientation				LB1			RB1	
Final Orientation				LS1			CS	
				2				
				LB1				
Total Energy	193.001							
van der Waals	131.687							
electrostatic	-189.157							
ΔEs	-73.784							
	-0.176							
	-79.43							

	H	H	Q	K	L	V	F	F
Initial Orientation				RS1			LB1	
Final Orientation				RS1			CS	
				3				
Total Energy	196.244							
van der Waals	133.714							
electrostatic	-186.587							
ΔEs	-70.541							
	1.851							
	-76.86							

	H	H	Q	K	L	V	F	F
Initial Orientation				LS1			RB1	
Final Orientation				LS1			CS	
				3				
Total Energy	178.179							
van der Waals	129.946							
electrostatic	-204.79							
ΔEs	-88.606							
	-1.917							
	-95.063							

	H	H	Q	K	L	V	F	F
Initial Orientation				RS2			LB1	
Final Orientation				RS2			CS	
				2				
				RS1				
Total Energy	182.372							
van der Waals	129.574							
electrostatic	-199.197							
ΔEs	-84.413							
	-2.289							
	-89.47							

	H	H	Q	K	L	V	F	F
Initial Orientation				LS2			RB1	
Final Orientation				LS1			LS2	
				LB1			LB1	
				LS2			CS	
Total Energy	161.637							
van der Waals	123.392							
electrostatic	-221.574							
ΔEs	-105.148							
	-8.471							
	-111.847							

	H	H	Q	K	L	V	F	F					H	H	Q	K	L	V	F	F	Val12
Initial Orientation				RB2			LB1					Initial Orientation				LB1			RB2		
Final Orientation				RB2			RB1					Final Orientation	LS1			LS1*			RS1		LS1
				RS1			CS									LNH*			RB2		C=O
				RNH			LB1									*-CH2-					
																RB1					
																RNH					
Total Energy	177.444											Total Energy	122.653								
van der Waals	123.22											van der Waals	115.562								
electrostatic	-191.461											electrostatic	-245.953								
ΔEs	-89.341											ΔEs	-144.132								
	-8.643												-16.301								
	-81.734												-136.226								

	H	H	Q	K	L	V	F	F					H	H	Q	K	L	V	F	F	Val12
Initial Orientation				LB2			RB1					Initial Orientation				RB1			LB2		
Final Orientation				LB1			LB1					Final Orientation				RB1					RS1
				LS2			CS									LB1					RB1
				LNH			RB1									RB2					
																LS2					
Total Energy	166.004											Total Energy	148.754								
van der Waals	122.824											van der Waals	116.267								
electrostatic	-206.523											electrostatic	-213.566								
ΔEs	-100.781											ΔEs	-118.031								
	-9.039												-15.596								
	-96.796												-103.839								

	H	H	Q	K	L	V	F	F	His6	Asp23			H	H	Q	K	L	V	F	F	Val12
Initial Orientation				LS2			RB2					Initial Orientation				RS2			LB2		
Final Orientation				LS2					LB2	RB2		Final Orientation	RB2			RB1			LB2		RS2
													RS2			RNH*			LS2		C=O
																RS2*					
																RB2*					
																*-CH2-					
Total Energy	164.095											Total Energy	137.992								
van der Waals	122.648											van der Waals	120.94								
electrostatic	-207.194											electrostatic	-230.69								
ΔEs	-102.69											ΔEs	-128.793								
	-9.215												-10.923								
	-97.467												-120.963								

	H	H	Q	K	L	V	F	F	Val12				H	H	Q	K	L	V	F	F	
Initial Orientation				LB2			RB2					Initial Orientation				RB2			LB2		
Final Orientation				LB2					LB2			Final Orientation				RS1					
				LS2												RNH					
				2												RB2					
Total Energy												Total Energy	187.968								
van der Waals												van der Waals	125.272								
electrostatic												electrostatic	-182.32								
ΔEs	-266.785											ΔEs	-78.817								
	-131.863												-6.591								
	109.727												-72.593								

	H	H	Q	K	L	V	F	F	Ala30				H	H	Q	K	L	V	F	F	
Initial Orientation				CS				LB1				Initial Orientation				CS				RB2	
Final Orientation	LS1			CS	LS1		RB1	LB1	LS1			Final Orientation	RS1			RS2				RB2	
	LS2			LS2*			RS1									2					
				LS1*												RB1*					
				LB1*												RS1*					
				*-CH2-												*-CH2-					
Total Energy	126.133											Total Energy	140.714								
van der Waals	111.017											van der Waals	118.665								
electrostatic	-245.26											electrostatic	-229.186								
ΔEs	-140.652											ΔEs	-126.071								
	-20.846												-13.198								
	-135.533												-119.459								

	H	H	Q	K	L	V	F	F					H	H	Q	K	L	V	F	F	
Initial Orientation				CS				LB2				Initial Orientation				LB1				RB1	
Final Orientation	LS2			LB1				LS1				Final Orientation				LB1			CS	RB1	
				LS1												LS1				CS	
				LS2												2					
				-CH2-																	
Total Energy	148.612											Total Energy	176.618								
van der Waals	121.812											van der Waals	120.18								
electrostatic	-218.016											electrostatic	-192.519								
ΔEs	-118.173											ΔEs	-90.167								
	-10.051												-11.683								
	-108.289												-82.792								

	H	H	Q	K	L	V	F	F					H	H	Q	K	L	V	F	F	
Initial Orientation				RB1				LB1				Initial Orientation				RS1				LB1	
Final Orientation				RB1								Final Orientation				RS1				CS	
				RS1												2					
				2																	
				CS																	
				-CH2-																	
Total Energy	190.534											Total Energy	216.461								
van der Waals	128.431											van der Waals	127.89								
electrostatic	-182.841											electrostatic	-154.375								
ΔEs	-76.251											ΔEs	-50.324								
	-3.432												-3.973								
	-73.114												-44.648								

	H	H	Q	K	L	V	F	F					H	H	Q	K	L	V	F	F	Gly29
Initial Orientation				LS1				RB1				Initial Orientation				RS2				LB1	
Final Orientation				LS1								Final Orientation				RS2				LS2	
				2												2					C=O
				LNH																	
Total Energy	191.889											Total Energy	187.178								
van der Waals	130.73											van der Waals	124.849								
electrostatic	-189.409											electrostatic	-184.491								
ΔEs	-74.896											ΔEs	-79.607								
	-1.133												-7.014								
	-79.682												-74.764								

	H	H	Q	K	L	V	F	F						H	H	Q	K	L	V	F	F	
Initial Orientation				LS2				RB1					Initial Orientation				LB1				RB2	
Final Orientation	LS1			RS2				CS					Final Orientation				RB1				RS1	
				2													LB1					
				LS1																		
				-CH2-																		
Total Energy	162.729												Total Energy	221.528								
van der Waals	121.575												van der Waals	121.916								
electrostatic	-204.122												electrostatic	-144.274								
ΔEs	-104.056												ΔEs	-45.257								
	-10.288													-9.947								
	-94.395													-34.547								

	H	H	Q	K	L	V	F	F	Lys28	Gly29	Ala30			H	H	Q	K	L	V	F	F	Gly29
Initial Orientation				RB2				LB1					Initial Orientation				LB2				RB1	
Final Orientation				RB2				CS	LS2	LS2	LB2		Final Orientation				LS2			LS1	RB1	RS1
				RS2				RS2	-CH2-	C=O							LNH				CS	C=O
				2																		
Total Energy	181.219												Total Energy	201.879								
van der Waals	117.983												van der Waals	120.153								
electrostatic	-187.109												electrostatic	-167.679								
ΔEs	-85.566												ΔEs	-64.906								
	-13.88													-11.71								
	-77.382													-57.952								

	H	H	Q	K	L	V	F	F						H	H	Q	K	L	V	F	F	
Initial Orientation				RB1				LB2					Initial Orientation				LS1				RB2	
Final Orientation	LS1			RB1			RB2	LB2					Final Orientatior	LB2			LS1					
				LB1													LB2					
				LNH													-CH2-					
				-CH2-													LNH					
Total Energy	134.689												Total Energy	201.297								
van der Waals	122.29												van der Waals	124.167								
electrostatic	-242.395												electrostatic	-164.561								
ΔEs	-132.096												ΔEs	-65.488								
	-9.573													-7.696								
	-132.668													-54.834								

	H	H	Q	K	L	V	F	F						H	H	Q	K	L	V	F	F	
Initial Orientation				RS1				LB2					Initial Orientation				LS2				RB2	
Final Orientation	LB1			RB2	LS1		RB2	LS1					Final Orientation				LS2			LB2		
	LS1			RNH													2					
	LS2			LB1*													LB2					
				LNH*																		
				LS1*																		
Total Energy	109.025			*-CH2-									Total Energy	191.03								
van der Waals	107.904												van der Waals	126.745								
electrostatic	-256.692												electrostatic	-179.443								
ΔEs	-157.76												ΔEs	-75.755								
	-23.959													-5.118								
	-146.965													-69.716								

	H	H	Q	K	L	V	F	F	Val12					H	H	Q	K	L	V	F	F	
Initial Orientation				RS2				LB2					Initial Orientation				LB2				RB2	
Final Orientation				RS2					RB2				Final Orientation				LB2					
																	LS2					
																	2					
Total Energy	188.368												Total Energy	187.913								
van der Waals	129.187												van der Waals	130.381								
electrostatic	-192.801												electrostatic	-194.418								
ΔEs	-78.417												ΔEs	-78.872								
	-2.676													-1.482								
	-83.074													-84.691								

	H	H	Q	K	L	V	F	F	Glu11					H	H	Q	K	L	V	F	F	
Initial Orientation				RB2				LB2					Initial Orientation									
Final Orientation				RS2				LB2	RB2				Final Orientation									
									C=O													
Total Energy	169.882												Total Energy									
van der Waals	122.387												van der Waals									
electrostatic	-198.266												electrostatic									
ΔEs	-96.903												ΔEs	-266.785								
	-9.476													-131.863								
	-88.539													109.727								

The gas phase results of solapsone and the 1BA4 conformer of Aβ

	H	H	Q	K			H	H	Q	K
Initial Orientation	RB1	CS				Initial Orientatio	CS	RB1		
Final Orientation	RS1	RB1				Final Orientatior	LS1	RS1	LS1	
	RS2	RS2					LS2	LB1	-CH2-	
	-CH2-	RS1						LS1		
	RB2							-CH2-		
Total Energy	58.557					Total Energy	51.504			
van der Waals	89.502					van der Waals	89.289			
electrostatic	-251.858					electrostatic	-260.135			
ΔEs	-114.282					ΔEs	-121.335			
	-12.188						-12.401			
	-103.12						-111.397			

	H	H	Q	K			H	H	Q	K
Initial Orientation	LB1	CS				Initial Orientatio	CS	LB1		
Final Orientation	LS1	LB1				Final Orientation	LB1	LS1		
		LS1					LB1			
		CS					LS2			
		RB1					LS1			
							CS			
							RB1			
Total Energy	96.697					Total Energy	60.492			
van der Waals	95.478					van der Waals	90.116			
electrostatic	-220.32					electrostatic	-249.545			
ΔEs	-76.142					ΔEs	-112.347			
	-6.212						-11.574			
	-71.582						-100.807			

	H	H	Q	K			H	H	Q	K
Initial Orientation	RS1	CS				Initial Orientatio	CS	RS1		
Final Orientation	RB2	RS1				Final Orientation	LB1	RS1		
	RS1						LS2	RS2		
	-CH2-						LS1			
Total Energy	93.394					Total Energy	46.285			
van der Waals	96.09					van der Waals	92.471			
electrostatic	-226.367					electrostatic	-267.826			
ΔEs	-79.445					ΔEs	-126.554			
	-5.6						-9.219			
	-77.629						-119.088			

	H	H	Q	K			H	H	Q	K
Initial Orientation	LS1	CS				Initial Orientatio	CS	LS1		
Final Orientation	LS1	LB1				Final Orientatior	CS	LS1		
	LS2	CS						2		
	LB2	LS1								
Total Energy	76.3					Total Energy	117.647			
van der Waals	91.861					van der Waals	99.895			
electrostatic	-237.156					electrostatic	-202.545			
ΔEs	-96.539					ΔEs	-55.192			
	-9.829						-1.795			
	-88.418						-53.807			

	H	H	Q	K			H	H	Q	K
Initial Orientation	CS	RS2				Initial Orientatio	RS2	CS		
Final Orientation	RB1	RS2				Final Orientatior	RS2	LS2		
	RB1							CS		
	CS							RB1		
	RS1									
	RS2									
	-CH2-									
Total Energy	67.278					Total Energy	65.596			
van der Waals	93.671					van der Waals	92.098			
electrostatic	-250.015					electrostatic	-249.362			
ΔEs	-105.561					ΔEs	-107.243			
	-8.019						-9.592			
	-101.277						-100.624			

	H	H	Q	K			H	H	Q	K
Initial Orientation	LS2	CS				Initial Orientatio	CS	LS2		
Final Orientation	LS2	LB1				Final Orientation	LB1	LS2		
		LS2					LS2	LS1		
		RB1					-CH2-			
		RS2					LS1			
							CS			
							RS2			
Total Energy	49.668					Total Energy	49.632			
van der Waals	90.52					van der Waals	89.955			
electrostatic	-261.678					electrostatic	-263.924			
ΔEs	-123.171					ΔEs	-123.207			
	-11.17						-11.735			
	-112.94						-115.186			

	H	H	Q	K			H	H	Q	K
Initial Orientation	RB1	LB1				Initial Orientatio	LB1	RB1		
Final Orientation	RS1	LS1				Final Orientation	LS1	RS1		
	RB1	LNH					LNH			
	RNH	LB1					LB1			
Total Energy	96.848					Total Energy	105.56			
van der Waals	96.731					van der Waals	99.375			
electrostatic	-220.586					electrostatic	-214.764			
ΔEs	-75.991					ΔEs	-67.279			
	-4.959						-2.315			
	-71.848						-66.026			

	H	H	Q	K					H	H	Q	K	
Initial Orientation	LB1	RS1						Initial Orientatio	RS1	LB1			
Final Orientation	LS1	RS1						Final Orientatior	RS1	RB1			
	LB1									RS1			
Total Energy	102.181							Total Energy	85.121				
van der Waals	98.617							van der Waals	97.976				
electrostatic	-219.235							electrostatic	-234.908				
ΔEs	-70.658							ΔEs	-87.718				
	-3.073								-3.714				
	-70.497								-86.17				

	H	H	Q	K					H	H	Q	K	
Initial Orientation	LS1	RB1						Initial Orientatio	RB1	LS1			
Final Orientation	LS1	RB1						Final Orientatior	RB1	LB1			
	CS	RB1							RS1	LS1			
	-CH2-	RS1							CS				
	LB1	RS2											
		CS											
Total Energy	209.058							Total Energy	218.113				
van der Waals	78.677							van der Waals	84.208				
electrostatic	-61.878							electrostatic	-57.123				
ΔEs	36.219							ΔEs	45.274				
	-23.013								-17.482				
	86.86								91.615				

	H	H	Q	K	Tyr10	Val12			H	H	Q	K	Leu17
Initial Orientation	LB1	RS2						Initial Orientatio	RS2	LB1			
Final Orientation	LB1	RS2			LB2	LS2		Final Orientatior	RS2	LB1			LS2
	LB2				LS2	-CH-				LS2			LS1
	LS2									RB1			
	CS												
	RB1												
Total Energy	208.765							Total Energy	205.855				
van der Waals	75.665							van der Waals	76.45				
electrostatic	-60.089							electrostatic	-62.094				
ΔEs	35.926							ΔEs	33.016				
	-26.025								-25.24				
	88.649								86.644				

	H	H	Q	K	Tyr10	Val12			H	H	Q	K	Leu17
Initial Orientation	RB1	LS2						Initial Orientatio	LS2	RB1			
Final Orientation	LS2	LB1			RB1	CS		Final Orientatior	LS2	RB1			RS2
	CS	LS2			RS1	C=O				RS2			
	-CH-	LS1			CS					CS			
	RS2				RS2								
Total Energy	194.27							Total Energy	214.612				
van der Waals	66.239							van der Waals	81.186				
electrostatic	-68.591							electrostatic	-58.479				
ΔEs	21.431							ΔEs	41.773				
	-35.451								-20.504				
	80.147								90.259				

	H	H	Q	K	Leu17				H	H	Q	K	Tyr10
Initial Orientation	RB2	LB1						Initial Orientatio	LB1	RB2			
Final Orientation	RB2	LB1			LS1			Final Orientatior	LB2	RB2			LB2
	RS1	RB1							RS2	RS2			
	RNH	LNH							RB1				
		LS1							LS2				
Total Energy	73.437							Total Energy	73.048				
van der Waals	89.365							van der Waals	88.647				
electrostatic	-240.78							electrostatic	-242.243				
ΔEs	-99.402							ΔEs	-99.791				
	-12.325								-13.043				
	-92.042								-93.505				

	H	H	Q	K	Tyr10	Val12			H	H	Q	K	
Initial Orientation	LB2	RB1						Initial Orientatio	RB1	LB2			
Final Orientation	LS2	LB1	RS1		LB2	LB2		Final Orientatior	LB1	LB2			
	LB2	RS1				C=O			LB1	LS1			
		-CH2-							RS1				
		RB1							RNH				
		LNH							RB1				
									LNH				
									LS1				
									-CH2-				
									LB2				
Total Energy	56.516							Total Energy	55.957				
van der Waals	84.58							van der Waals	87.039				
electrostatic	-255.417							electrostatic	-257.496				
ΔEs	-116.323							ΔEs	-116.882				
	-17.11								-14.651				
	-106.679								-108.758				

	H	H	Q	K	Leu17				H	H	Q	K	
Initial Orientation	LS2	RS2						Initial Orientatio	RS2	LS2			
Final Orientation	LB1	CS	CS		RS1			Final Orientation	RS1	LS2			
	LS2	-NH-	-CH2-						RS2	2			
		RB1								LS1			
		RS1											
		RS2											
Total Energy	46.422							Total Energy	34.012				
van der Waals	87.705							van der Waals	94.786				
electrostatic	-261.284							electrostatic	-268.751				
ΔEs	-126.417							ΔEs	-138.827				
	-13.985								-6.904				
	-112.546								-120.013				
	H	H	Q	K					H	H	Q	K	
Initial Orientation	LS2	RB2						Initial Orientatio	RB2	LS2			
Final Orientation	LS2	RB2						Final Orientation	RB2	LS2	LB2		
		RS2							RS2				
Total Energy	82.34							Total Energy	73.028				
van der Waals	95.516							van der Waals	91.085				
electrostatic	-235.324							electrostatic	-239.595				
ΔEs	-90.499							ΔEs	-99.811				
	-6.174								-10.605				
	-86.586								-90.857				
	H	H	Q	K					H	H	Q	K	
Initial Orientation	LB2	RS2						Initial Orientatio	RS2	LB2			
Final Orientation	LB2	RS1						Final Orientation	RB1	LS1	RS2		
	LS2	RS2							RB1	LS2	-CH2-		
	RS2								RS2				
									RS1				
Total Energy	55.26							Total Energy	31.009				
van der Waals	89.078							van der Waals	88.676				
electrostatic	-255.213							electrostatic	-278.353				
ΔEs	-117.579							ΔEs	-141.83				
	-12.612								-13.014				
	-106.475								-129.615				
	H	H	Q	K					H	H	Q	K	
Initial Orientation	LB2	RB2						Initial Orientatio	RB2	LB2			
Final Orientation		RS2						Final Orientation	LS2	LS2	LB2		
									-CH2-	2			
									RB1				
									RNH				
									RB2				
Total Energy	129.247							Total Energy	45.514				
van der Waals	100.869							van der Waals	85.74				
electrostatic	-192.59							electrostatic	-262.022				
ΔEs	-43.592							ΔEs	-127.325				
	-0.821								-15.95				
	-43.852								-113.284				
	H	H	Q	K	Val12	Phe19			H	H	Q	K	Val12
Initial Orientation	LB2			RB2				Initial Orientatio	RB2			LB2	
Final Orientation	LB2				LB2	RNH		Final Orientation	RB2				RS2
	LB2					RB1			RS2				
									2				
Total Energy	129.4							Total Energy	121.016				
van der Waals	93.808							van der Waals	94.307				
electrostatic	-186.148							electrostatic	-196.402				
ΔEs	-43.439							ΔEs	-51.823				
	-7.882								-7.383				
	-37.41								-47.664				

	L	V	F	F	His14				L	V	F	F	His14			
Initial Orientation	RB1	LB1						Initial Orientatio	LB1	RB1						
Final Orientation	RS1	CS			RB1			Final Orientation	LS1	CS			LB2			
					RS1				LB1				LS1			
													LNH			
													LB1			
													-CH2-			
Total Energy	118.131							Total Energy	113.995							
van der Waals	92.892							van der Waals	90.721							
electrostatic	-194.04							electrostatic	-198.745							
ΔEs	-54.708							ΔEs	-58.844							
	-8.798								-10.969							
	-45.302								-50.007							
	L	V	F	F	His13	His14			L	V	F	F	Asp1	His13	His14	Lys16
Initial Orientation	LB1	RB2						Initial Orientatio	RB1	LB2						
Final Orientation	LB1	RB2			LS2	LS2		Final Orientation	LB1			RB2	RB2	RS1	RS1	RB2
		RS2			C=O				RB1				(NH3+)	C=O		
									RNH							
Total Energy	86.05							Total Energy	104.78							
van der Waals	88.259							van der Waals	80.966							
electrostatic	-210.979							electrostatic	-202.437							
ΔEs	-86.789							ΔEs	-68.059							
	-13.431								-20.724							
	-62.241								-53.699							

	L	V	F	F	His14			
Initial Orientation	LB2	RB2						
Final Orientation	LB2				LS2			
					LB2			
Total Energy	115.186							
van der Waals	93.243							
electrostatic	-199.81							
ΔEs	-57.653							
	-8.447							
	-51.072							

	L	V	F	F	His14			
Initial Orientatio	RB2	LB2						
Final Orientatior	RB2				RNH			
					RS1			
Total Energy	119.352							
van der Waals	97.056							
electrostatic	-199.512							
ΔEs	-53.487							
	-4.634							
	-50.774							

	L	V	F	F
Initial Orientation	LB2		RB2	
Final Orientation				
Total Energy	142.266			
van der Waals	94.929			
electrostatic	-163.845			
ΔEs	-30.573			
	-6.761			
	-15.107			

	L	V	F	F	His13	His14	Gln15
Initial Orientatio	RB2		LB2				
Final Orientation					RS1	RS2	RS1
					-CH2-	RS1*	-NH-
					*NH of backbone		
Total Energy	90.016						
van der Waals	87.713						
electrostatic	-224.71						
ΔEs	-82.823						
	-13.977						
	-75.972						

	L	V	F	F	His14
Initial Orientation	LB1			RB1	
Final Orientation	LB1			CS	LS1
	LS1				
Total Energy	116.575				
van der Waals	95.35				
electrostatic	-204.571				
ΔEs	-56.264				
	-6.34				
	-55.833				

	L	V	F	F	His14
Initial Orientatio	RB1			LB1	
Final Orientatior	CS			LB1	RS1
	RB1			LS2	
	RS1			LS1	
				CS	
Total Energy	90.413				
van der Waals	85.8				
electrostatic	-210.786				
ΔEs	-82.426				
	-15.89				
	-62.048				

	L	V	F	F	His14	Val24
Initial Orientation	LB1			RB2		
Final Orientation	LB1	LB2			LS1	RB2
		LS1				
Total Energy	90.126					
van der Waals	87.55					
electrostatic	-207.677					
ΔEs	-82.713					
	-14.14					
	-58.939					

	L	V	F	F	His14
Initial Orientatio	RB2			LB1	
Final Orientatior	RS2			LB1	RS2
	RNH				
	RB1				
Total Energy	83.54				
van der Waals	91.234				
electrostatic	-238.553				
ΔEs	-89.299				
	-10.456				
	-89.815				

	L	V	F	F	Ala21	Val24	Gly25	Lys28
Initial Orientation	LB2			RB1				
Final Orientation				RB1	LS2	CS	LS2	LS1
					C=O	LB1		2
						LS2		
Total Energy	106.982							
van der Waals	89.116							
electrostatic	-205.72							
ΔEs	-65.857							
	-12.574							
	-56.982							

	L	V	F	F	His14
Initial Orientatio	RB1			LB2	
Final Orientatior	RB1	RS2		LB2	RS2
				LS2	
Total Energy	85.416				
van der Waals	90.606				
electrostatic	-224.832				
ΔEs	-87.423				
	-11.084				
	-76.094				

	L	V	F	F	His14	Val24
Initial Orientation	LB2			RB2		
Final Orientation	LB1				LB2	RB2
					LS1	
Total Energy	101.663					
van der Waals	89.005					
electrostatic	-197.487					
ΔEs	-71.176					
	-12.685					
	-48.749					

	L	V	F	F	His14
Initial Orientatio	RB2			LB2	
Final Orientatior	CS			LB2	RB1
	RB1				RS2
	RS2				
Total Energy	87.753				
van der Waals	87.539				
electrostatic	-222.651				
ΔEs	-85.086				
	-14.151				
	-73.913				

	L	V	F	F	Gln15	Glu22
Initial Orientation		RB1	LB1			
Final Orientation		RB1	CS		CS	CS
			LB1			
Total Energy	162.268					
van der Waals	94.02					
electrostatic	-152.466					
ΔEs	-10.571					
	-7.67					
	-3.728					

	L	V	F	F	Gln15
Initial Orientation		LB1	RB1		
Final Orientation					LB1
					RB1
Total Energy	145.532				
van der Waals	92.425				
electrostatic	-172.129				
ΔEs	-27.307				
	-9.265				
	-23.391				

	L	V	F	F	Gln15			
Initial Orientation		RB2	LB1					
Final Orientation			LB1		RS1			
			LNH		RNH			
					RB1			
					-CH2-			
Total Energy	148.005							
van der Waals	94.063							
electrostatic	-167.867							
ΔEs	-24.834							
	-7.627							
	-19.129							

	L	V	F	F				
Initial Orientation		LB2	RB1					
Final Orientation								
Total Energy	158.662							
van der Waals	95.996							
electrostatic	-159.285							
ΔEs	-14.177							
	-5.694							
	-10.547							

	L	V	F	F				
Initial Orientation		RB2	LB2					
Final Orientation								
Total Energy	151.415							
van der Waals	97.767							
electrostatic	-170.271							
ΔEs	-21.424							
	-3.923							
	-21.533							

	L	V	F	F	His13	His14	Gln15	
Initial Orientation		LB2	RB2					
Final Orientation		LB2			LS2	LS2*	LS2	
						LB2	-CH2-	
					*NH of backbone			
Total Energy	84.855							
van der Waals	94.306							
electrostatic	-214.875							
ΔEs	-87.984							
	-7.384							
	-66.137							

	L	V	F	F	His14	Gln15		
Initial Orientation		RB1		LB1				
Final Orientation	LB1	RB1			RB1*	RS1		
		RS1			RNH*			
					RS1*			
					*-CH2-			
Total Energy	83.393							
van der Waals	83.406							
electrostatic	-209.628							
ΔEs	-89.446							
	-18.284							
	-60.89							

	L	V	F	F	His13	Lys16	Val24	Lys28
Initial Orientation		RB2		LB1				
Final Orientation	LB2			LB1	LB2	LB2	RS1	RS1
				RB1	C=O	-CH2-		2
Total Energy	83.581							
van der Waals	84.588							
electrostatic	-228.304							
ΔEs	-89.258							
	-17.102							
	-79.566							

	L	V	F	F	Lys16			
Initial Orientation		LB2		RB1				
Final Orientation	LNH			RB1	RB2			
	LB1				-CH2-			
Total Energy	116.875							
van der Waals	88.908							
electrostatic	-196.447							
ΔEs	-55.964							
	-12.782							
	-47.709							

	L	V	F	F				
Initial Orientation		RB2		LB2				
Final Orientation								
Total Energy	163.769							
van der Waals	101.134							
electrostatic	-157.239							
ΔEs	-9.07							
	-0.556							
	-8.501							

	L	V	F	F	His14	Ala21	Val24	Lys28
Initial Orientation		LB2		RB2				
Final Orientation	LB1	LB1			LS1	RB1	RB2	RB2
	LNH	LB2				CS		RS2
						LB1		2
Total Energy	55.789							
van der Waals	79.391							
electrostatic	-239.524							
ΔEs	-117.05							
	-22.299							
	-90.786							

	L	V	F	F	His13	His14	Gln15	
Initial Orientation			LB2	RB2				
Final Orientation					LS1	LS1*	LS1*	
						2	*NH of backbone	
					*NH of backbone			
Total Energy	60.454							
van der Waals	91.271							
electrostatic	-240.247							
ΔEs	-112.385							
	-10.419							
	-91.509							

	L	V	F	F	Gln15	Ala21	Val24	
Initial Orientation			RB2	LB2				
Final Orientation		RB2			RB2	LB2	LB2	
Total Energy	136.813							
van der Waals	91.7							
electrostatic	-177.595							
ΔEs	-36.026							
	-9.99							
	-28.857							

	L	V	F	F
Initial Orientation				
Final Orientation				
Total Energy				
van der Waals				
electrostatic				
ΔEs	-172.839			
	-101.69			
	148.738			

	H	H	Q	K	L	V	F	F	
Initial Orientatio	RB2				LB1				
Final Orientation	LB2	LB1			LS1	CS			
	RNH	RB1			LB1				
	-CH2-								
	RS1								
Total Energy	61.165								
van der Waals	86.679								
electrostatic	-246.655								
ΔEs	-111.674								
	-15.011								
	-97.917								

	H	H	Q	K	L	V	F	F	
Initial Orientatio	RB1				LB2				
Final Orientation	RB1	RB2	LS1		LB2				
	RNH	LS1							
	RS1	-CH2-							
Total Energy	56.318								
van der Waals	83.38								
electrostatic	-257.313								
ΔEs	-116.521								
	-18.31								
	-108.575								

	H	H	Q	K	L	V	F	F	
Initial Orientatio	RS1				LB2				
Final Orientation	RNH	LB1			LS1	LS1			
	-CH2-	RB1							
	RS1	LS1							
	RB2	-CH2-							
		RNH							
		RS2							
Total Energy	45.409								
van der Waals	83.151								
electrostatic	-250.324								
ΔEs	-127.43								
	-18.539								
	-101.586								

	H	H	Q	K	L	V	F	F	Val12
Initial Orientatio	RS2				LB2				
Final Orientation	RB2	LS1							RB2
	RS2	LS2							
Total Energy	62.73								
van der Waals	92.683								
electrostatic	-254.314								
ΔEs	-110.109								
	-9.007								
	-105.576								

	H	H	Q	K	L	V	F	F	
Initial Orientatio	RB2				LB2				
Final Orientation	RB2					LB2			
	RS2								
Total Energy	84.994								
van der Waals	93.999								
electrostatic	-231.121								
ΔEs	-87.845								
	-7.691								
	-82.383								

	H	H	Q	K	L	V	F	F	
Initial Orientatio	LB1					RB2			
Final Orientation	LS1	RS1							
	LB1	2							
Total Energy	79.08								
van der Waals	95.775								
electrostatic	-240.959								
ΔEs	-93.759								
	-5.915								
	-92.221								

	H	H	Q	K	L	V	F	F	
Initial Orientatio	RB1					LB2			
Final Orientation	RB1	RB1	LB2						
	RS1	RNH	LS1						
		RS1	-CH2-						
Total Energy	74.05								
van der Waals	87.654								
electrostatic	-236.844								
ΔEs	-98.789								
	-14.036								
	-88.106								

	H	H	Q	K	L	V	F	F	
Initial Orientatio	RS1					LB2			
Final Orientation	RB1	RB2	LB2			LB2			
	RNH	RS2							
	RS1								
	RB2								
Total Energy	81.336								
van der Waals	90.921								
electrostatic	-237.859								
ΔEs	-91.503								
	-10.769								
	-89.121								

	H	H	Q	K	L	V	F	F	Val12
Initial Orientatio	LB2				RB1				
Final Orientation	LB2	RB1			RS1				LS1
	LB2	RB1							C=O
	LS1	LB1							
	LNH	RNH							
	-CH2-	LNH							
Total Energy	70.625								
van der Waals	81.856								
electrostatic	-240.314								
ΔEs	-102.214								
	-19.834								
	-91.576								

	H	H	Q	K	L	V	F	F	
Initial Orientatio	LB1				RB2				
Final Orientation	RB1	RB1			RB2			RB2	
	-CH-	RNH							
	LB1	LB1							
	LNH	LNH							
	-CH2-	LB2							
	LS1								
Total Energy	58.805								
van der Waals	83.758								
electrostatic	-252.226								
ΔEs	-114.034								
	-17.932								
	-103.488								

	H	H	Q	K	L	V	F	F	
Initial Orientatio	LS2				RB2				
Final Orientation	LB1	RB2							
	LB1	RB2							
	LS1	RS2							
	LS2	LS2							
Total Energy	43.815								
van der Waals	83.7								
electrostatic	-261.414								
ΔEs	-129.024								
	-17.99								
	-112.676								

	H	H	Q	K	L	V	F	F	
Initial Orientatio	LB2				RB2				
Final Orientation	LS1	LS2							
	LS2								
	-CH2-								
	LB2								
Total Energy	65.645								
van der Waals	91.462								
electrostatic	-248.838								
ΔEs	-107.194								
	-10.228								
	-100.1								

	H	H	Q	K	L	V	F	F	
Initial Orientatio	LB1					RB1			
Final Orientation	LB2	LS1							
	LB2								
	LS1								
	-CH2-								
Total Energy	73.304								
van der Waals	89.925								
electrostatic	-238.298								
ΔEs	-99.535								
	-11.765								
	-89.56								

	H	H	Q	K	L	V	F	F	
Initial Orientatio	RB2					LB1			
Final Orientation	RS1	LS2	RB1		LS2	LB1			
	RB2	LB1*	-CH2-		LNH	CS			
		RB1*			LB1				
		*-CH2-							
		RB2							
Total Energy	44.197								
van der Waals	79.605								
electrostatic	-260.716								
ΔEs	-128.642								
	-22.085								
	-111.978								

	H	H	Q	K	L	V	F	F	
Initial Orientatio	LS1					RB2			
Final Orientation	LB2								
	LS1								
Total Energy	94.552								
van der Waals	93.009								
electrostatic	-221.431								
ΔEs	-78.287								
	-8.681								
	-72.693								

	H	H	Q	K	L	V	F	F	
Initial Orientatio	LS2					RB2			
Final Orientation	LB1	LS2	RS1						
	LS1	RS2	-CH2-						
	LS2								
Total Energy	28.467								
van der Waals	89.315								
electrostatic	-282.822								
ΔEs	-144.372								
	-12.375								
	-134.084								

	H	H	Q	K	L	V	F	F					H	H	Q	K	L	V	F	F		
Initial Orientatio	RS2					LB2						Initial Orientatio	LB2					RB2				
Final Orientation	RB2	LS2				LS2						Final Orientatio	LS1	LS2								
	RB2					LB2							LS2									
	RS2																					
Total Energy	58.363											Total Energy	66.939									
van der Waals	91.724											van der Waals	92.339									
electrostatic	-244.101											electrostatic	-247.012									
ΔEs	-114.476											ΔEs	-105.9									
	-9.966												-9.351									
	-95.363												-98.274									

	H	H	Q	K	L	V	F	F					H	H	Q	K	L	V	F	F		
Initial Orientatio	RB2					LB2						Initial Orientatio	RS1						LB1			
Final Orientation	RS1	RS2	RS2									Final Orientatio	RS2									
	RS2	-NH-	-CH2-										RS1									
		RS1																				
Total Energy	57.193											Total Energy	102.313									
van der Waals	88.596											van der Waals	94.259									
electrostatic	-254.476											electrostatic	-213.006									
ΔEs	-115.646											ΔEs	-70.526									
	-13.094												-7.431									
	-105.738												-64.268									

	H	H	Q	K	L	V	F	F	Val12				H	H	Q	K	L	V	F	F		
Initial Orientatio	LS1						RB1					Initial Orientatio	RS2						LB1			
Final Orientation	LS1		CS						LS1			Final Orientatio	RB2		CS							
	LS2		LB1										RS2									
			LS1																			
			-CH2-																			
Total Energy	87.65											Total Energy	118.472									
van der Waals	89.147											van der Waals	96.917									
electrostatic	-224.592											electrostatic	-200.701									
ΔEs	-85.189											ΔEs	-54.367									
	-12.543												-4.773									
	-75.854												-51.963									

	H	H	Q	K	L	V	F	F	Val12				H	H	Q	K	L	V	F	F	Tyr10	Val12
Initial Orientatio	LS2						RB1					Initial Orientatio	LB1						RB2			
Final Orientation	LB1	LS2							CS			Final Orientatio	LB1	RS1	RB2						LB1	RB1
	LS1	-CH2-											RB1		RB1						LB2	
	LS2												LS1		-CH2-							
													RS1*									
													RNH*									
													*-CH2-									
													LNH									
Total Energy	69.356											Total Energy	59.036									
van der Waals	88.823											van der Waals	81.856									
electrostatic	-239.656											electrostatic	-252.491									
ΔEs	-103.483											ΔEs	-113.803									
	-12.867												-19.834									
	-90.918												-103.753									

	H	H	Q	K	L	V	F	F					H	H	Q	K	L	V	F	F		
Initial Orientatio	RB2						LB1					Initial Orientatio	LB2						RB1			
Final Orientation	RB2	RS2	RB1									Final Orientatio	LB2	LS1	LB1*							
	RS2		-CH2-										LB2	-CH2-	LS1*							
	-CH2-												LS1		*-CH2-							
Total Energy	87.187											Total Energy	79.02									
van der Waals	92.175											van der Waals	90.268									
electrostatic	-223.281											electrostatic	-231.478									
ΔEs	-85.652											ΔEs	-93.819									
	-9.515												-11.422									
	-74.543												-82.74									

	H	H	Q	K	L	V	F	F	Tyr10	Val12			H	H	Q	K	L	V	F	F	Tyr10	
Initial Orientatio	RB1						LB2					Initial Orientatio	LS1						RB2			
Final Orientation	RS2	LS2	LS2*						RB2	RS2		Final Orientatio	LS1						RB2		LB2	
	RB1	-NH-	LB2*						RS2	C=O			LNH									
	LB1		*-CH2-																			
	LS2																					
Total Energy	47.983											Total Energy	122.161									
van der Waals	79.444											van der Waals	95.128									
electrostatic	-255.122											electrostatic	-196.864									
ΔEs	-124.856											ΔEs	-50.678									
	-22.246												-6.562									
	-106.384												-48.126									

	H	H	Q	K	L	V	F	F					H	H	Q	K	L	V	F	F		
Initial Orientatio	RS1						LB2					Initial Orientatio	LS2						RB2			
Final Orientation	RB1	RB2	LB2									Final Orientatio	LB2									
	RNH	RS2											LB2									
	RS1												LS2									
	RS2																					
	-CH2-																					
Total Energy	70.962											Total Energy	121.95									
van der Waals	89.509											van der Waals	97.295									
electrostatic	-244.389											electrostatic	-196.376									
ΔEs	-101.877											ΔEs	-50.889									
	-12.181												-4.395									
	-95.651												-47.638									

	H	H	Q	K	L	V	F	F					H	H	Q	K	L	V	F	F		
Initial Orientatio	RS2						LB2					Initial Orientatio	LB2						RB2			
Final Orientation	LS2	LS2	LS2									Final Orientatio	LB2									
	RS2	-CH2-	-CH2-										LB2									
													LS2									
Total Energy	69.706											Total Energy	125.985									
van der Waals	93.609											van der Waals	97.298									
electrostatic	-247.599											electrostatic	-193.075									
ΔEs	-103.133											ΔEs	-46.854									
	-8.081												-4.392									
	-98.861												-44.337									

	H	H	Q	K	L	V	F	F
Initial Orientatior	RB2						LB2	
Final Orientation	RB2							
	RS2							
Total Energy	126.919							
van der Waals	99.951							
electrostatic	-193.923							
ΔEs	-45.92							
	-1.739							
	-45.185							

	H	H	Q	K	L	V	F	F
Initial Orientatio	LB1							RB2
Final Orientatior	RB1	LB1		RS1	RB2			RB2
	C=O	LB1		-CH2-	RS1			
	LB1	RB1						
	LS1	LNH						
		LB2						
Total Energy	52.733							
van der Waals	79.168							
electrostatic	-250.912							
ΔEs	-120.106							
	-22.522							
	-102.174							

	H	H	Q	K	L	V	F	F	Val12
Initial Orientatior	LB2							RB1	
Final Orientation	LB2	LB1			RB1				LS1
	LNH*	LS2							C=O
	LS1*	LNH							
	LB1*								
	*C=O								
Total Energy	78.806								
van der Waals	85.051								
electrostatic	-229.886								
ΔEs	-94.033								
	-16.639								
	-81.148								

	H	H	Q	K	L	V	F	F
Initial Orientatio	RS1							LB2
Final Orientatior	RS1	RB1			LB2			LB2
	RB2	RNH						
		RS1						
Total Energy	75.512							
van der Waals	83.702							
electrostatic	-236.505							
ΔEs	-97.327							
	-17.988							
	-87.767							

	H	H	Q	K	L	V	F	F	Tyr10
Initial Orientatior	LS2							RB2	
Final Orientation	LB2	RS2			RS2				LB2
	LS2	LS2							
	LS1								
Total Energy	76.833								
van der Waals	86.242								
electrostatic	-230.882								
ΔEs	-96.006								
	-15.448								
	-82.144								

	H	H	Q	K	L	V	F	F
Initial Orientatio	LS1							RB2
Final Orientatior	LB1	LB1						
	LS1	LNH						
		LS2						
		LB2						
Total Energy	71.035							
van der Waals	87.388							
electrostatic	-241.853							
ΔEs	-101.804							
	-14.302							
	-93.115							

	H	H	Q	K	L	V	F	F	Tyr10	Val12
Initial Orientatior	RS2							LB2		
Final Orientation	LB1	LB1			LB2			LB2	CS	CS
	C=O	RB1			LS2			LS2		C=O
	CS	RS2								
	-CH-									
	RB1									
	RS1									
	RS2									
	-CH2-									
Total Energy	33.253									
van der Waals	77.853									
electrostatic	-267.576									
ΔEs	-139.586									
	-23.837									
	-118.838									

	H	H	Q	K	L	V	F	F	Tyr10	Val12
Initial Orientatio	LB2									
Final Orientatior	LS2	LB1			RS2					
	LB2	LS2								
Total Energy	88.918									
van der Waals	94.401									
electrostatic	-225.639									
ΔEs	-83.921									
	-7.289									
	-76.901									

	H	H	Q	K	L	V	F	F
Initial Orientatior	RB2							LB2
Final Orientation	RB2	RS2						LB2
	RB2	RNH						
	RS2	RB1						
Total Energy	93.758							
van der Waals	90.425							
electrostatic	-219.729							
ΔEs	-79.081							
	-11.265							
	-70.991							

	H	H	Q	K	L	V	F	F
Initial Orientation								
Final Orientation								
Total Energy								
van der Waals								
electrostatic								
ΔEs	-172.839							
	-101.69							
	148.738							

Initial Orientation		RS1				LB1			
Final Orientation	RS1	RS1	CS			LB1			
Total Energy	67.177								
van der Waals	93.082								
electrostatic	-236.645								
ΔEs	-105.662								
	-8.608								
	-87.907								

Initial Orientation		LS1				RB1			
Final Orientatior	LS1	LS2				CS			
	-CH2-	LS1							
Total Energy	79.963								
van der Waals	91.367								
electrostatic	-231.204								
ΔEs	-92.876								
	-10.323								
	-82.466								

	H	H	Q	K	L	V	F	F	Ala21
Initial Orientation		RS2				LB1			
Final Orientation		RS2	LS2		RS2	CS			CS
					RS1	LB1			
					RB1	LS2			
Total Energy	111.273								
van der Waals	87.794								
electrostatic	-198.159								
ΔEs	-61.566								
	-13.896								
	-49.421								

	H	H	Q	K	L	V	F	F
Initial Orientation		RB1				LB2		
Final Orientatior	LS1	RS1	LB2					
		RB1						
		RNH						
Total Energy	68.121							
van der Waals	91.202							
electrostatic	-249.395							
ΔEs	-104.718							
	-10.488							
	-100.657							

	H	H	Q	K	L	V	F	F
Initial Orientation		LB2				RB1		
Final Orientation		LB2	RB1		LS1			
		LNH						
		LS1						
		-CH2-						
Total Energy	83.561							
van der Waals	91.674							
electrostatic	-233.95							
ΔEs	-89.278							
	-10.016							
	-85.212							

	H	H	Q	K	L	V	F	F
Initial Orientation		LB1				RB2		
Final Orientation	RS1	LB1	RS2*					
		RB1	RB2*					
		LS2	*-CH2-					
		RS2						
		-NH-						
		LNH						
		RS2						
		-CH2-						
Total Energy	38.376							
van der Waals	85.242							
electrostatic	-269.744							
ΔEs	-134.463							
	-16.448							
	-121.006							

	H	H	Q	K	L	V	F	F
Initial Orientation		RB2				LB1		
Final Orientation	RS1	RS1				LB1		
	-CH2-	RNH						
Total Energy	100.876							
van der Waals	88.86							
electrostatic	-211.088							
ΔEs	-71.963							
	-12.83							
	-62.35							

	H	H	Q	K	L	V	F	F
Initial Orientation		LS2				RB2		
Final Orientation	LB2	LS2				RB2		
	LS2							
	LS1							
Total Energy	64.935							
van der Waals	88.577							
electrostatic	-247.344							
ΔEs	-107.904							
	-13.113							
	-98.606							

	H	H	Q	K	L	V	F	F
Initial Orientation		RS2				LB2		
Final Orientation	RB2	RS2						
	RB2	RB1						
	RS2							
Total Energy	99.026							
van der Waals	93.462							
electrostatic	-217.4							
ΔEs	-73.813							
	-8.228							
	-68.662							

	H	H	Q	K	L	V	F	F
Initial Orientation		LB2				RB2		
Final Orientation	LS1	LB1	LB2		RB1			
		RB1						
		RS1						
		RNH						
Total Energy	72.003							
van der Waals	95.356							
electrostatic	-245.075							
ΔEs	-100.836							
	-6.334							
	-96.337							

	H	H	Q	K	L	V	F	F
Initial Orientation		RB2				LB2		
Final Orientation	RS1	RB2						
		RS1						
Total Energy	87.313							
van der Waals	93.729							
electrostatic	-229.453							
ΔEs	-85.526							
	-7.961							
	-80.715							

	H	H	Q	K	L	V	F	F
Initial Orientation		RS1				LB2		
Final Orientation	LS1	LB1	LB2		RB1			
		RB1						
		RS1						
		RNH						
Total Energy	59.375							
van der Waals	86.952							
electrostatic	-253.898							
ΔEs	-113.464							
	-14.738							
	-105.16							

	H	H	Q	K	L	V	F	F
Initial Orientation		LS2					RB2	
Final Orientation	LS2	LS2	RB2				RB2	
		-NH-	-CH2-					
		LB2						
Total Energy	75.776							
van der Waals	92.442							
electrostatic	-244.431							
ΔEs	-97.063							
	-9.248							
	-95.693							

	H	H	Q	K	L	V	F	F
Initial Orientation		RB2					LB2	
Final Orientation	RB1	RB2	LB2					
	RNH	RS2						
	RS2	2						
	RB2							
Total Energy	84.008							
van der Waals	93.357							
electrostatic	-234.649							
ΔEs	-88.831							
	-8.333							
	-85.911							

	H	H	Q	K	L	V	F	F
Initial Orientation		LB2					RB2	
Final Orientation	LS2	LB2						
		LS2						
Total Energy	90.738							
van der Waals	99.005							
electrostatic	-230.813							
ΔEs	-82.101							
	-2.685							
	-82.075							

	H	H	Q	K	L	V	F	F
Initial Orientation		RS1						LB1
Final Orientation		RS1						LS1
								LB1
Total Energy	120.925							
van der Waals	96.663							
electrostatic	-197.317							
ΔEs	-51.914							
	-5.027							
	-48.579							

	H	H	Q	K	L	V	F	F
Initial Orientation		LS1					RB1	
Final Orientation		LS1			LB1		RB1	
Total Energy	103.22							
van der Waals	93.435							
electrostatic	-211.732							
ΔEs	-69.619							
	-8.255							
	-62.994							

	H	H	Q	K	L	V	F	F
Initial Orientation		RS2						LB1
Final Orientation		RS2						CS
								LB1
								LS2
Total Energy	110.769							
van der Waals	92.29							
electrostatic	-206.663							
ΔEs	-62.07							
	-9.4							
	-57.925							

	H	H	Q	K	L	V	F	F
Initial Orientation		LS2						RB1
Final Orientation		LS2			CS			CS
								RB1
								RS1
								RS2
Total Energy	97.658							
van der Waals	91.722							
electrostatic	-215.972							
ΔEs	-75.181							
	-9.968							
	-67.234							

	H	H	Q	K	L	V	F	F
Initial Orientation		RB2						LB1
Final Orientation		RS1			RS1			LS1
		RNH			RB1			
Total Energy	118.235							
van der Waals	93.997							
electrostatic	-200.757							
ΔEs	-54.604							
	-7.693							
	-52.019							

	H	H	Q	K	L	V	F	F
Initial Orientation		LB1						RB2
Final Orientation		LS1			RS1			RS1
		LB1						
Total Energy	106.354							
van der Waals	93.124							
electrostatic	-207.283							
ΔEs	-66.485							
	-8.566							
	-58.545							

	H	H	Q	K	L	V	F	F
Initial Orientation		LB2						RB1
Final Orientation		LB2			LNH			RB1
		LB2			LS1			LB1
		LS1						
Total Energy	100.768							
van der Waals	88.499							
electrostatic	-212.689							
ΔEs	-72.071							
	-13.191							
	-63.951							

	H	H	Q	K	L	V	F	F
Initial Orientation		RB1						LB2
Final Orientation	RS1	RS1			LS1			LB2
		RNH						
		RB1						
Total Energy	88.689							
van der Waals	92.401							
electrostatic	-225.716							
ΔEs	-84.15							
	-9.289							
	-76.978							

	H	H	Q	K	L	V	F	F
Initial Orientation		LS1						RB2
Final Orientation		LB1						RB2
		LNH						
		LS1						
Total Energy	108.582							
van der Waals	94.042							
electrostatic	-202.537							
ΔEs	-64.257							
	-7.648							
	-53.799							

	H	H	Q	K	L	V	F	F	Tyr10
Initial Orientation		RS1						LB2	
Final Orientation		RS1							RB2
		RNH							-CH2-
Total Energy	122.783								
van der Waals	94.693								
electrostatic	-195.088								
ΔEs	-50.056								
	-6.997								
	-46.35								

	H	H	Q	K	L	V	F	F
Initial Orientation		LS2						RB2
Final Orientation		LB2						
		LS2						
Total Energy	134.879							
van der Waals	97.158							
electrostatic	-184.045							
ΔEs	-37.96							
	-4.532							
	-35.307							

	H	H	Q	K	L	V	F	F
Initial Orientation		RS2						LB2
Final Orientation	RS1	LB1						
		RB1						
		RS1						
		RS2						
Total Energy	68.703							
van der Waals	90.949							
electrostatic	-244.829							
ΔEs	-104.136							
	-10.741							
	-96.091							

	H	H	Q	K	L	V	F	F
Initial Orientation		LB2						RB2
Final Orientation		LB2						
		LS2						
Total Energy	132.275							
van der Waals	98.64							
electrostatic	-188.44							
ΔEs	-40.564							
	-3.05							
	-39.702							

	H	H	Q	K	L	V	F	F
Initial Orientation		RB2						LB2
Final Orientation								
Total Energy	161.765							
van der Waals	101.325							
electrostatic	-159.29							
ΔEs	-11.074							
	-0.365							
	-10.552							

	H	H	Q	K	L	V	F	F
Initial Orientation								
Final Orientation								
Total Energy								
van der Waals								
electrostatic								
ΔEs	-172.839							
	-101.69							
	148.738							

	H	H	Q	K	L	V	F	F	Glu11
Initial Orientation				LB2			RB2		
Final Orientation									
Total Energy	165.398								
van der Waals	96.469								
electrostatic	-153.822								
ΔEs	-7.441								
	-5.221								
	-5.084								

	H	H	Q	K	L	V	F	F
Initial Orientation				RB2			LB2	
Final Orientation								RB2
								-CH2-
Total Energy	163.082							
van der Waals	98.685							
electrostatic	-156.454							
ΔEs	-9.757							
	-3.005							
	-7.716							

The gas phase results of solapsone and the 1IYT conformer of Aβ

	H	H	Q	K				
Initial Orientatio	CS	RB1						
Final Orientatior	LS1	RS1						
	LB1							
Total Energy	79.919							
van der Waals	90.169							
electrostatic	-227.953							
ΔEs	-54.132							
	-6.101							
	-48.506							

	H	H	Q	K	Leu17			
Initial Orientatio	RS1	CS						
Final Orientatior	RS2	CS			RS1			
	RS1							
Total Energy	69.833							
van der Waals	88.674							
electrostatic	-238.345							
ΔEs	-64.218							
	-7.596							
	-58.898							

	H	H	Q	K	Leu17			
Initial Orientatio	CS	RS1						
Final Orientatior	RS1	RS1			RB1			
	CS				CS			
Total Energy	64.87							
van der Waals	85.112							
electrostatic	-236.159							
ΔEs	-69.181							
	-11.158							
	-56.712							

	H	H	Q	K	His6	Tyr10		
Initial Orientatio	LS1	CS						
Final Orientatior	LS1	CS				CS		
					RS1	RB1		
Total Energy	43.494							
van der Waals	80.399							
electrostatic	-256.129							
ΔEs	-90.557							
	-15.871							
	-76.682							

	H	H	Q	K	Leu17			
Initial Orientatio	CS	LS1						
Final Orientatior	RB1	LS1		RS2	CS			
	CS	2						
	RS2							
Total Energy	29.176							
van der Waals	82.041							
electrostatic	-283.223							
ΔEs	-104.875							
	-14.229							
	-103.776							

	H	H	Q	K	His6	Tyr10	Leu17	
Initial Orientatio	RS2	CS						
Final Orientatior	RS2	CS			LS2	CS	RS1	
	RS1							
Total Energy	21.227							
van der Waals	78.56							
electrostatic	-275.029							
ΔEs	-112.824							
	-17.71							
	-95.582							

	H	H	Q	K	Gly9	Tyr10		
Initial Orientatio	CS	RS2						
Final Orientatior	CS	RS2			RS1	RS1		
					C=O			
Total Energy	71.26							
van der Waals	89.849							
electrostatic	-235.977							
ΔEs	-62.791							
	-6.421							
	-56.53							

	H	H	Q	K	Tyr10			
Initial Orientatio	LS2	CS						
Final Orientatior	LS2	CS			CS			
	LS1							
Total Energy	53.846							
van der Waals	85.845							
electrostatic	-251.601							
ΔEs	-80.205							
	-10.425							
	-72.154							

	H	H	Q	K	Gly9	Tyr10	Val12	Leu17
Initial Orientatio	CS	LS2						
Final Orientatior	RB1	LS1		RS1	LS2	LS2	RS2	LS1
	LB1			RS2	C=O	-CH-		
	LB1			-CH2-				
	LS1							
Total Energy	-12.899							
van der Waals	75.904							
electrostatic	-305.236							
ΔEs	-146.95							
	-20.366							
	-125.789							

	H	H	Q	K	Gly9	Tyr10	Leu17	
Initial Orientatio	CS	RB2						
Final Orientatior	RB1	RS2			RS1	RS1	RS2	
	RS1				C=O	-CH-		
	CS							
Total Energy	52.193							
van der Waals	82.429							
electrostatic	-247.844							
ΔEs	-81.858							
	-13.841							
	-68.397							

	H	H	Q	K	Gly9	Tyr10	Leu17	
Initial Orientatio	CS	LB2						
Final Orientatior	LB1	LS1			LS2	LS2	LS1	
	LB1				C=O	-CH-		
	CS							
	LS2							
	LS1							
	-CH2-							
Total Energy	53.912							
van der Waals	83.631							
electrostatic	-245.373							
ΔEs	-80.139							
	-12.639							
	-65.926							

	H	H	Q	K	Phe20			
Initial Orientatio	LB1	RB1						
Final Orientatior	LB1	RS1		LS2	LB2			
	LS2			-CH2-	LS2			
	LS1				-CH2-			
	RB1							
	RS1							
	-CH2-							
Total Energy	-4.182							
van der Waals	75.97							
electrostatic	-292.821							
ΔEs	-138.233							
	-20.3							
	-113.374							

	H	H	Q	K	Gly9	Tyr10		
Initial Orientatio	RB1	LB1						
Final Orientatior	RS1	LS1			CS	LS1		
	CS				C=O			
	-CH2-							
	RB1							
Total Energy	68.296							
van der Waals	87.177							
electrostatic	-235.337							
ΔEs	-65.755							
	-9.093							
	-55.89							

	H	H	Q	K	Gly9			
Initial Orientatio	RS1	LB1						
Final Orientatior	RB1	LS1			CS			
	RNH				C=O			
	RS1							
Total Energy	55.058							
van der Waals	87.365							
electrostatic	-252.526							
ΔEs	-78.993							
	-8.905							
	-73.079							

	H	H	Q	K		
Initial Orientatio	LB1	RS1				
Final Orientatior	LS1	RS1				
	LB1					
	LNH					
Total Energy	57.833					
van der Waals	90.694					
electrostatic	-251.347					
ΔEs	-76.218					
	-5.576					
	-71.9					

	H	H	Q	K	Tyr10		
Initial Orientatio	LS1	RB1					
Final Orientation	LS1	RS1			RS1		
	LNH	2					
	LB1						
Total Energy	53.479						
van der Waals	90.318						
electrostatic	-257.083						
ΔEs	-80.572						
	-5.952						
	-77.636						

	H	H	Q	K	Gly9	
Initial Orientatio	RB1	LS1				
Final Orientatior	RB1				CS	
	RB1					
	RS1					
	2					
	CS					
Total Energy	62.64					
van der Waals	89.396					
electrostatic	-245.465					
ΔEs	-71.411					
	-6.874					
	-66.018					

	H	H	Q	K	Tyr10	Val12	Leu17
Initial Orientatio	RS2	LB1					
Final Orientation	RB1	LB1			LS2	RS2	CS
	RB1	LS2					
	RS1						
	RS2						
	CS						
Total Energy	24.131						
van der Waals	80.617						
electrostatic	-275.346						
ΔEs	-109.92						
	-15.653						
	-95.899						

	H	H	Q	K
Initial Orientatio	LB1	RS2		
Final Orientatior	LB1	RS2		LS2
	LS2			
	RB1			
Total Energy	16.144			
van der Waals	81.2			
electrostatic	-291.016			
ΔEs	-117.907			
	-15.07			
	-111.569			

	H	H	Q	K	Val12	Leu17
Initial Orientatio	RB1	LS2				
Final Orientation	RB1	LB2		RS1	RS2	LS2
	LS2	LS2		RS2		LB1
	LB1			-CH2-		CS
	RNH					
	RS2					
Total Energy	1.033					
van der Waals	76.119					
electrostatic	-294.243					
ΔEs	-133.018					
	-20.151					
	-114.796					

	H	H	Q	K	Tyr10	Leu17
Initial Orientatio	LS2	RB1				
Final Orientatior	LB2				RS2	LB2
	LS2	RS2				
Total Energy	62.674					
van der Waals	86.64					
electrostatic	-241.725					
ΔEs	-71.377					
	-9.63					
	-62.278					

	H	H	Q	K	Gly9	Tyr10	Leu17	Phe20
Initial Orientatio	LB1	RB2						
Final Orientation	LB1	RB2		LS2*	RS2	RS2	LS2	LB2
	RB1	RS2		LS1*	C=O			LS2
	RB1			*-CH2-				-CH2-
	LS2							
Total Energy	-4.977							
van der Waals	68.419							
electrostatic	-293.092							
ΔEs	-139.028							
	-27.851							
	-113.645							

	H	H	Q	K	Gly9	Tyr10
Initial Orientatio	RB2	LB1				
Final Orientatior	RB1	LB1			RS1	RS1
	-CH2-	LNH			C=O	LB1
	RNH					
	RS1					
	RB2					
Total Energy	52.512					
van der Waals	83.921					
electrostatic	-250.131					
ΔEs	-81.539					
	-12.349					
	-70.684					

	H	H	Q	K	Leu17	Phe20
Initial Orientatio	RB1	LB2				
Final Orientation	RB1	LB2		RS1	LB2	RB2
	LB1			2		RS1
	LB1					-CH2-
	RS1					
	LNH					
Total Energy	10.046					
van der Waals	76.225					
electrostatic	-284.797					
ΔEs	-124.005					
	-20.045					
	-105.35					

	H	H	Q	K	Tyr10	Leu17
Initial Orientatio	LB2	RB1				
Final Orientatior	LS2	RB1			RS2	LB2
		RS2				
Total Energy	57.831					
van der Waals	82.263					
electrostatic	-245.693					
ΔEs	-76.22					
	-14.007					
	-66.246					

	H	H	Q	K	Tyr10	Leu17	Phe20
Initial Orientatio	LS2	RS2					
Final Orientation	LB1	RB2		LS2	RS2	LS2	LB2
	LS2	RS2		-CH2-		RB2	LS2
	LS1						-CH2-
	RB1						
Total Energy	-10.185						
van der Waals	70.925						
electrostatic	-295.197						
ΔEs	-144.236						
	-25.345						
	-115.75						

	H	H	Q	K	Tyr10
Initial Orientatio	RS2	LS2			
Final Orientatior	RS1	LS2			LB2
	RS2				
Total Energy	48.454				
van der Waals	89.394				
electrostatic	-258.855				
ΔEs	-85.597				
	-6.876				
	-79.408				

	H	H	Q	K	Tyr10	Leu17
Initial Orientatio	RB2	LS2				
Final Orientation	RS2	LS2		RS2	LS2	RS2
	RB1			-CH2-	LB2	
Total Energy	42.699					
van der Waals	82.431					
electrostatic	-256.771					
ΔEs	-91.352					
	-13.839					
	-77.324					

	H	H	Q	K	Gly9	Tyr10
Initial Orientatio	LS2	RB2				
Final Orientation	LS2	RB2		LS2	RS2	RS2
	LB1	RS2		-CH2-	C=O	
Total Energy	15.759					
van der Waals	78.615					
electrostatic	-281.18					
ΔEs	-118.292					
	-17.655					
	-101.733					

	H	H	Q	K	Tyr10
Initial Orientatio	LB2	RS2			
Final Orientation	RB1	RB2			RS2
	RB1	RS2			
	LS2				
	LB1				
	RNH				
Total Energy	27.488				
van der Waals	81.765				
electrostatic	-271.13				
ΔEs	-106.563				
	-14.505				
	-91.683				

	H	H	Q	K	Val12	Leu17
Initial Orientatio	RS2	LB2				
Final Orientation	RB1	LS2		RS2	RS2	CS
	RS2	RB2		-CH2-		LB1
	LB1			RS1		LS2
	LS2					
Total Energy	1.448					
van der Waals	75.24					
electrostatic	-289.997					
ΔEs	-132.603					
	-21.03					
	-110.55					

	H	H	Q	K	Tyr10	Val12	Leu17
Initial Orientatio	RB2	LB2					
Final Orientation	RB1	LB2		RB2	LB2	RB2	LS2
	LS2	LS2		RS2			
	-CH2-						
	LB1						
	RNH						
	RS2						
Total Energy	13.129						
van der Waals	82.502						
electrostatic	-289.395						
ΔEs	-120.922						
	-13.768						
	-109.948						

	H	H	Q	K	Leu17	Phe20
Initial Orientatio	LB2	RB2				
Final Orientation	LB1	RB2		LS2	LS2	LB2
	LS2			-CH2-		
	LS1			LS1		
Total Energy	29.373					
van der Waals	81.394					
electrostatic	-274.649					
ΔEs	-104.678					
	-14.876					
	-95.202					

	H	H	Q	K	Gly9
Initial Orientatio	RS1	LS1			
Final Orientation	RB1	LS1			CS
	RB1				C=O
	RS1				
	2				
	CS				
Total Energy	62.646				
van der Waals	89.018				
electrostatic	-246.122				
ΔEs	-71.405				
	-7.252				
	-66.675				

	H	H	Q	K	Tyr10
Initial Orientatio	LS1	RS1			
Final Orientation	LB1	RS1			RS1
	LB1	2			
	LS1				
	LNH				
Total Energy	54.25				
van der Waals	90.727				
electrostatic	-255.316				
ΔEs	-79.801				
	-5.543				
	-75.869				

	H	H	Q	K	Phe20
Initial Orientatio	CS			RB1	
Final Orientation	LS2			RB1	CS
	2			RS1	
	CS			CS	
				-CH2-	
				RNH	
Total Energy	56.401				
van der Waals	88.369				
electrostatic	-253.717				
ΔEs	-77.65				
	-7.901				
	-74.27				

	H	H	Q	K	Val12
Initial Orientatio	RB1			CS	
Final Orientation	RS1		LS1	LS2	LS1
				2	LB1
				LS1	
				-CH2-	
Total Energy	24.174				
van der Waals	86.919				
electrostatic	-276.744				
ΔEs	-109.877				
	-9.351				
	-97.297				

	H	H	Q	K	His6	Gly9	Val12
Initial Orientatio	CS			LB1			
Final Orientation	LB1			LS2	RS1	RB1	LS1
	CS			LS1	2		
	LS1			-CH2-			
Total Energy	16.137						
van der Waals	82.946						
electrostatic	-290.213						
ΔEs	-117.914						
	-13.324						
	-110.766						

	H	H	Q	K	Val12	Phe20
Initial Orientatio	LB1			CS		
Final Orientation	LS1			RB1	LS1	RS1
	LNH			RS1		
				CS		
Total Energy	54.842					
van der Waals	86.058					
electrostatic	-252.337					
ΔEs	-79.209					
	-10.212					
	-72.89					

	H	H	Q	K
Initial Orientatio	CS			RS1
Final Orientation	RS1			RS1
				RB2
Total Energy	53.008			
van der Waals	92.514			
electrostatic	-260.178			
ΔEs	-81.043			
	-3.756			
	-80.731			

	H	H	Q	K
Initial Orientatio	RS1			CS
Final Orientation	RS1			LB1
				RB1
Total Energy	51.602			
van der Waals	91.329			
electrostatic	-259.109			
ΔEs	-82.449			
	-4.941			
	-79.662			

	H	H	Q	K	Val12
Initial Orientatio	LS1			CS	
Final Orientation	LS1			LB1	LS1
				LS1	
				-CH2-	
Total Energy	68.479				
van der Waals	90.507				
electrostatic	-242.829				
ΔEs	-65.572				
	-5.763				
	-63.382				

	H	H	Q	K	His6	Gly9	Val12				H	H	Q	K	Val12	
Initial Orientatio	CS			LS1						Initial Orientatio	RS2			CS		
Final Orientatior	LB1			LS1	RS1	RB1	LS1			Final Orientatior	RB2			CS	RS1	
	CS			-CH2-							RS2			RS2	RS2	
	LS1			LB2										-CH2-		
Total Energy	32.293									Total Energy	55.155					
van der Waals	85.296									van der Waals	85.409					
electrostatic	-272.405									electrostatic	-249.43					
ΔEs	-101.758									ΔEs	-78.896					
	-10.974										-10.861					
	-92.958										-69.983					

	H	H	Q	K	Arg5	His6	Gly9	Val12			H	H	Q	K	Val12	Leu17
Initial Orientatio	CS			RS2						Initial Orientatio	CS			LS2		
Final Orientatior	RB1			RS2	LS2	LS2	LB1	CS		Final Orientatior	RB1			LS2	LS1	RB2
	RS1				-CH2-	LS1	CS	RS2			CS			LS1		
	CS						C=O				RS2					
Total Energy	6.904									Total Energy	22.546					
van der Waals	78.723									van der Waals	81.632					
electrostatic	-294.446									electrostatic	-275.363					
ΔEs	-127.147									ΔEs	-111.505					
	-17.547										-14.638					
	-114.999										-95.916					

	H	H	Q	K							H	H	Q	K	His6	Val12
Initial Orientatio	LS2			CS						Initial Orientatio	CS			RB2		
Final Orientatior	LS2			RB1						Final Orientatior	RB1			RS1*	LS2	RS2
				RS2							CS			RS2*	LB2	
											RS1			*-CH2-		
											RS2					
Total Energy	44.988									Total Energy	2.809					
van der Waals	93.035									van der Waals	78.983					
electrostatic	-264.15									electrostatic	-292.317					
ΔEs	-89.063									ΔEs	-131.242					
	-3.235										-17.287					
	-84.703										-112.87					

	H	H	Q	K	Val12						H	H	Q	K	Val12	
Initial Orientatio	RB2			CS						Initial Orientatio	LB2			CS		
Final Orientatior	RB2			RB1	RS1					Final Orientatior	LS1			LB1	LS2	
	RS2			RS2							LS2			CS		
	RS1			-CH2-							LB2			LS1		
				CS										-CH2-		
Total Energy	41.649									Total Energy	43.22					
van der Waals	83.75									van der Waals	83.588					
electrostatic	-262.5									electrostatic	-258.689					
ΔEs	-92.402									ΔEs	-90.831					
	-12.52										-12.682					
	-83.053										-79.242					

	H	H	Q	K	Val12						H	H	Q	K	Phe20	
Initial Orientatio	CS			LB2						Initial Orientatio	RB1			LB1		
Final Orientatior	LB1			LS2	LS1					Final Orientatior	RS1			LB1	LB1	
	CS			LS1							RB1			LS2		
				-CH2-										2		
														CS		
														-CH2-		
														LS1		
Total Energy	51.248									Total Energy	54.912					
van der Waals	87.368									van der Waals	84.584					
electrostatic	-252.954									electrostatic	-251.043					
ΔEs	-82.803									ΔEs	-79.139					
	-8.902										-11.686					
	-73.507										-71.596					

	H	H	Q	K	Val12						H	H	Q	K	Leu17	
Initial Orientatio	LB1			RB1						Initial Orientatio	LB1			RS1		
Final Orientatior	LS1			RS1	CS					Final Orientatior	LS2			RB2	LS1	
	LB1			RB1							LS1			RS1		
				-CH2-							LB1					
				RNH												
Total Energy	50.425									Total Energy	38.73					
van der Waals	85.324									van der Waals	86.76					
electrostatic	-249.865									electrostatic	-268.341					
ΔEs	-83.626									ΔEs	-95.321					
	-10.946										-9.51					
	-70.418										-88.894					

	H	H	Q	K							H	H	Q	K	Val12	Phe20
Initial Orientatio	RS1			LB1						Initial Orientatio	RB1			LS1		
Final Orientatior	RS1			LS1						Final Orientatior	RS1			LB1		CS
											RB1			LS2		
														2		
														CS*		
														LS1*		
														*-CH2-		
Total Energy	55.039									Total Energy	24.879					
van der Waals	90.879									van der Waals	81.741					
electrostatic	-256.152									electrostatic	-274.183					
ΔEs	-79.012									ΔEs	-109.172					
	-5.391										-14.529					
	-76.705										-94.736					

	H	H	Q	K	Phe20			
Initial Orientatio	LS1			RB1				
Final Orientatior	LB1			RS1	RS1			
	LNH							
	LS1							
Total Energy	64.891							
van der Waals	88.925							
electrostatic	-239.909							
ΔEs	-69.16							
	-7.345							
	-60.462							

	H	H	Q	K	Phe19	Phe20	Asp23	
Initial Orientatio	RS2			LB1				
Final Orientatior	RS2			LB2	LB2	LB2	LB2	
				LS2				
Total Energy	47.257							
van der Waals	87.375							
electrostatic	-262.318							
ΔEs	-86.794							
	-8.895							
	-82.871							

	H	H	Q	K
Initial Orientatio	LS2			RB1
Final Orientatior	LS2			RS2
				RB1
Total Energy	52.185			
van der Waals	92.676			
electrostatic	-256.223			
ΔEs	-81.866			
	-3.594			
	-76.776			

	H	H	Q	K	Phe19			
Initial Orientatio	RB2			LB1				
Final Orientatior	RS1			LB1	LS1			
				RS1				
				-CH2-				
				LNH				
Total Energy	42.634							
van der Waals	86.276							
electrostatic	-260.555							
ΔEs	-91.417							
	-9.994							
	-81.108							

	H	H	Q	K	Ser8	Gly9	Val12	Phe20
Initial Orientatio	LB2			RB1				
Final Orientation				RS1	LS1	LS1	LS1	RB2
						LB2		
						C=O		
Total Energy	45.259							
van der Waals	84.771							
electrostatic	-264.673							
ΔEs	-88.792							
	-11.499							
	-85.226							

	H	H	Q	K
Initial Orientatio	RS2			LS2
Final Orientatior	RS2			LS2
Total Energy	50.319			
van der Waals	93.366			
electrostatic	-258.572			
ΔEs	-83.732			
	-2.904			
	-79.125			

	H	H	Q	K	Gly9	Val12	Asp23
Initial Orientatio	RB2			LS2			
Final Orientatior	RS2			LS2	RS2	RS2	LB2
	RB2			2			
				LB2			
Total Energy	50.179						
van der Waals	87.529						
electrostatic	-253.992						
ΔEs	-83.872						
	-8.741						
	-74.545						

	H	H	Q	K	Val12		
Initial Orientatio	LB1			RS2			
Final Orientatior	LS2			RS1	RS2		
				RS2			
				-CH2-			
Total Energy	27.089						
van der Waals	87.617						
electrostatic	-276.079						
ΔEs	-106.962						
	-8.653						
	-96.632						

	H	H	Q	K	Gly9	Leu17	
Initial Orientatio	RB1			LS2			
Final Orientatior	RB1	RS2		LS2	RS1	RS2	
	RS1			LS1	C=O		
	RS2						
	-CH2-						
	RB2						
Total Energy	-1.703						
van der Waals	78.302						
electrostatic	-301.325						
ΔEs	-135.754						
	-17.968						
	-121.878						

	H	H	Q	K	Val12	Leu17	Phe20
Initial Orientatio	LB1			RB2			
Final Orientation	RB1			RB2	RS1	LS1	RB2
	LB1			RS1			
	LS1			-CH2-			
	LNH						
Total Energy	27.217						
van der Waals	77.044						
electrostatic	-274.204						
ΔEs	-106.834						
	-19.226						
	-94.757						

	H	H	Q	K	Ser8	Gly9	Val12	Phe20
Initial Orientatio	RB1			LB2				
Final Orientation	RB1			LB2	RB2	RS1	RB2	LB2
	LS1			LS1		C=O		
	LB1			-CH2-		RB2		
Total Energy	33.825							
van der Waals	77.079							
electrostatic	-266.754							
ΔEs	-100.226							
	-19.191							
	-87.307							

	H	H	Q	K	Val12
Initial Orientatio	LS2			RS2	
Final Orientation	LS2			LB2	RS2
				RS1	
				RS2	
Total Energy	37.844				
van der Waals	88.41				
electrostatic	-268.524				
ΔEs	-96.207				
	-7.86				
	-89.077				

	H	H	Q	K	Gly9	Phe20	Asp23
Initial Orientatio	LS2			RB2			
Final Orientatior	LS2			RB2	LB2	RS2	RB2
				RS2		RB2	
				2			
Total Energy	56.112						
van der Waals	88.319						
electrostatic	-249.953						
ΔEs	-77.939						
	-7.951						
	-70.506						

	H	H	Q	K	Phe20
Initial Orientatio	RS2			LB2	
Final Orientatior	RS2			LS2	LB2
				LB2	
Total Energy	52.996				
van der Waals	89.688				
electrostatic	-252.309				
ΔEs	-81.055				
	-6.582				
	-72.862				

	H	H	Q	K
Initial Orientatio	LB2			RS2
Final Orientatior	LS2			RS2
	LB2			
Total Energy	38.652			
van der Waals	89.765			
electrostatic	-273.567			
ΔEs	-95.399			
	-6.505			
	-94.12			

	H	H	Q	K	Val12	Phe19	Phe20
Initial Orientatio	LB2			RB2			
Final Orientation	LS1			RS2	LS2	RB2	RS2
	LS2				LB2		
	LB2						
Total Energy	36.741						
van der Waals	81.336						
electrostatic	-260.261						
ΔEs	-97.31						
	-14.934						
	-80.814						

	H	H	Q	K	Leu17
Initial Orientatic	RB2			LB2	
Final Orientatior	RB1			LS1	RB2
	RS2			:LS2	
	RNH				
	LS2				
Total Energy	22.304				
van der Waals	82.649				
electrostatic	-279.982				
ΔEs	-111.747				
	-13.621				
	-100.535				

	H	H	Q	K	Gly9	Tyr10
Initial Orientation		LB2		RB2		
Final Orientatior	RB1	LB2		RB2	LB1	LS1
				RS2	LNH*	-CH-
					LS1*	
					*-C=O	
Total Energy	21.104					
van der Waals	82.649					
electrostatic	-280.512					
ΔEs	-112.947					
	-13.621					
	-101.065					

	H	H	Q	K	Phe20
Initial Orientation		RB2		LB2	
Final Orientatior	RB1	RB2		LB2	LB2
	RB1			LS2	
	LB1			-CH2-	
Total Energy	32.459				
van der Waals	85.255				
electrostatic	-270.934				
ΔEs	-101.592				
	-11.015				
	-91.487				

	RB1	LB1				
Initial Orientatio	RB1	LB1				
Final Orientation	RNH				RS1	RB1
						RS1
Total Energy	53.292					
van der Waals	86.839					
electrostatic	-250.126					
ΔEs	-80.759					
	-9.431					
	-70.679					

	LB1	RB1				
Initial Orientation	LB1	RB1				
Final Orientation	LS2				LS2	
	LB1					
	CS					
Total Energy	58.901					
van der Waals	84.746					
electrostatic	-244.344					
ΔEs	-75.15					
	-11.524					
	-64.897					

	L	V	F	F
Initial Orientatio	LB2	RB2		
Final Orientation				
Total Energy	125.239			
van der Waals	95.226			
electrostatic	-187.076			
ΔEs	-8.812			
	-1.044			
	-7.629			

	L	V	F	F
Initial Orientation	RB2	LB2		
Final Orientation				
Total Energy	128.191			
van der Waals	96.221			
electrostatic	-185.226			
ΔEs	-5.86			
	-0.049			
	-5.779			

	L	V	F	F
Initial Orientatio	RB2		LB2	
Final Orientation				
Total Energy	118.778			
van der Waals	87.812			
electrostatic	-188.442			
ΔEs	-15.273			
	-8.458			
	-8.995			

	L	V	F	F	His14
Initial Orientation	LB2		RB2		
Final Orientation	LB2				LB2
					-CH-
Total Energy	118.59				
van der Waals	89.987				
electrostatic	-190.482				
ΔEs	-15.461				
	-6.283				
	-11.035				

	L	V	F	F	His13	Lys16
Initial Orientatio	LB1			RB1		
Final Orientation	LB1			RB1	LB1	CS
					CS	-CH2-
					LS1	
Total Energy	75.191					
van der Waals	83.098					
electrostatic	-222.942					
ΔEs	-58.86					
	-13.172					
	-43.495					

	L	V	F	F	Val12	His13	His14	Lys16
Initial Orientation	RB1			LB1				
Final Orientation	CS			LS2	LS1	LB1	RS1	LS2*
	RB1					LS1		LS1*
						LNH		*-CH2-
						RB1		
						RS1		
						-CH2-		
Total Energy	1.575							
van der Waals	74.935							
electrostatic	-287.032							
ΔEs	-132.476							
	-21.335							
	-107.585							

	L	V	F	F	His13	Lys16	
Initial Orientatio	LB1			RB2			
Final Orientation	RS1				RS2	RS1	
	RNH				RS1	-CH2-	
	RB1				RNH		
	LB1						
Total Energy	41.024						
van der Waals	82.062						
electrostatic	-261.466						
ΔEs	-93.027						
	-14.208						
	-82.019						

	L	V	F	F	His13	Lys16	
Initial Orientation	RB2			LB1			
Final Orientation	RS2			CS	LS2	LS2	LS1
	RNH			LB1	LB2		LB1
	RB1						LNH
Total Energy	29.676						
van der Waals	77.512						
electrostatic	-267.83						
ΔEs	-104.375						
	-18.758						
	-88.383						

	L	V	F	F	His13	His14	Lys16
Initial Orientatio	RB1			LB2			
Final Orientation	RS2			LS2	LB1	RS2	LS2
	RB1			LB2	LS1		LS1
					CS		-CH2-
					LS2		
Total Energy	12.498						
van der Waals	73.702						
electrostatic	-282.131						
ΔEs	-121.553						
	-22.568						
	-102.684						

	L	V	F	F	His13	Lys16	
Initial Orientation	RB1			RB1			
Final Orientation	CS				RS2	RS2	RS1
	LB1					RB1	RS2
	LS2						-CH2-
Total Energy	11.655						
van der Waals	76.704						
electrostatic	-285.944						
ΔEs	-122.396						
	-19.566						
	-106.497						

	L	V	F	F	His13		
Initial Orientatio	RB2			LB2			
Final Orientation	RB2				RS2		
	RS2						
Total Energy	88.702						
van der Waals	91.856						
electrostatic	-222.142						
ΔEs	-45.349						
	-4.414						
	-42.695						

	L	V	F	F	His13	Leu34	
Initial Orientation	LB2			RB2			
Final Orientation					LS1	RS2	
Total Energy	98.232						
van der Waals	90.396						
electrostatic	-212.502						
ΔEs	-35.819						
	-5.874						
	-33.055						

	L	V	F	F			
Initial Orientation		LB1	RB1				
Final Orientation			RS2				
Total Energy	124.754						
van der Waals	91.78						
electrostatic	-185.84						
ΔEs	-9.297						
	-4.49						
	-6.393						

	L	V	F	F	Gln15		
Initial Orientation		RB1	LB1				
Final Orientation		RB1	LS1		CS		
Total Energy	124.147						
van der Waals	90.158						
electrostatic	-185.17						
ΔEs	-9.904						
	-6.112						
	-5.723						

	L	V	F	F			
Initial Orientation		RB2	LB2				
Final Orientation							
Total Energy	128.667						
van der Waals	95.046						
electrostatic	-183.495						
ΔEs	-5.384						
	-1.224						
	-4.048						

	L	V	F	F			
Initial Orientation		LB2	RB2				
Final Orientation							
Total Energy	126.202						
van der Waals	94.501						
electrostatic	-186.161						
ΔEs	-7.849						
	-1.769						
	-6.714						

	L	V	F	F	Val24		
Initial Orientation		LB2		RB2			
Final Orientation					RB2		
Total Energy	105.84						
van der Waals	90.737						
electrostatic	-204.134						
ΔEs	-28.211						
	-5.533						
	-24.687						

	L	V	F	F	Val24	Lys28	Met35
Initial Orientation		RB2		LB2			
Final Orientation					LB2	LS1	LS1
						2	
Total Energy	80.593						
van der Waals	86.676						
electrostatic	-226.071						
ΔEs	-53.458						
	-9.594						
	-46.624						

	L	V	F	F	Lys16	Ala30	
Initial Orientation			RB1	LB1			
Final Orientation			RNH		RS1	LB2	
			RS1		2	LS1	
					RB1		
Total Energy	78.207						
van der Waals	86.398						
electrostatic	-225.705						
ΔEs	-55.844						
	-9.872						
	-46.258						

	L	V	F	F	His13	Lys16	Asp23
Initial Orientation			LB1	RB1			
Final Orientation			LS2	CS	RS1	LB1	CS
			LS1	RB1		LS1	
			LB1	RS2		LNH	
						RB1	
						RS1	
						-CH2-	
Total Energy	37.833						
van der Waals	75.397						
electrostatic	-261.177						
ΔEs	-96.218						
	-20.873						
	-81.73						

	L	V	F	F			
Initial Orientation			LB2	RB2			
Final Orientation				RB2			
Total Energy	117.344						
van der Waals	95.06						
electrostatic	-194.279						
ΔEs	-16.707						
	-1.21						
	-14.832						

	L	V	F	F			
Initial Orientation			RB2	LB2			
Final Orientation							
Total Energy	130.336						
van der Waals	96.283						
electrostatic	-183.672						
ΔEs	-3.715						
	0.013						
	-4.225						

	H	H	Q	K	L	V	F	F		
Initial Orientatio	CS				RB1					
Final Orientation	LB1				RB1					
	LS2									
	LS1									
	-CH2-									
Total Energy	66.844									
van der Waals	84.715									
electrostatic	-239.142									
ΔEs	-67.207									
	-11.555									
	-59.695									

	H	H	Q	K	L	V	F	F		
Initial Orientatio	CS				LB1					
Final Orientation	RB1			RS1	LS1					
	RS2									
	LB1									
	LS1									
	-CH2-									
Total Energy	9.379									
van der Waals	83.754									
electrostatic	-293.748									
ΔEs	-124.672									
	-12.516									
	-114.301									

	H	H	Q	K	L	V	F	F		
Initial Orientatio	RB1				LB1					
Final Orientation	RB1			LS1	LS1					
	RS2									
	LB1									
	LS1									
	-CH2-									
Total Energy	10.204									
van der Waals	84.045									
electrostatic	-293.046									
ΔEs	-123.847									
	-12.225									
	-113.599									

	H	H	Q	K	L	V	F	F		
Initial Orientatio	LB1				RB1					
Final Orientation	LS1			LS2	RB1			CS		
	LB1			2						
Total Energy	51.212									
van der Waals	85.265									
electrostatic	-254.493									
ΔEs	-82.839									
	-11.005									
	-75.046									

	H	H	Q	K	L	V	F	F		
Initial Orientatio	RS1				LB1					
Final Orientation	RB1	LS1		RB2	RS1			RS1		
	RS2			RS2*	LB1			-CH2-		
	RS1			RS1*						
	CS			*-CH2-						
Total Energy	23.682									
van der Waals	75.599									
electrostatic	-272.739									
ΔEs	-110.369									
	-20.671									
	-93.292									

	H	H	Q	K	L	V	F	F		
Initial Orientatio	LS1				RB1					
Final Orientation	LS1				RB1					
	LNH									
	LB1									
Total Energy	92.076									
van der Waals	91.852									
electrostatic	-217.952									
ΔEs	-41.975									
	-4.418									
	-38.505									

	H	H	Q	K	L	V	F	F	Ala21	
Initial Orientatio	RS2				LB1					
Final Orientation	RS2			RS1	RB1			RS1	CS	
					CS					
Total Energy	39.8									
van der Waals	80.655									
electrostatic	-260.73									
ΔEs	-94.251									
	-15.615									
	-81.283									

	H	H	Q	K	L	V	F	F		
Initial Orientatio	LS2				RB1					
Final Orientation	LB1			LS2	RS2					
	CS									
	LS1									
Total Energy	45.783									
van der Waals	87.014									
electrostatic	-261.583									
ΔEs	-88.268									
	-9.256									
	-82.136									

	H	H	Q	K	L	V	F	F	Tyr10	Val12
Initial Orientatio	LB1				RB2					
Final Orientation	LB1	RB2		LB1*	RB1				RS2	LS2
	LS1	RS2		LS2*					C=O	
	RS2			*-CH2-						
	-CH2-			LB2						
	RB1									
	LS2									
Total Energy	7.279									
van der Waals	75.279									
electrostatic	-286.565									
ΔEs	-126.772									
	-20.991									
	-107.118									

	H	H	Q	K	L	V	F	F
Initial Orientatio	RB2				LB1			
Final Orientation	RB2				RB1			
	RS1				LB1			
	RNH							
	RB1							
	-CH2-							
Total Energy	74.023							
van der Waals	82.311							
electrostatic	-227.599							
ΔEs	-60.028							
	-13.959							
	-48.152							

	H	H	Q	K	L	V	F	F	Val12
Initial Orientatio	RB1				LB2				
Final Orientation	LB1			RB2	LB2			RB2	RS1
	RB1								
	RNH								
	LNH								
	LS1								
	-CH2-								
Total Energy	29.606								
van der Waals	78.955								
electrostatic	-272.141								
ΔEs	-104.445								
	-17.315								
	-92.694								

	H	H	Q	K	L	V	F	F	Ala21
Initial Orientatio	LB2				RB1				
Final Orientation	LB1				RS2			RB2	RB2
	LS2				CS				RS2
Total Energy	66.542								
van der Waals	78.777								
electrostatic	-231.777								
ΔEs	-67.509								
	-17.493								
	-52.33								

	H	H	Q	K	L	V	F	F
Initial Orientatio	LS2				RB2			
Final Orientation	LB1	RS2		LB2	RS2			LB2
	LS1			LS2	RB1			LS2
	CS							-CH2-
	LS2							
Total Energy	8.075							
van der Waals	77.121							
electrostatic	-284.229							
ΔEs	-125.976							
	-19.149							
	-104.782							

	H	H	Q	K	L	V	F	F
Initial Orientatio	RS2				LB2			
Final Orientation	RB2				LS2			
	RS2				LB2			
Total Energy	74.534							
van der Waals	88.056							
electrostatic	-232.745							
ΔEs	-59.517							
	-8.214							
	-53.298							

	H	H	Q	K	L	V	F	F
Initial Orientatio	RB2				LB2			
Final Orientation	RS2				RB2			
	RB2							
Total Energy	83.202							
van der Waals	93.067							
electrostatic	-226.942							
ΔEs	-50.849							
	-3.203							
	-47.495							

	H	H	Q	K	L	V	F	F
Initial Orientatio	LB2				RB2			
Final Orientation	LS2			LS2	RS2			
	LS1			-CH2-	RB2			
Total Energy	33.861							
van der Waals	85.809							
electrostatic	-269.205							
ΔEs	-100.19							
	-10.461							
	-89.758							

	H	H	Q	K	L	V	F	F	
Initial Orientatio	LS2					RB2			
Final Orientation	LB1	RS2		LS2	LS2			LB2	
	LS1	-CH-		-CH2-	RB1				
	LS2				RB2				
Total Energy	16.516								
van der Waals	73.67								
electrostatic	-274.942								
ΔEs	-117.535								
	-22.6								
	-95.495								

	H	H	Q	K	L	V	F	F	
Initial Orientatio	RB2					LB2			
Final Orientation									
Total Energy	119.99								
van der Waals	91.978								
electrostatic	-189.873								
ΔEs	-14.061								
	-4.292								
	-10.426								

	H	H	Q	K	L	V	F	F	Val12
Initial Orientatio	LS2						RB2		
Final Orientation	LS1			RS2			RB2	RS2	LB2
	LB2								LS2
	LS2								
Total Energy	37.047								
van der Waals	81.637								
electrostatic	-259.676								
ΔEs	-97.004								
	-14.633								
	-80.229								

	H	H	Q	K	L	V	F	F	
Initial Orientatio	RB2						LB2		
Final Orientation	RB2			LB1			LB2	CS	
	RS2			LS2			LS2		
				2					
				CS					
				RS2					
				-CH2-					
Total Energy	28.883								
van der Waals	81.001								
electrostatic	-271.1								
ΔEs	-105.168								
	-15.269								
	-91.653								

	H	H	Q	K	L	V	F	F	
Initial Orientatio	CS							RB2	
Final Orientation	RB1			RS2	RS1			RS1	
	CS			RS1				RB2	
	RS1			-CH2-					
Total Energy	43.322								
van der Waals	80.036								
electrostatic	-257.37								
ΔEs	-90.729								
	-16.234								
	-77.923								

	H	H	Q	K	L	V	F	F	Val12
Initial Orientatio	RS1							LB1	
Final Orientation	RS2			RB1				LS1	RS1
				RS1				LB1	
				-CH2-				CS	
Total Energy	50.923								
van der Waals	82.805								
electrostatic	-253.044								
ΔEs	-83.128								
	-13.465								
	-73.597								

	H	H	Q	K	L	V	F	F	Asp23
Initial Orientatio	LS2							RB1	
Final Orientation	LS2			RS2			RS2	CS	RS2
								RB1	
								RS2	
Total Energy	72.224								
van der Waals	87.336								
electrostatic	-233.883								
ΔEs	-61.827								
	-8.934								
	-54.436								

	H	H	Q	K	L	V	F	F	
Initial Orientatio	RB2							LB1	
Final Orientation	RS1			LB1	RS1			LB1	
	RNH			LNH				CS	
	RB1			LS2					
				-CH2-					
Total Energy	35.054								
van der Waals	81.703								
electrostatic	-266.864								
ΔEs	-98.997								
	-14.567								
	-87.417								

	H	H	Q	K	L	V	F	F	Ala21
Initial Orientatio	RS2					LB2			
Final Orientation	RB2				RB1	LB2			LS2
	RS2								LB2
Total Energy	77.355								
van der Waals	83.779								
electrostatic	-228.792								
ΔEs	-56.696								
	-12.491								
	-49.345								

	H	H	Q	K	L	V	F	F	
Initial Orientatio	LB2					RB2			
Final Orientation	LS2								
	LB2								
Total Energy	72.544								
van der Waals	90.09								
electrostatic	-235.001								
ΔEs	-61.507								
	-6.18								
	-55.554								

	H	H	Q	K	L	V	F	F	
Initial Orientatio	RS2						LB2		
Final Orientation	RB2			LS2			LB2		
	RS2								
Total Energy	45.847								
van der Waals	90.248								
electrostatic	-263.351								
ΔEs	-88.204								
	-6.022								
	-83.904								

	H	H	Q	K	L	V	F	F	Val12
Initial Orientatio	LB2						RB2		
Final Orientation	LB2			LS1			RB2		LS2
	LS2			LS2					
				-CH2-					
Total Energy	40.571								
van der Waals	85.58								
electrostatic	-266.728								
ΔEs	-93.48								
	-10.69								
	-87.281								

	H	H	Q	K	L	V	F	F	
Initial Orientatio	CS							LB2	
Final Orientation	LB1			LS1	LS2			LB2	
	CS			LS2					
	LS2			-CH2-					
Total Energy	45.795								
van der Waals	83.012								
electrostatic	-259.482								
ΔEs	-88.256								
	-13.258								
	-80.035								

	H	H	Q	K	L	V	F	F	Val12
Initial Orientatio	LS1							RB1	
Final Orientation	LS1			CS				CS	LS2
				LS2				RS1	LS1
				-CH2-					
				LB1					
Total Energy	50.248								
van der Waals	83.073								
electrostatic	-250.771								
ΔEs	-83.803								
	-13.197								
	-71.324								

	H	H	Q	K	L	V	F	F	
Initial Orientatio	LB1							RB2	
Final Orientation	RB1			RB2	LS1			RB2	
	LS1			RNH	LNH				
	-CH2-			-CH2-	LB1				
	LB1								
	RNH								
	RS1								
Total Energy	17.699								
van der Waals	76.58								
electrostatic	-277.275								
ΔEs	-116.352								
	-19.69								
	-97.828								

	H	H	Q	K	L	V	F	F	Val12
Initial Orientatio	LB2							RB1	
Final Orientation	LB2			LB1				RB1	LS1
				LNH*					
				LS1*					
				*-CH2-					
Total Energy	61.416								
van der Waals	84.25								
electrostatic	-243.192								
ΔEs	-72.635								
	-12.02								
	-63.745								

	H	H	Q	K	L	V	F	F	Gly9	Val12
Initial Orientatio	RB1							LB2		
Final Orientation	RB1								RS1	RNH
	RNH									RS1
										RB2
Total Energy	59.5									
van der Waals	85.837									
electrostatic	-246.252									
ΔEs	-74.551									
	-10.433									
	-66.805									

	H	H	Q	K	L	V	F	F	F
Initial Orientatio	LS1								RB2
Final Orientation	LS1			RB2					
				RS1					
				RNH					
Total Energy	48.456								
van der Waals	89.351								
electrostatic	-255.801								
ΔEs	-85.595								
	-6.919								
	-76.354								

	H	H	Q	K	L	V	F	F	Val12	Leu34
Initial Orientatio	RS1							LB2		
Final Orientation	RNH							LB2	RB2	LS1
	RS1									
Total Energy	59.9									
van der Waals	85.314									
electrostatic	-244.907									
ΔEs	-74.151									
	-10.956									
	-65.46									

	H	H	Q	K	L	V	F	F	F	Val12
Initial Orientatio	LS2								RB2	
Final Orientation	LS2			RS2					RB2	LB2
	LB2								RS2	
Total Energy	70.777									
van der Waals	87.763									
electrostatic	-240.671									
ΔEs	-63.274									
	-8.507									
	-61.224									

	H	H	Q	K	L	V	F	F
Initial Orientatio	RS2							LB2
Final Orientation	RS2			LS1				LB2
				-CH2-				
				LS2				
Total Energy	40.148							
van der Waals	89.025							
electrostatic	-264.186							
ΔEs	-93.903							
	-7.245							
	-84.739							

	H	H	Q	K	L	V	F	F	F
Initial Orientatio	RB2								LB2
Final Orientation	RS1			RS2	RS2				
	RS2				RB2				
	RB2								
Total Energy	53.454								
van der Waals	89.181								
electrostatic	-254.633								
ΔEs	-80.597								
	-7.089								
	-75.186								

	H	H	Q	K	L	V	F	F
Initial Orientatio	LB2							RB2
Final Orientation	LS2			LS1*	LB2			LB2
	LS1			LB2*				
	LB2			*-CH2-				
Total Energy	52.391							
van der Waals	83.546							
electrostatic	-251.279							
ΔEs	-81.66							
	-12.724							
	-71.832							

	H	H	Q	K	L	V	F	F	Tyr10
Initial Orientation		CS			RB1				
Final Orientation	RS1	CS			RS1				CS
		RB1							
		LB1							
Total Energy	77.259								
van der Waals	85.844								
electrostatic	-226.598								
ΔEs	-56.792								
	-10.426								
	-47.151								

	H	H	Q	K	L	V	F	F	Gly9
Initial Orientation		CS			LB1				
Final Orientation	RS1				LS1				RS1
									C=O
Total Energy	65.282								
van der Waals	86.499								
electrostatic	-239.921								
ΔEs	-68.769								
	-9.771								
	-60.474								

	H	H	Q	K	L	V	F	F
Initial Orientation		LS1			RB1			
Final Orientation	CS	LS1			RB1			
Total Energy	90.871							
van der Waals	89.245							
electrostatic	-215.035							
ΔEs	-43.18							
	-7.025							
	-35.588							

	H	H	Q	K	L	V	F	F	Tyr10
Initial Orientation		RS1			LB1				
Final Orientation		RS1			CS				RS1
Total Energy	93.142								
van der Waals	90.004								
electrostatic	-213.537								
ΔEs	-40.909								
	-6.266								
	-34.09								

	H	H	Q	K	L	V	F	F	Ala21
Initial Orientation		RS2			LB1				
Final Orientation	CS	RS2			RS2			LS2	LB2
	RS2								
	-CH2-								
Total Energy	46.934								
van der Waals	78.427								
electrostatic	-249.746								
ΔEs	-87.117								
	-17.843								
	-70.299								

	H	H	Q	K	L	V	F	F	Gly9	Tyr10
Initial Orientation		LS2			RB1					
Final Orientation	RB1	LS1		RS2	CS				LS2	LS2
	LB1				LS1				C=O	C=O
	LS2									
Total Energy	-3.793									
van der Waals	77.299									
electrostatic	-298.029									
ΔEs	-137.844									
	-18.971									
	-118.582									

	H	H	Q	K	L	V	F	F	Tyr10
Initial Orientation		RB2			LB1				
Final Orientation		RB2			LB1				RB2
Total Energy	100.22								
van der Waals	89.63								
electrostatic	-206.262								
ΔEs	-33.831								
	-6.64								
	-26.815								

	H	H	Q	K	L	V	F	F	Tyr10
Initial Orientation		LB1			RB2				
Final Orientation	RS1	LB2			RNH				LS1
		C=O			RB2				
		LS1							
		LNH							
		LB1							
Total Energy	71.514								
van der Waals	83.954								
electrostatic	-236.534								
ΔEs	-62.537								
	-12.316								
	-57.087								

	H	H	Q	K	L	V	F	F			
Initial Orientation		LB2			RB1						
Final Orientation	RB2	LB2			LS2						
	RS2	LB2									
		LS2*									
		RS2*									
		*-CH2-									
Total Energy	48.644										
van der Waals	78.75										
electrostatic	-249.049										
ΔEs	-85.407										
	-17.52										
	-69.602										

	H	H	Q	K	L	V	F	F	Tyr10		
Initial Orientation		RS1			LB2						
Final Orientation		RS1			LB2			LB2	RS1		
					LB1						
Total Energy	72.577										
van der Waals	83.363										
electrostatic	-232.262										
ΔEs	-61.474										
	-12.907										
	-52.815										

	H	H	Q	K	L	V	F	F	Tyr10		
Initial Orientation		RS2			LB2						
Final Orientation		RB2			LS2				RB2		
		RB2									
		RS2									
		LS2									
Total Energy	65.24										
van der Waals	88.055										
electrostatic	-240.398										
ΔEs	-68.811										
	-8.215										
	-60.951										

	H	H	Q	K	L	V	F	F	Tyr10	Ala21	Val24
Initial Orientation		LB2			RB2						
Final Orientation	LS1	LB2			LB1			RB2	LB2	RB2	RB2
	-CH2-	LB2			LNH						
		LS1			LS1						
Total Energy	57.091										
van der Waals	78.053										
electrostatic	-243.77										
ΔEs	-76.96										
	-18.217										
	-64.323										

	H	H	Q	K	L	V	F	F	Tyr10		
Initial Orientation		CS				LB2					
Final Orientation		LB1			LS1				CS		
		CS									
		LS2									
Total Energy	83.418										
van der Waals	87.137										
electrostatic	-221.167										
ΔEs	-50.633										
	-9.133										
	-41.72										

	H	H	Q	K	L	V	F	F			
Initial Orientation		LS1				RB1					
Final Orientation		CS			CS	CS					
		C=O			LB1						
		LB1			LS1						
		LS1									
Total Energy	78.18										
van der Waals	83.27										
electrostatic	-223.074										
ΔEs	-55.871										
	-13										
	-43.627										

	H	H	Q	K	L	V	F	F	Gly9	Tyr10	Ala21
Initial Orientation		RB2				LB1					
Final Orientation	RS2	RNH		LS2	RB1			LB2	RB2	RB2	LB2
	RB2	RS1			RS2				C=O	-CH-	LNH
	-CH2-	RB2									
Total Energy	24.442										
van der Waals	69.829										
electrostatic	-267.783										
ΔEs	-109.609										
	-26.441										
	-88.336										

	H	H	Q	K	L	V	F	F	Tyr10		
Initial Orientation		LB2				RB1					
Final Orientation		LB2			LS1	RB1			LB2		
		LNH									
Total Energy	86.978										
van der Waals	85.075										
electrostatic	-216.206										
ΔEs	-47.073										
	-11.195										
	-36.759										

	H	H	Q	K	L	V	F	F	Tyr10
Initial Orientation		RB1			LB2				
Final Orientation		RS1							RS1
		2							
Total Energy	99.823								
van der Waals	90.082								
electrostatic	-207.01								
ΔEs	-34.228								
	-6.188								
	-27.563								

	H	H	Q	K	L	V	F	F	Tyr10
Initial Orientation		LS2			RB2				
Final Orientation		LS2			RB2				LS2
					RS2				LB2
Total Energy	95.016								
van der Waals	89.821								
electrostatic	-210.211								
ΔEs	-39.035								
	-6.449								
	-30.764								

	H	H	Q	K	L	V	F	F	Tyr10
Initial Orientation		RB2			LB2				
Final Orientation	LS2	RB2							RS2
		RB2							RB2
		RS2							
Total Energy	49.356								
van der Waals	86.846								
electrostatic	-254.233								
ΔEs	-84.695								
	-9.424								
	-74.786								

	H	H	Q	K	L	V	F	F	Tyr10
Initial Orientation		CS				RB2			
Final Orientation		RB1			RS2	RB2			CS
		RS1			RB2				
		RS2							
Total Energy	90.963								
van der Waals	80.522								
electrostatic	-210.739								
ΔEs	-43.088								
	-15.748								
	-31.292								

	H	H	Q	K	L	V	F	F	
Initial Orientation		RS1				LB1			
Final Orientation		RS1							
Total Energy	98.591								
van der Waals	92.959								
electrostatic	-211.82								
ΔEs	-35.46								
	-3.311								
	-32.373								

	H	H	Q	K	L	V	F	F	Ala21
Initial Orientation		LS2				RB1			
Final Orientation		LS2				CS			RS2
Total Energy	96.793								
van der Waals	89.176								
electrostatic	-210.347								
ΔEs	-37.258								
	-7.094								
	-30.9								

	H	H	Q	K	L	V	F	F	
Initial Orientation		LB1				RB2			
Final Orientation						RB2			
Total Energy	80.491								
van der Waals	91.347								
electrostatic	-226.847								
ΔEs	-53.56								
	-4.923								
	-47.4								

	H	H	Q	K	L	V	F	F	
Initial Orientation		RB1				LB2			
Final Orientation		RB1			RB2				
Total Energy	81.747								
van der Waals	88.262								
electrostatic	-225.136								
ΔEs	-52.304								
	-8.008								
	-45.689								

	H	H	Q	K	L	V	F	F	Tyr10	
Initial Orientation		LS1				RB2				
Final Orientation		LS1				RB2			LB2	
		LB2							LS1	
		LNH								
Total Energy	92.823									
van der Waals	88.827									
electrostatic	-215.378									
ΔEs	-41.228									
	-7.443									
	-35.931									

	H	H	Q	K	L	V	F	F	Tyr10	
Initial Orientation		RS1				LB2				
Final Orientation		RS1							RS1	
		RNH								
Total Energy	94.166									
van der Waals	90.885									
electrostatic	-213.501									
ΔEs	-39.885									
	-5.385									
	-34.054									

	H	H	Q	K	L	V	F	F	Tyr10	
Initial Orientation		LS2				RB2				
Final Orientation		LS2							LS2	
Total Energy	87.259									
van der Waals	90.433									
electrostatic	-220.125									
ΔEs	-46.792									
	-5.837									
	-40.678									

	H	H	Q	K	L	V	F	F
Initial Orientation		RB2				LB2		
Final Orientation								
Total Energy	114.157							
van der Waals	93.784							
electrostatic	-197.683							
ΔEs	-19.894							
	-2.486							
	-18.236							

	H	H	Q	K	L	V	F	F	Tyr10	Glu11
Initial Orientation		RS1					LB2			
Final Orientation		RB1	LNH						RS1	LB1
		RNH	LB1							CS
		RS1								RB1
Total Energy	107.027									
van der Waals	80.675									
electrostatic	-197.082									
ΔEs	-27.024									
	-15.595									
	-17.635									

	H	H	Q	K	L	V	F	F	Tyr10
Initial Orientation		RB2					LB2		
Final Orientation		RB2							RB2
Total Energy	116.207								
van der Waals	93.486								
electrostatic	-197.504								
ΔEs	-17.844								
	-2.784								
	-18.057								

	H	H	Q	K	L	V	F	F
Initial Orientation		LB2						
Final Orientation		LB2						
		LB2						
Total Energy	115.821							
van der Waals	88.545							
electrostatic	-189.184							
ΔEs	-18.23							
	-7.725							
	-9.737							

	H	H	Q	K	L	V	F	F	Tyr10
Initial Orientation		LS2					RB2		
Final Orientation		LB2					RB2		LS2
		LB2							
		LS2							
Total Energy	100.979								
van der Waals	86.363								
electrostatic	-207.483								
ΔEs	-33.072								
	-9.907								
	-28.036								

	H	H	Q	K	L	V	F	F	Tyr10
Initial Orientation		LS1						RB2	
Final Orientation	RB1	LS1		RS1	LB1			RB2	
	LB1			2	LNH			RS1	
	LS1							-CH2-	
	-CH2-								
Total Energy	14.568								
van der Waals	75.263								
electrostatic	-276.299								
ΔEs	-119.483								
	-21.007								
	-96.852								

	H	H	Q	K	L	V	F	F
Initial Orientation		RS1						LB2
Final Orientation	RB2	RS1			RNH			
					RB1			
					LB1			
Total Energy	51.215							
van der Waals	78.204							
electrostatic	-251.737							
ΔEs	-82.836							
	-18.066							
	-72.29							

	H	H	Q	K	L	V	F	F	Tyr10
Initial Orientation		LS2						RB2	
Final Orientation	LS2	LS2			LS2			RB2	LB2
	-CH2-	LB2							
Total Energy	68.98								
van der Waals	85.366								
electrostatic	-235.079								
ΔEs	-65.071								
	-10.904								
	-55.632								

	H	H	Q	K	L	V	F	F
Initial Orientation		RS2						LB2
Final Orientation	LS2	RS1		LS2	LS2			LB2
	LS1	RS2		-CH2-	RS2			LS2
	LB1							-CH2-
Total Energy	9.754							
van der Waals	79.295							
electrostatic	-285.866							
ΔEs	-124.297							
	-16.975							
	-106.419							

	H	H	Q	K	L	V	F	F
Initial Orientation		LB2						
Final Orientation								
Total Energy	109.895							
van der Waals	91.704							
electrostatic	-197.193							
ΔEs	-24.156							
	-4.566							
	-17.746							

	H	H	Q	K	L	V	F	F
Initial Orientation		RB2						LB2
Final Orientation	RS2	RB2			RB2			LB2
	-CH2-	RB2						
		RS2						
Total Energy	66.026							
van der Waals	83.891							
electrostatic	-237.137							
ΔEs	-68.025							
	-12.379							
	-57.69							

	H	H	Q	K	L	V	F	F	Ser8	Glu11	Val12
Initial Orientation		LB2					RB1				
Final Orientation			LNH	RS1				RS1	RB2	LB2	RB2
			LB1								
			RB1								
			RNH								
Total Energy	78.218										
van der Waals	78.163										
electrostatic	-223.347										
ΔEs	-55.833										
	-18.107										
	-43.9										

	H	H	Q	K	L	V	F	F	Gly9	Ala21	Val24	Lys28
Initial Orientation								LB2				
Final Orientation	RB2	RS1			RNH				RB2	LS1	LB2	LB2
					RB1				C=O			
					LB1							
Total Energy	51.215											
van der Waals	78.204											
electrostatic	-251.737											
ΔEs	-82.836											
	-18.066											
	-72.29											

	H	H	Q	K	L	V	F	F	Val12
Initial Orientation				RB1	LB1				
Final Orientation	RB1			RB2	LS1				RS1
				RS1*					
				RNH*					
				*-CH2-					
Total Energy	56.963								
van der Waals	84.211								
electrostatic	-246.525								
ΔEs	-77.088								
	-12.059								
	-67.078								

	H	H	Q	K	L	V	F	F
Initial Orientation				RS1	LB1			
Final Orientation	CS			RS1				
	RB1			RB1				
				-CH2-				
Total Energy	71.655							
van der Waals	87.512							
electrostatic	-233.177							
ΔEs	-62.396							
	-8.758							
	-53.73							

	H	H	Q	K	L	V	F	F
Initial Orientation				RS2	LB1			
Final Orientation	RB1	LS2		RS2	CS			
	LS2				LS1			
	-CH2-							
Total Energy	7.462							
van der Waals	81.9							
electrostatic	-289.927							
ΔEs	-126.589							
	-14.37							
	-110.48							

	H	H	Q	K	L	V	F	F	Val12
Initial Orientation				RB2	LB1				
Final Orientation	RB1			RB2	LB1			CS	
	RNH			RB1*				RB1	
	RS1			RNH*				RB2	
				*-CH2-					
Total Energy	42.173								
van der Waals	77.288								
electrostatic	-257.001								
ΔEs	-91.878								
	-18.982								
	-77.554								

	H	H	Q	K	L	V	F	F	
Initial Orientation				LB2	RB1				
Final Orientation	LB1			LB2	RS2	RB2		LB2	
	LS2			LS2	RB1				
				-CH2-					
Total Energy	50.974								
van der Waals	78.384								
electrostatic	-246.862								
ΔEs	-83.077								
	-17.886								
	-67.415								

	H	H	Q	K	L	V	F	F	Val12
Initial Orientation				RS2	LB2				
Final Orientation	LB2			RB1	LS2			LB1	RS2
	LS2			RS1	LB2			LS1	
				RS2*					
				LS2*					
				*-CH2-					
Total Energy	16.126								
van der Waals	76.822								
electrostatic	-280.832								
ΔEs	-117.925								
	-19.448								
	-101.385								

	H	H	Q	K	L	V	F	F	Val12
Initial Orientation				LB2	RB2				
Final Orientation	RS2			LB1	RS2			CS	LS2
				LNH				LB1	
				LS2					
				-CH2-					
Total Energy	33.563								
van der Waals	85.354								
electrostatic	-271.632								
ΔEs	-100.488								
	-10.916								
	-92.185								

	H	H	Q	K	L	V	F	F
Initial Orientation				LB1	RB1			
Final Orientation	RB1			LS1	RS1			CS
	RNH			LB1	RB1			
	LB1			-CH2-				
	LNH							
Total Energy	37.019							
van der Waals	82.135							
electrostatic	-272.413							
ΔEs	-97.032							
	-14.135							
	-92.966							

	H	H	Q	K	L	V	F	F
Initial Orientation				LS1	RB1			
Final Orientation	LB1			LS1	RS1			
	RB1							
	RNH							
Total Energy	38.815							
van der Waals	84.757							
electrostatic	-271.108							
ΔEs	-95.236							
	-11.513							
	-91.661							

	H	H	Q	K	L	V	F	F
Initial Orientation				LB1	RB2			
Final Orientation	RS2			LB1	RS2			RB1
	RB2			LS2	RB2			
				LNH				
				RS2				
				-CH2-				
Total Energy	23.709							
van der Waals	78.428							
electrostatic	-274.36							
ΔEs	-110.342							
	-17.842							
	-94.913							

	H	H	Q	K	L	V	F	F	Val12
Initial Orientation				RB1	LB2				
Final Orientation	LB2			RS2	LB2		RS2	LS1	RB1
	LS2			LS2	LS2				
	LB1			-CH2-					
Total Energy	8.517								
van der Waals	76.027								
electrostatic	-280.887								
ΔEs	-125.534								
	-20.243								
	-101.44								

	H	H	Q	K	L	V	F	F	Asp23
Initial Orientation				LS2	RB2				
Final Orientation	RS2			LS2	RS2		LB2	RB2	LB2
				LB2	RB2				
Total Energy	38.409								
van der Waals	80.003								
electrostatic	-260.684								
ΔEs	-95.642								
	-16.267								
	-81.237								

	H	H	Q	K	L	V	F	F	Val12
Initial Orientation				RB2	LB2				
Final Orientation	LB1			RS1	LS2				RB2
	RS2			RS2	LB2				RS2
	LNH			-CH2-					
	LB2								
	-CH2-								
Total Energy	22.004								
van der Waals	82.303								
electrostatic	-277.767								
ΔEs	-112.047								
	-13.967								
	-98.32								

	H	H	Q	K	L	V	F	F
Initial Orientation				RB2		LB2		
Final Orientation			LS2	RS2			RB2	
			LB2	RB2			RB1	
							LB1	
Total Energy	69.53							
van der Waals	83.006							
electrostatic	-233.739							
ΔEs	-64.521							
	-13.264							
	-54.292							

	H	H	Q	K	L	V	F	F	Val12			H	H	Q	K	L	V	F	F	
Initial Orientation				LB2		RB2					Initial Orientation				CS			RB1		
Final Orientation			RB1	LB2			LB1		LS1		Final Orientation	LS1			LB1			RS1	LB2	
				LS1			CS								LS1*					
				-CH2-			RB1								LNH*					
				LNH											*-CH2-					
															RB1					
Total Energy	65.753										Total Energy	42.235								
van der Waals	80.162										van der Waals	82.418								
electrostatic	-237.979										electrostatic	-260.461								
ΔEs	-68.298										ΔEs	-91.816								
	-16.108											-13.852								
	-58.532											-81.014								

	H	H	Q	K	L	V	F	F	Val12			H	H	Q	K	L	V	F	F	Val12
Initial Orientation				CS			LB1				Initial Orientation				RB1			LB1		
Final Orientation				RB1			LS1		RS1		Final Orientation	RS1			LB1			LS1		RS1
				RS2			CS					RS2			RS2					
				CS								RB2			-CH2-					
				RS1																
				-CH2-																
Total Energy	55.47										Total Energy	13.807								
van der Waals	85.598										van der Waals	81.129								
electrostatic	-251.039										electrostatic	-285.249								
ΔEs	-78.581										ΔEs	-120.244								
	-10.672											-15.141								
	-71.592											-105.802								

	H	H	Q	K	L	V	F	F				H	H	Q	K	L	V	F	F	Asp23
Initial Orientation				LB1			RB1				Initial Orientation				RS1			LB1		
Final Orientation	LS1			LB1			RS1	LB2			Final Orientation				RB1			LB1		CS
				LNH											RNH			CS		
				LS1											RS1			RB1		
				-CH2-											-CH2-					
Total Energy	50.137										Total Energy	79.257								
van der Waals	86.258										van der Waals	89.235								
electrostatic	-255.901										electrostatic	-228.17								
ΔEs	-83.914										ΔEs	-54.794								
	-10.012											-7.035								
	-76.454											-48.723								

	H	H	Q	K	L	V	F	F				H	H	Q	K	L	V	F	F	
Initial Orientation				LS1			RB1				Initial Orientation				RS2			LB1		
Final Orientation				LS1			RB1				Final Orientation				RB1			LB1		
				LNH			CS								RNH			RB1		
							LB1								RS2					
															-CH2-					
Total Energy	86.843										Total Energy	67.171								
van der Waals	90.184										van der Waals	85.633								
electrostatic	-223.7										electrostatic	-233.86								
ΔEs	-47.208										ΔEs	-66.88								
	-6.086											-10.637								
	-44.253											-54.413								

	H	H	Q	K	L	V	F	F	Val12			H	H	Q	K	L	V	F	F	
Initial Orientation				LS2			RB1				Initial Orientation				LB1			RB2		
Final Orientation	LS1		RB2	LB1			RS2		LS2		Final Orientation	LS1		RS1	RB1			RB2	LB2	
	LS2			CS											LB1			RS1		
	LB2			RB1											RS1*			-CH2-		
				LS1											RNH			RNH		
				-CH2-											LNH*			RB1		
															LS1*					
															*-CH2-					
Total Energy	25.861										Total Energy	16.924								
van der Waals	80.154										van der Waals	73.618								
electrostatic	-273.351										electrostatic	-279.528								
ΔEs	-108.19										ΔEs	-117.127								
	-16.116											-22.652								
	-93.904											-100.081								

	H	H	Q	K	L	V	F	F	Val12			H	H	Q	K	L	V	F	F	
Initial Orientation				RB2			LB1				Initial Orientation				RB1			LB2		
Final Orientation	RB2		LS2	RB1			LB1		RS2		Final Orientation	RS2			RB1			LB2	RB2	
	RS2		LB2	LB1			LNH								LS2			LS2		
				RS2			LS1								2					
				-CH2-			LB2								RS2					
															-CH2-					
Total Energy	23.031										Total Energy	24.056								
van der Waals	75.841										van der Waals	81.324								
electrostatic	-269.362										electrostatic	-275.906								
ΔEs	-111.02										ΔEs	-109.995								
	-20.429											-14.946								
	-89.915											-96.459								

	H	H	Q	K	L	V	F	F				H	H	Q	K	L	V	F	F	
Initial Orientation				LB2			RB1				Initial Orientation				LS2			RB2		
Final Orientation	LB2		RB2	LB1			RS2				Final Orientation				LS2			RS2		
	LS2			LS2			CS											RB2		
				-CH2-																
Total Energy	52.479										Total Energy	65.608								
van der Waals	82.673										van der Waals	85.755								
electrostatic	-252.529										electrostatic	-234.425								
ΔEs	-81.572										ΔEs	-68.443								
	-13.597											-10.515								
	-73.082											-54.978								

	H	H	Q	K	L	V	F	F	
Initial Orientation				RS2			LB2		
Final Orientation	RS2			RB1			LB2	RB2	
				LS2			LS2		
				LB1					
				RS2					
				-CH2-					
Total Energy	18.122								
van der Waals	76.043								
electrostatic	-276.203								
ΔEs	-115.929								
	-20.227								
	-96.756								

	H	H	Q	K	L	V	F	F
Initial Orientation				RB2			LB2	
Final Orientation	RS2			RB1			LS2	RB2
				LS2			LB2	
				2				
				RS2				
				-CH2-				
Total Energy	23.823							
van der Waals	79.669							
electrostatic	-271.643							
ΔEs	-110.228							
	-16.601							
	-92.196							

	H	H	Q	K	L	V	F	F	Val12
Initial Orientation				LB2			RB2		
Final Orientation	LS1			RB1			RB2		LS2
	LS2			LS1					
	LB2			-CH2-					
Total Energy	4.929								
van der Waals	77.427								
electrostatic	-290.83								
ΔEs	-129.122								
	-18.843								
	-111.383								

	H	H	Q	K	L	V	F	F	Leu34
Initial Orientation				CS				RB1	
Final Orientation	LS1			LS1				RS1	RB2
				-CH2-					
				LS2					
Total Energy	36.753								
van der Waals	82								
electrostatic	-261.531								
ΔEs	-97.298								
	-14.27								
	-82.084								

	H	H	Q	K	L	V	F	F
Initial Orientation				CS				LB1
Final Orientation				RB1			RS1	LB1
				RS2				
				2				
				CS				
Total Energy	83.264							
van der Waals	90.21							
electrostatic	-223.895							
ΔEs	-50.787							
	-6.06							
	-44.448							

	H	H	Q	K	L	V	F	F
Initial Orientation				LB1				RB1
Final Orientation	LS1			LB1				CS
				LS2				
				LS1				
				-CH2-				
Total Energy	42.564							
van der Waals	82.957							
electrostatic	-257.212							
ΔEs	-91.487							
	-13.313							
	-77.765							

	H	H	Q	K	L	V	F	F
Initial Orientation				RB1				LB1
Final Orientation	RS1			RB1				RB1
				RNH				LB1
				RS1				
				-CH2-				
				RB2				
Total Energy	56.54							
van der Waals	82.067							
electrostatic	-246.773							
ΔEs	-77.511							
	-14.203							
	-67.326							

	H	H	Q	K	L	V	F	F
Initial Orientation				RS1				LB1
Final Orientation	RS1			RB2				RB1
				RS1				LB1
				-CH2-				
				RNH				
				RB1				
Total Energy	56.549							
van der Waals	81.96							
electrostatic	-247.355							
ΔEs	-77.502							
	-14.31							
	-67.908							

	H	H	Q	K	L	V	F	F
Initial Orientation				LS1				RB1
Final Orientation				LB1				CS
				LS2				
				LS1				
				-CH2-				
Total Energy	56.821							
van der Waals	87.112							
electrostatic	-247.198							
ΔEs	-77.23							
	-9.158							
	-67.751							

	H	H	Q	K	L	V	F	F
Initial Orientation				RS2				LB1
Final Orientation	RS2			RB1				LS2
				RS1				LB1
				RS2				CS
				-CH2-				
Total Energy	41.902							
van der Waals	80.786							
electrostatic	-257.144							
ΔEs	-92.149							
	-15.484							
	-77.697							

	H	H	Q	K	L	V	F	F	Val12
Initial Orientation				LS2				RB1	
Final Orientation				LS1				RS2	LS2
				LS2				CS	
				-CH2-					
Total Energy	51.52								
van der Waals	84.903								
electrostatic	-256.272								
ΔEs	-82.531								
	-11.367								
	-76.825								

	H	H	Q	K	L	V	F	F
Initial Orientation				LB1				RB2
Final Orientation	RS1		LS2	LB1			LS2	RS2
	RS2		LB2	RS2*			-CH2-	
				LS2*			LB2	
				*-CH2-				
Total Energy	1.705							
van der Waals	75.513							
electrostatic	-289.474							
ΔEs	-132.346							
	-20.757							
	-110.027							

	H	H	Q	K	L	V	F	F	Val12
Initial Orientation				RB2				LB1	
Final Orientation	LB2			RB1	LS2			LS2	RS2
	LS2			LS2*				LB1	
				CS				CS	
				RS1					
				RS2*					
				*-CH2-					
Total Energy	22.219								
van der Waals	75.341								
electrostatic	-272.583								
ΔEs	-111.832								
	-20.929								
	-93.136								

	H	H	Q	K	L	V	F	F	Val12
Initial Orientation				RB1				LB2	
Final Orientation	LB1			RB2	LS1		RS1	LB2	RB1
	LS1			LS1*					
				LNH*					
				LB1*					
				RNH*					
				RS1*					
				*-CH2-					
Total Energy	9.794								
van der Waals	66.254								
electrostatic	-285.952								
ΔEs	-124.257								
	-30.016								
	-106.505								

	H	H	Q	K	L	V	F	F	Val12
Initial Orientation				LB2				RB1	
Final Orientation			LB2	LB1			LB2	RS1	LS2
				RB1				RNH	
				LNH				RB1	
				LS2					
				-CH2-					
Total Energy	41.947								
van der Waals	79.667								
electrostatic	-256.988								
ΔEs	-92.104								
	-16.603								
	-77.541								

	H	H	Q	K	L	V	F	F	Leu34
Initial Orientation				RB2				LB2	
Final Orientation				RNH					LB2
				RS1					
				-CH2-					
				RB2					
Total Energy	64.62								
van der Waals	86.16								
electrostatic	-239.393								
ΔEs	-69.431								
	-10.11								
	-59.946								

	H	H	Q	K	L	V	F	F	Val12
Initial Orientation				LB2				RB2	
Final Orientation			LB2	LB1			LB2	RS2	LS2
				RB1				RB1	
				LS2					
				LB2					
				-CH2-					
Total Energy	30.947								
van der Waals	75.833								
electrostatic	-262.36								
ΔEs	-103.104								
	-20.437								
	-82.913								

The gas phase results of solapsone and the 1Z0Q conformer of β-amyloid

	H	H	Q	K	Gly9	Tyr10
Initial Orientatio	CS	LB1				
Final Orientatio	RS1	LS1		RS1	CS	CS
	RB1			2	C=O	-CH-
	CS					
Total Energy	139.591					
van der Waals	117.425					
electrostatic	-261.241					
ΔEs	-104.985					
	-4.277					
	-101					

	H	H	Q	K	L	V	F	F	Val12
Initial Orientation				LB2				RB2	
Final Orientation			LB2	LB1			LB2	RS2	LS2
				RB1				RB1	
				LS2					
				LB2					
				-CH2-					
Total Energy	30.947								
van der Waals	75.833								
electrostatic	-262.36								
ΔEs	-103.104								
	-20.437								
	-82.913								

	H	H	Q	K	Gly9	Tyr10
Initial Orientatio	LB1	CS				
Final Orientation	CS	CS		LS1	CS	
	-CH2-	-NH-		LS2	-CH2-	
	LB1	RS1				
	LS1					
Total Energy	135.765					
van der Waals	109.219					
electrostatic	-260.637					
ΔEs	-108.811					
	-12.483					
	-100.396					

	H	H	Q	K	Leu17
Initial Orientatio	CS	RS1			
Final Orientatio	CS	RS1		RS2	RS2
	RS1			-CH2-	
	-CH2-				
	LB1				
	RB1				
Total Energy	161.738				
van der Waals	109.638				
electrostatic	-233.306				
ΔEs	-82.838				
	-12.064				
	-73.065				

	H	H	Q	K	Gly9
Initial Orientation	RS1	CS			
Final Orientation	RS2	LS1		RS1	RS2
	RS1	LS2			C=O
Total Energy	110.047				
van der Waals	109.653				
electrostatic	-284.095				
ΔEs	-134.529				
	-12.049				
	-123.854				

	H	H	Q	K
Initial Orientatio	CS	LS1		
Final Orientatio	RB1	LS2		RS1
	RS1	LS1		RB1
	RS2			RNH
Total Energy	105.307			
van der Waals	110.471			
electrostatic	-291.8			
ΔEs	-139.269			
	-11.231			
	-131.559			

	H	H	Q	K	Tyr10
Initial Orientation	LS1	CS			
Final Orientation	LS1	RB1		LB1	CS
	CS	RS2		LS2	-CH2-
	-CH2-	CS		2	
		-NH-		LS1	
		RS1			
Total Energy	108.858				
van der Waals	104.221				
electrostatic	-287.616				
ΔEs	-135.718				
	-17.481				
	-127.375				

	H	H	Q	K	Gly9	Tyr10
Initial Orientatio	CS	RS2				
Final Orientatio	LB1	RS2		LS2	CS	CS
	LS1	RS1		2	C=O	-CH2-
	LS2			RS2		
				-CH2-		
Total Energy	99.511					
van der Waals	109.292					
electrostatic	-293.141					
ΔEs	-145.065					
	-12.41					
	-132.9					

	H	H	Q	K	Leu17
Initial Orientation	RS2	CS			
Final Orientation	RS2	LB1		RS1	CS
		LS1		CS	
		CS		-CH2-	
Total Energy	113.757				
van der Waals	105.47				
electrostatic	-278.627				
ΔEs	-130.819				
	-16.232				
	-118.386				

	H	H	Q	K	Leu17				H	H	Q	K	Gly9	Tyr10	
Initial Orientatic	CS	LS2						Initial Orientatio	LS2	CS					
Final Orientatio	CS	LS2		LS1*	LS1			Final Orientatior	LS2	RS1			LB2	LS1	
	RB1			LB1*					LB2				C=O	-CH2-	
	RS2			*-CH2-										LS2	
				CS										-CH-	
Total Energy	130.683							Total Energy	139.606						
van der Waals	104.379							van der Waals	112.806						
electrostatic	-263.265							electrostatic	-257.474						
ΔEs	-113.893							ΔEs	-104.97						
	-17.323								-8.896						
	-103.024								-97.233						

	H	H	Q	K	Gly9	Tyr10			H	H	Q	K	Gly9		
Initial Orientatic	CS	LB2						Initial Orientatio	RB1	LB1					
Final Orientatio	LB1	LS2		LS1	CS	LS2		Final Orientatior	RB1	LS2		LS1	RB1		
	LS1	LS1		-CH2-	C=O	-CH2-			RNH	LS1			C=O		
	-CH2-	-CH-							RS1						
	CS								RB2						
Total Energy	160.629							Total Energy	106.001						
van der Waals	108.539							van der Waals	105.858						
electrostatic	-231.106							electrostatic	-288.005						
ΔEs	-83.947							ΔEs	-138.575						
	-13.163								-15.844						
	-70.865								-127.764						

	H	H	Q	K					H	H	Q	K	Gly9		
Initial Orientatic	LB1	RB1						Initial Orientatio	LB1	RS1					
Final Orientatio	LS1	RS1		LS2				Final Orientatior	LB1	RS1		LS2	LS1		
				2					CS	CS		2	C=O		
				LB1					-CH2-	-CH-		CS			
				-CH2-					LS1			-CH2-			
									LS2						
Total Energy	132.501							Total Energy	121.79						
van der Waals	117.442							van der Waals	110.988						
electrostatic	-274.526							electrostatic	-275.435						
ΔEs	-112.075							ΔEs	-122.786						
	-4.26								-10.714						
	-114.285								-115.194						

	H	H	Q	K	Gly9				H	H	Q	K	Gly9	Tyr10	Leu17
Initial Orientatic	RS1	LB1						Initial Orientatio	RB1	LS1					
Final Orientatio	RS1	LS1		RNH	RS1			Final Orientatior	RS1	LS2		LS1	RS1*	CS	LS1
					C=O				RB1	LS1		-CH2-	RB1*	-CH2-	
													*C=O		
Total Energy	142.499							Total Energy	134.4						
van der Waals	117.472							van der Waals	106.173						
electrostatic	-257.406							electrostatic	-260.158						
ΔEs	-102.077							ΔEs	-110.176						
	-4.23								-15.529						
	-97.165								-99.917						

	H	H	Q	K					H	H	Q	K	Gly9	Tyr10	
Initial Orientatic	LS1	RB1						Initial Orientatio	LB1	RS2					
Final Orientatio	RS1	CS		LB1				Final Orientatior	LB1	RS2		LS2	CS	CS	
	CS	-CH-		LS2					LS1	RS1		2	C=O	-CH2-	
	-CH2-			2					LS2			RS2			
	LB1			CS								-CH2-			
	LS1			-CH2-											
				LS1											
Total Energy	126.537							Total Energy	98.47						
van der Waals	114.699							van der Waals	104.359						
electrostatic	-279.398							electrostatic	-292.452						
ΔEs	-118.039							ΔEs	-146.106						
	-7.003								-17.343						
	-119.157								-132.211						

	H	H	Q	K	Leu17				H	H	Q	K	Tyr10		
Initial Orientatic	RS2	LB1						Initial Orientatio	RB1	LS2					
Final Orientatio	RS2	LS2		RS1	CS			Final Orientatior	RS2	LS2			LS2		
		LB1		RS2									-CH2-		
		CS													
Total Energy	121.293							Total Energy	153.461						
van der Waals	105.592							van der Waals	112.18						
electrostatic	-272.75							electrostatic	-244.615						
ΔEs	-123.283							ΔEs	-91.115						
	-16.11								-9.522						
	-112.509								-84.374						

	H	H	Q	K	Gly9	Tyr10	Leu17	Val18
Initial Orientatio	LS2	RB1						
Final Orientation	LB1	RB1		LB2	LS1	CS	RS2	RS2
	LS2	CS		LS2	C=O	-CH2-		
	LS1	-CH2-						
		RS1						
		RS2						
Total Energy	99.12							
van der Waals	100.016							
electrostatic	-291.072							
ΔEs	-145.456							
	-21.686							
	-130.831							

	H	H	Q	K	Gly9
Initial Orientation	RB2	LB1			
Final Orientation	RB2	LS2		RS2	RB2
	RS2	2		-CH2-	C=O
	-CH2-	RS2			
		-CH-			
Total Energy	151.844				
van der Waals	111.73				
electrostatic	-243.709				
ΔEs	-92.732				
	-9.972				
	-83.468				

	H	H	Q	K	Tyr10
Initial Orientatio	LB1	RB2			
Final Orientation	RB1	RB2			RS2
	LS2	RS2			-CH2-
	LB1				
	CS				
Total Energy	128.469				
van der Waals	104.222				
electrostatic	-263.496				
ΔEs	-116.107				
	-17.48				
	-103.255				

	H	H	Q	K	Gly9
Initial Orientation	LB2	RB1			
Final Orientation	LB2	RB1		LS1	LB2
	LS1	RS1		-CH2-	C=O
	LNH	LB1			
	LB1	-CH-			
	-CH2-	RNH			
Total Energy	129.111				
van der Waals	107.682				
electrostatic	-257.711				
ΔEs	-115.465				
	-14.02				
	-97.47				

	H	H	Q	K	Gly9	Tyr10
Initial Orientatio	RB1	LB2				
Final Orientation	LB1	LB2		RS2	LB1	LS1
	RB1	LS1		RB1	C=O	LNH*
	RB1					LB1*
	LNH					*-CH2-
	-NH-					
	RNH					
Total Energy	107.413					
van der Waals	97.731					
electrostatic	-275.241					
ΔEs	-137.163					
	-23.971					
	-115					

	H	H	Q	K	Tyr10
Initial Orientation	LS2	RS2			
Final Orientation	LS2	RB1		LB2	CS
	LS1	RS1		LS2	-CH2-
		RS2			
Total Energy	106.184				
van der Waals	107.614				
electrostatic	-285.376				
ΔEs	-138.392				
	-14.088				
	-125.135				

	H	H	Q	K	Leu17
Initial Orientatio	RS2	LS2			
Final Orientation	RB2	LS2		RS1	CS
	RS2			RS2*	
				RB1*	
				CS*	
				*-CH2-	
Total Energy	114.822				
van der Waals	106.717				
electrostatic	-279.908				
ΔEs	-129.754				
	-14.985				
	-119.667				

	H	H	Q	K
Initial Orientation	RB2	LS2		
Final Orientation	RB2	LS2		RS2
	RS2	LB2		2
Total Energy	135.755			
van der Waals	115.866			
electrostatic	-267.65			
ΔEs	-108.821			
	-5.836			
	-107.409			

	H	H	Q	K	Val18
Initial Orientatio	LS2	RB2			
Final Orientation	LS2	RB2		LS2	RB2
	LS1				
Total Energy	107.914				
van der Waals	105.287				
electrostatic	-282.698				
ΔEs	-136.662				
	-16.415				
	-122.457				

	H	H	Q	K	Val18
Initial Orientation	LB2	RS2			
Final Orientation	LB2	RB2		LS1	RB2
	LS2	RS2		LB2	
	LB1			LNH	
				-CH2-	
Total Energy	126.265				
van der Waals	104.686				
electrostatic	-272.779				
ΔEs	-118.311				
	-17.016				
	-112.538				

	H	H	Q	K	Leu17	Val18
Initial Orientatio	RS2	LB2				
Final Orientation	RB2	LB2		RB1	LS2	LS2
	RS2	LS2		RS2		
Total Energy	124.503					
van der Waals	109.776					
electrostatic	-276.707					
ΔEs	-120.073					
	-11.926					
	-116.466					

	H	H	Q	K	Gly9	Tyr10
Initial Orientation	RB2	LB2				
Final Orientation	RS2	LB2		RS1	RB2	RS2
		LS2		RS2	C=O	-CH-
		2				
Total Energy	125.792					
van der Waals	107.557					
electrostatic	-265.71					
ΔEs	-118.784					
	-14.145					
	-105.469					

	H	H	Q	K	Gly9	Val18			H	H	Q	K
Initial Orientatio	LB2	RB2						Initial Orientatio	LS1	RS1		
Final Orientatio	LB2	RB2			LB2	RB2		Final Orientation	LB1	RS1		LB1
		RS2			C=O				LNH	RB1		
									LS1			
Total Energy	195.363							Total Energy	152.459			
van der Waals	115.52							van der Waals	110.378			
electrostatic	-209.836							electrostatic	-246.619			
ΔEs	-49.213							ΔEs	-92.117			
	-6.182								-11.324			
	-49.595								-86.378			

	H	H	Q	K	Tyr10				H	H	Q	K
Initial Orientatio	RS1	LS1						Initial Orientatio	CS			RB1
Final Orientatio	RS1	LS1		RS1	CS			Final Orientation	RB1			RS2
	RB1	LB1		RNH	-CH2-				CS			2
		LNH										RS1
												-CH2-
Total Energy	129.888							Total Energy	170.62			
van der Waals	106.317							van der Waals	118.265			
electrostatic	-269.602							electrostatic	-232.103			
ΔEs	-114.688							ΔEs	-73.956			
	-15.385								-3.437			
	-109.361								-71.862			

	H	H	Q	K					H	H	Q	K
Initial Orientatio	RB1			CS				Initial Orientatio	CS			LB1
Final Orientatio	RS1			LS1				Final Orientation				LS1
Total Energy	176.809							Total Energy	174.098			
van der Waals	120.924							van der Waals	122.367			
electrostatic	-228.247							electrostatic	-232.98			
ΔEs	-67.767							ΔEs	-70.478			
	-0.778								0.665			
	-68.006								-72.739			

	H	H	Q	K					H	H	Q	K
Initial Orientatio	LB1			CS				Initial Orientatio	CS			RS1
Final Orientatio	LS1			RB1				Final Orientation	RB1			RS2
	2			RS1					CS			RS1
Total Energy	167.609							Total Energy	171.734			
van der Waals	116.064							van der Waals	116.536			
electrostatic	-233.674							electrostatic	-231.866			
ΔEs	-76.967							ΔEs	-72.842			
	-5.638								-5.166			
	-73.433								-71.625			

	H	H	Q	K					H	H	Q	K
Initial Orientatio	RS1			CS				Initial Orientatio	CS			LS1
Final Orientatio	RS1			RS2				Final Orientation	LB1			LB2
									LNH			LS1
									LS1			-CH2-
Total Energy	167.973							Total Energy	159.814			
van der Waals	116.407							van der Waals	117.038			
electrostatic	-232.764							electrostatic	-244.256			
ΔEs	-76.603							ΔEs	-84.762			
	-5.295								-4.664			
	-72.523								-84.015			

	H	H	Q	K					H	H	Q	K
Initial Orientatio	LS1			CS				Initial Orientatio	CS			RS2
Final Orientatio	LS1			RB1				Final Orientation	RB1			RS2
				RS1					CS			2
				RS2					RS1			RS1
Total Energy	162.074							Total Energy	153.152			
van der Waals	115.997							van der Waals	117.156			
electrostatic	-239.528							electrostatic	-251.64			
ΔEs	-82.502							ΔEs	-91.424			
	-5.705								-4.546			
	-79.287								-91.399			

	H	H	Q	K					H	H	Q	K
Initial Orientatio	RS2			CS				Initial Orientatio	CS			LS2
Final Orientatio	RS1			LB1				Final Orientation	CS			LB2
	RB1			RB1					LS2			LS2
	RS2			LS2								2
				CS								
				-CH2-								
Total Energy	142.735							Total Energy	179.787			
van der Waals	110.352							van der Waals	120.458			
electrostatic	-252.207							electrostatic	-224.119			
ΔEs	-101.841							ΔEs	-64.789			
	-11.35								-1.244			
	-91.966								-63.878			

	H	H	Q	K				H	H	Q	K	
Initial Orientatio	LS2			CS			Initial Orientatio	LB1			RB1	
Final Orientatio	LS2			CS			Final Orientation	LB1			RS1	
	LS1							LS1			2	
Total Energy	170.648						Total Energy	177.117				
van der Waals	120.774						van der Waals	119.216				
electrostatic	-236.567						electrostatic	-226.636				
ΔEs	-73.928						ΔEs	-67.459				
	-0.928							-2.486				
	-76.326							-66.395				
	H	H	Q	K				H	H	Q	K	
Initial Orientatio	RB1			LB1			Initial Orientatio	LB1			RS1	
Final Orientatio	RS1			LS1			Final Orientation	LB1			RS2	
				2				CS			2	
				LB1				RB1			RS1	
				LNH							-CH2-	
Total Energy	171.583						Total Energy	151.125				
van der Waals	118.557						van der Waals	114.134				
electrostatic	-233.045						electrostatic	-245.77				
ΔEs	-72.993						ΔEs	-93.451				
	-3.145							-7.568				
	-72.804							-85.529				
	H	H	Q	K				H	H	Q	K	
Initial Orientatio	RS1			LB1			Initial Orientatio	RB1			LS1	
Final Orientatio	RS1			LS1			Final Orientation	LB1			LS1	
				2				LS1				
Total Energy	173.34						Total Energy	161.759				
van der Waals	120.502						van der Waals	117.462				
electrostatic	-231.449						electrostatic	-240.766				
ΔEs	-71.236						ΔEs	-82.817				
	-1.2							-4.24				
	-71.208							-80.525				
	H	H	Q	K				H	H	Q	K	Gly9
Initial Orientatio	LS1			RB1			Initial Orientatio	LB1			RS2	
Final Orientatio	LS1			RS1			Final Orientation	LS2			RS2	LS2
											2	
											RS1	
Total Energy	174.046						Total Energy	150.38				
van der Waals	119.63						van der Waals	114.488				
electrostatic	-230.882						electrostatic	-251.666				
ΔEs	-70.53						ΔEs	-94.196				
	-2.072							-7.214				
	-70.641							-91.425				
	H	H	Q	K				H	H	Q	K	
Initial Orientatio	RS2			LB1			Initial Orientatio	RB1			LS2	
Final Orientatio	RS2			LS2			Final Orientation	LB1			LS2	
				2				CS			2	
				LS1				RS2				
Total Energy	148.389						Total Energy	153.37				
van der Waals	120.747						van der Waals	116.054				
electrostatic	-255.85						electrostatic	-248.262				
ΔEs	-96.187						ΔEs	-91.206				
	-0.955							-5.648				
	-95.609							-88.021				
	H	H	Q	K	Phe19			H	H	Q	K	Gly9
Initial Orientatio	LS2			RB1			Initial Orientatio	LB1			RB2	
Final Orientatio	LS2			RS2	RB2		Final Orientation	LB1			RB2	LS1
	2			RB1	RS2			RS1			RS1	C=O
								RB1			RNH	
								LNH				
								LS1				
Total Energy	147.54						Total Energy	157.675				
van der Waals	113.929						van der Waals	110.979				
electrostatic	-253.465						electrostatic	-245.245				
ΔEs	-97.036						ΔEs	-86.901				
	-7.773							-10.723				
	-93.224							-85.004				
	H	H	Q	K				H	H	Q	K	Ser8	Gly9
Initial Orientatio	RB2			LB1			Initial Orientatio	RB1			LB2		
Final Orientatio	RNH			LB1			Final Orientation	LB1			LB2	RS1	RB1
	RS1			RB1				RB1			LS1		
	RB2							RB1			-CH2-		
								RNH			LNH		
								RS2					
Total Energy	167.219						Total Energy	146.163				
van der Waals	114.611						van der Waals	107.697				
electrostatic	-233.144						electrostatic	-250.387				
ΔEs	-77.357						ΔEs	-98.413				
	-7.091							-14.005				
	-72.903							-90.146				

	H	H	Q	K	Val12			H	H	Q	K		
Initial Orientation	LB2			RB1			Initial Orientation	RS2			LS2		
Final Orientation	LS1			RB1	LS1		Final Orientation	RS2			LS2		
	LNH			LB1							2		
	LB2												
Total Energy	163.53						Total Energy	164.19					
van der Waals	113.7						van der Waals	119.593					
electrostatic	-241.377						electrostatic	-241.015					
ΔEs	-81.046						ΔEs	-80.386					
	-8.002							-2.109					
	-81.136							-80.774					
	H	H	Q	K				H	H	Q	K		
Initial Orientation	LS2			RS2			Initial Orientation	LS2			RB2		
Final Orientation	LS2			RS2			Final Orientation				RS2		
											LS2		
											RNH		
Total Energy	167.65						Total Energy	153.85					
van der Waals	121.36						van der Waals	114.193					
electrostatic	-239.456						electrostatic	-246.025					
ΔEs	-76.926						ΔEs	-90.726					
	-0.342							-7.509					
	-79.215							-85.784					
	H	H	Q	K	Gly9			H	H	Q	K		
Initial Orientation	RB2			LS2			Initial Orientation	LB2			RS2		
Final Orientation	RB2			LS2	RB2		Final Orientation	LB2			RS2		
	RS2			2				LS2			2		
Total Energy	160.506						Total Energy	163.21					
van der Waals	116.154						van der Waals	119.236					
electrostatic	-244.352						electrostatic	-243.973					
ΔEs	-84.07						ΔEs	-81.366					
	-5.548							-2.466					
	-84.111							-83.732					
	H	H	Q	K				H	H	Q	K	Gly9	
Initial Orientation	RS2			LB2			Initial Orientation	RB2			LB2		
Final Orientation	RS1			LS2			Final Orientation	RS2			LS2	RB2	
	RS2			LB2									
Total Energy	131.291						Total Energy	166.436					
van der Waals	111.018						van der Waals	116.234					
electrostatic	-266.759						electrostatic	-234.492					
ΔEs	-113.285						ΔEs	-78.14					
	-10.684							-5.468					
	-106.518							-74.251					
	H	H	Q	K	Phe19			H	H	Q	K		
Initial Orientation	LB2			RB2			Initial Orientation	LS1			RS1		
Final Orientation	LS2			RS2	RB2		Final Orientation	LB1			RB1		
				RB2				LS1			RS2		
								CS			RS1		
								RB1			-CH2-		
Total Energy	164.18						Total Energy	148.441					
van der Waals	116.998						van der Waals	113.402					
electrostatic	-239.442						electrostatic	-252.67					
ΔEs	-80.396						ΔEs	-96.135					
	-4.704							-8.3					
	-79.201							-92.429					
	H	H	Q	K				H	H	Q	K	Tyr10	
Initial Orientation	RS1			LS1			Initial Orientation		CS		RS2		
Final Orientation	RB1			LB1			Final Orientation	RS2	LS1		RS2	LS2	
	RS1			LS1				CS	CS		RS1		
	CS			LS2				-CH2-	-CH-		CS		
				CS							-CH2-		
				-CH2-									
Total Energy	167.224						Total Energy	110.367					
van der Waals	112.638						van der Waals	106.661					
electrostatic	-234.371						electrostatic	-285.894					
ΔEs	-77.352						ΔEs	-134.209					
	-9.064							-15.041					
	-74.13							-125.653					
	H	H	Q	K				H	H	Q	K	Tyr10	Leu17
Initial Orientation		CS		LS2			Initial Orientation		LS2		CS		
Final Orientation	LB1	RS1		LS2			Final Orientation	RS2	LS2		RB1	LS2	LS1
	CS	CS						LS2	-CH-		RS1	-CH2-	
	-CH2-	-CH-						-CH2-	LB2		LS1		
											-CH2-		
Total Energy	122.67						Total Energy	98.547					
van der Waals	113.245						van der Waals	106.866					
electrostatic	-274.571						electrostatic	-292.232					
ΔEs	-121.906						ΔEs	-146.029					
	-8.457							-14.836					
	-114.33							-131.991					

	H	H	Q	K	Tyr10			
Initial Orientation		RS1		LB1				
Final Orientation	LB2	RS1		LS1	RS1			
				2	-CH2-			
				LNH				
				LB1				
Total Energy	133.918							
van der Waals	110.293							
electrostatic	-263.54							
ΔEs	-110.658							
	-11.409							
	-103.299							

	H	H	Q	K
Initial Orientation		LS1		RB1
Final Orientation	RS1	LS1		RS1
				RB1
				-CH2-
				RNH
Total Energy	138.077			
van der Waals	115.228			
electrostatic	-264.279			
ΔEs	-106.499			
	-6.474			
	-104.038			

	H	H	Q	K	Tyr10
Initial Orientation		RB2		LB1	
Final Orientation	RS2	RB2		LB1	RS2
				LNH	-CH-
				LS2	
Total Energy	144.288				
van der Waals	112.962				
electrostatic	-252.207				
ΔEs	-100.288				
	-8.74				
	-91.966				

	H	H	Q	K	Leu17
Initial Orientation		LB2		RB1	
Final Orientation		LB2		LB1	LS2
				RB1	
				LS2	
				-CH2-	
Total Energy	170.308				
van der Waals	112.966				
electrostatic	-227.995				
ΔEs	-74.268				
	-8.736				
	-67.754				

	H	H	Q	K	Gly9	Tyr10	Leu17	Val18
Initial Orientation		RS2		LS2				
Final Orientation	LB1	RS1		LS2	CS	CS	RS2	RS2
	LS1	RS2		2	C=O	-CH2-		
	CS							
Total Energy	94.272							
van der Waals	106.029							
electrostatic	-295.616							
ΔEs	-150.304							
	-15.673							
	-135.375							

	H	H	Q	K	Tyr10
Initial Orientation		LS2		RS2	
Final Orientation	RS2	LB2		RS1	LB2
		LB2		RS2	
		LS2			
Total Energy	125.96				
van der Waals	112.307				
electrostatic	-268.282				
ΔEs	-118.616				
	-9.395				
	-108.041				

	H	H	Q	K	Leu17
Initial Orientation		LS2		RB2	
Final Orientation		LB2		RS2	RS2
		LB2		2	
		LS2		RB1	
				RNH	
Total Energy	156.298				
van der Waals	111.346				
electrostatic	-249.523				
ΔEs	-88.278				
	-10.356				
	-89.282				

	H	H	Q	K	Leu17
Initial Orientation		RB2		LS2	
Final Orientation	RS2	RS2		LS2	RB2
	-CH2-	-CH-		2	
		RB2		LB1	
				RS2*	
				RB2*	
				*-CH2-	
Total Energy	143.851				
van der Waals	107.336				
electrostatic	-251.926				
ΔEs	-100.725				
	-14.366				
	-91.685				

	H	H	Q	K	Val18
Initial Orientation		RS2		LB2	
Final Orientation	LB1	RB2		LB2	RB2
	CS	RS2		LS2	
	-CH2-	CS			
	LS2	-CH-			
Total Energy	132.362				
van der Waals	107.8				
electrostatic	-264.558				
ΔEs	-112.214				
	-13.902				
	-104.317				

	H	H	Q	K	Leu17	Val18
Initial Orientation		LB2		RS2		
Final Orientation	RB2	LB2		RS2	CS	LB2
	RS1	LNH		2		
				CS		
				-CH2-		
				RB1		
Total Energy	116.633					
van der Waals	104.698					
electrostatic	-275.832					
ΔEs	-127.943					
	-17.004					
	-115.591					

	H	H	Q	K	Val18	Ala21
Initial Orientation		LB2		RB2		
Final Orientation	RB2	LNH		RS2	LB2	LB2
	RS1	LS1		2		
	RNH			RB1		
	RB1			-CH2-		
Total Energy	112.239					
van der Waals	103.129					
electrostatic	-280.205					
ΔEs	-132.337					
	-18.573					
	-119.964					

	H	H	Q	K	Val18
Initial Orientation		RB2		LB2	
Final Orientation		RB2		LS2	RB2
		RS2		LB2	
Total Energy	159.255				
van der Waals	115.368				
electrostatic	-240.963				
ΔEs	-85.321				
	-6.334				
	-80.722				

	L	V	F	F	His14					L	V	F	F	His14	Lys16
Initial Orientation	RB1	LB1							Initial Orientation	LB1	RB1				
Final Orientation	RS1	LB1			LS1				Final Orientation	LB1				RS1	LS1
	RB1				2					LS1					-CH2-
					LB1										
Total Energy	194.286								Total Energy	178.555					
van der Waals	114.552								van der Waals	111.697					
electrostatic	-198.761								electrostatic	-221.045					
ΔEs	-50.29								ΔEs	-66.021					
	-7.15									-10.005					
	-38.52									-60.804					

	L	V	F	F	His14	Lys16				L	V	F	F	His14	Lys16
Initial Orientation	LB1	RB2							Initial Orientation	RB1	LB2				
Final Orientation	LB1	RB2			RB2	LS2			Final Orientation	RB1	LB2			LB2	RS1
	RB1				RS2	2				LB1				LS1	2
						LB1									RNH
						-CH2-									
Total Energy	161.249								Total Energy	156.156					
van der Waals	110.053								van der Waals	107.952					
electrostatic	-233.708								electrostatic	-249.603					
ΔEs	-83.327								ΔEs	-88.42					
	-11.649									-13.75					
	-73.467									-89.362					

	L	V	F	F	His14					L	V	F	F	His14	
Initial Orientation	LB2	RB2							Initial Orientation	RB2	LB2				
Final Orientation		RB2			RB2				Final Orientation					LB1	
					RS2										
					2										
Total Energy	203.694								Total Energy	204.651					
van der Waals	116.965								van der Waals	114.236					
electrostatic	-198.312								electrostatic	-195.208					
ΔEs	-40.882								ΔEs	-39.925					
	-4.737									-7.466					
	-38.071									-34.967					

	L	V	F	F						L	V	F	F	Lys16	
Initial Orientation	LB1		RB1						Initial Orientation	RB1		LB1			
Final Orientation	LB1								Final Orientation	RS1		CS	CS	RS1	
										RB1		LB1		2	
										CS				RNH	
														RB1	
Total Energy	231.76								Total Energy	199.369					
van der Waals	118.09								van der Waals	109.072					
electrostatic	-170.46								electrostatic	-203.717					
ΔEs	-12.816								ΔEs	-45.207					
	-3.612									-12.63					
	-10.219									-43.476					

	L	V	F	F	Lys16					L	V	F	F	Lys16	
Initial Orientation	RB2		LB1						Initial Orientation	LB1		RB2			
Final Orientation	RNH		LB1		RS2				Final Orientation	LS2				RS1	
					2					LB1				2	
														RB1	
														RNH	
Total Energy	193.33								Total Energy	196.046					
van der Waals	111.33								van der Waals	113.742					
electrostatic	-213.315								electrostatic	-207.25					
ΔEs	-51.246								ΔEs	-48.53					
	-10.372									-7.96					
	-53.074									-47.009					

	L	V	F	F	Val12	Gln15	Lys16			L	V	F	F	Lys16	
Initial Orientation	LB2		RB1						Initial Orientation	RB1		LB2			
Final Orientation	LB2		RB1	LS2	RB2	RB2	RB1		Final Orientation	RB1				LS2	
	LS2		RS2			-CH2-	RB2							2	
							-CH-								
Total Energy	164.34								Total Energy	189.562					
van der Waals	102.523								van der Waals	116.235					
electrostatic	-226.591								electrostatic	-214.268					
ΔEs	-80.236								ΔEs	-55.014					
	-19.179									-5.467					
	-66.35									-54.027					

	L	V	F	F	Lys16				L	V	F	F		
Initial Orientation	RB2		LB2					Initial Orientation	LB2		RB2			
Final Orientation	RB2				RS2			Final Orientation						
	RS2													
Total Energy	191.274							Total Energy	230.29					
van der Waals	116.744							van der Waals	119.106					
electrostatic	-215.099							electrostatic	-175.843					
ΔEs	-53.302							ΔEs	-14.286					
	-4.958								-2.596					
	-54.858								-15.602					

	L	V	F	F	Lys16				L	V	F	F	Lys16	
Initial Orientation	LB1			RB1				Initial Orientation	RB1			LB1		
Final Orientation	LS1			RS1	LS1			Final Orientation	CS			LS1	RS1	
	LNH				2				RB1			LB1		
									RS1			CS		
Total Energy	195.942							Total Energy	198.721					
van der Waals	115.771							van der Waals	111.209					
electrostatic	-207.059							electrostatic	-203.974					
ΔEs	-48.634							ΔEs	-45.855					
	-5.931								-10.493					
	-46.818								-43.733					

	L	V	F	F					L	V	F	F	Lys16	
Initial Orientation	RB2			LB1				Initial Orientation	LB1			RB2		
Final Orientation				RB1				Final Orientation				RB2	LS1	
				LB1									LB1	
Total Energy	226.908							Total Energy	201.558					
van der Waals	115.31							van der Waals	113.045					
electrostatic	-174.796							electrostatic	-204.193					
ΔEs	-17.668							ΔEs	-43.018					
	-6.392								-8.657					
	-14.555								-43.952					

	L	V	F	F	Lys16	Lys28			L	V	F	F	Lys16	
Initial Orientation	LB2			RB1				Initial Orientation	RB1			LB2		
Final Orientation	LB2			RB1	LB2	RS1		Final Orientation	RS1				RB2	
				LB1		2			RNH				RS1	
						RNH							-CH2-	
Total Energy	167.303							Total Energy	191.881					
van der Waals	108.215							van der Waals	114.006					
electrostatic	-233.085							electrostatic	-205.315					
ΔEs	-77.273							ΔEs	-52.695					
	-13.487								-7.696					
	-72.844								-45.074					

	L	V	F	F					L	V	F	F		
Initial Orientation	RB2			LB2				Initial Orientation	LB2			RB2		
Final Orientation	RB2							Final Orientation						
Total Energy	240.958							Total Energy	241.945					
van der Waals	120.179							van der Waals	120.477					
electrostatic	-163.319							electrostatic	-162.149					
ΔEs	-3.618							ΔEs	-2.631					
	-1.523								-1.225					
	-3.078								-1.908					

	L	V	F	F	Gln15	Lys16			L	V	F	F		
Initial Orientation		LB2	RB1					Initial Orientation		RB2	LB2			
Final Orientation			RB1		LB2	RS2		Final Orientation						
			LB1											
			RNH											
Total Energy	200.011							Total Energy	210.003					
van der Waals	110.909							van der Waals	124.992					
electrostatic	-212.006							electrostatic	-202.226					
ΔEs	-44.565							ΔEs	-34.573					
	-10.793								3.29					
	-51.765								-41.985					

	L	V	F	F					L	V	F	F	His14	Ala21
Initial Orientation		LB2	RB2					Initial Orientation		RB2		LB1		
Final Orientation		LB2						Final Orientation	RS2			LB1	RB2	RNH
												LNH		RB1
Total Energy	213.07							Total Energy	209.598					
van der Waals	123.133							van der Waals	111.414					
electrostatic	-197.274							electrostatic	-187.31					
ΔEs	-31.506							ΔEs	-34.978					
	1.431								-10.288					
	-37.033								-27.069					

	L	V	F	F	His14		
Initial Orientation		RB2		LB2			
Final Orientation				LB2	RB2		
Total Energy	212.466						
van der Waals	116.952						
electrostatic	-189.568						
ΔEs	-32.11						
	-4.75						
	-29.327						

	L	V	F	F	His14	Lys16	Ala21	Glu22
Initial Orientation		LB2		RB2				
Final Orientation	LS1	LB2		RS2	LB2	LS1	LB2	LB2
	LNH			RB2	LS2	-CH2-	LB1	-CH2-
	LB1				LS1			
Total Energy	161.657							
van der Waals	104.25							
electrostatic	-233.256							
ΔEs	-82.919							
	-17.452							
	-73.015							

	L	V	F	F	Asp23	Val24	Lys28
Initial Orientation			LB1	RB1			
Final Orientation				RB1	CS	RS1	RB1
				CS		RB1	RS2
				-CH-			
Total Energy	172.908						
van der Waals	107.527						
electrostatic	-217.621						
ΔEs	-71.668						
	-14.175						
	-57.38						

	L	V	F	F	Val24	Lys28
Initial Orientation			RB1	LB1		
Final Orientation			RS1	LB1	LS1	LS1
				RB1		LNH
Total Energy	172.552					
van der Waals	110.958					
electrostatic	-223.017					
ΔEs	-72.024					
	-10.744					
	-62.776					

	L	V	F	F	Asp23	Val24	Lys28
Initial Orientation			RB2	LB1			
Final Orientation	LS2			RB2	RB2	RS2	RS2
				RS2			2
				RB1			RB2
				CS			
				LS2			
Total Energy	179.186						
van der Waals	108.954						
electrostatic	-216.636						
ΔEs	-65.39						
	-12.748						
	-56.395						

	L	V	F	F	Gln15
Initial Orientation			LB1	RB2	
Final Orientation			LB1	RB2	LB2
			LS2		
			LB2		
Total Energy	196.419				
van der Waals	113.229				
electrostatic	-203.164				
ΔEs	-48.157				
	-8.473				
	-42.923				

	L	V	F	F
Initial Orientation			LB2	RB1
Final Orientation				RS1
				RB1
Total Energy	227.137			
van der Waals	117.459			
electrostatic	-175.095			
ΔEs	-17.439			
	-4.243			
	-14.854			

	L	V	F	F	Lys16
Initial Orientation			RB1	LB2	
Final Orientation	LNH		RB1		LS1
	LS1		LB1		LB1
Total Energy	197.716				
van der Waals	108.556				
electrostatic	-202.957				
ΔEs	-46.86				
	-13.146				
	-42.716				

	L	V	F	F
Initial Orientation			RB2	LB2
Final Orientation				
Total Energy	226.642			
van der Waals	119.917			
electrostatic	-181.38			
ΔEs	-17.934			
	-1.785			
	-21.139			

	L	V	F	F	Lys28
Initial Orientation			LB2	RB2	
Final Orientation					RS1
					2
					RNH
Total Energy	197.573				
van der Waals	116.823				
electrostatic	-203.015				
ΔEs	-47.003				
	-4.879				
	-42.774				

	H	H	Q	K	L	V	F	F
Initial Orientatio	RS1				LB1			
Final Orientatior	RS1			RS1	LS1			
				RB1	LNH			
				-CH2-	LB1			
				RNH				
Total Energy	159.81							
van der Waals	117.508							
electrostatic	-242.976							
ΔEs	-84.766							
	-4.194							
	-82.735							

	H	H	Q	K	L	V	F	F
Initial Orientatio	LS1				RB1			
Final Orientatior	LS1			RB1	RS1			
				LB1				
Total Energy	148.251							
van der Waals	117.809							
electrostatic	-258.276							
ΔEs	-96.325							
	-3.893							
	-98.035							

	H	H	Q	K	L	V	F	F	Gly9
Initial Orientatio	LB1				RB2				
Final Orientatior	LNH			RS1					LS1
	LS1			RNH					
Total Energy	160.8								
van der Waals	110.705								
electrostatic	-238.069								
ΔEs	-83.776								
	-10.997								
	-77.828								

	H	H	Q	K	L	V	F	F	Gly9	Tyr10
Initial Orientatio	RB2				LB1					
Final Orientatior	RB2	RNH		LS1	LB1				RB2	RB2
		-CH-		LNH*					C=O	-CH2-
		RS1		LB1*						
				RB1*						
				*-CH2-						
Total Energy	136.874									
van der Waals	104.652									
electrostatic	-255.216									
ΔEs	-107.702									
	-17.05									
	-94.975									

	H	H	Q	K	L	V	F	F			
Initial Orientatio	RB1				LB2						
Final Orientatior	RS1										
Total Energy	188.254										
van der Waals	119.565										
electrostatic	-213.403										
ΔEs	-56.322										
	-2.137										
	-53.162										

	H	H	Q	K	L	V	F	F			
Initial Orientatio	LB2				RB1						
Final Orientatior	LB2			LS1	RB1						
	LNH			LS1							
	-CH2-										
	LS1										
Total Energy	163.546										
van der Waals	113.652										
electrostatic	-237.977										
ΔEs	-81.03										
	-8.05										
	-77.736										

	H	H	Q	K	L	V	F	F			
Initial Orientatio	LS1				RB2						
Final Orientatior	LB2	LB2		LB1	RB2						
	LS1	-CH-		RB1							
				LNH							
				RNH							
Total Energy	137.401										
van der Waals	107.183										
electrostatic	-264.718										
ΔEs	-107.175										
	-14.519										
	-104.477										

	H	H	Q	K	L	V	F	F			
Initial Orientatio	RS1				LB2						
Final Orientatior	RB2			RS2	LB2						
	RB1			RB1							
	RNH										
	RS1										
Total Energy	145.721										
van der Waals	107.642										
electrostatic	-251.977										
ΔEs	-98.855										
	-14.06										
	-91.736										

	H	H	Q	K	L	V	F	F			
Initial Orientatio	LS2				RB2						
Final Orientatior	LS2			LB1	RS2						
				RS2							
				-CH2-							
Total Energy	127.725										
van der Waals	109.474										
electrostatic	-265.921										
ΔEs	-116.851										
	-12.228										
	-105.68										

	H	H	Q	K	L	V	F	F			
Initial Orientatio	RS2				LB2						
Final Orientatior	RS2			LS2	LB2				RS1	RS2	
	RS1			LB1					C=O	-CH-	
										RB2	
										-CH2-	
Total Energy	127.705										
van der Waals	112.236										
electrostatic	-267.955										
ΔEs	-116.871										
	-9.466										
	-107.714										

	H	H	Q	K	L	V	F	F			
Initial Orientatio	LB2				RB2						
Final Orientatior											
Total Energy	234.875										
van der Waals	119.025										
electrostatic	-168.242										
ΔEs	-9.701										
	-2.677										
	-8.001										

	H	H	Q	K	L	V	F	F			
Initial Orientatio	RB2				LB2						
Final Orientatior	RS1			RS2	LS2				RB2		
	RS2			RB1					C=O		
Total Energy	148.457										
van der Waals	113.464										
electrostatic	-257.555										
ΔEs	-96.119										
	-8.238										
	-97.314										

	H	H	Q	K	L	V	F	F	Gly9	Tyr10	Ala21
Initial Orientatio	LS1					RB1					
Final Orientatior	LS1	RB1		LB1	CS	RB1			LS1	LS1	RS1
		LB1		LS2					C=O	-CH-	
		CS		2							
		RNH		CS							
				-CH2-							
Total Energy	125.601										
van der Waals	102.169										
electrostatic	-262.568										
ΔEs	-118.975										
	-19.533										
	-102.327										

	H	H	Q	K	L	V	F	F			
Initial Orientatio	RB2					LB2					
Final Orientatior	LS2	LS1		RS1	LS2				LB1		
				RS2					CS		
				2							
Total Energy	108.835										
van der Waals	105.351										
electrostatic	-285.602										
ΔEs	-135.741										
	-16.351										
	-125.361										

	H	H	Q	K	L	V	F	F			
Initial Orientatio	LB2					RB2					
Final Orientation		RB2			RB2	RB2					
Total Energy	211.82										
van der Waals	114.733										
electrostatic	-190.424										
ΔEs	-32.756										
	-6.969										
	-30.183										

	H	H	Q	K	L	V	F	F			
Initial Orientatio	LS1						RB1				
Final Orientatior	LS1			LS2			LNH				
							CS				
Total Energy	144.693										
van der Waals	112.524										
electrostatic	-251.125										
ΔEs	-99.883										
	-9.178										
	-90.884										

	H	H	Q	K	L	V	F	F			
Initial Orientatio	RS1						LB1				
Final Orientatior	RS1		CS	RB1			CS				
			-CH2-	RS2			LB1				
				RS1			LS1				
				CS							
				C=O							
Total Energy	162.892										
van der Waals	109.207										
electrostatic	-231.074										
ΔEs	-81.684										
	-12.495										
	-70.833										

	H	H	Q	K	L	V	F	F			
Initial Orientatio	LB1						RB2				
Final Orientatior	LB1			LS2			RB2				
	LNH										
	LS1										
Total Energy	152.117										
van der Waals	106.486										
electrostatic	-243.86										
ΔEs	-92.459										
	-15.216										
	-83.619										

	H	H	Q	K	L	V	F	F	Val12		
Initial Orientatio	RB2						LB1				
Final Orientatior	RB2			RS1					RB2		
				2							
				RNH							
Total Energy	166.199										
van der Waals	115.723										
electrostatic	-239.148										
ΔEs	-78.377										
	-5.979										
	-78.907										

	H	H	Q	K	L	V	F	F			
Initial Orientatio	RB1						LB2				
Final Orientatior	RB1			LS2			LB2				
	RS2			2							
Total Energy	156.212										
van der Waals	112.105										
electrostatic	-240.948										
ΔEs	-88.364										
	-9.597										
	-80.707										

	H	H	Q	K	L	V	F	F	Val12		
Initial Orientatio	LB2						RB1				
Final Orientatior	LB2			RB1					LS1		
	LS1			LB1							
				RNH							
				-CH2-							
Total Energy	127.698										
van der Waals	109.278										
electrostatic	-267.899										
ΔEs	-116.878										
	-12.424										
	-107.658										

	H	H	Q	K	L	V	F	F			
Initial Orientatio	LS1				RB2						
Final Orientatior	LB1			LS2					CS		
	LNH								LB1		
	LS1										
Total Energy	143.235										
van der Waals	107.775										
electrostatic	-249.145										
ΔEs	-101.341										
	-13.927										
	-88.904										

	H	H	Q	K	L	V	F	F
Initial Orientatio	RS1						LB2	
Final Orientatior	RS1			LB1			LB2	
	2							
Total Energy	170.614							
van der Waals	117.987							
electrostatic	-232.644							
ΔEs	-73.962							
	-3.715							
	-72.403							

	H	H	Q	K	L	V	F	F
Initial Orientatio	LS2						RB2	
Final Orientatior	LS2			RS2			RB2	
				RB2				
Total Energy	159.764							
van der Waals	114.119							
electrostatic	-238.264							
ΔEs	-84.812							
	-7.583							
	-78.023							

	H	H	Q	K	L	V	F	F
Initial Orientatio	RS2						LB2	
Final Orientatior	RS1			RS2			LB2	
	RS2							
Total Energy	135.225							
van der Waals	115.564							
electrostatic	-267.739							
ΔEs	-109.351							
	-6.138							
	-107.498							

	H	H	Q	K	L	V	F	F
Initial Orientatio	RB2						LB2	
Final Orientatior	RS1			LNH			LB2	
	RB2							
	RS2							
Total Energy	150.552							
van der Waals	117.159							
electrostatic	-255.13							
ΔEs	-94.024							
	-4.543							
	-94.889							

	H	H	Q	K	L	V	F	F
Initial Orientatio	LB2						RB2	
Final Orientatior	LNH	LB2		RB1			RB2	
	LS1	-CH-		LB1				
	LB2			LB2				
	-CH2-			-CH2-				
Total Energy	143.735							
van der Waals	111.761							
electrostatic	-252.841							
ΔEs	-100.841							
	-9.941							
	-92.6							

	H	H	Q	K	L	V	F	F
Initial Orientatio	LB2						RB2	
Final Orientatior	LB2			LS2	RS2			
	LS2			LNH	RB2			
				LB1				
Total Energy	166.637							
van der Waals	113.907							
electrostatic	-234.523							
ΔEs	-77.939							
	-7.795							
	-74.282							

	H	H	Q	K	L	V	F	F
Initial Orientatio	RB2							LB2
Final Orientatior	RS2			LB1	LB2			LB2
	RB2			RB1	LS1			
				RS2				
Total Energy	146.922							
van der Waals	110.396							
electrostatic	-251.276							
ΔEs	-97.654							
	-11.306							
	-91.035							

	H	H	Q	K	L	V	F	F	Tyr10	Lys28
Initial Orientation		CS			RB1					
Final Orientation		LB1							CS	RS1
		LB1							-CH2-	2
		LS1								
		CS								
		-CH2-								
		LS2								
Total Energy	139.226									
van der Waals	107.27									
electrostatic	-251.961									
ΔEs	-105.35									
	-14.432									
	-91.72									

	H	H	Q	K	L	V	F	F	Tyr10
Initial Orientation		CS			LB1				
Final Orientation		LB1							CS
		LB1							
		LS1							
		CS							
		-CH2-							
		LS2							
Total Energy	180.587								
van der Waals	114.075								
electrostatic	-222.078								
ΔEs	-63.989								
	-7.627								
	-61.837								

	H	H	Q	K	L	V	F	F	His6	Tyr10
Initial Orientation		CS			RB2					
Final Orientation	RS2	RB1							LS2	LB1
		RB1								CS
		RS1								RS2
		RS2								-CH2-
		-CH2-								
Total Energy	125.618									
van der Waals	104.951									
electrostatic	-260.079									
ΔEs	-118.958									
	-16.751									
	-99.838									

	H	H	Q	K	L	V	F	F	Tyr10
Initial Orientation		CS			LB2				
Final Orientation		LB1		LS1	LB2	LS2			CS
		LS2		-CH2-					
		CS							
		-CH2-							
		LS1							
		-CH-							
Total Energy	144.585								
van der Waals	109.131								
electrostatic	-247.972								
ΔEs	-99.991								
	-12.571								
	-87.731								

	H	H	Q	K	L	V	F	F
Initial Orientation		RB1			LB1			
Final Orientation		RS1			LS1			
Total Energy	193.612							
van der Waals	116.732							
electrostatic	-208.82							
ΔEs	-50.964							
	-4.97							
	-48.579							

	H	H	Q	K	L	V	F	F
Initial Orientation		LB1			RB1			
Final Orientation		LS2			RS1			
		LB1						
Total Energy	196.56							
van der Waals	116.449							
electrostatic	-203.336							
ΔEs	-48.016							
	-5.253							
	-43.095							

	H	H	Q	K	L	V	F	F
Initial Orientation		RS1			LB1			
Final Orientation		RS1						
Total Energy	199.718							
van der Waals	118.785							
electrostatic	-207.434							
ΔEs	-44.858							
	-2.917							
	-47.193							

	H	H	Q	K	L	V	F	F
Initial Orientation		LS1			RB1			
Final Orientation		LS1		RS1	RB1			
		2		2	RNH			
				RB1				
				-CH2-				
Total Energy	174.681							
van der Waals	113.922							
electrostatic	-231.044							
ΔEs	-69.895							
	-7.78							
	-70.803							

	H	H	Q	K	L	V	F	F	
Initial Orientation		RS2			LB1				
Final Orientation		RS2		CS	LS2				
				-CH2-	LS1				
					LB1				
Total Energy	170.96								
van der Waals	115.096								
electrostatic	-230.888								
ΔEs	-73.616								
	-6.606								
	-70.647								

	H	H	Q	K	L	V	F	F	
Initial Orientation		LS2			RB1				
Final Orientation		LS2			CS				
					RB1				
Total Energy	179.174								
van der Waals	115.093								
electrostatic	-221.564								
ΔEs	-65.402								
	-6.609								
	-61.323								

	H	H	Q	K	L	V	F	F	
Initial Orientation		LB1			RB2				
Final Orientation		LB1		RS1	RB2				
		LS1		-CH2-					
Total Energy	178.192								
van der Waals	112.803								
electrostatic	-219.722								
ΔEs	-66.384								
	-8.899								
	-59.481								

	H	H	Q	K	L	V	F	F	
Initial Orientation		RB2			LB1				
Final Orientation		RB2			LB1			LB1	LB2
		LS2			LB1			LB2	
		LB1*							
		*-CH2-							
Total Energy	158.538								
van der Waals	106.371								
electrostatic	-238.411								
ΔEs	-86.038								
	-15.331								
	-78.17								

	H	H	Q	K	L	V	F	F	Glu22
Initial Orientation		RB1			LB2				
Final Orientation		LS2		LS2	LB2				RB2
		RS2		-CH2-	LS2				
Total Energy	168.751								
van der Waals	107.625								
electrostatic	-223.984								
ΔEs	-75.825								
	-14.077								
	-63.743								

	H	H	Q	K	L	V	F	F	Tyr10
Initial Orientation		LB2			RB1				
Final Orientation	LS1	LB2		LS1	RS1				LS1
	-CH2-	LS1		-CH2-	RB1				-CH-
		-CH-							
Total Energy	160.103								
van der Waals	108.186								
electrostatic	-237.017								
ΔEs	-84.473								
	-13.516								
	-76.776								

	H	H	Q	K	L	V	F	F	
Initial Orientation		LS2			RB2				
Final Orientation		LB2			RB2				LB2
		LB2							
		LS2							
Total Energy	196.786								
van der Waals	115.584								
electrostatic	-204.162								
ΔEs	-47.79								
	-6.118								
	-43.921								

	H	H	Q	K	L	V	F	F	
Initial Orientation		RS2			LB2				
Final Orientation		RS2		LB2					
				LS2					
Total Energy	166.669								
van der Waals	113.785								
electrostatic	-226.407								
ΔEs	-77.907								
	-7.917								
	-66.166								

	H	H	Q	K	L	V	F	F	
Initial Orientation		RB2			LB2				
Final Orientation		RB2							
		RS2							
Total Energy	193.975								
van der Waals	118.191								
electrostatic	-212.378								
ΔEs	-50.601								
	-3.511								
	-52.137								

	H	H	Q	K	L	V	F	F	
Initial Orientation		LB2			RB2				
Final Orientation		LS2							LB2
		LB2							
Total Energy	196.406								
van der Waals	115.722								
electrostatic	-207.449								
ΔEs	-48.17								
	-5.98								
	-47.208								

	H	H	Q	K	L	V	F	F	
Initial Orientation		RB2					LB2		
Final Orientation									
Total Energy	243.903								
van der Waals	120.118								
electrostatic	-162.583								
ΔEs	-0.673								
	-1.584								
	-2.342								

	H	H	Q	K	L	V	F	F	
Initial Orientation		LB2					RB2		
Final Orientation									
Total Energy	248.63								
van der Waals	119.979								
electrostatic	-151.408								
ΔEs	4.054								
	-1.723								
	8.833								

	H	H	Q	K	L	V	F	F	
Initial Orientation		LS1						RB1	
Final Orientation		LS1			CS	LS1		RS1	
		2							
Total Energy	195.091								
van der Waals	114.03								
electrostatic	-201.888								
ΔEs	-49.485								
	-7.672								
	-41.647								

	H	H	Q	K	L	V	F	F	
Initial Orientation		LB1						RB2	
Final Orientation		LS1			RB1				
		LB1			RS1				
Total Energy	191.612								
van der Waals	113.542								
electrostatic	-203.88								
ΔEs	-52.964								
	-8.16								
	-43.639								

	H	H	Q	K	L	V	F	F	Ala21
Initial Orientation		RB2						LB1	
Final Orientation		RB2			LB2			LB1	RB1
Total Energy	221.174								
van der Waals	114.127								
electrostatic	-178.988								
ΔEs	-23.402								
	-7.575								
	-18.747								

	H	H	Q	K	L	V	F	F	Ala21
Initial Orientation		RB1						LB2	
Final Orientation		RS1							LB1
Total Energy	189.882								
van der Waals	116.382								
electrostatic	-217.454								
ΔEs	-54.694								
	-5.32								
	-57.213								

	H	H	Q	K	L	V	F	F	
Initial Orientation		LS1						RB2	
Final Orientation		LS1			RS1				
					RNH				
Total Energy	195.862								
van der Waals	115.556								
electrostatic	-207.55								
ΔEs	-48.714								
	-6.146								
	-47.309								

	H	H	Q	K	L	V	F	F	
Initial Orientation		RS1						LB2	
Final Orientation		RS1							
Total Energy	197.571								
van der Waals	114.946								
electrostatic	-198.882								
ΔEs	-47.005								
	-6.756								
	-38.641								

	H	H	Q	K	L	V	F	F	Val24
Initial Orientation		LS2						RB2	
Final Orientation		LS2				LS2			RB2
		2							
		LB2							
Total Energy	193.896								
van der Waals	113.618								
electrostatic	-203.469								
ΔEs	-50.68								
	-8.084								
	-43.228								

	H	H	Q	K	L	V	F	F
Initial Orientation		RS2						LB2
Final Orientation		RS2			LS2			
Total Energy	201.567							
van der Waals	117.327							
electrostatic	-199.607							
ΔEs	-43.009							
	-4.375							
	-39.366							

	H	H	Q	K	L	V	F	F
Initial Orientation		RB2						LB2
Final Orientation		RB2						
		RS2						
Total Energy	200.391							
van der Waals	119.23							
electrostatic	-201.534							
ΔEs	-44.185							
	-2.472							
	-41.293							

	H	H	Q	K	L	V	F	F
Initial Orientation		LB2						RB2
Final Orientation		LS2						
		LB2						
Total Energy	200.265							
van der Waals	116.54							
electrostatic	-200.836							
ΔEs	-44.311							
	-5.162							
	-40.595							

	H	H	Q	K	L	V	F	F
Initial Orientation				CS	RB1			
Final Orientation	LS2			LB1	RS1			
				LS1*				
				RB1				
				RS1*				
				*-CH2-				
Total Energy	148.76							
van der Waals	113.861							
electrostatic	-252.041							
ΔEs	-95.816							
	-7.841							
	-91.8							

	H	H	Q	K	L	V	F	F	Val12
Initial Orientation				CS	LB1				
Final Orientation	RS2			RB1					RS1
	RS1			RS1					
				-CH2-					
Total Energy	148.531								
van der Waals	112.791								
electrostatic	-251.384								
ΔEs	-96.045								
	-8.911								
	-91.143								

	H	H	Q	K	L	V	F	F
Initial Orientation				RB1	LB1			
Final Orientation				RS1	CS			
				2	LB1			
				RNH				
				RB1				
Total Energy	194.844							
van der Waals	120.668							
electrostatic	-210.997							
ΔEs	-49.732							
	-1.034							
	-50.756							

	H	H	Q	K	L	V	F	F
Initial Orientation				LB1	RB1			
Final Orientation				LB1	RS1			RS1
				LS2	RB1			
				2				
				LS1				
				-CH2-				
Total Energy	159.296							
van der Waals	114.511							
electrostatic	-241.318							
ΔEs	-85.28							
	-7.191							
	-81.077							

	H	H	Q	K	L	V	F	F
Initial Orientation				RS1	LB1			
Final Orientation				RS1	CS			LS1
				2				
				RB1				
Total Energy	192.163							
van der Waals	119.621							
electrostatic	-211.749							
ΔEs	-52.413							
	-2.081							
	-51.508							

	H	H	Q	K	L	V	F	F
Initial Orientation				LS1	RB1			
Final Orientation				LB1	RB1			
				LS2				
				2				
				LS1				
				-CH2-				
Total Energy	164.666							
van der Waals	114.47							
electrostatic	-236.204							
ΔEs	-79.91							
	-7.232							
	-75.963							

	H	H	Q	K	L	V	F	F
Initial Orientation				RS2	LB1			
Final Orientation				RB1	LS2			LS1
				RS1	LB1			
				RS2	CS			
Total Energy	165.726							
van der Waals	114.659							
electrostatic	-234.27							
ΔEs	-78.85							
	-7.043							
	-74.029							

	H	H	Q	K	L	V	F	F
Initial Orientation				LS2	RB1			
Final Orientation				LS2	RS2		RS2	RS2
				2			RB2	RB2
Total Energy	172.668							
van der Waals	111.733							
electrostatic	-222.956							
ΔEs	-71.908							
	-9.969							
	-62.715							

	H	H	Q	K	L	V	F	F
Initial Orientation				LB1	RB2			
Final Orientation	RS1	RS2		LS2				
	RS2	RB2		LB1				
	-CH2-			RS2				
				-CH2-				
Total Energy	114.522							
van der Waals	109.928							
electrostatic	-284.903							
ΔEs	-130.054							
	-11.774							
	-124.662							

	H	H	Q	K	L	V	F	F
Initial Orientation				RB2	LB1			
Final Orientation				RB2	LB1			
				RS2				
Total Energy	195.63							
van der Waals	116.705							
electrostatic	-205.997							
ΔEs	-48.946							
	-4.997							
	-45.756							

	H	H	Q	K	L	V	F	F			H	H	Q	K	L	V	F	F	
Initial Orientation				RB1	LB2					Initial Orientation				LB2	RB1				
Final Orientation				LB1	LB2					Final Orientation				LB1	RNH				
				RB1										LNH	RB1				
				LNH*															
				LS1*															
				*-CH2-															
Total Energy	162.287									Total Energy	203.41								
van der Waals	114.769									van der Waals	115.398								
electrostatic	-242.039									electrostatic	-201.393								
ΔEs	-82.289									ΔEs	-41.166								
	-6.933										-6.304								
	-81.798										-41.152								

	H	H	Q	K	L	V	F	F			H	H	Q	K	L	V	F	F	
Initial Orientation				LS2	RB2					Initial Orientation				RS2	LB2				
Final Orientation	LS2	RS2		LS2	RS2					Final Orientation	RB2			RS2	LB2				
				LS1							RS2			RB1	LS2				
				LB1										RS1					
				RS2															
				-CH2-															
Total Energy	121.887									Total Energy	169.22								
van der Waals	113.119									van der Waals	114.423								
electrostatic	-277.752									electrostatic	-235.432								
ΔEs	-122.689									ΔEs	-75.356								
	-8.583										-7.279								
	-117.511										-75.191								

	H	H	Q	K	L	V	F	F			H	H	Q	K	L	V	F	F	
Initial Orientation				LB2	RB2					Initial Orientation				RB2	LB2				
Final Orientation				LS2	RB2			RB2		Final Orientation	RB2			RB1	LB2				
					RS2						RS2			CS	LS2				
														LB1					
														-CH2-					
														RS2					
Total Energy	178.578									Total Energy	161.177								
van der Waals	117.844									van der Waals	112.116								
electrostatic	-224.83									electrostatic	-233.026								
ΔEs	-65.998									ΔEs	-83.399								
	-3.858										-9.586								
	-64.589										-72.785								

	H	H	Q	K	L	V	F	F			H	H	Q	K	L	V	F	F	Tyr10
Initial Orientation				LB1		RB2				Initial Orientation				RB1		LB2			
Final Orientation	RS2	RS2		LB1						Final Orientation	LS1	LB2		RB1	LS2	LB2			LS1
	-CH2-	-CH-		LS2							LB1	LS1		LB1	LB2				-CH2-
		RB2		LNH							LNH	-NH-		RNH					
				RS2							-CH2-			LNH					
				-CH2-										-CH2-					
Total Energy	131.997									Total Energy	142.465								
van der Waals	109.864									van der Waals	105.045								
electrostatic	-261.229									electrostatic	-248.714								
ΔEs	-112.579									ΔEs	-102.111								
	-11.838										-16.657								
	-100.988										-88.473								

	H	H	Q	K	L	V	F	F			H	H	Q	K	L	V	F	F	Ala21
Initial Orientation				LS2		RB2				Initial Orientation				RS2		LB2			
Final Orientation	LS2	RB2		LS2		RB2				Final Orientation	RS1	LS1		RS2	LS1	LS1			LB2
		RS2		LNH							RNH	LB2		2		LB2			
				LB1							RB1								
				RS2															
				-CH2-															
Total Energy	122.12									Total Energy	118.876								
van der Waals	112.056									van der Waals	106.614								
electrostatic	-274.468									electrostatic	-276.187								
ΔEs	-122.456									ΔEs	-125.7								
	-9.646										-15.088								
	-114.227										-115.946								

	H	H	Q	K	L	V	F	F	Ala21		H	H	Q	K	L	V	F	F	
Initial Orientation				RB2		LB2				Initial Orientation				LB2		RB2			
Final Orientation	RS1	LB2		RS2		LB2			LB2	Final Orientation		RB2		LS2					
				RB1								RS2		LB2					
				RNH															
Total Energy	125.774									Total Energy	152.234								
van der Waals	108.748									van der Waals	115.229								
electrostatic	-267.813									electrostatic	-245.883								
ΔEs	-118.802									ΔEs	-92.342								
	-12.954										-6.473								
	-107.572										-85.642								

	H	H	Q	K	L	V	F	F			H	H	Q	K	L	V	F	F	
Initial Orientation				CS			RB1			Initial Orientation				CS			LB1		
Final Orientation				LS1			RS1			Final Orientation				RB1	CS				
				2										RS1					
														CS					
														RS2					
Total Energy	207.682									Total Energy	171.397								
van der Waals	119.986									van der Waals	114.218								
electrostatic	-200.146									electrostatic	-229.993								
ΔEs	-36.894									ΔEs	-73.179								
	-1.716										-7.484								
	-39.905										-69.752								

	H	H	Q	K	L	V	F	F
Initial Orientation				CS			RB2	
Final Orientation				RB1	RS1		RS2	
				RS1				
				RS2				
Total Energy	197.374							
van der Waals	116.266							
electrostatic	-207.208							
ΔEs	-47.202							
	-5.436							
	-46.967							

	H	H	Q	K	L	V	F	F
Initial Orientation				CS			LB2	
Final Orientation				LB1				
				LS1				
				LS2				
Total Energy	186.299							
van der Waals	117.813							
electrostatic	-215.419							
ΔEs	-58.277							
	-3.889							
	-55.178							

	H	H	Q	K	L	V	F	F
Initial Orientation				RB1			LB1	
Final Orientation	RS1			RB1				
				RS1				
				RS2				
Total Energy	157.162							
van der Waals	113.685							
electrostatic	-242.832							
ΔEs	-87.414							
	-8.017							
	-82.591							

	H	H	Q	K	L	V	F	F
Initial Orientation				LB1			RB1	
Final Orientation	LS1			LS1			RS1	
	LS2			2				
Total Energy	169.272							
van der Waals	119.2							
electrostatic	-233.396							
ΔEs	-75.304							
	-2.502							
	-73.155							

	H	H	Q	K	L	V	F	F
Initial Orientation				RS1			LB1	
Final Orientation	RS1			RS2				
	2							
Total Energy	159.948							
van der Waals	119.623							
electrostatic	-243.4							
ΔEs	-84.628							
	-2.079							
	-83.159							

	H	H	Q	K	L	V	F	F
Initial Orientation				LS1			RB1	
Final Orientation				LS1				
				2				
				LNH				
Total Energy	192.522							
van der Waals	119.997							
electrostatic	-211.935							
ΔEs	-52.054							
	-1.705							
	-51.694							

	H	H	Q	K	L	V	F	F
Initial Orientation				RS2			LB1	
Final Orientation				RS1			CS	
				RS2				
				2				
Total Energy	185.586							
van der Waals	117.783							
electrostatic	-218.594							
ΔEs	-58.99							
	-3.919							
	-58.353							

	H	H	Q	K	L	V	F	F
Initial Orientation				LS2			RB1	
Final Orientation				LS2				
Total Energy	192.351							
van der Waals	117.623							
electrostatic	-211.533							
ΔEs	-52.225							
	-4.079							
	-51.292							

	H	H	Q	K	L	V	F	F
Initial Orientation				LB1			RB2	
Final Orientation				LB1			RNH	
				LNH				
Total Energy	190.876							
van der Waals	115.247							
electrostatic	-212.534							
ΔEs	-53.7							
	-6.455							
	-52.293							

	H	H	Q	K	L	V	F	F
Initial Orientation				RB2			LB1	
Final Orientation				RS1				
				RNH				
Total Energy	203.322							
van der Waals	114.455							
electrostatic	-201.592							
ΔEs	-41.254							
	-7.247							
	-41.351							

	H	H	Q	K	L	V	F	F
Initial Orientation				RB1			LB2	
Final Orientation	RS1			RS2			LS2	
				LB1			LB2	
Total Energy	132.817							
van der Waals	114.731							
electrostatic	-265.211							
ΔEs	-111.759							
	-6.971							
	-104.97							

	H	H	Q	K	L	V	F	F
Initial Orientation				LB2			RB1	
Final Orientation				LB2	LS2			
				LS2				
Total Energy	191.069							
van der Waals	114.698							
electrostatic	-212.215							
ΔEs	-53.507							
	-7.004							
	-51.974							

	H	H	Q	K	L	V	F	F
Initial Orientation				LS2			RB2	
Final Orientation	LS2			LS2			RS2	
				LB1			RB2	
Total Energy	174.215							
van der Waals	116.574							
electrostatic	-226.624							
ΔEs	-70.361							
	-5.128							
	-66.383							

	H	H	Q	K	L	V	F	F
Initial Orientation				RS2			LB2	
Final Orientation	RS1			LB1			LB2	
	RS2			RB1				
				RS2				
				-CH2-				
Total Energy	119.08							
van der Waals	113.42							
electrostatic	-279.964							
ΔEs	-125.496							
	-8.282							
	-119.723							

	H	H	Q	K	L	V	F	F
Initial Orientation				RB2			LB2	
Final Orientation	RS1			RB1				
	RS2			RS2				
				-CH2-				
Total Energy	144.843							
van der Waals	112.278							
electrostatic	-251.977							
ΔEs	-99.733							
	-9.424							
	-91.736							

	H	H	Q	K	L	V	F	F
Initial Orientation				LB2			RB2	
Final Orientation	LS2			LS2				
	LB2			LS1				
Total Energy	164.467							
van der Waals	116.009							
electrostatic	-235.955							
ΔEs	-80.109							
	-5.693							
	-75.714							

	H	H	Q	K	L	V	F	F	Val12
Initial Orientation				CS				RB2	
Final Orientation	LS2			LB1	RS2		RS2	RB2	LS2
	LS1			LS2					
				-CH2-					
Total Energy	142.078								
van der Waals	106.753								
electrostatic	-255.052								
ΔEs	-102.498								
	-14.949								
	-94.811								

	H	H	Q	K	L	V	F	F
Initial Orientation				RS1				LB1
Final Orientation				RS1				LS1
				2				
Total Energy	203.182							
van der Waals	116.061							
electrostatic	-196.609							
ΔEs	-41.394							
	-5.641							
	-36.368							

	H	H	Q	K	L	V	F	F
Initial Orientation				LB1				RB2
Final Orientation				LS1			RS1	RB2
				LB1				
				LNH				
Total Energy	195.371							
van der Waals	117.58							
electrostatic	-206.786							
ΔEs	-49.205							
	-4.122							
	-46.545							

	H	H	Q	K	L	V	F	F
Initial Orientation				RB1				LB2
Final Orientation				RS1				
				2				
				RNH				
				RB1				
Total Energy	190.747							
van der Waals	120.251							
electrostatic	-212.815							
ΔEs	-53.829							
	-1.451							
	-52.574							

	H	H	Q	K	L	V	F	F
Initial Orientation				LS1				RB2
Final Orientation				LS1				
				LNH				
				LB2				
				-CH2-				
Total Energy	185.155							
van der Waals	117.83							
electrostatic	-217.566							
ΔEs	-59.421							
	-3.872							
	-57.325							

	H	H	Q	K	L	V	F	F
Initial Orientation				LS2				RB2
Final Orientation	LS2			LS2				
				RB1				
				LNH				
Total Energy	175.851							
van der Waals	118.061							
electrostatic	-227.405							
ΔEs	-68.725							
	-3.641							
	-67.164							

	H	H	Q	K	L	V	F	F
Initial Orientation				RB2				LB2
Final Orientation				RB2				LB2
				RS2				
				2				
Total Energy	200.04							
van der Waals	118.514							
electrostatic	-203.77							
ΔEs	-44.536							
	-3.188							
	-43.529							

	H	H	Q	K	L	V	F	F
Initial Orientation				CS				LB2
Final Orientation				LS2	LS2		LS2	LB2
				LB1			LS1	LS2
								-CH2-
Total Energy	189.807							
van der Waals	109.772							
electrostatic	-208.218							
ΔEs	-54.769							
	-11.93							
	-47.977							

	H	H	Q	K	L	V	F	F
Initial Orientation				LS1				RB1
Final Orientation				LS1	LB1		CS	CS
				2				-CH2-
								RB1
								RS1
Total Energy	198.741							
van der Waals	111.434							
electrostatic	-199.89							
ΔEs	-45.835							
	-10.268							
	-39.649							

	H	H	Q	K	L	V	F	F
Initial Orientation				RB2				LB1
Final Orientation				RB2	RS1			LB1
				RS1				
				2				
Total Energy	191.594							
van der Waals	112.661							
electrostatic	-218.147							
ΔEs	-52.982							
	-9.041							
	-57.906							

	H	H	Q	K	L	V	F	F
Initial Orientation				LB2				RB1
Final Orientation				LB2				CS
Total Energy	206.743							
van der Waals	111.73							
electrostatic	-199.399							
ΔEs	-37.833							
	-9.972							
	-39.158							

	H	H	Q	K	L	V	F	F
Initial Orientation				RS1				LB2
Final Orientation				RS1	LB1			
				2				
				RB1				
				RNH				
Total Energy	192.02							
van der Waals	117.668							
electrostatic	-209.561							
ΔEs	-52.556							
	-4.034							
	-49.32							

	H	H	Q	K	L	V	F	F
Initial Orientation				RS2				LB2
Final Orientation				RS2				LS2
				2				LB2
Total Energy	191.221							
van der Waals	119.17							
electrostatic	-210.86							
ΔEs	-53.355							
	-2.532							
	-50.619							

	H	H	Q	K	L	V	F	F
Initial Orientation				LB2				RB2
Final Orientation				LB2				
				LS2				
				2				
Total Energy	201.232							
van der Waals	122.045							
electrostatic	-205.845							
ΔEs	-43.344							
	0.343							
	-45.604							